NIRS

HIMAC

NIRS-M-103
HIMAC-008

Proceedings of NIRS International Seminar on the Application of Heavy Ion Accelerator to Radiation Therapy of Cancer in connection with XXI PTCOG Meeting

Edited by
Tatsuaki Kanai
Eiichi Takada

November 14 - 16, 1994

National Institute of Radiological Sciences

9-1, Anagawa 4-chome, Inage-ku, Chiba-shi 263 JAPAN

Proceedings of NIRS International Seminar on the Application of Heavy Ion Accelerator to Radiation Therapy of Cancer in connection with XXI PTCOG Meeting

Edited by
Tatsuaki Kanai
Eiich Takada

November 14 - 16, 1994

National Institute of Radiological Sciences
9-1, Anagawa 4-chome, Inage-ku, Chiba-shi 263 JAPAN

International Seminar Organization

Advisory Committee

Chairman : K. Morita(NIRS)

Vice Chairman: K. Kawachi(NIRS)
A. Akanuma(NIRS)
M. Goitein(MGH)
H. Ikeda(National Cancer Center)
T. Inada(U. Tsukuba)
A. Itoh(Cancer Institute)
S. Kimura(Hyogo Medical Center for Adults)
T. Kumatori(Radiation Effects Association)
K. Mori(Japan Atomic Industrial Forum)
R. Mukherjee(IAEA)
N. Nohara(NIRS)
Y. Ohtsu(NIRS)
N. Suzuki(U. Tokyo)
K. Tatsumi(NIRS)
H. Tsujii(NIRS)

Local Organizing Committee

Chairman : K. Kawachi
K. Ando
M. Endo
Y. Furusawa
H. Imazeki
T. Kanai (Editor)
S. Kato
T. Nakano
J. Mizoe
M. Murakami
F. Soga
E. Takada (Editor)

Acknowledgements

The organizing committee would like to express their gratitude to various sponsors and organizations for the support of the seminar, in particular,

International Atomic Energy Agency,
Proton Therapy Co-Operative Group,
Japan Atomic Industrial Forum, Inc.
International Science Foundation,
Japan International Cooperation Agency.

Organizing Committee

contents

3. Poster

4. Proton Therapy and Facility

5. Biology I

6. Biology II

7. Clinical Results and Protocols

8. Beam Delivery and Dosimetry

9. Treatment Planning

10. Projects and Status II

11. Perspectives

12. Closing

Appendix

Opening

Opening Address

Director General of National Institute of Radiological Sciences
Yasuo Hirao, Ph.D.

Ladies and Gentlemen:

I would like to have a great honor to deliver the opening address of the NIRS International Seminar on the "Application of Heavy Ion Accelerator to Radiation Therapy of Cancer" here today.

We, NIRS, are very much pleased to have such the nice and many participants of prominent experts in the field of charged particle therapy and related biology in the world. At the planning stage of this seminar, PTCOG (proton therapy cooperative group) decided kindly to bring the XXI meeting to Japan, and then, we decided to hold in conjunction with PTCOG XXI meeting.

We are also very much encouraged to hear that IAEA has a strong interest in the particle therapy as an important field of application of radiation in the life-science. This seminar, therefore, is cooperated with IAEA (International Atomic Energy Agency) Consultant's Meeting on the "Application of High-LET Radiation in Cancer Treatment". We appreciate very much the warmest consideration of IAEA.

Another great help for this seminar is owing to Japan Atomic Industrial Forum. Inc. (JAIF). Because JAIF is also interested in an application of the particle accelerator in medicine, which is one of the important activities in the field of peace application of nuclear energy. JAIF supports an industrial accelerator research group to promote a newly coming-up field, such as medical particle accelerator. These activities are also very effective to bring up heavy particle therapy in Japan.

By the way, our heavy ion medical facility, HIMAC, has just started its clinical trial of cancer treatment. Japanese government, especially STA (Science and Technology Agency), made the greatest possible support for this project. Furthermore, I believe that this project was strongly supported by the international research cooperation and encouragement between all of you. I wish to make this seminar the opportunity to express my gratitude, and I would like to expect further fostering of the international research collaboration using HIMAC.

The HIMAC itself is just at the commissioning stage and only realized some simple and basic mode among many kinds of capability, in other words, only at a milestone of our goal. New hospital corresponding to HIMAC is still under construction. Therefore, further suggestions and comments from various (medical and biological) sides are quite important and helpful for our side.

I sincerely hope that this international seminar will be quite informative and fruitful, and will give a future prospect to the charged particle therapy.

Historical Aspects of Heavy Ion Radiotherapy

Mudundi R. Raju
Life Sciences Division, Los Alamos National Laboratory, Los Alamos NM

Summary

Historical developments of heavy-ion radiotherapy including cooperation between Japan and United States along with some personal reflections are presented.

Introduction

My research career started out with an interest to pursue neutron capture therapy and Bragg peak therapy while I was still a graduate student in nuclear physics in India. I never could have imagined then that I would ever have the honor of presenting a main lecture to a distinguished audience like this. I thank the organizers for giving me this opportunity.

I had the pleasure of being associated with the developments of heavy particle therapy since 1961, starting as a postdoctoral fellow at Massachusetts General Hospital, Boston, then at Lawrence Berkeley Laboratory during 1963-1971 and, finally, Los Alamos National Laboratory since 1971. I also had the opportunity to participate in some of the US-Japan, US-EORTC and US-USSR cooperative meetings.

I will try to present to you some of the historical aspects of heavy ion radiotherapy. The developments of other heavy particles such as, neutrons, pions and protons, in radiotherapy, are also related to some of the aspects of heavy ion radiotherapy. Although my presentation is mainly on heavy ions, I will bring some aspects of other heavy particles within the context of my presentation.

Historical developments

Dr. Cornelius Tobias was primarily instrumental in initiating the heavy ion therapy program . His interest in heavy ions dates back to his graduate student days at Berkeley. In 1938, Dr. Louis Alvarez, his thesis advisor, began to wonder why everyone was accelerating protons, deuterons and helium and not heavier nuclei. As Alvarez was interested in using a bigger projectile, he put some carbon into the 37-inch cyclotron and was able to attain a very unsteady stream of fast carbon particles. The thesis project of Dr. Tobias was an attempt to accelerate carbon nuclei at the 60-inch cyclotron. He soon found out that Alvarez was using the wrong gas, methane, in the arc ion source. Methane produced a large number of hydrogen ions, which apparently overwhelmed the carbon ions in the arc. One day, Dr. Tobias tried carbon dioxide. This yielded clean resonating beams of carbon and, alternatively, of oxygen. He became quite excited because he recognized that this could be the beginning of nuclear science with heavy ions. His thesis in 1942 was entitled "High Energy Carbon Particles". This thesis, like most other nuclear physics research during the war, became classified as soon as it was written. He studied nuclear interactions with carbon using nuclear emulsions and found multiple-pronged events. The laboratory decided to use the 60-inch cyclotron for producing more plutonium during the second world war and, hence, the experiments of Tobias were stopped. As a graduate student, he also assisted the fast neutron therapy program conducted by Stone and Lawrence. After the war, in 1950, his thesis was unclassified and was published as a laboratory report (UCRL 1039). Dr. Tobias, in a talk to the American Physical Society, proposed the idea of using a linear accelerator as an injector to a cyclotron for producing high-energy heavy ions.

Zirkle had already demonstrated, in 1935, big biological effects of alpha particles from polonium and, subsequently, with fast

neutrons[10]. Since the protons did not produce biological effects much different from X-rays, it was then thought that heavy ions had all the advantages of protons and, in addition, they also had a high-LET effect.

Rationale of heavy ions in radiotherapy

The rationale for the use of heavy ions in radiotherapy comes from the study of low-energy heavy-ion effects on cultured cells by Paul Todd at Berkeley using the low-energy heavy-ion accelerator (HILAC) and the Lloyd Skarsgard, Deering and Rice from Yale University HILAC during the early 1960's. The rationale was that the radioresistance of the tumors could be due to the presence of hypoxic tumor cells and/or the tumor cells in radioresistant phases of the cell cycle[2,8,9]. The earlier studies by Barendsen using low-energy alpha particles from polonium indicated that the OER of 3-Mev alpha particles was close to unity. The low-energy heavy-ion studies also indicated that the OER for carbon ions with energy of about 10 Mev/u was also very close to unity, and there was practically no variation of radiosensitivity as a function of cell cycle. Unlike for fast neutrons and protons, from a radiobiologic point of view, there is a large variation in heavy-ion effects with both energy and energy modulation required to treat large tumors. The extrapolation of the effects observed at low energies to high energy turned out to be a lot more complicated and the expectations of achieving very low OER were not materialized.

High energy heavy ion beams

Heavy ions with ranges adequate for radiotherapy were not available until 1974, when two existing accelerators at Lawrence Berkeley Laboratory, the heavy ion linear accelerator (HILAC) and the Bevatron were modified and connected together to accelerate heavy ions to energies suitable for heavy ion radiotherapy. This combined facility was known as Bevalac and this was the only biomedical heavy-ion facility in the world, until its eventual shutdown in 1993.

Soon after the availability of high-energy heavy-ion beams, an extensive series of radiobiological experiments were conducted at Berkeley[1]. I had the privilege of conducting radiobiological experiments for the first time using radiotherapeutically appropriate heavy-ion beams, by broadening their narrow Bragg peaks to 10 cm width[4]. These results surprised everyone, because of the expectations based on the data of low-energy heavy ion beams. The OER of carbon ions at the centre of the 10 cm wide peak, for example, was found to be higher than the OER of fast neutrons. In those days, there was an undue emphasis on OER. We also found that the reduction in variation of radiosensitivity as a function of cell cycle after exposure to therapeutically relevant heavy-ion beams is not anywhere near that obtained with low-energy heavy-ion beams[5,6]. These results were not popular among heavy-ion enthusiasts at that time.

US-Japan cooperation

High energy physicists in spite of their big egos, in the best interests of science, have developed an international scientific culture that enabled them to work together beyond their national boundaries. Dr. Wilson, the proponent of protons in radiotherapy, also played a major role in promoting this international culture in high-energy physics. Particle therapy benefited from this culture. Even during the cold war, international collaboration in particle therapy flourished and took advantage of high-energy physics facilities around the world.

US-Japan cooperation in this field was established nearly 20 years ago by the US

National Cancer Institute and the corresponding organizations in Japan, under the leadership of Dr. Glenn Sheline. This cooperation started out with fast neutrons. In the 1970's, there were competing proposals for building pion and heavy-ion facilities in Japan, and a total neglect of protons. The thinking was that pions and heavy ions have all of the advantages of protons and, in addition, they have the high-LET advantage. I had the privilege of attending the US-Japan cooperation meeting in 1979. I felt, at that time, the need to stress the importance of building proton facilities while continuing research with the existing heavy-ion and pion facilities in the US, Canada and Switzerland. I also proposed the importance of having young Japanese physicists and radiation oncologists working in the above facilities, who would then provide guidance on the basis of their first hand experience and knowing the needs of Japan. The Japanese leaders must have thought along similar lines because, within a year, I was pleased to see Japanese physicists, radiobiologists and radiation oncologists working in Los Alamos, Vancouver and Villigen. I am also pleased to see that Dr. Tsujii, who worked in Los Alamos as well as in Villigen, is now heading the clinical program here at HIMAC. The particle radiotherapy programs in Japan are in the hands of experienced people and we wish them every success in their challenging endeavors.

Some reflections

Most of the experience with heavy ions at Berkeley was with neon ions. We have more experience with pions than with carbon ions. Our radiobiological data show some similarities in radiobiological effects between carbon ions and pions. There are no plans (and, probably, there never will be) to build biomedical pion facilities in the world, because of cost. There is a need to analyze the clinical data obtained from Los Alamos, Vancouver and Villigen. Such data will have some relevance to light ions such as carbon.

Dose localization and flexibility in beam delivery made considerable differences in reducing the morbidity of the treatment with fast neutrons. The morbidity of proton treatment can be expected to be further reduced with proton gantries now being used at Loma Linda. The heavy-ion beams, in principle, can have considerably lower treatment morbidity than fast neutrons especially with the treatment flexibility now being introduced at HIMAC.

The results with protons as well as with fast neutrons in the treatment of locally advanced prostate cancer, are impressive[3,7]. The effectiveness of fast neutrons in treating well-differentiated tumors was demonstrated convincingly. There is a suggestion that proton boost compared to X-ray boost, is more effective only on proliferating prostate tumors[7]. Heavy ions may be useful in treating prostate tumors, both proliferative as well as non-proliferative, by choosing different heavy ions. Recent developments in sophisticated imaging techniques helped to make use of the excellent dose distributions of heavy charged particles. Because of the biological complexities of tumors and their variations from patient to patient, the optimum utilization of high- LET beams requires considerable research effort in developing predictive assays to identify tumors that have better prognoses for high LET. The clinical experience with fast neutrons is relevant to heavy ions with regard to the potential applications of high-LET radiations. The clinical experience with fast neutrons gained by Dr. Tsunomoto and his colleagues at Chiba, and with protons by Dr.Tsujii at Tsukuba, should help the heavy-ion program at HIMAC. In principle, for the tumors that are found to be treated better with fast neutrons compared to conventional radiations, heavy ions should be better than fast neutrons because of their good localization characteristics. An international and cooperative effort is required to find the appropriate role for heavy ions in radiotherapy.

I am pleased that the IAEA is also involved in organizing this International meeting. Human talent is not restricted only to the developed countries. I hope that the IAEA will play a supporting role in giving an opportunity to the talented physicists, radiobiologists and radiation oncologists from developing countries to work in heavy-ion programs in Chiba and Darmstadt. This in turn, could stimulate further developments in the field of radiation oncology.

I would like to conclude with a philosophical note, which we need to keep in mind when we are engaged in high technology to improve the quality of life. High technology has a way controlling us rather than to be a useful tool under our control to improve the quality of life for everybody. While we are engaged in sophisticated technology in improving results of cancer treatment, it is also equally important to see that at least, standard forms of treatment are available for every cancer patient in the world. To alleviate human suffering using high technology, it is not enough just to be technically competent, but one also needs to be a good person, which is much harder, as beautifully expressed by Kenzaburo Oe in his Nobel Prize lecture. Thank you for your attention.

REFERENCES

1. Blakely, E.A.; Ngo, F.Q,H.; Curtis, S.B.; Tobias, C.A. Heavy-ion radiobiology: Cellular studies. Adv. Radiat. Biol. 11:295-378; 1984.
2. Deering, R.A., and Rice, R. Heavy-ion irradiation of Hela cells. Radiat. Res. 17: 774-786; 1962.
3. Laramore, G.E.; Krall, J.M.; Thomas, F.J.; Russell, K.J.; Maor, M.H.; Hendrickson, F.R.; Martz, K.L.; Griffin, T.W.; Davis, L.W. Fast neutron radiotherapy for locally advanced prostate cancer. Final report of an RTOG randomized clinical trial. Am. J. Clin. Oncol. 16 (2); 164-167; 1993.
4. Raju, M.R.; Amols, H.I.; Bain, E.; Carpenter, S.G.; Cox, R.A.; Robertson, J.B. Heavy particle comparative study. Part III. OER and RBE. Brit. J. Radiol. 51: 712-719; 1978.
5. Raju, M.R.; Bain, E.; Carpenter, S.G.; Walters, R.A.; Jett, J.H., Howard, J. Powers-Risius, P. Effects of Argon Ions on Synchronized Chinese Hamster Cells. Radiat. Res. 84: 152-157; 1980.
6. Raju, M.R.; Carpenter, S.G.; Tokita, N.; Howard, J. Effect of Neon Ions on synchronized Chinese hamster cells. Int. J. Rad. Biol. 48: 271-276; 1985.
7. Shipley, W.U.; Verhey, L.J.; Munzenrider, J.E.: Suit, H.D.; Urie, M.M.; McManus, P.L.; Young, R.H.; Shipley, J.W.; Zietman, A.L.; Biggs, P.J., Heney, N.M., Goitein, M. Advanced prostate cancer: The results of a randomized comparative trial of high dose irradiation boosting with conformal protons compared with conventional dose irradiation using photons alone. Am. Soc. of Therap. Radiol. and Oncol.; October 6, 1994.
8. Skarsgard, L.D.; Pujara, C.M.; Richardson, S.S. The effect of high LET radiations on recovery and radiation sensitivity throughout the cell cycle in mammalian cells. In abstracts of the Third International Congress on Radiation Research, Cortina di Ampezzo, p.204; June 26-July 2, 1966.
9. Todd, P.W. Reversible and irreversible effects of ionizing radiations on the reproductive integrity of mammalian cells cultured in vitro. Ph.D. Thesis, Lawrence Radiation Laboratory, Berkeley, CA, report UCRL-11614: 1964.
10. Zirkle, R.E. Bilogical effectiveness of alpha particles as a function of ion concentration induced in their paths. Am. J. Cancer. 23:558-567: 1935.

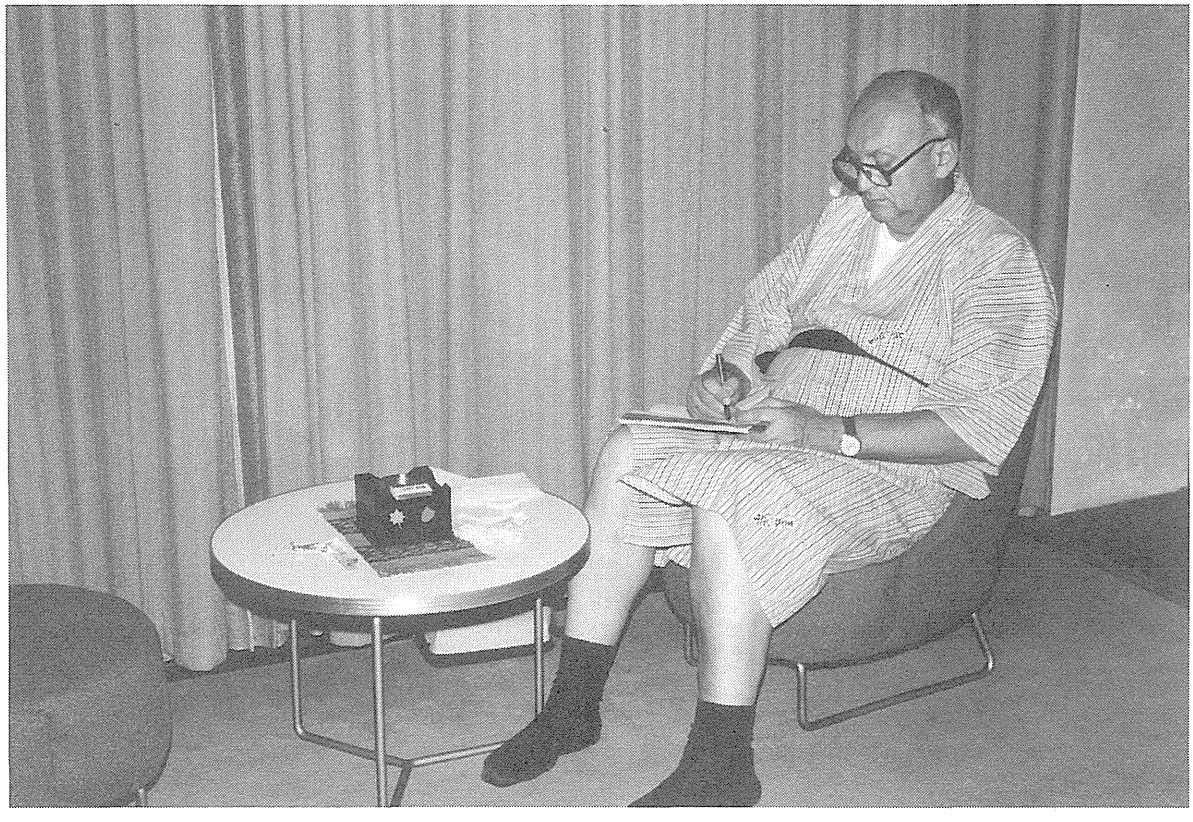

Prof. C.A. Tobias (picture taken by the author during U.S.-Japan Cooperative Meeting held in KYOTO in May, 1979, while sharing room in SUMIYA RYKON Hotel.

HIMAC

Overview of the HIMAC Construction
- A decade history -

K.Kawachi
National Institute of Radiological Sciences
4-9-1, Anagawa, Inage-ku, Chiba-shi 263, JAPAN

The present report aims to introduce a background to come to choose a heavy ion accelerator for cancer therapy and a progress of the HIMAC construction project. The latter part is divided into two categories. One is a design study of HIMAC for about four years of beginning. Another is a progress of manufacturing of accelerator system and of building construction for latter six years. The former part is a history of preparation period to make a proposal of heavy ion accelerator for cancer therapy.

Introduction

The National Institute of Radiological Sciences (NIRS) has been put a great deal of effort into the research and development in the radiation therapy of malignant tumors and radiation diagnosis of diseases more than 35 years. During this history, particle radiation therapy using the fast neutrons from the NIRS medical cyclotron has been carried out since 1975 in place of the commonly used type of radiation for far advanced and highly incurable cancers. At this time in United State, the large field size helium ions treatment was started in the Lawrence Berkeley Laboratory using BEVALAC and protons was started in Massachusetts General Hospital using Harvard cyclotron. In 1977, carbon and neon ion beam treatments were started at the BEVALAC and helium ion beam treatments were continued at the 184 in cyclotron. In 1979, the proton therapy was started at NIRS using medical cyclotron and adopted a sophisticated spot beam scanning method. Some of these results indicated significant improvements in the local control rate for tumors involving selected organs. These cases were closely related to the excellent physical dose distribution of protons and higher biological effectiveness of neutrons. Furthermore, based on the prospective results of heavy ion research work at LBL using BEVALAC and the recent progress in accelerator technology, we believed that heavy ion beams would become significantly superior to the most effectively used conventional radiation. The first proposal of a heavy ion medical accelerator was prepared in 1980 based on the above experiences and circumstance in those days.

Design study of HIMAC

Since 1981, death caused by cancer has been the highest rank in Japan. Therefore, the cancer control was one of the most important subjects and the people of Japan very much hoped that positive action should be taken by the government. In 1983, it happened an unlocked for piece of luck that the Cabinet Council for Cancer Control decided to carry out "Comprehensive 10-year Strategy for Cancer Control". The Japanese Government gave the utmost priority for the realization of cancer control and put into operation this strategy from 1984. As a part of this strategy, NIRS decided to promote a project for the construction of HIMAC.

In 1984, NIRS again carried out a feasibility study on heavy ion medical accelerator along the first proposal of 1980. The out line of the feasibility study is as follows;

(1) Investigation and data analysis of existing heavy ion accelerator.
(2) Selection of the most suitable heavy ion medical accelerator by theoretical analysis and computer simulation.

a. Physical design study and to select the most suitable accelerator complex.
b. Technical evaluation of accelerator shielding design.
c. Study on the layout of the accelerator complex and its building.
d. Design policy on the accelerator control, operation and maintenance.
e. Investigation on electric power supplying

facility.

f. Technical investigation of beam delivery system for patient's positioning and irradiation.

In 1985, Conceptual design study of accelerator facility was ordered to four Japanese companies, which have several experiences to manufacture the accelerators, under the direction of the NIRS staff with dividing the accelerator design into four major parts as follows:

(1) Injector system: ion sources, pre-injector, injector and those beam transport system.
(2) Main accelerator I: Synchrotron magnets and those power supplies.
(3) Main accelerator II: Injection system, extraction system, RF accelerating cavity and vacuum system.
(4) High energy beam transport system and beam delivery system for irradiation.

The first NIRS international workshop on heavy ion medical accelerator was held in 1986 just after finishing the conceptual design study. The aim of this workshop was as follows:

(1) To make a better understanding on the actual circumstance of heavy ion accelerator in the world.
(2) To discuss with the experts from overseas on the results of the conceptual design study.
(3) To stimulate Japanese accelerator physicists, engineers and manufacturers involving this project.

In this workshop, two important changes were proposed for the former specification and design studies. The maximum accelerating energy was changed from 600 MeV/u to 800 MeV/u due to emphasize the importance of silicon ions which is indispensable to treat a deep seated and radio-resistant tumor. The original idea on double ring synchrotron was also proposed in this workshop.

Overview of HIMAC Construction
- Design Study -

Fiscal year	Contents
1984	Beginning of "Comprehensive 10-year Strategy for Cancer Control"
	Feasibility study of medically dedicated heavy ion accelerator.
1985	Conceptual design study of heavy ion medical accelerator.
	NIRS International Workshop on heavy ion medical accelerator.
1986	Fundamental design study
	Building design study
1987	Detailed design study of HIMAC
	Final design of HIMAC building

In the fundamental design study of HIMAC, a design of the double ring synchrotrons was adopted according to the following reasons.

(1) It is possible to reduce a repetition rate per ring, which is necessary to satisfy the specification of dose rate. The higher repetition rate of synchrotron has involved a technical difficulty because s slow extraction was strongly required to synchrotron operation for the precise dose control.
(2) The reactive power fluctuation rate is greatly reduced by operating both synchrotron ring with phase difference of one half period.

A building design study was also started in 1986. The important works the radiation shielding study are estimation of neutron source or yield from the interaction with beam line devices and heavy ions and of transmission of high energy neutrons.

Accelerator manufacture and building construction

From 1987, manufacturing of the injector system including ion sources was ordered and started the manufacturing. The other parts of facility was continued the detailed design study. Division of Accelerator research was established in this year to proceed properly the construction project of HIMAC. In 1988, a main synchrotron ring was ordered and building construction was also started in November and excavated the land.

In 1989, a high energy beam transport system were ordered. The third tank of Alvarez linac appeared at a factory. In the building construction, a concrete placing of 2nd basement was made in this year. The rest parts of HIMAC, such as 2nd synchrotron ring,

irradiation beam delivering system, general control system, were ordered in 1990. Building construction of 1st basement and first floor was made in this year.

In the summer of 1991, the 2nd NIRS international workshop was held at Chiba as one of the satellite meeting of the world congress of medical physics and biomedical engineering. All the attendants visited a construction site of the HIMAC building and went down to the 2nd basement of injector area with rain shoes and a hard hat. Some of mechanical and electrical system, cooling system, and power supplies were installed in the building.

In early 1992, the injector system was made a start of installation in to the HIMAC building in spite of worse air conditioning with high humidity. In the latter half of this year, the most of parts were also installed in the building.

In March of 1993, a beam acceleration was started at injector system and the ions were accelerated up to the energy of 6 MeV/u. The total facility including the fine and precise setting up of all devices was completed in September of 1993. The beam commissioning was started from November of 1993, and 230 MeV/u helium ions were delivered to the treatment room by the end of 1993.

After an examination of radiation safety of the HIMAC facility, pre-clinical studies were started from February of 1994. The clinical trial at the HIMAC was started from June of 1994 using carbon beams. Fortunately, the project made a good progress more than we had expected. The detail discussion will be presented in the following papers.

Overview of HIMAC Construction
- Manufacture & Construction -

	Accelerator	Building
1987	Injector	
1988	Synchrotron I	Excavation of the land
1989	High energy beam transport system	Concrete placing 2nd basement
1990	Synchrotron II	1st basement & 1st floor
	Irradiation system	
1991	Installation of injector	Mechanical & electrical system Cooling & power supplies
1992		Installation of the others
1993	Beam acceleration Completed	
1994	Clinical trial was started in June	

HIMAC ACCELERATOR

S. Yamada, H. Ogawa, T. Murakami, A. Kitagawa, Y. Sato, J. Yoshizawa,
K. Sato*[1], A. Itano*[2], M. Kumada, M. Kanazawa, K. Noda,
T. Kohno, M. Sudou*[3], M. Torikoshi*[4], K. Ueda*[5] and K. Kawachi

National Institute of Radiological Sciences
4-9-1 Anagawa, Inage-ku, Chiba 263, Japan

Abstract

A heavy ion synchrotron complex, HIMAC, consists of two types of ion sources, two types of linacs, a couple of synchrotron rings, long and complicated beam transport lines, three treatment rooms and four experimental rooms. The maximum energy of the HIMAC synchrotron is designed to be 800 MeV/u for light ions with q/A = 1/2 so that the residual range of silicon ions reaches about 30 cm in a human body. The beam tests of the accelerator system started in November 1993 and is successfully completed in February 1994. After about four months tests of the irradiation system and the biological experiments, the clinical trials started on June 21 using a 290 MeV/u carbon beam.

This paper describes the design parameters and the present status of HIMAC.

Introduction

HIMAC is the first heavy ion synchrotron complex dedicated to the medical use[1],[2]. The maximum energy of HIMAC is designed to be 800 MeV/u for light ions with q/A = 1/2 so that silicon ions reach 30 cm deep in a human body. Ion species of He, C, Ne, Si *etc.* are required for the clinical treatment. In the facility, there are three treatment rooms one of which has both vertical and horizontal beam lines. The other two treatment rooms are equipped with a vertical and a horizontal beam lines, respectively.

The design study of HIMAC started in 1984, and it takes about ten years to get the first beam from the synchrotron. Construction of the accelerator and buildings lasted for six years. The first clinical trials have been successfully completed for three patients in August 1994. It takes about 90 seconds for a single fractional treatment with 290 MeV/u carbon beam, while the precise patient-fixing procedure requires about 25 minuets. Three fractions per week and total of 18 fractions for each patient were planned to destroy perfectly tumor cells.

*[1] Present address: RCNP, Osaka University.
*[2] Present address: Government of Hyougo Pref.
*[3] Present address: Accelerator Engineering Co.
*[4] Mitsubishi Electric Co.
*[5] Accelerator Engineering Cooperation

General description of HIMAC

The major design parameters of the HIMAC facility are summarized in table 1 and a cut away view of the facility is shown in Fig.1. The upper ring provides a vertical beam of 600 MeV/u max. to the treatment rooms A and B, and a horizontal beam with the same energy to the experimental room for biology. The extracted

Table 1: Parameters of the HIMAC facility

Ion species	from ^{4}He to ^{40}Ar
Maximum energy	800 MeV/u (q/A=1/2)
Minimum energy	100 MeV/u
Beam intensity*	1.2×10^{10} pps for ^{4}He
	2.0×10^{9} ^{12}C
	8.5×10^{8} ^{20}Ne
	4.5×10^{8} ^{28}Si
	2.7×10^{8} ^{40}Ar
Beam duration	400 ms
Repetition rate	1/2 Hz for each ring
Beam emittance	10 π mm mrad
Momentum spread	< $\pm$0.2%
Irradiation facility	
Treatment room	1 (Horizontal beam)
	1 (Vertical beam)
	1 (Horizontal & vertical)
Experimental room	4
Beam characteristics	
Field size	22 cm (Max. diameter)
Dose uniformity	$\pm$2%
Maximum range	30 cm
Dose rate	5 Gy/min.
Field broadening	Wobbler scanning

*Extracted beam intensity per ring.

beam from the lower ring (800 MeV/u max.), on the other hand, goes horizontally to the treatment rooms B and C, and experimental room for physics and general purposes. Since the upper high energy beam transport (HEBT) line and the lower HEBT line intersect with each other, the output beam of the lower synchrotron can be provided vertically to the treatment rooms A and B. There are two other experimental rooms for the medium energy (6 MeV/u) experiments and for the radioactive beam experiments. A beam line for generating the radioactive beam will be installed in near future.

In the following sections, brief descriptions are given for major components of HIMAC.

Injector

The injector[3] consists of two types of ion sources, a PIG and a 10 GHz ECR sources, two types of linacs, a 100 MHz RFQ and a 100 MHz Alvarez linacs, a debuncher to reduce the momentum spread of the output beam, and beam transport lines connecting them.

A PIG source is a hot cathode type and operated in a very short pulse with a relatively long time interval[4]. Such an operation increases appreciably an arc impedance resulting in a high arc voltage. The performance of the PIG source is excellent as indicated in table 2.

An ECR source is energized with a 10 GHz microwave source of 2 kW max. and equipped with a sextupole permanent magnet of 9 kG at a pole tip.[5] The output beam intensities are satisfactory for the treatments as listed in table 3. In the daily operation for the clinical treatment, the ECR source is preferable because of the easiness of the source operation.

An RFQ linac accelerates heavy ions with $q/A \geq 1/7$ from 8 keV/u to 800 keV/u. The RFQ is a conventional four vane type and operated at 100 MHz. Since the length of the RFQ vane is very large comparing with the tank diameter, a filed distribution must be carefully tuned along longitudinal direction. About 40 side tuners are introduced for this purpose and realize very small field error of 4.9% and 2.6% for longitudinal and transverse directions, respectively. An acceptance and an accelerating rate are 0.6 π mm・mrad (normalized) and 0.76 MV/m, respectively.

The RFQ is followed by an Alvarez type linac (DTL) operated with the same frequency of 100 MHz. The transverse phase space matching between the RFQ and the DTL is accomplished with a quadrupole magnet quadruplet installed in a 1.9 m long beam transport line. The DTL tank is 24 m long and separated into three independent rf cavities. The diameters of the cavities are about

Table 2: Performance of the PIGIS (eμA).

Ion	A	1+	2+	3+	4+	5+	6+	7+	8+
He	4	**>12,000**	**3,000**						
C	12	**1,000**	**5,000**	**(3,000)**	**700**	**20**			
N	14		**3,200**	**2,800**	**1,200**	**200**			
O	16		2,000	**2,300**	**(3,000)**	**300**	**30**		
Ne	20		2,000	**3,800**	**800**	**(400)**	**20**		
Si	28			400	**600**	**300**	**50**	**10**	
Ar	40			1,500	1,900	1,800	**1,300**	**400**	**200**

Boldface characters indicate ions available for the linac.

Table 3: Performance of the ECRIS (eμA).

Ion	A	1+	2+	3+	4+	5+	6+	7+	8+	9+	10+	11+	12+	13+
H	1	**2,500**												
He	4	**3,200**	**2,100**											
C	12		**470**	—	**430**	**50**								
N	14		**790**	**590**	**340**	**180**	**23**							
O	16		660	**470**	**(440)**	**280**	**130**	**15**						
Ne	20		622	**700**	**680**	**(600)**	**220**	**54**	**10**	**1**				
Ar	40				380	340	345	**270**	**235**	**65**	**(38)**	**2**	**1**	
Kr	84								70	55	37	22	**12**	**6**

Boldface characters indicate ions available for the linac.

2 m and change with one cavity to the next, in order to obtain reasonable values for transit time factors. Since a transverse emittance of the output beam from the RFQ is thoroughly small, a FODO type focusing sequence is adopted for Q-magnets in the drift tubes. The magnets have laminated cores and are excited with a very low flat-top-duty of 0.3%.

At the output end of the DTL, a 100 $\mu g/cm^2$ thick carbon stripping foil is inserted to improve a charge to mass ratio of the ions. Only one stripping stage is adopted at a relatively high ion energy of 6 MeV/u because of the reliability of the system and of advantages for future expansion to the acceleration of heavier ions. In table 4, major parameters of the injector are summarized.

Table 4: Injector specifications.

Ion species	^{4}He to ^{40}Ar
Charge to mass ratio	≥ 1/7
Ion source type	PIG & ECR
Linac frequency	100 MHz
Repetition rate	3 Hz max.
Duty factor	0.3% max.
Acceptance	0.6 π mm·mrad (normalized)
RFQ linac	
Input/Output energy	8 / 800 keV/u
Vane length	7.3 m
Cavity diameter	0.59 m
Max. surface field	205 kV (1.8 Kilpatrick)
Peak rf power	260 kW (typical)
Alvarez linac	
Input/Output energy	0.8 / 6.0 MeV/u
Total length	24 m (3 rf cavities)
Cavity diameter	2.20 / 2.18 / 2.16 m
Average axial field	1.8 / 2.2 / 2.2 MV/m
Shunt impedance	31 ~ 46 MΩ/m (effective)
Max. surface field	150 kV/cm (1.3 Kilpatrick)
Peak rf power	840 / 830 / 770 kW (typical)
Focusing sequence	FODO (5.1 kG/cm max.)
Output beam emittance	≤ 1.5 π mm·mrad (normalized)
Momentum spread	≤ ± 0.1%

Synchrotron

The main accelerator of HIMAC consists of two independent synchrotron rings. The two ring structure of the synchrotron makes it possible to provide a treatment room simultaneously with a horizontal and a vertical beams having different energies. As a future extension, two stage acceleration of the heavier ions is planned. In table 5, main parameters of the synchrotron are summarized.

A multiturn injection scheme is adopted to increase the circulating beam current by a factor of 20. A third order resonant extraction is also adopted to realize a rather long beam duration of 400 ms.

Table 5: Synchrotron specifications

General	
Type	Separated function
Accelerated particles	He ~ Ar
Output energy	100 - 800 MeV/u (q/A=1/2)
Ring diameter	41.3 m (12 cells, 6 s-per.)
Repetition rate	0.3 - 1.5 Hz
Injection	
Injection energy	6 MeV/u
Injected emittance (H/V)	264 / 26.4 π mm-mrad
No. of injected turns	40
Magnet system	
Focusing order	FODO
Betatron tunes (H/V)	3.75 / 3.25
No. of bend. ma	12 (24 tons each)
Bending field	0.11 - 1.5 T
No. of quad. mag	24 (3.2 tons each)
Quad. gradient	0.54 - 7.4 T/m
Rise/Flat-top time	0.7 / 0.5 s (typical)
Straight sections	
No. sections (long/short)	2 / 4
Length (long/short)	5.0 / 0.8 m
Acceleration system	
No. of cavities	1
Frequency range	1.0 - 8.0 MHz
Acceleration voltage	11 kV
RF power input	25 kW (max.)
Momentum acceptance	± 0.2%
Vacuum system	
Chamber material	SUS 316L (0.3 mm thick)
Baking temperature	200 °C
Average pressure	1×10^{-8} torr
Pumps	SIP, TGP, TMP
Extraction system	
Type	Slow (1/3 resonance)
Beam spill	400 ms at 600 MeV/u

A pulse magnet located in a MEBT line switches the output beam of the injector linac to the upper and lower synchrotron rings. The two synchrotron rings are operated independently from each other except that the magnets must be excited 180° out of phase. The synchrotron is a separated function type with a FODO type focusing structure. The ring consists of 12 unit cells, whereas the superperiodicity of the ring is 6. A bending angle and a radius of the dipole magnet are 30° and 6.5 m, respectively. The dipole field changes from 0.11 T at injection energy to 1.5 T

at maximum with a ramping rate of 2 T/s (max).

The rf system is required to realize a wide frequency range from 1 to 8 MHz. The energy gain per charge is estimated to be 10 kV for ions with a charge to mass ratio of 1/2. A fully digital control system (sampling rate of 500 kHz) is adopted for the feed back loop of the phase and the beam position. The rf frequency is essentially varied with a B-clock pulse generated at every 0.2 G change in bending field. The control system works very well and even a very low intensity beam of a few hundred particles per second ca be stably accelerated without $\Delta\phi$ and Δr feedback loops.

Comissioning and beam performance

The first beam from the injector has been obtained in late March 1993 with singly charged He ions. Beam tests have been begun for dual synchrotron rings in November 1993 with doubly charged He ions. The ions were accelerated to 230 MeV/u with a repetition rate of 1/2 Hz for each ring. Tests of the slow extraction from both rings were successfully completed in December and the extracted beams were transported to three treatment rooms within a few days. The length of the extracted beam spill was typically 300 ms.

After careful tuning of the whole system including the measurements of biomedical effects of the carbon ions, clinical trials of the heavy ion cancer therapy started in late June 1994 with 290 MeV/u carbon beam. Three patients were treated excellently in the first series of the clinical trials extended for 8 weeks.

The accelerated ion species and energies with the upper and the lower rings (referred as U-ring and L-ring, respectively) are summarized in table 6. Since the clinical trials use only carbon ions at the present stage, ion species tend to be partial to carbon. In Fig. 2, an example of oscilloscope signals is given for a bending magnet excitation pattern (top), a pulse magnet for beam extraction (2nd), beam signal in the synchrotron ring (3rd) and the extracted beam signal (bottom). In the signal of the extracted beam, the very big intensity fluctuation can be observed. This fluctuation is due mainly to a current ripple of the focusing magnet in the synchrotron ring, since no feedback system works to stabilize the extracted beam intensity.

Table 6: Accelerated ion species and energies

Ions	Energy (MeV/u)	Intensity of L-ring (pps)	Intensity of U-ring (pps)
$^{4}He^{2+}$	230	3.5×10^{9}	5.4×10^{9}
$^{12}C^{6+}$	80	—	3.6×10^{8}
$^{12}C^{6+}$	100	5.0×10^{8}	4.3×10^{8}
$^{12}C^{6+}$	230	7.0×10^{8}	1.2×10^{9}
$^{12}C^{6+}$	290	1.5×10^{9}	1.5×10^{9}
$^{12}C^{6+}$	330	3.6×10^{8}	1.0×10^{9}
$^{12}C^{6+}$	350	3.5×10^{8}	1.2×10^{9}
$^{12}C^{6+}$	430	3.6×10^{8}	3.3×10^{8}
$^{20}Ne^{10+}$	400	—	5.0×10^{8}
$^{20}Ne^{10+}$	430	4.0×10^{8}	—
$^{20}Ne^{10+}$	600	—	2.2×10^{8}

Future developments

This facility is open for many researchers who are interested in the heavy ion science as well as heavy ion therapy. The accelerator is required to accelerate heavier ions with a variety of energies and with high quality. In order to match these demands, third ion source of 18 GHz ECR source is now under developments. Ions from these three ion sources will be accelerated simultaneously with so called time sharing acceleration scheme and delivered to a medium energy experimental room, the upper synchrotron ring and the lower synchrotron ring.

A secondary beam will be available within a several years to investigate the possibility of precise check of the ion stopping position of positron emitters in a human body. The beam course will be open for other scientific fields.

References

[1] Y. Hirao *et. al.*, NIRS-M-89, 1992.

[2] K. Sato *et. al.*, European Particle Accelerator Conference, 1994, to be published.

[3] S. Yamada *et. al.*, 1994 Linac Conference, Tsukuba, Japan, p768.

[4] Y. Sato *et. al.*, Rev. Sci. Instrum., **63 (4)**, 2904 (1992).

[5] A. Kitagawa *et. al.*, Rev. Sci. Instrum., **65 (4)**, 1087 (1994).

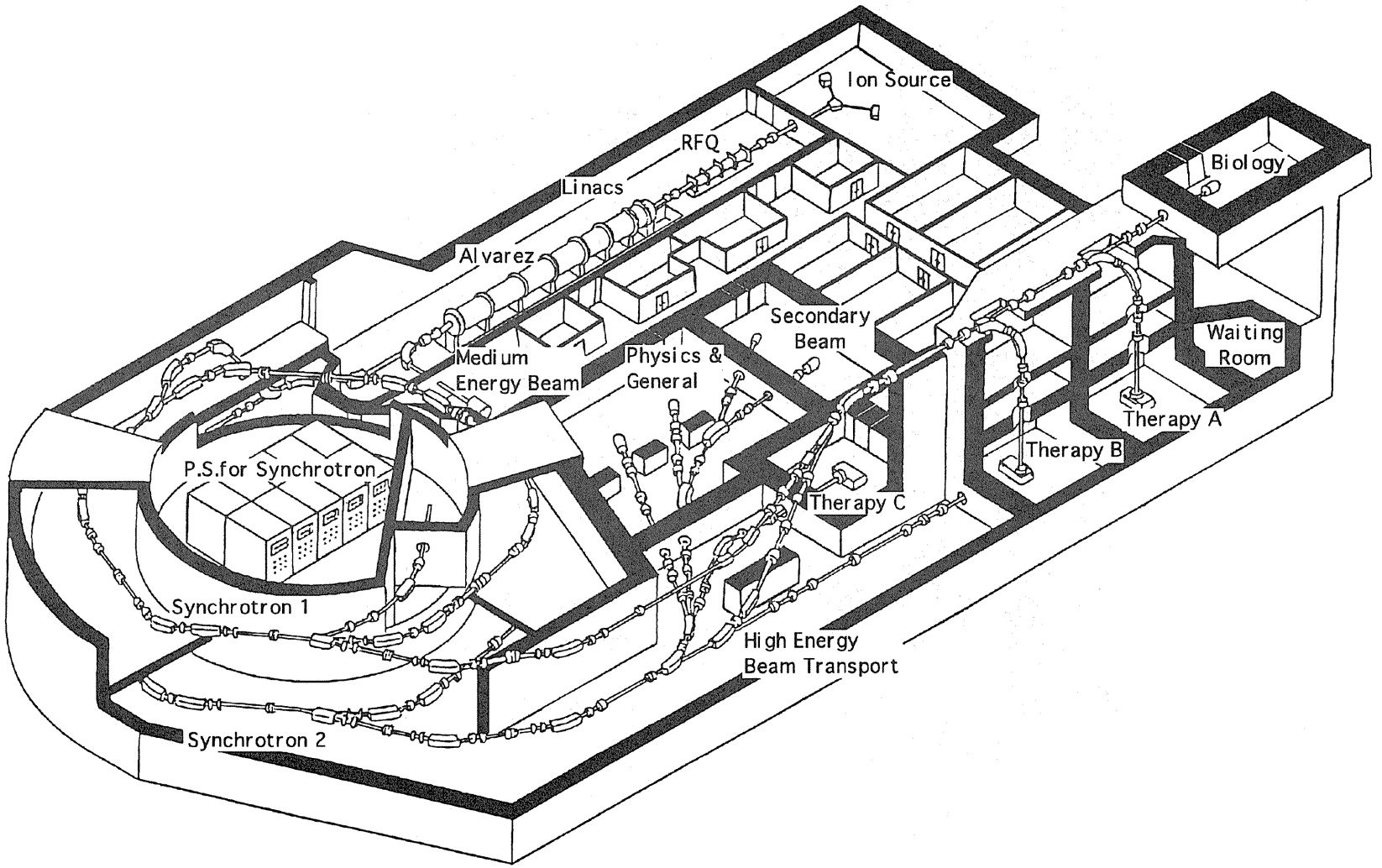

Fig. 1: A bird's eye view of the HIMAC facility.

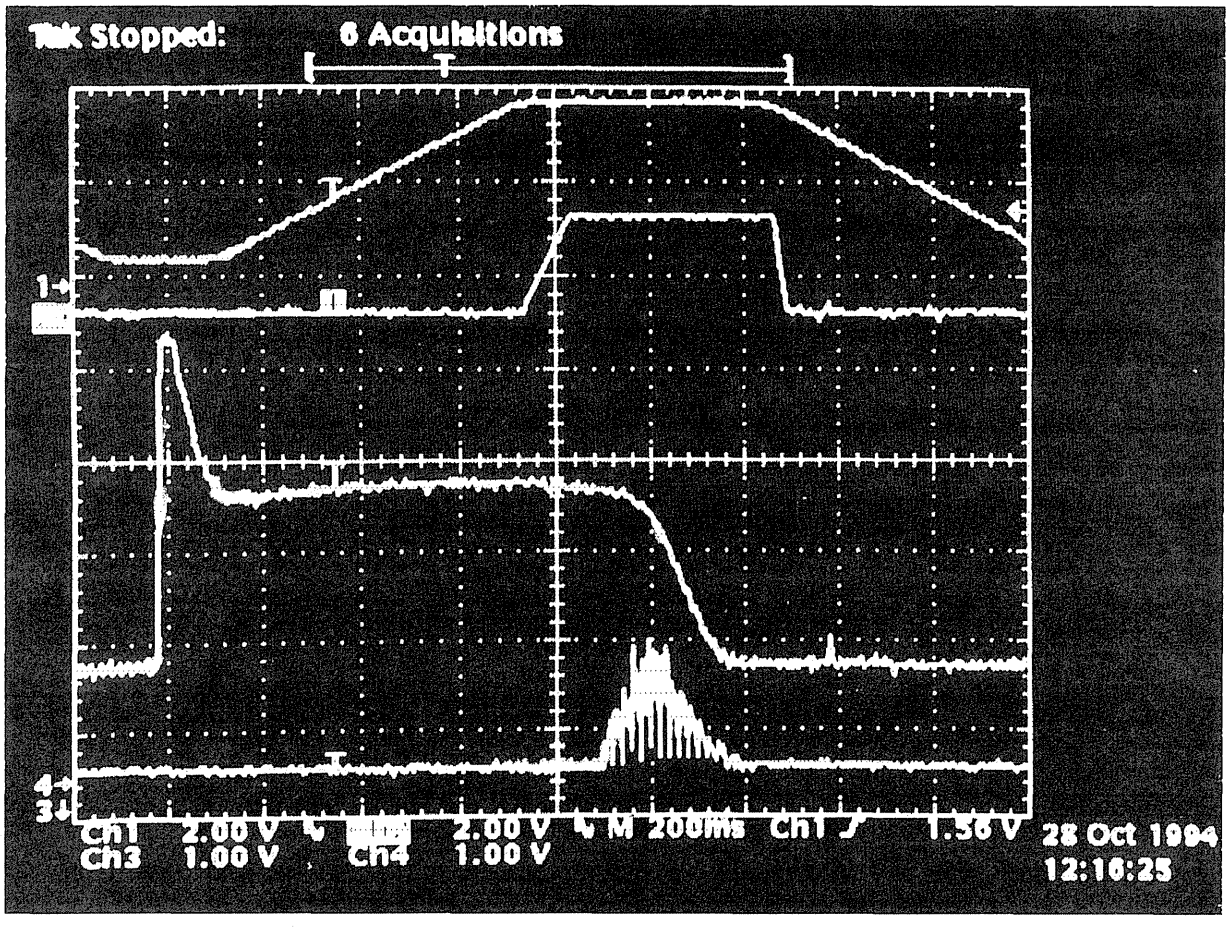

Fig. 2: A typical oscilloscope view of the synchrotron acceleration cycle: An excitation pattern of the synchrotron magnet (top), a bump field (2nd), a beam signal in the ring (3rd) and an extracted beam signal (bottom).

UPDATE STATUS OF HIMAC AND ITS FACILITY OPERATIONS

K. Ueda, K. Maeda, T. Nakamura, T. Fukushima, T. Kimura, Y. Satoh,M. Ishida, K. Murata, T. Aoki, R. Ohishi, Y. Ishikawa, K. Okumura, M. Sudou and I. Kobayashi.

Accelerator Engineering Corporation
10-14-302, 2-Chome Konakadai, Inage-ku, Chiba 263, Japan

Abstract

After long period of the construction and the installation, the commissioning of HIMAC started last autumn. It was successfully accomplished in March 1994, by mixed engineers team of NIRS, 4 companies of HIMAC manufacturers, and a new engineering company named Accelerator Engineering Corporation(AEC). From April 1994, only AEC operates whole HIMAC systems.

This report describes the outline of HIMAC and its facility operation at the time of Nov.1994. The 24 hours operation of HIMAC started from October. Every week, HIMAC beam in the day time from Tuesday to Friday is used for the cancer therapy in two treatment rooms, and the night time from Monday to Friday and day time of Saturday is used for biomedical and physical experiments.

Up to the present, the beam mainly used for the therapy is carbon 290MeV/N, with the intensity of 1.8×10^8pps for both A and B treatment rooms. Completely computerized control system for HIMAC can give very good operation performance, by the Parameter Operation File control method. Also we can easily change the course to each irradiation room, or change the energy and the intensity of the beam in short time. 7 AEC operators work in 2 shifts from Monday to Saturday.

Profile of AEC

Accelerator Engineering Corp.(AEC) was established in Nov. 1992, in Chiba, for the operation of HIMAC and its facilities. The history is shown in Fig.1. Now this company has 69 employees and 5 groups; each group is engaged in the operation and the maintenance of HIMAC; building utilities, injector, synchrotrons, beam transports, and medical facilities. During the final site tests before the HIMAC commissioning, engineers in this company had been cooperating with HIMAC manufactures which are Mitsubishi Electric Corp., Toshiba Corp., Sumitomo Heavy Industries Ltd., and Hitachi Ltd. These works turned out to give the basic technical training to this company. A selected technical team, the members are NIRS specialists, manufactures' and AEC's engineers started toward the accomplishment of heavy ion beam test. This March the commissioning was successfully completed, and since the beginning of April, we AEC have been solely in charge of the operation and the maintenance of HIMAC and its facilities. From this October, semi-regular operation of continuous 24 hours started in two shifts with 7 operators each.

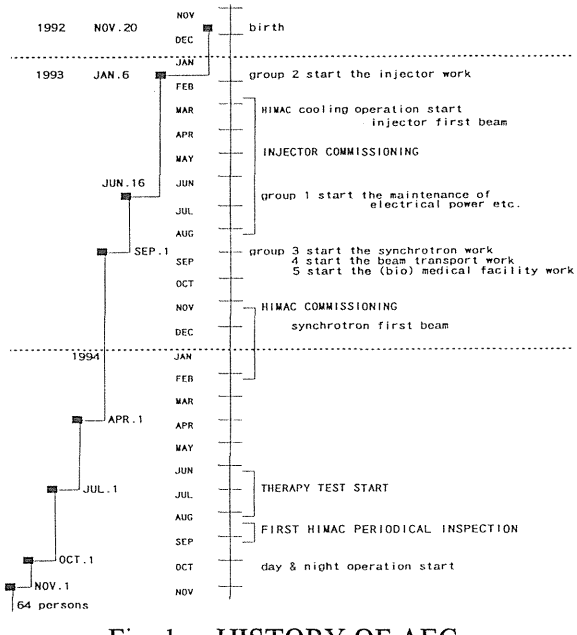

Fig. 1 HISTORY OF AEC

Each AEC group has individual task as follows, with cooperation of one another. The #1 group (G1) is responsible for the operation and the maintenance of HIMAC building utilities; the thermal source, the air conditioning, the ventilation, the water supply and drain, the sanitation, the fire protections, electric power distributor, the communication paging system etc.

The #2, #3 and #4 groups (G2,G3,G4) are responsible for the operation of the accelerator HIMAC; injector, synchrotrons and beam transports, respectively. Their works include daily, weekly and monthly check of whole machines of their corresponding area, continuous improvements of the essential components and adequate preparation for the consumption due to the span of life or troubles. The watch of whole information console and HIMAC cooling system are included in the task of G4. The #5 group (G 5) is in charge of the operation and the maintenance of bio and medical facilities. They make measurement and calibration with dose monitor before the irradiation for the therapy, and record and accumulate the data of irradiations. In addition, their maintenance work is similar as those of G2~G4.

The performance of AEC at present is as follows:

G1 works without holiday whole the year with 2 shifts. Workers of the day time from Monday to Friday is 6 persons. In the other time 3 persons work. 3 persons are engaged in the supervision and the operation of the HIMAC utilities in the building control room and other persons are engaged in the maintenance. G2, G3 and G4 work on the operation of HIMAC from Monday morning to Saturday night with 2 shifts of 7 operators according to the alternation schedule. Other persons work on the maintenance, improvement, tests, parts preparation and data accumulation and analysis etc. The G5 works mainly along the therapy schedule. On this schedule they are engaged in the dose measurement before the therapy and two persons are awaiting any troubles if happens in the midst of the therapy, for each treatment room. In the case of biomedical experiment usually performed in the night, one operator is on duty.

As mentioned above, the activity of the AEC covers almost all the area related to HIMAC only except the radiation safety control which is the business of an other company, Tokyo Nuclear Service Corp.. On this base NIRS will push forward with the essential task, therapy trials and many fundamental researches.

Weekly Schedule of HIMAC Operation

Fig 2 shows a typical weekly schedule of HIMAC operation. Day time from Tuesday to

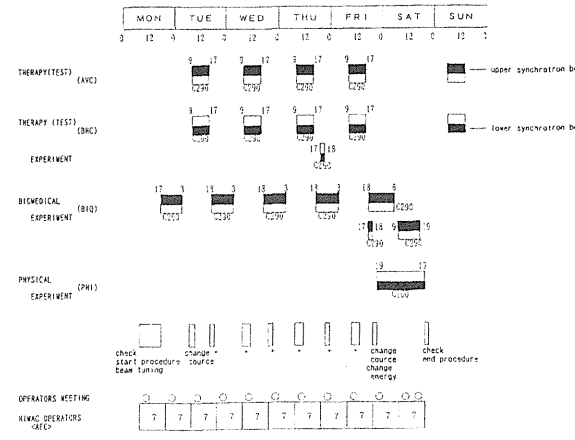

Fig. 2 A TYPICAL SCHEDULE

Friday, the C beam at the energy of 290 MeV/N is used for the therapy. Dose measurements for individual patients are done in the morning by AEC engineers, and in the afternoon the irradiation for these patients are done by the radiation technologist.

Two treatment rooms A and B are used for the cancer therapy. Room A has vertical line, and in the room B horizontal line is now used. After the therapy, upper synchrotron beam changes the course to the biomedical experimental room in the 2nd floor. From Monday to Friday night, many experiments are done until 3 o'clock in the morning. At the weekend, experiments on physics are done in experimental room for physics and general at the energy of 100 MeV/N of C and its beam intensity is 1.8×10^{8}pps. In the some case of these experiments extremely small beam is required.

Long range operation schedule is determined by NIRS machine time committee for HIMAC operation through several adjusting meeting of beam users, of course including the therapy or the therapy test. One or two weeks before practice, the final fine adjusted schedule is given to AEC. After this October, HIMAC is continuously operated from Monday morning to

Saturday night every week.

Monday morning HIMAC starts from the halt state only with the vacuum system and the computer system including related control systems being in action. With local switching and checking of power supplies and beam line devices, HIMAC operators on duty patrol over all the area of HIMAC accelerators. Owing to this patrol, they can find any little abnormal smell or sound, unusual rate of current or pressure, small leakage of water and oil. If any trouble is found, short time repair-work or exchange of spare parts can turn it back to the normal state. In the case of heavy trouble, they may call for the specialist service of the manufacturer. After this check and maintenance work, HIMAC will be operated in the accelerator control room on the required schedule.

From Monday morning to Saturday night, operators change at every 12 hours. At the time of change, take-over meeting is always held, so that the information of the operation condition is handed over to next team.

During the off duty time of beam service, operators can practice the trial of the expected beam specification such as the specimen of the particle, the beam energy or the beam intensity. They may register new Parameter File filled with parameters of all devices including the learned values of B, Q magnet currents.

These processes and results are transferred to the up-to-date operation manual, so that all AEC engineers will be able to provide the newly specified beam.

Operation Method of HIMAC

All operations of HIMAC can be done in the accelerator control room except several local switching for start-up or stop-down.

Fig. 3 shows the HIMAC control desks. From right to left the injector console, two synchrotron consoles, two beam. Five each console desk consists of two 20" color CRT and two 14" color CRT, and 3 encoders, interphones, oscilloscopes etc. 20" CRT is used mainly for information indication. 14" CRT is used mainly as operational touch cells. 3 encoders are used for any 3 devices tuning, which can be assigned in 14" CRT.

These configuration is same to the injector, the upper synchrotron, the lower synchrotron, the upper beam transport, the lower beam transport. Therapy irradiation control room is separated from here located near the treatment rooms in the second underground floor.

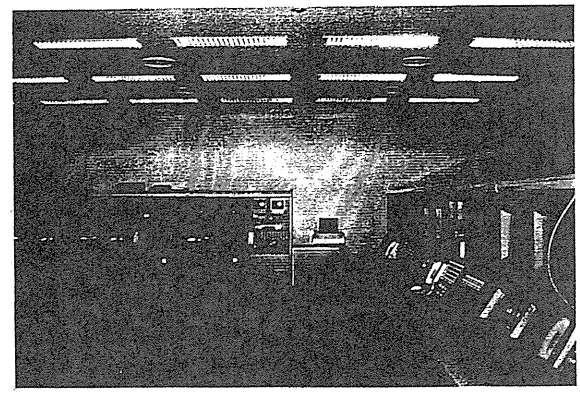

Fig. 3 HIMAC CONSOLE DESK

All control computers are connected one another by LAN network. For human safety, the hard wired Global Interlock system guards against any serious trouble.

Fig. 4 shows the outline of the computer

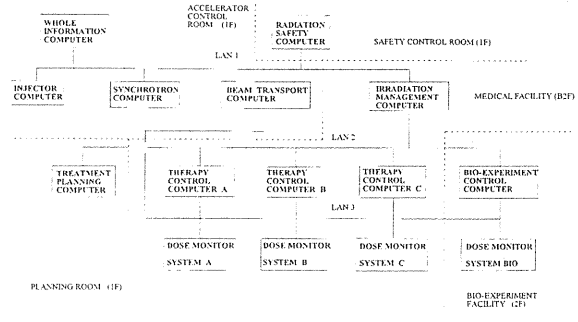

Fig. 4 OUTLINE OF HIMAC COMPUTER SYSTEM

network. Several different computers are used. But operation methods including CRT layout or touch cell layout are unified. From whole information console, an unified common Operation Parameter File will be able to be sent to every console for full automatically one-man operation in the near future, but now individual Operation Parameter Files are prepared in each 5 systems.

When one sees the operator in the injector console, the operational procedures are described in the following manner. Even when HIMAC is in halt state, computers are usually on with useful information on the CRT

At first, on the 14" CRT main menu, the

operator selects the "Operation Parameter File list", and the file list is shown on the 20" CRT and he chooses and loads the one which fits to the day program. This file is a set of individual Device Operation Parameter Files which correspond to all operation parameters of all kind of devices, or power supplies of the injector. Accordingly all devices go to run up to the parameter value. Every device operational status is shown in another 20" CRT layout by several colors; stop status is green, run status at the parameter value is yellow, transient status is green blink or yellow blink, trouble status is red, and forbidden status to operate is violet.

beam for medical use, so that the start up time becomes quite short. At the time of start-up, operators adjust the various parameters, looking at the output beam pulse waveform, the charge state distribution, the beam profile and the beam position.

After the satisfactory intensity and stability are confirmed, the beam is lead to the RFQ and the Alvarez (DTL) linacs by opening the beam line Faraday cup. RFQ and DTL linacs are almost free from tuning with little adjustment of the beam, in other words, the Operation Parameter File well functions. Between starting the ion source tuning and the beam delivering for

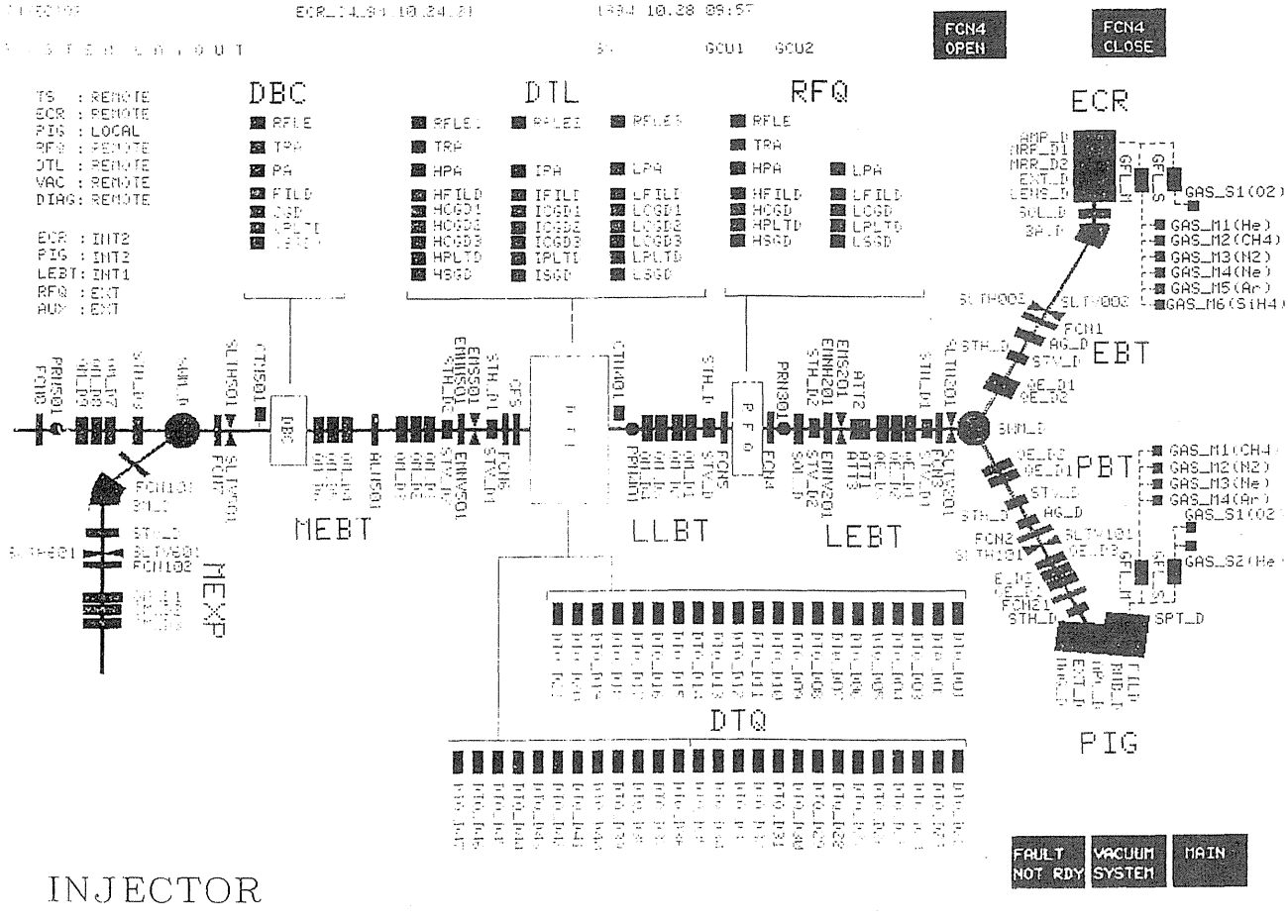

Fig. 5 GRAPHICAL LAYOUT OF INJECTOR

For the cancer therapy, usually the ECR ion source is used for C beam. In general, fine tuning is required in the ion source, however, this ion source is well constructed considering the

synchrotrons, it takes normally about 2 hours, which includes the parameter survey etc. Sometimes of urgent requests, it happens to take only 1 hour for delivering the beam to

synchrotrons.

Fig. 5 shows the injector layout on CRT, in which every device status is indicated in color as mentioned above .

Fig. 6 shows the beam waveform and Fig. 7 the beam profile at the downstream of the DTL.

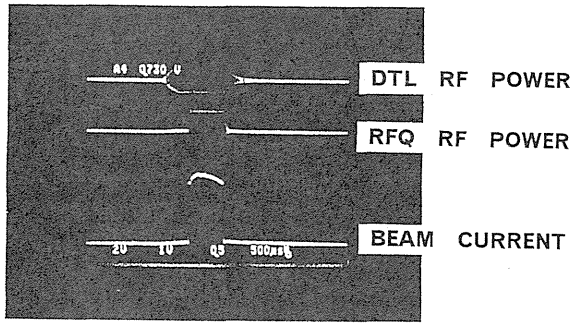

Fig. 6 BEAM CURRENT OF INJECTOR

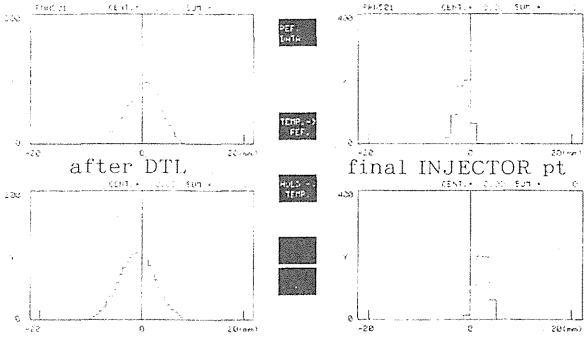

Fig. 7 BEAM PROFILE OF INJECTOR

The beam energy after the DTL is always measured, in real time through the analyzing magnet at the experimental room (midium energy experimental room) for the linac beam, where every one of two beam pulses are lead and the beam can be exactly adjusted to 6.0 MeV/N for C^{6+}. Delivering pulse beam to the upper and lower synchrotrons are alternatingly made, that is, one by every 2 seconds. The injector beam frequency is 2 H_Z.

The performance of C^{6+} beam pulse from the injector is about 700μs in width, 130eμA at the peak.

In the case of the synchrotron operation, the method is similar to the injector. The first procedure is the choice of an Operation Parameter File suitable to the requested specification.

Each synchrotron has its own parameter file. Both synchrotron Operation Parameter Files also include pattern figure indication of ring magnets. RF power into the accelerating cavity is controlled by the similar pattern figure. The master timing signal generated in the power supply at the synchrotron bending magnet controls all HIMAC devices including injector.

In most case, it is not necessary to make fine tuning concerning the acceleration energy or the beam profile adjustment after loading the Operation Parameter File. The beam intensity depends primarily on the ion source. Operators measure the beam intensity by the beam current integrator at the D shutter (DST) and observe the fine structure of the beam waveform by the fixed destructive scintillation monitor. Beam intensity is roughly controlled by the shadow mesh screen in the injector or the scraper in the synchrotron. Small intensity (faint) beam can be realized by the pattern modification of the ring magnets.

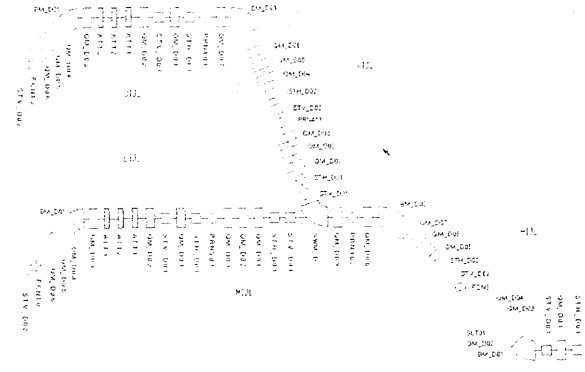

Fig. 8(a) GRAPHICAL LAYOUT OF SYNCHROTRON INJECTION LINE

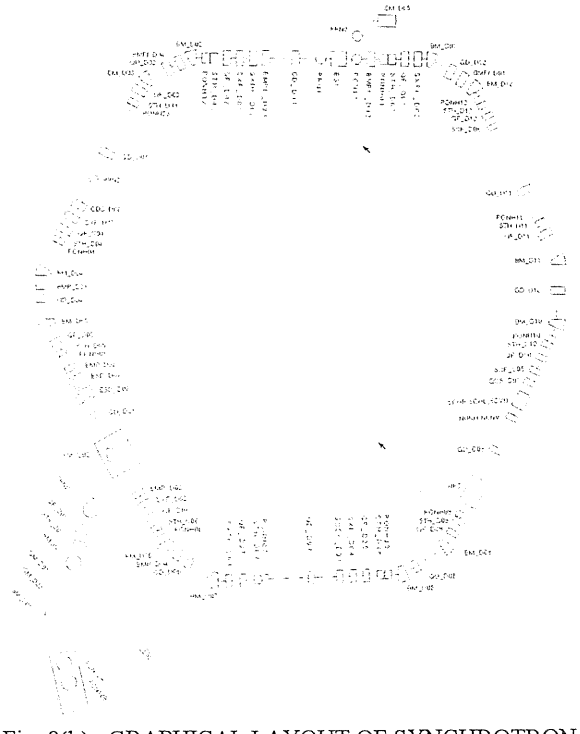

Fig. 8(b) GRAPHICAL LAYOUT OF SYNCHROTRON

Profiles of output beam and inner beam can be observed with the movable profile monitor.

Fig. 8. (a), (b) shows the layout of the synchrotron devices on CRT. Fig. 9 is a photo of the beam waveform. Fig. 10 shows the beam profile of the synchrotron. When the energy change is required, another prepared Operation Parameter File for the new energy is put in and within half an hour we can obtain a tuned new energy beam.

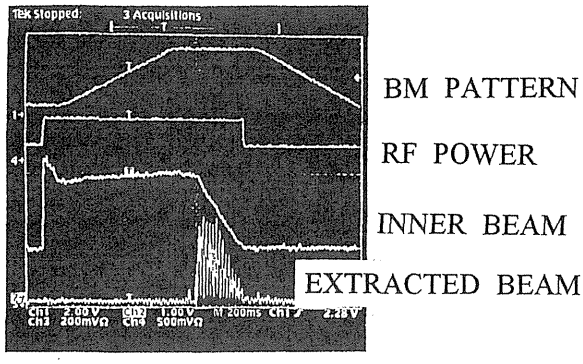

Fig. 9 BEAM WAVEFORM OF SYNCHROTRON

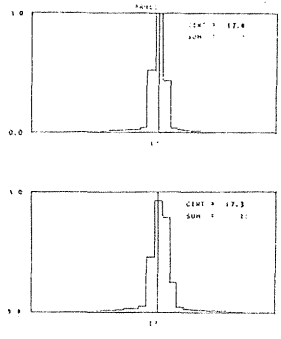

Fig. 10 BEAM PROFILE OF SYNCHROTRON

The operation of the high energy beam transport is almost same as well. Upper and lower beam transport is operated independently. Since there are so many transport lines connected to two synchrotrons, Operation Parameter File is corresponding to all beam courses which the beam can pass through with the exception of the branching point switching magnet. After the Operation Parameter File is set in, a beam course is selected to operate the switching magnet which guides the beam to the required course. Neutron shutter (NST) is located in front of each treatment room and experimental room.

The right (prority for action) to open the DST and the NST belongs basically to the beam transport console. When the Room-Ready Signal is sent from the irradiation management console which supervises the therapy and biomedical consoles, the NST can be opened through the touch panel.

Fig. 11 (a), (b) shows the layout of the upper and lower high energy beam transport on CRT.

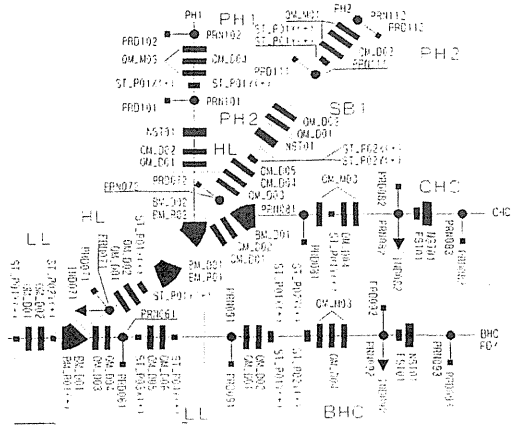

Fig.11(a) GRAPHICAL LAYOUT OF BEAM TRANSPORT HORIZONTAL LINE

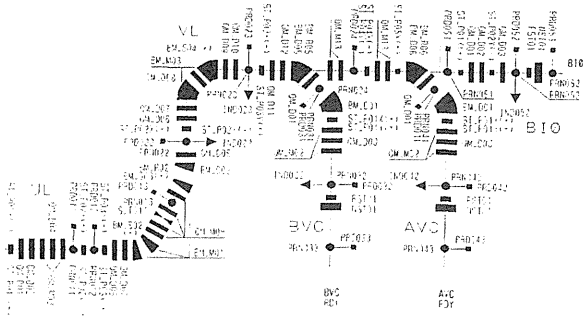

Fig.11(b) GRAPHICAL LAYOUT OF BEAM TRANSPORT VERTICAL LINE

Fig. 12 shows one example of the beam profile at the isocenter. After selecting beam course, the operators rarely need to do fine tuning.

In the case of changing course, necessary time to confirm the beam profile which can be delivered to the medical facilities, is about half an hour.

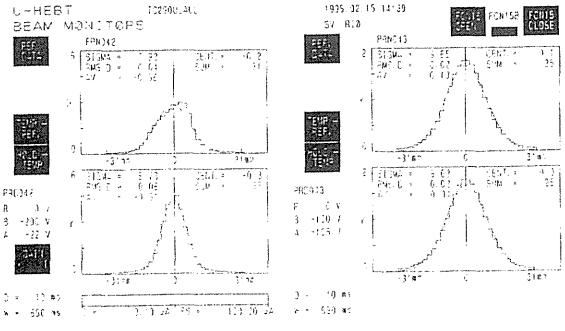

Fig. 12 BEAM PROFILE AT ISOCENTER

Ready beam to the treatment room or the biomedical room is left to stop at DST, and HIMAC operators wait for the request to open the DST from the irradiation management console.

In the case of therapy, before the irradiation to patients, radiation technologists need the corresponding dose measurement data to every patients which agree with the beam performance for the treatment planning. For the dose measurement or therapy, the action priority of the beam transportation to the treatment room which is realized by the opening or closing NST and DST is removed to the therapy console.
This right is transferred by the operator of the beam transport console only when necessary conditions in the side of therapy are satisfied and the request from the therapy console operator is acceptable.

Acknowledgments

From April 1994, HIMAC has been well operated on the schedule of the cancer therapy without any cancellation. We would like to thank many accelerator specialists at the Accelerator Research Division of NIRS headed by Dr. K. Kawachi for warmhearted guidance of HIMAC operation.

HIMAC beam delivery system
- Physical characteristics -

T.Kanai, H.Tomura, N.Matsufuji, S.Minohara, A.Fukumura, T.Hiraoka, Y.Furusawa, N.Miyahara, H.Koyama-Itoh, M.Endo, F.Soga and K.Kawachi
National Institute of Radiological Sciences, 4-9-1, Anagawa, Inage-ku, Chiba-shi, CHIBA 263 JAPAN

HIMAC was commissioned for pre-clinical experiments at the end of February, 1994. The clinical trial of the heavy-ion radiotherapy was also started at June 1994 after the pre-clinical experiments using the heavy-ion beam. In this paper, an irradiation system for the heavy-ion radiotherapy installed at HIMAC, the physical characteristics of the therapeutic beam and a choice of a carbon beam as the heavy-ion of the first clinical trial were discussed in detail. The accelerated beam was broadened by wobbler magnets and a scatterer in this system, and the spread-out Bragg peak was obtained by a bar ridge filter. Based on the biophysical properties of the heavy-ion beam, spread-out Bragg peaks were designed so that the biological dose (physical dose multiplied by RBE) was constant in the spread peak. A 290 MeV/u carbon beam was firstly used for the clinical trial of the heavy-ion radiotherapy. The fractionation schedule and the dose per fraction used in the neutron radiotherapy were applied for the heavy-ion radiotherapy using the carbon beam.

INTRODUCTION

Heavy-ion radiotherapy is expected to improve results of the radiation therapy because of its excellent dose localization and high LET effects of the biological responses. In expectation of the radiation therapy of the next generation, HIMAC (Heavy Ion Medical Accelerator in Chiba) was commissioned for pre-clinical experiments at the end of February in 1994. After three and half months of the pre-clinical experiments, the clinical trial of the heavy-ion therapy was started at June 24, 1994. Physical and biological experiments for the preparations of the heavy-ion radiotherapy had been performed using 135 MeV/u carbon and neon beams accelerated by RIKEN ring cyclotron[1,2]. We had investigated biological effectiveness of the carbon and neon beams on various biological systems and how to make the spread-out Bragg peak for the radiation therapy[1,2]. For the pre-clinical experiments just before the clinical trial using HIMAC beam, we ascertained the feasibility of the irradiation system and the bio-physical properties of the heavy-ion beams. We checked the uniformity of the irradiation field, dosimetry of the heavy-ion radiation field by three different methods, the physical and biological depth dose distributions of the spread-out Bragg peaks and so on.

In this report, first, the irradiation system of the HIMAC facility is described. Dosimetry of the heavy-ion beam are also discussed.

IRRADIATION SYSTEM

In the HIMAC facility, we have 3 treatment rooms, 1 biological experimental room, and a large general experimental hall. Treatment room A has a vertical beam line, C and biological experiment rooms have a horizontal beam line and room B has both beam lines. The irradiation systems of the beam lines are the same each other. Figure 1 illustrate an irradiation system of the HIMAC facility. The irradiation system comprises wobbler magnets, a scatterer, beam monitors, a range shifter, a ridge filter, collimators, patient positioning devices and a patient couch. In order to make a uniform

irradiation field, we used a pair of wobbler magnets and the scatterer. The range shifter is used for adjusting the peak position in the patient. The ridge filter is used for spreading out Bragg peak.

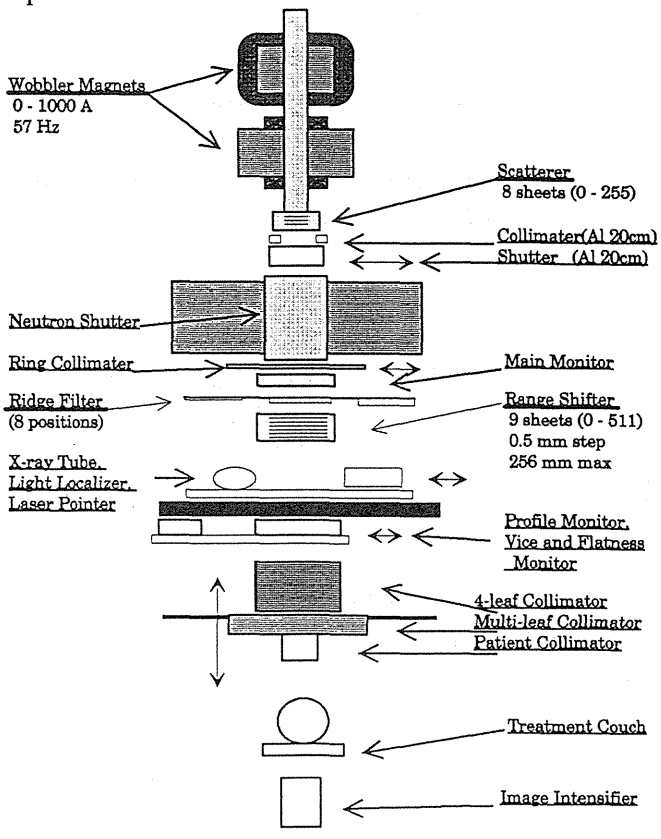

Fig. 1. Schematic layout of the irradiation system installed at HIMAC.

A conceptual method of making the uniform irradiation field is almost identical with the irradiation course of the RIKEN ring cyclotron facility[3]. The accelerated beam is focused on the iso-center of the irradiation course. The focused beam can draw a circular trace at the iso-center with the wobbler magnets. Then, the wobbled beam is scattered to make a uniform field at the iso-center. The repetition rate of the accelerated beam is 0.5 Hz. Width of the beam pulse is around 200 - 250 msec. The beam pulse has again a fine time structure. The pulse consists of 11-13 spikes with 50 Hz repetition. In order to make a uniform irradiation field with this spiked beam, the three spikes were distributed in a circular trace and rotate around 1/3 round in the one beam pulse. The large irradiation fields of diameters over 16 cm were obtained so that the difference between the intensities at the central part and the peripheral highest part was less than 2 % of the average intensity.

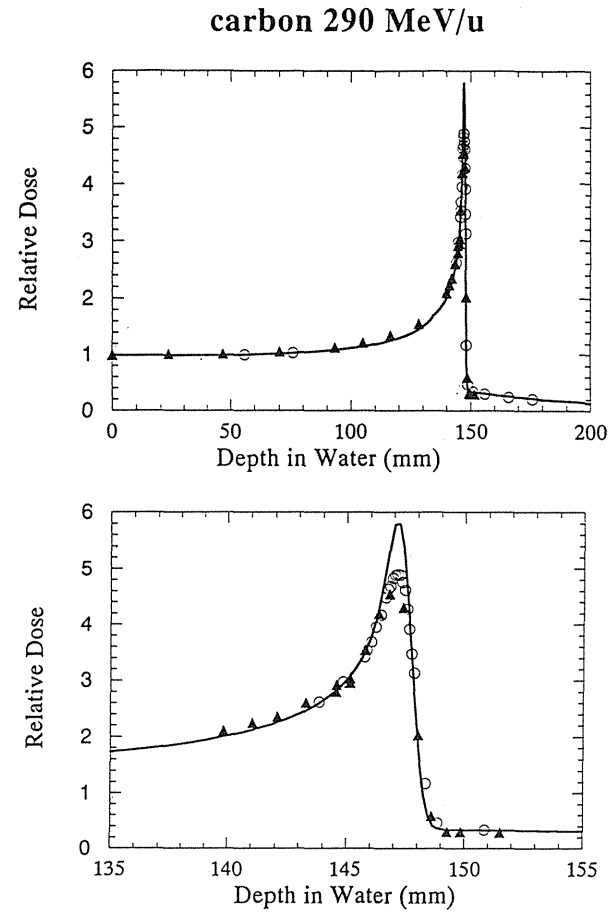

Fig. 2. Depth dose distribution of 290 MeV/u carbon in water.

DOSIMETRY

The dosimetry of the heavy-ion beam was checked by three different methods, such as an ionization chamber method, a fluence measurement method and measurement by silicon diode. From the Bragg-Gray theory of the ionization in the cavity, the absorbed dose of tissue irradiated with the heavy-ion beam can be obtained as follows;

$$D = \frac{Q_{IC}}{M_{IC}} W S_{t/g} K$$

where K is a correction factor for temperature, pressure of the gas in the cavity, ion recombination and so on. Q_{IC}, M_{IC}, $S_{t/g}$ and W in the equation are the ionization charge collected by the chamber, mass of the gas in the cavity chamber, stopping power ratio of tissue to gas and W value of the chamber gas for the heavy-ion, respectively. The W value of the air for the heavy-ions are assumed to be 35.2 eV, which is the same as that for high energy protons[4].

We developed a systematic method to obtain the absorbed doses for the cases of low and high energy heavy-ion radiation fields by the fluence measurement method[5]. Using a plastic scintillator, 5 mm in diameter, fluence of the heavy-ion beam at the entrance part in the depth dose distribution was measured. The dose at the entrance position of the depth dose distribution is obtained by multiplying the stopping power in water by the measured fluence of the heavy-ions.

The above method to obtain the absolute dose can be applied to very low energy heavy-ion beams and also applied to high energy heavy-ion beams[5].

We also measured the heavy-ion dose by silicon diode[6]. The response of the silicon diode was firstly calibrated by ^{60}Co gamma ray field. The dose calibration factor was derived by the collecting charge per unit absorbed dose in silicon in the ^{60}Co gamma ray field. The absorbed dose in silicon material for the heavy ion beams was obtained by the ionizing charge in the silicon detector for the heavy-ion radiation field divided by the derived dose calibration factor. The absorbed dose in water was obtained by multiplying the absorbed dose in silicon by a stopping power ratio of water to silicon.

Table 1 compares the results of the three methods. In case of the fluence method, the beam intensity was reduced to 1 x 10^6 particles per synchrotron pulse, which is 1/500 of the usual beam intensity. Because of the fine spikes in the synchrotron beam, the scintillation pulses in the scintillator were piled-up at that large intensity. The fluence measurement was checked by counting tracks in CR-39 track detector. The fluence measured by the two methods agreed within 1.2 %. From the table, the results of the heavy-ion dosimetry measured by the three different methods agreed within 5%. In case of the dosimetry by the ion chamber, there is uncertainty in the W value for the high energy carbon ion. If the W value is 33.7 eV, which is the W value for high energy electrons and gamma rays, it will give 4.5 % higher dose. In this clinical trial, the dosimetry by the ionization chamber method was tentatively adapted.

Table 1. Comparison of the three dosimetry

Fluence Measurements below 6.4 x 10^5 cpp (p/cm^2/monitor)

CR39	(2.050 +/- .017) x 10^5
Plastic Scintillator	(2.074 +/- .047) x 10^5

Ratio of the dose by the three dosimetries

Ionization Chamber	1.0
Fluence Method	0.958
Silicon Diode	0.973

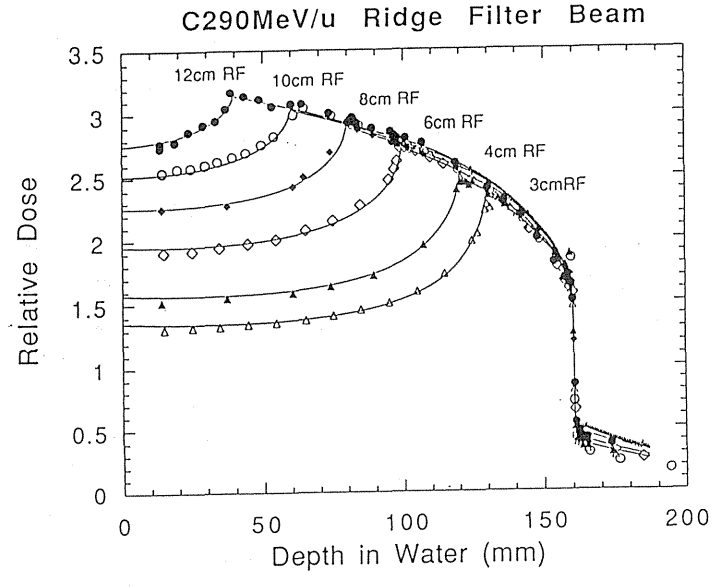

Fig. 3. Physical depth dose distributions of spread-out Bragg peaks using carbon 290 MeV/u beam.

PHYSICAL AND BIOLOGICAL DEPTH DOSE DISTRIBUTIONS OF CARBON BEAM

Fig. 2 shows the results of the depth dose distribution in water of carbon 290 MeV/u beam. Open circle and closed triangles in the figure are the relative ionization in water and in Lucite, respectively. The thickness of the Lucite is converted to water equivalent thickness. Solid line in the figure shows the result of a depth dose calculation, in which secondary and tertiary particle contributions are taken into consideration[1,7]. The calculated results agreed very well with the experimental results measured by the ionization chamber.

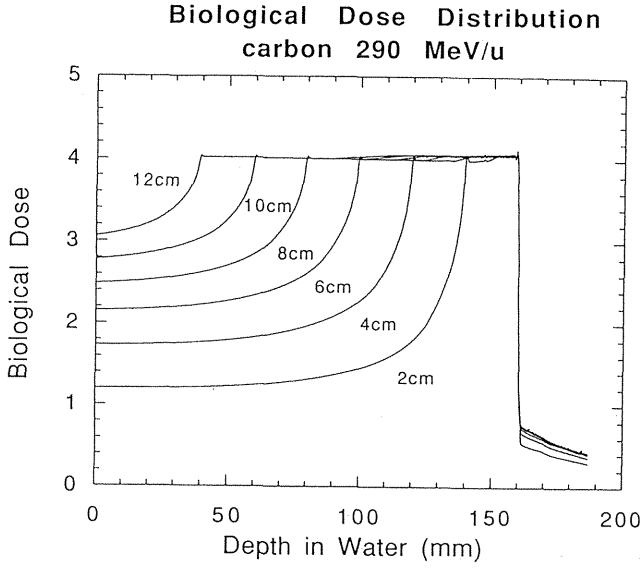

Fig. 4. Biological depth dose distributions of spread-out Bragg peaks using carbon 290 MeV/u beam.

Using not only the calculated depth dose distribution and LET distribution but also the biological responses of the carbon beams on HSG cells, the spread-out Bragg peak were designed as described in references[1,2]. The spread-out Bragg peak were made by putting a bar ridge filter in the beam course. Spacing of the each ridge is 5 mm, and it does not move during the irradiation. Due to multiple scattering in the ridge filter and the angular distributions of the wobbled beam, shade of the bar ridge filter was smeared out. Depth dose distributions of the spread-out Bragg peak are shown in Fig.3. The depth dose distributions were taken by changing Lucite thickness placed in front of the parallel plate ionization chamber. The Lucite thickness was again converted to water equivalent thickness. A calculated biological depth dose distribution is shown in Fig. 4.

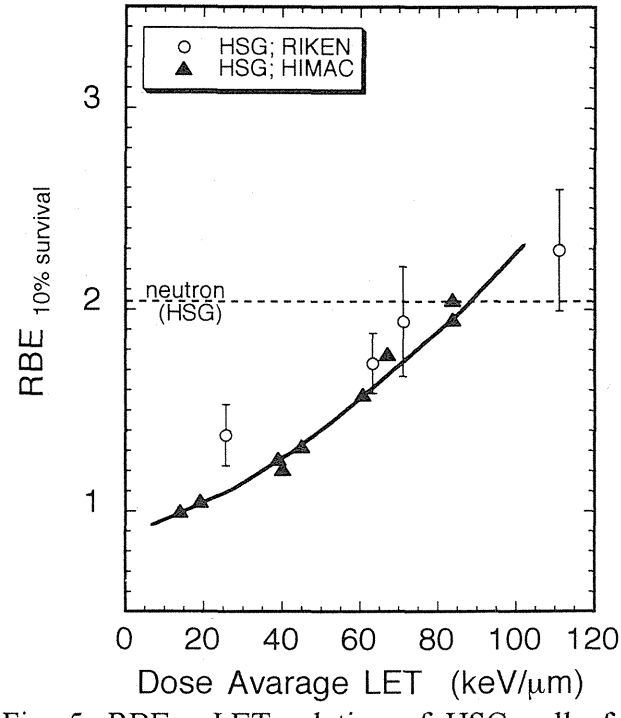

Fig. 5. RBE - LET relation of HSG cells for carbon beams of 290 MeV/u and 135 MeV/u. RBE for NIRS neutron beam is also shown by dashed line.

CHOICE OF CARBON FOR THE FIRST CLINICAL TRIAL

In the clinical application of the heavy-ion beam, it is necessary to select a sort of heavy-ion, treatment schedule of the treatment. At this moment, we don't have sufficient data about the treatment schedule for the heavy-ion radiation therapy. Fortunately, however, we have 20-year experiences of neutron radiotherapy, which can be said high LET radiotherapy. Then, it is reasonable to start the heavy-ion radiotherapy

with applying the treatment schedule of the neutron radiotherapy. Our strategy for the heavy-ion radiotherapy is set up as follows;

1. Find neutron-equivalent heavy-ion beam.
2. As a starting point, apply the treatment schedule of the neutron radiotherapy to that of heavy-ion radiotherapy.
3. Then, seek the optimum particle or treatment schedule for the heavy-ion radiotherapy.

As discussed in the reference[1], the survival curves for monoenergetic carbon beams of 65 keV/μm were very similar with those of the neutron beam at NIRS. For the proximal peak of the spread-out Bragg peak of 135 MeV/u carbon beam, the biological responses were similar with those of neutrons. The dose average LET for the proximal peak was also around 65 keV/μm.

Consequently, we have decided to select a carbon beam as the first heavy-ion to start the clinical trial of the heavy-ion radiotherapy. Using a code for calculating the depth dose distributions and the LET and fluence distributions of the heavy-ions in water or tissue materials[1,7], spread-out Bragg peaks were designed as shown in Fig. 3. RBE of the many biological systems were measured for the HIMAC spread-out Bragg peaks. In Fig. 5, the RBE of HSG cells were plotted against the dose averaged LET of the spread-out Bragg peak, in which width is 6 cm in water. Dashed horizontal line shows the RBE of the HSG cells for the neutron radiation. From this figure, we concluded 80 keV/μm carbon beam of spread-out Bragg peak was neutron-equivalent in terms of the biological responses. The neutron-equivalent LET of the spread-out beam was higher than the case of 135 MeV/u carbon beam. This may be because the spread-out beam using 290 MeV/u carbon contained a large amount of low LET components, and the LET spectrum of the beam spread over in very large range. The biological responses for the beam were less effective than those for the 135 MeV/u carbon beams which had low contamination's of fragmented light nuclei. Biological dose for the HSG cells for the spread-out Bragg peak is shown in Fig.6. Flat responses were obtained in the spread-out Bragg peak. The neutron equivalent position in the spread-out Bragg peak was around 8 mm up-stream from the distal peak of the spread-out Bragg peak.

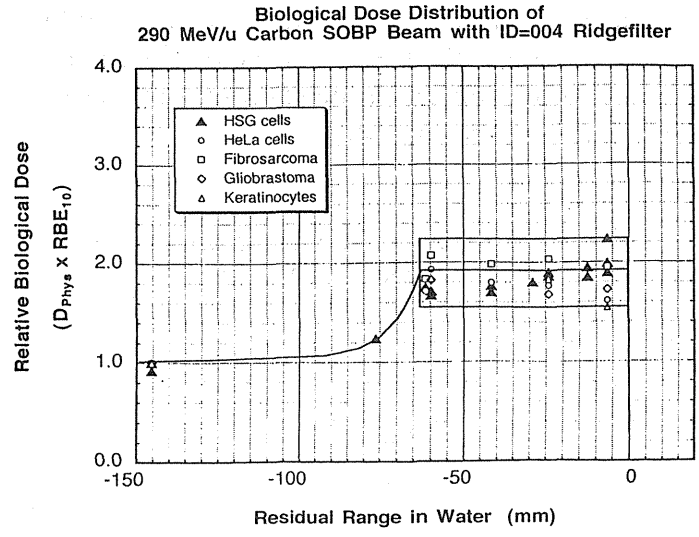

Fig. 6. Experimental results of the biological dose distribution of spread-out Bragg peak.

CONCLUSION

A heavy-ion irradiation system was designed and constructed at HIMAC facility for the clinical trials of heavy-ion therapy. For the first clinical trial of the heavy-ion radiotherapy with HIMAC beams, we have selected to use a beam of carbon 290 MeV/u and to start with an irradiation schedule of neutron therapy. Spread-out Bragg peaks were designed for the carbon beam to have uniform biological responses in the peak. The physical dose distributions of the beam agreed very well with the predicted depth dose distributions, and also the biological responses were satisfactorily flat in the spread-out Bragg peak. The heavy-ion dosimetry was checked by three different methods. The results of the dosimetries were coincided each other

within 5 %. From these feasibility studies of the irradiation system and bio-physical studies of the carbon beam, the clinical trial of the heavy-ion radiation therapy has been safely started at the HIMAC facility.

References

[1] T.Kanai et al., "Biological and physical proposals for a heavy-ion clinical trial.", Proceedings of Third Workshop on Physical and Biological Research with Heavy ions, (Edited by K.Ando and T.Kanai), HIMAC report (NIRS Publication), HIMAC-003,1-3, 1993.

[2] T.Kanai et al., "Preparatory studies for heavy-ion therapy.", Proceedings of the fifth Japan-China Joint Symposium on Accelerators for Nuclear Science and Their Applications, Oct.,1993, Osaka, Japan.

[3] T.Kanai, et al., "Irradiation of 135 MeV/u carbon and neon beams for studies of radiation biology.", HIMAC report (NIRS Publication), HIMAC-004, 1993.

[4] ICRU report 31, "Average energy required to produce an ion pair.", 1979.

[5] T.Kanai et al., "Dosimetry and Measured Differential W Values of Air for Heavy Ions", Radiation Research 135, 293-301 (1993).

[6] A.Fukumura et al., "Silicon diodes as detectors in relative dosimetry of heavy ions.", Proceedings of Third Workshop on Physical and Biological Research with Heavy ions, (Edited by K.Ando and T.Kanai), HIMAC report (NIRS Publication), HIMAC-003,1-3, 1993.

[7] L.Sihver et al., "Depth-dose and fluence distributions when using heavy ion beams", The proceedings of NIRS International Seminar on Application of Heavy Ion Accelerator on Radiation Therapy of Cancer in connection with XXI PTCOG Meeting., NIRS, Chiba, 14-16 Nov. 1994., HIMAC report, NIRS-M-103/HIMAC-008.

Preclinical Biology for HIMAC beam

K.Ando, T.Kanai, Y.Furusawa, M.Suzuki, S.Koike, K.Nemoto, M.Iizuka, N.Hori, A.Kamohara, Y.Kase, S.Matsushita, S.Sato, T.Nakano, A.Ishikawa, T.Kawase, T.Furuse, H.Ohtsu, M.Tomisawa, H.Aoyagi, J.Mizoe, S.Furukawa, K.Yoshikawa and H.Maezawa

Research Center for Charged Particle Therapy, Natl Inst Radiol Sci, chiba 263 Japan

Purpose:This study is to investigate the biological dose distribution of carbon-12 beams and to estimate a physical dose appropriate for clinical use. Materials and Methods: Five human cell lines cultured in vitro were irradiated by single doses of 290 MeV/u carbon-12 with a 6-cm width Spread-Out-Bragg-Peak (SOBP) and served for colony formation. C3H female mice aged 10-12 week old served for skin damage. Depilated right hind legs received either single or fractionated irradiations. Skin reaction score was given to individual mice every other day since 7 days after first irradiation, and 5 highest scores were averaged to use as a representative value for a group. Results:Relative biological effectiveness (RBE) of carbon SOBP for 10 % cell survivals , depending on cell lines, ranged from1.2 to 2.3 at proximal SOBP (40 keV/μm) and increased to 2.0 through 2.7 at distal SOBP (82 keV/μm). Isoeffect dose of skin dry desquamation showed an RBE of 2.3 at proximal SOBP and 3.2 at distal SOBP when 4 equal doses each were delivered for 4 days. Distribution of biological doses within SOBP was fairly homogeneous after fractionated irradiations or small dose per fraction , but showed a decline at mid through distal peaks after single irradiations or large dose per fraction. A position within SOBP which showed the same biological effectiveness as fast neutrons was designated here as the neutron-equivalent point. Cell kills for human salivary gland tumor cells(HSGc-C5) and mouse skin damage pinpointed the neutron-equivalent point at 80 keV/μm or 8 mm-upstream of the distal fall-off. Based on a calculation using (1)the neutron-equivalent point experimentally determined and (2)clinical data of fast neutrons (i.e., RBE=3.0; neutron dose per fraction =0.9 Gy), we estimated a physical dose of 1.133 Gy at 3.0 cm apart from the fall-off(i.e., middle SOBP) suitable for clinical trial. Conclusions: Biological dose was homogeneously distributed within a 6-cm SOBP carbon beam (290 MeV/u). A carbon dose of 1.133 Gy at middle SOBP was recommended as a fraction size in clinical trial which planned to use 3 fractions per week for 6 weeks.

key words: Carbon-12, Biological dose, Spread-Out-Bragg-Peak

INTRODUCTION

A synchrotron accelerator HIMAC has recently been installed in National Institute of Radiological Sciences. We selected Carbon-12 with 290 MeV/u as initial beams for clinical trial, because this beam would provide biological effectiveness similar to fast neutrons which have been used for therapy and biology at NIRS for more than 20 years. Knowledge accumulated through fast neutrons could predict responses of patients who receive new particle beams, and thus would be useful to estimate dose size appropriate for carbon-12.

The purpose of the present study is to inspect biological dose distribution of SOBP of carbon-12 and to estimate a physical dose suitable for clinical trial as well. Biological endpoints employed here were cell survivals and skin reaction . As initial patients for carbon therapy were planned to be selected for head and neck malignancies, and fast neutrons have been proven effective against parotid tumors, a human salivary gland tumor cell line was employed here. As skin is inevitably included in irradiation field, mouse skin reaction was also investigated.

MATERIALS AND METHODS

Cells and mice

Five cell lines of all human origin were used. These were HeLa S3 epitheloid carcinoma, HT1080 fibrosarcoma, T98 glioblastoma, HSGc-C5 salivary gland carcinoma and HK human keratinocytes. HSGc-C5 cells were kindly supplied by Dr. Kanemitsu Shirasuna at Osaka University. Cells being grown in Eagles MEM supplemented with 10 % fetal bovine serum were plated into 24-sq.cm plastic culture bottles(Nunc) 24-48 hrs before irradiation. Each bottle was placed in a hollow made on a Lucite plate which was set on a remote controlled translator, and irradiated individually by single doses of carbon-12.beams C3H female mice aged 10-12 week old served for skin irradiation. Hair on right hind legs of mice were removed by applying depilatory(Shiseido) 9-10 days before irradiation. With pentobarbital anesthesia and taping, five mice were immobilized on a Lucite plate. Right hind legs were placed in a rectangular field of 28- x 100-mm, and received either single or fractionated irradiations.

Irradiation

Carbon-12 particles were accelerated by HIMAC synchrotron up to 290 MeV/u. The beam was laterally spread by a thin scatter (lead and tantalum) and two wobbling magnets, which , in turn, provided a uniform physical dose distribution for a circular field with 10 cm in diameter. For longitudinal spread, an aluminum wedge filter biologically designed by T.Kanai(1) was used and provided 6-cm width SOBP (Fig.1). A physical dose declined to approximate 50 % when the irradiation position moved from the edge of proximal SOBP to distal SOBP. LET of 290 MeV/u carbon-12 was 15 keV/μm at the entrance of 6-cm SOBP, and gradually increased to 20 keV/μm along with

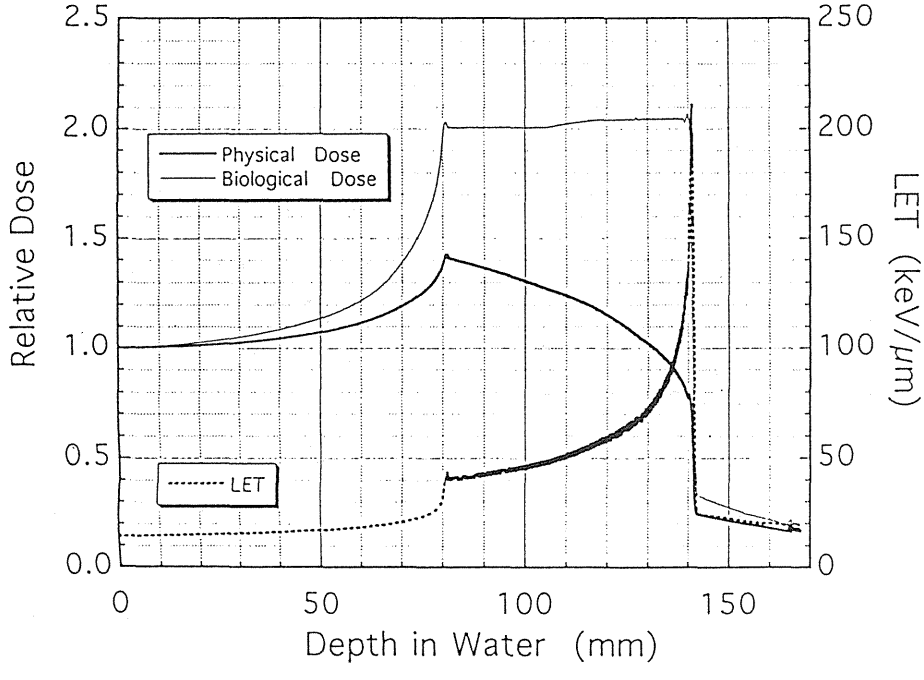

Fig.1 Dose and LET Distribution for 290MeV/u C-12

8-cm beam path. The proximal edge of SOBP locating at 9-cm path possessed an LET of 40 keV/μm. LET increased with beam path and reached to 200 keV/μm or over at 15-cm path which corresponded to distal fall-off of SOBP.

Biological experiments were conducted in Therapy B room using horizontal beam with a dose rate of 0.3-0.5 Gy/min. Irradiation field was made by a brass collimator. Irradiation position was adjusted by a Lucite range shifter. For calculating relative biological effectiveness (i.e., RBE) of carbon beam, 200 kVp X rays (0.8 Gy/min with 0.5 mm Al + 0.5 mm Cu filter) and Cs-137 γ rays (1.6 Gy/min at an FSD of 21 cm) were used for cells and skin irradiation, respectively. Also used here as a reference beam was cyclotron fast neutrons(13 MeV) which were produced by bombarding a thick beryllium target with 30 MeV deuterons.

Endpoints

Irradiated cells were trypsinized and replated into plastic dishes, and incubated for 13days before fixation and staining. Plating efficiencies of unirradiated cells were 90-95 % for all cell lines. Skin reaction of irradiated legs were scored every other day according to a modified Aizawa's method(2), starting from Day 7 of initial irradiation up to Day 35. Highest 5 scores for an individual mouse were averaged and used as a representative value of an experimental group consisting of five mice.

RESULTS

Cell survivals

Survival curves for five cell lines were obtained after single irradiations of carbon-12 at various SOBP positions (Fig.2). RBEs of carbon-12 SOBP relative to X rays were calculated at 10 % survivals.

Dose response for skin reaction

Skin reactions after single dose irradiations at SOBP positions were obtained for doses ranging from 3 Gy to 28 Gy(Fig.3). We examined five SOBP positions (40, 50, 60 ,80 and 100 keV/μm), gamma rays and fast neutrons. Dose response curves were obtained for each radiation qualities, and RBEs were calculated by comparing between high LET and gamma rays at an iso-effect score of 2.5 which represented dry desquamation, a well tolerable skin damage.

Skin reactions after daily fractionated dose irradiations at SOBP positions were also obtained (Fig.4). A total dose were equally divided into four fractions, each of which was consecutively delivered for four days.

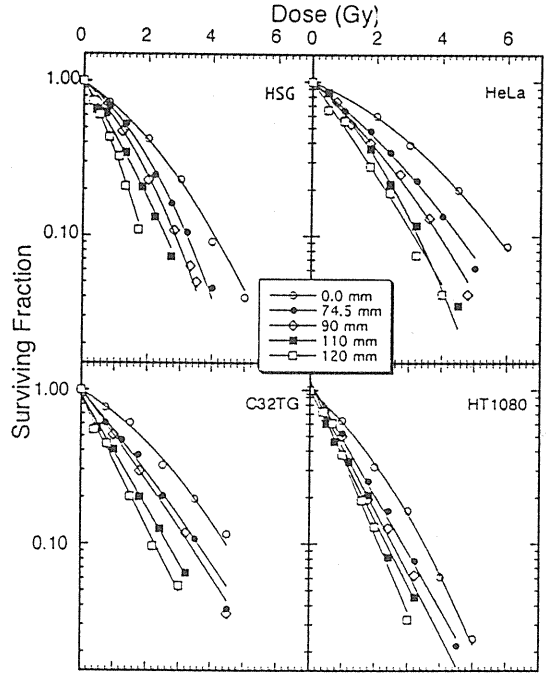

Fig.2 Cell kill effects of C-12 with 6Cm SOBP.

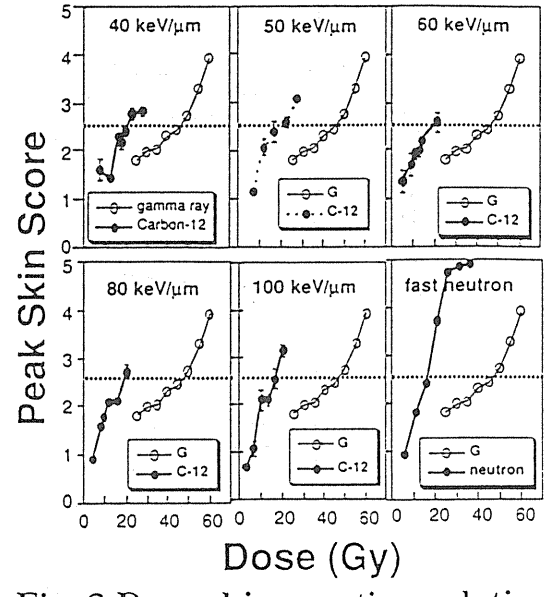

Fig. 3 Dose-skin reaction relations after single radiations with 290MeV/u carbon-12 (6cm SOBP)

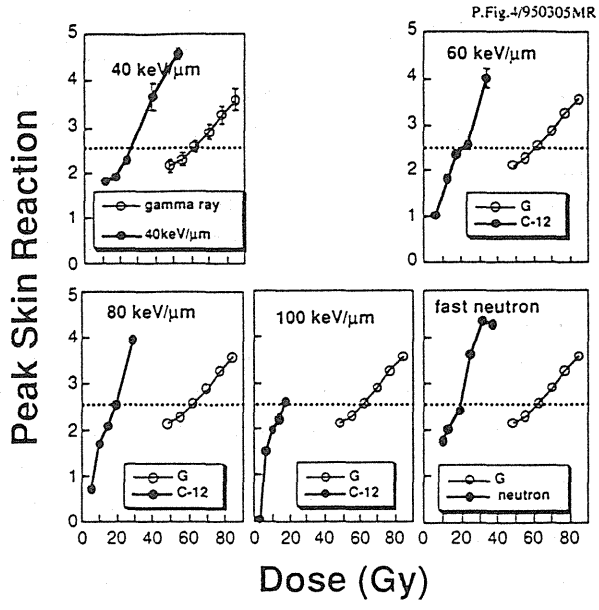

Fig.4 Dose-skin reaction relations after 4-daily radiations with 290MeV/u carbon-12 (6cmSOBP)

RBEs of carbon-12 SOBP after single irradiations

RBE values of carbon-12 SOBP after single irradiations relative to X rays were plotted in Fig.5 for 10 % cell kills. At given LET, RBEs varied depending on cell lines; e.g., HSGc-C5 cells showed an RBE of 1.0 at 20 keV/μm while HK cells showed an RBE of 1.7.

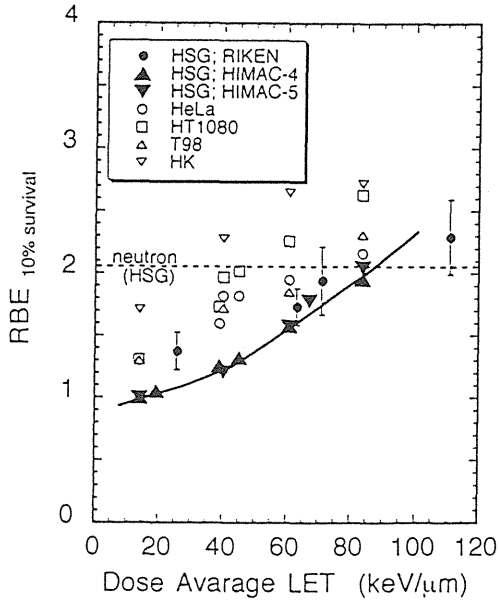

Fig.5 BRE of C-12 with 6 CM SOBP for five human cell lines.

RBEs increased with increase of LET for all cell lines, and showed the largest value of 2.7 for HK cells at 82 keV/μm. Fig. 6 shows RBEs of SOBP relative to gamma rays for skin reaction. The RBE of SOBP was 2.0 for entrance (15 keV/μm), and gradually increased up to 2.7 at near distal fall-off of 100 keV/μm.

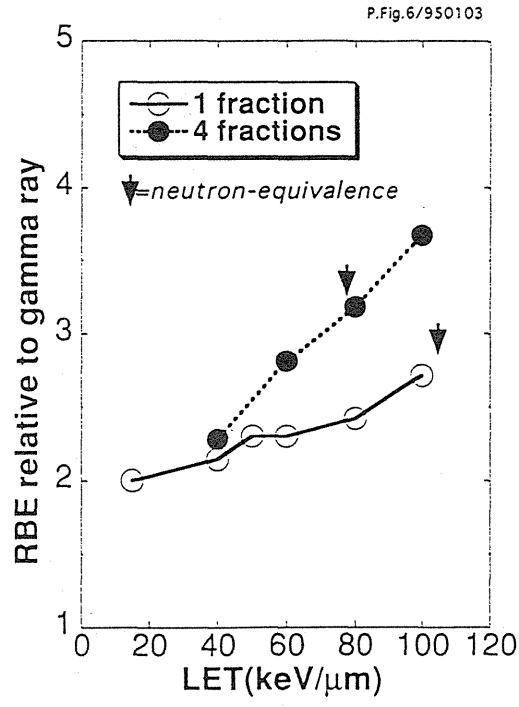

Fig.6 RBE of 6cm SOBP Carbon-12 for Skin Dry Desquamation
LET Dependence

RBEs of carbon-12 after fractionated irradiations:

Skin reactions after fractionated irradiations of carbon-12 SOBP were compared with those after fractionated gamma rays. RBE of proximal SOBP (40 keV/μm) for fractionated irradiations was 2.25 (Fig.6).which was similar to that for single irradiations. With increase of LET or beam path, RBE of carbon SOBP with fractionated irradiations increased steeply and largely in such that an RBE after fractionated irradiations at 100 keV/μm was 3.65 , and much larger than that after single irradiations,i.e., 2.7.

Dependence of RBE on dose

RBEs for skin dry desquamation obtained by single and fractionated experiments were plotted on dose per fraction (Fig.7). The dependence of RBE on dose was more prominent for higher LET of carbon SOBP. Neutrons showed a particular dose dependence of RBE in such that RBE remained high at large doses.

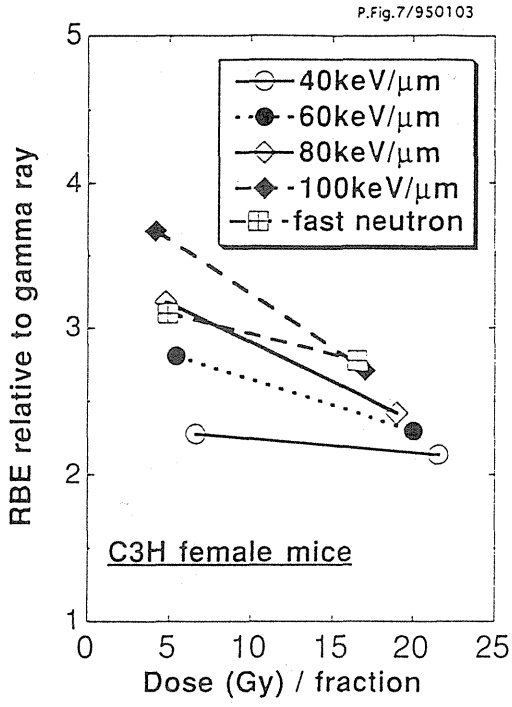

Fig.7 RBEs of C-12 SOBP for Skin Dry Desquamation

Distribution of biological dose within SOBP

Biological effectiveness of an SOBP is determined by dose and RBE at given position. As RBEs at various positions were experimentally obtained, biological effectiveness at the position could be calculated as the products of physical dose and RBE, and expressed as biological dose with a dimension of Gy. RBEs for cultured cells obtained at a 10% iso-survival(Fig.2) were multiplied by a physical dose at the corresponding SOBP position, and resultant biological doses were plotted against depth (Fig.8)

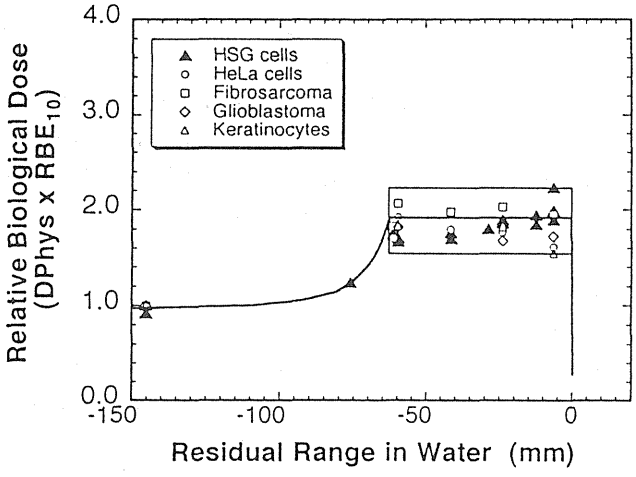

Fig.8 Biological dose distribution of C-12 6CM SOBP for cell kills.

As we normalized physical doses to entrance of SOBP, biological doses shown here had no dimension. Biological doses for 5 cell lines within SOBP showed a mean value of 1.9 and ranged from 1.6 to 2.2, i.e., 15% of the mean value.

Biological doses for skin reaction at 42, 45, 48, 55, 65 and 80 keV/μm, which corresponded to edge of proximal SOBP, 1-cm down stream of proximal edge, 2-cm, 3-cm, 4-cm and 5-cm, respectively, were also calculated from Fig.6, and plotted against path of SOBP where we normalized physical doses to proximal SOBP (Fig.9). Homogeneous distribution was obtained for skin reaction after fractionated irradiations, but not for single irradiations; biological dose distribution for single irradiations was similar to physical dose distribution in such that biological dose of 2.2 at proximal SOBP decreased down to 1.7 at distal SOBP(i.e., 1-cm upstream of distal fall-off).

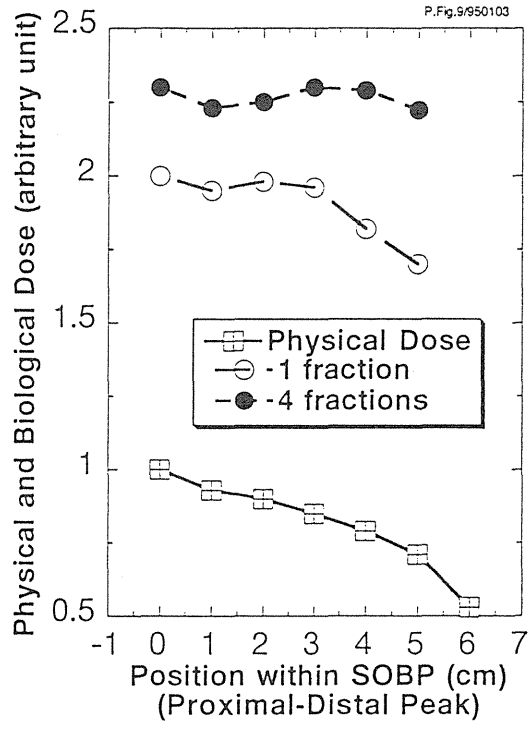

Fig.9 Physical and Biological Dose Distribution within 6 cm SOBP

Estimation of carbon dose for clinical use

As clinical parameters for neutron therapy have been well investigated in our institute, it would be reasonable to use the same fractionation schedule of neutrons (3 fractions per week for 6 weejs) as of initial carbon therapy. We employed two methods to estimate a carbon

dose recommendable for clinical trial; i.e., neutron-equivalent method and RBE method. Table 1 shows procedures employed in these two methods.

(Fig.5). Mouse skin dry desquamation indicated that 75 keV/μm was the neutron-equivalent point for fractionated irradiations (Fig.6). These two neutron-equivalent points narrowed down to

Table 1

Procedure to estimate a carbon dose for clinical trial

	(A)neutron-equivalent method	(B)RBE method
(1)	80 keV/μm of 6 cm SOBP =8 mm upstream of the fall-off =neutron-equivalent point	
(2)	clinical parameters of neutron therapy dose/fraction=0.9 Gy	photon TDF for 3 f / week x 6 weeks =3.0 Gy
(3)		Biological dose =3.0 GyE
(4)	Physical dose of SOBP is represented at 3.0 cm upstream of the fall-off (middle SOBP)	
(5)	carbon dose at (4) = *1.133 Gy*	RBE of mouse skin at (4) =2.6
(6)	Biological dose in neutron therapy =0.9 Gy x 3.0(RBE) =2.7 GyE	carbon dose at (4) =3.0 Gy / 2.6 = *1.15 Gy*
(7)	RBE at (4) = 2.7 Gy / 1.133 Gy = 2.38	

In neutron-equivalent method, biological data were used only for pinpointing the SOBP position which was biologically identical to fast neutrons(Fig.10). First, we selected HSGc-C5 among five in vitro cell lines to derive the neutron-equivalent point. This is because that the first patient in carbon clinical trial had parotid gland tumor to be treated with, and that HSGc-C5 is a human salivary gland tumor cell line.

The neutron-equivalent point within SOBP for cultured HSGc-C5 cells was 82 keV/μm

determine the SOBP position; we determined 80 keV/μm and 8 mm upstream of the distal fall-off as the neutron-equivalent point clinically usable. Second, neutron therapy used 0.9 Gy neutron dose per fraction for a total of 18 fractions(3). Third, we presumed that middle SOBP would be the most appropriate position to chose for physical dose of the SOBP. As neutron-equivalent position was 8 mm upstream of the distal fall-off, and as carbon dose at this position would be 0.9 Gy which was used in neutron

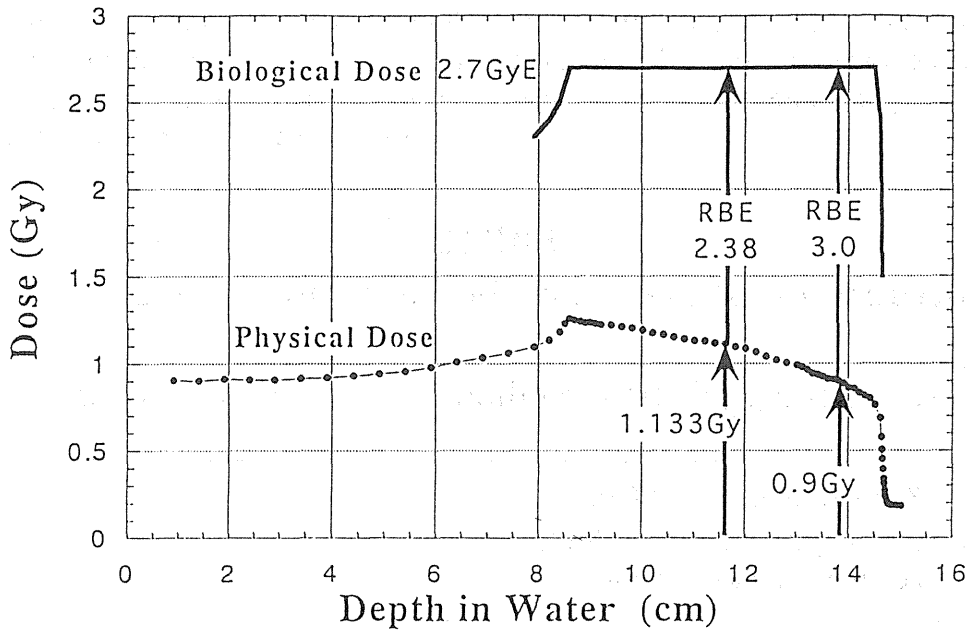

Fig.10 Neutron-equivalent method used for estimating a carbon dose suitable in clinical trial

therapy, carbon dose at middle SOBP (i.e., 3.0-cm upstream of the distal fall-off) was physically determined to be 1.133 Gy. Fourth, RBE of carbon dose of 1.133 Gy was calculated to be 2.38. Neutron therapy used an RBE of 3.0 which results in an biological dose of neutron as 0.9 Gy x 3.0=2.7 Gy-equivalent. An RBE of 2.38 for a carbon dose 1.133 Gy could then be obtained by 2.7 Gy-equivalent /1.133 Gy.

In RBE method, photon TDF value and mouse skin RBE were used to determine carbon dose. First, clinical trial of carbon therapy would employ 3 fractions per week for 6 weeks, a schedule identical to neutron therapy used in NIRS. TDF value for photon in this fractionation schedule is 3.0 Gy(4). Second, we presumed that middle SOBP would be the most appropriate position to chose for physical dose of the SOBP. Third, skin RBE of fractionated carbon ions was 2.6 at middle SOBP (Fig.6). Fourth, carbon dose at middle SOBP (i.e., 3.0-cm upstream of the distal fall-off) was then biologically determined by a formula 3.0 Gy/2.6 and was 1.15 Gy. As two methods reached to calculated doses similar to each other (i.e., 1.133 Gy and 1.15 Gy), we concluded to recommend 1.13 Gy as a carbon dose for clinical use where 3 fractions per week and a total of 18 fractions would be used for the first patient.

DISCUSSION

We have investigated biological effectiveness of high LET beams on cell kills, tumor controls and normal tissue damage, using fast neutrons produced by NIRS cyclotron (5-7) and , more recently, 135 MeV/u carbon ions produced by ring cyclotron at RIKEN (8-10). The followings have been disclosed by these investigation. First, RBE of high LET beams depends on materials, endpoints, dose size, and fractionation schedule. Second, charged particles are different from neutrons in dose localization. A tissue behind the distal fall-off of Bragg Peak remains intact, and develops no detectable damage during observation period(11). Third, LET measurement has been methodologically established for pure beams of charged particles, but is not yet for SOBP and neutrons.

RBEs of carbon-12 290 MeV/u with 6-cm SOBP varied depending on cell line (Fig.5). Magnitude of variation seems to be larger at distal SOBP than proximal SOBP. As LET at distal SOBP(1 cm upstream of fall-off) was 70-200 keV/μm and higher than that at proximal SOBP (Fig.1), difference of RBE among cell lines would be maximally expressed at distal SOBP. This variation would also be the case in

vivo; i.e., magnitude of response to carbon ions would be different from one tumor to another tumor and from one normal tissue to another normal tissue as well. Physiological condition including hypoxia and cell cycle distribution would also contribute to the variation. It is essential in future to individualize tissue response after high LET irradiation.

Biological dose was homogeneously distributed within SOBP for fractionated irradiations , but not for single irradiations (Fig.9). Difference between single and fractionated irradiations is expressed in the relation between RBE and dose size. RBE of SOBP against skin reaction depended on dose size and this dose dependence became prominent when LET increased (Fig.7). Survival curves for the target cells responsible to skin reaction may have a large shoulder at small dose region where RBE of high LET beams increases. As the wedge filter used here was designed to bring out 10% cell survivals, RBEs for skin would also meet this design at small dose.

In mechanistic point of view, neutrons and carbon ions are different in depositing energy to a cell. Carbon ions directly give energy to a cell while neutrons once react with atoms in a cell to produce secondary particles such as recoil protons which then give energy to a cell(12). This difference in energy deposition implies that variation of LET distribution for neutrons would be larger than that of carbon ions, and, if it were the case, then that a dose response curve for carbon ions might have a slope steeper than that for neutrons. In the present mouse skin experiments, however, we could not detect any significant difference between carbon ions and neutrons in dose response curves. The dose-RBE relation was in stead different between carbon ions and neutrons (Fig.7). Slope of the dose-RBE relation for neutrons was shallower than that for carbon SOBP with relevant LET, but similar to that for low LET of carbon SOBP. This implies that the shoulder region on the survival curve of target cells remains after neutron irradiation, but disappears after high LET of carbon SOBP.

In summary, We selected carbon-12 as a initial beam for heavy particle radiotherapy at NIRS. Carbon dose was here estimated by two methods, and recommended to clinical trial. Past neutron clinical trial in our institute provided us a clue to use neutron-equivalent method. As RBE method resulted in a conclusion similar to neutron-equivalent method, skin reactios of mice would further be applied to obtain fractionation parameters (e.g., α and β values) with clinical relevance. Studies on other normal tissues, transplanted tumors as well as cultured cells are now under investigation and would be reported in near future.

REFERENCES

1.Kanai,T.;Minohara,S.;Sudou,M.;Kohno,T.; Takada,E.;Soga,F.;Kawachi,K.;Furusawa,Y.; Fukutsu,K.;Eguchi-Kasai,K.;Itsukaichi,H.; Ohara,H.; Yatagai,F. Beam modulation for heavy ion radiotherapy. Proceedings of the second workshop on physical and biological research with heavy ions. ed.by Ando,K.; Kanai,T. NIRS-M-90, HIMAC-003, 1992

2.Aizawa,H.Relative biological effectiveness of fast neutrons, observed in the skin reaction of mice, after single and fractionated irradiation. Nipp.Act.Radiol.33(7), 602-616, 1973

3.Hall,E.J. Time, Dose , and fractionation in radiotherapy. Radiobiology for the radiologist 273-290, second edition, Harper & Row, Publishers, New York, 1978

4.Tsunemoto,H.;Morita,S.;Satoh,S.;Iino,Y.; Yoo,Y. Present status of fast neutron therapy in Asian countries. Strahlenther.Onkol.165, 330-336(Nr.4), 1989

5.Ando,K.;Koike,S.;Fukuda,N.;Kanehira,C. Independent effect of a mixed-beam regimen of fast neutrons and gamma rays on a murine fibrosarcoma. Radiat.Res.98, 96-106, 1984

6.Ando,k.;Koike,S.;Sato,S. Nonlinear survival curves for cells of solid tumors after large doses of fast neutrons and γ rays. Radiat.Res. 131, 157-161, 1992

7Ando,K.;Koike,S.;Fukuda,N.;Kanai,T.; Hiraoka,T.;Kawachi,K.;Jinnouchi,T. Effects of radiation qualities and 2 fractionated irradiation on radiation oral death. Nippon Acta Radiologica 43(2), 349-354, 1983

8.Ando,K.;Koike,S.;Kimoto,M.;Iizuka,M.;
Kiuchi,T.;Aruga,T.;Shimizu,W.;Sugita,T.;
Cho,C.K.;Kanai,T.;Kato,H.;Yatagai,F.
Tumor control probabilities and tumor growth
delay after accelerated carbon ions.
RIKEN Accel.Prog.Rep.26, 107, 1998

9.Ando,K.;Koike,S.;Fukutsu,K.;Kimoto,M.,
Iizuka,M.;Kiuchi,T.;Aruga,T.;Shimizu,W.;
Sugita,T.;Cho,C.K.;Kanai,T.;Furukawa,S.;
Kato,H.;Matsushita,S.;Furusawa,Y;Yatagai,F.
Effects of accelerated carbon ions on normal
tissues and tumors in experimental animals.
Proceedings of the second workshop on
physical and biological research with heavy
ions. ed.by Ando,K.;Kanai,T. 42-43,
NIRS-M-90, HIMAC-003, 1992

10.Ando,K.;Koike,S.; Iizuka,M.;Aruga,T.;
Hori,N.;Shimizu,W.;Sugita,T.;Murayama,S.;
Kanai,T.;Minohara,S.;Sudo,M.;Yatagai,F.
Effects of high LET radiation on murine skin
and tumors. Proceedings of the third
workshop on physical and biological research
with heavy ions. ed.by Ando,K;Kanai,T.
61-63,NIRS-M-99, HIMAC-006, 1993

11.Ando,K.;Fukutsu.K.;Tatsuzaki,H.;Yatagai,F.
Downsizing effect of irradiated volume on
normal tissue injuries.RIKEN Review No.4,
Focused on heavy ion science and technology.
43-44, 1994

12.Raju,M.R. Physical aspects of fast neutrons.
Heavy particle radiotherapy, 93-102,
Academic Press, London, 1980

TREATMENT PLANNING SYSTEM AT HIMAC - PRESENT FACILITY AND FUTURE PROSPECTIVE

MASAHIRO ENDO, PH.D., HIROKO KOYAMA-ITO, PH.D., SHIN-ICHI MINOHARA, PH.D., NOBUYUKI MIYAHARA, PH.D., HIROMI TOMURA, PH.D. AND TATSU-AKI KANAI, PH.D.

Division of Accelerator Physics and Engineering, National Institute of Radiological Sciences, Anagawa, Chiba, 263 JAPAN

Full use of advantages of heavy ions needs a treatment plan which enables to concentrate sufficient dose to a target region and spare surrounding critical organs. A powerful computer support is necessary to make such a plan because it is an iterative process in which we need real-time display of images including three-dimensional (3D) models, and need high-speed computation of 3D dose distributions. HI-PLAN (Heavy Ion Plan) is our treatment planning system which is constructed on modern graphical workstations with UNIX and X Window. It enables a standard treatment planning process and determination of irradiation parameters at HIMAC. In this paper we describe the software specifications, system architecture, hardware platforms and operation examples of the present version of HI-PLAN together with the future prospective.

INTRODUCTION

The use of heavy ions in radiation therapy may provide a therapeutic gain to deeply seated radioresistant tumors as a result of an improved dose distribution and a potential biologic advantage. Full use of such advantages of heavy ions needs a treatment plan that enables to concentrate sufficient dose to a target region and spare surrounding critical organs.

In treatment planning, firstly a target region is interactively inputted onto a three dimensional (3D) XCT image. Then irradiation fields are set so as to give prescribed dose to the target region and spare surrounding critical organs. A dose distribution is calculated for the fields, and a calculation result is observed on the displayed images.

If the dose distribution is not satisfied, above process is repeated to different fields. In this paper we will describe our treatment planning system with which we can perform above processes at HIMAC(1).

SOFTWARE SPECIFICATION

In our treatment planning system, the following functions are available.

1. Consecutive XCT images (100 slices maximum) are transferred via ethernet and converted to the format of the treatment planning system.
2. The XCT images are displayed on a monitor in one or multi-frame format and observed with diagnostic image quality. Slices are changed at a speed of more than one frame per second (depending on hardware).
3. Coronal and saggital sections are reformatted from transverse XCT images and displayed simultaneously.
4. Contours of a target and surrounding critical organs are interactively inputted onto XCT images. Some contours (body outline, lung and bone) can be automatically extracted by a threshold method.
5. The contours are reformatted and displayed on the coronal and saggital sections mentioned in the process 3.
6. A 3D model of the target and organs is generated from the contours, and then displayed. Surface and/or wire-frame models are available.
7. The 3D model is displayed as if viewers' eye were placed on the upstream of the beam (beam's eye view). The view point can be instantly changed so as to select the beam direction which makes the best separation of the target and critical organs. This process is called virtual simulation.
8. A beam outline is defined as a contour of projected target on a plane perpendicular to the beam direction, plus a margin. A patient collimator is designed so that an outline of the patient collimator is the same as the beam outline. If a multi-leaf collimator is necessary (large field case), leaf openings are determined so that leaves are cir-

cumscribed to the beam outline. Though these processes are automatically made, the results can be manually modified.

9. Milling depths of compensator are calculated so that range end of heavy ion beam is matched to distal edge of target. Inhomogenities of tissues are corrected using a calibration curve relating CT number and water equivalent length per pixel.

10. Control parameters of beam delivery and shaping devices such as scatterer thickness, wobbler currents are calculated from beam specification (beam size, beam range in the body, target thickness etc.), which are obtained in the processes 8 and 9.

11. A 3D dose distribution is calculated and displayed as isodose contours on transverse CT images as well as on reformatted coronal and/or sagittal sections. Isodose surfaces can be superimposed on the 3D model of target and critical organs.

12. Dose volume histograms (DVH) are calculated and displayed for the target and critical organs.

13. Digitally reconstructed radiograms (DRR) (2) are calculated and displayed from the beam direction and from the direction perpendicular to it. The contour of projected target, the outline of patent (or multi-leaf) collimator and landmarks are superimposed on each DRR, which is used for patient positioning.

14. Outline of patient collimator and thicknesses of compensator are numerically described and transferred to computer aided designing and machining (CAD/M) terminal, at which those data are converted to a standard format and used to fabricate the patient collimator and compensator with a numerically controlled (NC) milling machine.

15. Control parameters of beam delivery and shaping devices together with DRRs for positioning aid are transferred to a HIMAC irradiation room computer.

16. Major displayed images with overlays (such as dose distributions and DRRs) are saved for a meeting of treatment chart rounds. Images can be presented as hard copies or on a large screen video projector.

SYSTEM ARCHITECTURE AND HARDWARE

Fig.1 illustrates system architecture that we built in order to realize such specification as mentioned in the previous section. Hardware platforms are so called graphics workstations (TITAN 750 and Indigo2). Firstly we started to produce treatment planning software on TITAN 750 and this system is now used to clinical trials. Because TITAN 750 is now an old machine due to rapid progress of computer technology, we are preparing to move to Indigo2 (Silicon Graphics Inc.). Table 1 shows specifications of TITAN 750 and Indigo2. Indigo 2 is roughly three times faster than TITAN 750 in calculation and rendering speed.

The operating systems (OS) of the both computers are UNIX with X Window libraries (X lib and X toolkit). OSF/Motif is used as graphical user interface (GUI) in Indigo2. 3D graphics libraries are Dore (Dynamic Object Rendering Environment) and AVS (Application Visualization System) for TITAN 750, and GL for Indigo2. Dr. View is a general purpose medical image processing software system, on which our treatment planning system named HI-PLAN (Heavy Ion Plan) is constructed.

IRRADIATION PARAMETERS AND DOSE CALCULATION

Finely focused mono-energy beam just after extraction from the accelerator should be broadened in space and energy and be shaped to match a target volume before irradiating a patient. It is made by irradiation devices which consist of wobbler magnets (horizontal and vertical pair), a scatterer, a ring collimator, a ridge filter, a range shifter, a 4-leaf collimator, a multi-leaf collimator, a compensator and a patient collimator aligned from upstream. In our system we should determine control parameters of these devices as one process of treatment planning. Because the detail logic of determining the irradiation parameters are too complicated to mention here, we will describe the essence of the process.

Firstly a beam outline is defined as a contour of projected target on a plane perpendicular to the beam direction, plus a margin. Beam diameter d is defined as the maximum diameter of the beam outline. Water equivalent lengths (WEL) from upstream of beam to proximal and distal edges of target w1 and w2 are calculated by transforming pixel CT-numbers to WEL and integrating them along a beam path, where w1 and w2 are functions of coordinates (y,z) shown in Fig2.

Using these two parameters, residual range R, maximum thickness of target W and thicknesses of compensa-

tor T(y,z) are calculated as follows.

$$R = \max \{w2(y,z)\}$$

$$W = \max \{w2(y,z)-w1(y,z)\}$$

$$T(y,z) = R-w2(y,z)$$

Then irradiation parameters are calculated from combination of d,R and W. For example SOBP width of ridge filter is determined from W and range shifter thickness is determined from R. Depth dose distribution is also selected from the ridge filter and beam diameter d.

Dose calculation is made just after determination of irradiation parameters using ray-tracing algorithm. Wp(x,y) is calculated as water equivalent length to dose calculation point P(x,y) along beam path, where Wp(x,y) includes thickness of compensator T(y,z0) (z0 is z coordinate of dose calculation point). That is

$$Wp(x,y) = T(y,z0) + Wp'(x,y) ,$$

where Wp'(x,y) is water equivalent length within a patient body. Dose value at point P is as follows.

$$Dp = Dr \times P(Wp-R+R0) \times S(dy)$$

where Dr is SOBP dose, P is percent depth dose (100% at SOBP center). R0 is maximum range of the beam. S(dy) is a factor between 0 and 1 that shows penumbra at collimator edge. dy is length between point P to collimator edge along y direction. Function S(y) is given by the error function.

RESULTS

Phantom experiment

In order to examine accuracy of dose calculation, dose values of several points in a head phantom were measured to therapeutic beams and compared with calculated ones. Dosimeters, a PTW chamber and semiconductors were inserted into a hole of 1 cm diameter drilled from left lower jaw to left upper jaw in the phantom. A treatment planning was made to irradiate a target including the dosimeters by horizontal opposed fields. In the planning the maximum physical dose was set to 1.00 Gy. The results are shown in Table 2, and indicate that differences between calculated and measured values were approximately 2% for the left-right field that passed only soft tissues and that those were approximately 5% for the right-left field that passed bones and teeth as well as soft tissues.

Planning example

Fig.4 shows a target contour inputted interactively onto a CT image of a patient with lung cancer. Fig.5a) shows a 3D model of the target and critical organs of the same patient as Fig.4. The target and cord are shown in surface format, while left and right lungs are shown in wireframe format. Fig.5b) shows the same model from a slightly different view angle. From this view separation of the target and cord is better than the other view. Fig.6 shows isodose contours on the CT image. Fig.7 shows isodose contours on the CT image and reformatted saggital and coronal images. Fig.8 shows a DRR with landmarks, a projected target contour and a collimator outline. This image is used for patient positioning.

DISCUSSION

In the present time we just started making a treatment plan with the system mentioned above, though it satisfies only basic requirements. Future developments will include following functions.

1. At present we can only make a treatment plan with a constant thickness of range shifter and fixed aperture of collimator. However our irradiation devices can change range shifter thickness and collimator aperture continuously during irradiation, which enables 3D dynamic conformal therapy. We will implement a function to make a treatment plan and to determine irradiation parameters of such therapy.
2. We can only use XCT images for inputting a target contour with the present system. However the target may be delineated better by MRI or PET images. Dose calculation needs XCT images because only CT-number can be related to water equivalent length. Therefore precise registration of XCT and PET/MRI images is necessary. This technique is called image correlation (3), which recently has been developed in the field of conventional and proton therapy. This function will be implemented in the near future.
3. We are now using a ray tracing algorithm (4) to calculate dose distributions. It does not take effects of multiple scattering into account except penumbras at a collimator

edge. Recently some authors have proposed methods that take multiple scattering into account (5). They showed their method might be useful to dose calculations in highly heterogeneous regions that contain tissue/air or tissue/bone interfaces. We are now developing our own algorithm that enables a precise estimation of multiple scattering not only in patient but also in beam shaping devices.

4. It is a tedious task to input contours of critical organs onto consecutive XCT images. At present only the contours of body, lung and bone can be extracted automatically by a threshold method. We will implement more sophisticated algorithms for automated extraction of critical organ contours, which are efficient for kidney, liver, rectum, bladder etc..

5. Treatment data are now archived separately in treatment planning computers and in a HIMAC irradiation room computer. They are now archived with a backup function standard to UNIX. A user makes a substantial effort to incorporate treatment data. We are now developing a treatment data base in which all treatment data including image data are archived, and retrieved more easily.

REFERENCES

1. Kawachi, K.; Kanai, T.; Endo, M. et al. Radiation oncological facilities of the HIMAC. J. of JASTRO 1:19-29, 1989
2. Sherouse, G.W.; Novins, K.N. et al. Computation of digitally reconstructed radiographs for use in radiotherapy treatment planning. Int. J. Radiation Oncology Bio. Phys. 18:651-658, 1990
3. Pelizzari, C.A.; Chen, G.T.Y.; Spelbring, D.R.; Accurate three dimensional registration of CT, PET, and/or MR images of the brain. J. Comput. Assist. Tomogr. 13:20-26, 1989
4. Chen, G.T.Y.; Singh, R.P.; Castro, J.R. et al. Treatment planning for heavy ion radiotherapy. Int. J. Radiation Oncology Bio. Phys. 5:1809-1819, 1979
5. Petti, P.L. Differential-pencil-beam dose calculations for charged particles. Med. Phys. 19:137-149

Table 1 Hardware platforms.

TITAN 750 V (KUBOTA COMPUTER)	
Main Memory	**128 MB**
Magnetic Disk	**1.5 GB + 1.0 GB**
CPU Speed	**32 MIPS**
Rendering Speed	**400 Kvector/sec**
Indigo−2 (Sillicon Graphics Inc.)	
Main Memory	**128 MB**
Magnetic Disk	**2 GB**
CPU Speed	**85 MIPS**
Rendering Speed	**1.2 Mvector/sec**

Table 2 Comparison between calculated and measured values.

L − R			
	Calculated(A)	Measured(B)	B/A
CH1	0.93 Gy	0.918	98.7 %
CH2	0.98	1.002	102.2
CH3	0.98	0.986	100.6
PTW	0.85	0.862	101.4
R − L			
	Calculated(A)	Measured(B)	B/A
CH1	0.94 Gy	0.892 Gy	94.6 %
CH2	0.89	0.960	107.9
PTW	0.96	0.951	99.1

Fig.1 System architecture.

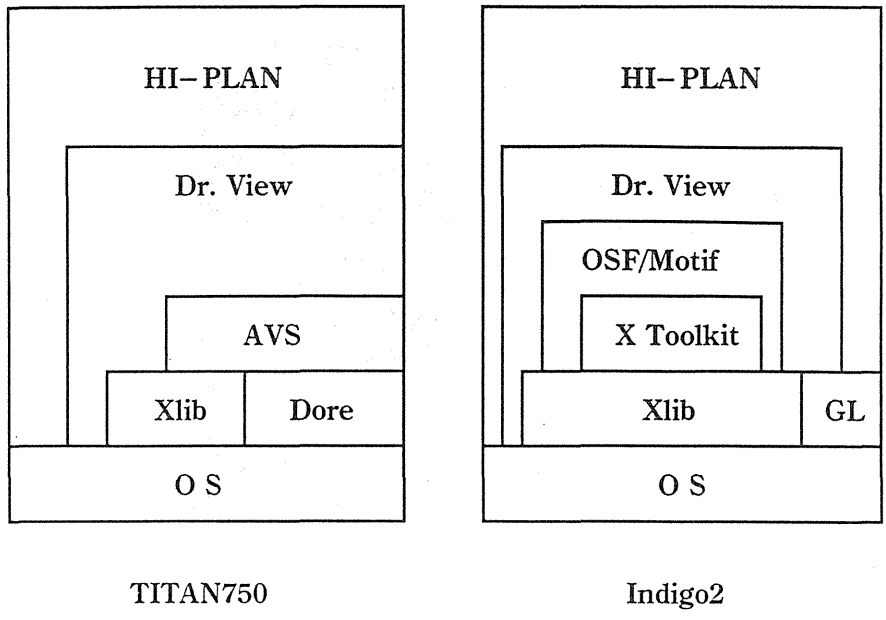

Fig.2 WEL from upstream of beam to proximal and distal edges of target.

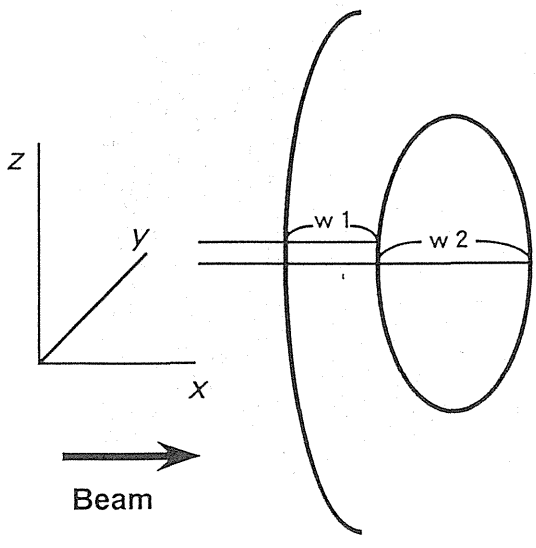

Fig.3 Dose calculation (Ray tracing algorithm).

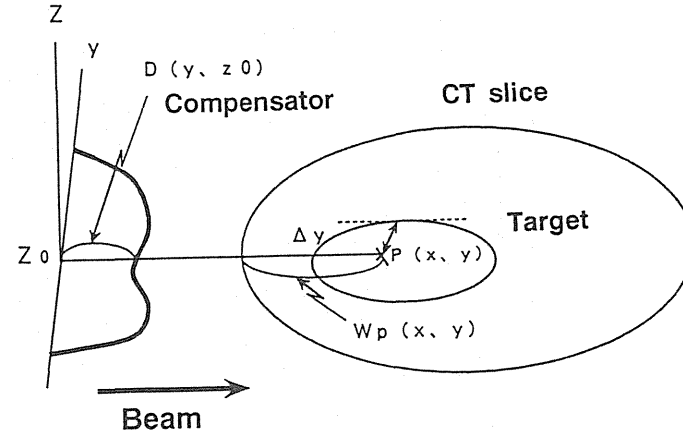

Fig.4 Contours of target and critical organs on CT image.

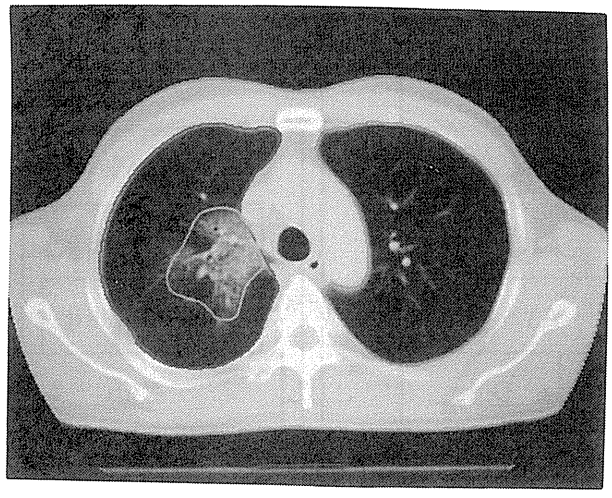

Fig.5 Virtual simulation. Perspective views of target and critical organs from beam source. View angles are slightly changed between a) and b).

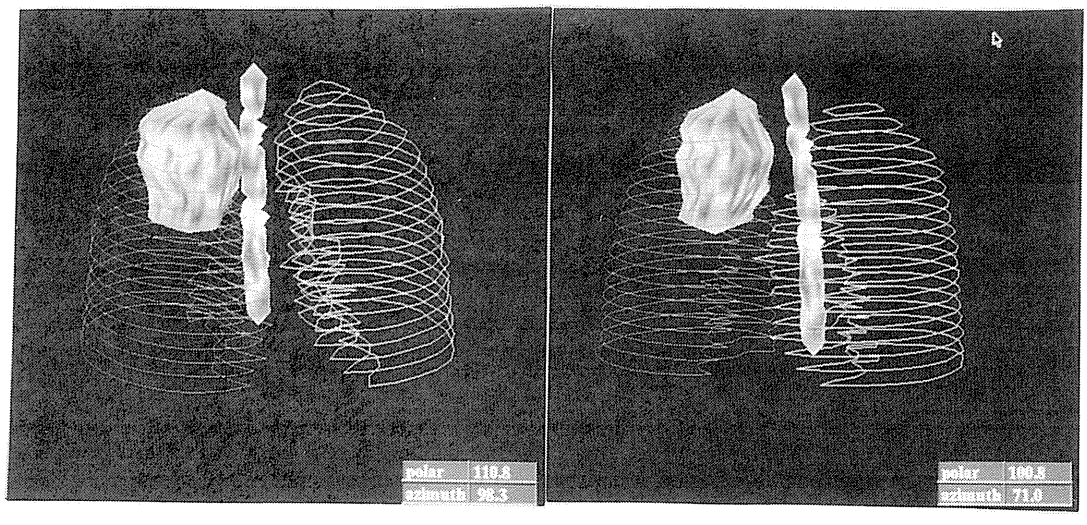

Fig.6 Dose distributions (Isodose contours) on CT image.

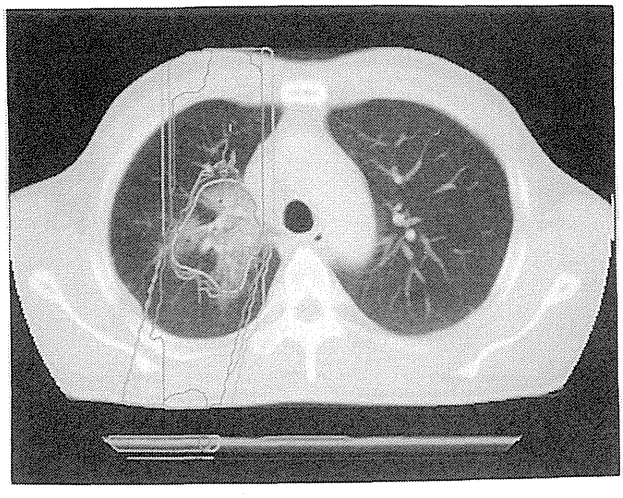

Fig.7 Dose distributions (Isodose contours) on CT image and reformatted images.

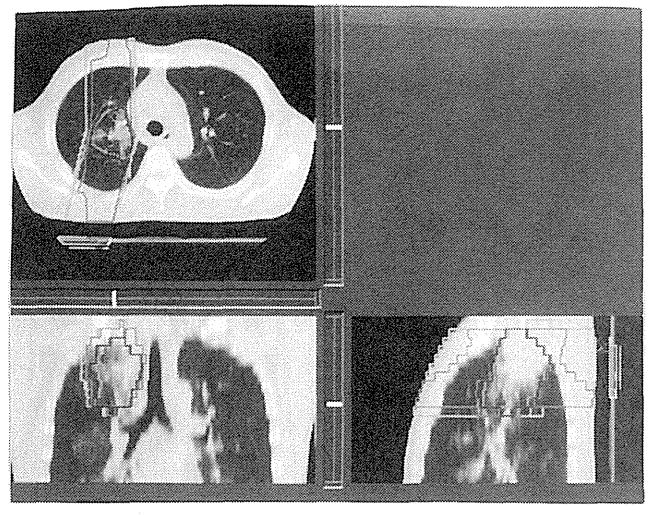

Fig.8 Digitally reconstructed radiograph (DRR) with a target projection and an outline of multi-leaf collimator.

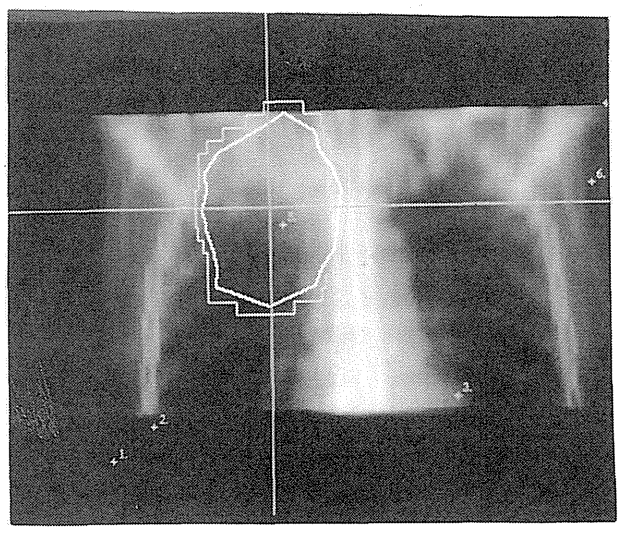

Project and Status I

THE MASSACHUSETTS GENERAL HOSPITAL NORTHEAST PROTON THERAPY CENTER BOSTON, MASSACHUSETTS[1]

ALFRED SMITH, PH.D., MICHAEL GOITEIN, PH.D., HERMAN SUIT, M.D., D. PHIL., STANLEY DURLACHER, JACOB FLANZ, PH.D., KENNETH GALL, PH.D., ANNE LEVINE, STANLEY ROSENTHAL, PH.D., SUSAN WOODS

Department of Radiation Oncology, Massachusetts General Hospital
Boston, Massachusetts 02114, USA

The Northeast Proton Therapy Center (NPTC) is being built on the main campus of Massachusetts General Hospital in Boston, Massachusetts.The NPTC is scheduled to begin patient treatments in the third quarter of 1998. The proton accelerator will be a fixed energy 235 MeV cyclotron capable of delivering 300 nA continuously. An energy selection system, consisting of a degrader and energy analyzer, will permit rapid (2 sec.) energy changes. The facility will have three treatment rooms with the provision for expansion to a fourth treatment room in the future. Up to two treatment rooms will be outfitted with isocentric beam delivery gantries. Initially, the third room will house an eye treatment station, a stereotactic intracranial treatment station, and a combination large-field treatment and experimental station. The beam delivery nozzles will include both a passive scattering and beam wobbling systems. The treatment /patient positioning system will permit rapid and accurate patient set-up and treatment delivery. In addition to the treatment control system, the facility will have an overall computer control system for the accelerator control and beam monitoring and an overall safety system to ensure personnel and patient safety. The NPTC is designed to treat 1000 patients per year with a large percentage of patients being entered into research protocols. The cost of the facility is approximately $46 million US dollars which is being shared between the National Cancer Institute and the Massachusetts General Hospital.

Radiation therapy, Proton therapy, Heavy charged particles, Proton Accelerator

INTRODUCTION

Massachusetts General Hospital (MGH) in collaboration with the Massachusetts Eye and Ear Infirmary (MEEI) has been treating patients at the Harvard Cyclotron Laboratory (HCL) for more than 30 years. Over six thousand patients have been treated at HCL using the 160 MeV proton beam. The approximate distribution of patients is: single-fraction stereotactic intracranial treatments - 50%; Uveal Melanomas - 33%; and large-field treatments - 17%. Among the large-field treatments the most common sites treated have been chordomas and chondrosarcomas of the skull base and cervical spine, soft tissue sarcomas, brain, head and neck, and prostate. The clinical research program has achieved increased local control without concomitant increases in morbidity in the chordoma/chondrosarcoma and uveal melanoma protocols and in the treatment of arteriovenous malformations. The early results in other treatment sites is encouraging. Our clinical results have led us to the conclusion that a modern proton treatment facility will provide opportunities for success at other disease sites and also

provide the capacity to treat additional patients in those disease sites for which protons have been proven to be superior to photons.

THE NORTHEAST PROTON THERAPY CENTER

The Northeast Proton Therapy Center (NPTC) will be located on the main campus of the Massachusetts General Hospital. The status of this project has been described in two previous reports (1,2). The NPTC site is immediately adjacent to clinical buildings of the MGH and the MEEI and therefore the NPTC will be integrated into a major hospital setting. The building will provide approximately 23,429 net square feet of program space including: three treatment rooms (up to two with gantries and one with horizontal beams); beam transport lines; integrated control system; immobilization fabrication and storage areas; mechanical, electrical, and vacuum shops; treatment planning facilities; offices and conference facilities; and storage areas. The treatment floor of the building is underground, and pits for the gantries extend below that floor. All patient activities will take place on the treatment floor. The offices, treatment planning areas and conference rooms will be on the first floor (ground level). Although the treatment floor is underground there will be skylights and a two-story lobby/waiting room area which will provide generous natural light to this space. The facility will be designed so as to be capable of subsequent expansion to four treatment rooms, three of which can contain gantries, the remaining room being a fixed field room. In the original configuration of three treatment rooms, the horizontal beam room will be capable of being fitted with a gantry.

Figure 1 shows the ground-level exterior elevation of the NPTC while Figures 2 and 3 show the first and second floors, respectively. Figure 4 provides views of the cyclotron vault (upper view) and a treatment room with gantry and patient positioner.

The facility will have the capacity to treat at least 1,000 patients per year (or approximately 16,000 treatment fractions per year) at the rate of about 65 patients per day.

The NPTC will be a regional resource for the northeast region of the United States which has a population base of 38 million people within a radius of 250 miles of Boston. We have encouraged affiliations with academic medical centers from each of the six New England states and from Albany, New York. These affiliations will enhance the opportunities for proton therapy, for both individual investigator and collaborative research; improve patient access; and achieve a broad referral base. Affiliated institutions may participate in clinical research studies, participate in clinical rounds, tumor conferences and continuing education, and explore the potential for establishing a telecommunications treatment planning network.

CLINICAL SPECIFICATIONS FOR THE NEW FACILITY

One of our first steps was to develop clinical specifications for the new facility. It was our belief that all performance and functional specifications should flow directly from the clinical requirements. We worked with the Lawrence Berkeley Laboratory heavy ion therapy and accelerator groups in the development of the clinical specifications. It is important to note that the specifications did not specify the implementation - that is, for example, they did not specify the type of accelerator (synchrotron or cyclotron, etc.) nor the type of gantry (corkscrew or compact, etc.). Rather, they defined what the proton beam characteristics at the patient must be. The vendor was left with the flexibility to decide how the requirements would be achieved. This approach provided the widest possible scope for potential vendors and provided MGH with the best possible range of choices and cost-performance trade-offs. The detailed clinical specifications have been published (3); Table I gives a summary of the most important ones. The acceptance tests of the equipment will be designed to test whether or not the clinical specifications have been achieved.

Table I

Summary of clinical specifications

	Preferred specification	Minimum specification
Range in Patient	32 g/cm^2 maximum 3.5 g/cm^2 minimum	28 g/cm^2 maximum 5.0 g/cm^2 minimum
Average dose rate	A beam intensity sufficient to treat a 25 x 25 cm field at a depth of 32 g/cm^2, modulated over the full depth, to a dose of 2 Gy in 1 minute or less.	A beam intensity sufficient to treat a 25 x 25 cm field at a depth of 28 g/cm^2, modulated over the full depth, to a dose of 2 Gy in 4 minutes or less.
Field size	Fixed: $\geq$ 40 x 40 cm Gantry: $\geq$ 40 x 30 cm	Fixed: $\geq$ 28 x 28 cm Gantry: $\geq$ 26 x 22 cm
Dose uniformity	$\pm$ 2.5% over treatment field	$\pm$ 4% over treatment field
Distal dose fall-off 80-20%	Not more than 0.1 g/cm^2 > physical limit from range straggling of a monoenergetic beam.	Not more than 0.6 g/cm^2
Lateral penumbra	Not more than 2 mm over the penumbra due to multiple scattering in the patient.	Not more than 4 mm over the penumbra due to multiple scattering in the patient.
Time to switch energy in one room.	$\leq$ 2 sec.	
Treatment beam availability	> 95%	

THE BUILDING AND EQUIPMENT PROCUREMENT PROCESS

The Building

After extensive discussion, the NPTC staff concluded that an integrated approach to the design and construction of the facility would be to the overall advantage of the project. As a result, the request for proposals (RFP), issued in November 1992, solicited proposals from teams which possessed expertise in project management and systems integration as well as proven capabilities in design, engineering, and construction.

Proposals from each of six prequalified teams were received in March 1993. After technical and cost evaluation, three of the proposals were deemed to be in the competitive range. Discussions and further interviews were held with these teams, and the team led by Bechtel Corporation was selected in June and a contract was signed in August, 1994. Bechtel, providing project management services and construction management, is teamed with Tsoi/Kobus & Associates, Architect; McNamara/Salvia Inc., Structural Engineering; McPhail Associates, Geotechnical Engineering; and John Moriarty & Associates, Construction Contractor. Bechtel provided preliminary design services through an early services agreement. The project is using the design/build approach for the building. The architectural design, engineering, and construction management services are being carried out under a fixed

price contract while the construction will be completed under a guaranteed maximum price (GMP) contract.

The Equipment

An RFP was issued in December, 1992, to select a vendor to design, fabricate, install and commission an integrated proton therapy system for a fixed price. The major items which were requested included the proton accelerator, beam transport and switching systems, fixed horizontal beams in one treatment room, isocentric gantries in each of two treatment rooms, patient positioners, a beam dump, and an integrated control system consisting of accelerator, treatment, and safety components. A process was developed which included the use of outside technical experts, to make a technical evaluation of the proposals received and to assist MGH in selecting a vendor.

Six vendors were prequalified to submit proposals and three vendors submitted a total of four proposals - two for synchrotrons and two for cyclotrons. Two of the four proposals were determined to be in the competitive range according to their combined technical and cost scores. After a final round of proposal clarifications and discussions, MGH selected IBA, a Belgian firm, teamed with General Atomics (USA) and a contract was signed with IBA in April of 1994.

The proton therapy equipment is comprised of a number of elements:

a. A 235 MeV isochronous cyclotron, able to deliver beams of up to 1.5 mA, but hardware-limited at 300 nA in order to limit the maximum possible dose rate to the patient. This accelerator has been under development by IBA for over three years, in collaboration with Sumitomo Heavy Industries of Japan.

b. An energy selection system (ESS) which reduces the 235 MeV beam extracted from the cyclotron to a beam of any desired pre-selected lower energy within a two second time frame. The ESS also provides control over the energy spread and emittance of the lower energy beam, and with instrumentation, verifies the properties of the resulting beam. It also includes a beam dump.

c. A beam transport and switching system (BTSS) connecting the exit of the ESS to the entrance points of the isocentric gantries and the fixed beam lines, using achromatic bends.

d. A large-throw, in plane, isocentric gantry. The gantry optics consist of a 45 degree upward bend, then a number of quadrupole magnets, followed by a 135 degree bending magnet. These are followed by a "nozzle' which includes devices for beam position, shape, and intensity monitoring, for beam spreading both laterally (using passive and wobbling elements) and in depth, and for beam shaping using apertures and range modifying compensators.

e. Three or more fixed horizontal beam lines. The optics and construction of these are closely related to the BTSS. In one treatment room there will be three horizontal beam lines, one for eye treatments, one for intracranial, stereotactic treatments.

f. A computer-based integrated control system which includes the accelerator control unit (ACU), and a number of independent, but networked, therapy control stations. Through the network, each of the treatment control stations can also take control of the PLC-based ACU controlling the cyclotron, the beam line and the gantry optics.

g. A global safety system independent of the control system. This system will be responsible for the protection of patients, personnel, and the public, from exposure to potential radiation and other hazards. The safety system will use a combination of hardwired interlocks and independent PLC's to achieve a safety level meeting applicable standards.

h. An articulated patient positioning system which will provide support for patients and, in conjunction with the gantry, enable the proton beam to be accurately directed to any target within the body.

PROJECT MILESTONES

The overall project milestones are outlined in Table II.

Table II.

Project Milestones

Date	Milestone
June, 1995	Building construction begins
November, 1996	Building construction completed
November, 1994	Equipment construction begins
August, 1997	Equipment installation complete
November, 1997	Equipment acceptance complete
July, 1998	Equipment commissioning complete
August, 1998	**First patient treated.**

REFERENCES

1. Smith, A.; Goitein, M.; Durlacher, S.; Flanz, J.; Levine, A.; Reardon, P.; Woods, S. The Massachusetts General Hospital Northeast Proton Therapy Center. In Hadrontherapy in Oncology, U. Amaldi and B. Larsson, editors. Elsevier Science B. V: 138-144; 1994.

2. Flanz J.; Durlacher, S.; Goitein, M.; Levine, A.; Reardon, P.; Smith, A. Overview of the MGH-Northeast Proton Therapy Center Plans and Progress. Nucl Instr. Meth. in Phys. Res. B 00 (1995) NIB0341.

3. Gall, K.; Verhey, L.; Alonso, J.; Castro, J.; Collier J.; Chu, W.; Daftari, I.; Goitein, M.; Kubo, H.; Ludewigt, B.; Munzenrider, J.; Petti, P.; Renner, T.; Rosenthal, S.; Smith, A.; Staples, J.; Suit, H.; Thornton, A. State of the Art? New proton medical facilities for the Massachusetts General Hospital and the University of California Davis Medical Center, Nucl. Instr. Meth. in Phys. Res. 1993; B79:881-4.

Supported in part by grants CA 56931 and CA 59267 from the National Cancer Institute, Department of Health and Human Services, Bethesda, Maryland, USA

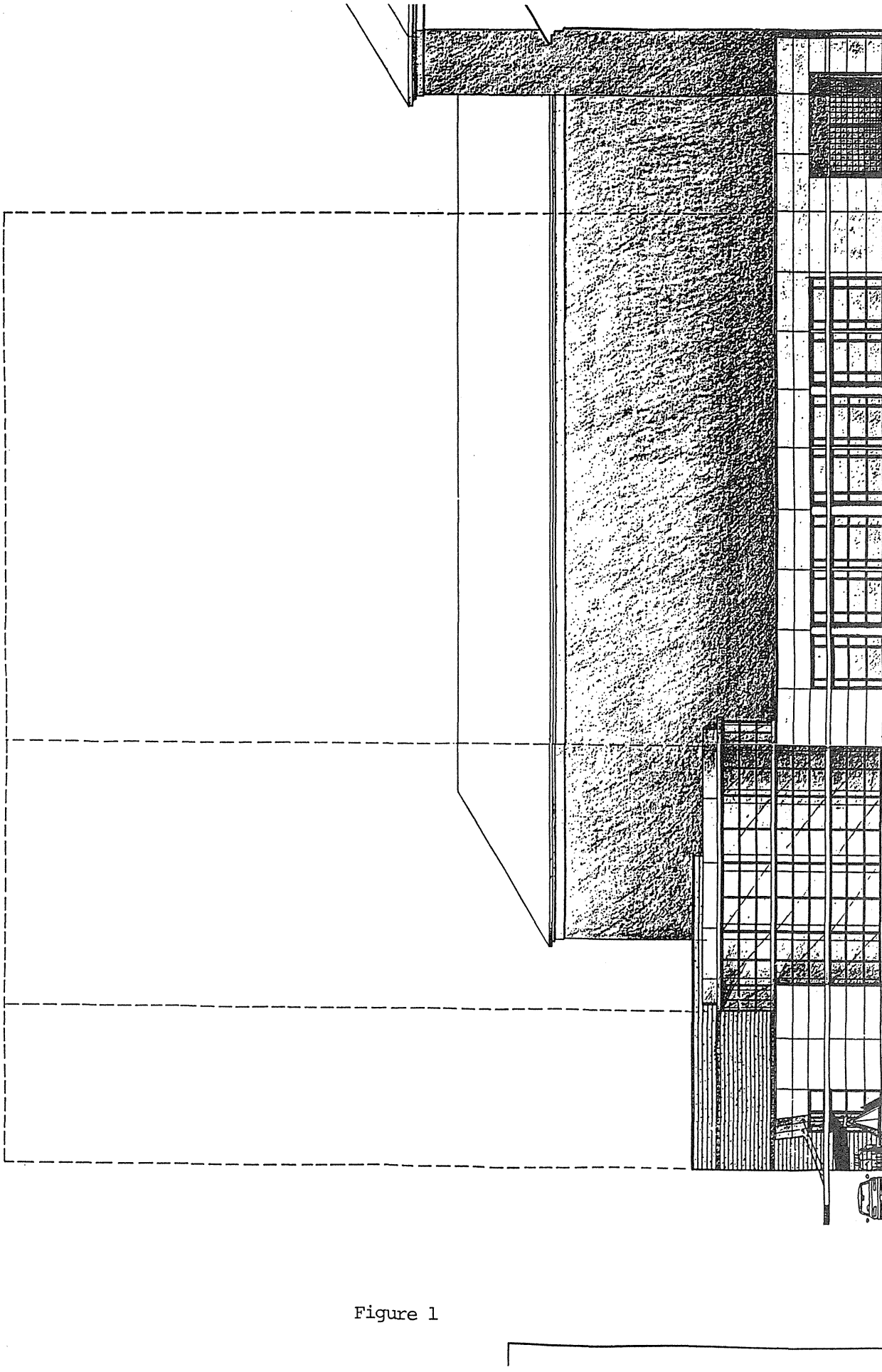
MGH: NORTHEAST PROTON THERAPY CENTER
FRUIT STREET ELEVATION

Figure 1

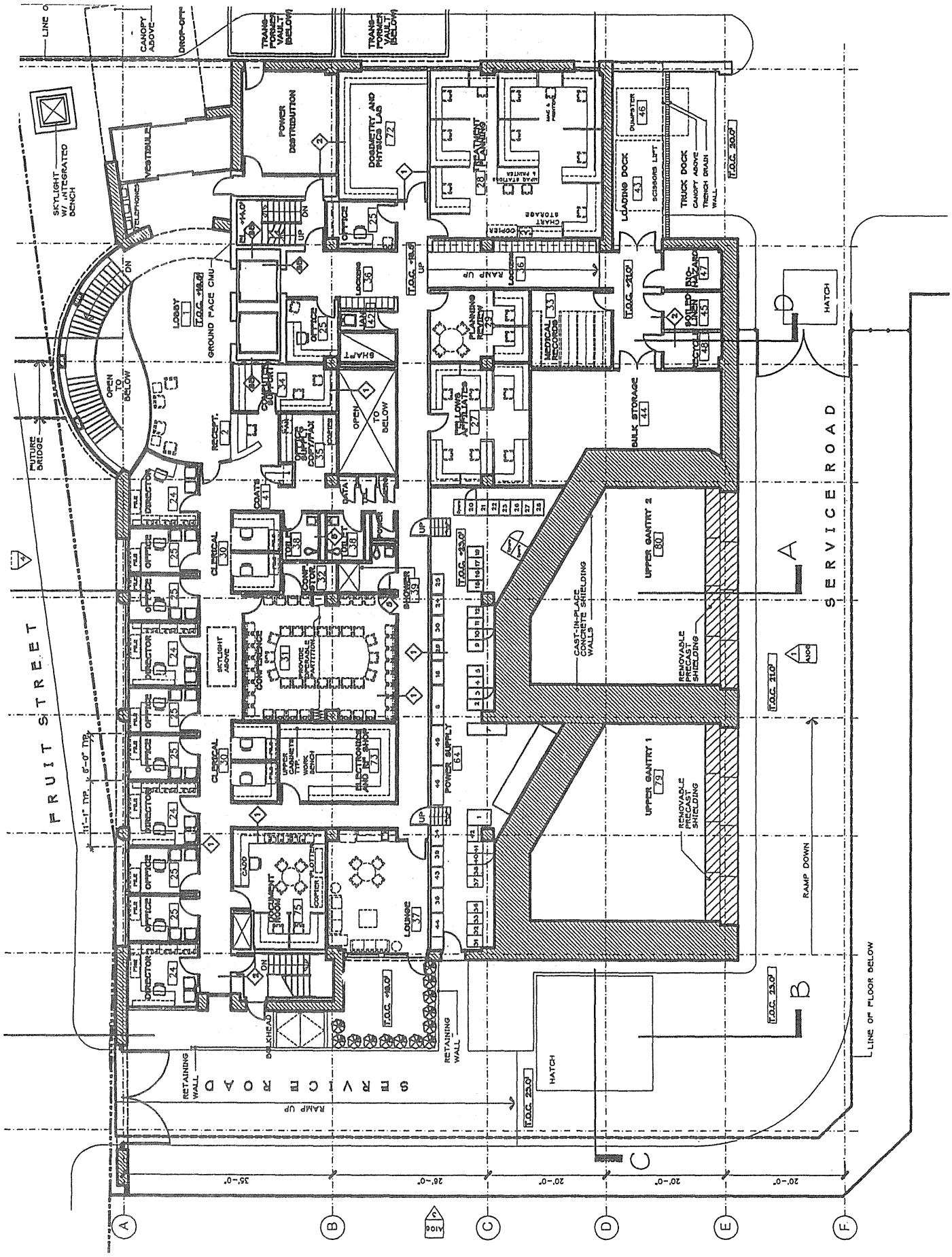
FRUIT STREET
SERVICE ROAD
SERVICE ROAD
LOBBY
RECEPT.
CLERICAL
CLERICAL
DIRECTOR
OFFICE
SKYLIGHT ABOVE
CONFERENCE
POWER DISTRIBUTION
DOSIMETRY AND PHYSICS LAB
TREATMENT PLANNING
LOADING DOCK
TRUCK DOCK
UPPER GANTRY 1
UPPER GANTRY 2
CAST-IN-PLACE CONCRETE SHIELDING WALLS
REMOVABLE PRECAST SHIELDING
BULK STORAGE
MEDICAL RECORDS
LOUNGE
POWER SUPPLY
RAMP UP
RAMP DOWN
HATCH
RETAINING WALL
LINE OF FLOOR BELOW
FUTURE BRIDGE
SKYLIGHT W/ INTEGRATED BENCH
GROUND FACE CMU
OPEN TO BELOW
A
B
C
D
E
F

Figure 2

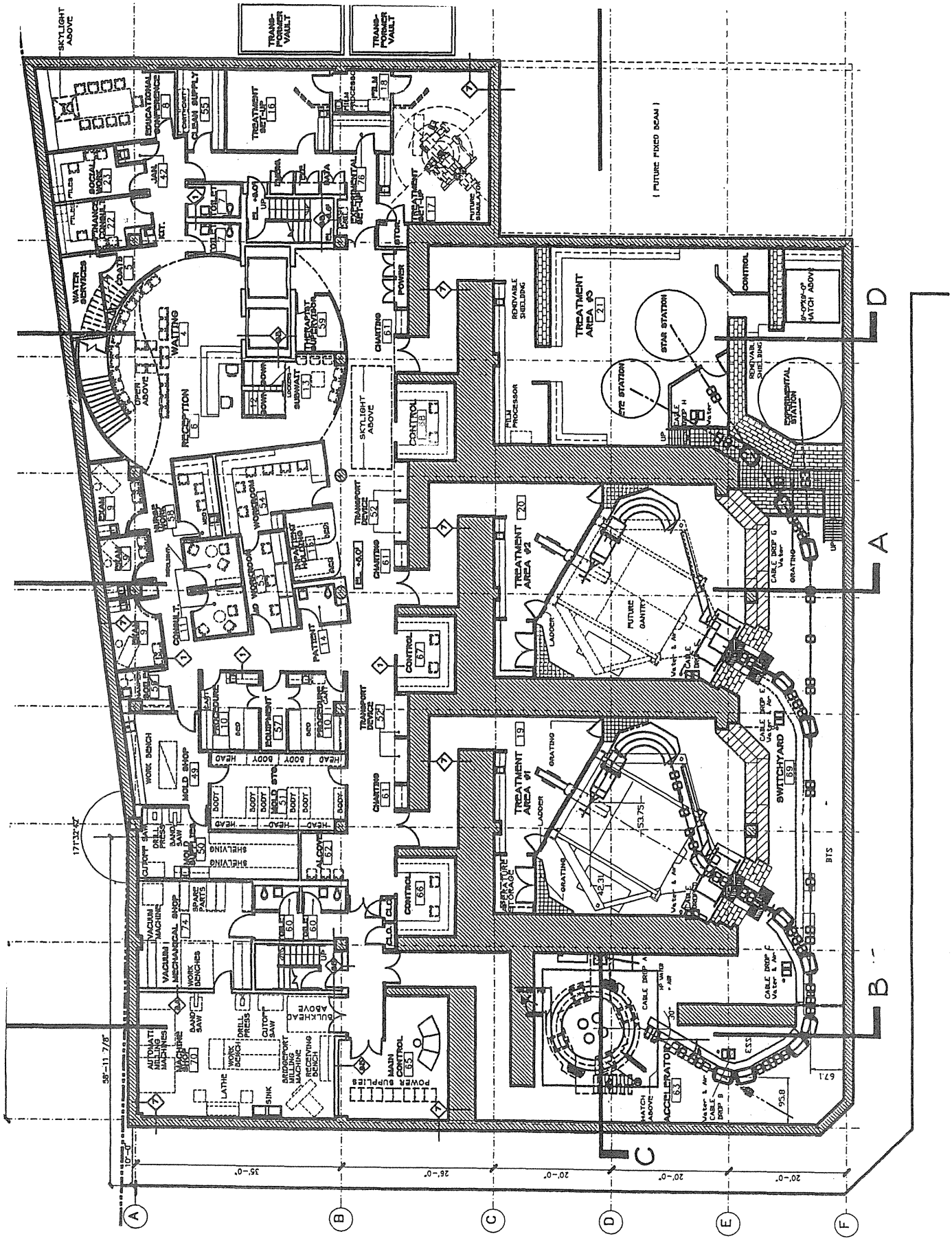
SKYLIGHT ABOVE
TRANS-FORMER VAULT
TRANS-FORMER VAULT
TREATMENT SET UP 16
CLEAN SUPPLY 55
EDUCATIONAL CONFERENCE 8
FILM PROCESSOR 18
TREATMENT SET UP 17
FUTURE SIMULATOR
(FUTURE FIXED BEAM)
WATER SERVICES
WAITING 4
RECEPTION 6
THERAPIST PROCEDURE 59
SUBWAIT 13
CHARTING 61
POWER
REMOVABLE SHIELDING
TREATMENT AREA #3 21
STAR STATION
CONTROL
MATCH ABOVE
CONTROL 38
TRANSPORT DEVICE 52
WORKROOM 54
PATIENT 14
CONSULT 11
NURSE WORK 58
BAN 9
ROOF 57
PROCEDURE 10
EQUIPMENT 57
PROCEDURE 10
TRANSPORT DEVICE 32
CONTROL 67
TREATMENT AREA #2 20
FUTURE GANTRY
LADDER
CABLE DROP G
GRATING
SWITCHYARD 69
TREATMENT AREA #1 19
FUTURE STORAGE
CONTROL 66
MOLD SHOP 49
WORK BENCH
SHELVING
ALCOVE 62
SPARE PARTS
VACUUM MECHANICAL SHOP 74
VACUUM MACHINE
WORK BENCHES
BAND SAW
DRILL PRESS
CUTOFF SAW
ABOVE
BULKHEAD
AUTOMATI MACHINES
WORK BENCH 70
LATHE
SINK
BRIDGEPORT MILLING MACHINE
RECEIVING BENCH
MAIN CONTROL 65
POWER SUPPLIES
ACCELERATOR 63
CABLE DROP B
CABLE DROP F
BTS
35'-0"
26'-0"
20'-0"
20'-0"
20'-0"
A
B
C
D
E
F

Figure 3

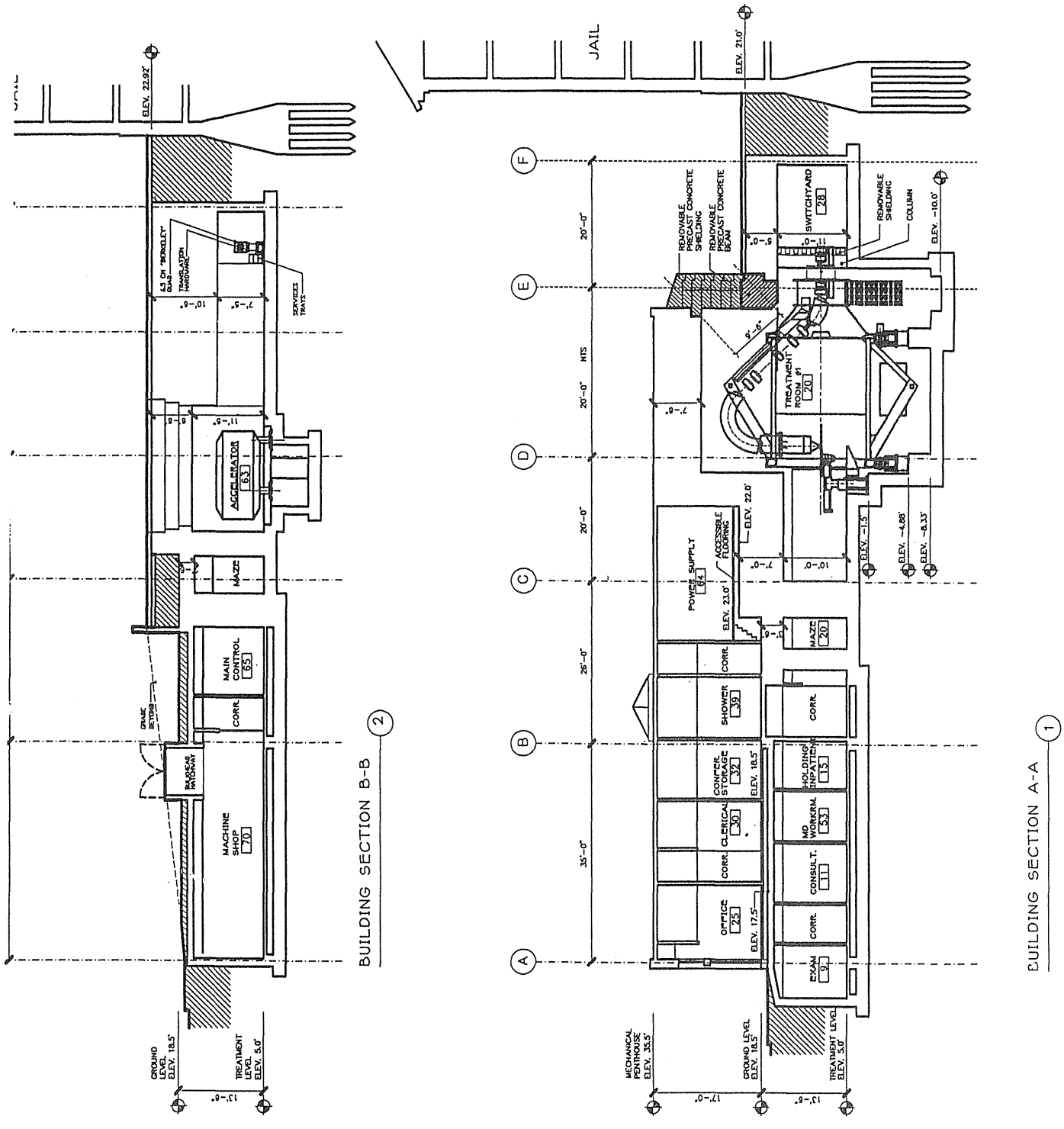
BUILDING SECTION B-B
BUILDING SECTION A-A
JAIL
ELEV. 22.92'
ELEV. 21.0'
ACCELERATOR
MAZE
MAIN CONTROL
CORR.
MACHINE SHOP
GROUND LEVEL ELEV. 18.5'
TREATMENT LEVEL ELEV. 5.0'
SERVICES TRAYS
REMOVABLE PRECAST CONCRETE SHIELDING
REMOVABLE PRECAST CONCRETE BEAM
SWITCHYARD
REMOVABLE SHIELDING
COLUMN
TREATMENT ROOM #1
POWER SUPPLY
ACCESSIBLE FLOORING
SHOWER
CONFER. STORAGE
CLERICAL
OFFICE
CONSULT.
MD WORKRM.
HOLDING/INPATIENT
EXAM
MECHANICAL PENTHOUSE ELEV. 33.5'
NTS

Figure 4

The proton therapy system for MGH's NPTC: equipment description and progress report

Yves Jongen
Ion Beam Applications s.a. (IBA)
Chemin du Cyclotron, rue J.E. Lenoir 6
B-1348 Louvain-la-Neuve, Belgium

Abstract

At the beginning of 1994, the Massachusetts General Hospital (MGH) of the Harvard Medical School in Boston, MA, USA, a pioneer in proton therapy since 1959, selected a team leaded by IBA to supply the proton therapy equipment of its new Northeast Proton Therapy Centre (NPTC). The present paper presents the equipment being build for the NPTC.

1. Introduction

IBA has integrated the technologies developed for its low and medium energy cyclotrons into a high energy system dedicated to proton therapy. The objective was to meet all the clinical specifications of a state-of-the-art proton therapy facility in the most simple, reliable and cost effective manner. The main elements of the IBA integrated system are the following: a compact 235 MeV isochronous cyclotron, a short energy selection system transforming the fixed energy beam extracted from the cyclotron into a variable energy beam, one or more isocentric gantries fitted with a nozzle, a system consisting of one or more horizontal beam lines, a global control system including an accelerator control unit and several independent but networked therapy control stations, a global safety management system independent of the global control system, and a robotic patient positioning system. This equipment was selected by MGH for the NPTC.

2. The IBA team and the NPTC project

The different steps of the project, from the call for proposals to the selection of IBA, were the following:

- the request for proposals was dated December 1992;
- six qualified vendor teams were selected in March 1993;
- three proposals were introduced in June 1993;
- in August 1993 the hospital announced that the budget was limited to 17.64 MUSD. As all the proposals were above this limit, cost reduction suggestions were requested;
- based on the revised proposals, the vendors list narrowed to two in October 1993. One of them was a team

composed, among others, by IBA and General Atomics (GA);
- the IBA/GA team was finally selected in January 1994, with IBA as the prime contractor;
- the contract was signed in April, 26, 1994.

The cyclotron steel was cast in August 1994 and the machining started in October 1994. The first beam is expected to be produced, in the IBA factory, in March 1996. The building should be ready in November 1996 and the equipment delivery and installation will start at that date. The system acceptance tests on site are expected to be performed in October 1997, and the first patient should be treated in April 1998.

As already mentioned, IBA is the prime contractor and is in charge of the system integration, the accelerator and the control system. General Atomics is responsible for the beam transport, the gantries and the patient positioner, while Sumitomo Heavy Industries is in charge of part of the accelerator design and design review. The University of Louvain is responsible for part of the nozzle design, the development of selected electronic modules and chambers, and part of the design review. A number of specialists well-known for their competence in these fields were asked to act as consultants to the team.

3. A cyclotron based proton therapy system

The main elements composing the proton therapy system for the NPTC are the following:

- a 235 MeV isochronous cyclotron, able to deliver beams of up to 1.5 μA, but hardware-limited at 300 nA in order to limit the maximum possible dose rate to the patient.

- an energy selection system transforming the fixed energy beam extracted from the cyclotron into a variable energy beam (235 to 70 MeV range) provided with energy spread and emittance limitations and verification.

- a beam transport and switching system connecting the exit of the energy selection system to the entrance points of a number of gantries and fixed beam lines.

- isocentric gantry(ies) fitted with a nozzle, and a system consisting of two horizontal beam lines, the large field one being equipped with a nozzle. For beam spread-out on the gantries and on the large field line, both beam scattering and beam wobbling are available.

- a robotic patient positioning system. Combined with the gantry, the equipment provides complete 4π coverage of the patient.

- a global control system including, in addition to an "accelerator control unit", several independent, but networked "therapy control stations". Through the network, each of these irradiation control systems can also take control of the accelerator control unit controlling the cyclotron, the beam line and the gantry optics.

- a global safety management system independent of the control system. This safety management system uses a combination of hardwired

interlocks and independent PLC's to achieve a safety level meeting applicable standards.

4. Why a fixed energy, isochronous cyclotron?

The advantages of this system, and in particular of the choice of a cyclotron for proton acceleration, are the following:

- Simplicity, reliability and operability. An isochronous cyclotron is probably the simplest and most inexpensive way to produce 235 MeV protons. This technology is well-known and widespread. The cyclotron operates CW (continuous wave). The machine parameters are constant in time and only five (possibly seven) of them are adjustable. None of these parameters requires operator tuning during machine operation or during the morning start-up: reference values are stored by the control system and fine-tuned using well developed computer algorithms. Fast computer algorithms are not required as there is no time-critical tunings but only the need to compensate for slow drifts.

- Scanning ready. The high intensity, continuous extracted beam can be intensity controlled from the ion source within 15 μsec turn on/turn off time, and only 30 μsec separate the time of the beam living the source and reaching the patient. The beam is, for these reasons, perfectly suited for beam scanning and wobbling. The high available intensity easily allows respiration gating without extending treatment times, even for very large fields.

- Safety. The extracted beam is characterised by a fixed energy, a low energy dispersion and a fixed, low emittance. The accelerator is unable to produce an extracted beam with incorrect energy, energy dispersion or emittance pattern. The safety system ensures the safety of the patient and personnel.

- Maintainability. The cyclotron splits at the median plane allowing easy maintenance: the upper yoke can be raised in minutes by hydraulic jacks, giving free access to all machine components. Thanks to the moderate vacuum requirements and the generous pumping system, full energy beam can be resumed less than 30 minutes after the start of pump-down. The room temperature cyclotron technology allows short repair times.

Figure 1 presents a schematic view of the IBA cyclotron while figure 2 shows the complete system. Additional details concerning this system may be found in (1), (2) and (3).

5. The energy selection system

The energy variability of the system is achieved by means of a carbon wedge used as an energy degrader. As a result of the energy degradation, there is an increase in emittance and energy spread. Emittance slits are therefore used to define the emittance of the transmitted beam, while an analysing magnet system limits the energy spread. Energy changes are completed in two seconds, using

laminated magnets and quadrupoles. Figure 3 presents a view of the energy selection system.

6. The beam transport system

The beam transport and switching system connects the exit of the energy selection system to the entrance points of the gantries and the fixed beam lines. All bends are achromats. At strategic points along the beam transport system, the beam characteristics are monitored by grid ionisation chambers. This information can be used for automatic tuning. Figure 4 shows the beam transport system equipment.

7. The gantry

The NPTC equipment includes one complete isocentric gantry (the installation of a second one is foreseen as a possible upgrade). The gantry is an achromatic system. Its optics can be tuned for either beam scattering/wobbling or for pencil beam scanning. As for the energy selection system and the beam transport system, the use of laminated magnets and quadrupoles allows for energy changes in two seconds. Figure 5 presents a view of the gantry room.

8. The nozzles

The isocentric gantry and one of the horizontal beam lines, the large field one, will be fitted with nozzles. The functions of the nozzles include the 3-D beam shaping to irradiate the target volume at a constant dose, the beam monitoring and dosimetry, the help for patient positioning and field alignment verification, and the support of patient specific devices. The proposed design provides a static lateral beam spreading system, based on a double scattering method. The provision of 6-position barrels for the two scatterers and a six-track, fully compensated modulating wheel combined with the gating of the beam in synchronism with the wheel rotation allow versatile and reliable operation at a large span of field areas, ranges and modulation depths with optimum dose uniformity. A 1m long space, just after the scatterer/range modulator, is used for the installation of the X-Y beam sweeping magnets. The nozzle is equipped with several dose monitoring devices (transmission ionisation chambers) at different locations in the beam. The snout of the nozzle is telescopic to allow the final collimator and the bolus to be placed as close as possible to the patient, minimising deterioration of the penumbra. Figure 6 presents the different elements of this nozzle.

9. The patient positioning system

The patient positioner which will equip the gantry room is a robotic system allowing rotations around a virtual axis. It offers high precision, stability and reproductibility. Combined with the gantry, the equipment provides complete 4p coverage of the patient. It has a patient load/unload position. Figure 7 presents a side view of the gantry and patient positioner, while figure 8 shows a plan view of the patient positioner.

References

1. Y. Jongen *et al*, "Progress report on the IBA-SHI small cyclotron for cancer therapy", *Nuclear Instruments and Methods in*

Physics Research B79 (1993) 885-889

2. "The IBA Proton Therapy System", Brochure describing the Proton Therapy System proposed by Ion Beam Applications s.a., available upon request from IBA, Chemin du Cyclotron, rue J. Lenoir 6 - B 1348 Louvain-la-Neuve - Belgium

3. Y. Jongen *et al*, "New features in the design of the IBA-SHI proton therapy facility", Proceedings of the EPAC 94, London, May 1994

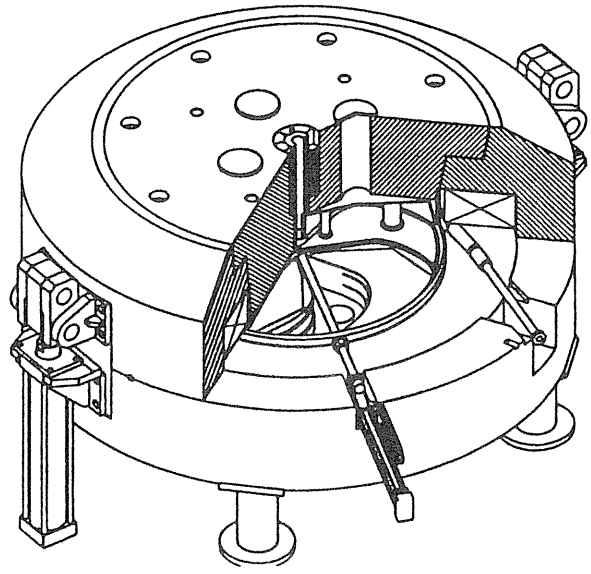

(a)

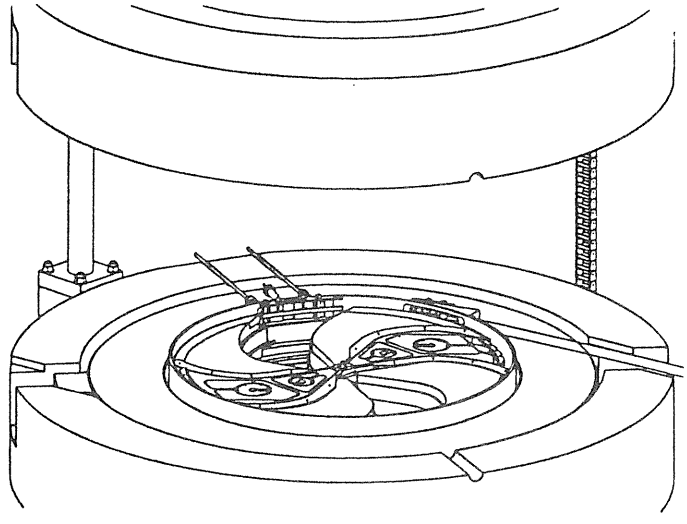

(b)

Figure 1. Schematic view of the IBA 235 MeV cyclotron (a). This cyclotron splits at the median plane allowing easy maintenance (b).

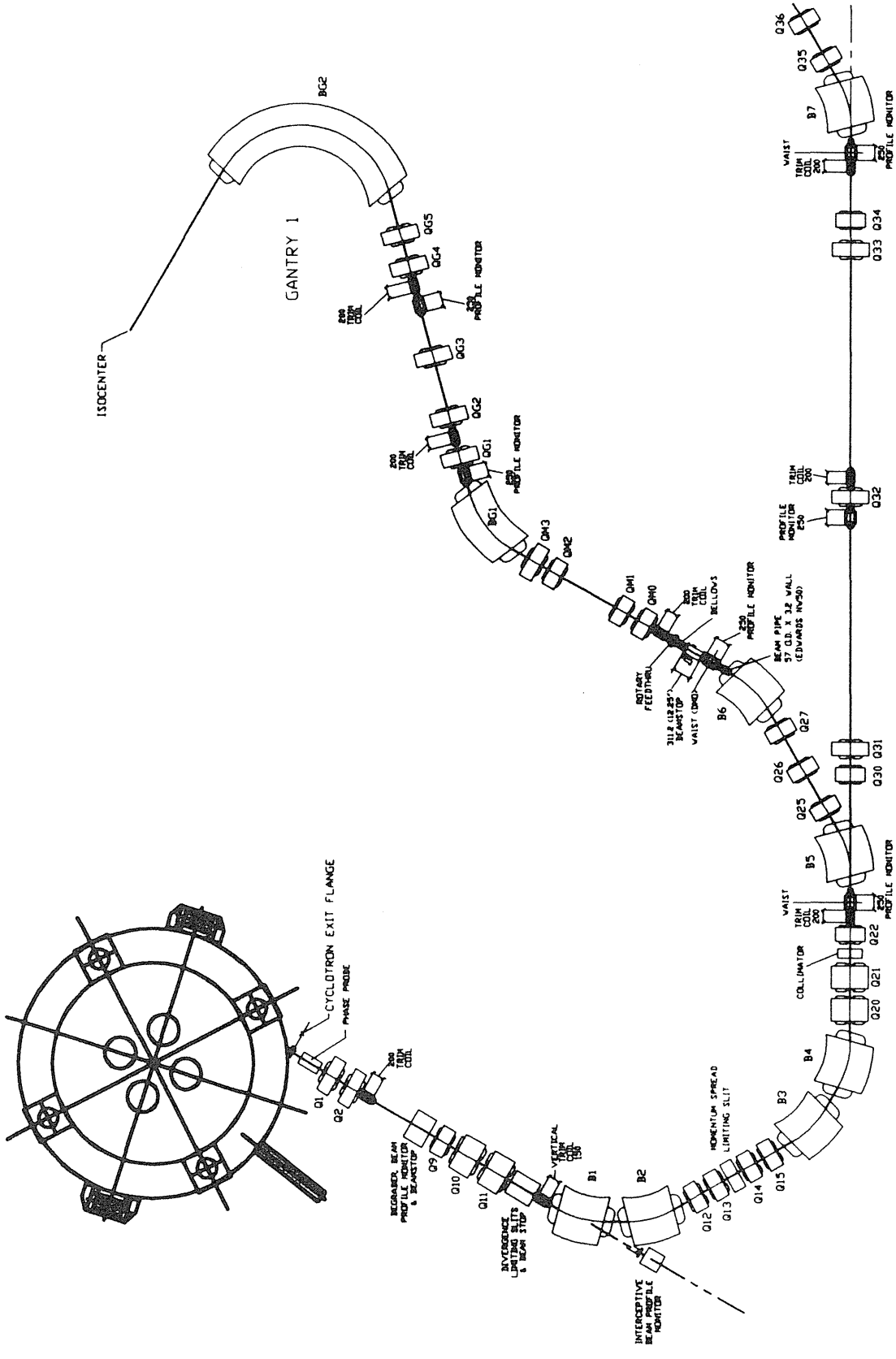

Figure 2. Part of the Proton Therapy equipment for the NPTC.

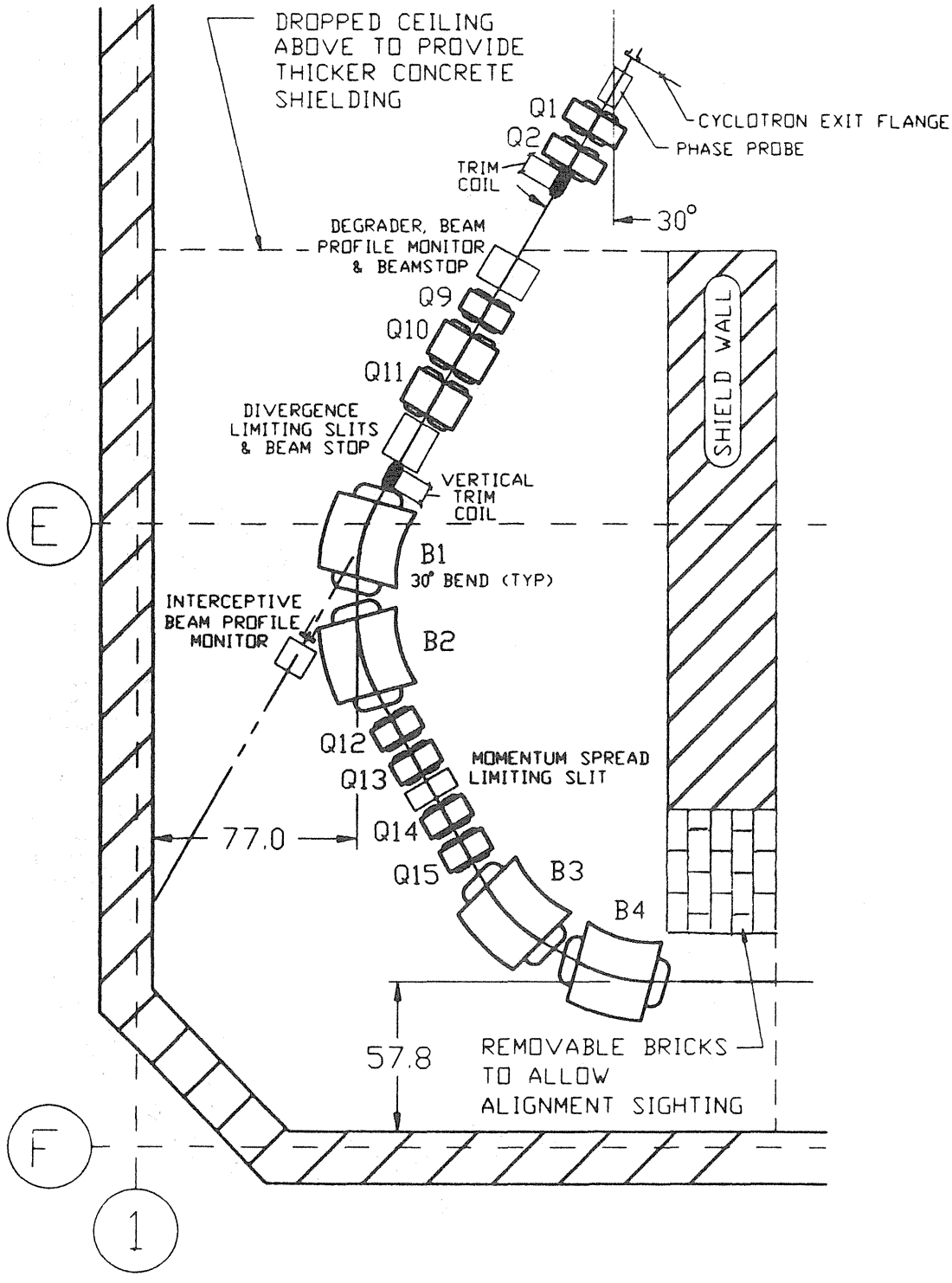

Figure 3. The Energy Selection System.

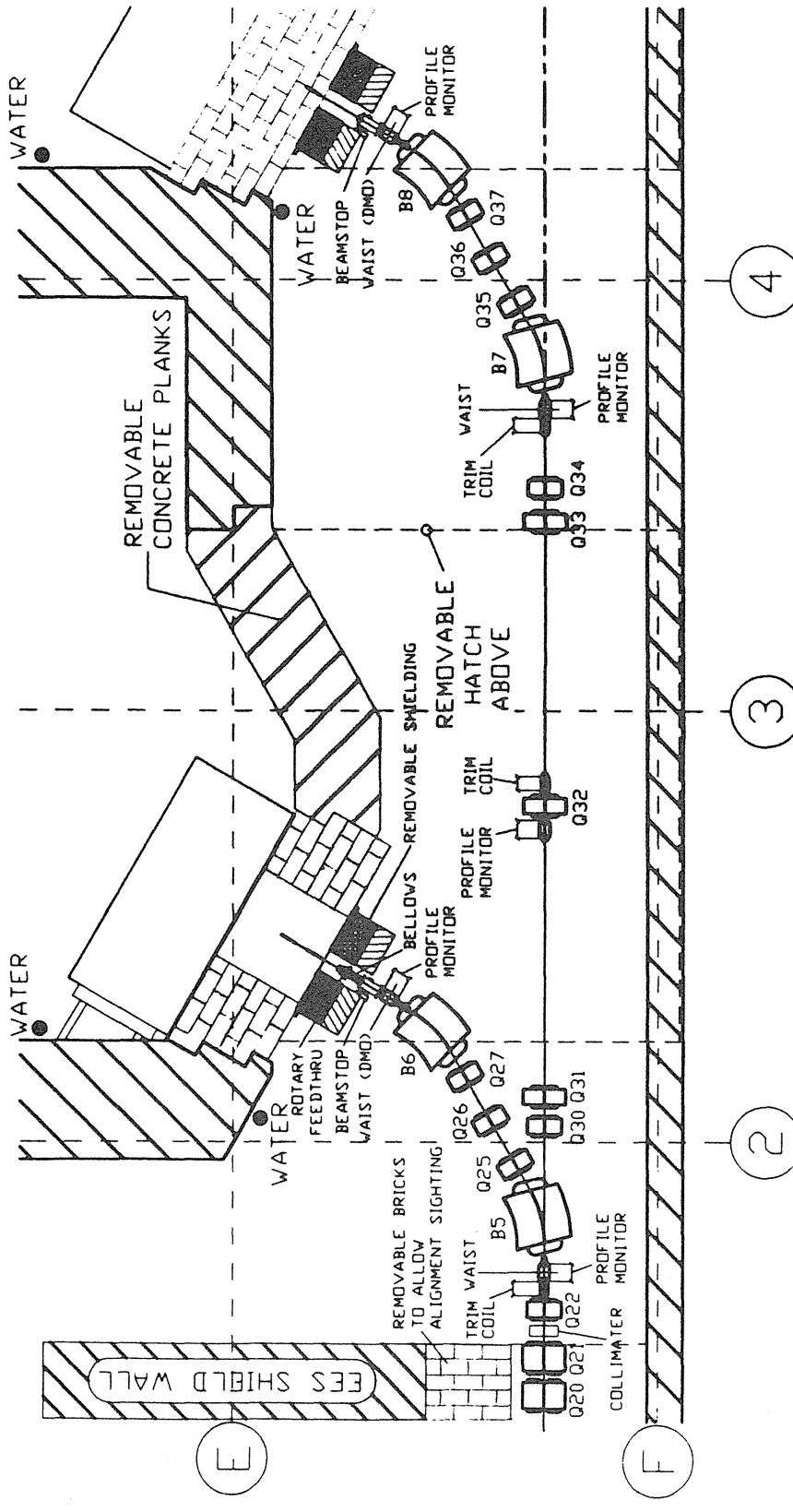

Figure 4. The Beam Transport System equipment.

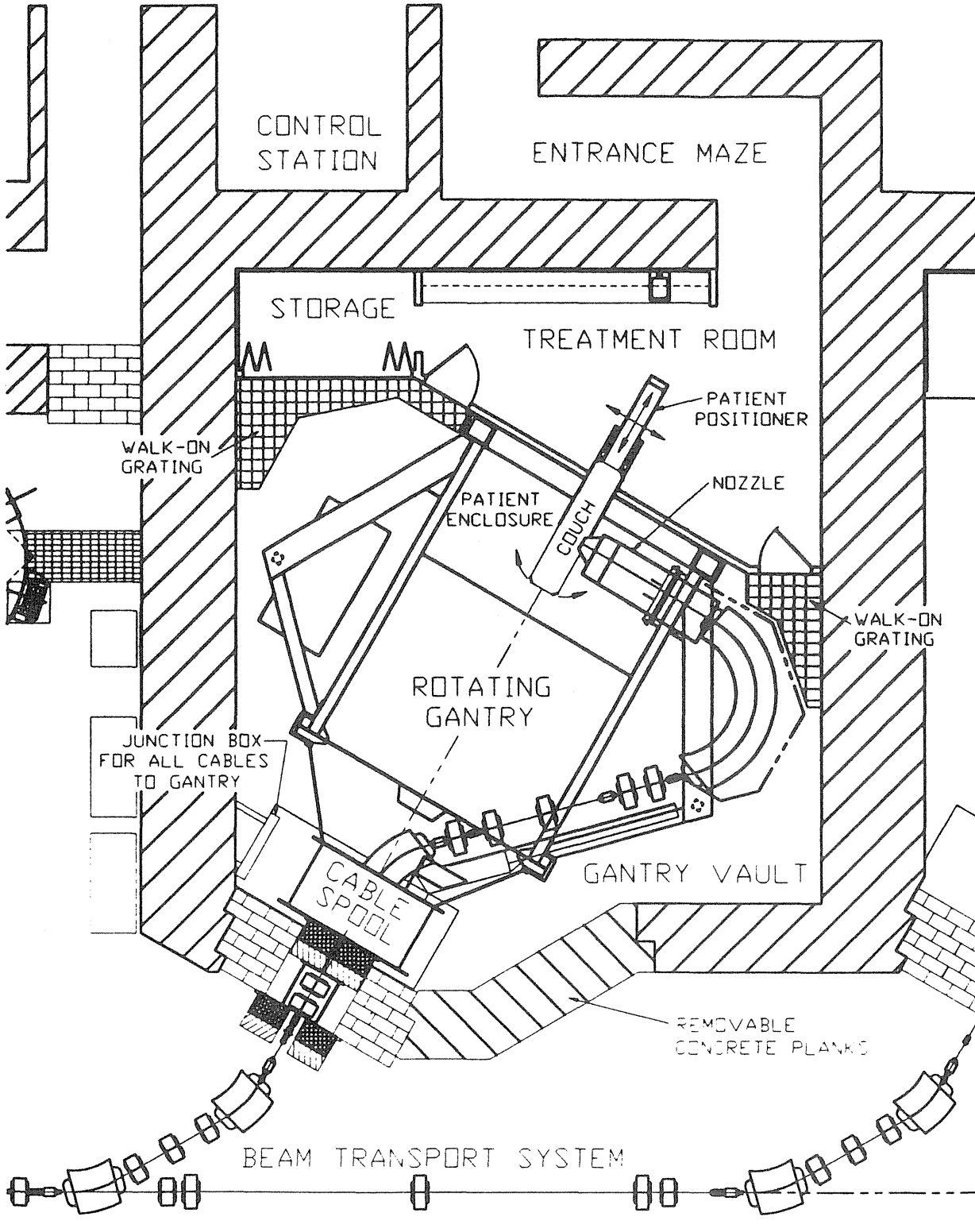

Figure 5. View of the Gantry room equipment.

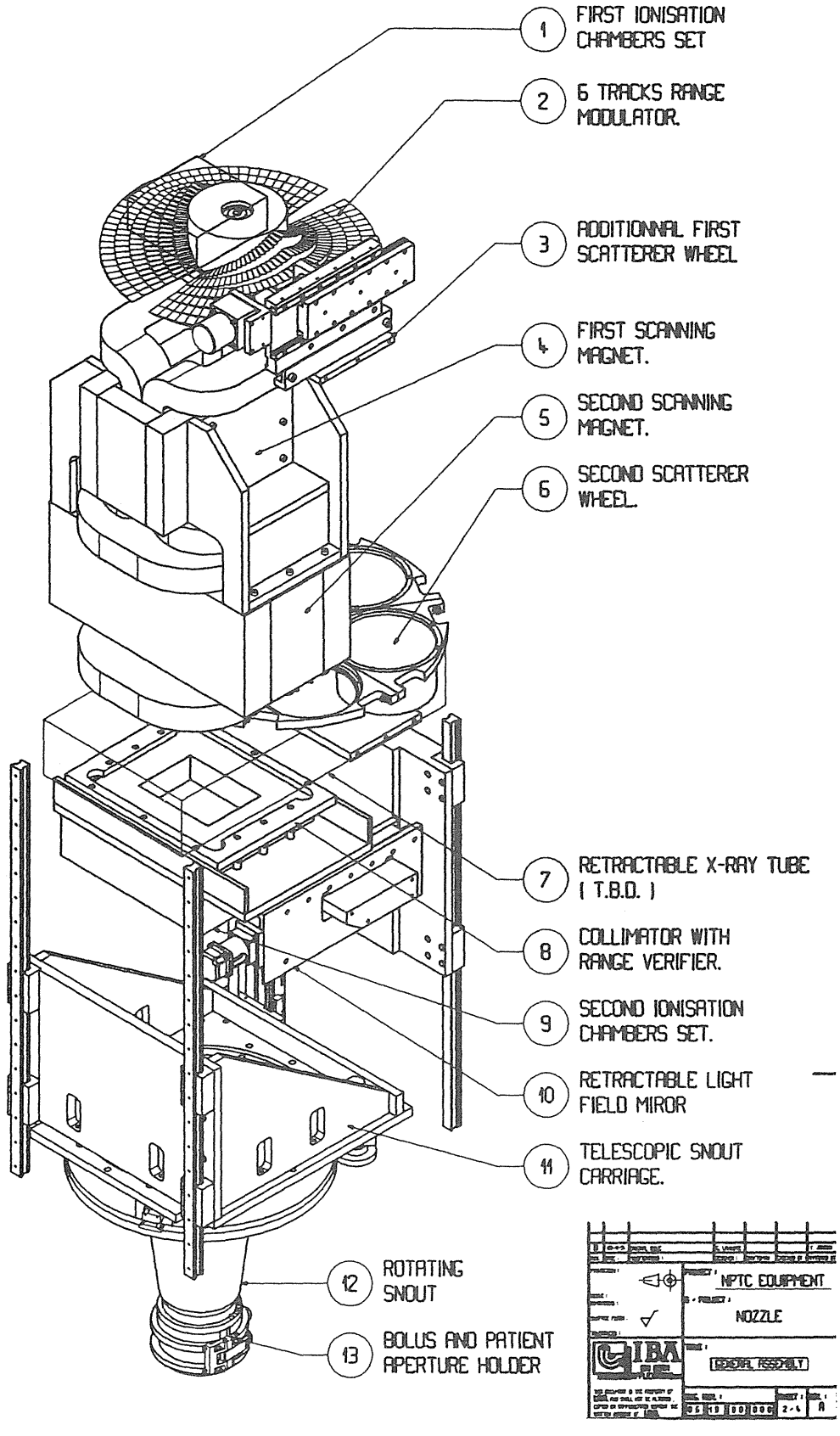

Figure 6. The Nozzle.

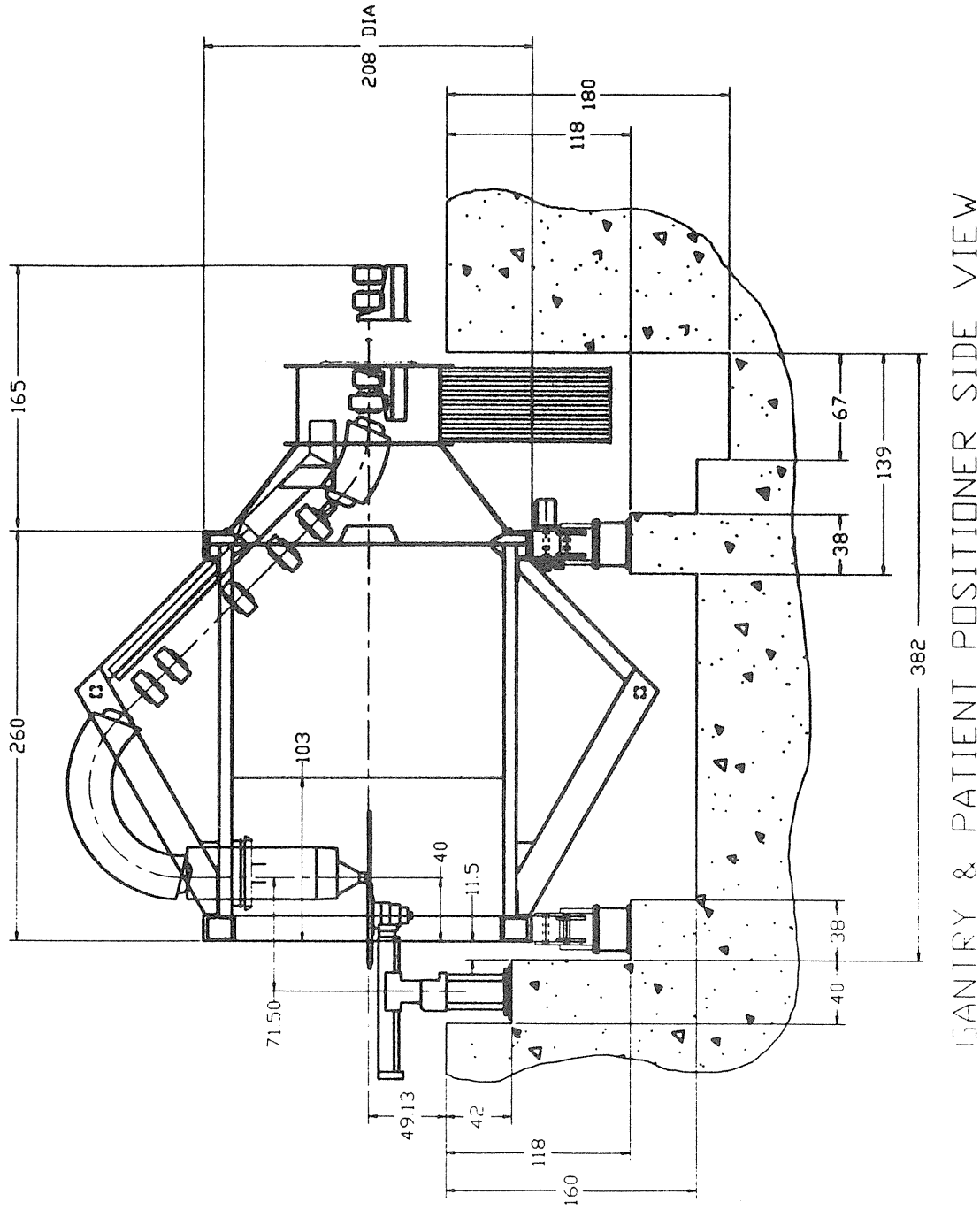

Figure 7. Side view of the Gantry and Patient Positioner.

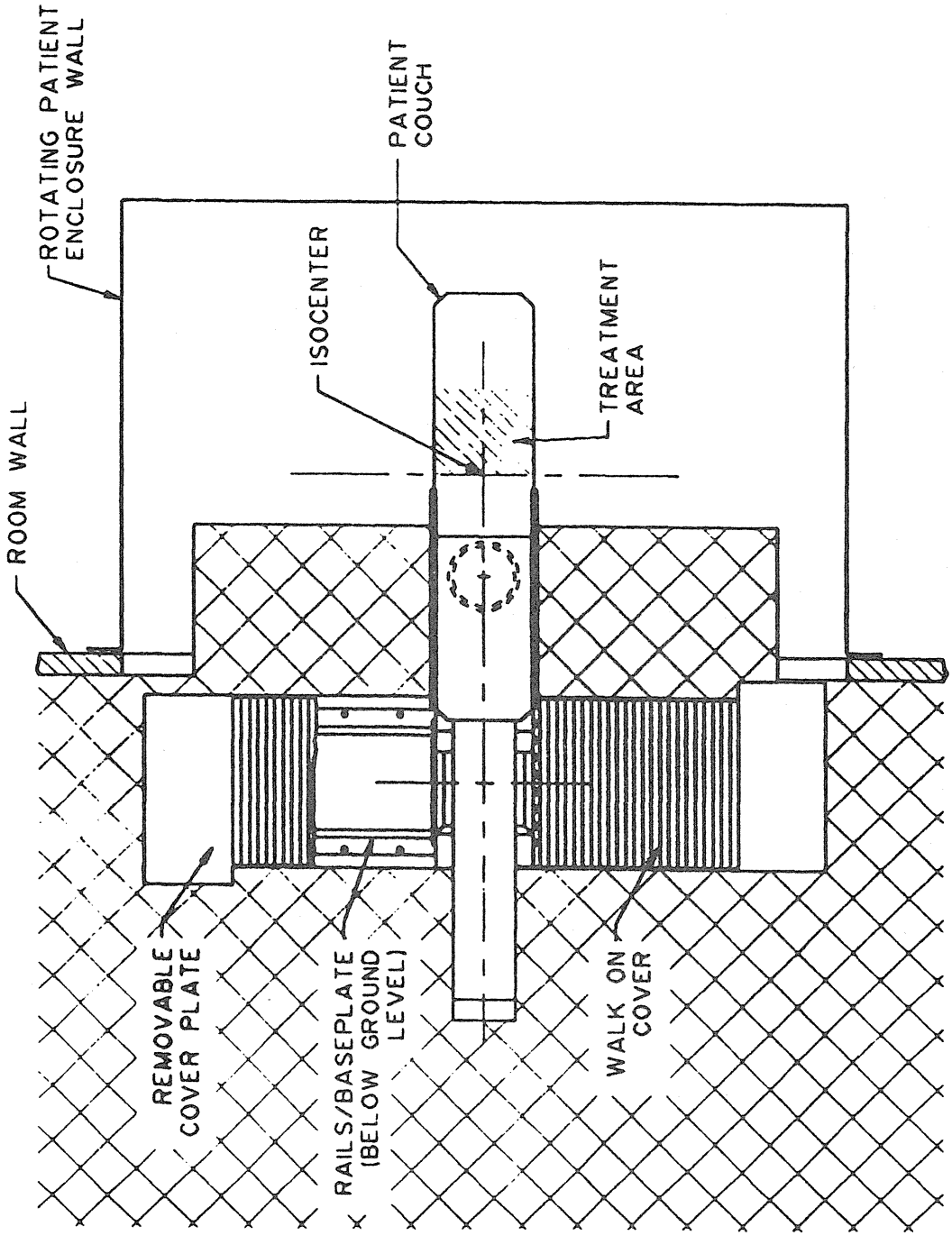

Figure 8. Plan view of the Patient Positioner.

Heavy Ion Therapy at GSI

G. Kraft for the heavy ion therapy collaboration of GSI Darmstadt,
Radiological Clinic Heidelberg,
DKFZ Heidelberg, FZ Rossendorf
Germany

Abstract

As the result of a joint proposal of the GSI Darmstadt, together with the Radiological Clinic and the Cancer Research Center, both at Heidelberg, a unit for particle therapy is presently under construction at the heavy ion synchrotron SIS at Darmstadt. It is planed to treat approximately 70 patients a year with carbon ions starting in summer 1996. In contrast to the existing particle therapies, a tumor conform treatment will be realised using an intensity controlled rasterscan. Therefore, the beamline to the radiation unit has been equipped with a special diagnosis to guarantee the quality of the beam at the entrance of the rasterscanner. Fast and position-sensitive counters in front of the patient will monitor and control the intensity and position of the beam which is deflected by the rasterscanner. In addition an interactive PET system will be used to monitor the distribution of the stopping particles inside the patient.

A detailed knowledge of the physical and biological properties of the charged particle beam is indispensable for an application of the rasterscan system. Due to nuclear collisions the primary flux is decreasing with penetration depth and lower-Z fragments having different biological efficiency are built up. Therefore extensive studies both, theoretical and experimental have been performed aiming at the production of a biological isoeffect in an irregulary shaped 3 dimensional target volume. The resulting physical and biological models will be integrated into the existing treatment planning system at the cancer research center, Heidelberg. For the patient treatment the medical responibility including diagnosis, patient selection and treatment planning will be centered at the radiological clinic at Heidelberg.

Introduction

Presently optimal condition for a tumor therapy using heavy charged particles exist at the German heavy ion research center GSI: The heavy ion accelerator SIS (1) is able to accelerate heavy charges particles from deuterons to uranium to energies of more than 1 GeV/u. These energies and the corresponding particle ranges exceed the requests of radiotherapy that is mostly bound to the lighter ions like carbon or neon in an energy range of 500 MeV/u and below. For these lighter ions, intensities up to 10^9 particles can be obtained from the heavy ion synchrotron SIS that are also greater than requested by therapy.

Long time before the high energetic ions became available at GSI, an intense program on the understanding of the particle action in biological material was started, using the low energy beam of the Unilac that accelerates all ions up to energies of 20 MeV/u (2). At the Unilac the response of different cells and subcellular structures like DNA and chromosomes has been studied in numerous experiments in which more than one hundred thousand biological samples have been exposed and analysed. These experiments yielded a quantitative understanding of the action of particles having an elevated linear energy transfer (LET). In addition, physics experiments exploring the structure of the individual particle tracks as well as the behaviour of macroscopic particle beams penetrating through matter were performed. The microscopic description of the particle tracks together with an advanced biological knowledge was the basis of an unified model, a synthesis of track structure and microdosimetry approaches, describing the biological response to particles with

great accurancy (3). Fragmentation and scattering experiments yielded a quantitative physical characterization of particle beams (4). Based on such a long preparation lasting over more than 10 years it was possible to propose a heavy ion therapy (5) using a completely different method for patient treatment compared to all the existing particle therapies: In the heavy ion therapy at GSI (HITAG) a pencil beam is used to fill an irregular target volume by irradiating each volume element by an appropriate number of particles that has been calculated to obtain the desired biological effect. This method of target conform treatment of any irregularily shaped tumor in expected to exploit the properties ions heavier than protons to a maximal extend, but the clinical experience has to justify the applied effort (Fig.1).

The intensity controlled rasterscan

For the tumor conform dose delivery a magnetic scanning system is used for the lateral beam deflection and an for the range variation an active energy variation by the accelerator has been studied in preclinical experiments in the biology cave at SIS.

To start with the second point: in various experiments it has been shown that an energy variation from pulse to pulse, i.e. within two seconds, is possible at the synchrotron SIS including the tuning of the beamline to the experimental cave (6). Fig. 2 shows a scanning system pattern taken with four different energies delivered within a time sequence of three seconds from energy to energy.
The first point, the lateral beam deflection represents more difficult problem for tumor conform treatment: because any treatment of the distal layers pre-irradiates the proximal layers partially the proximal layers have to be covered inhomogenously in order to achieve a homogenous dose or inactivation effect in the target volume. In addition, beam fluctuations from the accelerators have to be compensated to achieve the desired particle number in each pixel.

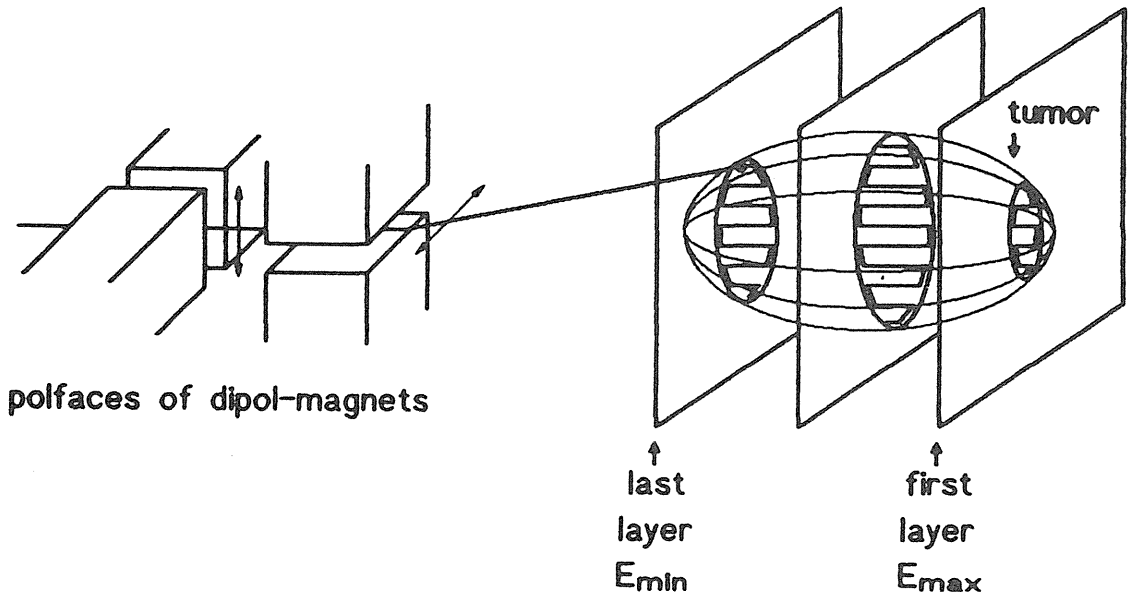

Figure 1: Schematic view of the magnetic scanning system. The tumor volume is dissected in layers of equal particle range and each layer is treated separatly by "painting" the necessary dose with a pencil beam.

Two different strategies, raster- and pixelscan, have been proposed to cope with these problems and extensive calculation have shown (6) that with both approaches, the same quality of particle covering of any irregular shaped volume can be obtained. Moreover, in the practical realisation both methods become very similar: For pixelscanning an optimal pathway is obviously the connection between neighboring pixels, i.e. a more or less continuous pathway. For raster scanning the given pathway has to be digitized into coordinates, i.e. pixels that can be stored in a computer. The only remaining difference between the two solutions is whether the beam has to be turned off while moving from pixel to pixel.

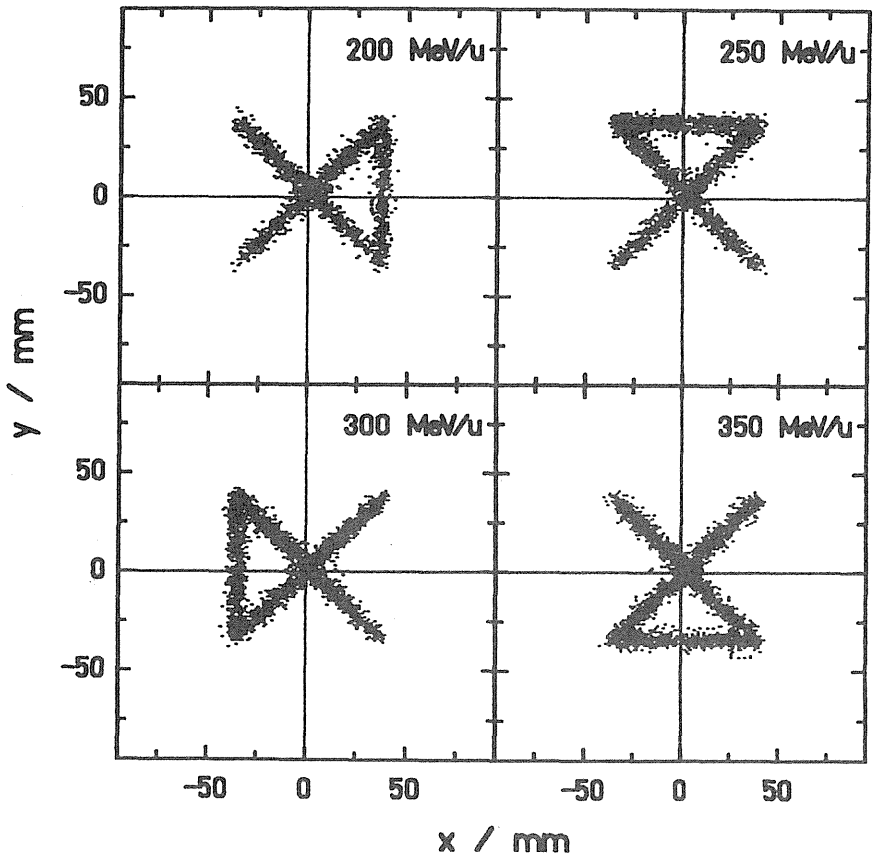

Figure 2: By combining beam scanning and energy variations simple figures are produced to test the performance of the scanning system and the qualtiy of the beam. The energy was changed in the accelerator from pulse to pulse within 3 seconds and the beam line was tuned in the same rhythm.

When the distance between consecutive pixels is much smaller than the diameter of the beam, the dose delivered during moving from pixel to pixel is small and the beam has not to be interrupted. Slight over or under exposures of one pixel can be compensated during exposure of the next pixel.

A digitized version of an intensity controlled rasterscan, has been realized at the biophysics cave at GSI (details are given in (6)). In this set up the beam is guided by two magnets in x- and y-position and the beam intensity is measured by means of a transmission counter.

The beam path of one range-slice is dissected into a maximum of 16.000 pixels and the writing velocity (maximum 1 cm/msec.) of the beam is controlled by an ionization

chamber as transmission counter. The use of a transmission counter to control the writing velocity has been demonstrated to be also a very elegant and efficient method to cope with the intensity fluctuations of the beam as extracted from the accelerator. First experiments demonstrated that particle coverings with a homogenity of 5 % or better can be produced although the incoming beam has large intensity fluctuations (fig. 3). But in the same way any inhomogenous distribution can be produced with the same accuracy if required. This is important when a 3-dimensional volume has to be exposed to an given isodose or isoeffect where in the midsection low intensities are required but higher intensities at the borderline.

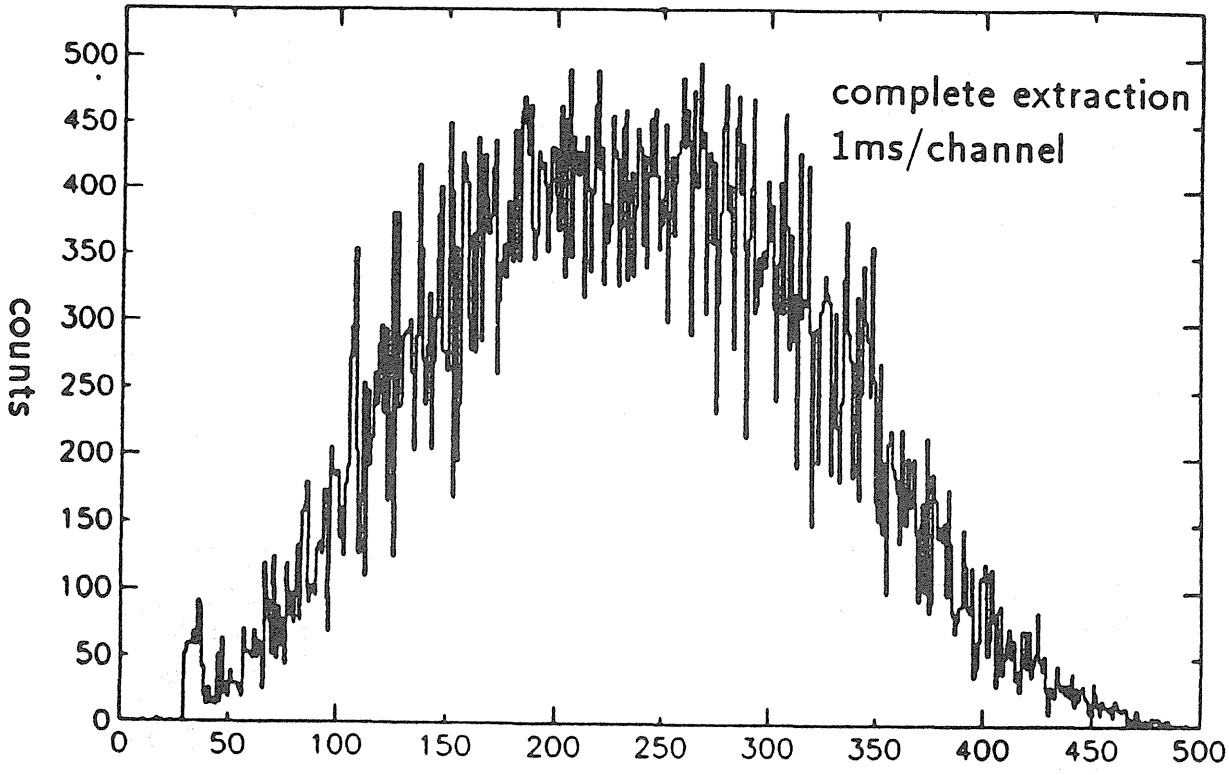

Figure 3:
Time profile of the extracted beam of the SIS. The beam intensity is given as a function of the extraction time. The feed back system of the rasterscan is able to adjust the writing velocity to these fluctuations.

The application of inhomogenous exposures has been used in a 3-dimensional simulation of a spherical isodose. In this experiment, in a water tank as tissue equivalent material a spherical volume of 6 cm in diameter in a depth between 9 and 15 cm was exposed to an isodose of carbon ions (7). CR 39 nuclear track detectors immersed in the water were used to record the dose. 30 particle energies were necessary to produce the variation in depth and for each particle range up to several hundred pixels were irradiated. The particle covering in the equatorial plane and a photograph of the total exposed volume are shown in figure 4a and b. The results of this experiments fully confirm the expectation that tumor conform treatment can be performed by an intensity controlled raster scan system. In the mean time this technique has been extended to the treatment of more irregulary shaped target volumes.

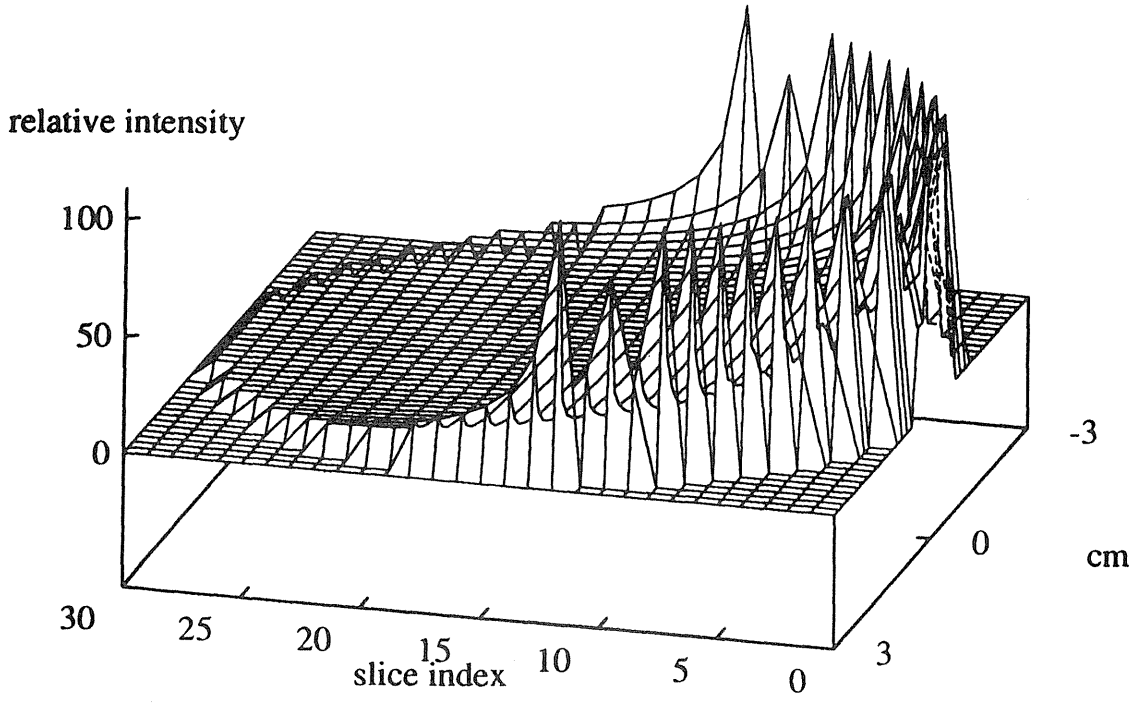

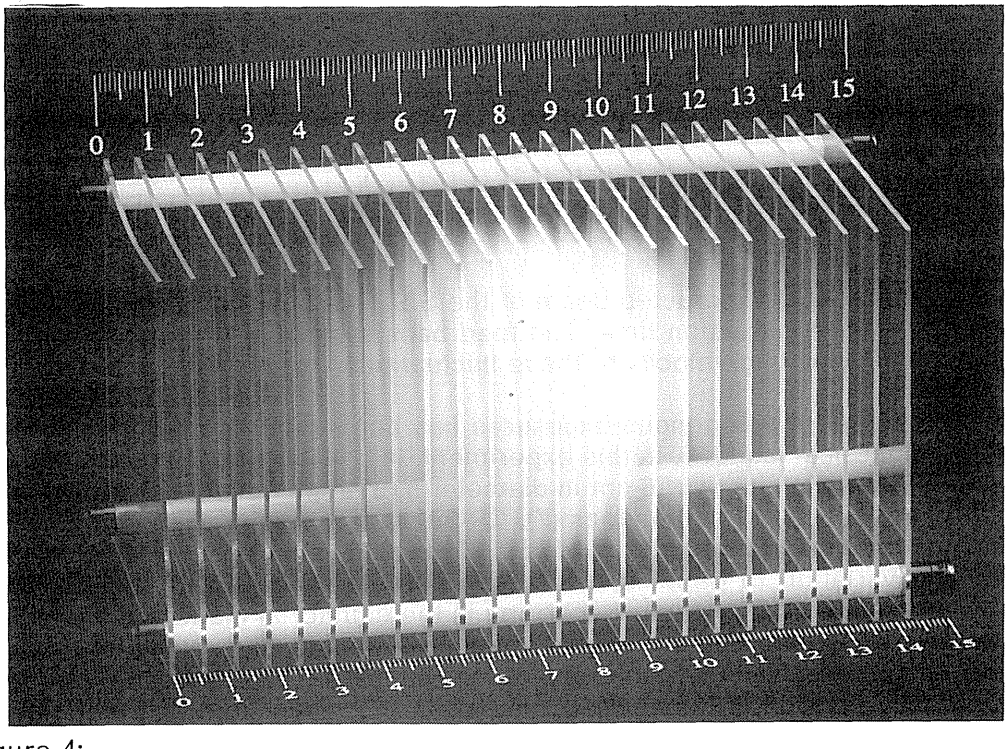

Figure 4:
A volume of 6 cm in diameter in a depth of 15 cm of water was exposed to a spherical isodose.
a.) the particle covering in the equatorial plane of the volume
b.) photographs of a recording of the dose by nuclear track detectors. A small dose is visible in the entrance channel at the left side.

On-line control of the beam by PET techniques

A precise beam delivery needs precise control. Heavy ions can be monitored using the production of radioactive isotopes that decay by positron emission. It has been demonstrated in phantom measurements that β^+ radioactivity produced by a stabil beam is sufficient to monitor the stopping points of the projectile ions (6). Beams of stabil ions undergo nuclear reactions like projectile and target fragmentation. Most likely are stripping reactions leading to lighter ions a fraction of which are β^+ isotopes. In the case of target fragmentation, these β^+ emitters are smeared out over the particle path. For the projectile fragmentation the β^+ isotopes have nearly the same range due to their similar mass to charge ratio and a strongly forward peaked reaction kinematics. The β^+ annihilation can be localized by the coincident detection of the two 511 keV gamma quanta in two adjacent gamma-cameras. Because the positrons are emitted isotropically with respect to the beam direction, the center of the observed distribution of positron emission corresponds to the stopping point of the radioactive isotope.

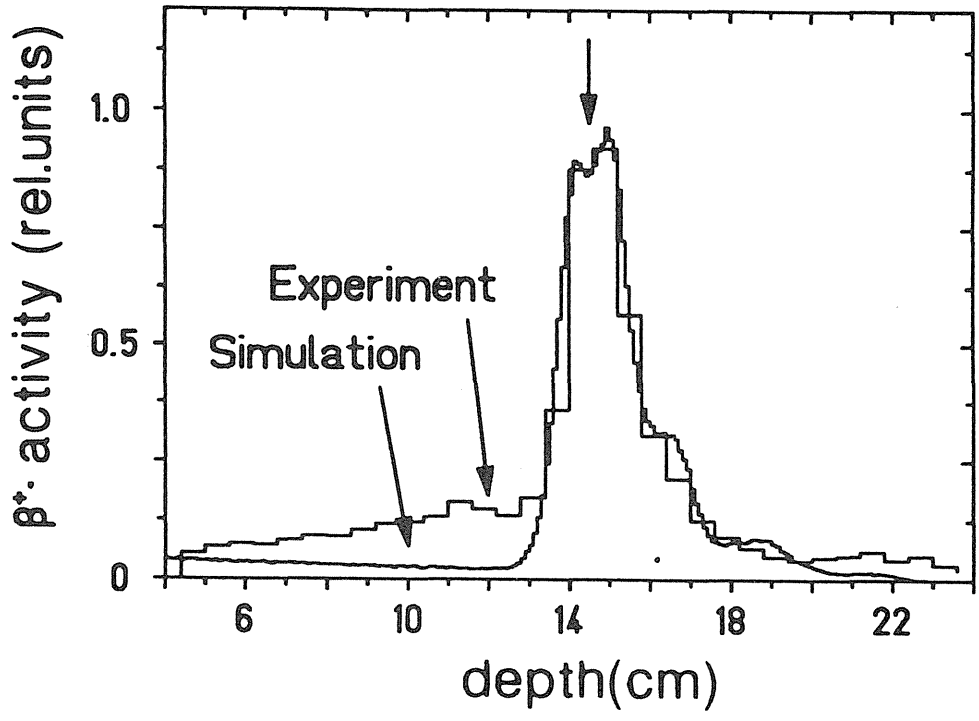

Figure 5:
Measured and calculated profiles of β^+ emitting isotopes that are compared with the range of the primary stabil ^{20} Ne beam as indicated by an arrow.

In figure 5 the induced β^+ activity by a ^{19}Ne beam implanted into a plastic block is compared with the calculated range distribution and with the range of the primary ^{20}Ne beam. From the β^+ distribution the range of the stabil Ne-ions can be calculated with high accuracy and compared to the treatment planning.

Physical and biological beam characterisation

A detailed knowledge of the physical and biological interaction of the beam with the target material is extremly important when using the beam scanning methods to achieve a tumor conform target volume: In an arbitaryly shaped target volume the

composition of the particle field differs from one position to the next. This is due, first to the fact that beams of different energies have to be superimposed in order to achieve the desired depth distribution (fig. 6). Therefore particles of different energies contribute to the biological effect in each point. Secondly the nuclear fragmentation of the primary beam changes the composition in atomic number to a large extend. For a penetration depth of 15 cm in tissue, approximately 50 % of the primary carbon ions went through nuclear reactions, in which lighter fragments are produced (9). Therefore, in each target point the particle field consists of various contributions of particles having atomic numbers from the primary ions down to protons and having a complex energy distribution.

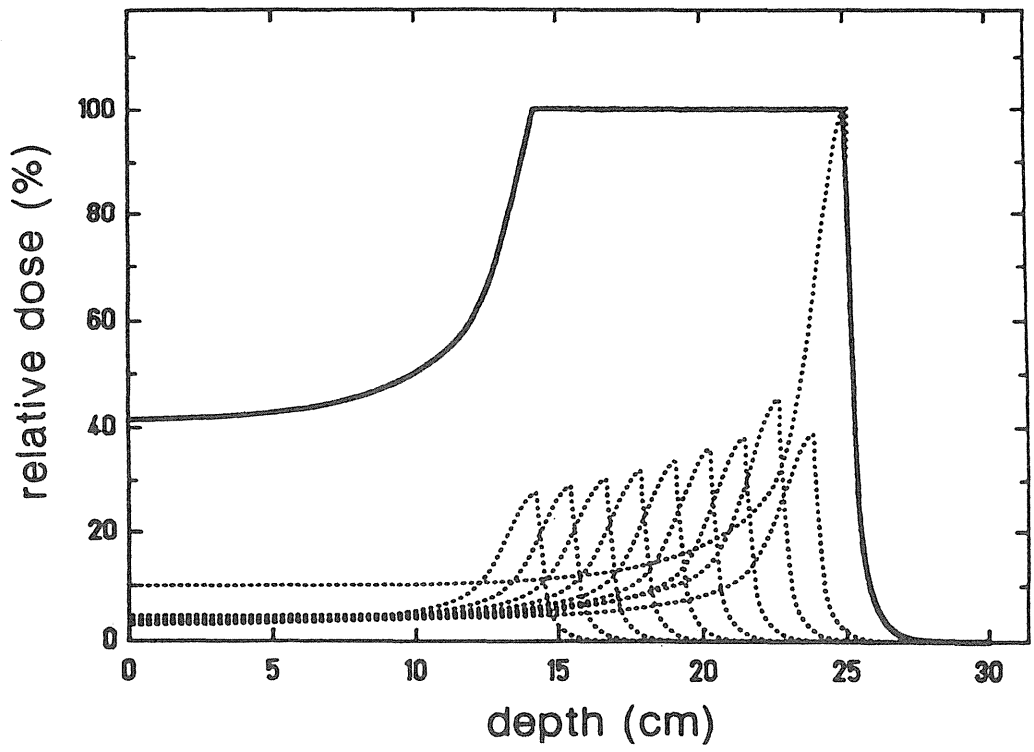

Figure 6:
Schematic superposition of individual Bragg peaks in order to produce a homogenous dose distribution over an extended target volume.

Extended measurements of beam fragmentation in thick water targets have been performed at the fragment seperator (FRS) at GSI (10). Because of the double separation mode of the FRS, it was possible to produce all isotopes of medical interest simultanously in a first target and to follow then their fragmentation in a tissue equivalent target using a complex analysis system for energy and atomic number (9). These measurements showed that fragmentation in the second and third generation, i.e. the fragmentation of the reaction products contributes significantly to the total amount of reaction products (fig.7).

Based on a proper parametrisation of the beam fragmentation and taking into account the energy loss and straggling of these ions, the dose D(x,y,z) deposited by such a particle distribution can be calculated. But the dose distribution cannot be used to calculate directly the biological effect, because the relative biological efficiency RBE(x,y,z) is also a strong function of the atomic number and energy of the particles (3). In order to determine a proper RBE in each target point the origine of the given dose in atomic number and energy has to be known.

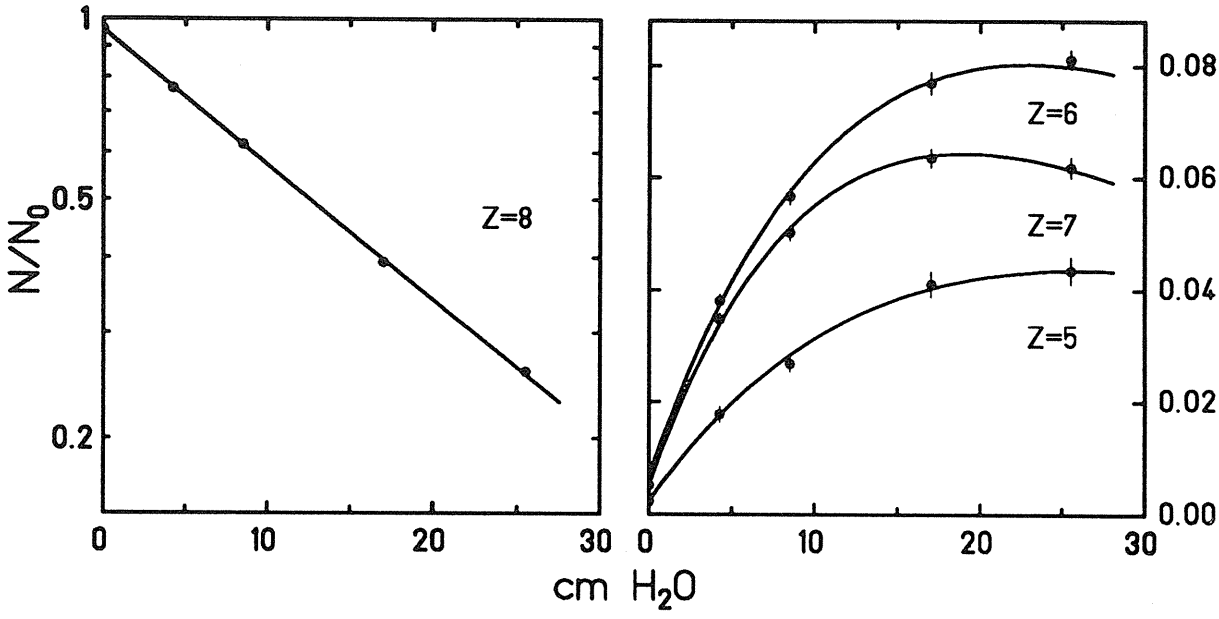

Figure 7:
Nuclear fragmentation of heavy ions. The decrease of the primary ions by the nuclear reaction as function of the penetration depth is shown at the left side and the build up of the heavier reaction products with increasing penetration depth in water at the right side.

In reality, the situation is even more complex because the RBE depends also on biological parameters like the dose level and dose fractionation scheme and most important, on the type of the tissue. A solution of this problem is only possible using an elaborate theoretical approach (3) as it is described in detail by Michael Scholz in this issue.

Technical realisation of the HITAG project

The heavy ion synchrotron SIS is capable to produce the medical relevant ions with intensities of some 10^9 particles per spill. This flux is sufficient to produce a dose of a few Gray per liter within five to ten spills i.e. in 10 to 20 seconds.

The energy from SIS can be changed from pulse to pulse. Because of the high flexibility of the SIS it is planned to perform patient treatment in time-sharing with the physics experiments in four periods of a few weeks per year and to operate the SIS with two different ion sources, one running with carbon for patient treatment, the other with any other ion for physical experiments. Using the rasterscan method, the treatment of one a fraction should be accomplished within five minutes or less, while the patient positioning lasts much longer (20-40 minutes). Therefore, the deadtime for the physics experiments will be in order of 5 to 10 minutes per hour.

In order to minimize possible conflicts between the physical experiments and medical treatment, a medical cave has been constructed that will be connected to an annex (fig.8) housing a control room for the beam delivery and other rooms necessary for physicians and patients like waiting rooms, examination rooms and offices. However, the main examination and diagnosis of the patient will be performed at the radiological clinic Heidelberg before treatment.

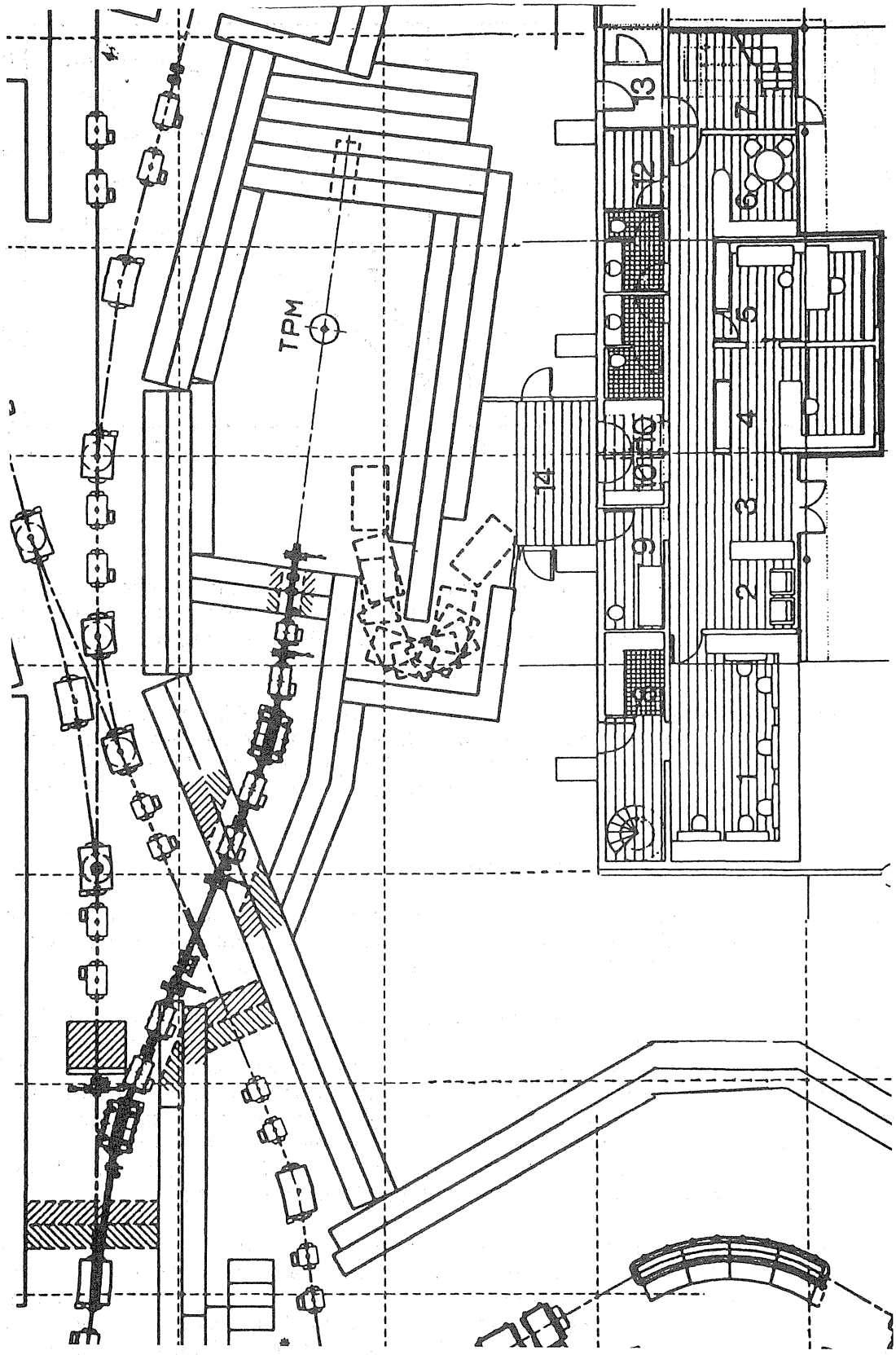

Figure 8:
Medical cave at the SIS with beam line and an annex for the control room and medical rooms.

Safety system

Because of the use of a pencil beam having a high local efficiency for cell killing, special precautions have to be taken to guarantee that the beam has always the desired specifications and is located in the target volume at the correct position. Therefore, a set of detectors and controls will be installed to trace the beam. In order to have no uncontrolled movement of the beam at the entrance of the scanner magnets during extraction, the beam line between accelerator and scanning magnets is set to a non-dispersive (achromatic) transport of the beam. This is especially necessary for the last part of the transport system where the beam is bent into the medical cave from the main beam line by two symetric dipol magnets and pairs of quadrupols, symmetric to the dipol magnets. Thus an intermediate focus is produced between the dipols that is a correct image of the final focus in the patient. Location and diameter of the beam can be monitored in a non- destructive way using scintillator paddels as beam scratchers at the intermediate focus.
In addition, a set of two independent position sensitve counters just in front of the patient monitor the beam during exposure. One of these detectors, a multiwire chamber measures the localisation of the center of the beam and its diameter within 100 μsec, these data are compared with the precalculated irradiation pattern within less than a half millisecond. It has been confirmed experimentally that the time needed to stop the extraction of the beam by a control signal from the rasterscan is less than a half millisecond. This means that the beam can be interrupted within 1 millisecond in the case of a failure. In the abortion time, less than a milli Gy is deposited per liter assuming an operation of 2 Gy per 10 second. This is much less than a physian takes care of conventional treatment. A sensitive ionization chamber is proposed for clinical dosimetry, measuring the absolute dose in each position of the patient entrance. The data of these transmission detectors together with the previously reported PET system guarantees a precise control of the deposited dose.
Another important saftey requirement is the asymetric layout of the rasterscan system: If the magnets of the scanning system are not powered, the beam will pass by the patient and will stop in a beam dump. Only if the scan magnets are powered correctly the beam is directed to the patient. In the unexpected case of a failure of the scanning system, the beam will automatically move out of the patient.

In addition to these special saftey features for using scaned pencil beams, the usual precaution for radiation safety will be obied, but the major point for the beam distribution system used in the HITAG-Project is the on-line local control of beam quality and location compared to the previously defined values. Because of the fast beam deflection this comparison has to be independent from the human intervention.

Time perspective

In the proposal for the HITAG project it was expected to start with patient treatment in 1996. At the time being (end of 1994) the concrete shielding of the medical cave is completed and the beam line components has been installed. It is expected to start with first test of the complete system in spring 1995. The PET system is presently in test at Rossendorf and the components for treatment planning are expected to be included into an existing treatment plan from the German Cancer Research Center. Experiments in which the in vitro results will be transferred to extended tissues are planned also for the year 1995 as well as animal experiments for normal tissue response. From mid of 1995 the interplay of all hardware components and the treatment programs will be tested in shame treatments of an andropomorph phantoms or in animal experiments. If sufficient beam time will be available for the preparative experiments of the therapy in 1995, there seem to be no general objections to start the proposed patient treatment in 1996.
Note: Parts of this manuscript have be presented and published in other conferences.

References

1. SIS eine Beschleunigeranlage für relativistische schwere Ionen, Darmstadt, GSI July 1979

2. G. Kraft, Radiobiological effects of very heavy ions, Nucl. Science Appl. 3 1-28, 1987

3. M. Scholz, G. Kraft, A parameter-free track-structure model for heavy ion action cross sections, In: Biophysical Modelling of Radiation Effects, K.H. Chardwick, G. Moschini, M.N. Varma (eds.), Bristol, Philadeplphia, New York 1992

4. I. Schall, Untersuchung der Kernfragmentierung leichter Ionen, PhD Thesis 1994 TH Damrstadt

5. G. Kraft, G. Gademann, Einrichtung einer experimentellen Strahlentherapie bei der GSI Darmstadt, GSI Report 93-23 1993

6. Th. Haberer, W. Becher, D. Schardt, G. Kraft, Magnetic scanning system for heavy ion therapy, Nucl. Instr. Meth., A330 291, 1991

7. U. Weber, GSI Nachrichten, 1993 11 6

8. W. Enghardt, W.D. Fromm, H. Geissel, H. Keller, G. Kraft, A. Magel, P. Manfraß, G. Müzenberg, F. Nickel, J. Pawelke, D. Schardt, C. Scheidenberger, M. Sobiella, The spatial distribution of positron-emitting nuclei generated by relativistic light ions, Phys. Med. Biol., 37 2127, 1992

9. I. Schall, D. Schardt, G. Kraft, A. Magel, M.F. Mohar, G. Münzenberg, F. Nickel, C. Scheidenberger, W. Schwab, E. Kankeleit, A. Fukumura, Nuclear fragmentation of light ion beams in water, GSI, 93-1, 337

10. H. Geissel et al, The Fragment Separator at SIS, Nucl. Inst. Meth B70, 286-301, 1992

11. G. Kraft, Radiobiological and physical basis for radiotherapy with protons and heavier ions, Strahlenther. Onkol., 166 10, 1990

WORLD EXPERIENCE IN PROTON/ION THERAPY IN 1994

JANET M. SISTERSON,
Cyclotron Laboratory, Harvard University, Cambridge Massachusetts.

There are sixteen operating proton therapy centers world-wide in 1994. By July 1994, proton beams had been used to treat ~14,000 patients world-wide for both benign and malignant disease. Six centers are located in Europe, four in the United States, three in Russia, two in Japan and one in South Africa. Accelerators originally designed for other purposes and adapted for radiation therapy are the usual source of proton beams, only one center has an accelerator designed and built for the hospital environment. At six centers where the accelerator has a maximum energy of <100 MeV, only a limited number of sites can be treated. The only clinical program using helium and heavier ions ended in 1992 after ~ 2500 patients had been treated when the Bevalac at the Lawrence Berkeley Laboratory in California was shut down. HIMAC at Chiba, Japan, due to start patient treatments in 1994 will provide the next ion beam therapy experience.

Introduction

From 1954 to July 1994, ~14,000 patients world wide have been treated with proton beams for both benign and malignant disease. The estimated cumulative patient totals for all proton therapy facilities are shown in Figure 1. The increased interest in proton therapy over the past decade is evident and reflects the promising long-term follow up results that are now becoming available (1). World wide there has been only one clinical program using heavy ions at the Lawrence Berkeley Laboratory, University of California where helium ions have been used to treat ~ 2000 patients and heavier ions to treat ~500 patients (1).

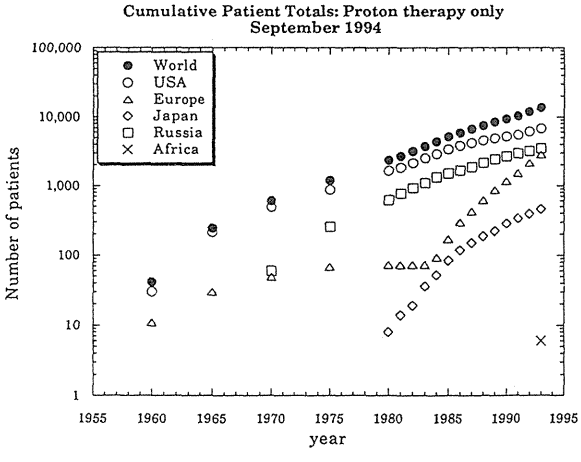

Figure 1. Estimated cumulative patient totals, compiled August 1994.

Proton Therapy Facilities

There are 16 operating proton therapy facilities in 1994 (2). Through 1993, an estimated 13558 patients world wide had been treated with proton beams. Figure 2 shows the percentage of patients treated at each institution since the start of proton therapy in 1954.

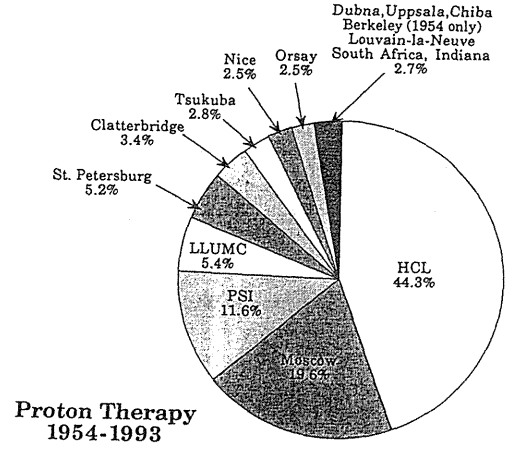

Figure 2. World wide proton therapy experience at all centers operating since 1954.

The increase in the number of operating centers in recent years can be seen in Figure 3. It is projected that there might be nearly 30 operating centers by the year 2000. Most operating facilities are located at research centers and use accelerators designed for nuclear research or neutron therapy. LLUMC has the first facility designed specifically for proton radiation therapy and located in a hospital. Several of the proposed new proton therapy facilities will be in a hospital setting while others will be at research institutions with dedicated proton therapy beam lines (2). Three of these new facilities are expected to start patient treatments in 1995; these are at TRIUMF, University of British Columbia, Canada; a new beamline at PSI, Switzerland and the Berlin Eye Treatment Facility. A fourth facility at MGH, Boston USA, is funded and construction is scheduled to start in 1995 with the first patient treatment expected in 1998.

Several of the proposed facilities hope to be able to have light/heavy ion beams as well as proton beams. Other facilities will have only light/heavy

ions. HIMAC at Chiba, Japan which will only have heavy ions is scheduled to begin patient treatments in 1994. The other heavy ion facility at GSI, Darmstadt, Germany plans for the first patient treatment in 1996.

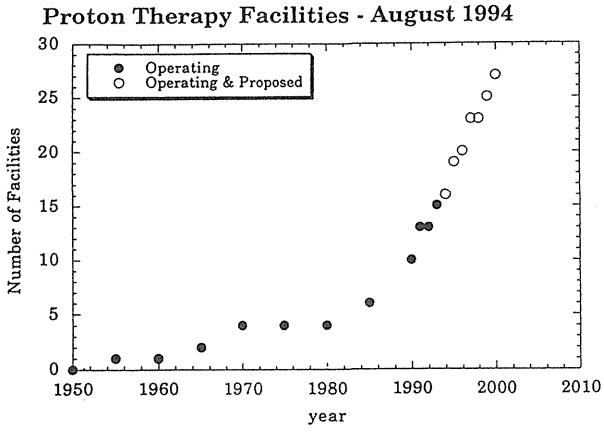

Figure 3. The cumulative number of facilities operating per year. Estimates for the projected figures are extracted from information in Particles 14 (2).

Annual patient statistics for 1993

Patient statistics are available for the 15 proton therapy facilities that were operating in 1993. An estimated total of ~1637 patients were treated world wide in 1993; 37.1% of these treatments took place in the USA, 42.5% in Europe. 16.1% in Russia, 3.9% in Japan and 0.4% in South Africa.

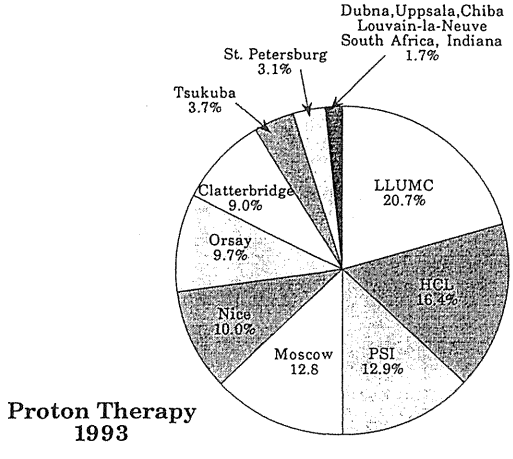

Figure 4. World wide proton therapy experience at all centers operating in 1993.

Figure 4 shows the percentage of patients in 1993 treated at each operating institution. Over 90% of the patients were treated at 7 centers. It should be noted that several centers are at research facilities where beam time is available on a limited basis. This is reflected both in the annual patient load and also the type of diseases that can be treated. During 1993, 10 patients or less were treated at 6 centers, 50-60 patients were treated at 2 centers, ~150-170 patients were treated at 3 centers and 200-350 patients treated at 4 centers.

There are three major categories of patient treatments:-

(1) Single fraction intracranial treatments
(2) Fractionated therapy for ocular melanoma.
(3) Fractionated therapy for many categories of both benign and malignant disease.

Figure 5 shows the cumulative world experience in these three major categories *excluding* the 2662 patients treated from 1969-1993 at Moscow (patients were treated in all three major categories) and the 21 patients (four had single fraction treatments, none were treated for uveal melanoma and 17 had fractionated therapy for several diagnoses) treated from 1991-1993 at Louvain-la-Neuve; detailed annual statistics were not available from these institutions at this time. The early series of patient treated at Berkeley (30 patients treated in 1954-1955 with protons), Uppsala and Dubna are also excluded.

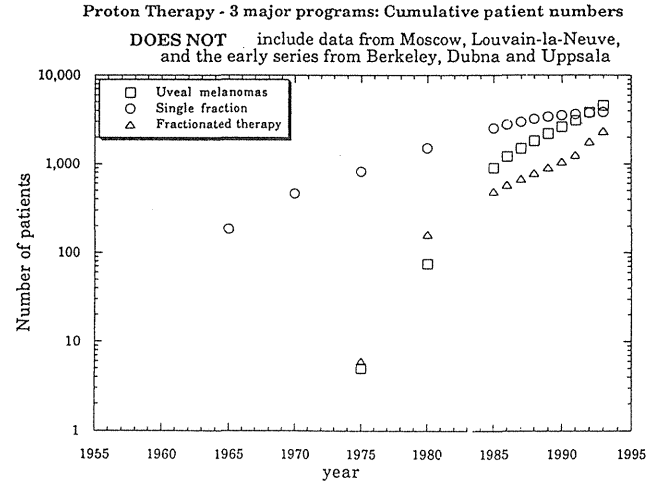

Figure 5. Cumulative patient numbers for the three major categories excluding data from Moscow and Louvain-la-Neuve and the early series from Berkeley, Uppsala and Dubna.

Figure 6 shows the cumulative total patient data for fractionated therapy and for selected sites within this category. As in Figure 5, the data from Moscow, Louvain-la-Neuve and the early series from Berkeley, Uppsala and Dubna are omitted.

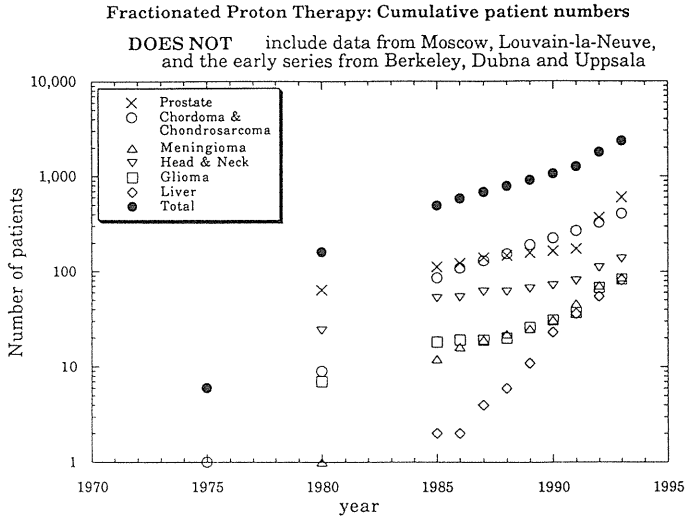

Figure 6. Cumulative patient data for fractionated proton therapy and the principal sites treated in this category excluding data from Moscow and Louvain-la-Neuve and the early series from Berkeley, Uppsala and Dubna.

Conclusions

Proton and ion beams can be used to advantage to shape the dose distribution very precisely to the target volume allowing as much sparing as possible of adjacent sensitive structures. The long term follow-up results that are now available are leading to the increased interest world wide in developing new proton and ion facilities, particularly in a hospital setting.

References

1) Munzenrider, J.E.; Crowell, C. Charged Particles. In: Radiation Oncology, Technology and Biology, eds., P. M. Mauch and J. S. Loeffler, (W. B. Saunders Company, Philadelphia,), p34-55; 1994.
2) Sisterson, J. M. ed. Particles 14, July 1994.

Poster

Heavy Ion Medical Accelerator Project by Hyogo Prefecture Government

A. Itano, S. Hidaka, Y. Hishikawa, K. Ishida, H. Karashima, M. Kato
Public Health and Environment Department, Hyogo Prefecture Government
10-1 Shimoyamatedori, 5-chome, Chuo-ku, Kobe-shi, Hyogo-ken 650, JAPAN

S. Hukumoto
National Laboratory for High Energy Physics
Oho 1-1, Tsukuba-shi, Ibaraki-ken 305, JAPAN

A. Mizobuchi
Institute for Nuclear Study, University of Tokyo
2-1 Midori-cho, 2-chome, Tanashi-shi, Tokyo 188, JAPAN

A. Noda
Institute for Chemical Research, Kyoto University
Gokanoshou, Uji-shi, Kyoto-fu 611, JAPAN

Y. Hirao, K. Kawachi, S. Yamada
National Institute of Radiological Sciences
9-1 Anagawa, 4-Chome, Inage-ku, Chiba-shi, Chiba-ken 263, JAPAN

Abstract **- A project to construct a heavy ion medical accelerator facility for cancer therapy in five years is expected to start from 1995 by Hyogo prefecture government. The site will be located near SPring-8 synchrotron radiation facility in Harima Science Garden City, about 75 km north-west of Kobe city, Japan. Beam particles include proton, helium and carbon. Beam energy ranges are 70 - 230 MeV/u for proton and helium, and 70 - 320 MeV/u for carbon. The beam intensities are required to satisfy the dose rate of 5 Gy/min for treatment volumes of 15 cmϕ field size and of fully extended spread out Bragg peak (SOBP) over the maximum beam range. The facility will have a horizontal line, a vertical line and an oblique (45°) line for helium and carbon beams, and two isocentric gantry lines for proton beam.**

Hyogo prefecture government had been engaged in a construction of Harima Science Garden City, which has about 2000 ha surface and is located about 75 km north-west of Kobe-city. The location is shown in Fig. 1. As the major facilities in the city, a synchrotron radiation facility SPring-8 and a charged particle therapy facility had been planned. The Spring-8 is now under construction by the Institute of Physical and Chemical Research (RIKEN) and the Japan Atomic Energy Research Institute (JAERI) of the Science and Technology Agency (STA). As a Heavy Ion Medical Accelerator in Chiba (HIMAC) of the National Institute of Radiological Sciences (NIRS) was commissioned this spring [1] and the clinical trials were successfully started [2], the Hyogo prefecture government has decided to start the construction of the charged particle therapy facility from next year. This is the first charged particle therapy facility in Japan that is constructed by a non-national but a prefedture government level. This year a basic design study of the facility starts under a financial support by the government.

Beam particles include proton, helium and carbon. Beam energy ranges are 70 - 230 MeV/u for proton and helium, and 70 - 320 MeV/u for carbon. The beam intensities are required to satisfy the dose rate of 5 Gy/min for treatment volumes of 15 cmϕ field size and of fully extended spread out Bragg peak (SOBP) over the maximum beam range. The facility will have a horizontal line, a vertical line and an oblique (45°) line for helium and carbon beams, and two isocentric gantry lines for proton beam. One of the gantry lines is for future extension. One beam line for physical and/or biological experiment is also anticipated. Table 1 summarizes the clinical requirement and physical specifications of the charged particle beams. From the results of the basic design some reconsideration of the requirements on beam intensities and field size may be done to bring about a simpler and more compact design of the facility. Some options for future extensions and upgrades will be studied. In next year a detailed design of the accelerator and the buildings will start. Clinical trials are expected to start in the year 2000. The project will be executed in close collaboration with NIRS. Medical imaging using the synchrotron radiation light from SPring8 is anticipated. Table 2 shows the time schedule of the construction.

References

[1] S. Yamada, "HIMAC Accelerator -- Performance and Feature.", These proceedings, 1994.
[2] H. Tsujii, "COMMENCING HEAVY-ION CLINICAL TRIAL AT HIMAC.", These proceedings, 1994.

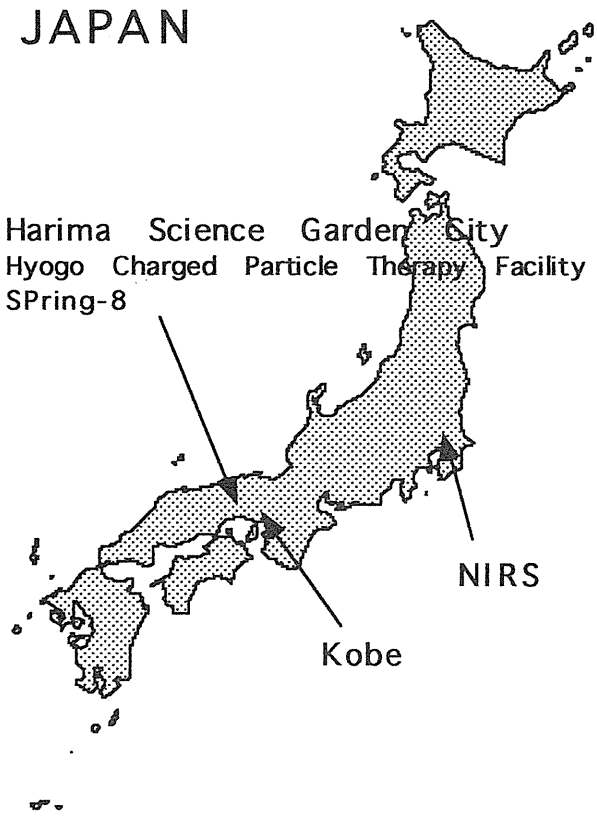

Fig. 1 Location of the Harima science garden city in Hyogo prefecture.

Table 1 Clinical Requirement and Physical Specifications of Charged Particle Beams

Particles	Proton, Helium and Carbon
Energy Range	70 - 230 MeV/u for p & He 70 - 320 MeV/u for C
Beam Intensity	7.2×10^{10} pps for p 1.8×10^{10} pps for He 1.2×10^{9} pps for C
Dose Rate	5 Gy/min for treatment volumes of 15cmϕ field size and of fully extended Spread Out Bragg Peak(SOBP)
Beam Range	40 - 300 mm for p and He 13 - 200 mm for C
Field homogeneity	± 2% (over treatment field)
Field size	30cmx15cm by magnetic wobbling 15cmx15cm by double scattering method 15cm x15cm for gantry
Displacement of beam axis	± 2mm (from isocentre)
Irradiation rooms	One horizontal line One Vertical line One oblique line(45°) Two gantries for proton
Spill length	400ms
Repetition rate	0.5Hz for He and C 1 Hz for proton

Table 2 Construction Time Schedule.

Budget year	Accelerator, beam delivery and instrumentation	Accelerator building and conventional plants	Hospital	Service utilitiy (hotel,dwelling)
1994	Basic design			
1995	Design and Construction	Design		
1996	Construction	Construction	Design	Design
1997			Construction	Construction
1998	Installation	Commissioning	Commissioning	
1999	Commssioning		Pre-test	Commissioning
2000	Routine Beam Operation		Clinical trial	

•*Poster Session 3:*

MEASUREMENTS OF HEAVY ION BEAM QUALITIES

N. MATSUFUJI, T. KANAI, H. TOMURA, T. KOHNO,
A. FUKUMURA, F. SOGA AND K. KAWACHI

Division of Accelerator Physics and Engineering, National Institute of Radiological Sciences, Anagawa, Chiba 263 JAPAN

The basic beam qualities of carbon 135 MeV/nucleon, 290 MeV/nucleon and neon 135 MeV/nucleon were measured at NIRS Heavy Ion Medical Accelerator and RIKEN Ring Cyclotron Facility. Measurements were carried based on ΔE-E counter telescope method with using a beam monitor scintillator, a coincidence scintillator, a proportional counter, a silicon semiconductor detector and a BGO scintillator.
As results, fragment particles were identified by ΔE-E or ΔE-ΔE 2-dimensional plots. Fluence spectra of fragment particles were derived and compared with the result of calculation. Macroscopic reaction cross sections between target and incident beam were deduced from these fluence spectra.

Fragmentation, HZE particle, Fluence, Counter-Telescope

INTRODUCTION

When shifting the range of heavy ion therapy beam at HIMAC, bombardments between incident beam and range-shifter, made of lucite plates, cause spallation reactions. As a result, incident nuclei are broken into some fragmented particles. It is important to know about the qualities of the beam such as the composition of the beam and/or the contribution of each fragmented nuclide to the total spectra of LETs to make our treatment-planning more precise. For this purpose, beam qualities were measured for tcarbon 290 MeV/nucleon, 135 MeV/nucleon and neon 135 MeV/nucleon beams.

METHODS

Figure 1 shows a schematic diagram of a detector system. The system was based on the ΔE-E counter-telescope method. A beam monitor made of a thin plate of plastic scintillator was located at the most upstream position to count the number of incident particles. A coincidence detector was composed of a plastic scintillator of 5.0 mm in diameter and positioned at the downstream of the lucite range shifter to distinguish the event of fragmented particles from that of noises. A proportional counter with tissue-equivalent gas was equipped to estimate the energy transferred to cells. A Si semiconductor detector was used as a ΔE counter to measure the energy loss ΔE in the detector. At the end of the beam line, a BGO scintillator was utilized as an E counter to measure total energy E. To stop incident beam within E counter, two different sizes of BGO detector were used. One had a cylindrical BGO crystal of 15.0 mm in diameter and 15.0 mm in length, and was employed for the measurements of the beams of 135 MeV/nucleon carbon or neon. The other was composed of larger BGO crystal of rectangular form in the size of 40.0 mm in width and height and 300.0 mm in length, and was utilized for the measurement of the more energetic beam, 290 MeV/nucleon carbon.
Fragmented particles were measured with this system by changing the thickness of lucite plate variously.

Signals from a Si-ΔE detector, a LET counter and a BGO-E detector were fed to NIM standard ADC modules when coincidence-logic was accepted. Data were then collected by a personal computer and recorded to magneto-optical disk in list-mode.

Measurements were carried out in biological experimental room and treatment room B of HIMAC, and in E5 experimental room of RIKEN ring cyclotron accelerator facility. In both facilities, uniform irradiation field (±5%) of about 15 cm in diameter was achieved by scatterers and wobbler magnets.

RESULTS AND DISCUSSION

Figure 2 illustrates an example of E-ΔE scatter plots for the incidence of carbon beam. The thickness of the target was 28.97 mm in water-equivalence. The abscissa represents the total

energy E measured by BGO detector and the ordinate denotes the energy loss ΔE from Si semiconductor detector. Each belt in the figure represents the kind of fragmented particle. The most upper band corresponds to the group of carbon and consequently the lowest one is the group of helium. A band of hydrogen is not clear because of the insufficiency of the length of the E counter to stop energetic hydrogen fragments. From this figure, fragmented particles are well discriminated by the kind of nuclide.

Fluence spectra of each nuclide were derived by normalizing the number of particles included in each belt of E-ΔE scatter plots with the number of incident particles. The fluences of each nuclide were displayed in fig.3(290 MeV/nucleon carbon beam), fig.4(135 MeV/nucleon carbon beam) and fig.5(135 MeV/nucleon neon beam). The values calculated by Sihver(1) are also plotted for the sake of comparison.

Macroscopic reaction cross sections between incident beam and target Σ were deduced by the fluence spectrum of incident nuclide. The Σ is expressed as an exponent of following equation:

$$\frac{N}{N_0} = \exp(-\Sigma x) \ ,$$

where x is the thickness of the target, N_0 is the number of incident particles and N is the number of survived incident particles. Results are summarized in table 1.

Table 1. Macroscopic reaction cross sections with a lucite target (m^{-1}).

Beam	Experiment	Calculation
C 290MeV/nucleon	5.29	5.49
C 135MeV/nucleon	6.71	5.14
Ne 135MeV/nucleon	8.52	7.06

CONCLUSION

These results indicate that incident heavy ion particles are more disintegrative comparing with calculational expectations. Precise analyses for the reason of this tendency and other beam qualities such as LET spectra for each nuclide are now in progress.

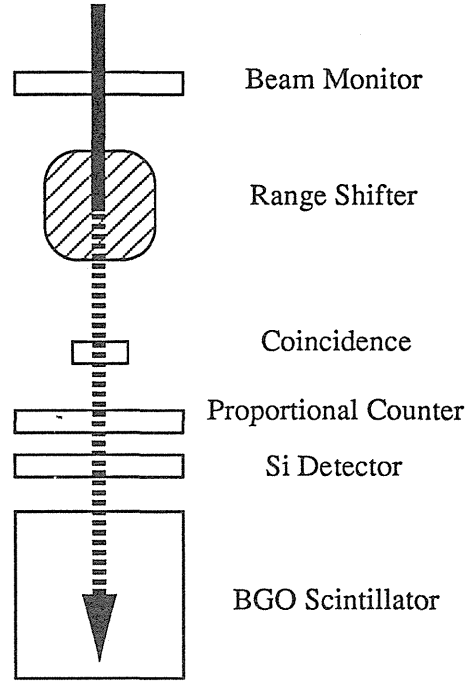

Fig. 1. The schematic view of the detector system.

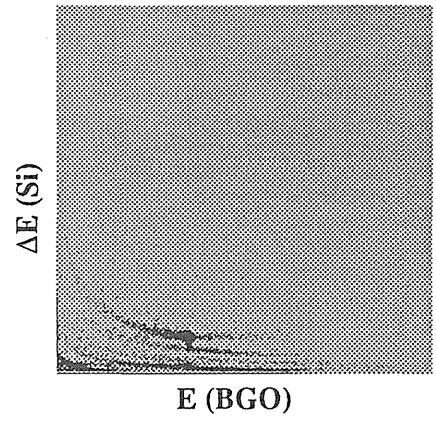

Fig 2. E-ΔE 2-dimensional plot for the incidence of 135 MeV/nucleon carbon beam to the lucite range shifter of 26.67 mm in water-equivalent thickness.

ACKNOWLEDGEMENTS

The authors acknowledge the courtesy of Dr. L. Sihver of his presentation of calculational results.

REFERENCE

1. Sihver L. Depth-Dose and Fluence Distributions When Using Heavy Ion Beams. The Proceedings of the Application of Heavy Ion Accelerator to Radiation Therapy of Cancer(PTCOG XXI), to be published.

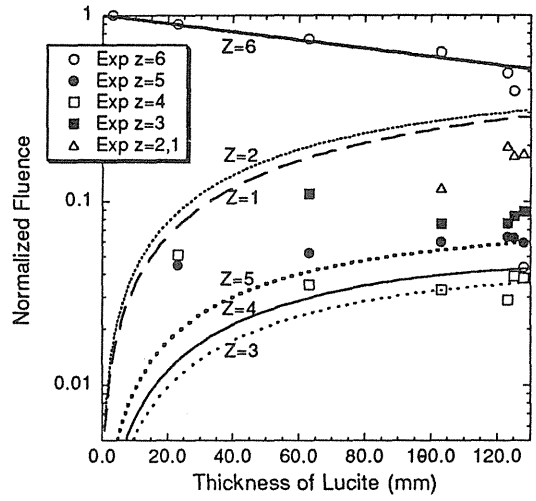

Fig. 3 Fluence spectra of fragments for the incidence of 290 MeV/nucleon carbon beam.

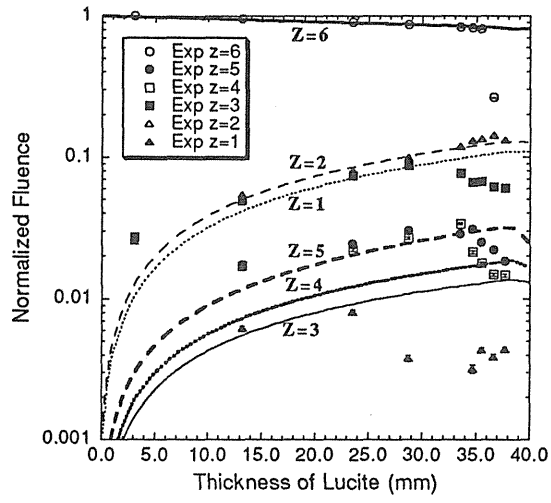

Fig. 4 Fluence spectra of fragments for the incidence of 135 MeV/nucleon carbon beam.

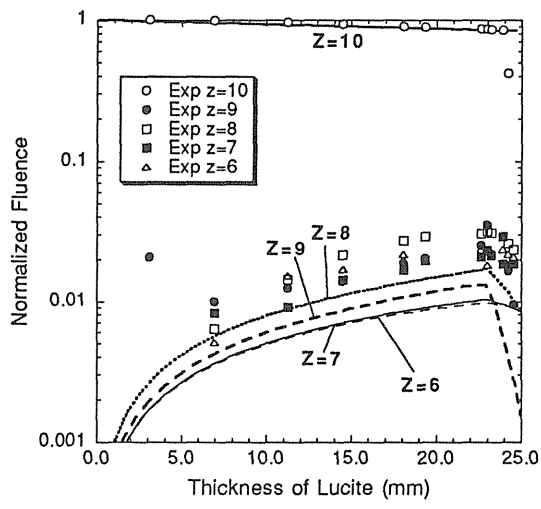

Fig. 5 Fluence spectra of fragments for the incidence of 135 MeV/nucleon neon beam.

RESULTS OF PENUMBRA MEASUREMENTS IN HIMAC

H. TOMURA, T. KANAI, M. ENDO, N. MATSUFUJI, F. SOGA, N. MIYAHARA, S. MINOHARA, H. KOYAMA-ITOH AND K. KAWACHI

Division of Accelerator Physics and Engineering, National Institute of Radiological Sciences, 9-1, Anagawa 4-chome, Inage-ku, Chiba-shi 263 JAPAN

Penumbras in HIMAC clinical ports were measured. These results agree well with the calculation of the distribution function taking account of beam wobbling and multiple-scattering for the average energy at a range modulator.

INTRODUCTION

In the application of the heavy ion beam to the radiation therapy, it is very important to estimate the penumbra size of the radiation field. In the clinical port of HIMAC (Heavy Ion Medical Accelerator in Chiba), the thickness of the scatterer and range shifter, wobbler radius, and other conditions are changed to obtain the flat distribution in the target region for each patient (1). Therefore, it is very important to develop unified semi-empirical equations for the size of the penumbra in such various radiation conditions.

It has been explained that the penumbra size is related to the variance of beam angle (2), and the width of radiation field is related to the beam angle. These quantities are much important for the dose distribution of pencil beam (2-5) as information of initial distribution.

In this report we described the measured penumbra size and development of theoretical equation for the penumbra.

EXPERIMENTAL PROCEDURE

The flatness of radiation field was made using the wobbler and the scatterer (1). When range-shifter was used, the scatterer thickness was changed to keep distribution width of multiple scattering

Lateral dose distribution of radiation field was measured with KODAK X-film. Some results were compared to those with diode detector. These results by two methods nearly agreed.

The experimental data were parameterized as (i) width of radiation field of 50 % intensity, W_{50}, and (ii) Lateral dose falloff from 80 % to 20 %, $P_{80\to 20}$. These parameters were shown in Fig. 1.

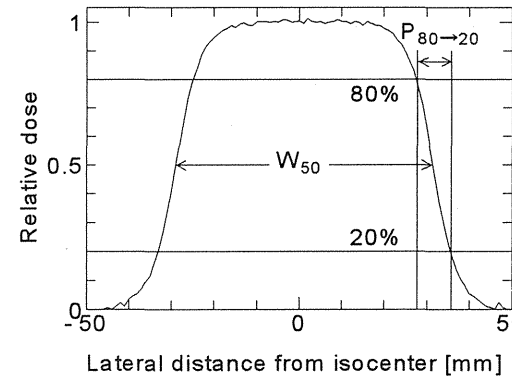

Fig. 1. Measured quantities, W_{50} and $P_{80\to 20}$

RESULT AND DISCUSSION

Lateral dose falloff $P_{80\to 20}$ and field size W_{50} were proportional to distance from the isocenter to collimator position. In addition, lateral dose falloff was proportional to thickness of the scatterer and range-shifter, and field size was proportional to the distance and collimator width. After taking the data in the many different geometrical conditions by using the Carbon beam at 290 MeV/u, the experimental results were empirically fitted by the form of

$$P_{80\to 20} \approx 0.8 + (1.72 + 0.0574 \cdot T)\frac{L_c}{37} \quad \text{[mm]}$$

and

$$W_{50} \approx W + 4\frac{W}{100}\frac{L_c}{37},$$

where T is thickness of bolus, W and L_c are width and distance of collimator from isocenter.

The lateral dose falloff $P_{80\to 20}$ and the field size W_{50}

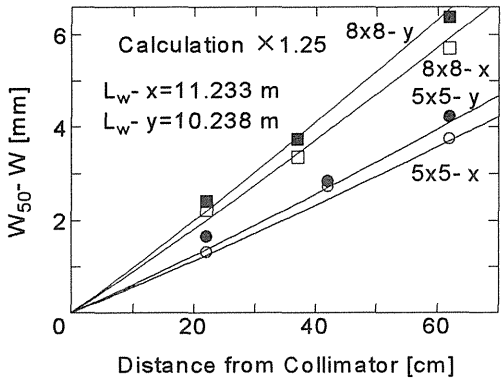

Fig. 2. The closed and opened boxes show the radiation size W_{50} of x and y direction in the case of the $8\times8\,\mathrm{cm}^2$ collimator. Circle symbols show those of the $5\times5\mathrm{cm}^2$ collimator. The solid line displays 1.25 times the calculated value.

were analyzed in the formalism of DPB (differential pencil beam) method (2-5). The distribution of beam is written as the function $F(x,y,\phi_x,\phi_y)$ of lateral axis, x and y, and projected angle to the axis, ϕ_x and ϕ_y. In the case of uniform field, the average $\bar{\phi}=\overline{\phi_x}=\overline{\phi_y}$ and variance $\sigma_\phi=\sigma_{\phi_x}=\sigma_{\phi_y}$ of projected angle at a local position (x, y) are defined as the form of

$$\bar{\phi}=\bar{\phi}(x,y)=\frac{\int_{-\infty}^{\infty}\phi_x d\phi_x\int_{-\infty}^{\infty}d\phi_y F(x,y,\phi_x,\phi_y)}{\int_{-\infty}^{\infty}d\phi_x\int_{-\infty}^{\infty}d\phi_y F(x,y,\phi_x,\phi_y)} \qquad \text{(Eq. 1)}$$

and

$$\sigma_\phi{}^2=\overline{\left(\phi_x-\overline{\phi_x}\right)^2}$$
$$=\frac{\int_{-\infty}^{\infty}\left(\phi_x-\overline{\phi_x}\right)^2 d\phi_x\int_{-\infty}^{\infty}d\phi_y F(x,y,\phi_x,\phi_y)}{\int_{-\infty}^{\infty}d\phi_x\int_{-\infty}^{\infty}d\phi_y F(x,y,\phi_x,\phi_y)}\ . \qquad \text{(Eq. 2)}$$

The local average (Eq. 1) were distinguished from the full space average $\langle\phi\rangle=\langle\phi_x\rangle$ given as the form of

$$\langle\phi\rangle=\iiiint\phi_x\,F(x,y,\phi_x,\phi_y)\,dx\,dy\,d\phi_x\,d\phi_y\ . \qquad \text{(Eq. 3)}$$

Neglecting the expansion of field size, lateral dose falloff $P_{80\to20}$ and the field size W_{50} are given by the following form of

$$P_{80\to20}\approx2\,\mathrm{Erf}^{-1}(0.2)\,\sigma_\phi L_c\approx1.64\,\sigma_\phi L_c$$

$$W_{50}\approx W+2\bar{\phi}\,L_c\ .$$

Eyges (6) gave the solution of Fermi's approximation (7) for the small-angle multiple-scattering, including the energy loss. The solution can be shown by the form of

$$F_s(x,\phi)=\frac{1}{2\pi D}\exp\left[\frac{\langle\phi^2\rangle_s x^2-2\langle x\phi\rangle_s x\phi+\langle x^2\rangle_s\phi^2}{D}\right],$$

where $\langle\phi^2\rangle_s$, $\langle x\phi\rangle_s$, $\langle x^2\rangle_s$ and D at the depth z are calculated from the following equations;

$$\begin{cases}\langle\phi^2\rangle_s=\int_0^z\frac{d\langle\phi^2\rangle_s}{dz'}dz'\\ \langle x\phi\rangle_s=\int_0^z(z-z')\frac{d\langle\phi^2\rangle_s}{dz'}dz'\\ \langle x^2\rangle_s=\int_0^z(z-z')^2\frac{d\langle\phi^2\rangle_s}{dz'}dz'\\ D=\langle\phi^2\rangle_s\langle x^2\rangle_s-\langle x\phi\rangle_s{}^2\end{cases}$$

These values satisfied the relation (Eq. 3). The local moments of the distribution F_s are shown by using the following terms.

$$\begin{cases}\bar{\phi}_s=\frac{\langle x\phi\rangle_s}{\langle x^2\rangle_s}x\\ \sigma_{s\phi}{}^2=\frac{D}{\langle x^2\rangle_s}\end{cases} \qquad \text{(Eq. 4)}$$

This shows that the definitions of (Eq. 1) and (Eq. 2) satisfy the DPB results. Considering (Eq. 4), the average distance from any material to the isocenter is defined as $L_s\equiv\langle x^2\rangle_s/\langle x\phi\rangle_s$. In this case average angle is represented as $\bar{\phi}_s=x/L_s$.

The distribution function for both multiple-scattering and wobbling, $F_{\mathrm{all}}(x,y,\phi_x,\phi_y)$, is calculated as

$$F_{\mathrm{all}}(x,y,\phi_x,\phi_y)=\frac{1}{2\pi}\int_0^{2\pi}F_s\left(x-R_w\cos\theta,\phi_x-\frac{R_w}{L_w}\cos\theta\right)$$
$$\times F_s\left(y-R_w\sin\theta,\phi_y-\frac{R_w}{L_w}\sin\theta\right)d\theta\ .$$

In this report we neglect energy distribution due to range modulator, and use average thickness.

The average angle (Eq. 1) for the distribution F_{all} was calculated as the form of

$$\overline{\phi_r}=\frac{r}{L_s}-R_w\left(\frac{1}{L_s}-\frac{1}{L_w}\right)\frac{I_1\left(rR_w/\langle x^2\rangle_s\right)}{I_0\left(rR_w/\langle x^2\rangle_s\right)},$$

where $r=\sqrt{x^2+y^2}$ is the radial distance from central beam to center of the wobblers, L_w is the wobbler distance from isocenter to center of the wobblers, R_w is the radius of wobbler trajectory at isocenter and $I_n(z)$ is the modified Bessel function given as $I_n(z)=(-i)^n J_n(iz)$. Assuming the flatness of radiation field, the average angle was approximately expressed as the form of

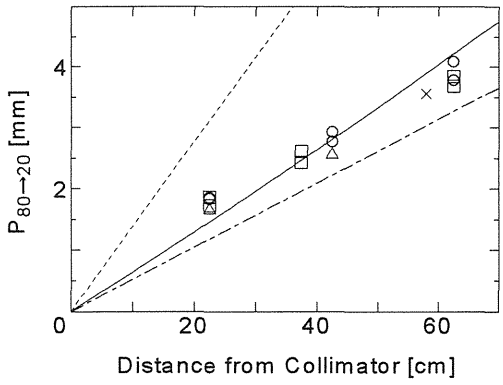

Fig. 3. Symbols show experimental results of penumbra for a $8\times8\,\mathrm{cm}^2$ collimator. Solid line shows penumbra calculated from the local variance (Eq. 5). The dot line shows penumbra estimated for the broad beam with uniform distribution. The dot-dash line shows that calculation from only Fermi-Eyges distribution corresponding to (Eq. 4).

$$\overline{\phi_r} = \frac{r}{L_w}\ .$$

In this form the average angle correspond only to the wobbler distance. The Fig. 2 shows the comparison between the approximation and experimental data in case of 8×8 and $5\times5\mathrm{cm}^2$ collimators. The calculated value was multiplied by factor of 1.25. The deviation of the factor 1.25 cannot be clarified so far, nevertheless the dependence coming from the different distance between L_{w-x} and L_{w-y} are well reproduced by this simple calculation.

The beam angle variance (Eq. 2) for the distribution function F_{all} was given as the form of

$$\sigma_\phi{}^2 = \frac{D}{\langle x^2\rangle} + \langle x^2\rangle\left(\frac{1}{L_s} - \frac{1}{L_w}\right)^2 \quad \text{(Eq. 5)}$$

assuming flatness of the radiation field. Fig. 3 shows the comparison between result of this estimation and experimental one. Solid line shows the penumbra estimated from (Eq. 5). This result was compared with that estimated for only Fermi-Eyges distribution, (Eq. 4), (dot-dash line) and with that for the broad beam with spatially-uniform distribution, where the local variance is given as the form of $\sigma_\phi{}^2 = \langle\phi^2\rangle_s$, (dot line). The simple calculation which correspond to (Eq. 5) agreed to experimental data.

CONCLUSION

The lateral dose falloff and field size were measured. They were proportional to the distance from the collimator. The lateral dose falloff was proportional to the distance from the collimator and absorber thickness, and the field size was to the distance and size of collimator. They were compared to the locally-difined average value and variance of angle of incident beam, considering the average beam energy and field flatness. The width deviates 25% between experimental data and calculation. The penumbra data is well reproduced by the model calculation.

REFERENCES

1. Kanai, T.; Tomura, H.; Matsufuji, N.; Minohara, S.; Fukumura, A.; Hiraoka, T.; Furusawa, Y.; Miyahara, N.; Koyama-Itoh, H.; Endo, M.; Soga, F.; Kawachi, K. HIMAC beam delivery system - Physical characteristics -. in this issue.
2. Hogstrom, K. R.; Mills, M. D.; Almond, P. R. Electron beam dose calculations. Phys. Med. Biol. 26:445-459:1981
3. Lax, I.; Brahme, A. Electron beam dose planning using Gaussian beams. Acta Radiat. Oncol. 3:75-85:1985
4. Jette, D. Electron dose calculation using multiple-scattering theory. A. Gaussian multiple-scattering theory. Med. Phys. 15:123-137:1988
5. Yu, C. X.; Ge, W. S.; Wong, J. W. A multiray model for calculating electron pencil beam distribution. Med. Phys. 15:662-671:1981
6. Eyges, L. Multiple scattering with energy loss. Phys. Rev. 74:1534:1948
7. Rossi, B.; Greisen, K. Cosmic-Ray Theory. Rev. Mod. Phys. 13:240-309:1941.

A COMPACT PROTON SYNCHROTRON WITH A COMBINED FUNCTION LATTICE FOR MEDICAL USE

KAZUO HIRAMOTO, PH.D., JUNICHI HIROTA, PH.D., MASATSUGU NISHI, PH.D.
Energy Research Laboratory, Hitachi, Ltd.
2-1, Omika-cho, 7-Chome, Hitachi-shi, Ibaraki-ken, 319-12, Japan

MAMORU KATANE, HIROAKI SAKURABATA
Hitachi Works, Hitachi, Ltd.
1-1, Saiwai-cho, 3-Chome, Hitachi-shI, Ibaraki-ken, 317, Japan

AKIRA NODA, PH.D., YOSHIHISA IWASHITA, PH.D. AND MAKOTO INOUE, PH.D.
Nuclear Science Research Facility, Institute for Chemical Research,
Kyoto University, Gokanoshou, Uji-shi, Kyoto-fu, 611, Japan

Abstract

A compact proton synchrotron dedicated for cancer therapy is presented. In the synchrotron, the number of quadrupole magnets is reduced by employing the combined function bending magnets. The proton beam is slowly extracted with use of the nonlinear betatron resonance after acceleration to the required energy level. In the slow extraction, transverse perturbation by the radio frequency is applied to make the beam diffuse and cross over the separatrix of the nonlinear resonance while the operating point is kept constant relative to the resonance. This scheme realizes a simple and low emittance beam extraction with a high duty factor. Furthermore, a new irradiation scheme for treatment is presented in which the proton beam is expanded in the deflecting plane of the bending magnets of the treatment gantry and scanned normal to the deflecting plane. Since this scheme does not employ scatterers, loss of the beam can be significantly reduced.

Proton Therapy, Bragg Peak, Combined Function Synchrotron, Untuned RF Cavity, Slow Beam Extraction, Gantry

I. Introduction

A high energy proton beam has been successfully applied to cancer treatments (Ref. for example 1,2) and sixteen proton therapy centers are presently being operated worldwide(3). In cancer therapy, it is expected that varying the energy of the proton beam is necessary when treating a different depth in the tissue because the proton beam shows a relatively sharp Bragg peak. Then, a synchrotron seems to have an advantage as an accelerator for cancer therapy because it is easy to change the acceleration energy of the charged particle beams. In the medical proton synchrotron, simple operating schemes are needed for acceleration, extraction and irradiation etc. because the medical accelerator system must be used in daily treatments. Considering this condition, we present a new synchrotron design for proton therapy in which the combined function lattice, a new type of the untuned accelerating cavity and a simple resonant extraction scheme(4,5) are employed. The combined function lattice has an advantage of simple operation for the beam acceleration, although this is gained at the expense of flexibility in selecting operating points in the separated function lattice(2,7). The present untuned accelerating cavity employs a new method for RF power feeding, that is, the RF power is fed separately to each Ni-Zn ferrite core to obtain a higher gap voltage. In the extraction, a transverse perturbation by radio frequency is applied to make the beam diffuse in the transverse direction and exceed the separatrix of the resonance of the betatron oscillations. Hereafter, we call this scheme the diffusion-resonant extraction. This diffusion-resonant extraction has a feature that the operating point of the synchrotron and the deflection angle of the electrostatic deflector are kept constant. The diffusion-resonant extraction has another feature that the time integrated emittance of the extracted beam can be kept low in comparison with that by the conventional extraction scheme varying the operating point and the deflection angle of the deflector(4-6). Finally, we present a new irradiation scheme in which the beam is defocused, with flattening of the distribution in the deflecting plane, and swept across this plane. Since this scheme does not employ scatterers, loss of the beam can be significantly reduced.

II. Synchrotron System Design

A. Lattice and Machine Parameters

The main machine parameters of the designed synchrotron are listed in Table 1. In the present synchrotron, a proton beam of 7 MeV is injected from a linac to the synchrotron. The maximum beam energy reached is 230MeV. After the acceleration, the beam is extracted by the diffusion-resonant extraction. These procedures are repeated at 0.5Hz.

Fig. 1 shows the lattice of the designed synchrotron. The synchrotron consists of two kinds of combined function bending magnets, BF and BD. The deflection angle of each bending magnet is 45 degrees. The maximum magnetic field of the bending magnets is 1.44 T, which results in the curvature radius of 1.62m. These magnets are excited in series. The n-indices of the magnets BF and BD are determined so as to satisfy the horizontal tune $\nu x=1.75$ and

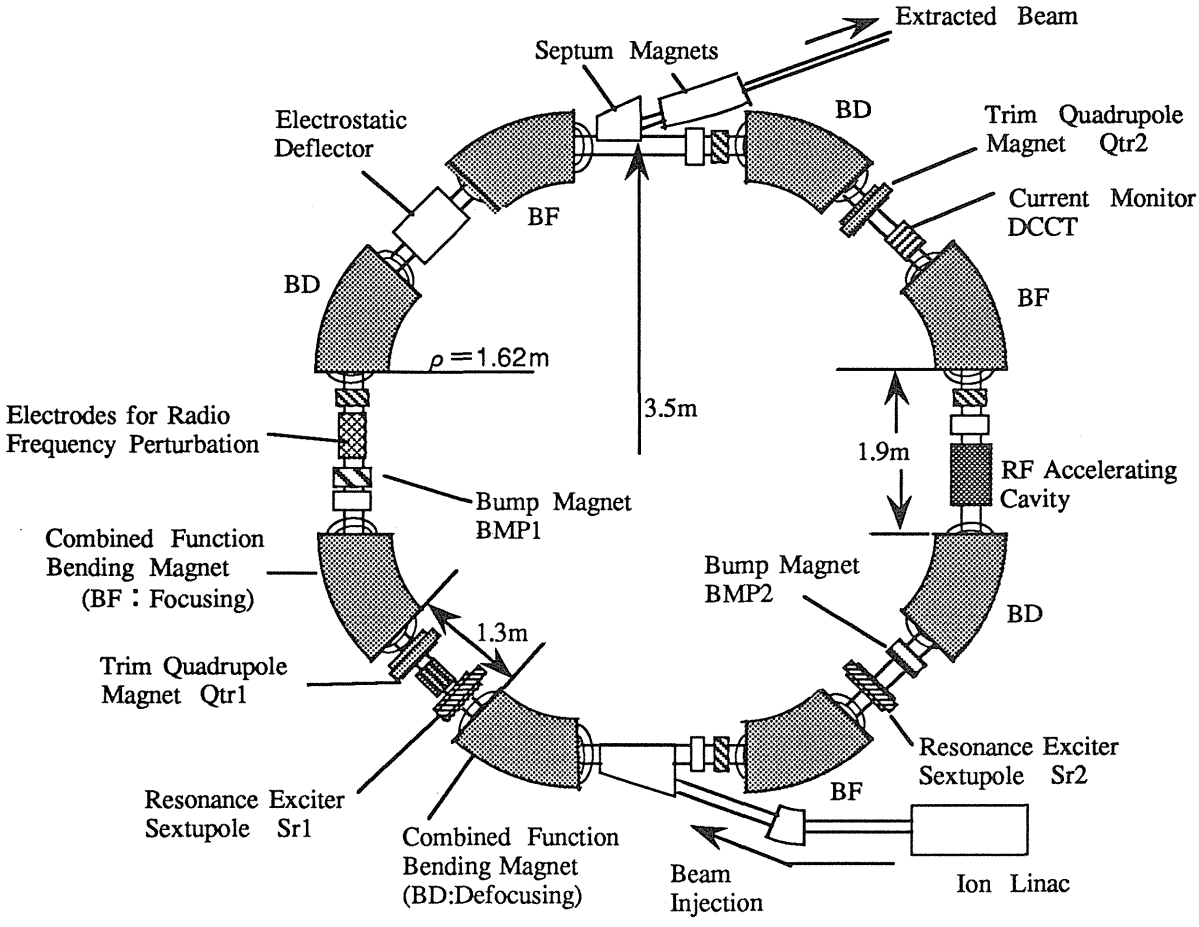

Fig. 1 Configuration of the Proton Synchrotron

Table 1 Machine Parameters

Circumference(m)	22.9
Injection Energy (MeV)	7
Max. Energy(MeV)	230
Super Period	4
Tune	
νx	1.75
νy	0.85
Bending Magnet	
Deflection Angle(deg)	45
Curvature Radius(m)	1.62
Max. Field Strength (T)	1.44
BD K($1/m^2$)	0.344
n	0.904
BF K($1/m^2$)	-0.228
n	-0.599
Twiss Parameters	
βx, max (m)	10.8
βy, max (m)	7.8
η, max (m)	2.2

the vertical tune νy=0.85. These tune values are chosen so as to avoid structure resonance for the betatron oscillations. If needed, fine control of the betatron tune can be done using the trim quadrupole magnets Qtr1 and Qtr2.

B. Injection

Beam injection into the synchrotron is done during about 20 revolution periods in a multi-turn injection scheme using the two injection bump magnets, BMP1 and BMP2. We assume that the phase space density is diluted almost half compared with the injected beam, then the circulating beam current is about 10 times as large as the injection current from the linac.

C. Acceleration

The current of the bending magnets is ramped to keep the beam orbit unchanged as the beam energy increases. The revolution frequency of the beam also goes up as the velocity of the beam increases. The beam is accelerated by the radio frequency (RF) accelerating cavity, whose frequency should be proportional to the revolution frequency. The RF cavity employs Ni-Zn ferrite cores and is untuned. Since the untuned RF cavity does not need any control of the resonant frequency, the control system can be significantly simplified. Generally, the gap voltage of the untuned cavity is relatively low, because of the small Q value and the impedance mismatch between the RF power source and the RF cavity. In the present cavity, the impedance mismatching is improved by feeding the RF power to each ferrite core separately, and then the higher

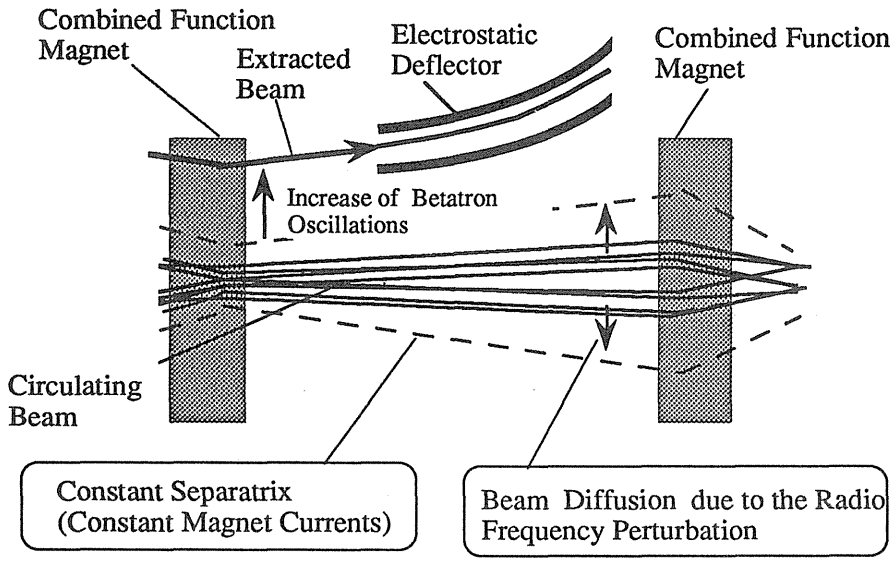

Fig. 2 Principle of the Diffusion-Resonant Extraction

gap voltage is achieved at the same input RF power. We expect the gap voltage of about 500V, which is required for the acceleration, can be easily obtained at rather low power level. The length of the designed untuned cavity is about 0.4 m.

D. Extraction

One of the features of the present synchrotron is that a low emittance beam can be extracted slowly by a very simple operating scheme, that is, the diffusion-resonant extraction scheme. The diffusion-resonant extraction and the beam behavior in the horizontal plane is schematically shown in Fig.2. A schematic time chart of the extraction is shown in Fig.3. The separatrix for the resonance is generated after Ts, that is, the end of the acceleration, by using the two sextupole magnets Sr1 and Sr2, and decreasing the horizontal betatron tune to 1.67. According the scheme shown in Fig. 2, the separatrix is kept constant during the extraction by the operation that the field strengths of all of the magnets are kept constant. On the other hand, the transverse radio frequency perturbation with a certain frequency width is applied to the beam to make it diffuse and exceed the separatrix of the resonance. The frequency of this perturbation ranges from 0.66fr to 0.68fr, where fr is the revolution frequency of the beam around the synchrotron. Since this frequency range covers the width of the frequencies of the betatron oscillations, which occurs due to the momentum spread of the beam etc., the beam diffuses and the particles exceeding the separatrix are extracted. During the extraction, the strength of the radio frequency perturbation is slightly increased to obtain the flat beam spill. The needed maximum voltage of the radio frequency perturbation is about 50V for the beam energy of 230MeV.

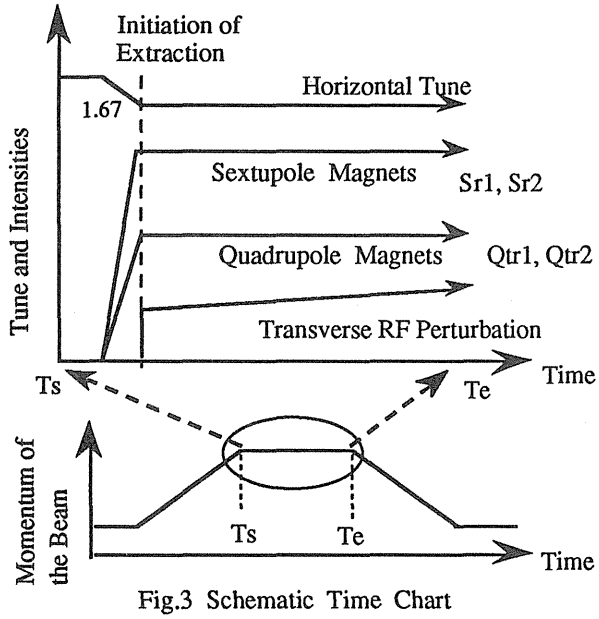

Fig.3 Schematic Time Chart

The particles are extracted horizontally through the electrostatic deflector and the septum magnet. By the merit of keeping the constant separatrix, the orbit gradients of the extracted particles are almost constant throughout the extraction process without dynamic control of the magnets(4). Because of this effect, time integrated emittance can be kept low. This effect has been also studied experimentally in TARN II (5) and HIMAC(6).

Furthermore, the intermittent structure of the extracted current can be improved significantly even under the condition that the magnet current includes a low frequency ripple(6,8). In the conventional extraction done by varying the separatrix size, the number of the extracted particles per unit time is expressed as NV where N(1/mm) is the number of particles on the separatrix in the phase space and V(mm/s) the speed of varying separatrix size. Since V is small in this scheme, its value is modulated by the ripple of the magnet current. This results in the intermittent extraction. In the diffusion-resonant extraction, the number of the extracted particles per unit time is expressed as NVrf where Vrf(mm/s) is the speed of the diffusion on the separatrix. Because of the characteristics of the diffusion, the value of N is small. Then, a relatively large value of Vrf is needed to obtain a sufficient flux exceeding the separatrix. As the result, the separatrix change due to the magnet current ripple does not make the extraction flux vary so significantly.

E. Irradiation

The extracted particles are transported to the treatment room. The present system employs a new scheme for expanding the irradiation field in the treatment room as follows. (i)The beam is defocused in the deflecting plane of the treatment gantry by quadrupole magnets. (ii) The beam distribution in the deflecting plane is flattened by a nonlinear

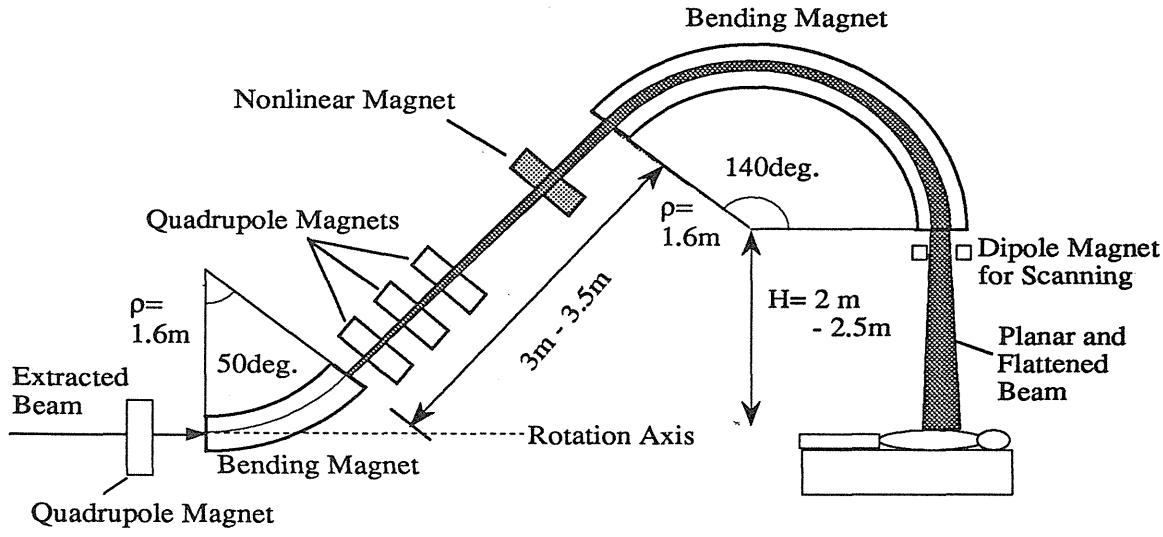

Fig. 4 The Gantry for Treatments Using A New Irradiation Scheme

magnet such as an octupole magnet. (iii) The beam is swept by the dipole magnet across the deflecting plane. Fig. 4 shows an example of the gantry to which the present scheme is applied. The beam distribution in the deflection plane just before the patient is shown in Fig. 5. It is found that the width of the uniformity within 2.5% is about 15cm for the case using octupole and duodecapole magnetic fields. For the case using only octupole magnetic field, the width having the same uniformity as the previous one slightly decreases. Since a square irradiation field is obtained by sweeping across the deflection plane, the beam should be collimated before the patient. One of the features is that the beam loss can be reduced in comparison with the scheme using scatterers. Another feature is that adequate selection of sweeping speed might realize a flat intensity distribution in the square irradiation field even under the condition that the intermittent extraction current occurs.

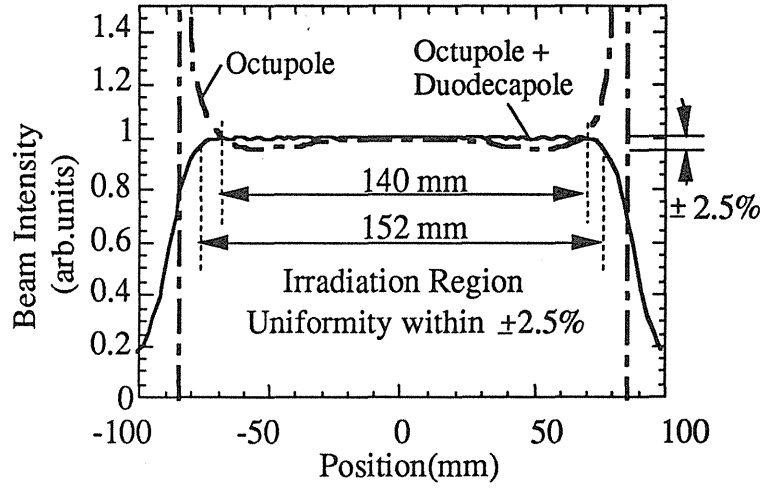

Fig. 5 Beam Distribution in the Deflecting Plane

III. Conclusion

We presented a compact proton synchrotron system for cancer therapy. In the synchrotron, a combined function lattice was applied with a new type of the untuned accelerating cavity in which the RF power is fed separately to each Ni-Zn ferrite core. The accelerated beam is slowly extracted by using a transverse radio frequency perturbation of a narrow bandwidth. Control of the synchrotron is simple, and a low emittance beam can be extracted. The time structure of the extracted current is improved even under the condition that the magnets have current ripples of low frequency.

We also presented a new irradiation scheme which employs defocusing a beam in the deflecting plane in the gantry and sweeping it perpendicularly to the plane. The distribution of the beam is flattened in the deflecting plane by the nonlinear magnet. Then beam loss, occurring in the case using scatterers, can be avoided.

References

1. H. Tsujii, et al., Proc. of NIRS International Workshop on Heavy Charged Particle Therapy and Related Subjects, p82, Chiba, Japan, 1991
2. J. M. Slater, et al., ibid., p73
3. J.M. Sisterson, Abstracts of the XX PTCOG Meeting, p19(1994)
4. K. Hiramoto, et al., Nucl. Instrum. Methods. A322, p154 (1992)
5. M. Tomizawa, et al., Nucl. Instrum. Methods. A326, p399 (1993)
6. K. Noda, et al., "Beam Test on Ring Property in HIMAC Synchrotron", Proc. of the European Particle Accelerator Conference, London, U.K., 1994 (in press)
7. G. Cesari, et al., CERN/PS/91-08(DI), 1991
8. K. Hiramoto, et al., Proc. of the Particle Accelerator Conference, p309, Washington D.C., USA, 1993

Application of the dual-ring double scattering method for proton field enlargement to beam with finite emittance

Yoshihisa Takada
Institute of Applied Physics, University of Tsukuba, Tsukuba, Ibaraki, Japan

Abstract

A novel beam spreading method using the dual-ring 2nd scatterer was proposed to obtain the uniform field required for proton cancer therapy. [1] It enables us to obtain such a uniform circular region of about 20 cm in diameter in short length (3 m) with higher efficiency (37%) for zero- or small-emittance beam. The range loss due to the scatterers is about 4 cm in water. We successfully applied this technique to the 237 MeV proton beam with relatively large emittance(100 π mm.mrad(2σ)). The 1st scatterer is made from 2.5 mm-thick hard lead (lead with 4% Sb). After scattered there, the proton beam is incident on the dual-ring; the inner disk made from 4.5 mm-thick hard lead and the surrounding outer ring made from 12.3 mm-thick aluminum. For fine adjustment of the scatterer parameters, 0.6 mm-thick stainless sheet covers whole region of the dual-ring. The boundary radius of the dual-ring is 23.2 mm. The distance between the 1st scatterer and the end plane is 3.300 m, and that between the 1st and the 2nd scatterers is 76.1 cm. Although the combination of scatterers is designed for zero-emittance beam, it can be applied to beam with large emittance if we adjust the longitudinal position of the 2nd scatterer 5 cm before the initially designed position for zero-emittance beam. The effect of the boundary on the Bragg curves at various positions is unnoticeable. The shapes of lateral field distributions are nearly the same along the various longitudinal positions of the Bragg curve. The beam misalignment effect on the lateral distribution was measured and found to be rather large as expected from the calculation. Therefore the real time monitoring of the beam distribution is required and the precise beam steering on the center of the dual ring is necessary. The effect of the possible third scatterer like range shifter and ridge filter was measured. It was found that up to 15 cm-thick water equivalent material placed 1.2 m before the end plane can be inserted with little reduction of the usable circle.[1] Therefore a few types of dual-rings should be prepared and can be changed quickly to cover the wide range of the range shifter and the ridge filter. Since the beam profile on the 2nd scatterer determines the final distribution, control of the longitudinal position of the dual-ring or of the 1st scatterer will serve to obtain the uniform field distribution when the other materials like the range shifter and the ridge filter are inserted in the beam line. Precise control of the lateral position of the dual-ring will serve to recover the small misalignment effect on the lateral beam distribution.

Introduction

High energy proton beam has been used as a powerful modality of cancer treatment using the advantage of depth-dose distribution. Sixteen facilities in the world are now conducting proton therapy and the number will increase. Since a large uniform field is required for cancer

treatment, it is necessary to transform the small beam of Gaussian shape to large uniform field. For that purpose, a number of methods were proposed and used. Out of them, double scattering method using an annular stopper was widely used for its simplicity, stability and reliability.[2] Other methods use scanning techniques to form a large uniform field by painting the field with the Gaussian beam. However such methods required the control of the spill structure of the extracted beam to obtain the uniform beam and an elaborate beam monitoring and safety system. The problems about the scattering system are as follows.

1. low efficiency of beam use (at most 27-30%).
2. long distance required for field formation (5 m).
3. range loss in the scatterers.
4. degradation of lateral penumbra of the irradiation field due to the scattering in the scatterers
5. additional exposure of the fast neutron from the scatterer and beam collimators.

Despite of these demerits, this method has been used as a practical method of obtaining the large uniform field required for cancer therapy. The object of this study was to improve this method to some extent. We devised a novel method of double scattering using the dual-ring second scatterer. By this method the beam utilization efficiency increased up to 37% and the distance required for field formation can be reduced to about 3 m with the range loss of about 4 cm in water in the scatterers.

Principle of this method

Figure 1 shows the arrangement of scatterers and figure 2 the formed proton field by this method. The details of the method are described in the separate paper.[1] The proton beam scattered by the 1st scatterer impinges on the dual-ring second scatterer. The dual-ring consists of an inner disk made from heavy metal and an outer ring made from lighter metal. Protons are scattered more strongly in the inner disk than in the outer ring. By selecting proper materials it is possible to form uniform central region yet keeping the same energy losses in the inner and outer scatterers. Although this method was considered for zero-emittance or small-emittance beam, it can be also applied to the beam with larger emittance if we adjust the related scatterer parameters by moving the dual-ring along the beam line.

Experimental Results

We performed the experiment to confirm the validity of applying this method to the beam with finite emittance. We used the 237 MeV proton beam of PMRC(Proton Medical Research Center), University of Tsukuba, located inside the National Laboratory for High Energy Physics (Often called KEK). Figure 3 shows the experimental setup. The distance between the 1st scatterer and the end plane is 3.300 m. The 1st scatterer is placed at the exit of brass collimator of 67 mm in depth with a cylindrical hole of 20 mm in diameter and is made from 2 mm-thick hard lead with 4% Sb. The second scatterer is a dual-ring; the inner disk made from 4.5 mm-thick hard lead with 4% Sb, and the outer ring made from 12.3 mm aluminum. The boundary radius of the dual-ring is 23.2 mm. For fine adjustment of the scatterer parameters, an additional 0.6 mm-thick

stainless sheet covers the entire region of the dual-ring. The dual-ring was placed 761 mm from the 1st scatterer. Since the beam emittance is 100 π mm.mrad(2σ), the position is 50 mm upstream of the optimum position for the hypothetical initial beam of zero-emittance. Using this combination of scatterers we obtained the uniform proton field of 21 cm in diameter with ±2-3%p-p non-uniformity. We used a silicon detector having a sensible region of 2 mm by 2 mm to measure the relative dose distribution of the proton field in water. For compensation of the beam intensity fluctuation during the experiment, another silicon detector was placed off-axis of the beam line about 60 cm before the end plane.

Figure 4 shows lateral proton distributions on the end plane for three different positions of the dual-ring. The shoulder of the distribution increases as the dual-ring moves to downstream of the nominal position. Figure 5 shows lateral beam distributions along the Bragg curves. The entrance position of the Bragg curve is the nominal end point. The shapes of the distributions are nearly the same. Figure 6 shows the Bragg curves at different positions of the usable circle of the beam field on the end plane. Noticeable difference cannot be seen. This means that the energy losses in the inner disk and outer ring are the same and the boundary effect of the dual-ring is unnoticeable. Figure 7 shows the misalignment effect of the beam. By moving the brass collimator in horizontal direction we obtained the effective misalignment of the beam on the dual-ring. The effect is rather large as can be expected from calculations. If we permit ±3% nonuniformity, the tolerable angular error of the beam centroid is around 1 mrad. Therefore precise beam alignment will be required together with the on-line monitoring of the beam flatness. Figure 8 shows the comparisons between the experiments and Monte Carlo calculations. We used the formula for multiple Coulomb scattering by Lynch and Dahl.[3] For fitting of the experimental data with calculations, a few percent lower values of the scattering strengths fitted the data well. Since the formula by Lynch and Dahl[3] has an error of a few percent, experimental results agree with the calculations within the expected error. Figure 9 shows the effect of possible third scatterer like a range shifter and a ridge filter on the lateral field distribution. We used aluminum of thicknesses of 4 cm and 8 cm as the 3rd scatterer placed 52~54 cm before the end plane.

Summary

Flat beam field can be obtained in short length (about 3 m) by the double scattering method using the dual-ring 2nd scatterer with high efficiency of beam utilization(37%).

Although we used the scatterers designed for the zero-emittance beam, it can be used for the proton beam with large emittance (100 π mm.mrad(2σ)) if we moved the dual-ring 5 cm upstream of the beam line, which resulted in adjustment of contributions of protons scattered in the inner disk and the outer ring of the dual-ring. The longitudinal position control of the dual-ring or of the 1st scatterer also serves to control the beam profile on the dual-ring, which results in keeping the good field homogeneity when the other scatterers like a range shifter or a ridge filter modifying the effective scatterer parameters are inserted. For wider coverage of range shifter parameter, the scattering effect in the range shifter should be combined with that in the variable-thickness 1st scatterer. When the thickness of the range shifter made from low-Z

material increases, the thickness of the 1st scatterer made from high-Z material decreases to compensate the increase of the scattering strength in the range shifter.

Precise alignment of beam on the center of the dual-ring is important to keep good homogeneity of the field distribution because this method is rather sensitive to the misalignment of beam. Typically less than 1 mrad of alignment error of the beam centroid direction will be required. Therefore fine control of lateral position of the 2nd scatterer may be effective to align the beam precisely on the center of the dual-ring. Further it is important to monitor the flatness of the proton field distribution on line to confirm the field homogeneity quickly.

In order to obtain the uniform region of 20 cm in diameter with ±2% non-uniformity, about 4 cm range loss in water occurs in the scatterers for 237 MeV proton beam. Therefore it is necessary to determine the maximum proton energy keeping in mind this range loss in the scatterers when we determined the maximum size of usable field and the maximum proton range. The thickness of scatterers are roughly proportional to square of the required field size.

In summary, the dual-ring double scattering method was proved to be an efficient and simple method of obtaining the flat proton distribution in short length. Therefore it can be installed in the proton rotating gantry.

References

1. Y.Takada: Japn. J. of Appl. Phys. 33 (1994) 353.
2. A.M.Koehler, R.J.Schneider and J.M.Sisterson: Med. Phys. 4 (1977) 297.
3. G.R.Lynch and O.I.Dahl: Nucl. Instrum. & Methods B 58 (1991) 6.

Figure Captions

1. Arrangement of scatterers of the dual-ring double scattering method
2. Distributions of the beam field formed by the dual-ring double scattering method: (a) total distribution, (b) contribution of the inner second scatterer, (c) that of the outer second scatterer and (d) the cross sectional view of the total distribution with the contributions of the inner and outer scatterers.
3. Experimental setup of the dual-ring double scattering method.
4. Lateral beam distributions for three cases of different longitudinal positions of the second scatterer.
5. Lateral beam distributions along Bragg curves. The entrance position of 0.4 cm is the nominal plane of the field formation.
6. Bragg curves at various lateral positions within the usable circle.
7. Effect of misalignment. The position of the collimator and the 1st scatterer was moved in horizontal direction to simulate the effect of the beam misalignment.
8. Comparisons of the experimental data with the results of Monte Carlo calculation. Left graph is the comparison of the lateral beam distribution with the calculation and right graph is that of the data of observing the misalignment effect with the calculation.
9. Effect of the 3rd scatterer on the lateral field distribution.

Arrangement of scatterers for the dual-ring double scattering method.

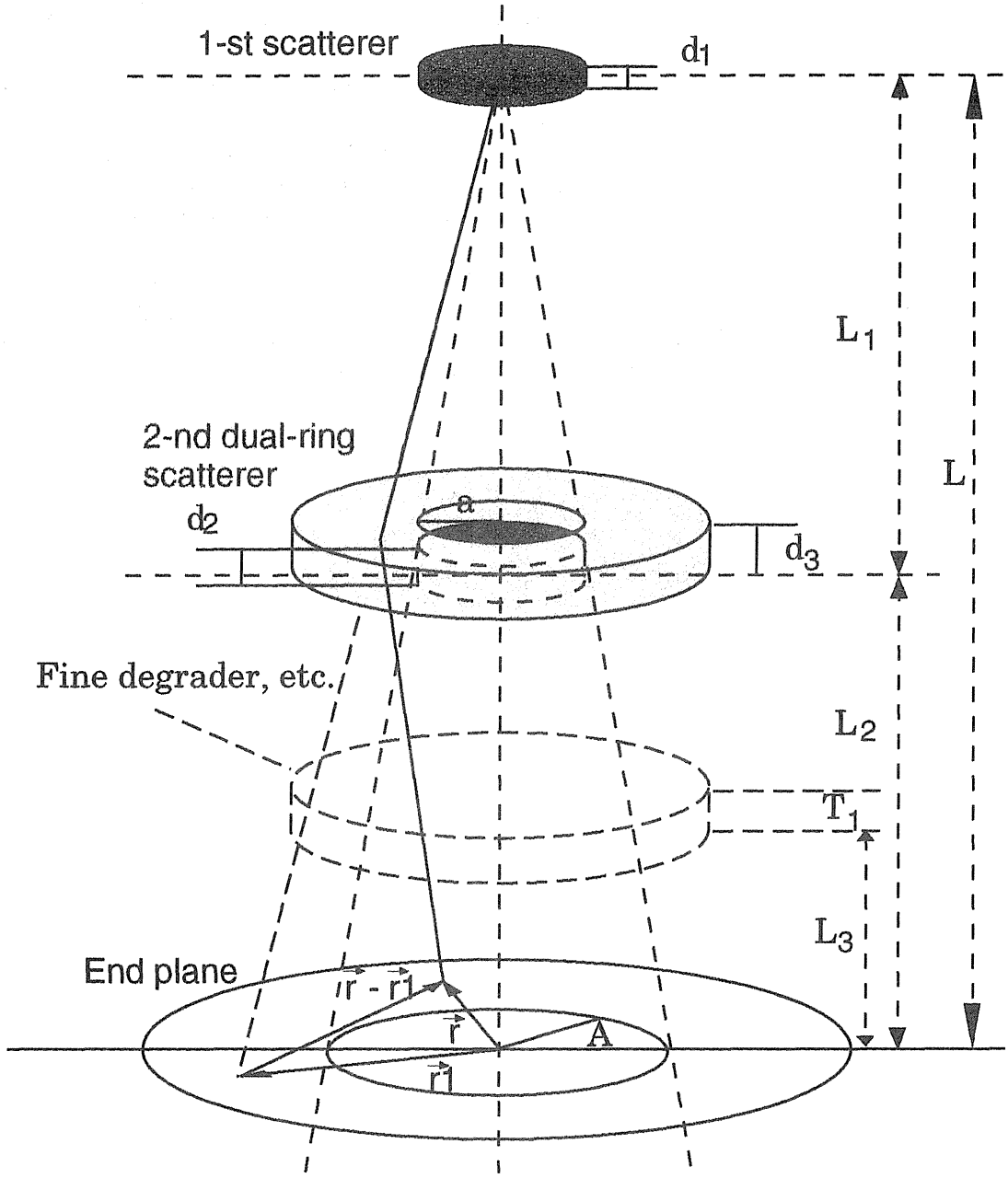

Fig.1

Proton Field Formation by the Dual-Ring Double Scattering Method

(The 1st and the 2nd inner scatterers are made from lead, and the 2nd outer scatterer from aluminum.)

(a) Total distribution

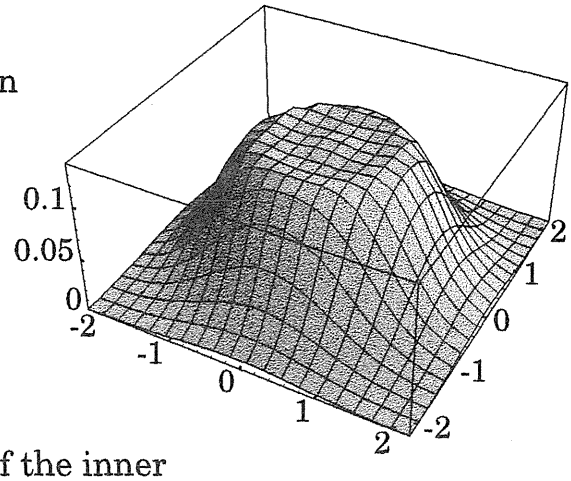

(b) Contribution of the inner second scatterer

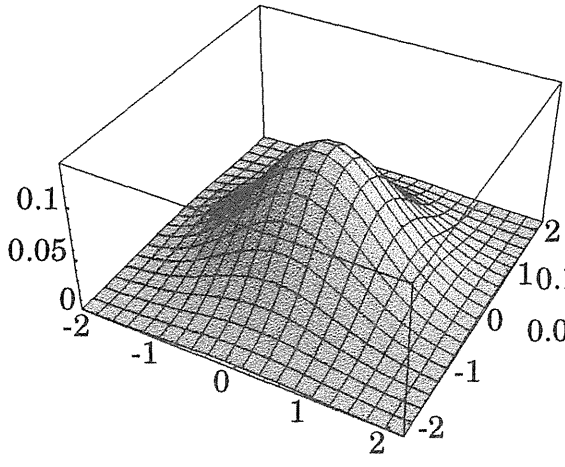

(c) Contribution of the outer second scatterer

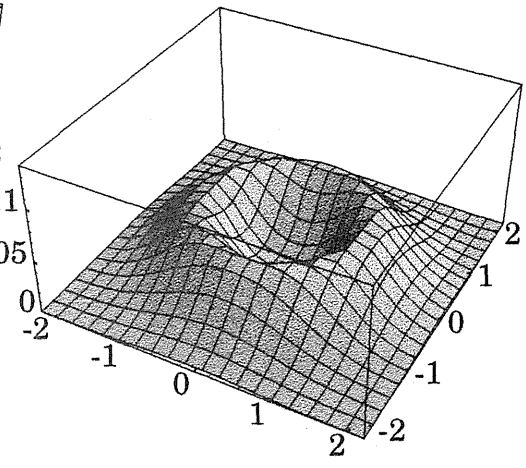

(d) Cross sectional view of the total distribution (Contributions of the inner and outer rings are displayed.)

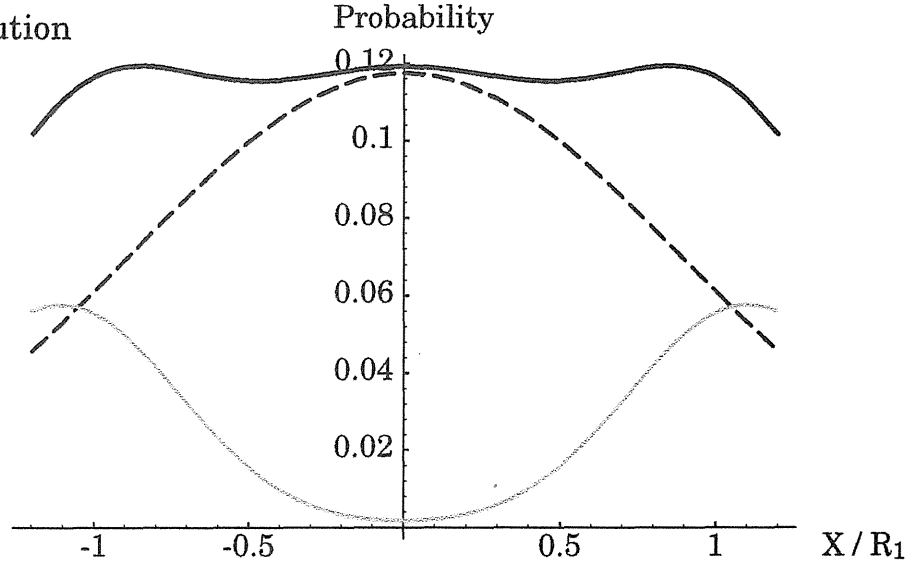

Fig.2

Experimental Setup of Dual-Ring Double Scattering Method

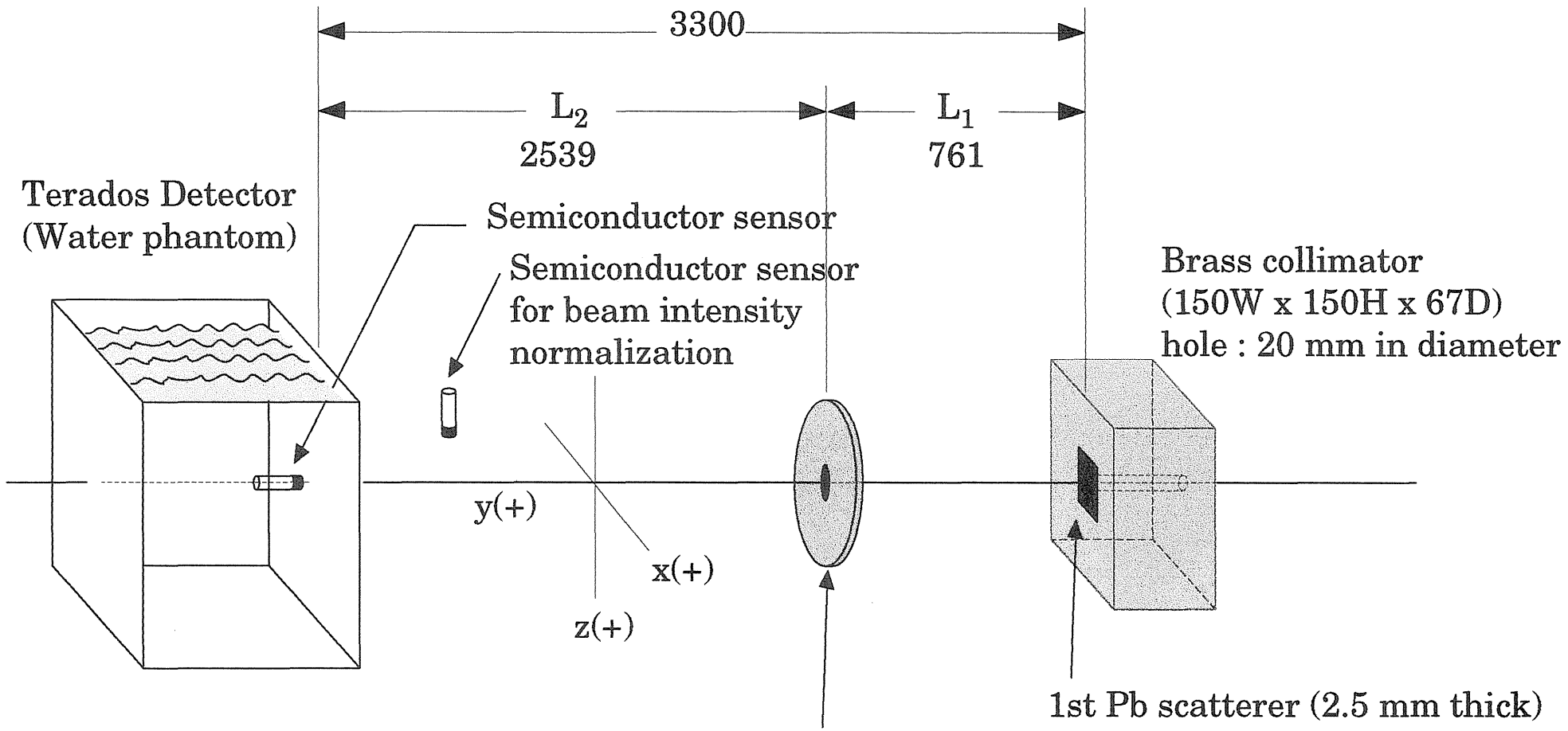

Fig.3

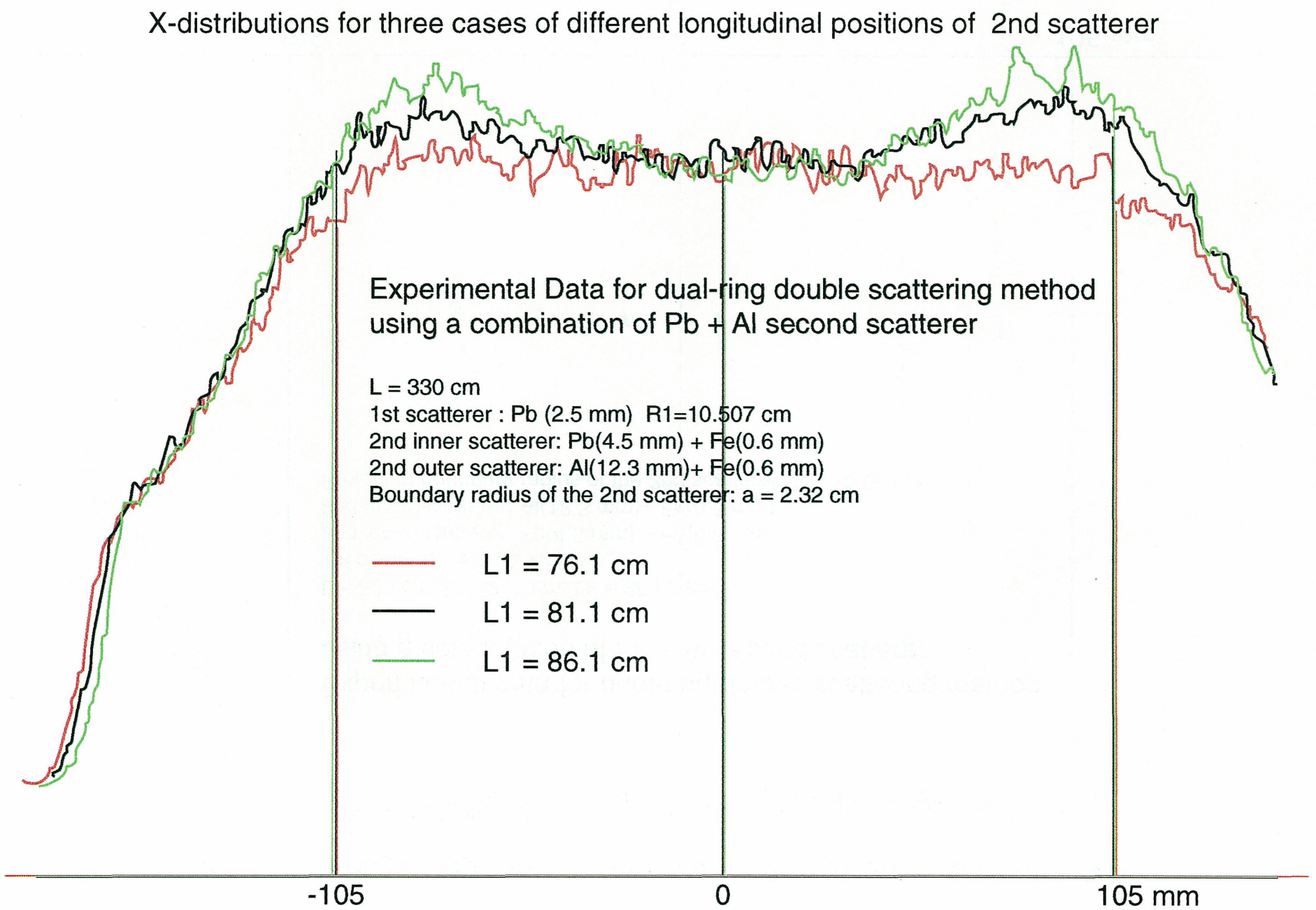
X-distributions for three cases of different longitudinal positions of 2nd scatterer
Experimental Data for dual-ring double scattering method using a combination of Pb + Al second scatterer
L = 330 cm
1st scatterer : Pb (2.5 mm) R1=10.507 cm
2nd inner scatterer: Pb(4.5 mm) + Fe(0.6 mm)
2nd outer scatterer: Al(12.3 mm)+ Fe(0.6 mm)
Boundary radius of the 2nd scatterer: a = 2.32 cm
L1 = 76.1 cm
L1 = 81.1 cm
L1 = 86.1 cm
-105
0
105 mm

Fig.4

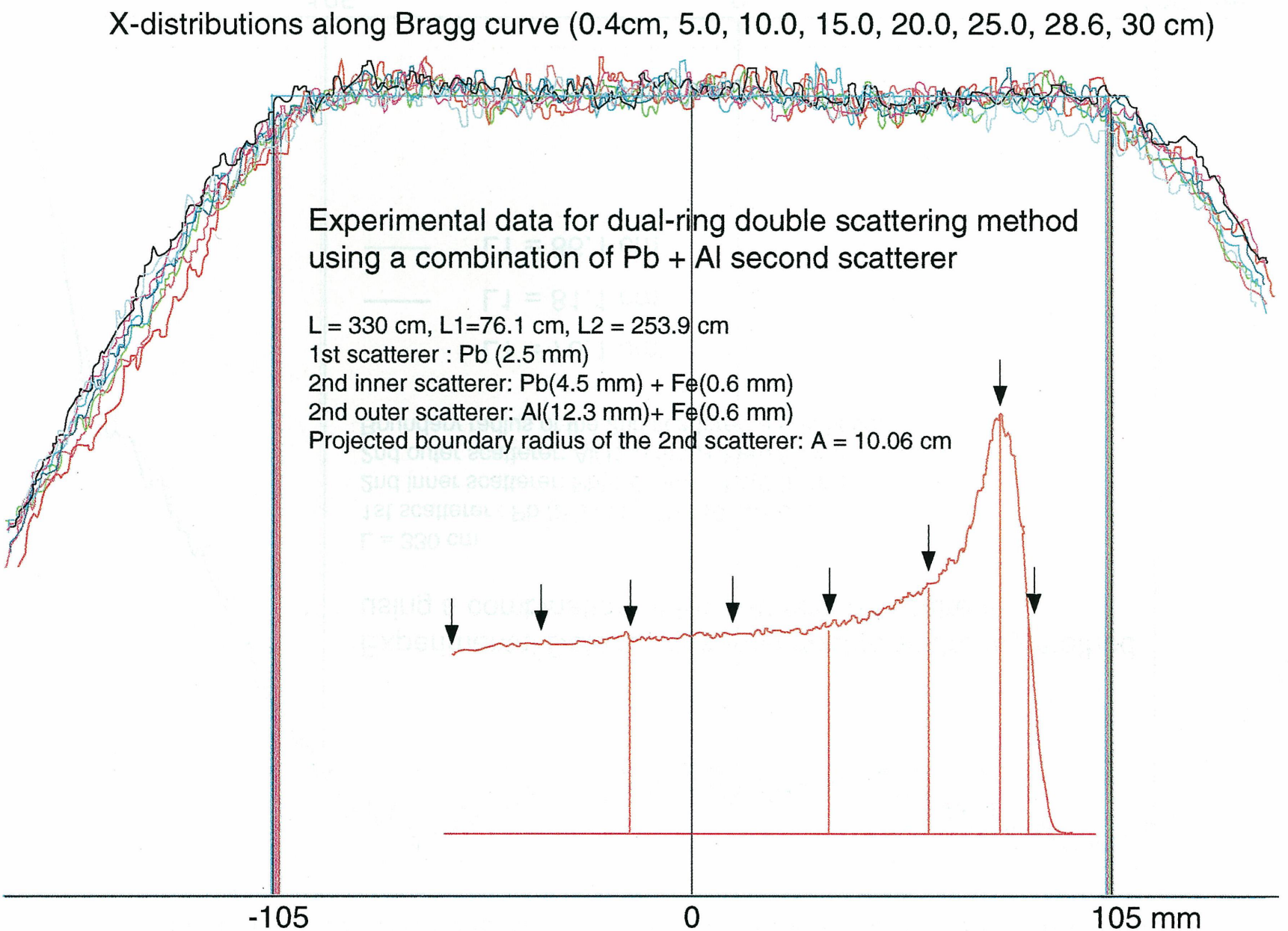
X-distributions along Bragg curve (0.4cm, 5.0, 10.0, 15.0, 20.0, 25.0, 28.6, 30 cm)
Experimental data for dual-ring double scattering method using a combination of Pb + Al second scatterer
L = 330 cm, L1=76.1 cm, L2 = 253.9 cm
1st scatterer : Pb (2.5 mm)
2nd inner scatterer: Pb(4.5 mm) + Fe(0.6 mm)
2nd outer scatterer: Al(12.3 mm)+ Fe(0.6 mm)
Projected boundary radius of the 2nd scatterer: A = 10.06 cm
-105
0
105 mm

Fig.5

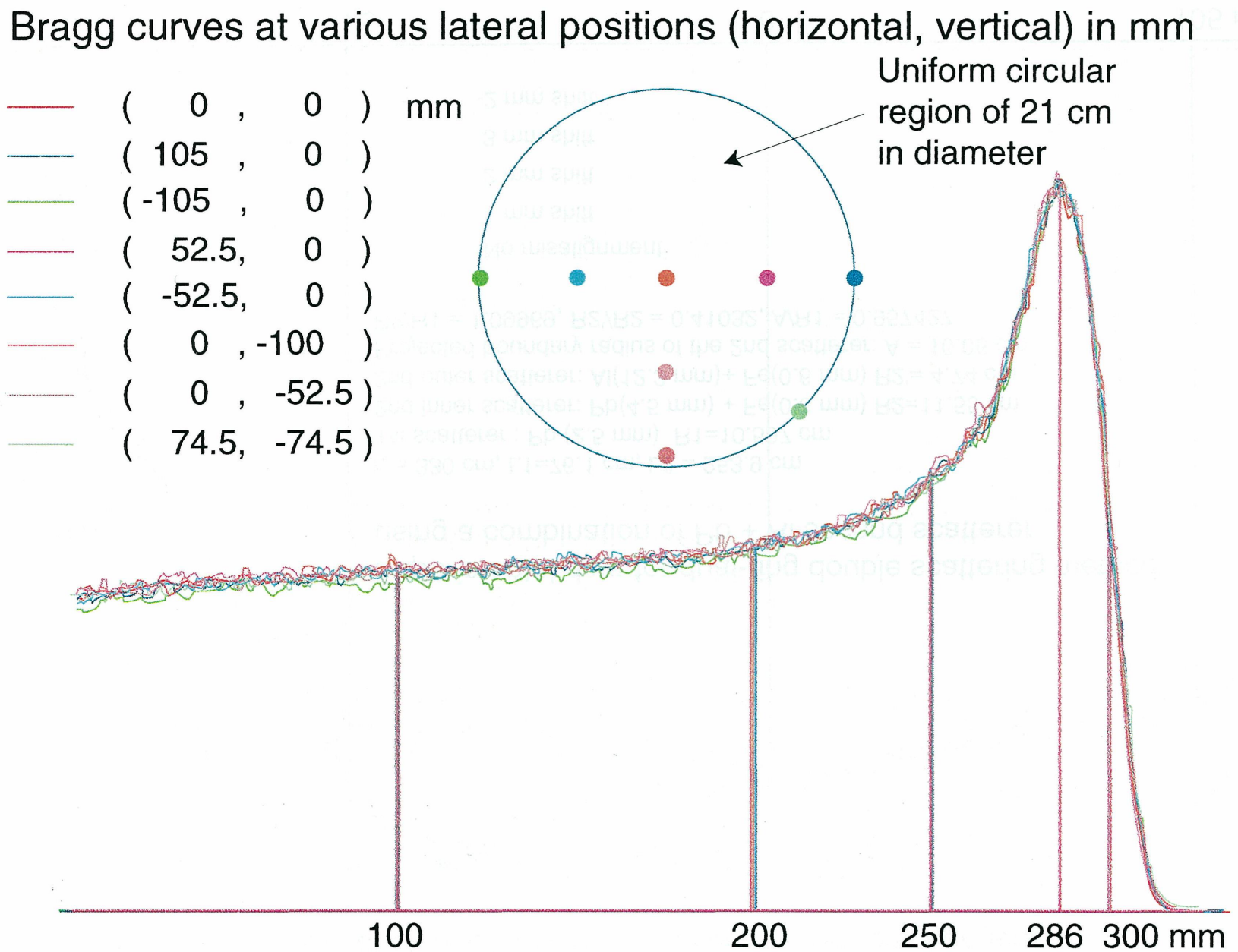
Bragg curves at various lateral positions (horizontal, vertical) in mm
(0 , 0) mm
(105 , 0)
(-105 , 0)
(52.5, 0)
(-52.5, 0)
(0 , -100)
(0 , -52.5)
(74.5, -74.5)
Uniform circular region of 21 cm in diameter
100
200
250
286
300 mm

Fig.6

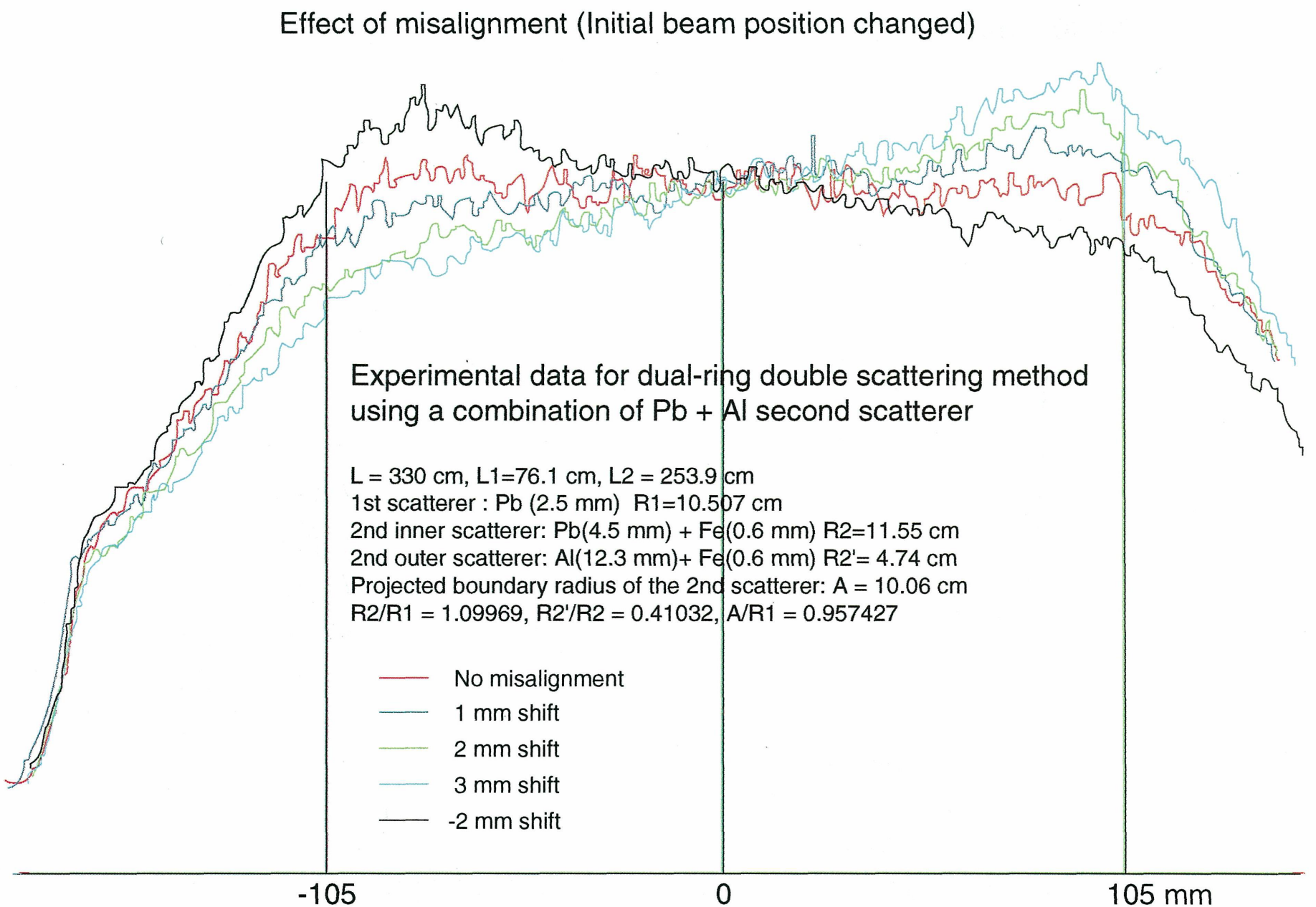
Effect of misalignment (Initial beam position changed)
Experimental data for dual-ring double scattering method
using a combination of Pb + Al second scatterer
L = 330 cm, L1=76.1 cm, L2 = 253.9 cm
1st scatterer : Pb (2.5 mm) R1=10.507 cm
2nd inner scatterer: Pb(4.5 mm) + Fe(0.6 mm) R2=11.55 cm
2nd outer scatterer: Al(12.3 mm)+ Fe(0.6 mm) R2'= 4.74 cm
Projected boundary radius of the 2nd scatterer: A = 10.06 cm
R2/R1 = 1.09969, R2'/R2 = 0.41032, A/R1 = 0.957427
No misalignment
1 mm shift
2 mm shift
3 mm shift
-2 mm shift
-105
0
105 mm

Fig.7

Comparison with the Monte Carlo simulation

Comparison of experimental data with the result of Monte Carlo simulation (L1=76.1 cm)

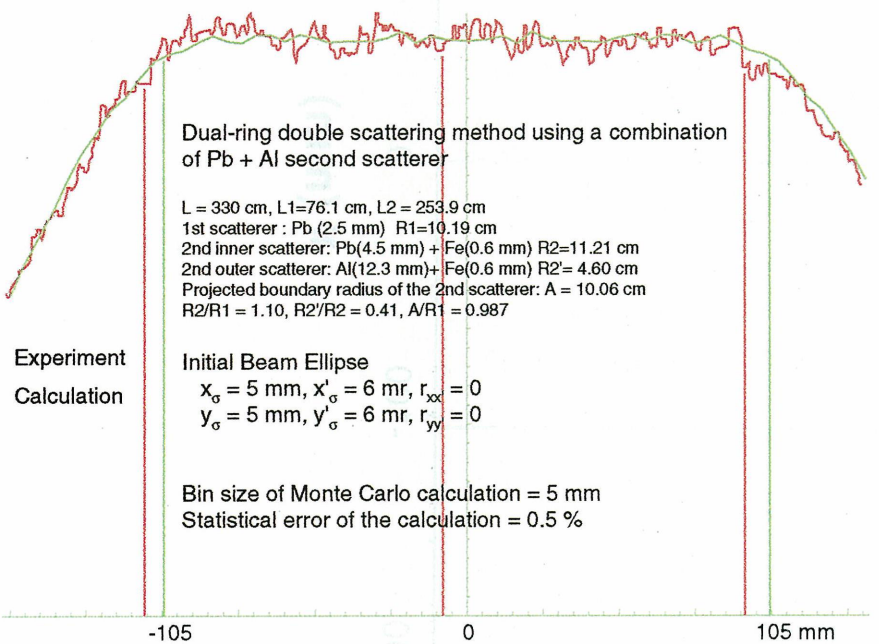

Misalignment effect of dual-ring double scattering method shift of beam center at the 1st scatterer = +3 mm

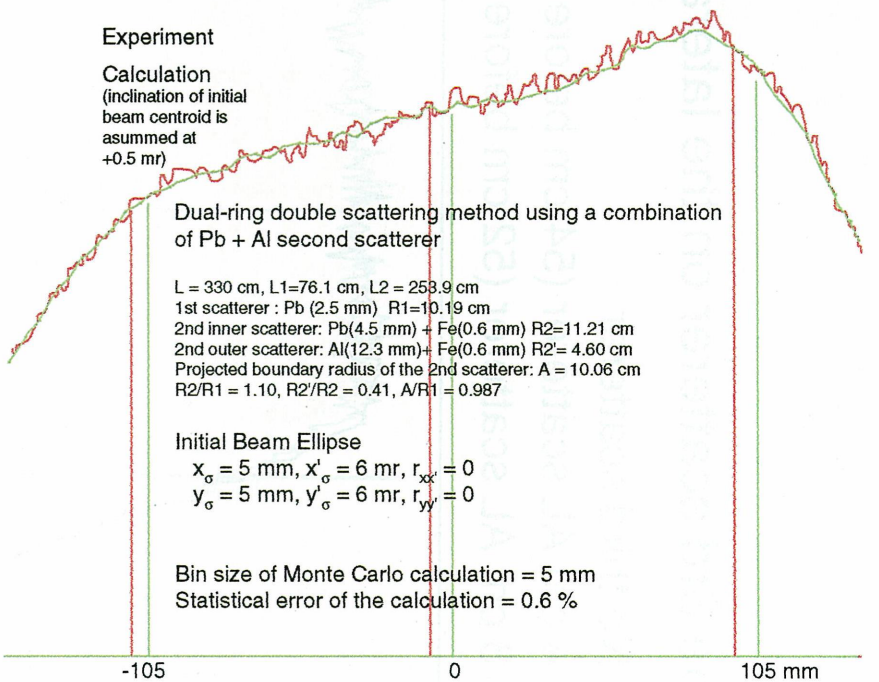

Fig.8

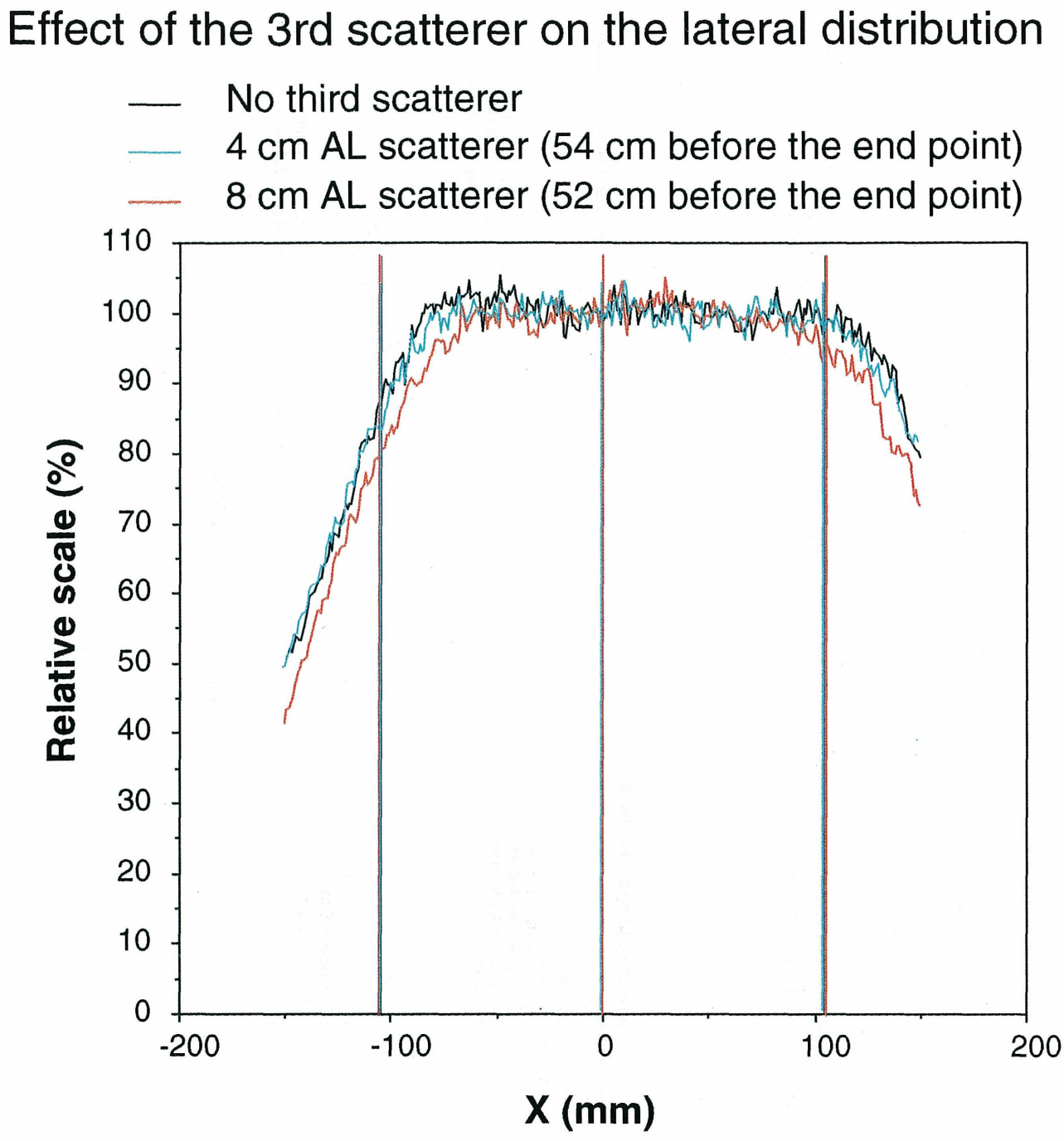
Effect of the 3rd scatterer on the lateral distribution
No third scatterer
4 cm AL scatterer (54 cm before the end point)
8 cm AL scatterer (52 cm before the end point)
Relative scale (%)
110
100
90
80
70
60
50
40
30
20
10
0
-200
-100
0
100
200
X (mm)

Fig.9

PROTON BEAMS SOLVE INVERSE PROBLEM BY HALVES

M.F.Lomanov
The Institute of Theoretical and Experimental Physics, B. Cheremuskinskaya 25, Moscow, 117259, Russia.

The objective of proton therapy is the complication-free control of tumor regression. Two approaches to this problem are possible. Usually it is a choise of the most optimal source, beam modalities and treatment technique. In contrast to this direct way, an inverse problem is based on the desirable dose distribution in patient to deduce an optimal set of irradiation conditions.

A.Brahme (1) has explained the impossibility of a general inverse problem solution. Namely, this solution needs a component with negative weighting coefficient (impossible for conventional irradiation). Our aim is to show that the use of protons and heavy charged particles nearly solves this theorem. Symbolically it is shown in Fig.1. Let A, D be input and output points of two opposite photon beams penetrating a body, and B, C be similar points at a target surface. The proton dose field ABC is equivalent to subtraction of an opposite proton field DC from the constant photon dose track ABCD. This picture can be rotated in space and it overlaps many dosimetric situations like a desired inverse problem solution.

Let us mention some practical examples of this solution. As usual, Fredholm integral equations of the first kind are used in inverse problem (2). A calculation method for ridge filter used to modify a Bragg curve in the desired depth dose distribution was developed and usually it can define the filter profile in explicit functional presentation. In this case (3) integral Volterra equation is solved, instead of many iterations or Monte Carlo calculation (both integral equations are linear, but limits are constant only in Fredholm integral).

Dose field calculation in inhomogeneous media can also be simplified. A direct solution has been made by means of Monte Carlo calculation for a long bone plate ('sliver') parallel to the beam (4).
In contrast, the inverse problem proceeds from the dose field desired, and a compensator profile could be calculated by means a corresponding Fredholm equation. For algorithm verification, we use the *axial* dose field (4) and fit some parameters of the integral equation. The equation with this fit was used to calculate transversal dose distribution which appears also in satisfactory coincidence with the Monte Carlo result (4).

From these few examples it is clear that proton beams have some new potentialities to dose planning simplification. It is not unlikely, that this kind of linearization of calculation methods can be repeated for heavy ion beams, even for study of isoeffective dose distribution.

Author wishes to thank Professor R.Martin for valuable discussion which resulted in addition remarks for this item after its oral presentation.

REFERENCES

1. A.Brahme, J.-E.Roos, I.Lax. Solution of an integral equation encountered in radiation therapy. Phys.Med.Biol. 10: 1221–1229: 1982.
2. A.Brahme, P.Kallman, B.Lind. Optimization of proton and heavy ion therapy using an adaptive inverse algorithm. Radiother.& Onc.15:189–197;1989.
3. M.F.Lomanov. A series of inverse problems in proton therapy planning (in press).
4. M.Goitein, J.M.Sisterson. The influence of thick inhomogeneities on charged particle beams. Rad.Res.74: 217–230: 1978.

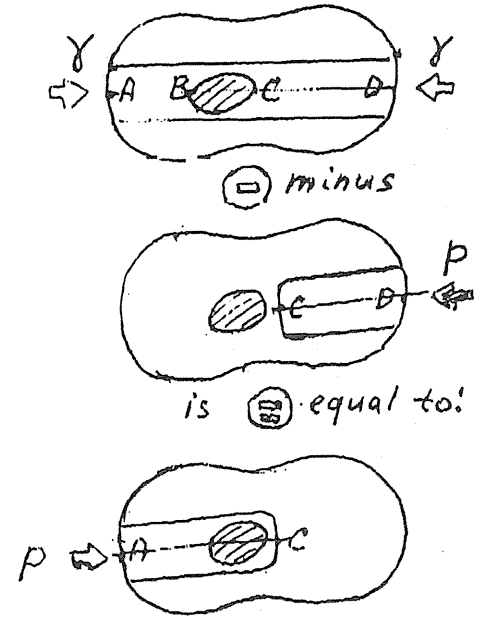

Fig.1.

The leakage of protons between plane collimator leaves in a multileaf collimator

Erik Grusell[1],Anders Montelius[2]

1. Dept. of Oncology, University Hospital, Akademiska sjukhuset, S-751 85 Uppsala, Sweden
2. Dept. of Hospital Physics, University Hospital, Akademiska Sjukhuset, S-751 85 Uppsala, Sweden

Abstract.

It is shown experimentally and theoretically that the leakage of protons between the leaves of a multiblade collimator can be reduced to acceptable levels by a proper machining of the leaves. If the opening between the collimator leaves is 20 micrometers, the maximum surface dose behind the collimator is shown to be less than 1 percent of the dose in the field under typical circumstances and never more than 9 percent. This maximum surface dose is attained in an area which is 0.5 percent of the total area covered by the collimator, and is lower at some depth in tissue because of the multiple scattering of the protons. When the treatment is fractionated, the dose from the protons leaking between collimator is spread out over a larger area and the mean dose behind the collimator is correspondingly lowered.

1. Introduction.

As protons come into routine clinical use in radiotherapy, the need arises for beam shaping devices similar to those used in photon radiotherapy, such as multileaf collimators. Different designs have been proposed to ensure that no particles can go between adjacent leaves of such a collimator, of which some examples are shown in figure 1, (Chu et al 1993). In the present investigation it is shown experimentally and theoretically that the dose behind a proton collimator made of plane leaves that are properly machined and put together can be made tolerable. It is shown that the maximum surface dose behind the interface between two collimator leaves can be kept below a few percent of the maximum surface dose. The area affected by this dose is very small compared to a normal treatment area, and during a fractionated treatment the dose will be spread out over a larger area, thus making the relative surface dose outside the treatment area even smaller.

2. Materials and methods.

One pair of collimator leaves was used in the investigation. They were made of brass, and had an extension of 60 mm, in the direction of the beam. They were machined by standard techniques to a surface flatness and roughness of better than 20 micrometers. This means that the opening between the metal blocks is less than this value.

The passage of particles between the collimator leaves was tested in a 180 MeV proton beam from the synchrocyclotron at the Svedberg laboratory. The range of these particles in brass is 39 mm (ICRU 1993). In order to make the experimental conditions as clean as possible, a broad beam was obtained with a single lead scattering foil close to the exit window, of

thickness 31 mg/cm^2. After the scattering foil the beam passed through 2 m of air and one transmission ionisation chamber.

The slit between the two collimator leaves was aligned to the centre of the area where the proton beam hit the scatterer, which was a spot of approximately 10 mm diameter as viewed on a luminiscent plate.

Dose profiles were then measured in air, 18 mm behind the surface of the collimator, with a silicon diode dosimeter, 2.5 mm in diameter, (Scanditronix, Uppsala, Sweden). This was done for different spacings between the collimator leaves. The experimental setup is shown in figure 2.

3. Theory.

Assume a broad particle beam with an angular spread of $\overline{\theta^2}$ to be incident on an opening of large length and width x between two collimator leaves. Let the extension of the collimator in the direction of the beam be t, and assume x<<t. Let Θ be the angle between the direction of motion of a particle and the beam axis, and Θ_x the projected angle on the x-z plane. Let $f_{\Theta x}$ be the probability density function of Θ_x, and assume a normal probability distribution, with mean zero and variance 0.5 $\overline{\theta^2}$. Then the probability density function of Θ_x is:

$$f_{\Theta x}(u) = \frac{1}{\sqrt{\pi\overline{\theta^2}}} \exp(-\frac{u^2}{\overline{\theta^2}}) \qquad (1)$$

The particles appearing after the collimator can, in the first approximation, be divided into three categories (see figure 3):
a) particles that do not enter the collimator opening, but pass some distance in the collimator and after that leave through the exit opening.
b) particles that enter the collimator opening and exit without touching the collimator,
c) particles that enter the collimator opening and after that pass some distance through the collimator.
The fraction of the particles that hit the entrance of the opening and pass through without hitting the collimator will be:

$$P_1(x) = \frac{1}{x} \int_0^x \int_{-\frac{s}{t}}^{\frac{x-s}{t}} f_{\Theta x}(u)\, du\, ds \qquad (2)$$

These particles will have the full energy of the beam and a narrow angular distribution. Particles from group c), i.e. particles that enter the opening and hit the collimator where the remaining distance in the collimator is less than the range, will have a lower energy than the original beam and a wider angular distribution due to multiple scattering in the collimator. Let r be the range of the particles in the collimator material. The fraction of the particles that enter the opening of the collimator and then hit the collimator wall where the distance to the downstream surface is less than r is:

$$P_2(x) = \frac{2}{x} \int_0^x \int_{\frac{x-s}{r}}^{\frac{x-s}{t-r}} f_{\Theta x}(u)\, du\, ds \qquad (3)$$

In the first approximation we assume that these particles all appear after the collimator. They will contribute to the surface dose, but due to their energy spread their number will decrease with increasing depth in the phantom, and the dose will decrease with depth also because of their angular spread.
Particles from group a) will be important only for wide collimator openings, beacause for a narrow opening they will have a large chance of hitting the opposite collimator wall before exiting. As we in this work are interested only in very narrow openings, they can be neglected.
To be able to calculate the integrals in equations (2) and (3) we must know $\overline{\theta^2}$. For the beam used in the present investigation, $\overline{\theta^2}$ can be calculated with the Fermi-Eyges transport theory (Brahme et al 1981):

$$\overline{\theta^2} = \overline{\theta_l^2} - \frac{(\overline{r\theta_l})^2}{\overline{r_l^2}} \qquad (4)$$

where

$$\overline{\theta_l^2} = \overline{\theta_0^2} + lT_{air} \qquad (5)$$

$$\overline{r\theta_l} = l\overline{\theta_0^2} + \tfrac{1}{2}l^2 T_{air} \qquad (6)$$

$$\overline{r_l^2} = \overline{r_0^2} + l^2\overline{\Theta_0^2} + \tfrac{1}{3}l^3 T_{air} \qquad (7)$$

Here $\overline{\theta_0^2}$ is the sum of the initial angular spread and the angular spread caused by the scattering foil, l is the distance from the scattering foil to the collimator entrance and T_{air} is the scattering power of air. It is assumed that there is no inital covariance of the spatial and angular distributions of the beam.

T_{air} and $\overline{\theta_0^2}$ can be calculated with the Moliére theory as given by Marion and Zimmerman. For a proton energy of 180 MeV this gives:

$$T_{air} = 4.8\ 10^{-8}\ cm^{-1} \qquad (8)$$

and $\overline{\theta_0^2} = 1.92\ 10^{-3}$ (9)

In equation (4) this gives:

$$\overline{\theta^2} = (0.0031)^2 \qquad (10)$$

4. Results.

Dose profiles measured perpendicular to the collimator slit for four different spacings are shown in figure 4. Because the detector is much wider than the distance between the collimator leaves, the narrow peak arising from protons going directly through the collimator opening cannot be resolved. As dicussed above, the detector signal arises mainly from protons from groups b and c. As the detector extension is known, the expected curve from a

narrow proton beam, i.e. protons from b can be calculated. Such a curve can be fitted to the central part of the measured curve, and in this way the contribution from these protons can be estimated. Results from this procedure are shown in table I. Because of the wide angular distribution of the protons of group a they will contribute much less to the maximum dose. As seen in table I, a maximum dose of 94 % was measured for an opening of 0.9 mm, and a dose of 29 % for an opening of 0.09 mm. With no spacers, i.e. an opening of less than 0.02 mm no measurable dose was obtained. It was estimated that an opening of 0.03 mm would have given a measurable response under the present conditions. It is seen that the measured values agree well with those calculated from the model presented above.

Table 1

distance between collimator leaves (mm)	measured relative penetration through opening	calculated relative penetration through opening
0,18	0,57	0,49
0,09	0,32	0,27
0,05	0,13	0,14
<0,020	<0,05	<0,06

5 Discussion.

It is shown above that the theoretical model presented in this report gives a good agreement with measured values of the dose of protons penetrating through a long and narrow opening in a collimator. By proper machining of the metal leaves of a multileaf collimator, it is possible to achieve a planeness which gives a maximum opening between two leaves of better than 20 micrometers over an area large enough for this purpose. As a worst case, we assume that the beam is monodirectional when exiting the vacuum and that it passes through 1 m of air. The angular spread of the beam at the collimator calculated from equation (4) is then:

$$\overline{\Theta^2} = (0.0021)^2 \qquad (10)$$

The penetration P_x through an opening of 20 micrometer in a 60 mm long collimator will then be given by equation (2), which with these values gives $P_x = 0.09$, i.e. a maximum of 9 % of the surface dose given in the treatment area can be expected behind the collimator. When it is considered that this is given to a 20 micrometer wide strip corresponding to 0.4 % of the total area behind a collimator blade of 5 mm width, it is clear that the effect of this dose is negligible. Furthermore, such a narrow beam will be quickly spread out by multiple scattering when passing through tissue, reducing the maximum dose below the surface even further. For fractionated treatments, it is unlikely that any given surface area will be affected more than during one fraction, so that the total dose increase to any surface element will be considerably lower than 9 %.

6. Conclusion

It is shown that by machining the collimator leaves to a surface planeness of 20 micrometers, the penetration of protons between the leaves of a multileaf collimator gives a negligible dose outside the treatment area.

REFERENCES

Chu W T Ludewigt B A and Renner T R 1993 Instrumentation for treatment of cancer using proton and light-ion beamsUniversity of California report no LBL-33403 UC-406

ICRU International Commission on Radiation Units and Measurements 1993. Stopping Powers and Ranges for Protons and Alpha Particles. Report ICRU 49. ICRU, Bethesda, MD.

Brahme A, Lax I and Andreo P 1981. Electron beam dose planning using discrete gaussian beams Acta Rad. Onc. 20 147-58

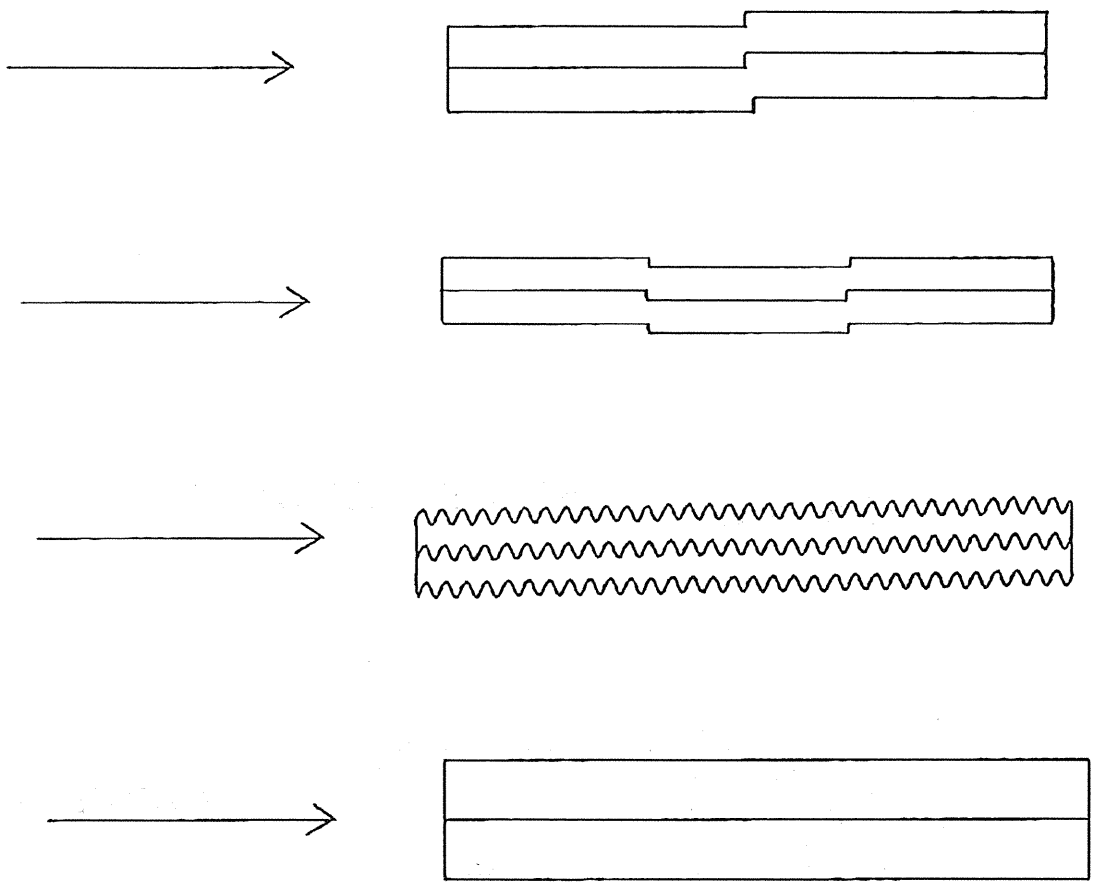

Figure 1

Different designs of the interface between adjacent collimator leaves.

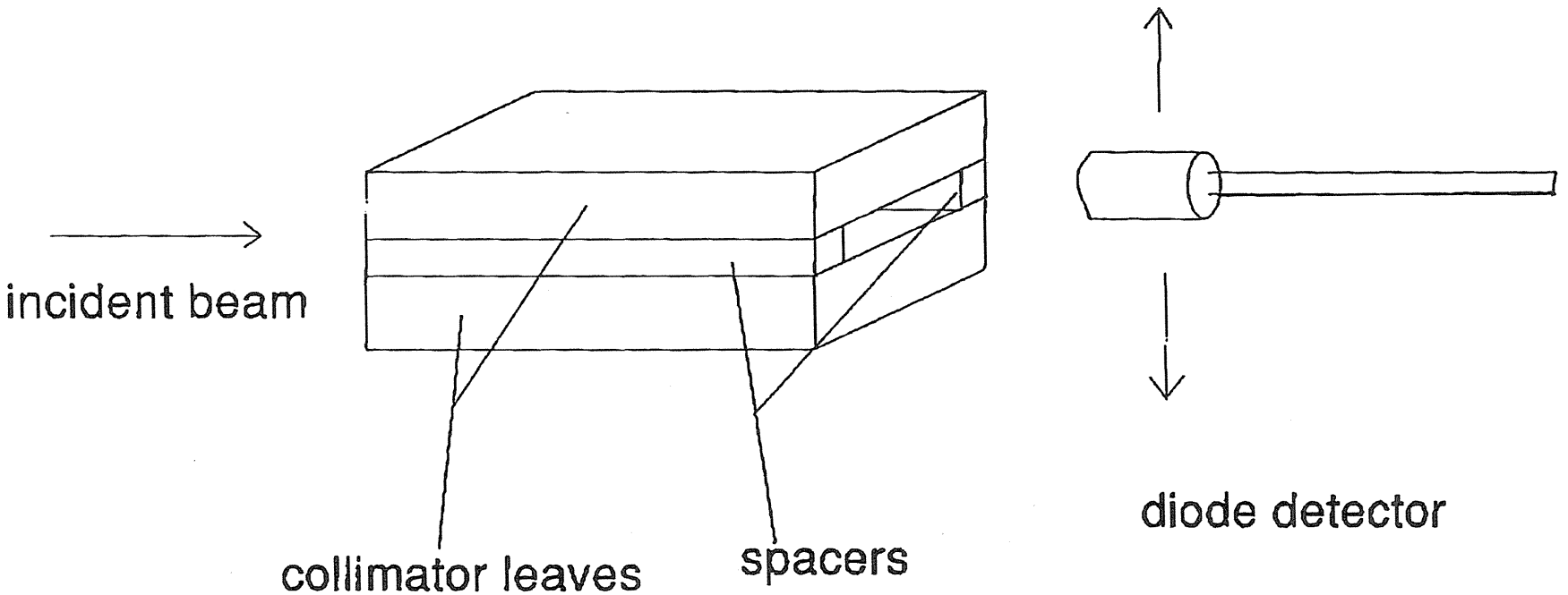

Figure 2

Schematic drawing of the experimental setup

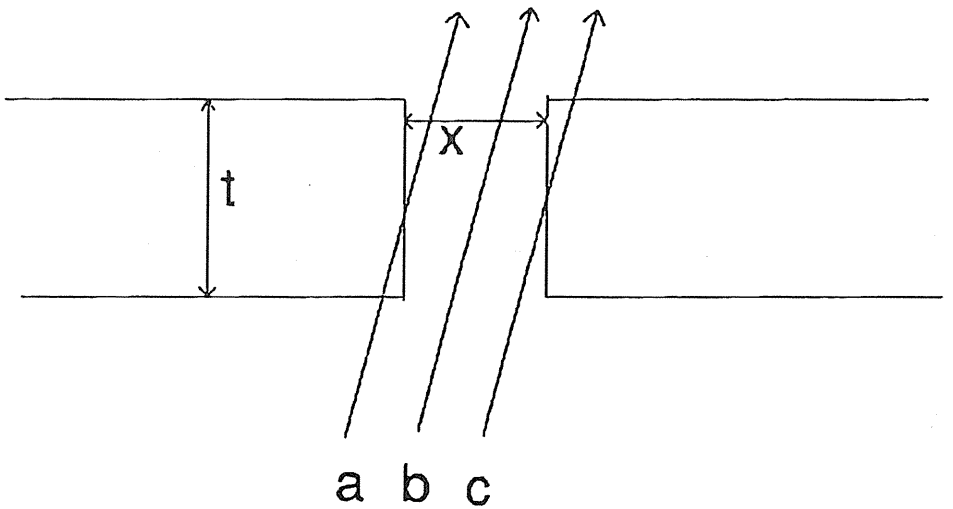

Figure 3

The main possibilities for a particle to penetrate the collimator

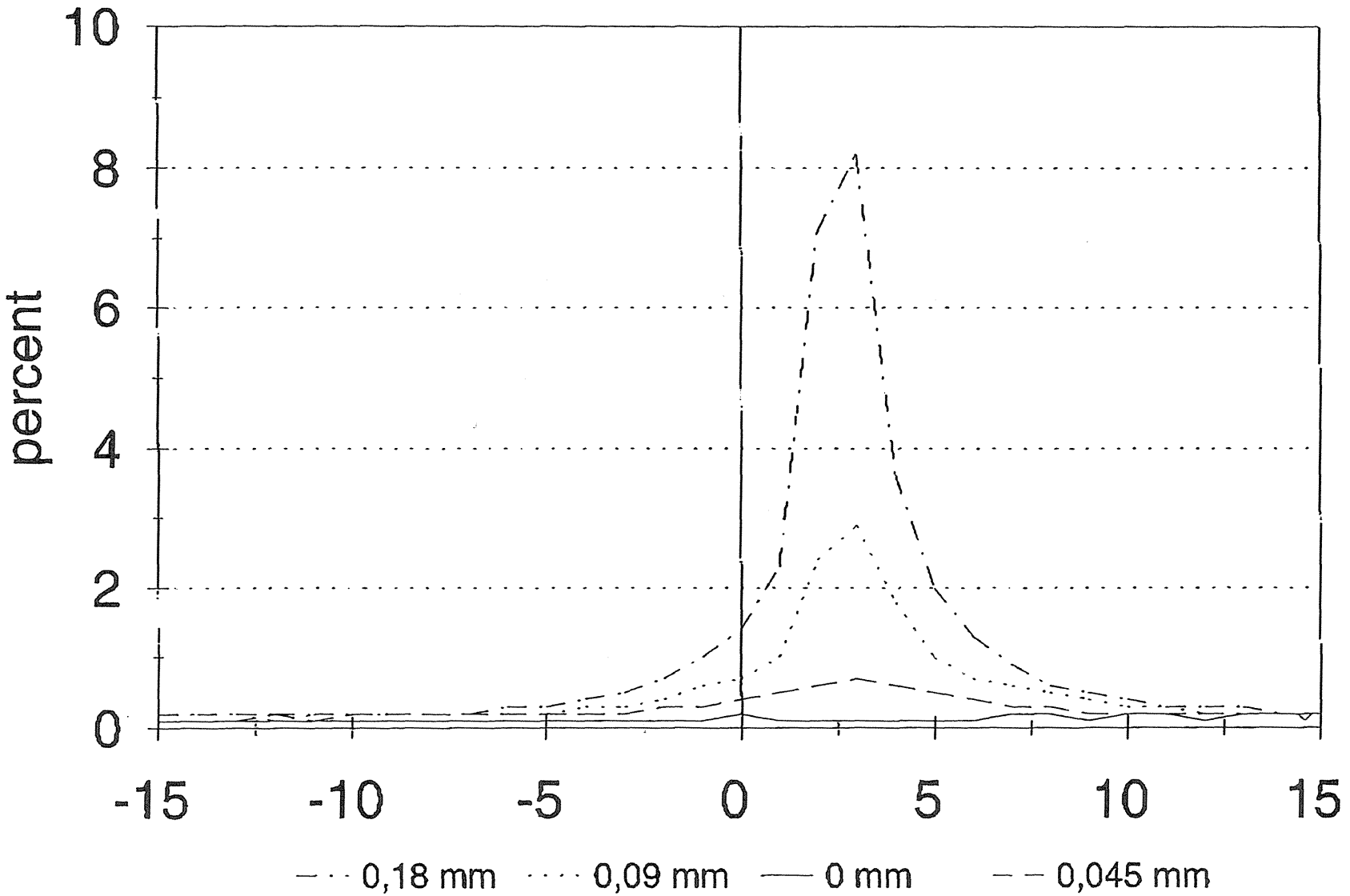

Figure 4 Measured profiles behind different collimator opening widths

PRELIMINARY MEASUREMENTS OF AUTO ACTIVATION OF ^{12}C BEAMS WITH A COMMERCIALLY AVAILABLE PET

TAKEHIRO TOMITANI, PH.D., KYOSAN YOSHIKAWA M.D., PH.D.†,
MITSUTAKA KANAZAWA, PH.D.‡, YASUHIRO WADA, B.A.* TATSUAKI KANAI, PH.D.‡

Division of Physics, Division of Radiation Medicine,† Division of Accelerator Research‡,
National Institute of Radiological Sciences, Chiba, Japan
Nuclear Product Group*, Siemens-Asahi Medical Technologies Ltd., Tokyo, Japan

Purpose: **In the heavy ion therapy, some of projectiles undergo fragmentation when they penetrate through target materials. Of these fragments, those deficient of neutrons will become positron emitters. Positron emitters can be measured non-destructively with positron emission tomography (PET) technique. What can be measured with PET is the distribution of the end points of positron emitting fragments that is broadened compared to that of primary particles. The yield of positron emitters is low due to low cross sections. The purpose of the present work is to investigate the broadening of end point distribution and the quality of the PET image of the activity generated by therapeutic dose.**

Methods and Material: **To separate various positron emitting isotopes of a variety of half lives, time spectra were measured with a time analyzer. To measure the end point distribution of ^{11}C, a polyethylene cylinder was irradiated with 290 MeV/u ^{12}C beams and the three-dimensional distribution was measured with a commercially available PET in an off-line way.**

Results: **From the time analyses of the activities, it turned out that activities exept ^{11}C decay away within 5 minutes after irradiation. The broadening of the end point distribution of ^{11}C was measured without ridge filter. The spatial spread was consistent with the distribution calculated from semi-empirical formula of fragmentation cross sections within the uncertainty due to the spatial resolution of PET. The effect of the primary beam broadening on the image quality was tested with ridge filters under the therapeutic irradiation condition. In spite of very poor statistics, the distribution forms distinct peak owing to the very high target to background contrast.**

Conclusion: **To separate ^{11}C activity from other positron emitting isotopes, we have to wait about 5 minutes after irradiation. The measurements on the auto activity, ^{11}C, in polyethylene target produced by ^{12}C beams revealed that the spatial resolution is 8~9 mm FWHM in a plane perpendicular to the beam direction, while that in the beam direction is further blurred by the spatial spread due to the variation of residual range of fragment which is dependent on the reaction point.**

Heavy ions, fragmentation, auto activation, PET.

INTRODUCTION

Heavy ions undergo fragmentation reactions on their passage through matter. Among various isotopes generated by fragmentation reaction, positron emitters are useful, since their distribution can be measured with positron emission tomography (PET) technique (1, 2). There are two types of fragmentation reactions, i.e., projectile fragmentation and target fragmentation. As to the projectile fragmentation, the velocity of the former almost remains unchanged through fragmentation reaction and hence projectile fragments have considerable residual range after fragmentation. Since the range of the secondary particle depends on the interaction point, the end points of positron emitters are dependent on the interaction positions.

Since target fragmentation is the reverse reaction of the projectile fragmentation, the velocity of the target fragment is close to that of the target nuclei and is almost zero, and hence the end points of this type of fragments are very close to the reaction points. Target fragments distribute from the entrance to the proximity of the end points of projectiles. The distribution of projectile fragments is limited in space and forms a peak of finite width so that it gives us some sort of information about the distribution of end points of projectiles.

The purposes of the present study are 1) to find out minimum time needed to cool down various positron emitting isotopes except ^{11}C, 2) to test the spatial spread of positron emitting projectile fragments in three dimensions in conjunction with the finite PET spatial resolution and 3) to see if the quality of the PET image obtained by therapeutic dose is useful in practice. The latter point is important, since fragmentation cross sections are of the order of 50 mb and the yield of positron emitters is low.

Table 1. Positron emitters generated from ^{12}C projectiles. In the third column, fragmentation cross sections are indicated as a measure of relative yield. In the cases of ^{11}C, ^{10}C, ^{9}C and ^{8}B, ^{12}C target is assumed with projectile energy of 100 MeV/u, while in the cases of ^{15}O, ^{14}O, ^{13}N and ^{12}N, ^{16}O target is assumed with the projectile energy of 100 MeV/u. In the latter case, the values were calculated from the reverse reactions.

Isotopes	Half lives	Cross sections (mb)
^{11}C	20.34 m	54
^{10}C	19.5 s	2
^{9}C	0.127 s	0.6
^{8}B	0.77 s	1.5
^{15}O	123 s	69
^{14}O	70.9 s	3
^{13}N	9.96 m	7
^{12}N	0.011 s	0.7

In the therapeutic study of HIMAC (Heavy Ion Medical Accelerator at Chiba)(3), ^{12}C beams were adopted. Therefore the discussions hereafter will be limited to the auto activation of ^{12}C. Possible positron emitters generated from ^{12}C projectiles through projectile fragmentation reactions and those generated from O in the target are shown in the first column of Table 1. Their half lives are listed in the second column of the table. Partial fragmentation cross sections at 100 MeV per nucleon are shown in the third column of the table as a measure of relative yield. The calculation of the partial fragmentation cross sections is based on the semi-empirical formula presented by L. Sihver et al. (4). At this energy range, the cross sections are almost constant.

METHODS AND MATERIALS

Time spectrum measurements

Various positron emitters are produced simultaneously through projectile fragmentation reactions. It is evident from Table 1 that among various positron emitters, only ^{11}C remains after 5 minutes from irradiation, since other positron emitters have shorter half lives. Preliminary experiments were performed with a polymethyl methacrylate block of 5 cm wide x 8 cm high x 10 cm deep irradiated with ^{12}C beams. Pair gamma rays were measured with a pair of BGO(Bismuth Germanate, $Bi_4Ge_3O_{12}$) detectors in coincidence. Data were recorded with a time analyzer. Typical time spectrum is shown in Fig. 1. By inspection, there are at least three components. The component of the longest half life apparently corresponds to ^{11}C ($\tau_{1/2}$ = 20.34 minutes). Other components decay away within 5 minutes after irradiation and this experimental data proves the above statement. The above statement was also confirmed by the non-linear regression analysis of the intensity of various positron emitting isotopes. Different isotopes of the same energy per nucleon have different range, so that, to measure the spatial distribution, it is necessary to distinguish isotope species. From the above preliminary experiment, we have to wait at least 5 minutes before the measurements. This inevitable time allows us off-line measurements in the sense that first we irradiated the sample and then carry it to PET locating remote to the experimental vault. The off-line method allows us the use of commercially available PET devices. In applying the off-line method to biological object, metabolism of the positron emitters in living objects must not be involved. This problem will be discussed later.

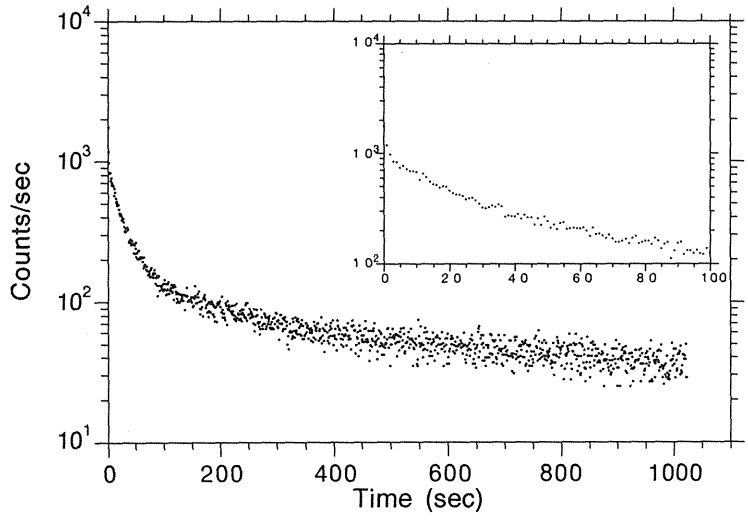

Fig. 1. Time spectrum of various positron emitters and the portion of time spectrum up to 100 seconds is enlarged in the inset.

Calculation of spatial distribution of ^{11}C

The distribution of ^{11}C end points in the beam direction was calculated using semi-empirical reaction cross section formula presented by L. Sihver, C. H. Tsao, R. Silberberg and T. Kanai (4). In the calculation, an energy degrader of 8 cm thick made of polymethyl methacrylate and a target of 7.5 cm thick made of polyethylene were assumed. In the calculation, primary beam attenuation and the secondary beam attenuation were taken into account, but the energy loss associated with the fragmentation reaction and the momentum spread in the beam direction were not taken into account. As to the former, Q-value is ~19 MeV and the error is about 0.6 % of the total energy of ^{11}C, 3.2 GeV. Hence the former factor may be negligible in the present case. As to the latter, the momentum spread in the beam direction can be estimated with the double differential cross section formula in eq.(1) cited from reference (5), that is,

$$\frac{d^2\sigma}{dEd\Omega} = C(\mu_f E_f)^{1/2} \exp\left\{-\mu_f\left(\frac{E_f \sin^2\theta}{\sigma_t^2} + \frac{E_f \cos^2\theta - 2(E_f\bar{E})^{1/2}\cos\theta + \bar{E}}{\sigma_p^2}\right)\right\}, \quad (1)$$

in which C is the normalization constant and μ_f, E_f and $\bar{E}$ are the mass, the kinetic energy and the most probable energy of the fragment, respectively. θ is the angle in laboratory system. σ_t and σ_p are the momentum spread in the direction tangential and parallel to the beam, respectively. From this formula, the energy spread due to fragmentation reaction turned out to be 2%. While spatial spread due to straggling was estimated to about 0.5 mm in the beam direction with eq.(2) cited from reference (6) and is negligible in the present situation.

$$\sigma_s = 0.0120\frac{R^{0.951}}{\sqrt{A}} \quad (2)$$

As to the momentum spread in the direction perpendicular to the beam direction can be estimated with eq.(1) and the angular spread was estimated to be 1.7° (FWHM) and the maximum deviation in the direction perpendicular to the beam direction is 150 mm times tan(1.7°) = 4.5 mm (FWHM). While, spatial spread due to multiple scattering in the direction perpendicular to the beam direction was estimated to about 1 mm from eq. (3) cited from reference (6) is negligible in the present situation.

$$\sigma_m = \frac{0.0294\, R^{0.896}}{Z^{0.207}\, A^{0.396}} \quad (3)$$

The calculated ^{11}C distribution of projectile fragments and target fragments is shown in Fig. 2.

Experimental setup of ^{12}C irradiation

Experimental setup of the irradiation used in the measurements of spatial distribution of ^{11}C fragments is schematically shown in Fig. 3. Polyethylene cylinder of 15 cm dia. x 10 cm long was irradiated, then the sample was transported to PET facility and ^{11}C activity distribution was measured with a PET.

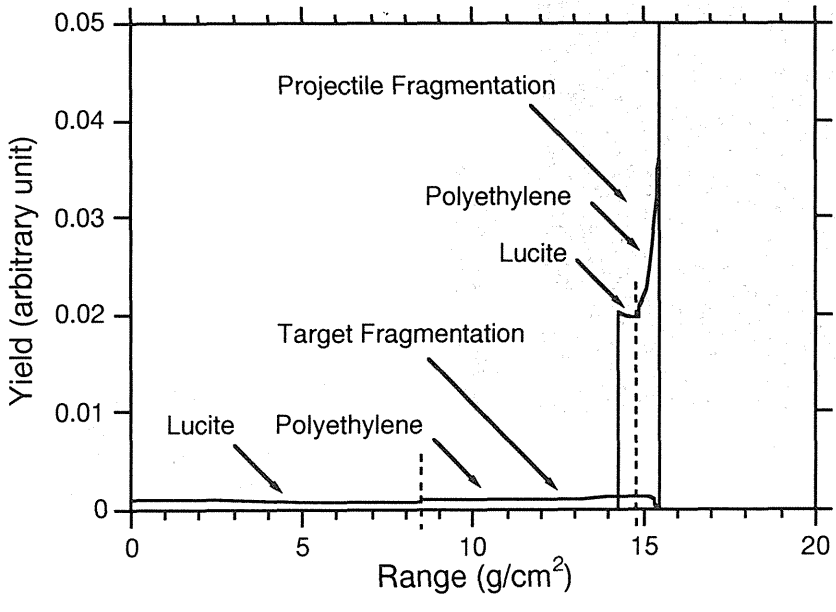

Fig. 2. Distribution of ^{11}C generated in the energy degrader and the polyethylene target.

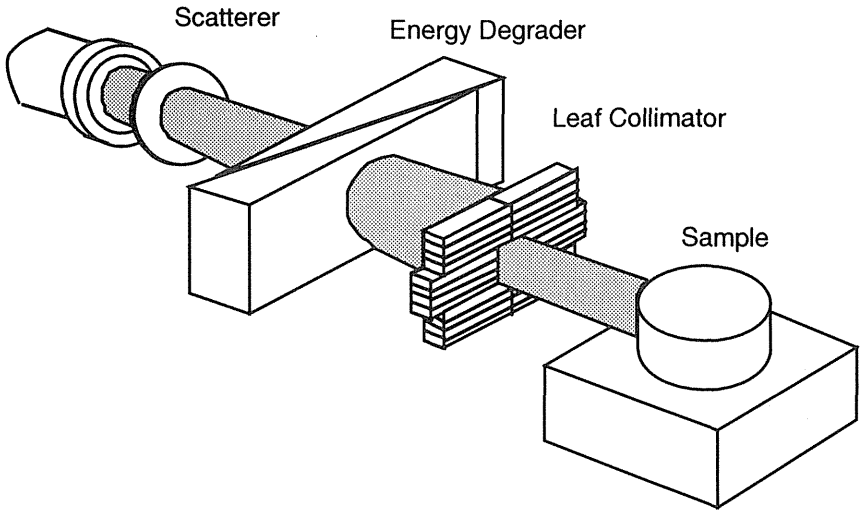

Fig. 3. Schematic drawing of experimental setup of auto activation measurement.

Transportation took about 5 minutes, which is in accordance with the above condition. Projectiles are ^{12}C 290 MeV/u (nominal). Primary beams were broadened in the direction perpendicular to the beam direction with a wobbler and further broadened with a Tl scatterer of 0.6 mm thick and a wobbler. The residual range of projectiles at the entrance of energy degrader is 14.5 cm in water. The beams were collimated to 1 cm wide x 1.3 cm high with a leaf collimator system. Aperture of the leaf collimator is adjusted continuously in one direction, while it is adjustable by 6.5 mm step in other direction. Energy degrader consists of two polymethyl methacrylate blocks of wedge shape. Its effective thickness is adjustable continuously. In addition to these, ridge filter was added to spread out the Bragg peak when volume irradiation was necessary.

PET nominal specification

The PET device used in the measurement is the model ECAT/EXACT 47*. Its transverse axial resolution is 6 mm FWHM at the center of field of view that degrades to 6.3 mm FWHM at 10 cm from the center. Its axial resolution is 5.4 mm at the center that degrades to 6.3 mm FWHM at 10 cm from the center. The device nominal sensitivity is 220 K cps/(μCi/ml in 20 cm dia. water cylindrical phantom of sufficient axial length). The spatial resolution deteriorates to 8~9 mm FWHM when HANN reconstruction filter is applied.

---

* Made by Siemens Gammasonics, Inc.

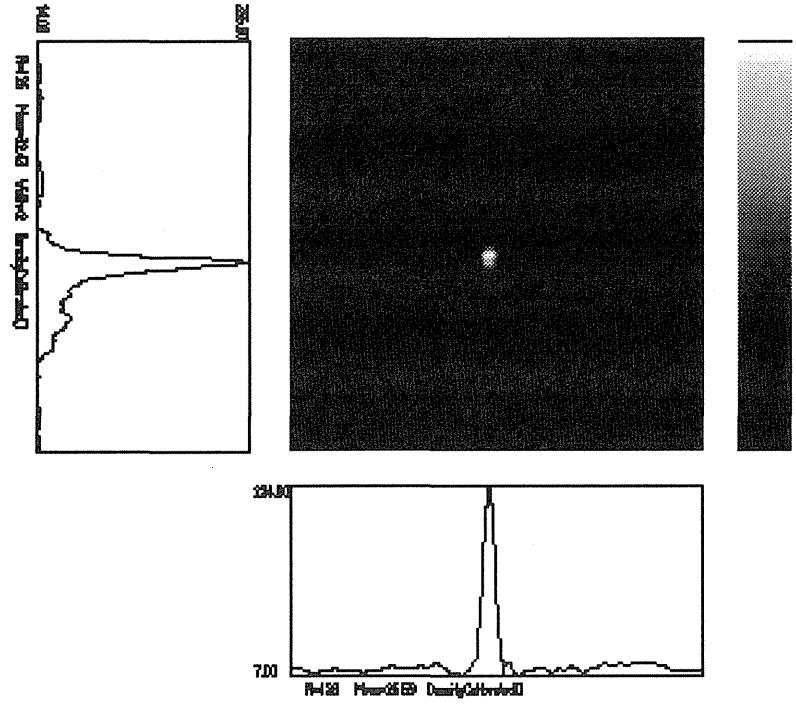

Fig. 4. ^{11}C distribution measured with PET in the polyethylene cylinder irradiated with 8 Gy of ^{12}C beam. Ridge filter was not set in.

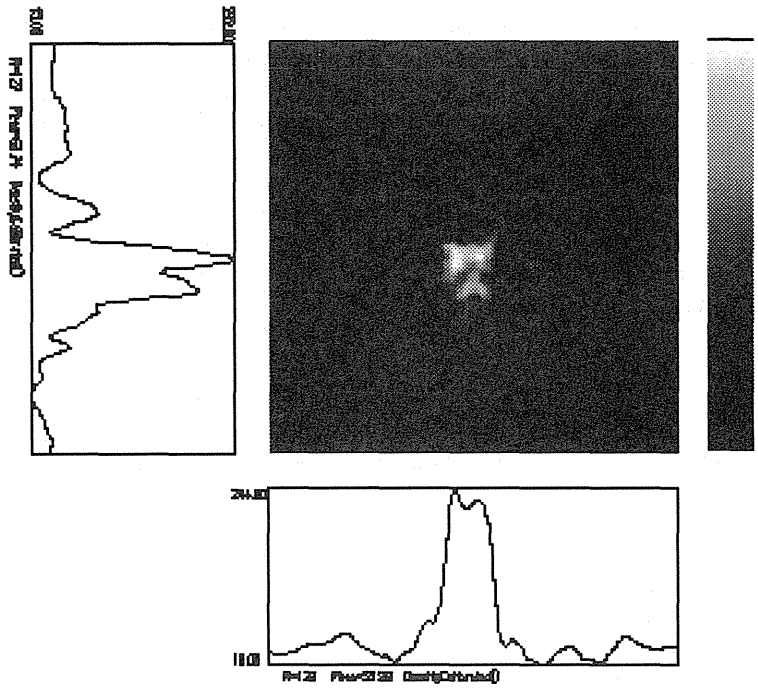

Fig. 5. ^{11}C distribution irradiated with 1.24 Gy of ^{12}C beam, which is one fractionation dose of the current therapeutic schedule. Ridge filter of 4 cm thick was set in.

Spatial distribution of ^{11}C generated from ^{12}C

To compare the above calculation, the distribution of ^{11}C in the polyethylene cylinder irradiated with 8 Gy of ^{12}C beam was measured with PET and the result is shown in Fig. 4. The ridge filter was not set in. Here 'dose' was defined as the one at the surface of the cylinder, since dose distribution without a ridge filter is strongly dependent on the spatial point along the beam direction. In this experiment, leaf collimator aperture was set to 1 cm x 1.3 cm. The beams are incident from the bottom to the top of the figure. The measurement time was 40 minutes. HANN filter was used in the reconstruction process.

To test the image quality under practical therapeutic condition, the distribution of ^{11}C in the same cylinder irradiated with 1.24 Gy of ^{12}C beam was measured and the result is shown in Fig. 5. This amount is one fractionational dose of the current therapeutic schedule. The beams are incident from the bottom to the top of the figure. Leaf collimator aperture was set to 4 cm x 4 cm. 4 cm thick ridge filter was set in. The measurement time was 40 minutes. HANN filter was also used in the reconstruction process.

RESULTS AND DISCUSSION

The profile along the beam direction of the measured ^{11}C distribution shown in the left side of Fig. 4 should be compared with the distribution calculated with the semi-empirical formula shown in Fig. 3. The component due to projectile fragmentation forms a peak with the spatial spread ~1.9 cm, which is roughly consistent with the theoretical value of 1.3 cm, if one takes account of the fact that the spatial resolution of PET in this direction is 0.8 cm FWHM with HANN reconstruction filter. The component due to target fragmentation is apparently seen in the figure. The ratio of it to the peak is rather higher than the estimated value. This might be due to the smearing effect of the finite spatial resolution of PET.

From the profile along the direction perpendicular to the beam direction shown in the lower part of Fig. 4, the spatial spread is about 1.6 cm, which is consistent with the leaf collimator aperture of 1.3 cm along with the spatial resolution of PET of 0.8 cm FWHM.

The yield of auto activity resulted from therapeutic dose, i.e., 1~2 Gy is of the order of 10 nCi/cm^3 and the measured events were ~5,000. This number should be compared with the number of events in PET images for diagnostic purposes, in which usually the number of events is of the order of 10^5 to 10^6. In spite of poor statistics, we can definitely see the distribution. The reason is high target/non-target contrast. In the case of diagnostic PET imaging, considerable fractions of pharmaceuticals remain in the blood volume as well as non-target tissues. On the other hand, in the case of auto activation, since positron emitters are almost concentrated around the therapeutic target volume, the activities in the non-target region are essentially zero and so target/non-target contrast is quite high. In spite of this, PET image quality is rather poor due to too few events. The applicability of this method to clinical purpose must be further examined carefully.

The yield of auto activation can be increased by raising primary particle energy, but the spread of end points also increases. With 290 MeV/u ^{12}C beams, the spread of ^{11}C in the beam direction is 1.3 cm. There might be some energy at which the yield and the spatial spread might be traded off.

The improvement of PET detection efficiency also increases the number of events. The PET device used in this experiment consists of a stack of ring detectors with cross coincidence facility with the adjacent rings and septa shields among the rings is incorporated so as to limit coincidence angle. In the case of PET called 'true three-dimensional PET,' septa shield is retractable and all possible coincidence pairs among rings are recorded. The efficiency can be increased by about a factor of 8 at a cost of the increase in scattered ray coincidence as well as chance coincidences. There are some technical difficulties in the image reconstruction algorithms and the reconstruction of images takes a hundred times more computation time. This difficulty is lessened in the present application, since the activity distribution is limited in space and target/non-target contrast is quite high and one can restrict the reconstruction field to smaller volume without any serious problems. Chance coincidence events can be eliminated by separate measurement facility but surely the subtraction of chance coincidence from prompt coincidence deteriorates statistics. This problem does not affect much in the application to auto activation measurements, since event rate is very low. A real problem associated with this technique is the increase of scattered ray coincidences. There are means to correct for scattered ray coincidences in the case of multi-stack of two dimensional rings, but, in the case of 'true three-dimensional PET,' the situation is much more complex and serious artifact may occur, since the correction algorithm deals with the low frequency components. This argument also holds for the application to auto activation measurement.

Chemical form and physiology of the auto activity inside the body are not known, however ^{11}C beams themselves damage tissues around their end points due to high LET and the clearance of ^{11}C may be different from that in normal tissue, with the exception that ^{11}C will come to stop inside blood vessels or blood pools. Roughly speaking, blood fraction by weight inside ordinary tissue may be ~10%. This fraction may be washed out in short time. This hypothesis must be examined by experiments on animals.

CONCLUSION

The possibility to use commercially available PET device to the measurements of the ^{11}C fragment induced by ^{12}C beams was tested. Due to low yield of fragmentation reaction, number of measured events were low. In spite of this, the distributions of ^{11}C can be clearly seen in the reconstructed image due to good target/non-target contrast. Nevertheless, quantification of the distributions of such poor statistics seems difficult and the applicability of the present method may be limited to the verification of positioning of the beams. Metabolism of induced ^{11}C in the target volume must be studied in order to apply the off-line method to clinical purposes.

REFERENCES

1. Enghardt, W.; Frommt, W.D.; Geisserl, H., Keller; H.; Kraft, G.; Magel, A.; Manfrass, P.; Munzenberg, G.; Nickel, F.; Pawelke, J.; Schardt, D.; Scheidenberger, C.; Sobiella, M. The spatial distribution of positron emitting nuclei generated by relativistic light ion beams in organic matter. Phys. Med. Biol. 37:2127-2131, August, 1992.
2. Tomitani, T.; Sudo, M.; Minohara, S.; Kohno, T.; Takada, E.; Sato, Y.; Kanai, T. Measurement of the distribution of auto activation in Lucite block. Proceedings of the Second Workshop on Physical and Biological Research with Heavy Ions, NIRS-M-90/HIMAC-003, pp.7-8, 1992.
3. Hirao, Y.; Ogawa, H.; Yamada, S.; Sato, Y.; Yamada, T.; Murakami, T.; Kitagawa, A.; Sato, K.; Itano, A.; Kumada, M.; Takada, E.; Kanazawa, M.; Noda, K.; Sudou, M.; Kawachi, K.; Soga, F.; Endo, M.; Kanai, T.; Minohara, S.; Koyama-Ito, H.; Kohno, T. Heavy ion medical accelerator in Chiba - A design summary and update-. NIRS-M-89, HIMAC-001, December, 1992.
4. Sihver, L.; Tsao, C. H.; Silberberg, R.; Kanai, T. Barghouty, A. F. Total reaction and partial cross section calculations in proton-nucleus ($Z_t \leq 26$) and nucleus-nucleus (Z_p and $Z_t \leq 26$). Phys. Rev. C 47:1225-1236, 1993.
5. Morjean, M.; Charvet, J. L.; Uzureau, J. L.; Patin, Y.; Peghaire, A.; Pranal, Y.; Sinopoli, L. Nuclear fragmentation processes in the $^{20}Ne+^{27}Al$ system at 30 MeV/A. Nucl. Phys. A438:547-563, 1985.
6. Tobias, C.A.; Fabrikant, J.I.; Benton, E.V.; Holley, W.R. Projection Radiography and tomography in 'Biological and medical research with accelerated heavy ions at the BEVALAC 1977-1980.' LBL-112200, 1980, pp.335-346.

Current status of clinical trials at PMRC, Tsukuba

Toshiyuki Okumura, Hiroshi Tsuji, Toshiya Chiba, Hirohiko Tsujii, Yuji Itai, Proton Medical Research Center (PMRC), Tsukuba, Ibaraki, Japan

The clinical trial of cancer treatment using 250MeV proton beams at PMRC has been conducted as extensively as ever. A total of 329 patients had received proton therapy as curative treatment until July 1994. Regarding current trend of treatment at PMRC, the increase of the number of treatment for primary liver cancer has been prominent in recent years.

We started our clinical study of proton therapy for primary liver cancer, that is hepatoma, in 1983 using very big treatment dose(70-85Gy/16-24fractions). Concerning irradiation technique, we developed the respiration-gated irradiation system(ReGIS), which is routinely used now, to minimize the irradiated volumes of the liver and to avoid bowel complications.

A total of 81 patients with hepatoma had undergone curative proton therapy by the end of 1993, and were followed up for more than 6 months. The preliminary result of the treatment for hepatoma is excellent and the number of patients has been increasing year by year. The local control rate of treated tumors is almost 90%(72/81) and no patients developed symptomatic radiation hepatitis or radiation-induced hepatic failure. The survival rate of our patients, despite including many inoperable ones, is comparable to that of patients treated surgically.

Successful results were not obtained only in hepatoma, but also in many other cancers, such as cancer of bladder, lung, esophagus, and so on.

Proton Therapy and Facility

Emerging International Consensus on Proton Dosimetry

Lynn J. Verhey, Ph.D.
University of California, San Francisco
Paper presented at PTCOG XXI in Chiba, Japan November, 1994

There is general agreement on the need for an international consensus on proton dosimetry. This need was recognized by the ICRU when they formed the Report Committee on Proton Dosimetry which is now in the final stages of report preparation. This Report will promote uniformity of standards for proton dosimetry which will provide a basis for comparison of clinical results and allow the development of meaningful multi-institutional clinical trials.

The timing of this Report coincides with increasing interest in the use of protons for clinical radiotherapy. Fortunately, it also coincides with an emerging international consensus on dosimetry techniques and on the values of most of the required dosimetric parameters. This presentation summarizes that emerging consensus and presents the broad outline of the recommendations of the forthcoming ICRU Report on Proton Dosimetry.

It is generally agreed that routine proton dosimetry will be based on the use of small, air-filled, tissue-equivalent ionization chambers, since these are generally available at all facilities and can be easily calibrated in a Co-60 beam by national standards laboratories. The absorbed dose should be determined in water or in a water-like phantom and specified to water. When possible, proton calibration factors which are obtained from Co-60 calibration factors, should be verified with more direct dosimetry techniques such as water calorimetry.

The proton-specific dosimetry factors which are needed to calculate the proton calibration factor, are the mass stopping power ratio from water to air and the w-value for protons in air. Although both these factors could be energy-dependent, an average value for therapy energies can be defined. The recommended mass stopping powers for protons are found in ICRU Report 49 (1993), entitled "Stopping Powers and Ranges for Protons and Alpha Particles". The w-value for protons is still under review by the ICRU Report Committee on Proton Dosimetry. The existing ICRU recommendation was presented in ICRU Report 31 (1979) based on an average of measurements at energies less than 2 MeV. That value was 35.2 J/C +/- 4%. Recent measurements have been performed at more relevant proton energies of from 20 MeV to 250 MeV and the resulting values for w-value span the range from 34.3 to 35.6 J/C, with an average of approximately 34.8 J/C +/- 2%. These new measurements of w-value, will allow us to recommend a new w-value with reduced uncertainty compared to the existing value.

The forthcoming ICRU Report on Proton Dosimetry will recommend a dosimetric technique and values for dosimetric factors which will be the basis for an international consensus on proton dosimetry. This consensus will allow proton facilities around the world to compare clinical results and to join together in clinical trials. If these clinical trials permit varying combinations of photons and protons, agreement on a single clinical value for RBE (relative biological efficiency) of protons relative to photons, must also be reached.

COMMISSIONING THE TRIUMF PROTON THERAPY FACILITY

E.W. BLACKMORE, J. VINCENT
TRIUMF, Vancouver, B.C., Canada V6T 2A3.

S. CHAVEZ, K. GARDEY, G. LAM, U. OELFKE, T. PICKLES
British Columbia Cancer Agency, Vancouver, B.C., Canada V5Z 4E6.

K. PATON
Department of Ophthalmology, University of British Columbia, Vancouver, B.C., Canada.

The Proton Therapy Facility (PTF) at TRIUMF will initially be used for treating uveal melanoma with 70 MeV protons. TRIUMF is a large multi-user research laboratory based on a 500 MeV H^- cyclotron which is capable of extracting simultaneously a number of proton beams of different energies and intensities. The PTF is installed on a beam line with a proton energy range of 65–120 MeV so other treatment sites can be contemplated. This paper describes the proton beam delivery system, the patient positioning system, the treatment control system and the commissioning tests carried out to date. First patient treatment is anticipated in early 1995.

INTRODUCTION

The design and development of the Proton Therapy Facility is a joint effort of the TRIUMF laboratory, the Physics and Developmental Radiotherapy Groups at the British Columbia Cancer Agency and the Department of Ophthalmology of the University of British Columbia. Particle therapy has been carried out at TRIUMF for more than a decade using negative pions produced by the high intensity proton beam from the cyclotron.[1] A phase III clinical trial with pions for two treatment sites, brain and prostate, is nearing completion based on randomizing approximately 300 patients. It is anticipated that the pion treatments will be terminated at the end of this trial and the effort of the group will concentrate on the use of protons for therapy.

The TRIUMF cyclotron is a unique particle accelerator for proton therapy as it can provide proton beams from 65–520 MeV with good energy resolution and with stable and easily controlled beam intensity. These advantages are offset by the fact that the cyclotron is a multi-user facility, so treatments must be compatible with the different operating regimes of the cyclotron.

The eye treatment facility is located on an existing beam line, BL2C, which has an energy range of 65–120 MeV. Nearby in the same room is a second beam line, BL1B, which has an energy range of 180–500 MeV and which has been used recently for radiation damage studies in electronics. This beam line could be modified for larger field treatments using 180–250 MeV protons at a future date.

The beam delivery and patient alignment systems which have been installed are similar to those used at existing eye treatment facilities.[2,3,4] The patient is treated in a seated position with the head immobilized with a face mask and bite block. However, there is enough flexibility in the arrangement to treat other sites to depths of 10 cm and with lateral beam sizes up to 8 cm diameter. In addition the treatment chair has six motorized degrees of freedom including full rotation about a vertical axis.

THE PROTON BEAM DELIVERY SYSTEM

The TRIUMF cyclotron[5] accelerates H^- ions to a peak energy of 520 MeV and to peak currents in excess of 150 μA for unpolarized beam operation. There is also a polarized source which delivers polarized H^- ions at lower intensities, presently about 5 μA. Typically unpolarized beam is scheduled for 24–30 weeks each year and polarized for 12–15 weeks. Initially the proton therapy facility would be available for treatments on a one week per month basis during either polarized or unpolarized operation.

The use of H^- ions allows for easy extraction of the beam by converting the beam to protons by passage through a thin foil as shown in Fig. 1. The extracted proton energy and intensity are varied by moving the stripping foil into the path of the circulating protons in the cyclotron with a mechanism which moves the foil in three orthogonal directions — R to select energy, L to centre the beam at the exit point, and Z to vary the

beam intensity. A variety of stripping foil shapes are available in a carousel on the extraction probe which can be used to provide stable beams from nanoamperes to the full output of the cyclotron. For proton therapy the stripping foil will in most cases be a 0.001" carbon wire for extracting beam currents at the nanoampere level if the circulating beam in the cyclotron is above 1 μA.

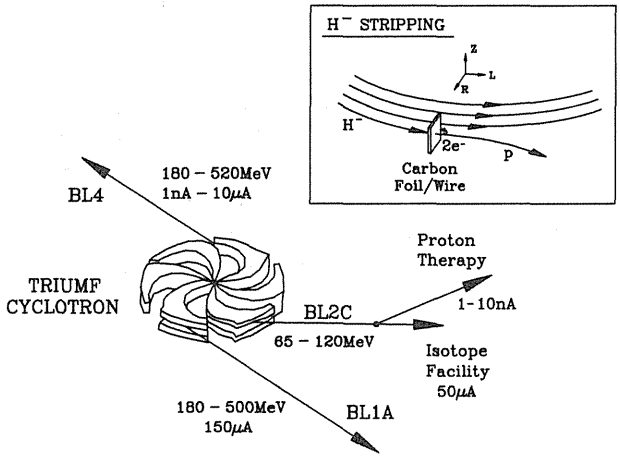

Figure 1: Beam extraction from the TRIUMF cyclotron using H^- stripping.

Although there is good experience in extracting reliable and stable low intensity beams which are 10^{-4} to 10^{-5} of the circulating beam intensity the proposed eye treatments will be done with an additional beam limiting device during unpolarized beam operation to ensure that the maximum circulating beam intensity in the cyclotron is limited to below 10 μA. With the standard 0.001" carbon wire stripper the maximum extracted beam intensity is limited to less than 0.5% of the circulating beam. The current required for treatment is in the range 3 nA to 10 nA which is easily achievable with partial insertion.

Beam line 2C which provides the protons to the therapy facility has two dipole magnets, five quadrupole magnets for beam focusing and three steering magnets for beam centring. A device called the Fast Shutter is the primary means of controlling the beam during patient treatment. It operates pneumatically with a turn-off time of 100 ms and a turn-on time of 200 ms. Typical treatment times will be 50–100 seconds. This beam shutter will be backed up by other devices which will stop the beam in less than 1 second. The Fast Shutter and back-up devices will be triggered either manually by an operator or automatically by the Treatment Control System. When the beam is stopped on the Fast Shutter the beam current can be read on the insulated beam stop so the operators will know the beam intensity prior to opening the Fast Shutter.

The required proton dose distribution is achieved using a passive scattering system and a rotating range modulator arranged as shown in Fig. 2. The first device after BL2C exits the vault wall is a Secondary Emission Monitor (SEM). This device measures the total proton beam current, does not saturate at high rates and is used as a beam rate monitor in the interlock system. The next device is a multiwire ionization chamber which provides the incoming beam profile and centring information. The beam is then defined by a first collimator/scatterer (typically 12 mm diameter aperture with 0.8 g/cm^2 thick lead). A second collimator located about 40 cm downstream stops a significant fraction of the scattered beam in the tails of the gaussian distribution with the central part passing through to the proton nozzle. Here the proton field shape is defined transversely by a patient dependent brass collimator to a maximum size of 25 mm diameter. The treatment position is approximately 10 cm downstream of the collimator.

Only about 2% of the incident proton beam is used for the treatment. The remaining beam is stopped in copper collimators which have some polyethylene added for neutron attenuation. Measurements have been made to show that the neutron dose to the patient from the protons stopping in the upstream collimators is less than 10^{-4} of the treatment dose. At 70 MeV with the lead scatterer and other material in the beam the maximum treatment depth is 32 mm in eye tissue. The treatment depth can be varied by a rotating wedge degrader or range shifter which is located between the first and second collimators. It is operated by a stepping motor with encoder readout. The range modulator which is just downstream of the range shifter rotates a plastic wheel which has been N/C machined to provide a flat spread out Bragg peak. The modulator wheel rotates at 240 RPM and has four modulations per rotation. A number of modulator wheels will be required to vary the width of the spread out Bragg peak over the required treatment depth of 5 to 25 mm in steps of 1 mm.

A diagnostic ion chamber which measures the total beam emerging from the first collimator is used to normalize the beam intensity for range shifter scans or for measuring the scattering function at the modulator position. The proton beam dose is monitored by a transmission ion chamber operating in air and located immediately upstream of the proton nozzle. The ion chamber consists of two transmission plates, one for an independent back-up and a set of quadrant plates to provide information on beam centring. The design aim is to provide dose uniformities both laterally and in

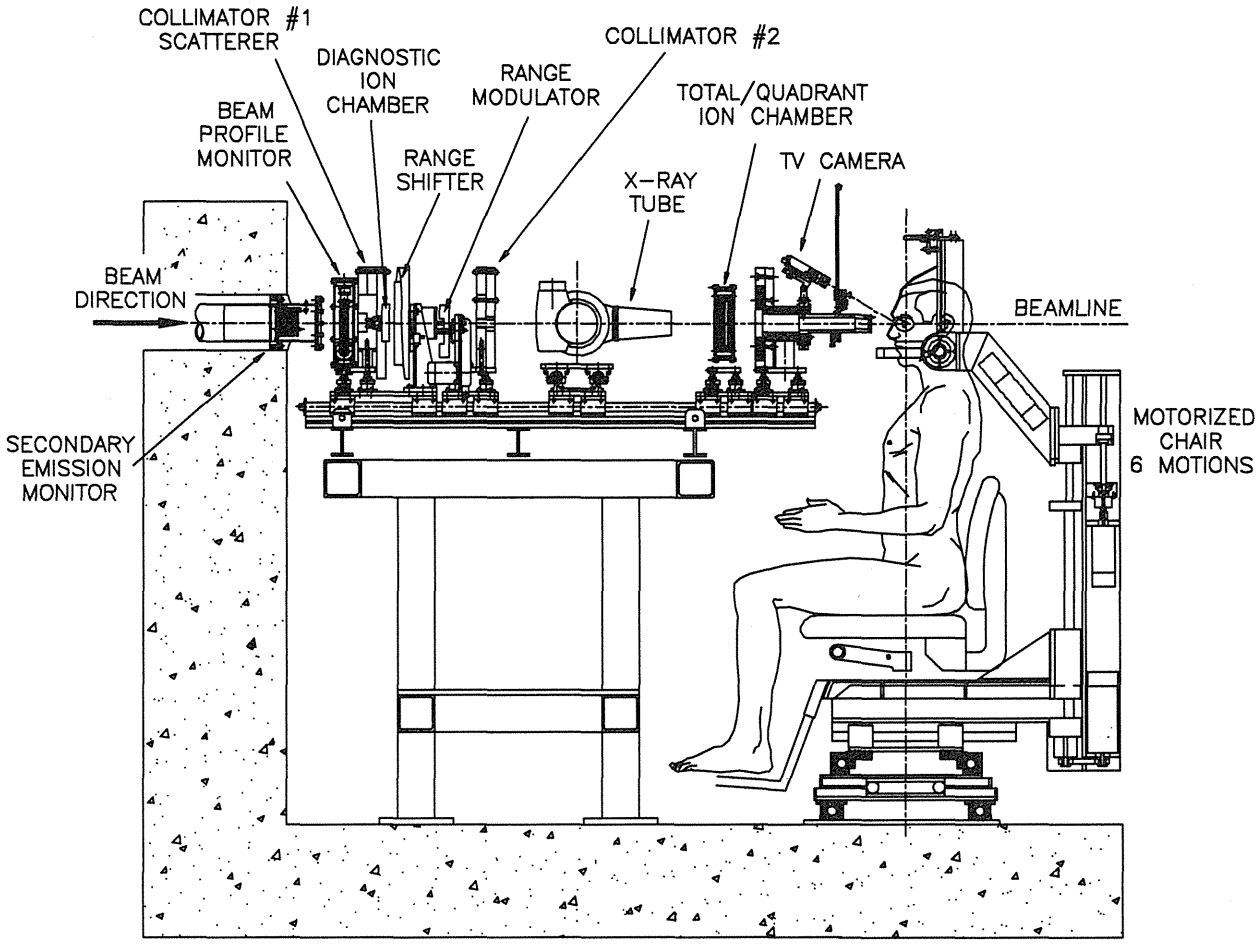

Figure 2: Arrangement of equipment for the proton beam delivery system.

depth at the 5% level. Measurements have shown that the beam distribution is relatively insensitive to beam focusing and steering and that the quadrant chamber is a useful diagnostic for changes in beam position.

The transmission ion chamber will be calibrated for each treatment against a reference ion chamber located at isocentre. The maximum dose rate of 15 Gy/minute is achieved with 5 to 10 nA of proton current on the first collimator, depending on amount of scattering and modulation.

PATIENT TREATMENT PROCEDURE

The method of patient alignment for treatment follows closely the techniques used at the other proton therapy facilities. The patient is seated in a treatment chair which has been constructed by a local company.[6] The patient is immobilized in a combination of a face mask made from Aquaplast material and a bite-block system. The treatment planning program EYEPLAN is used to determine the optimum orientation of the eye for therapy along with the collimator, modulation and proton range requirements.

Two orthogonal X-ray images are taken to establish the relationship of the tantalum clips, surgically placed on the eye to indicate tumour margins, to the treatment system landmarks. One X-ray tube is inserted onto the beam axis to view these clips through the proton nozzle for the axial or AP view and a second X-ray tube is mounted for a lateral view through the isocentre. Initially the X-ray images will be taken using Polaroid film with a Lanex intensifying screen but later a digital technique using an image intensifier may be developed. During treatment the patient's eye motion is monitored using a fixed focal length video camera with a shallow depth of field and magnified image in order to detect minor movements. This is focussed on the patient's eye and can track motion both laterally and parallel to the beam direction. The position of the eye is noted on the monitor screen for confirmation of the correct position during X-ray verification and treatment.

TREATMENT CONTROL SYSTEM

The treatment control system for TRIUMF's Proton Therapy Facility is modelled on the 500 MeV cyclotron's Central Control System. The system logic is carried out at three levels: high level in the Treatment Control Computer with interaction via an Xwindows terminal, NIM/CAMAC level using standard modules such as integrators, scalers, fanouts and TRIMAC microprocessor, and low level functions which are implemented in a Programmable Logic Controller and some custom hardware.

Ortec 439 current integrators with a sensitivity of 10^{-10} coulombs/pulse are used to read the Primary and Backup ion chambers. They are also used to read a diagnostic ion chamber and the diodes or miniature ion chambers used for scanning lateral and longitudinal profiles. The Primary and Backup ion chamber integrators, bias voltages and fanouts are in separately powered Nimbins. The SEM, Fast Shutter and Quadrant chamber currents are read out using a TRIUMF-built current-to-voltage amplifier followed by a voltage-to-frequency converter. The amplifiers have fixed gains of 10 nA/volt for the SEM and Fast Shutter and 100 nA/volt for the Quadrant chambers.

The integrator outputs are fanned out into CAMAC scalers and in some cases to visual scalers. A dedicated CAMAC scaler is used for dose monitoring and control, while a second CAMAC scaler is used for diagnostic studies. A TRIMAC microprocessor in the CAMAC crate reads the scaler information with a 100 ms cycle time and provides the logic information on dose completion, quadrant symmetry, SEM and Fast Shutter currents satisfactory, to the Programmable Logic Controller. The low level logic which generates the Fast Shutter control signals based on hardwired switches and the logic from the TRIMAC is implemented in a Programmable Logic Controller (PLC).

An independent hard-wired backup system which uses the second transmission foil on the ion chamber terminates the irradiation in the event of a failure of the primary system. The back-up dose is set by thumbwheels on a control panel and compared with the primary dose setting which is entered via a terminal to ensure that it is set 1% above. The backup system if activated inserts an independent beam blocker as well as the Fast Shutter.

The Treatment Control Computer is a MicroVAX 3400 and is used only for Proton Therapy applications. The primary display terminal has a number of dedicated display pages to allow the operator in input information about the patient treatment, to check the beam line settings and interlock status information and to check the ion chamber and quadrant chamber readings during treatment. In addition there are a number of detached processes that provide support for activities such as monitoring and reporting the dose count history, comparing the primary and backup dose setpoints, scanning the range shifter or 2D scanning device and providing graphic displays. There are also applications that have been developed for the cyclotron that are equally applicable to the treatment facility. These programs include display of the beam profile monitor, cyclotron parameter displays, and the like.

COMMISSIONING TESTS

The performance of the system and the beam monitoring devices has been checked during many weeks of beam operation thus far. The responses of the various beam monitoring devices have been studied. This includes the SEM, ion chambers, several types of diodes, a diamond detector and miniature ion chambers. Figure 3 shows the response of two different diodes, a BPW-34 optical diode and a 1N4007 conventional diode, as a function of total proton dose to determine the amount of pre-irradiation required before the

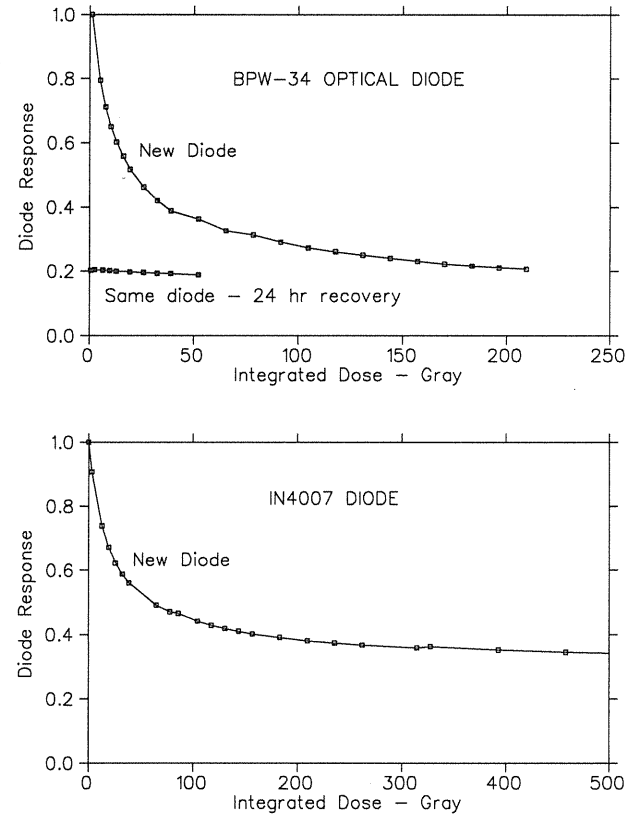

Figure 3: Response of new diodes to dose. The diode signals are normalized to the first reading taken.

response stabilizes. Lateral and longitudinal dose distributions have been measured by scanning a diode in a water box. The raw Bragg peak has been measured under different cyclotron operating conditions and beam line tunes and for different diodes. Figure 4 shows raw Bragg peaks as measured by different devices.

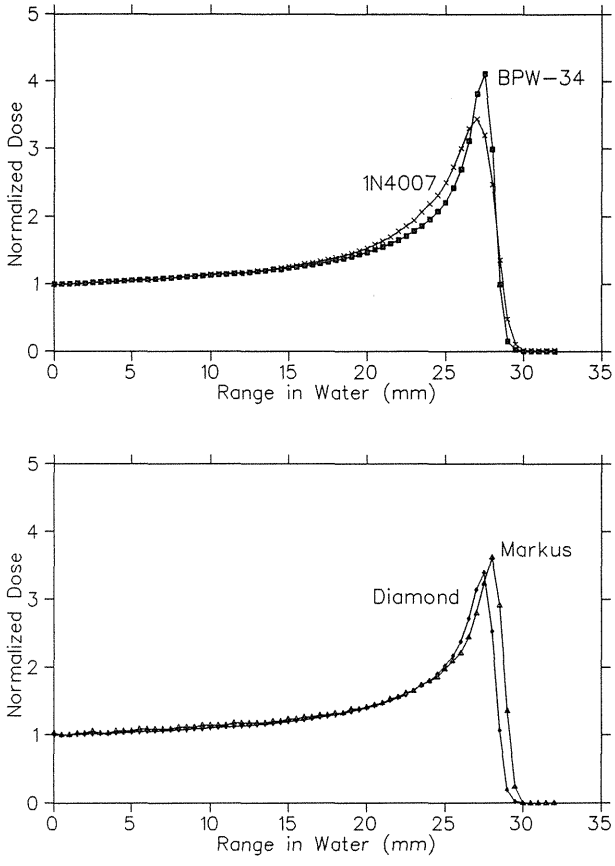

Figure 4: Raw Bragg peaks for 70 MeV protons as measured by different devices. The difference in shape is due to the size of the active volume of the device and the difference in position is due to the thickness of material in front of the device.

The design of modulators to provide a flat spread-out Bragg peak has been optimized and tested. Figure 5 shows a typical SOBP for several range shifter positions. The dosimetry data required for treatment planning have been measured and input into the EYEPLAN program.

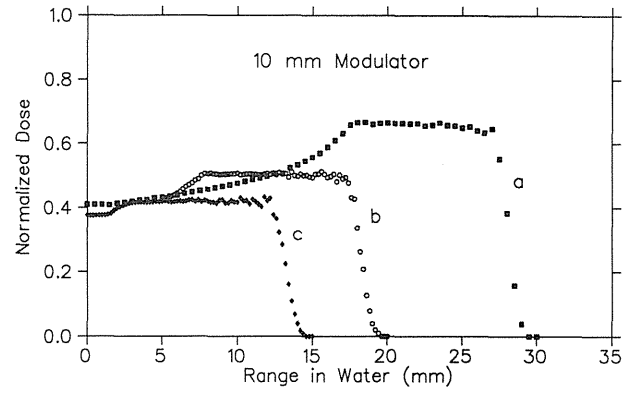

Figure 5: Typical spread out Bragg peaks using the same 10 mm modulator for different settings of the range shifter.

The Treatment Control System has been extensively tested to demonstrate that all interlocks and logic checks are functioning. The X-ray equipment has been tested both on phantoms and on volunteer patients who have eye clips in place as a result of treatments elsewhere. The patient treatment chair is essentially commissioned and the patient fixation devices tested.

The proton beam has been used to measure RBE in cultured V79-WRNE cells using the sliced gel technique.[7] A multifraction mouse foot experiment involving more than 100 separate irradiations has been carried out to measure the RBE relative to ^{60}Co. Both early and late effects will be studied.[8]

SUMMARY

The TRIUMF eye treatment facility has been fairly thoroughly commissioned over the past six months by carrying out a number of beam studies and checks to test the integrity of the system. Procedures for dose calibration have been established. The X-ray and alignment equipment have been installed and tested on volunteer patients. The EYEPLAN program has been used for a number of treatment simulations. The facility is presently undergoing safety reviews to permit first patient treatment early in 1995.

REFERENCES

1. Goodman, G.B., *et al.*: Pimeson Radiotherapy at TRIUMF. *J. Jpn. Soc. Ther. Radiol. Oncol.* **2**: 85–99, 1990.

2. Markovits, C., Jaccard, S. and Perret, C.: The Proton Beam Facility OPTIS for the Therapy of Ocular Tumors. *Proc. International Heavy Particle Therapy Workshop, Paul Scherrer Institute, Villigen, Switzerland*, September 1989, edited by Blattmann, H., PSI-Bericht, **69**: 134–139, 1990.

3. Suit, H.D., Goitein, M., Munzenrider, J., Verhey, L., Urie, M., Gragoudas, E., Koehler, A., Gottschalk, B., Sisterson, J., Tatsuzaki, H., *et al.*: Strahlentherapie und Onkologie, **166**: 40, 1990.

4. Bonnett, D.E., Kacperek, A. and Sheen, M.: The Clatterbridge Proton Therapy Facility. *Proc. International Heavy Particle Therapy Workshop, Paul Scherrer Institute, Villigen, Switzerland*, September 1989, edited by Blattmann, H., PSI-Bericht, **69**: 143–144, 1990.

5. Baartman, R. *et al.*: Status Report on the TRIUMF Cyclotron. *Proc. 10th Int. Conf. on Cyclotrons and their Applications, Michigan, USA*, 203, 1984.

6. Benchmark Engineering Inc., Vancouver, Canada.

7. Skarsgard, L.: Biological dosimetry for heavy charged particle beams using an in vitro system. *Proc. of this conference.*

8. Nemoto, K.: private communication.

The Proceedings of the NIRS International Seminar on the Application of Heavy Ion Accelerator to Radiation Therapy of Cancer.

PTCOG XXI Meeting at Chiba, Japan
14-16 November 1994.

Developments at the Clatterbridge Cyclotron Unit

A. Kacperek, M.A. Sheen, R.D. Errington, J. Kongerud
(Clatterbridge Centre for Oncology)
and
J Hungerford (London), B Damato (Liverpool)
I Rennie (Sheffield)

1. PATIENT TREATMENTS

Up to November 1994, a total of 560 eye patients, referred from three ophthalmological centres, have been treated with protons at Clatterbridge. Of these, 549 patients had choroidal and ciliary body melanoma. Five patients have been treated for choroidal haemangioma with a dose of 18 Gy in four daily fractions. Superficial treatments have given to three iris and three conjunctival melanomas. Two of the conjunctival treatments were given as boosts (25 Gy in five fractions) following electron therapy. The approximate throughput rate is 140 patients per annum and is equally distributed between large (>10 mm wide, >5 mm high) and small (<10 mm wide, <5 mm high) tumours. The first long-term follow-up study, including late-effects will be presented in January at Moorfields. A fourth referral centre has commenced suturing Ta clips following an understanding of the high quality of the clinical measurements (including ultra-sound) required for the treatment planning process.

2. PROTON RADIOBIOLOGY

The following radiobiological research plan has been established and will in the first instance involve the following groups, Clatterbridge Cancer Research Trust, Institute of Cancer Research (Sutton), Dublin Institute of Technology. Collaboration with european radiobiology groups is envisaged.

i) Radiobiological dosimetry intercomparisons (using a standard, well understood, cell-line such as V79). This to determine

ii) The effect of proton irradiation of mammalian cells (RBE of eg humour tumour cells, HX138 and HX142, ocular melanoma lines, V79 and CHO).

iii) Proton radiobiology of vascular endothelial cells to investigate changes in the permeability of endothelial monolayers. The work will consider the determination of meaningful non-clonogenic 'end-points' and has been stimulated by the proposed treatment of age-related macular degeneration, and the necessity of deriving the appropriate proton dose especially as the treatment will use essentially the Bragg peak, a region of high LET. A knowledge of the effective RBE is therefore essential.

3. RE-INVESTIGATION OF PROTON FIELD OUTPUT FACTORS*

Due to the increasing use of smaller treatment fields, the effects of collimator shape and diameter on proton dosimetry were experimentally investigated. The use of standard field conditions (fixed collimator and ion-chamber) for proton dosimetry may not be appropriate. Other factors such as the type of detector (diodes, ion-chamber) and proton energy were also examined. Previous work did not describe adequately the clinical irradiation conditions (1). Preliminary results show significant changes in dose with collimator diameters of < 8 mm but little affected by field shape.

*M.Sc. Dissertation, Leeds University, 1995. T. Chapman.

(1) Bonnett, D E, Kacperek, A, Sheen, M A, Goodall, R. and Saxton, T E 1993 The 62 MeV proton beam for the treatment of ocular melanoma at Clatterbridge. British Journal of Radiology 66, 907-914.

4. USE OF MAGNETIC RESONANCE (MR) IMAGING TO IMPROVE CLINICAL EYE DATA**

As reported at the PTCOG IXX meeting, several patients with sutured tantalum clips, and with ambiguous clinical eye data were scanned on an NMR scanner (at the MRI Unit, CCO). This work has two main objectives. First, by using the clip coordinate information available from orthogonal X-ray images, and developing a transformation technique it has been possible to eliminate spurious artefacts from the MR eye images and thus verify the clip positions with respect to the tumour. Second, the development of a further transformation matrix using MRI clip and tumour coordinates will allow direct comparison with surgical data. In addition, this technique may be further developed to include information on irregular eye and tumour shapes.

**M.Sc. Dissertation, Surrey University, 1994, A. Flynn. (Performed in collaboration with J. Brunt of the MRI scanning unit at the CCO).

Recent Developments at COSY-Jülich

U. Linz, Forschungszentrum Jülich GmbH, Jülich, Germany

On April 1,1993 the cooler synchrotron and storage ring COSY-Jülich was officially inaugurated. COSY has primarily been built as accelerator for medium energy physics but it is intended to apply its favorable properties to therapy, as well.

Fully developed, COSY will be able to accelerate protons from 40 MeV injection energy up to 2.5 GeV. COSY is also designed for heavier ions such as carbon, oxygen and neon in the medically necessary intensity and energy range (approx. 10^8 particles/s and E=400-500 MeV/n). This option, however, will not be exploited during the first years of operation. COSY is still in an early phase of operation. Machine development is not yet finished.

At present, COSY can store approx. $5x10^{10}$ protons and accelerates them up to the maximum momentum of 3.3 GeV/c or 2.5 GeV kinetic energy. Extraction has presented considerable difficulties with extraction efficiencies in the order of 0.1%. In the meantime 10^8 protons/burst have been measured externally, but cycle time is still in the range of several seconds. The projected beam intensity is approx. $5x10^9$ protons/s at maximum energy and $2x10^{10}$ s^{-1} at 200 MeV, respectively, which corresponds to approx. 3 Gy $l^{-1}min^{-1}$.

Other design parameters of COSY (1) which are of interest for therapeutic application of the accelerator including ultraslow extraction (spill times up to 1000 s), low beam emittance (2.5 πmm•mrad vert. and horiz.) and a high momentum stability during beam pulses ($\Delta p/p= 10^{-3}$) have yet to be achieved.

Although the medical programme at COSY (COSY-med) has suffered somewhat from the delay in machine development, the experimental area for the radiation physics programme could be finished and in early November the first beam was directed to this target site. Beam characterization including profile measurements, beam composition (fraction of neutrons, secondary charged particles, photons) and absolute dose of beams of various energies are now to start using a water or a double wedge solid phantom and various detector types (TEPC, Si-diode, microstrip detectors). The results will be compared to calculated data from MC-simulations. Both calculated and experimental data will be used as input into biophysical models. These studies will set the platform for in vitro cell culture experiments on survival and metabolic activity and subsequent in vivo investigations in small lab animals concerning tumor and normal tissue response.

The general concept of the medical program at COSY which has been described before (2) is still valid. However, for the time being the technical physics program which comprises design and development of the second medical beam line, i.e., the actual therapy site, and the infrastructure program have been put

on hold for budgetary reasons and until COSY is closer to routine operation. This means that, even though experiments at the medical test area will go on, it will be impossible to meet our original schedule which projected the first patient treatment for the end of 1996.

References

(1) U. Linz and R. Maier, A first concept to use the Cooler Synchrotron COSY-Jülich for cancer therapy. Proc. of the 3rd European Particle Accelerator Conference EPAC 92, Berlin, March 24-28, 1992, pp. 1672-1673.

(2) U. Linz, Plans and status of the ion beam therapy project at COSY-Jülich. Proc. of the Int. Symp. on Hadron Therapy, Como, Oct. 18-21, 1993, to be publ.

Biology I

An RBE study of a proton beam at University of Tsukuba. (vs. Co-60)

Hideo Tatsuzaki, M.D., Ph.D.[1], Toshiyuki Okumura, M.D.[2], Hiroshi Tsuji, M.D.[2], Yoshinori Hayakawa, Ph.D.[2], Takehiko Mori[3], Akira Maruhashi, Ph.D.[2], Hiroshi Fuji, M.D.[1], Mitsuhiko Kawashima, M.D.[1], Toshiya Chiba, M.D.[2], Yuji Itai, M.D., Ph.D[1], and Hirohiko Tsujii, M.D., Ph.D[2]

[1]Department of Radiation Oncology, Institute of clinical medicine, University of Tsukuba, Tennoudai, Tsukuba, Ibaraki 305 Japan. [2]Proton Medical Research Center, University of Tsukuba. [3]Suzuka Medical Technology Collage.

Abstract: The objective of this study was to determine the RBE value of a proton beam of the University of Tsukuba. A 250 MeV proton beam was compared with Co-60 gamma rays. C_3H mice were irradiated on the leg and skin contractions were observed after 250 days by tattoo method. The irradiation was performed with ten fractions over 11 elapsed days. As preliminary data, the result indicated the RBE value of 1.02 to 1.03.

Introduction

In spite of the emerging use of a proton beam in cancer treatment, there still exists the controversy about RBE of a proton beam. Two Japanese proton treatment center currently use the RBE value of 1.0, while those in U. S. A. or Europe use RBE value of 1.1. As the proton beam at Proton Medical Science Center, University of Tsukuba has relatively high original energy, 250 MeV, it can have low RBE compared with other facilities.

Because usual fraction size of proton treatment is 3 to 4 Gy, it is important to use lower dose in experiment when determining RBE. Furthermore, fractionated irradiation is used in clinical treatments in most of the cases. Thus, fractionated biological experiment is suitable. In this study, irradiation was performed with fractionation. We use late reaction of a normal tissue as an end-point to derive the RBE value.

Materials and methods

Animals:

Twelve weeks old, female C3H/He Slc mice were used for this experiment.

Radiation:

Proton irradiation was performed at the Proton Medical Research Center, the University of Tsukuba. A proton beam was derived from a 500 MeV booster synchrotron at the National Laboratory for High Energy Physics. The beam was bent to vertical direction by a 90 degree-magnet after degraded to 250 MeV. A 6 mm lead scatterer was installed 5 m upstream from the objective. A ridge filter was used to alter the depth-dose characteristic of the beam to achieve a Spread Out Bragg Peak (SOBP). The flat-top of the SOBP extended over 9 cm in water. A mix-DP absorber and a water bath fine degrader were placed in position to modulate the penetration depth. Objectives, or mice, were set at the middle portion of the SOBP. The proton flux was collimated to a 2.5 cm X 25 cm slit shaped beam with a brass collimating block before reaching the objective.

The absorbed dose was measured by a tissue-equivalent chamber that was calibrated with ^{60}Co. Since the proton beam was a pulse beam, ion recombination correction was also considered. At the time of irradiation, a transmission chamber was used as a monitor. The dose rate was 1.5 to 2 Gy/min.

Standard irradiation as control was performed by gamma-rays from a ^{60}Co tele-therapy unit. The source target distance was 80 cm. The beam was collimated to a 2.5 cm X 25 cm slit shape. The dose was measured by an ionization chamber that had been calibrated with ^{60}Co. The dose rate was 1.2 Gy/min.

1 cm thick Mix-R plates were placed on the skin surface as a build up bolus. The right lower legs of mice were irradiated under anesthesia (65 mg/kg pentobarbital, i.p.).
The fractionated irradiation was carried out in 10 fractions over 11 elapsed days.

Observation and data analysis:

Skin contraction was used as an end point. Seven days before irradiation, both hint legs were shaved with razor blade. Two tattoo points were injected in the shaved area. They were observed after 250 days. The distance of tattoos were measured and the skin contraction were calculated. Non-irradiated side was used as a standard (0 % contraction).

Result

Fig. shows skin contraction rates at the 250th day after irradiation. Data points were fitted by linear lines and RBE was derived at 2 reaction levels. As preliminary data, the RBE was 1.02 at 30 % skin contraction level and 1.03 at 40 % skin contraction level.

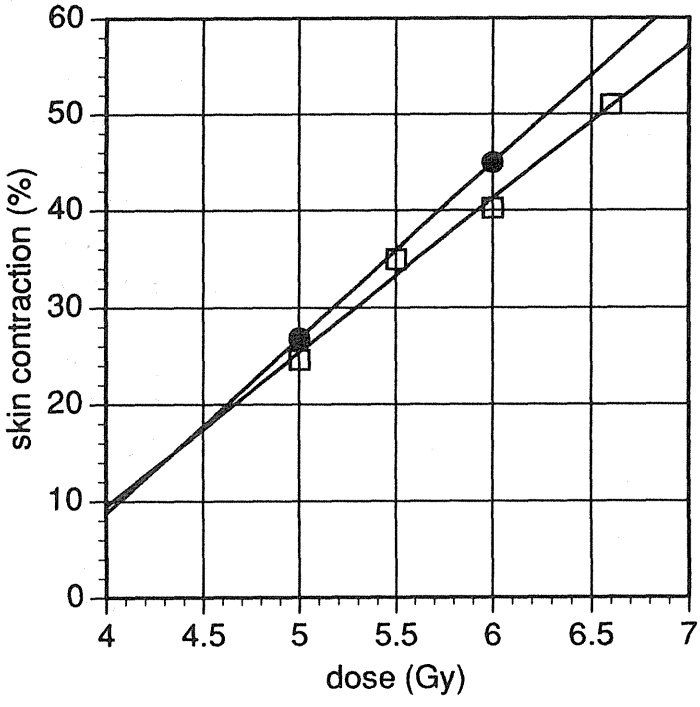

Fig. Skin contraction at the 250th day after 10 fraction irradiation. Close circles show a proton beam, while open squares show Co-60. Doses were indicated by the dose in a fraction, thus total doses were ten times greater.

ASSESSMENT OF ACUTE AND LATE EFFECTS TO HIGH-LET RADIATION

ELEANOR A. BLAKELY, PH.D.[1] AND JOSEPH R. CASTRO, M.D.[1,2]

Lawrence Berkeley Laboratory[1], Life Sciences Division, University of California, Berkeley, CA 94720 USA; and University of California[2], San Francisco School of Medicine, Department of Radiation Oncology, San Francisco, CA 94143 USA

We have begun to reassess late tissue effects available from the Charged Particle Cancer Radiotherapy program at Berkeley. Our quantitative approach is limited in the analysis of these Phase I/II studies by not having equivalent patient numbers for each of the particle beams studied, by not having completely comparable follow-up times, by variations in the sizes of the fields compared, by variations in the skin scoring photographic documentation available from the patient charts, and by variations in the fractionation sizes, numbers and schedules. Despite these limitations, preliminary evidence demonstrates acute skin reactions with a shift to increasing lower dose per fraction per field for the maximum skin reactions of helium, carbon and neon ions compared to electrons. Comparisons with skin reactions from low-energy neutrons indicate that Bragg peak carbon ions (initial energy 308 MeV/nucleon) are slightly less effective than 7.5 MeV neutrons. Bragg peak neon ions (initial energy 670 MeV/nucleon) corrected for differences in reference radiation are slightly more effective than 7.5 MeV neutrons. Bragg peak silicon ions (initial energy 670 MeV/nucleon) result in an enhanced acute skin reaction, and a premature appearance of late effects that may indicate a significantly different mechanism of damage and/or repair.

INTRODUCTION

Little clinical information is available on the assessment of acute and late effects of normal tissues to high-LET charged particles. With the closure of the clinical treatment program at the Berkeley Bevalac Facility in 1992, the U.S. National Cancer Institute has supported a follow-up of the approximately 1300 patients who received charged particle radiotherapy for cancer at the Lawrence Berkeley Laboratory during the period from 1975-1992. A systematic assessment of normal tissue reactions appearing early and later after exposure to high energy helium (225 Mev/u), carbon (308 MeV/u), neon (670 Mev/u) and silicon (670 MeV/u) ions is a part of this program. This is a report of some preliminary information obtained from this study.

The development of tissue damage after irradiation is known to depend on a number of factors, including whether or not the tissue is proliferating or consists of non-dividing or terminally differentiating tissues. Either type of tissue generally demonstrates a three phase response (early, intermediate and late) that is dependent on the dose and linear energy transfer (LET) of the radiation. (1) With exposure to radiations having LET values of about 100 keV/μm, the time course and severity of the reaction can shift. Frequently there is the appearance of earlier acute and late effects in both proliferative and non-proliferative tissue. The early induction period frequently is short and the rise to the maximum value is faster; the level of intermediate damage is higher, and the

Acknowledgements -This work was supported by the Director of the Office of Energy Research, Office of Health and Environmental Research, Division of Medical Applications and Biophysical Research of the U.S. Department of Energy under Contract No. DE-AC03-76SF00098 and by NIH grants CA 15184 and 19138. The authors would like to thank Cornelius A. Tobias for his suggestions to this manuscript.

time of appearance of late effects is earlier and the rate of any subsequent degeneration is faster (1).

Leith *et al*, (2) compiled a summary of normal tissue relative biological effectiveness (RBE) data from charged particle studies with experimental animals. At the same dose-averaged LET value, he reported a hierarchy of tissue responses, with for example, spinal cord having a much higher RBE value compared to intestinal crypt or skin. This was similar to observations made with neutrons by Field (3). It is important for clinical considerations to analyze RBE data from fractionated dose regimens.

Raju and Carpenter (4) evaluated the correlation between acute and late reactions to most of the available particle beams with a mouse foot skin model using plateau and Bragg Peak ions. They did not see any lack of correlation between the two. Acute effects were a good predictor of late effects. Both increased at high dose, but only single dose effects were measured.

This preliminary report summarizes PhaseI/II acute skin reaction studies that were completed for the purpose of selection of appropriate dose-fractions with charged particle beams at energies and LET values used for the first time for radiotherapy with the intent to eradicate underlying tumor. In the case of helium and silicon ions, correlative biological studies are also described. The analysis of late effects is still underway.

METHODS AND MATERIALS

Design of the study

We have deliberately selected the skin scores from patients, where due to the superficial location of their lesions, skin was not spared and received particle doses in the Bragg peak of the ions studied. The data therefore represent RBE estimates for normal tissues that could not be eliminated from the treatment volume.

Eligibility criteria

Only Phase I/II patients with locally advanced or metastatic disease who consented to the feasibility testing of charged particle exposures were included in the study.

Skin scoring

We have used an expanded 9-point scale (Table 1) to allow us to distinguish qualitative differences in erythema, and dry and moist desquamation. Electrons were used as a low-LET reference.

Table 1. CLINICAL SCORING FOR ACUTE SKIN IRRADIATION

1. No visible reaction
2. Minimal erythema
3. Moderate erythema
4. Minimal dry desquamation
5. Moderate dry desquamation (less than 1/2 field)
6. Marked dry desquamation (more than 1/2 field)
7. Moist desquamation (less than 1/2/ field)
8. Moist desquamation (more than 1/2 field)
9. Necrosis and/or ulceration

In vitro cell line and culture conditions

Asynchronously growing human T-1 cell fibroblasts (5,6) were used in the *in vitro* studies. There is a large data base in our laboratory with this cell line characterizing scattered, wobbled and scanned particle beams covering a range of atomic numbers from protons to uranium.

Particle exposure conditions

Cells were irradiated either in monolayers in tissue culture flasks filled with growth medium or in suspension under the conditions to be described later which simulated the patient irradiations under study. Dose-survival responses were obtained from single or sequential doses of the specified radiations.

In vitro survival measurement

A conventional colony-forming assay was used. After exposure the cells were trypsinized, resuspended, counted, plated, and incubated at 37°C for 11 days. Colony-forming was scored by staining the cultures with 1% methylene blue, and clones containing at least 50 cells were scored as survivors.

Data analysis

The dose-survival data were fitted to the linear-quadratic model of cell inactivation using programs written by Albright (7). These programs permit the calculation of radiobiological parameters and their 95% confidence intervals. The relative biological effectiveness (RBE) value for cell killing was determined from the ratio of the doses of helium Bragg peak ions to Bragg peak silicon ions 50% survival.

RESULTS AND DISCUSSION

Skin reactions

A compilation of the skin reactions to electrons, helium, carbon and neon is presented in Fig. 1. We detect dose-dependent shifts in the appearance and severity of the reactions on the 9 point scale covering 3 dose fraction sizes delivered in 10 fractions. We have emphasized the electron, helium, carbon and neon data because of its relevance to other ongoing programs. We do, however, have a small number of patients whose skin reactions were from heavier ions including silicon and argon. In that regard, one of the most dramatic tumor responses observed was in a patient treated with argon ions whose superficial tumor regressed significantly without any remarkable skin reaction. The data are obviously not statistically significant. However, we note that Blakely, *et al* (6) have previously observed in tissue cultures that argon beams reduce the radiobiological oxygen effect to a greater degree than any other beam studied is capable of doing. Further explorations with silicon or argon beams is clearly of interest to basic research.

To introduce the skin reaction data to heavier ions, we will describe a lung tumor patient whose multiple nodules were irradiated with an upper field of Bragg Peak high energy silicon ions, and whose deeper nodules were irradiated in a lower field with 225 MeV/nucleon helium ions (Fig. 2).

Radiobiology with a human fibroblast cell line in vitro was completed at the same time under the beam conditions of the patient treatment. The cell survival differences measured at the entrance and Bragg peak positions of each beam corresponding to the skin positions of interest are presented in Fig. 3. The right lower panel shows the enhanced killing of the silicon ions. The middle panel illustrates the confirmation of appropriate shaping of the ridge filters to yield isoeffectiveness at the dose fraction sizes selected.

A composite skin reaction photograph. is presented in Fig. 4. The photograph on the left was taken on the last day of treatment, The upper field was silicon, the lower field was helium. After three weeks, the middle photo, shows that the reactions were approximately equal, with perhaps the silicon field showing a little more color. However, at two months, the silicon field developed a significantly greater reaction and had a mottled appearance. It was difficult to assign a quantitative value to this acute skin response which included pigmentation changes suggestive of late skin reactions after low-LET radiations. The LET spectra of the silicon ion beam is presented in the lower panel of Fig. 5. The figure clearly indicates that the maximum dose-averaged LET number (84 keV/μm) actually represents a spread of LET values which complicates interpreting these data. Doses of plateau silicon ions with a significantly lower maximum dose-averaged LET value of 46 keV/μm did not cause this advanced late skin reaction in the single patient studied.

Table 2 indicates the relative silicon RBE values calculated from the *in vitro* cell experiments with Bragg peak silicon ions. The reference radiation was Bragg peak helium ions.

Table 2. RELATIVE SILICON RBE VALUES

	cells in vitro at 50% survival
Helium peak	
Silicon peak	3.2 ± 0.4

A preliminary analysis of the maximum clinical skin reactions as a function of physical dose per fraction per field

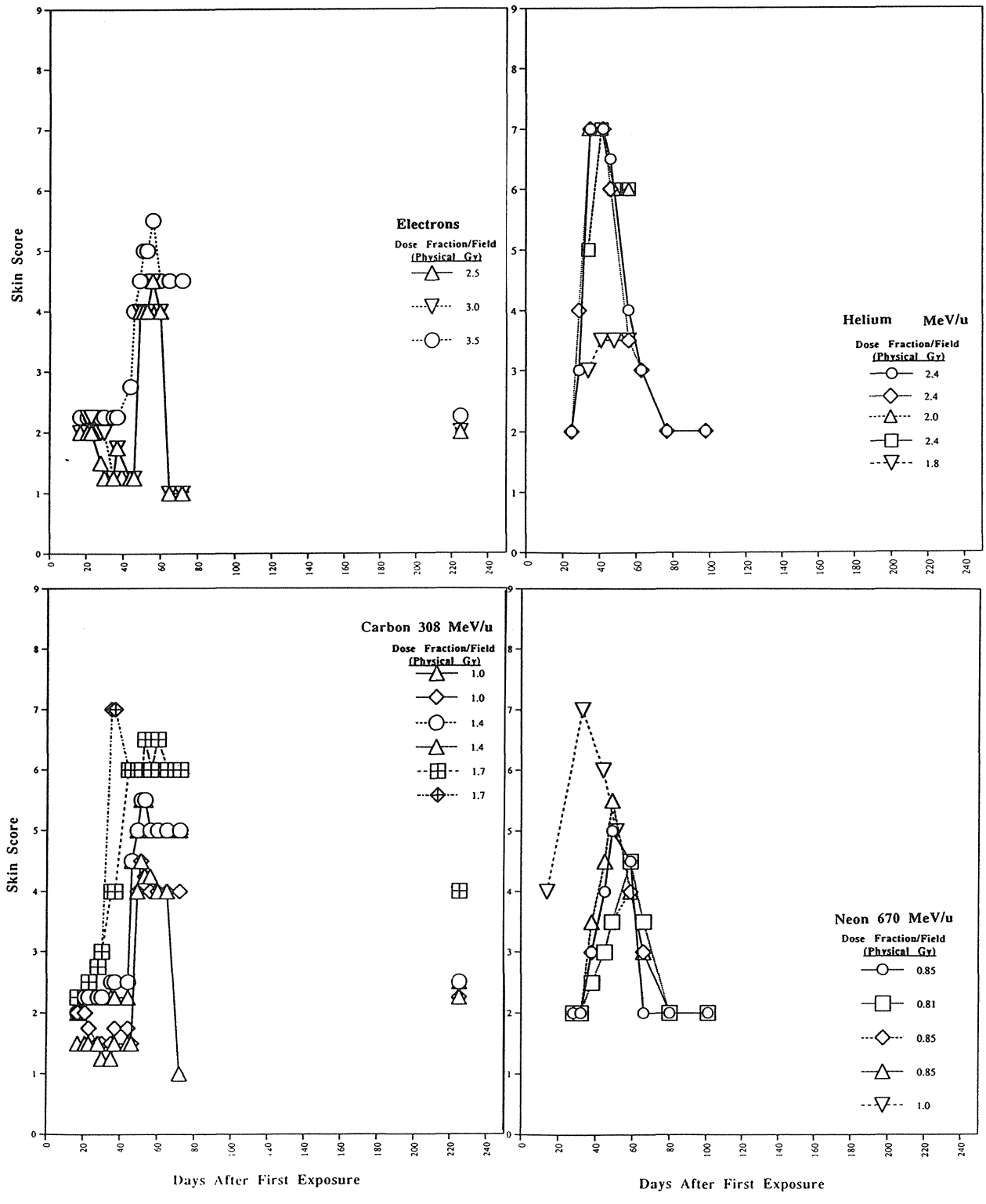

Fig. 1. Time course of maximum human skin responses to various accumulated dose fractions per treatment field of electrons, helium, carbon or neon ions. Note that data are from different dose fraction sizes and approximately equal fraction number, therefore total doses are not equivalent.

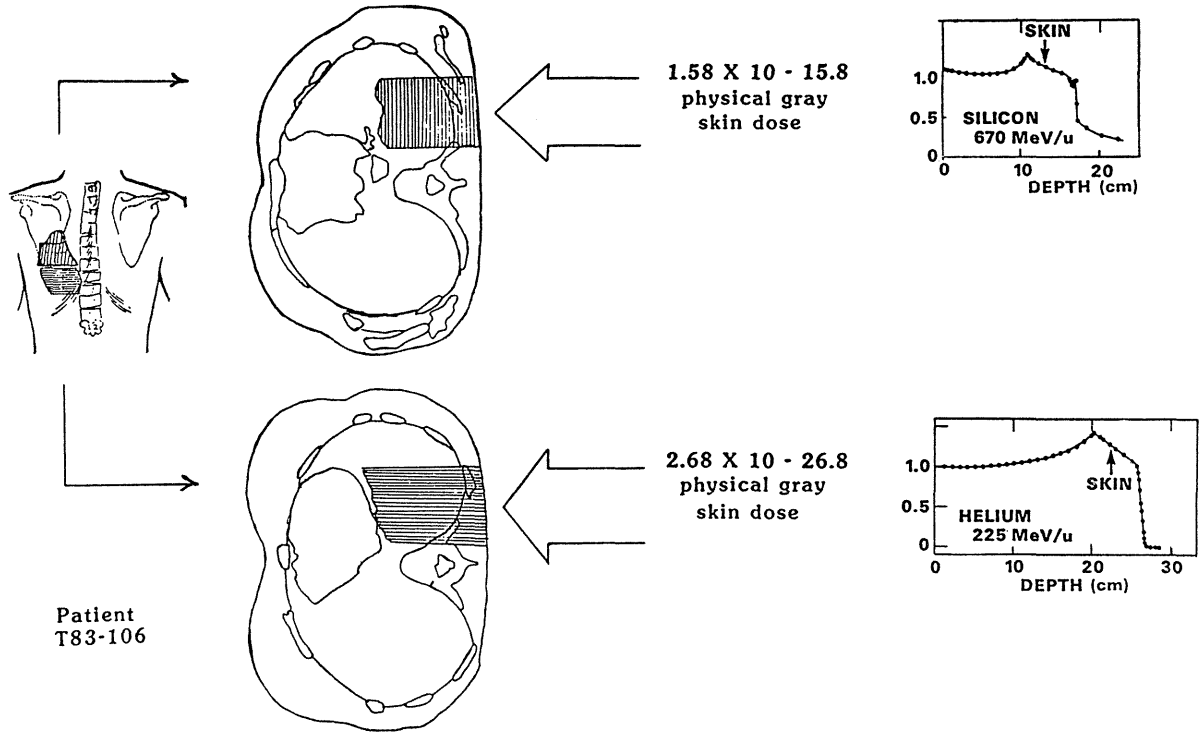

Fig. 2. Diagrammatic representation of two skin fields irradiated with either 225 MeV/u helium ions or 670 MeV/u silicon ions in a patient being treated for lung nodules with two matching fields.

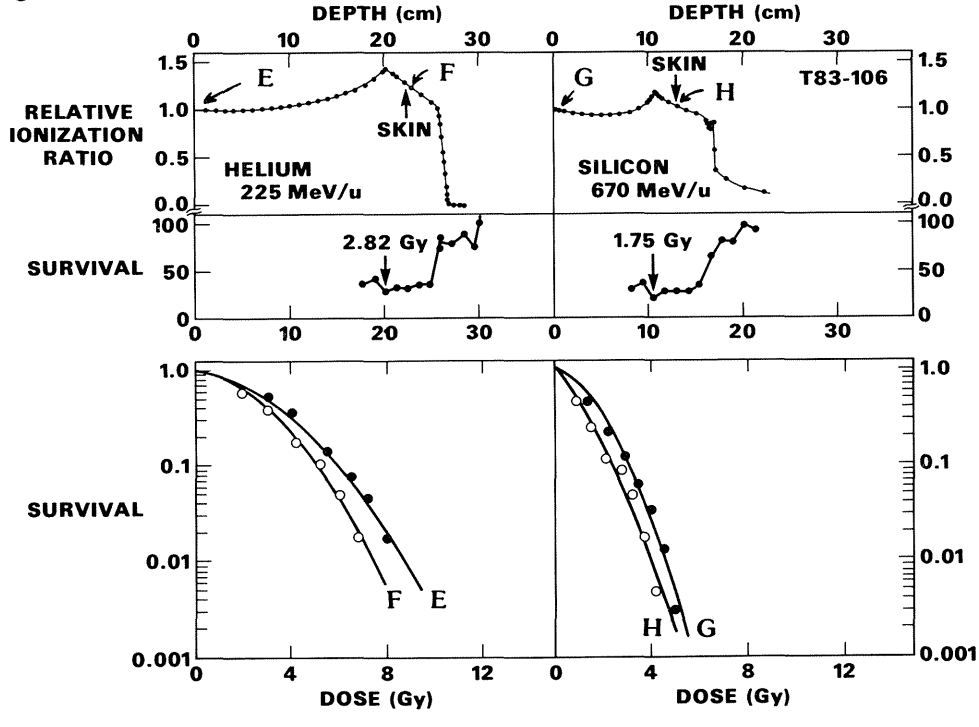

Fig. 3. Cellular survival measurements made at designated positions in the Bragg ionization curves of both a 225 MeV/u helium beam and a 670 MeV/u silicon ion beam using two biological techniques. (upper panel) Measured Bragg curves. (mid panel) Human T-1 cellular survival as a function of depth of penetration in water equivalent material after exposure to a dose fraction of 2.68 Gy helium or 1.58 Gy silicon ions. (lower panel) Survival curves measured at positions indicated in Bragg curves of each beam.

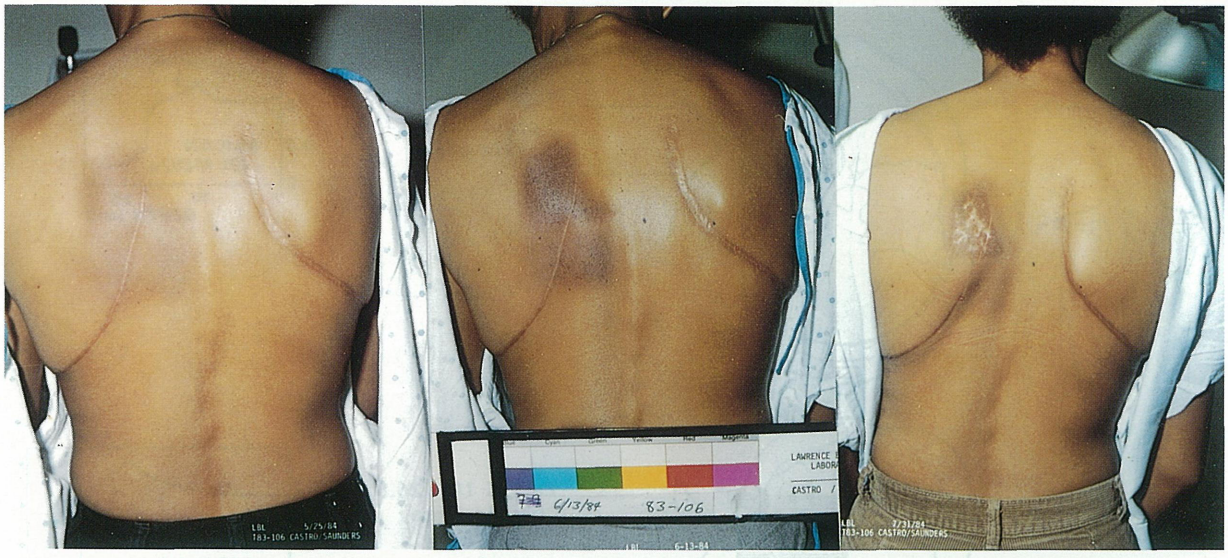

Fig. 4. Photographs illustrating skin reactions to doses of Bragg peak silicon ions and Bragg peak helium ions on adjacent fields on the last day of treatment (left), after three weeks (middle), and after two months (right panel). See text for further discussion.

studied is presented in Fig. 6. The electron response is shown on the right, with progressively steeper responses at lower dose fractions for helium peak, carbon peak and finally the steepest response was observed for Bragg peak neon ions. This kind of plot allows a RBE comparison in the middle of the skin scoring scale at the level of 4.5 - 5.0.

To put our data in perspective with some of the neutron RBE data, we have taken the plot of the RBE versus dose per fraction of 7.5 MeV neutrons by Field, *et al* (8) where a comparison is made of human skin responses at low doses per fraction to those obtained at higher doses per fraction in rat, pig and mouse skin.

Hopewell (9) has extended this analysis to higher energy fast neutron skin RBE values in the pig. The higher energy neutrons show a less steep slope than the 7.5 MeV neutrons. Only carbon and neon charged particle data have been added to this figure (shown as stars). The human skin data from carbon and neon peak exposures remarkably fall on the same line in this log/log plot. The three stars on the right of the lower line are from the fractionated carbon peak data of Leith, *et al* (10) with hamster skin.

The star with the filled symbol is the RBE value we have obtained in our analysis with 308 MeV/nucleon Bragg peak carbon ions on patient skin. The line of particle data lies lower than the 7.5 MeV neutron data line, but the low-LET reference was gamma photons for the neutron work, and was electrons or x-rays for the particle work. Correcting for this difference would shift the lower curve up slightly. The star with the open symbol is from our neon Bragg peak analysis. To our knowledge, there are no other available fractionated neon data from experimental animals.

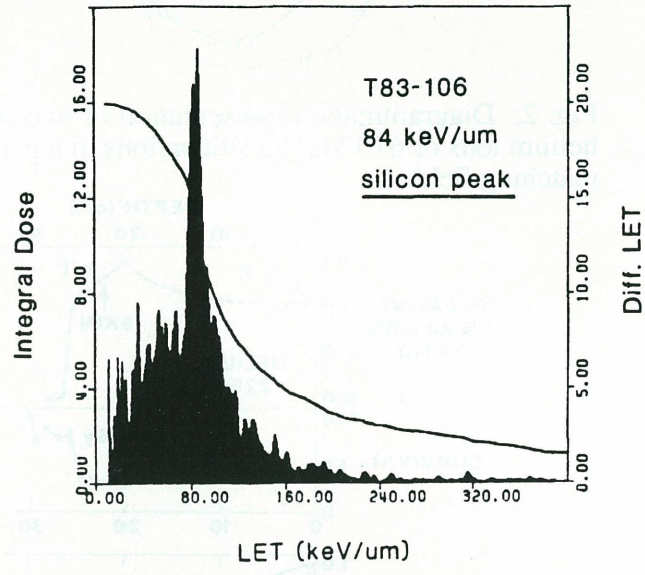

Fig. 5. Dose-average LET distribution from exposures of particle-sensitive CR39 plastic to the extended Bragg peak of a 670 MeV/u silicon ion beam. The peak LET value was 84 keV/μm in the Bragg peak as analyzed by E. Benton.

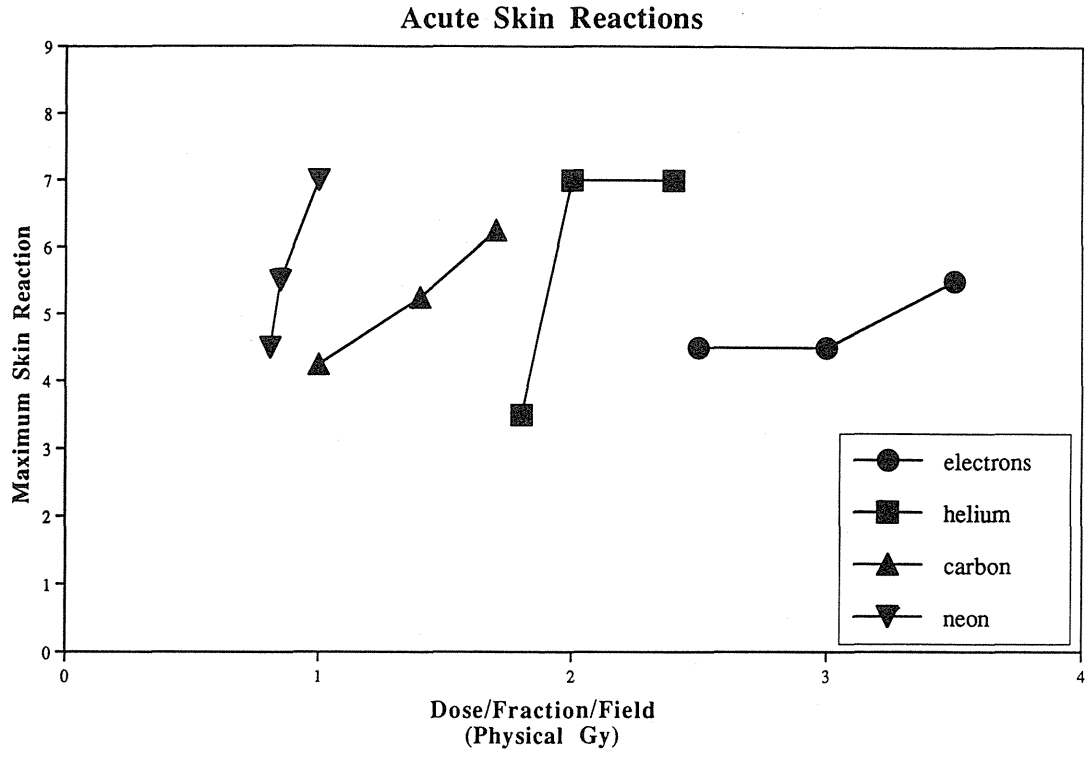

Fig. 6. Maximum human acute skin reaction versus dose per fraction per field of electrons, helium, carbon or neon ions.

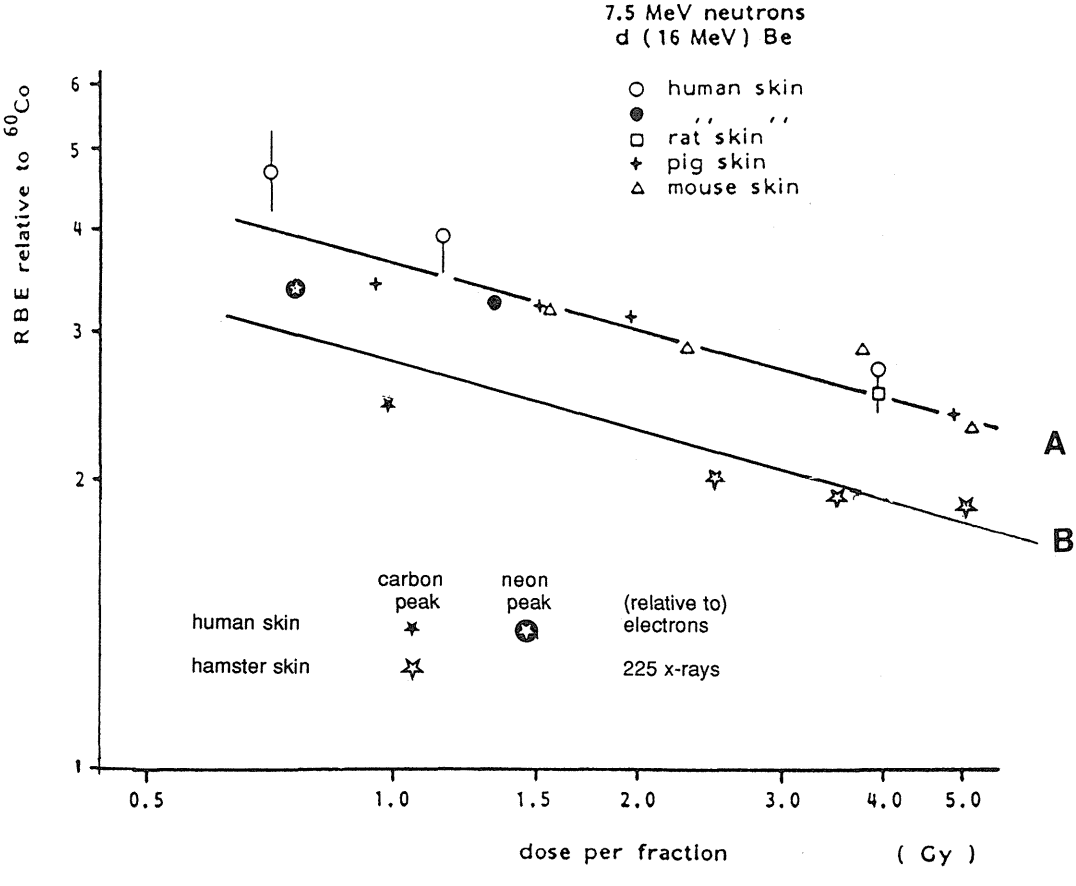

Fig. 7. RBE versus dose or dose per fraction for skin of different species, modified from Field, *et al* (8). Curve A represents neutron RBE data referenced to ^{60}Co radiation. Curve B represents carbon and neon RBE data referenced to electrons on xrays.

CONCLUSIONS

Carbon and neon skin reactions

We have begun a systematic reassessment of acute and late effects in cancer patients treated with charged particles. Preliminary comparisons indicate that Bragg peak carbon ions are slightly less effective than low energy neutrons (7.5 MeV). However, with normalization to similar low-LET reference radiations, carbon Bragg peak ions are nearly comparable to the neutrons. This conclusion about the acute effects of approximately 300 MeV/nucleon carbon ions is an independent qualitative confirmation of Ando's work with carbon ions presented at this Symposium. Bragg peak neon ions uncorrected for the RBE reference are more similar to the 7.5 MeV neutrons, which means that making this correction will shift the neon RBE to a value slightly more effective than the low energy neutron response.

Silicon ion skin reactions and radiobiology

Bragg Peak silicon ions demonstrate an enhanced acute skin reaction and a premature appearance of late effects, that perhaps speaks to the possibility of a significantly different biological mechanism of damage or repair. It is our opinion that normal tissue toxicities should be mapped out, port by port, with the physicians aware of critical normal tissue in each treatment field, and treatment planners accounting for tissue-specific, dose-dependent RBE values. This approach however will only be achievable when we have more information on the particle radiobiology of individual tissues.

Summary

High-LET charged particles have not had sufficient study to prove or disprove their merits in clinical therapy. However, despite promising tumor results (Linstadt, *et al* , 11, and Castro, 12), our follow-up studies have shown neon ions and silicon have had significant late effects on normal tissues. However, the observations presented in this paper should not necessarily mitigate against therapeutic applications of neon ions. Neon ions can provide deep tumor therapy with reduction of the radiobiological oxygen effect and of inherent radioresistance.

For the immediate future, we suggest that the carbon ion beam is to be preferred for further study of deep-seated tumors since it has biological dose localization advantages which are better than protons or neon ions. The ratio of dose in the tumor volume relative to the entrance region is maximized. A sufficient high-LET dose component is present to provide significant DNA damage, and suppression of radiation repair, maximized in the tumor because of the dose localization secondary to charged particles. Full use should be made of dynamic conformal therapy techniques to protect normal tissues and increase the dose in the tumor. We suggest that silicon ions would be advantageous for superficially-placed resistant tumors because of their high-LET advantage.

Techniques for predictive assays should be continued to be developed and tested in the clinic. These include tests of tumor growth kinetics, assays for inherent normal tissue and tumor radiosensitivity, assays of tumor hypoxia and assays to evaluate level and site of DNA damage. Combining these approaches may lead to individual patient profiles which will predict who might benefit from high-LET therapy, and how the selection of these patients should be made. A determined effort should be made to study tumor resistance at the genomic level and search for high-LET mechanisms that overcome this resistance. We anticipate that further follow-up and study of the patients treated with neon ions at LBL will contribute significantly to the rational use of heavy charged particles in the future.

REFERENCES

1. Lett, J.T.; Cox, A.B. and A.C. Lee, A.C. Selected examples of degenerative late effects caused by particulate radiations in normal tissues; TERRESTRIAL SPACE RADIATION AND ITS BIOLOGICAL EFFECTS, Eds. P. D. McCormack; C. E. Swenberg and H. Bucker; Plenum Publishing Corporation; 1988.
2. Leith, J.T.; Ainsworth, E. J. and Alpen, E. A. "Heavy ion radiobiology: normal tissue studies". Adv. Radiat. Biol. 10:191-236; 1983.
3. Field, S.B. Early and late normal tissue damage after fast neutrons. Int. J. Radiation Oncology Biol. Phys. 3:203-210; 1977.
4. Raju, M.R.; Carpenter, S. G. A heavy particle comparative study. Part IV: acute and late reactions British Journal of Radiology 51: 720-727; 1978.
5. Van der Veen, J., Bots, L. and Mes. A. Establishment of two human cell strains from kidney and reticule sarcoma of lung. Arch. Gesamte Virusforsch. 8:230-238; 1958.
6. Blakely, E. A.; Tobias, C.A.; Yang, T.C.H; Smith, K.C. and Lyman, J.T. Inactivation of human kidney cells by high-energy monoenergetic heavy-ion beams. Radiat. Res. 80:122-160; 1979.
7. Albright, N. Computer programs for the analysis of cellular survival data. Radiat. Res. 112:331-340; 1987.
8. Field, S. B.; Morgan, R. L. and Morrison, R. The response of human skin to irradiation with x-rays or fast neutrons. Int. J. Radiat. Oncol. Biol. Phys. 1, 481-488; 1976.
9. Hopewell, J.W.; Barnes, D.W. H. ; Robbins, E. C.; Sansom, J. M.; Young, C.M A. and Wiernik, G. The relative biological effectiveness of fractionated doses of fast neutrons (42 MeV $_{d\text{-}Be}$) for normal tissues in the pig II. Late effects on cutaneous and subcutaneous tissues British Journal of Radiology 63:760-770: 1990.
10. Leith, J.T.; Powers-Risius P.; Woodruff, K. H.; McDonald, M. and Howard, J. Response of the skin of hamsters to fractionated irradiation with xrays or accelerated carbon ions. Radiat. Res. 88:565-576; 1981.
11. Linstadt, D.; Castro, J. and Phillips, T. Results of the phase I-II neon trial at Lawrence Berkeley Laboratory. Int. J. Radiation Oncology Biol. Phys 20:761-769, 1991.
12. Castro, J.R. Heavy ion therapy: Bevalac epoch. In: Hadrontherapy In Oncology. Proceedings of the 1st International Symposium on Hadron Therapy. Como, Italy, October 1993. Elsevier Science B.V., pps. 208-216, 1994.

Calculation of survival in charged particle and neutron beams based on track structure

M. Scholz and G. Kraft
GSI/Biophysics, Planckstrasse 1, D-64291 Darmstadt, Germany

Introduction

Radiation fields used in charged particle tumor therapy are significantly more complex when compared to conventional photon fields. Due to the superimposition of beams with different penetration depth and due to the fragmentation of the primary beam while penetrating through matter, radiation quality may vary significantly throughout the irradiated volume. The relative biological efficiency (RBE) depends on the energy and LET distribution as well as on the biological endpoint and the level of the biological effect under consideration. Therefore, it is impossible to determine the radiobiological characteristics for all radiation fields used in the therapeutical practice. Instead, biophysical models have to be used in order to interpolate or extrapolate experimental data.
It has been shown, that the biological action of heavy ions can be predicted on the basis of the X-ray sensitivity and the microscopic distribution of energy deposition around the particle trajectories, i.e. track structure. [Scholz and Kraft 1992, Scholz and Kraft 1994]. More recently, these calculations have been extended in order to simulate irradiation of cells in complex radiation fields, i.e. including the superimposition of Bragg peaks and fragmentation effects. [Scholz et al. 1994]
In this contribution, the basic ideas of the model will be presented, and results of the calculation are compared with experimental data relevant for the application of charged particles in radiation therapy.

Basic principles of the model

The most significant difference between X-rays and charged particle radiation is their different spatial energy deposition pattern. Whereas with X-rays the dose is deposited nearly homogenous throughout the irradiated volume, the dose deposited by charged particles is concentrated in the region near their trajectory and shows a sharp decrease according to a $1/r^2$-law. The key question concerning charged particle irradiation is, whether high-LET specific effects like enhanced RBE or decreased OER can be attributed to these differences in the spatial energy deposition pattern.
In general, an enhanced effect of concentrated energy deposition as compared to a homogenous distribution can be already expected from the shouldered shape of X-ray survival curves, as is demonstrated in Fig. 1. Here, two possible ways to predict the effect of a high local dose in a small subvolume of the cell nucleus are compared. Based on the *average* dose of 2 Gy, a survival of approximatly 70% is expected. If, however, the prediction is based on the *local* dose of 10 Gy in 20% of the nucleus, a significantly lower survival is expected. A dose deposition of 10 Gy in the whole nucleus would lead to a survival probability of 2%. Assuming a homogenous distribution of radiosensitivity throughout the nucleus, each subvolume is expected to contribute equally to the total effect. Therefore,

partial irradiation of only 1/5 of the nucleus leads to a survival value $S_{1/5}$, so that

$$(S_{1/5})^5 = 0.02 \tag{1}$$

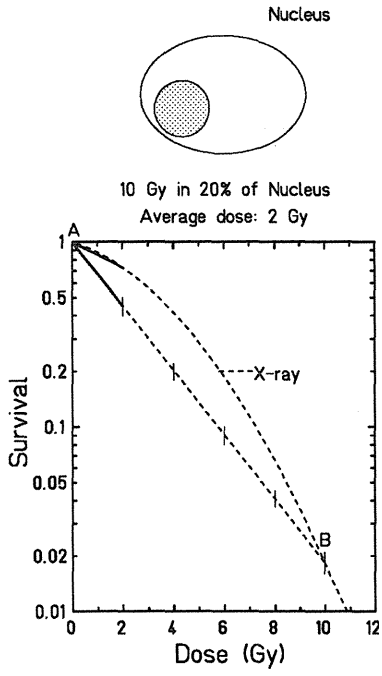

Fig. 1
Schematic explanation of biological action of local dose depositions

This condition is illustrated in Fig. 1 by dividing the straight line A-B into five equal intervals. As a result, the survival value based on the *local* dose deposition is expected to be approximatly 45%, which is significantly lower compared to the value based on the *average* dose deposition. This example already demonstrates, that the concentration of energy deposition is expected to show an enhanced efficiency compared to the homogenous deposition in any case, where the X-ray survival curve is shouldered.
The model calculations are based on the *local* dose and the corresponding *local* biological effect, as described above. The total biological effect, which is represented by the number of lethal events induced by a given local dose distribution D(x,y,z) inside the nucleus, is obtained by numerical integration of the local effect throughout the whole sensitive volume, i.e. the cell nucleus:

$$\overline{N_{lethal}} = \int_x \int_y \int_z \frac{ln\ S_X(D(x,y,z))}{V}\, dxdydz \tag{2}$$

where V is the volume of the nucleus and $S_X(D)$ represents the X-ray dose-effect curve. According to the Poisson statistics, the survival probability of a cell is given by the probability to carry no lethal event:

$$S = e^{-\overline{N_{lethal}}} \tag{3}$$

Results and Discussion

Fig. 2 shows a comparison of calculated and measured inactivation cross sections for V79 Chinese Hamster cells as a function of LET. In general, there is a good agreement between experimental and theoretical values. Deviations are mainly observed in the region from 100-300 $keV/\mu m$, where calculations underestimate the biological effect by approximatly 20-30%. However, it has to be pointed out, that the calculations are still based on several crude approximations as e.g. the same size and sensitivity for all cells of a asynchronous cell population. Better agreement is expected, if the cell cycle dependent size and sensitivity are taken into account.

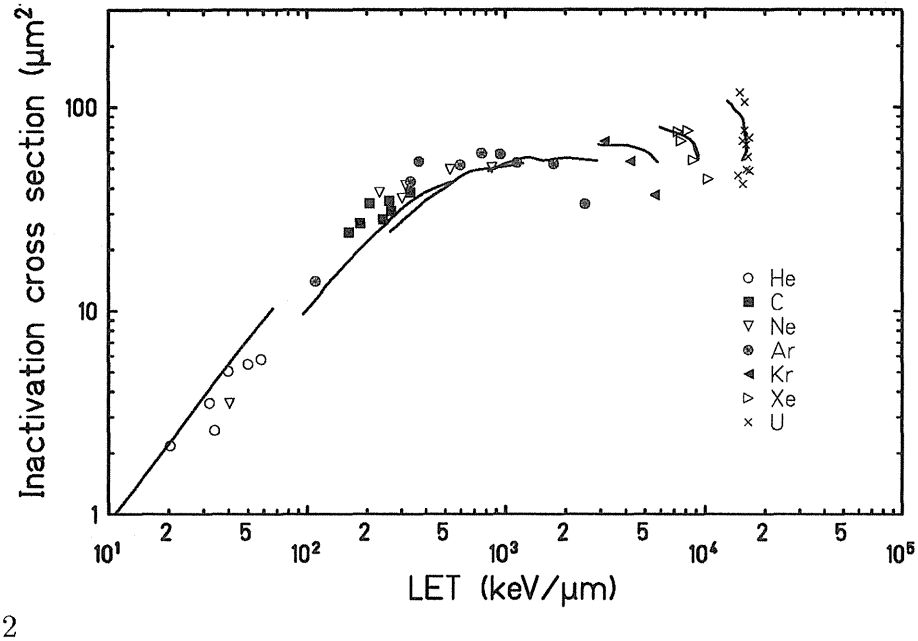

Fig. 2
Comparison of model calculations for inactivation cross sections σ_{inact} (full lines) with experimental results obtained with V79 Chinese hamster cells (symbols, redrawn from [Kraft 1987]).

Calculations shown in Fig. 2 are based on track segment conditions, i.e. defined energy and LET of the particles. The main goal for the development of our model, however, is to describe survival in complex irradiation fields, as they are used for charged particle radiotherapy. In general, these radiation fields consist of a superposition of particles with different energy and LET. In addition, for heavier particles like carbon, fragmentation effects have to be taken into account. Therefore, the model calculations have been extended to cover these complex fields as well (details are described in Scholz et al. 1994). Fig. 3 compares calculated and measured survival curves at different penetration depth in a water phantom. The contribution of lighter fragments increases with increasing penetration depth. The calculations are based on fragment spectra taken from a model which was adjusted to reproduce the experimental data [Haberer 1994]. It has to be pointed out, that survival values at 60mm penetration depth are higher than at 0mm penetration depth. This results from fragmentation processes and a corresponding decrease of primary particles, which overcompensate the increase of LET with penetration depth.
A similar situation, where highly complex charged particle fields are involved, is the case of neutron irradiation. Here, the biological effect is induced by the secondary charged particles produced by neutron irradiation. If these secondary particle spectra are known, the model is able to predict survival after neutron irradiation as well, as is shown in Fig. 4. Model predictions are compared with experimental data obtained by Eguchi-Kasai et al. (1994). As is demonstrated by this comparison, the model predicts survival after neutron irradiation even for different cell lines within a broad range of sensitivity against X-rays.

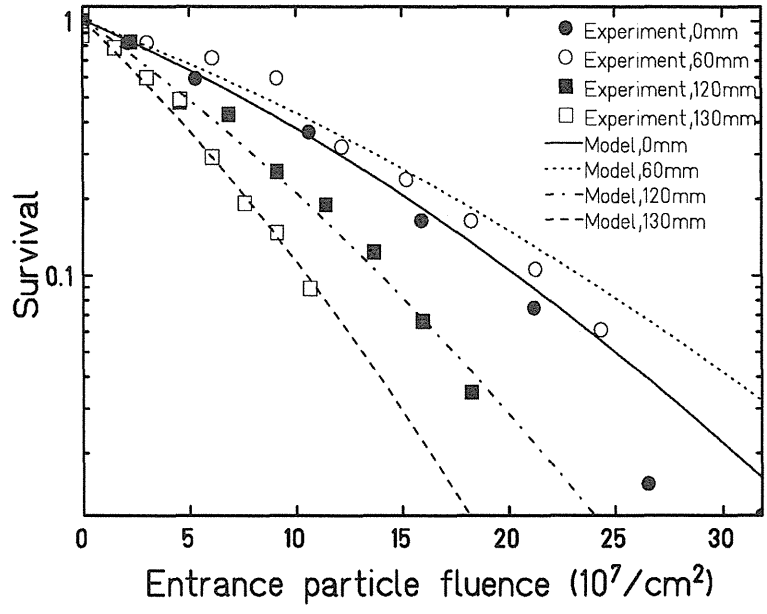

Fig. 3
Survival curves at different penetration depth of a 270 MeV/u carbon beam in water (symbols: experimental data; full lines: model calculations). Survival is plotted as a function of the particle fluence at 0mm penetration depth. Model calculations include the fragmentation of the primary beam.

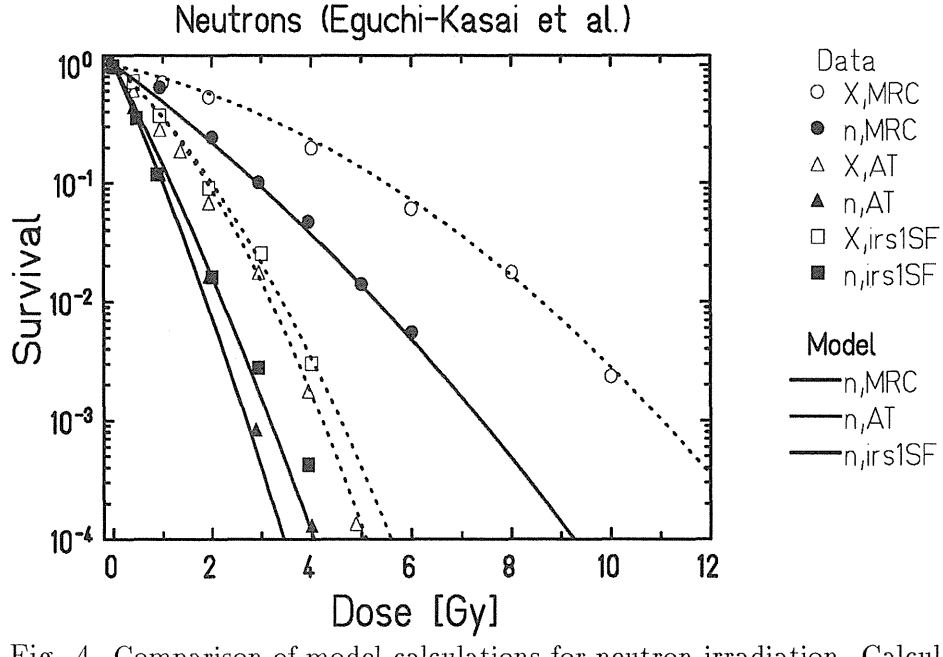

Fig. 4 Comparison of model calculations for neutron irradiation. Calculations are based on secondary charged particle spectra from [Morstin et al. 1985]. Experimental data were taken from [Eguchi-Kasai et al. 1994].

Conclusions

It has been shown, that cellular survival after charged particle irradiation can be predicted by model calculations based on the radial dose distribution of particle tracks. Good agreement is observed for track segment conditions as well as for complex charged particle fields, as they result for example from nuclear fragmentation of heavy particles or from recoil of target nuclei in neutron fields. Therefore, it is expected that the model is able to predict survival in extended Bragg peaks, as they are used for applications in charged particle radiotherapy, and that the model can be used in order to develop guidelines for the optimization of treatment modalities.

References

Eguchi-Kasai, K., Murakami M., Itsukaichi, H., Fukutsu, K., Kanai, T., Furusawa, Y., Sato, K., Ohara, H. and Yatagai, F., 1994, The role of DNA repair on cell killing by charged particles. Submitted to *Advances in Space Research*

Haberer, Th., 1994, Ph.D. Thesis, University of Heidelberg, GSI-Report 94-09

Kraft, G., 1987, Radiobiological effects of very heavy ions: inactivation, induction of chromosome aberrations and strand breaks. *Nuclear Science Applications* **3**, 1-28

Morstin, K., Dydejczyk, A. and Booz, J., 1985, High energy neutron interactions with tissues and tissue substitutes. In: Nuclear and Atomic Data for Radiotherapy and related Radiobiology (Proc. of Advisory Group Meeting, Rijswijk 1985) (IAEA, Vienna), 239-262

Scholz, M. and Kraft, G., 1992, A parameter free track structure model for heavy ion action cross sections. In: Biophysical Modelling of Radiation Effects. Edited by: K.H. Chadwick, G. Moschini and M.N. Varma (Adam Hilger, Bristol), 185-192

Scholz, M. and Kraft, G., 1994, Calculation of heavy ion inactivation probabilities based on track structure, X-ray sensitivity and target size. *Radiation Protection Dosimetry* **52**, 29-33

Scholz, M., Kraft-Weyrather, W. and Kraft, G., 1994, Calculation of cell survival in complex charged particle fields. Submitted to *Radiation and Environmental Biophysics.*

LET DEPENDENCE OF BIOLOGICAL EFFECTS BY ACCELERATED C ION BEAMS

MASAO SUZUKI*, MASAMI WATANABE**, TATSUAKI KANAI*, YOKO KASE*, FUMIO YATAGAI***, TAKESHI KATO# and SHO MATSUBARA##

* *National Institute of Radiological Sciences, 4-9-1 Anagawa, Chiba 263, Japan*
** *Nagasaki University, 1-14 Bunkyo-machi, Nagasaki 852, Japan*
*** *The Institute of Physical and Chemical Research, Saitama 351, Japan*
\# *School of Medicine, Osaka University, Osaka 565, Japan*
\#\# *Yokohama City University, 3-9 Fukuua Kanazawa-ku, Yokohama 236, Japan*

Purpose : In this study we investigated the LET dependence of cell death, mutation induction at the HPRT locus and the induction of chromatin breaks in normal human fibroblast cells irradiated by accelerated carbon ions.
Methods and Materials : Human embryonic fibroblast-like cells (HE20 cells) were irradiated by accelerated carbon-ion beams with various LETs. Cell death was detected by a colony- formation assay and mutation induction at the HPRT locus was measured by a 6-thioguanine(6TG) resistant colony-forming ability. Chromatin breaks and rejoining were measured by the procedure of premature chromosome condensation(PCC). DNA alteration was investigated as the deletion of 9 HPRT exons in 6TG-resistant clones detected by the multiplex PCR method.
Results : Cell death, mutation induction and induction of non-rejoining chromatin breaks had the same LET dependence. Carbon-ion beams of 110 and 124keV/μm were the most effective at all endpoints. The number of initially induced chromatin breaks, however, was independent of LET. The deletion spectrum of exons in the HPRT locus was LET-specific. Almost all of the mutants induced by 124keV/μm beams showed deletion of the entire locus, while all mutants induced by 230keV/μm beams showed no deletion.
Conclusion : These results suggest that the difference in the density distribution of the track of carbon-ion beams, the fragments with lower LETs and secondary electrons is responsible for the LET dependence of biological effects.

Normal human cells, Accelerated carbon-ion beams, PCC, HPRT locus, PCR

INTRODUCTION

It is well established that the biological effects of high LET radiation is more effective than that of low LET X or gamma rays. (1,2,3,4,5,6,7,8,9, 10,11,12,13,14,16,17). The LET dependence of these biological effects has been reported for various ions (2,4,5,7,8,15,18,19). These results indicated that the range of LET most effective in producing these effects was 100 to 200keV/μm.

In molecular studies, the mutation spectra of different types of radiation have been examined (20,21,22,23,24). There was no evidence that X or gamma rays and alpha-particles might show different mutation spectra. (21,24).

In this study, we investigated the LET dependence of cell death, mutation induction and chromatin damage in human cells irradiated by carbon-ion beams of different LETs and examined the molecular characterization of the HPRT locus in mutant clones induced by carbon-ion beams and ^{137}Cs gamma rays.

MATERIALS AND METHODS

Human embryonic (HE20) fibroblast-like cells (25) were used as target cells in this study. Mitotic XP2OS cells were also used as inducers of premature chromosome condensation(PCC). Both cell types were cultured in Eagle's minimum essential medium (MEM), supplemented with 0.2mM serine, 0.2mM aspartate, 1mM pyruvate and 10% fetal bovine serum (26) in a 5% CO_2 incubator at 37^{0}C.

Target HE20 cells were inoculated into 25cm^2 plastic flasks at 8x10^5 cells per flask 2 days before irradiation,by which time the cells were confluent, and about 90% were in G_1- or G_0-phase, as determined by flow cytometry (data not shown). The HE20 cells were irradiated by carbon-ion beams accelerated by the Riken Ring Cyclotron (RRC) at the Institute of Physical and Chemical Research and the cyclotron at the National Institute of Radiological Sciences (NIRS) in Japan. The details of the irradiation procedures

and dosimetry have been described elsewhere (27). Briefly, the fluence of the carbon-ion beam was measured using a plastic scintillator and the value of LET was measured using a proportional counter filled with tissue equivalent gas. The irradiation dose at the sample position was determined by multiplying the fluence by the LET value of the carbon-ion beams. We also monitored and controlled the irradiation dose using a parallel plate ionization chamber. The energies of the carbon-ion beam were 135 MeV/u (RRC) and 12 MeV/u (NIRS). Lucite absorbers were used to change LET. At the sample position, we estimated the LET_∞ values to be 22, 39, 68, 75, 110, 124, 148 and 230keV/μm. The dose rate was about 2 Gy/min for all of the carbon-ion beams. For a comparison, we irradiated target cells with ^{137}Cs gamma rays at a dose rate of 1.2 Gy/min. All irradiations were carried out at room temperature.

After irradiation, different numbers of target cells were immediately plated onto 100mm plastic dishes to form 60 to 70 colonies per dish for cell survival assay. The procedure for mutation assay have been described previous report (28). Briefly, sufficient number of cells were irradiated to ensure about $1x10^6$ cells survived each radiation dose. After irradiation cells were cultured in $75cm^2$ plastic flasks (T75) at a density of 1.5 to $2.0x10^6$ cells per T75 flask and subculture was carried out three times at 5 day intervals to allow expression of mutation. At the end of the expression period , $1x10^6$ cells were plated onto 20 dishes (100mm diameter) containing MEM supplemented with 40μM of 6TG. The mutation frequency was determined as the number of 6-thioguanine(6TG)-resistant colonies per 10^6 survivors. A mutant colony was randomly isolated from each set of dishes using a micropipette tip containing a small volume of complete medium. The isolated 6TG-resistant clones were cultured, then stored in liquid N_2 for molecular analysis.

Chromatin break induction was measured as fragmentation of prematurely condensed chromosomes. The procedure for induction of PCC has been described in detail elsewhere (14,29). Briefly, $1x10^6$ mitotic XP2OS cells produced by 6hr incubation in the presence of 0.1μg/ml demecolcine (Wako Pure Chemical Industries Ltd.) were mixed with an equal number of irradiated target cells in a polypropylene tube (Falcon 2059). The cell mixture was centrifuged at 200g for 5min and the pellet washed in 4ml PBS. After centrifugation at 200g for 5min, the pellet was exposed to 0.15ml of 50%(w/v) polyethyleneglycol (PEG M.W.=1540, Boehringer Mannheim GmbH, Germany) in 75mM Hepes for 1min, then 4ml of PBS was gently added to the tube and the cell suspension centrifuged at 200g for 5min. The pellet was resuspended in 5ml of MEM containing 0.1μg/ml demecolcine and incubated in a CO_2 incubator for 1hr. Subsequently, these cells were treated with 75mM KCl solution for 20min at room temperature and fixed with Carnoy's solution (methanol : acetic acid = 3:1). The cell suspension was dropped onto slides, air dried and stained with 5% Giemsa solution. PCC preparations of 50 cells were scored under a light microscope. In the study of the rejoining of chromatin breaks we incubated the cells, once fusion was complete, in MEM containing 0.1μg/ml demecolcine and 25μg/ml cycloheximide (Sigma) for 1hr in a CO_2 incubator (13) in order to inhibit rapid rejoining of chromatin breaks,.

The mutant cells ($1x10^6$) were placed in a microfuge tube and 100μl of K-buffer (50mM KCl, 10mM Tris HCl and 2.5mM $MgCl_2$, pH8.3), 1μl of 10mg/ml proteinase K and 0.5% Tween20 were added. After mixing, the tube was heated at 56^{0}C for 45min and at 95^{0}C for 10min. Five μl of this DNA solution (about 250ng) was used in the PCR reaction. Seven sets of primers were used in a multiplex PCR reaction to amplify exons 2 to 9 of the HPRT gene. DNA was mixed with 7 primer pairs in a total volume of 50μl of 67mM Tris HCl pH8.8, 6.7mM $MgCl_2$, 16.6mM $(NH_4)_2SO_4$,6.8μMEDTA, 5mM ß-mercaptethanol and 0.5 mM of each deoxyribonucleotide triphosphate. The mixture was heated at 95^{0}C for 5min to denature the DNA which was then annealed at 60^{0}C for 15min. Two units of *Taq* DNA polymerase (Promega Corporation) and 30μl of mineral oil were added. After preheating at 60^{0}C for 15min, the PCR reaction was performed for 30 cycles at 94^{0}C for 30sec/ 60^{0}C for 48sec/ 70^{0}C for 2min, followed by final extension at 70^{0}C for 7min, using a thermal cycler (Perkin-Elmer). The PCR products were analyzed by 4% agarose gel electrophoresis in TBE buffer (89mM Tris HCl, 89mM boric acid, 2mM EDTA, pH 8.0) at 8.3V/cm for 1hr at room temperature. The gel was stained with ethidium bromide (1μg/ml) for 1hr.

RESULTS

The dose-response curves for cell death in HE20 cells irradiated by carbon-ion beams and ^{137}Cs gamma rays are shown in Fig.1. Carbon-ion beams are more effective than ^{137}Cs gamma rays in producing cell death in HE20 cells and the RBE relative to ^{137}Cs gamma rays increases with LET up to about 100-120keV/μm, then decreases at higher LETs. The RBE values at 10% survival level are to be 1.90 for 22keV/μm, 2.13 for 39keV/μm, 2.36 for 68keV/μm, 2.75 for 75keV/μm, 3.57 for 110keV/μm, 3.57 for 124keV/μm, 3.00 for 148keV/μm and 2.75 for 230keV/μm.

Fig.2 shows that the mutation frequencies by carbon-ion beams steeply increase at low doses compared with ^{137}Cs gamma rays. The RBE, calculated as a ratio of doses that produced 100

mutants per 10^6 survivors, is 2.71 for 22 keV/μm, 3.10 for 39keV/μm, 3.61 for 68keV/μm, 5.00 for 75keV/μm, 7.22 for 110keV/μm, 7.32 for 124keV/μm, 4.64 for 148keV/μm and 5.00 for 230keV/μm.

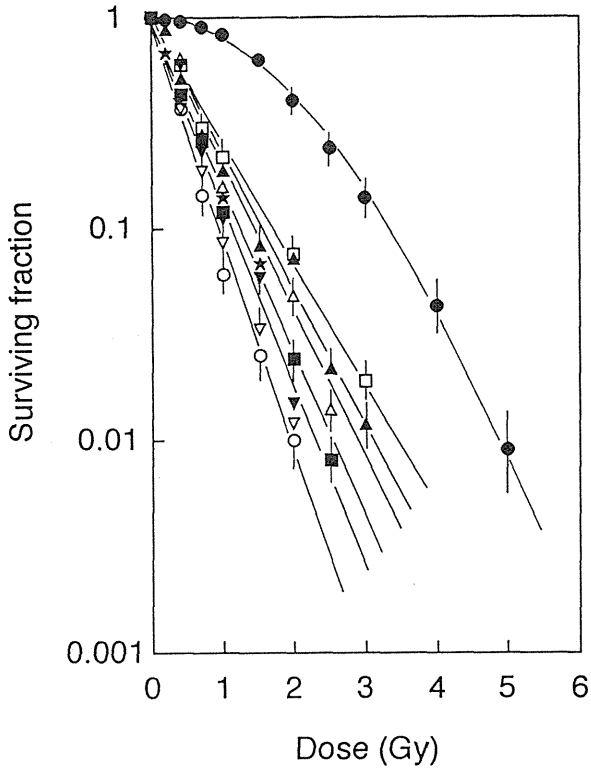

Fig.1 Dose-response curves for cell death irradiated by ^{137}Cs gamma rays (●), or carbon-ion beams at 22keV/μm (□), 39keV/μm (▲), 68keV/μm (△), 75keV/μm (■), 110keV/μm (○), 124keV/μm (▽), 148keV/μm (▼) and 230keV/μm (★). Results presented are the mean and standard error of three independent experiments. The curves are fitted by the method of least squares.

Fig. 3 shows the LET dependence for cell death and mutation induction (LET vs RBE). These curves show the maximum efficiency was in the LET range of 100 to 120 keV/μm. This LET dependence is consistent with previous reports on cell death (2,5,7,19), cell transformation (4,8) and DNA strand breaks (7,15,18).

Fig. 4 shows photomicrographs of prematurely-condensed chromosomes of control and 110keV/μm-beam-irradiated HE20 cells. In these photographs we observe 46 prematurely-condensed G_1/G_0 chromosomes in control HE20 cells (upper photograph), and 74 fragments in 110keV/μm-beam-irradiated (1Gy) cells (lower photograph). The yield of chromatin breaks per cell is estimated as the mean number of PCC fragments in excess of the mean number of control cells.

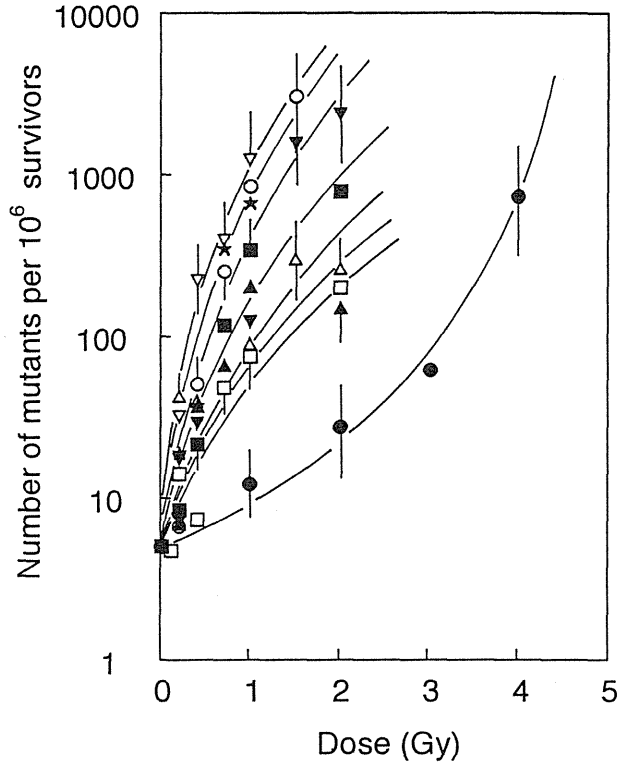

Fig.2 Dose-response curves of the frequency of HPRT-deficient mutants. Results presented are the mean and standard error of three independent experiments. The curves are fitted by eye. Symbols are the same as the Fig.1.

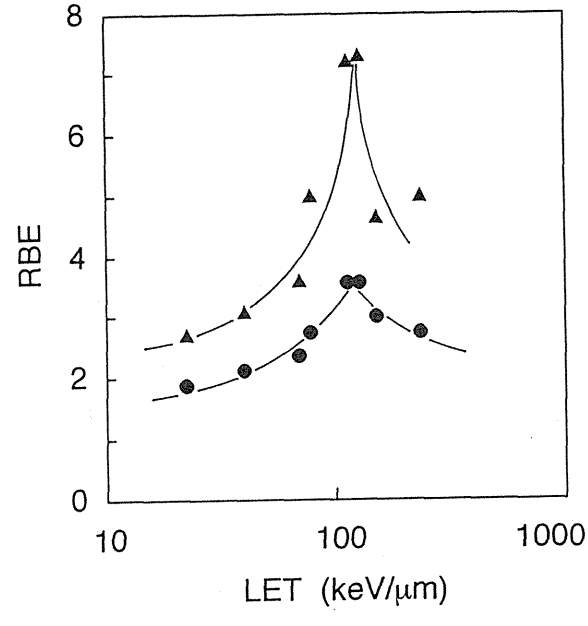

Fig.3 LET dependence (LET vs RBE) of cell death (●) and mutation induction (▲). Data are taken from figure 1 and figure 2.

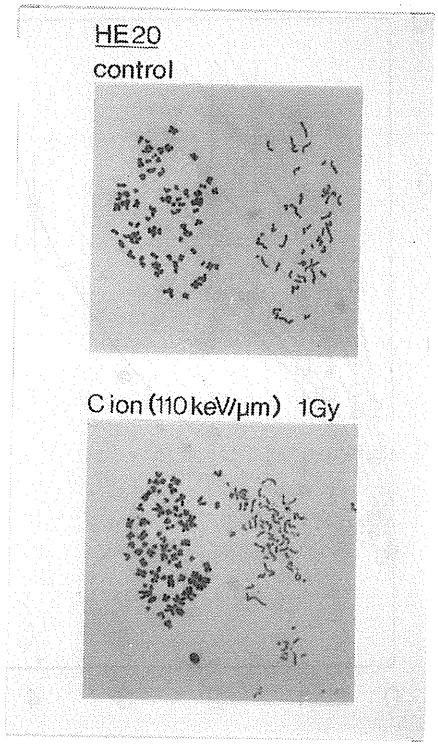

Fig.4 Photomicrographs of prematurely condensed chromosomes of control (upper) and 110keV/μm-beam-irradiated (1 Gy) HE20 cells (lower).

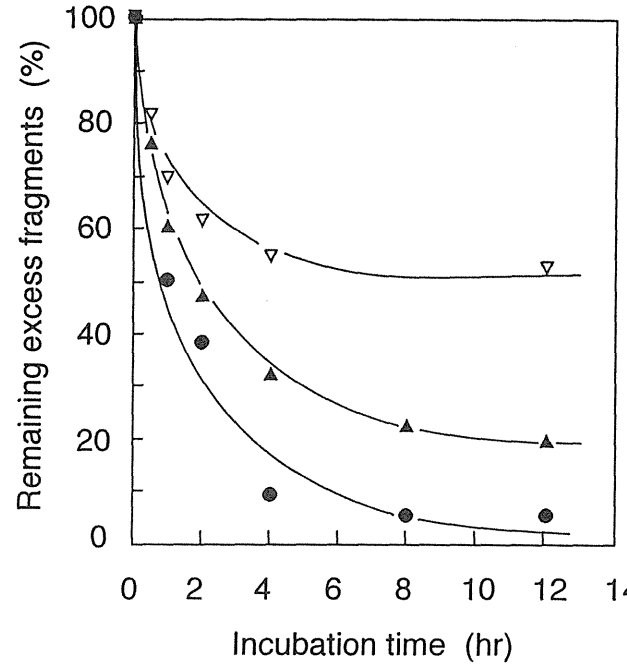

Fig.5 Rejoining time course of chromatin breaks after 4Gy irradiation of ^{137}Cs gamma rays (●), 3Gy of carbon ions at 39keV/μm (▲) and 124keV/μm (▽).

Fig. 5 shows the time course of the rejoining of chromatin breaks after 4Gy irradiation by ^{137}Cs gamma rays and after 3Gy irradiation by carbon-ion beams at 39keV/μm and 124keV/μm. About 50% of the initial breaks induced by gamma rays are rejoined 1hr after irradiation and about 95% of initial breaks are rejoined after 8hr of post-irradiation incubation, while only 50% of breaks induced by beams of 124keV/μm are rejoined after 8hr. These results suggest that the rejoining of PCC breaks occurs quickly.

To prevent the fast rejoining, we added cycloheximide (CHM) during the 1hr incubation after cell fusion, during which target chromatin is condensed. Fig. 6 shows the dose-response curves for the induction of chromatin breaks in both the absence (a) and presence of 25μg/ml CHM (b). The results indicate that the difference in the numbers of PCC breaks in cells between carbon-ion beams and gamma rays is reduced with the use of CHM. The number of PCC breaks caused by beams of 110keV/μm and 124keV/μm is the same in the absence and presence of CHM (15.3 breaks/Gy/cell in the presence of CHM and 15.1 breaks/Gy/cell in the absence of CHM), while different rates of induction are found in the presence or absence of CHM at lower LET radiations (9.7 breaks/Gy/cell in the presence of CHM and 5.5 breaks/Gy/cell in its absence in the case of ^{137}Cs gamma rays).

Table 1 shows the percentage of non-rejoining chromatin breaks in cells initially irradiated with 3Gy. About 93% of gamma-ray-induced PCC breaks rejoined, while only 50% of 110keV/μm- or 124keV/μm-beam-induced breaks do so.

The results are summarized in Fig.7. The difference in LET dependence is reduced with the use of CHM to avoid rejoining during the 1hr post-irradiation incubation time. The number of chromatin breaks per Gy per cell after 12hr of post-irradiation incubation is 0.69 for gamma rays and 7.3 to 7.6 for 110 to 124keV/μm beams.

Table 1 Non-rejoining fraction of PCCbreaks after 12hr post-irradiation incubation

Radiation	Non-rejoined fraction (%)
^{137}Cs gamma rays	7.1± 3.4
C ions (22keV/μm)	23.4 ± 5.4
C ions (39keV/μm)	19.0 ± 5.2
C ions (68keV/μm)	37.4 ± 5.1
C ions (110keV/μm)	49.7 ± 6.6
C ions (124keV/μm)	51.6 ± 7.2
C ions (148keV/μm)	34.3 ± 2.1
C ions (230keV/μm)	25.9 ± 6.7

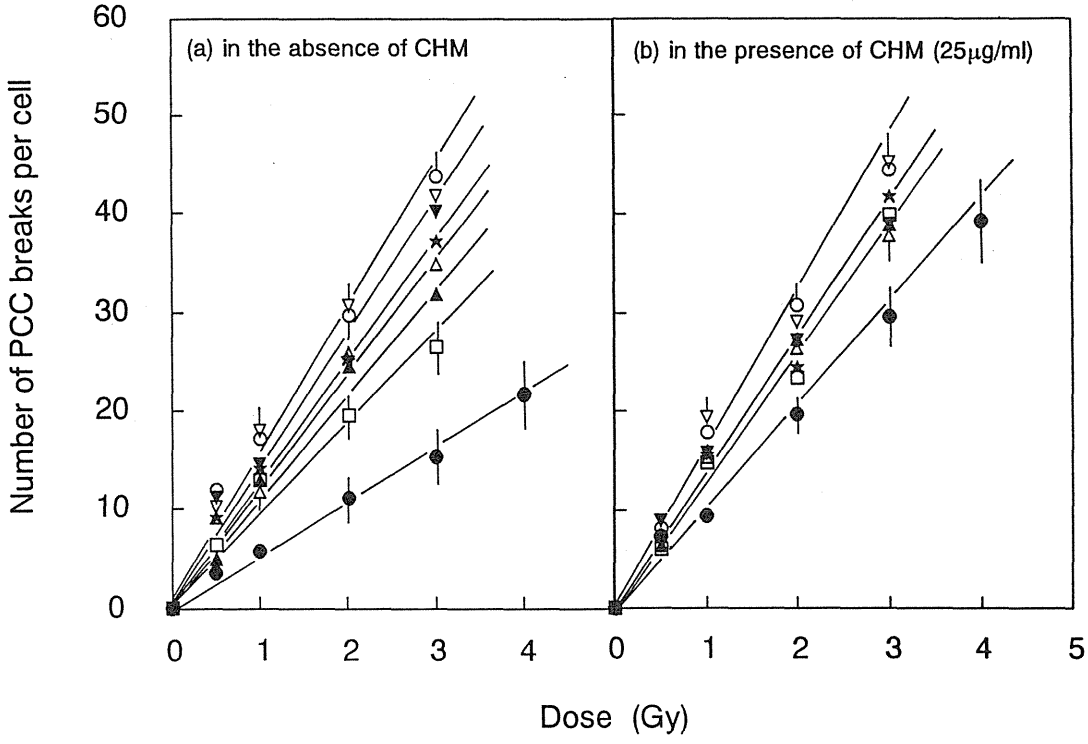

Fig.6 Dose-response curves of chromatin breaks detected as fragmentation of prematurely condensed chromosomes with PCC method in the absence (a) and presence of 25μg/ml CHM (b). Data presented are the mean and standard error of three independent experiments. The curves are fitted by the method of least squares. Symbols are the same as in Fig.1.

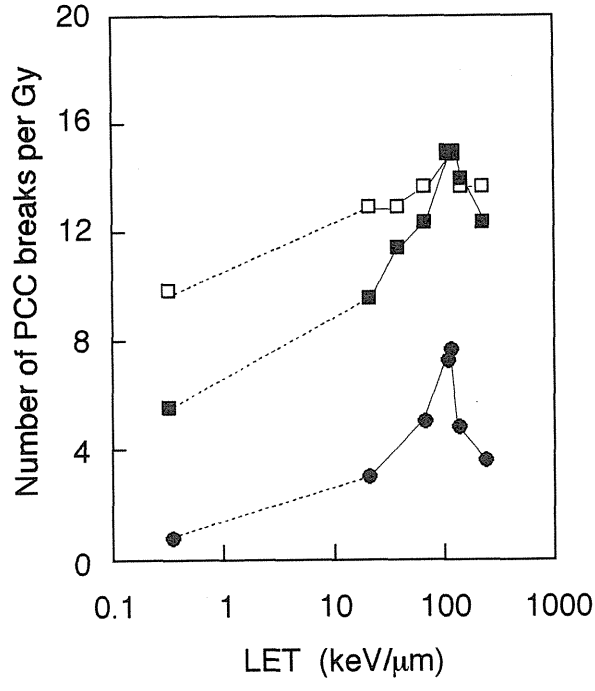

Fig.7 LET dependence of chromatin break induction. (□); initially induced breaks detected in the presence of 25μg/ml CHM, (■); number of breaks after 1hr of irradiation in the absence of CHM , (●); number of residual breaks after 12h of post-irradiation incubation. Points at 0.3keV/μm are for ^{137}Cs gamma rays. Data are taken from figure 6 and table 1.

Fig. 9 illustrates examples of the various types of mutants analyzed by gel electrophoresis. Table 2 summarizes the data obtained for all the 6TG-resistant mutants. About 30% of spontaneous and gamma-ray-induced mutants show no change in the band migration pattern. 10% of spontaneous mutants have total gene deletions, compared to almost 40% of the gamma-ray-induced mutants. In the case of mutants induced by carbon ions, however, the proportion of total gene deletion is dependent on the LET of the carbon-ion beams. Almost all of the mutants induced by 68 and 124keV/μm carbon-ion beams lacked any detectable HPRT-specific sequences and therefore are caused by a deletion of the entire locus, while no mutant induced by 230keV/μm carbon ions showed any deletion. In addition, there is a larger proportion of partial deletions in the spontaneous and gamma-ray mutants than among the carbon-ion mutants.

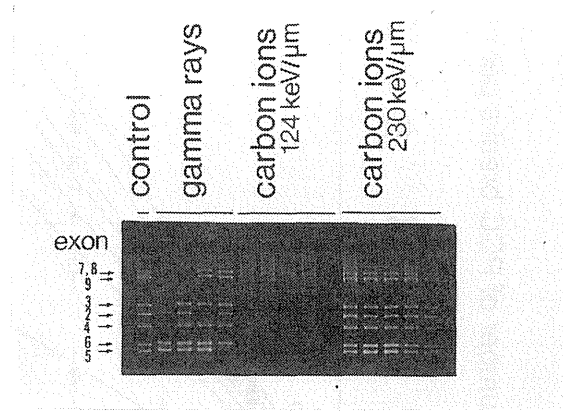

Fig.9 Photograph of gel electrophoresis with multiplex PCR products of 7 exon regions in the HPRT gene.

Table 2. Summary of the structure of the HPRT locus in spontaneous, ^{137}Cs gamma rays and carbon-ion induced mutants.

Radiation	Total mutants assayed	Number of mutants								
		No alteration	All exons deleted	Partial deletion[a)]						
				total	exon 2	3	4	5	6	7,8	9
Spontaneous	32	8	3	21	1	3	4	16	15	8	11
^{137}Cs gamma rays	42	13	18	11	1	0	8	8	8	10	10
C ions(39keV/μm)	12	4	2	6	2	1	1	2	2	1	1
C ions(68keV/μm)	14	0	14	0							
C ions(124keV/μm)	41	3	38	0							
C ions(230keV/μm)	32	32	0	0							

a); Some mutants show loss of more than one exon

DISCUSSION

We studied the LET dependence of cell death, mutation induction, chromatin break induction and rejoining of the breaks induced by various LETs of carbon-ion beams. Cell death, mutation induction and non-rejoining chromatin break induction all showed the same LET dependence with most effective peaks between 110 and 124keV/μm (Fig. 3 and 7), as reported previously (2,4,5,7,8,15,18,19).

The difference of frequency of induced chromatin breaks, measured under conditions which prevent the rejoining of breaks in the presence of CHM, was reduced when ^{137}Cs gamma rays or carbon-ion beams of various LETs are used. However, the number of chromatin breaks which remain after 12h of post-irradiation incubation was dependent on the LETs. These results suggest that, although the difference of the total number of breaks per cell per Gy produced among different LETs is small, the ratio of rejoinable and non-rejoinable breaks depends on the differing LETs. We suggest that non-rejoining chromatin breaks lead to cell death, explaining the close correlation between LET dependent cell

death and the presence of non-rejoining breaks.

However, since viable mutant cells are clearly not dead, it would seem that the LET dependence of mutation induction results from stable maintained chromatin damage caused by incorrect rejoining of breaks. To investigate this, it may be necessary to use techniques such as fluorescence *in situ* hybridization (FISH) (30).

In this study, we also observed the LET-specific effect on the deletion pattern of HPRT exons in C-ion-induced mutants. No exons were deleted in 230keV/μm-beam-induced mutants, while all exons were deleted in 93% of 124keV/μm-beam-induced mutants. It is surprising that 230keV/μm carbon ions produce no deletions, given the much greater energy deposition within the track. This result is not consistent with a previous report (24), in which it was found that, at equilethal doses, the mutant spectra produced by X rays or alpha-particles (121keV/μm) were very similar. However, it is not clear which component of the energy deposition pattern of heavy-ion tracks is responsible for mutation induction. We think that the LET dependence of our data is caused by the density distribution of projectile carbon ions per cell and secondary electrons produced by carbon ion tracks. Since large clusters of energy deposition from higher LET radiations may be predominantly lethal, only secondary electrons would be responsible for the mutations induced by 230keV/μm carbon ions.

REFERENCE

1. M. R. Raju, Human cell survival as a function of depth for a high-energy neon ion beam, *Radiation Research*, 46, 489-492 (1976).

2. R. Cox, J. Thacker, D.T. Goodhead and R.J. Munson, Mutation and inactivation of mammalian cells by various ionizing radiations, *Nature*, 267, 425- 427 (1977).

3. K. Eguchi, T. Inada, M.Yaguchi, S. Sato and I. Kaneko, Induction and repair of DNA lesions in cultured human melanoma cells exposed to nitrogen-ion beams, *International Journal of Radiation Biology*, 52, 115-123 (1987).

4. M. Suzuki, M. Watanabe, K. Suzuki, K. Nakano and I. Kaneko, Neoplastic cell transformation by heavy ions, *Radiation Research*, 120,468-476 (1989).

5. L.D.Skarsgard,B.A. Kihlman,L. Parker,C. M.Pujara and S. Richardson, Survival, chromosome abnormalities, and recovery in heavy-ion- and X-irradiated mammalian cells, *Radiation Research*, 7, 208-221 (1967).

6. C.Borek, E.J.Hall and H.H.Rossi, Malignant transformation in cultured hamster cells produced by X-rays, 430-keV monoenergetic neutrons, and heavy ions, *Cancer Res.* , 38, 2997-3005 (1978).

7. D.T. Goodhead, J. Thacker and R. Cox, Non-rejoining DNA breaks and cell inactivation, *Nature*, 272, 379-380 (1978).

8. T.C. Yang, L.M. Craise, M. Mei and C.A. Tobias, Neoplastic cell transformation by heavy charged particles, *Radiation Research*, 104,S-177-S-187 (1985).

9. T.K. Hei, K. Komatsu, E.J. Hall and M. Zaider, Oncogenic transformation by charged particles of defined LET, *Carcinogenesis*, 5, 747-750 (1988).

10. L. Hieber and C. Lucke-Huhle, PCC technique reveals severe chromatin lesions and repair in G2-arrested cells after alpha irradiation, *Experimental Cell Research*, 144,57-62 (1983).

11. M. Scholz, W. Kraft-Weyrather, S. Ritter and G. Kraft, Cell cycle delays induced by heavy ion irradiation of synchronous mammalian cells, *Adv. Space Res.*, 9,(10)91-(10)96 (1989).

12. J.S. Bedford and D.T. Goodhead, Breakage of human interphase chromosomes by alpha particles and X-rays, *International Journal of Radiation Biology*, 55,211-216 (1989).

13. E. Goodwin, T.E. Blakely, G. Ivery and S.C. Tobias, Repair and misrepair of heavy-ion-induced chromosomal damage, *Advances in Space Research*, 9,83-89 (1989).

14. M. Suzuki, M. Watanabe, K. Suzuki, K. Nakano and K. Matsui, Heavy ion-induced chromosome breakage studied by premature chromosome condensation (PCC) in Syrian hamster embryo cells, *International Journal of Radiation Biology*, 62,581-586 (1992).

15. R. Roots, T.C. Yang, L. Craise, E.A. Blakely and C.A. Tobias, Impaired repair capacity of DNA breaks induced in mammalian cellular DNA by accelerated heavy ions, *Radiation Research*, 78, 38-49 (1979).

16. D. Blocher, DNA double-strand break repair determines the RBE of α-particles, *International Journal of Radiation Biology*, 54,761-771 (1988).

17. J. Heilmann, H. Rink, G. Taucher-Scher and G. Kraft, DNA strand break induction and rejoining and cellular recovery in mammalian cells after heavy-ion irradiation, *Radiation Research*, 135, 46-55 (1993).

18. M.A. Ritter, J.E. Cleaver and C.A. Tobias, High-LET radiations induce a large proportion of non-rejoining DNA breaks, *Nature*, 266, 653-655 (1977).

19. L.S. Goldstein, T.L. Phillips, K.K. Fu, G.Y. Ross and L.J. Kane, Biological effects of accelerated heavy ions. I. Single doses in normal tissue, tumors, and cells *in vitro*, *Radiation Research*, 86,529-541 (1981).

20. A.W. Skulimowski, D.R. Turner, A.A. Morley, B.J.S. Sanderson and M. Haliandros, Molecular basis of X-ray-induced mutation at the HPRT locus in human lymphocytes, *Mutation Research*, 162,105-112 (1986).

21. J. Thacker, The nature of mutants induced by ionising radiation in cultured hamster cells. III. Molecular characterization of HPRT-deficient mutants induced by γ-rays or α–particles showing that the majority have deletions of all or part of the *hprt* gene, *Mutation Research*, 160, 267-275,(1986).

22. A. Kronenberg and J.B. Little, Molecular characterization of thymidine kinase mutants of human cells induced by densely ionizing radiation, *Mutation Research*, 211,215-224 (1989).

23. J.C. Fuscoe, L.J. Zimmerman, A. Fekete, R.W. Setzer and B.J.F. Rossiter, Analysis of X-ray induced HPRT mutations in CHO cells: Insertion and deletions, *Mutation Research*, 269,171-183 (1992).

24. S.Z. Aghamohammadi, T. Morris, D.L. Stevens and J. Thacker, Rapid screening for deletion mutations in the hprt gene using the polymerase chain reaction: X-ray and α-particle mutant spectra, *Mutation Research*, 269,1-7 (1992).

25. M. Watanabe, M. Suzuki, K. Suzuki, K. Nakano and K. Watanabe, Effect of multiple irradiation with low doses of gamma-rays on morphological transformation and growth ability of human embryo cells *in vitro*, *International Journal of Radiation Biology*, 62,711-718 (1992).

26. J.J. McCormick, S. Kateley-Kohler, M. Watanabe and V.M. Maher, Abnormal sensitivity of human fibroblasts from xeroderma pigmentosium variants to transformation anchorage independence by ultraviolet radiation, *Cancer Research*, 46,489-492 (1986).

27. T. Kanai, S. Minohara, M. Sudou, T. Kohno, E. Takada, F. Soga, K. Kawachi,Y. Furusawa, K. Fukutsu, K. Egchi-Kasai, H. Itsukaichi, H. Ohara and F. Yatagai, Beam modulation for heavy ion radiotherapy, *Proceedings of the Second Workshop on Physical and Biological Research with Heavy Ions*, 1-3, (1992).

28. M. Watanabe and M. Horikawa, Analysis of differential sensitivities of synchronized HeLa S3 cells to radiations and chemical carcinogens during cell cycle. Radiation- and chemical-carcinogen-induced mutagenesis, *Mutation Research*, 71, 219-231 (1980).

29. G.E. Pantelias and H.D. Maillie, A simple method for premature chromosome condensation induction in primary human and rodent cells using polyethyleneglycol, *Somatic Cell Genetics*, 9, 533-547 (1983).

30. J.M. Brown, J. Evans and M.S. Kovaca, The prediction of human tumor radiosensitivity *in situ* An approach using chromosome aberration detected by fluorescence *in situ* hybridization, *International Journal of Radiation Oncology Biology Physics*, 24,279-286 (1992).

Biology II

GENERAL CONSIDERATIONS IN THE BIOLOGICAL DOSIMETRY OF HEAVY CHARGED PARTICLE BEAMS AND USE OF THE GELATIN/CELL SORTER *IN VITRO* SYSTEM AT TRIUMF

L.D. Skarsgard[1,2], B.G. Wouters[1], G.K.Y Lam[2], U. Oelfke, and G.B. Goodman[3]

[1]Medical Biophysics Department, B.C. Cancer Research Centre, [2]Batho Biomedical Facility, TRIUMF, and [3]Developmental Radiotherapy, B.C. Cancer Agency, Vancouver, B.C., Canada

Biological dosimetry has become an essential precursor to the clinical application of any new type of radiation, and many different *in vivo* and *in vitro* systems have been used in an effort to determine what dose of the new modality will produce a biological effect equivalent to the particular dose of photons that is used in existing, conventional treatment for the tumour site in question. The "biological effect" could be tumour response or normal tissue damage. The relative biological effectiveness (RBE) of the new radiation is found to be specific to the test system (tissue, tumour, cells, etc.) used, however, and one should expect that clinical RBE values will also be specific to the tumour and normal tissue which is irradiated. The RBE can also be strongly dose-dependent. This raises questions about the usefulness of the concept of "cobalt-equivalent grays" (dose x RBE), if a given radiation cannot be characterized by a single RBE value. Despite these concerns, our experience with the pion beam at TRIUMF suggests that skin (mouse, pig, human) can be a very useful *in vivo* system, yielding RBE values which seem clinically relevant, at least for the two sites where we have extensive experience (brain and prostate).

With heavy charged particle beams one has the added complication that RBE increases with depth as the particles slow down. An *in vitro* biological dosimeter, using an appropriately chosen cell line, offers the most practical method for measurement of the RBE *vs.* depth profile of the beam, which can then be used to shape the physical dose profile to produce uniform biological effect. To date, such shaping of the physical depth dose has not been used for clinical proton beams, due to a lack of data and a presumption that RBE differences would be negligible. It should be noted that all other heavy ion beams used clinically have employed RBE-compensated depth dose profiles.

We have done RBE measurements on a modulated 70 MeV proton beam at TRIUMF, using a Chinese hamster V79 cell line. The gel technique which we developed earlier for pion beam studies was used, in combination with our cell sorter assay which allows more accurate determination of cell survival. Our preliminary measurements to date for a small proton stopping volume (approx. 8 cm^3, peak width 1.8 cm) show an average RBE in the stopping peak of 1.22 ± 0.12, for V79 WNRE cells, for doses > 3 Gy. The results suggest that the RBE increases at low dose and increases with depth, particularly at the distal edge of the distribution.

INTRODUCTION

It is a well-established tradition in experimental medicine that the implementation of a new treatment technique should draw, whenever possible, on our knowledge of and experience with the standard or conventional treatment which we are attempting to replace. This has certainly been true in radiation oncology in the testing of new types of radiation — clinical treatments have always been preceded by physical and biological measurements designed to ensure that the new modality will, at the outset, produce a therapeutic result and a complication rate no less favourable than the conventional treatment, at least. In the case of high LET radiations, where the dose effectiveness is generally greater than for x- or γ-rays, much effort has been devoted to measurements, using biological systems, designed to determine what dose (total dose or dose/fraction) of the new radiation should be used to produce the same effect as a particular dose of the conventional treatment. The ratio of these 2 doses is commonly used as the definition for the relative biological effectiveness (RBE) of the new radiation. Many

Reprint requests to L.D. Skarsgard: Department of Medical Biophysics, BCCRC, 601 West 10th Avenue, Vancouver, B.C. V5Z 1L3
Acknowledgements: It is a pleasure to acknowledge the assistance in this work of Kay Gardey and other TRIUMF staff associated with the operation and physical studies on the proton beam, as well as Art Sy, Deanna Acheson and Denise McDougal who assisted with the biological experiments and Linda Harris who typed the manuscript. This work was supported by the Woodward Foundation, The B.C. Cancer Foundation and by the National Cancer Institute of Canada with funds from the Canadian Cancer Society.

different biological test systems, both *in vivo* and *in vitro*, have been employed for such studies.

With heavy charged particle beams (heavy ions and pions, at least) there is the added complication that the dose effectiveness is not constant throughout the treatment volume, but increases with depth due to the changing dose deposition characteristics as the particles slow down. This requires the use of a biological "dosimeter" system which is capable of mapping this spatially dependent RBE. Such information is then used to shape the *physical dose* distribution so as to compensate for the changing RBE, to yield a uniform biological effect throughout the treatment volume.

An ideal biological dosimeter for charged particle beams, then, is one which meets the following basic requirements:

1. It should provide the necessary Relative Biological Effectiveness (RBE) information to allow determination of the particle beam dose that would be EQUIVALENT to a particular photon dose for
   - dose limiting normal tissues
   - tumour response

   for a particular treatment regime.
2. It should provide the RBE information necessary to create ISOEFFECTIVE dose throughout particle stopping distributions, where RBE varies with depth, for example.

Although many different and useful biological systems, both *in vivo* and *in vitro*, have been developed and applied to this problem, no single biological dosimeter has been able to satisfy all of the basic requirements above. In general, *in vivo* systems are required for 1) above, while for 2), *in vitro* systems are more practical. Among *in vivo* systems, perhaps the one most widely used to model early responding tissues has been skin, particularly the mouse foot skin reaction. Figure 1 represents RBE data for 16 MeV (d $\rightarrow$ Be^{+}) fast neutrons (relative to 250 kVp x-rays) summarized by Field and Hornsey (8) 2 decades ago. The figure shows the measured RBE *vs* dose per fraction from many authors,

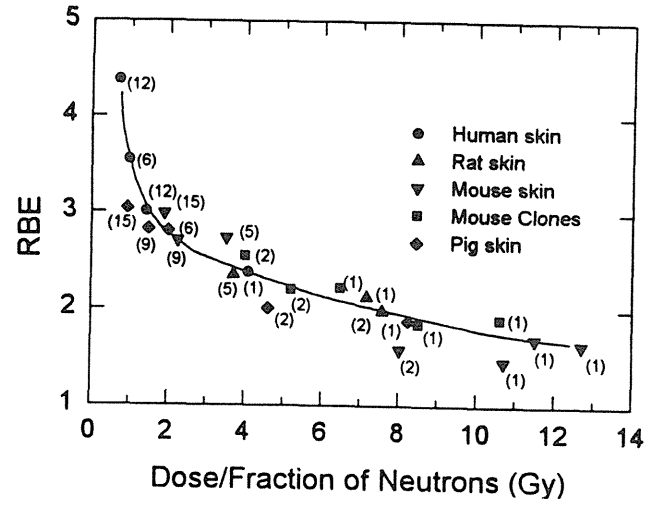

Fig. 1 RBE as a function of dose per fraction of neutrons (16 MeV deuterons on beryllium) for radiation damage to skin. The RBE is given relative to 250 kVp x-rays for human, pig, rat and mouse skin damage (for mouse, skin clone data are also included). The numbers in parentheses indicate the number of fractions used in each study. (Redrawn from Field and Hornsey(8)).

for human, pig, rat and mouse skin, irradiated with fractionated dose regimes. An impressive feature of these data is the good agreement between the results from different animal species. They also show very clearly the dependence of RBE on dose, for fast neutrons, which results primarily from reduced recovery from sublethal damage following neutron irradiation.

In similar pre-clinical studies of pion (π^- meson) beams at TRIUMF, we also observed a close correspondence between the RBE values derived from fractionated irradiation of mouse, pig and human skin (3-5,10,18,19,21,22,24). Thus, to the extent that skin is a dose-limiting normal tissue in radiation oncology, the dose response of skin reactions in experimental animals can be a very useful biological dosimeter for high LET radiations. With charged particle beams, however, skin will often not be a dose-limiting tissue, because of the favourable depth-dose characteristics of such radiations.

The relationships between the RBE of fast neutrons (16 MeV d $\rightarrow$ Be^{+}) and dose per fraction

for two other tissues, intestine and lung, are shown in figure 2,

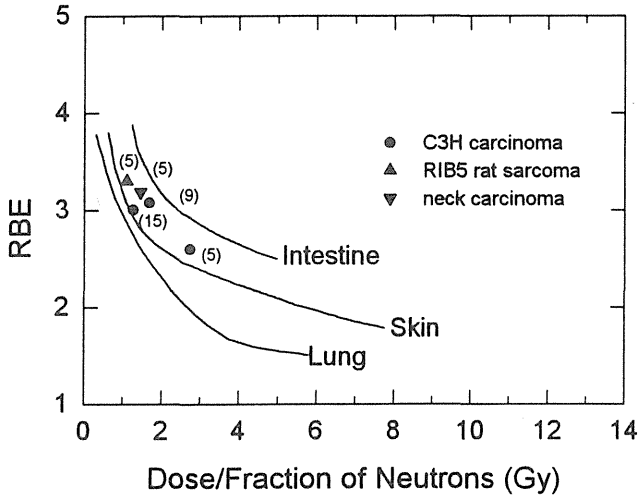

Fig. 2 RBE as a function of dose per fraction of neutrons (16 MeV deuterons on beryllium) for five or more fractions delivered to skin, intestine and lung. Data are also included for three tumours: C3H, RIB 5 and neck carcinoma. The numbers in parentheses again indicate the number of dose fractions. (Redrawn from Field (7)).

along with the skin response of figure 1. It can be seen that although the general nature of the response is similar for these tissues, there are significant *quantitative* differences between the 3 tissues. Also shown in this figure are RBE values measured for several experimental rodent tumours. These data, summarized by Field (7), again represent the work of several investigators. If the data of figure 2 are any indication at all of the way that RBE depends on the tissue being irradiated in *humans*, then we are faced with considerable uncertainty as to how we should define "equivalent dose" or "cobalt-equivalent dose" for a particular, high LET radiation — equivalent with respect to what? This situation is also illustrated by the recent neutron beam studies of Britten *et al.*, and Warenius *et al.* (2,32). Using fast neutrons from the Clatterbridge Cyclotron (62.5 MeV [$p \rightarrow Be^{+}$]) they compared the neutron and x-ray single dose responses for 30 different human tumour cell lines, representing a range of different histologies. Their work clearly showed that the RBE of neutrons differed widely for the different cell lines, as can be seen in Table 1, extracted from the data of Warenius *et al.*, (32) for 12 of those cell lines.

TABLE 1. THE RBE OF 62.5 MeV ($p \rightarrow Be^{+}$) FAST NEUTRONS *vs* 4 MeV PHOTONS, FOR VARIOUS HUMAN TUMOUR CELL LINES

Cell Line	Histology	RBE[1]
HX 142	Neuroblastoma	2.0
H 417	Small cell lung carcinoma	2.4
COLO 320	Adenocarcinoma colon	1.6
RT 112	Transit cell carcinoma bladder	3.6
A 549	Adenocarcinoma lung	2.8
NCTC	Normal skin epithelium	2.3
2780	Ovarian carcinoma	1.8
HT 29/5	Adenocarcinoma colon	2.4
HEP 2	Squamous carcinoma larynx	2.2
MEL 2	Melanoma	1.8
RPMI 7951	Melanoma	1.5
KB	Oral epidermoid carcinoma	1.8

[1] Calculated as D_{γ} / D_{n} at S = 0.1
Data from Warenius *et al.*, Radiother. Oncol. 30: 83-89 (1994).

A similar cell-line dependence of RBE was described by Ito *et al.*, using carbon ions accelerated at HIMAC (12). Data from studies with experimental animal tumours have also shown that the RBE can be different for different tumours. This has been observed for different high LET radiations, including pions: the work of Sakamoto *et al.* (14-16), Ogawa *et al.* (13) and Takai *et al.* (30) at TRIUMF, using murine tumours, yielded pion RBE values which were specific to the tumour system used. The RBE appeared to correlate (inversely) with tumour growth rate (13), consistent with the neutron investigations in human lung metastases of van Peperzeel *et al.* (31) and Batterman *et al.* (1). The important message of these results (and they represent just a few examples from a substantial literature on this subject) is that it is an oversimplification to attempt to characterize any high LET particle beam by a *single RBE value*. There is substantial evidence that the RBE is normal-tissue-specific and tumour-site-specific. And figures 1 and 2 indicate that it is dose-dependent too. Of course, with proton beams, which have much smaller RBE's than neutrons, one would expect that differences in RBE for different tissues will also be smaller. The differences are not likely to be insignificant, however, considering that a 10% error

in RBE and thus a 10% error in the calculated "equivalent dose" would be clinically unacceptable. The logical conclusion of this argument is that the clinical use of "equivalent dose" or "cobalt equivalent dose" in particle beam radiotherapy is only justified if it is based on clinical experience which, in effect, has established the value of the RBE for that tumour site and for the particular treatment protocol used. And the RBE derived in this way could relate either to a dose-limiting normal tissue (early or late effect) or to the tumour response. What we seem to be saying is that the patient is the ultimate petri dish.

With all of these qualifications about the significance of RBE, is there any point in laboratory measurements of RBE? The fact remains that some estimate of the RBE is essential before initiating clinical use of any new particle beam modality so that, despite their limitations, some laboratory studies of the effectiveness of the new particle beam, relative to photons, is hard to escape . At TRIUMF, clinical studies with pion beams were preceded by extensive studies of the comparative effects of pions and x-rays on skin, using a variety of fractionated regimes. It was found that mouse (3,4,18,21,22,24), pig (4,5,19) and human (10) skin all gave quite comparable results, consistent with figure 1, and the RBE obtained was approximately 1.5, for protocols using 10 - 15 fractions. This is the RBE value that was used to launch the clinical trials in 1982. It is interesting that more than 10 years later, the "best estimate" of the *clinical* RBE for fractionated pion treatment at TRIUMF, is also approximately 1.5, at least for the 2 sites for which we have extensive experience, glioblastoma and prostate carcinoma; sigmoidoscopy studies of the reaction of colon mucosa indicate that the RBE of fractionated pions is approximately 1.5 for this normal human tissue as well (9,11).

Laboratory measurements are also essential in order to produce particle beam dose distributions which are approximately isoeffective throughout the treatment volume, because of the change in RBE with depth. For this application, *in vitro* systems are the most practical, and they must provide a determination of RBE as a function of depth along the beam axis. The physical depth dose distribution is then shaped according to this RBE data to produce a biologically effective dose (dose x RBE) that is approximately constant throughout the treatment volume. The choice of cell line for such measurements is, again, important: if a cell line is chosen which has an unusually high or low RBE, in comparison to the relevant clinical endpoints (which could be normal tissue and/or tumour response) then one could end up with a shaped physical dose profile which is over- or under-compensated, respectively, for the depth dependence of the RBE. It is clear from Table 1 that at least some human tumour cell lines would be inappropriate for this purpose. We have used Chinese hamster cells for both our pion and our proton beam studies at TRIUMF. Some of the results of our studies with proton beams are described below.

METHODS AND MATERIALS

Biological System

The cell line used for these studies was the Chinese hamster V79-WNRE line, obtained from Dr. J.D. Chapman. It is a strain of the V79-379A line and can be grown in monolayer or in suspension, using MEM (+ 10% fetal bovine serum) or S MEM (+ 7% fetal bovine serum) growth medium, respectively. For experiments, cells were grown as monolayers, and harvested with 0.1% trypsin (4 min), followed by neutralization with MEM; this gave a very high proportion of single cells, desirable for cell sorting. After centrifugation, the cells were resuspended in 37°C medium containing 12% gelatin (G8, Fisher Scientific) at a concentration of approximately 7.5 x 10^5 cells/ml. At 37°C, this suspension was a viscous fluid which could be poured into ABS (acrylonitrile butadiene styrene) plastic tubes, 17.7 cm long, 1.2 cm in diameter and with a piston at one end. The tubes were then cooled to 0° C, sealed, and stored on ice until irradiation. For irradiation, the tubes were placed in a phantom, with the axis of the tube colinear with the axis of the proton beam. The phantom contained a mixture of glycerol and water, designed to have the same density and stopping power as the ABS plastic and the 12% gelatin. The purpose of this was to ensure that all particle paths encountered the same attenuation, even for protons scattered from points outside the gel. The

glycerol-water was maintained at 1-2°C, using a refrigerated circulating bath.

After irradiation, the gel tube was stored on ice while it was transported from TRIUMF to the Medical Biophysics labs. The gel was then extruded and sliced at 2 mm intervals using a taught wire (0.2 mm diameter) slicer (22,23,25). The gel slices were melted in 37° C medium and then a cell sorter (Becton-Dickinson 440) was used to deliver a known number of cells into a test tube for plating. Cells were identified on the basis of light scattering in the cell sorter, without the use of a cell stain (6). From each slice, three 10 cm petri dishes were plated for colony formation, which was scored in the conventional manner.

A cobalt-60 Theratron beam was beam was used as the comparison for RBE determinations. Irradiations were carried out with cells (from the same harvested population) in 12% gelatin, but in this case 0.5 ml of the suspension was loaded into 5 ml plastic test tubes which were irradiated and stored at ~ 0° C; after melting the gel at 37° C, samples were sorted and plated as above for proton irradiations.

Gel Preparation

It is necessary to dialyse the gelatin extensively to remove toxic products (presumably low molecular weight components such as amino acids, etc.) before preparation of the 12% gelatin-medium mixture. The process involves preparing a solution of 25% gelatin in cold serum-free medium, warming to 37° C for 10 min to aid mixing, and then heating to 70° C for 30-45 min until all of the gelatin is solubilized. The pH is then adjusted to 7.4 with 0.1 N NaOH and, while the solution is still hot, it can be filtered through a Millipore AP pre-filter (this removes some particulate material which can interfere with sorting). The solution is then autoclaved. While it is still warm, the gel solution is poured into dialysis tubes, the tubes are sealed to preserve sterility and the gel is dialysed at 4° C against serum-free growth medium for 1-2 weeks, with a daily change of dialysate. The cold dialysis procedure minimizes the uptake of fluid by the gel and results in a solution that is 15-20% gelatin at the end of dialysis. Medium is then added to produce the desired 12% gelatin solution.

Beam Characteristics and Dosimetry

The TRIUMF proton therapy facility provides a variable energy beam (65-120 MeV), which has a range of about 4 to 10 cm in water. It is used at present for the treatment of eye melanoma. The cyclotron is capable of delivering a very high intensity proton beam of the order of hundreds of μA, but for the present set of radiobiological experiments a current of 5 nA was used, which corresponds to a dose rate of the order of 5 Gy per minute. For the small field size used in these measurements, lateral uniformity was provided by simple beam scattering using a lead scatter foil placed at 1.2 m upstream and with a copper collimator placed at 10 cm from the irradiation sample, to select the central uniform dose region. A uniform depth dose profile was provided by the standard method of spreading out the Bragg peak using a lucite modulator wheel.

Proton dose was measured using a 0.05 cc thimble chamber, which was operated as an absolute dosimeter using a known chamber volume as calculated from the exposure calibration factor obtained from the calibration by an Accredited Dosimetry Calibration Lab. The measured dose was converted to proton dose in tissue using the appropriate W values and stopping power ratios for protons of the corresponding energy. The lateral dosimetry profiles were measured using a small silicon diode, while the depth dose profiles were measured using the parallel plate Markus chamber. The dectectors were mounted on a scanning system which uses stepping motors and has a precision of 0.05 mm.

RESULTS

Figure 3 shows the physical dose profiles, axial and transverse, of the modulated 70 MeV proton beam used in these preliminary studies at TRIUMF. The modulation was devised to yield a uniform dose over the depth range 14 to 30 mm. In figure 3a the vertical lines indicate the water-equivalent depth at the middle of the gel slices for which cell survival was measured. The last 3 slices, beyond 35 mm,

received no dose and these served as controls. Figure 3b shows that the procedure used for scattering and collimating the proton beam gives a transverse dose profile which is uniform across the gel tube.

Figure 4 shows a few examples of the cell survival profiles (survival *vs*. depth) obtained from gel tubes which received the indicated proton doses to the spread-out Bragg peak (SOBP). For each tube, the plating efficiency was obtained from the last 3 gel slices which received zero dose. The plating efficiency should be > 70%, close to the P.E. of ~ 80% which we normally observe in standard cell

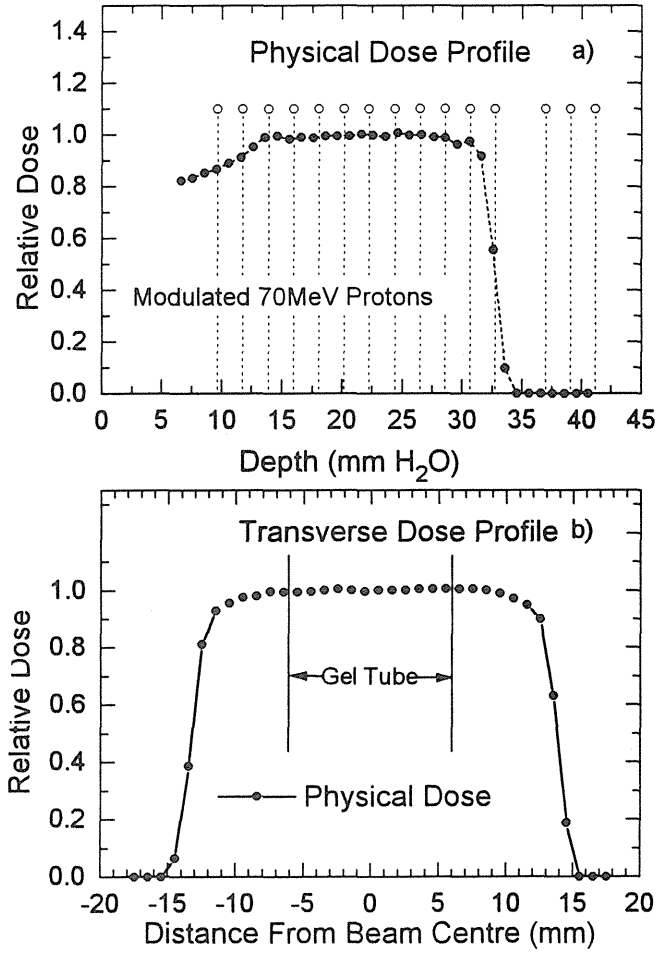

Fig. 3. a) Physical depth dose profile for a modulated beam of 70 MeV protons in water, measured at TRIUMF with a parallel plate Markus chamber

b) Dose profile transverse to proton beam axis, measured with a silicon diode.

sorting experiments, where there is no exposure to gelatin, no slicing and no prolonged 0° C storage. In this particular experiment, however, the P.E. was only ~ 60% due, presumably, to a shortened dialysis time (1 week). It can be seen that there is a consistent decrease in survival with increasing depth in these profiles, even though all of the 'peak' slices received essentially the same dose. This is particularly noticeable for the slice at the distal edge of the dose profile (depth 30.7 mm water), where cell survival drops more sharply. And this is not just the result of a somewhat higher dose at that depth. In fact, as can be seen from figure 3a, the physical dose to this slice is, if anything, slightly lower than for the rest of the peak slices. It should be noted that depth in gel has been converted to the stopping-power-equivalent depth in water in this plot.

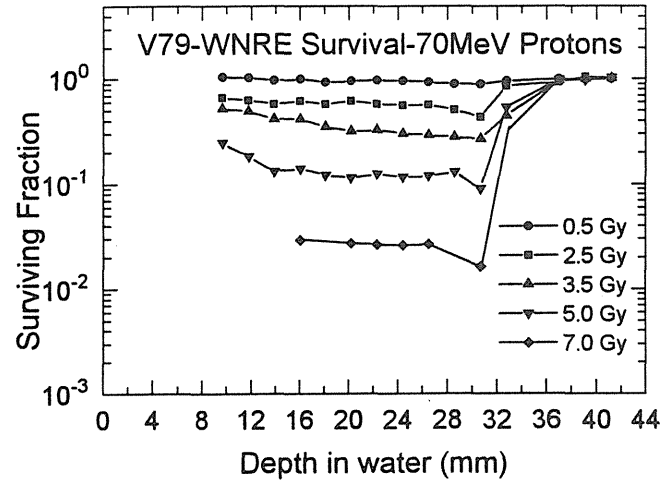

Fig. 4 V79 WNRE survival profiles for cells irradiated in gel tubes, using the proton beam shown in Figure 3. Each profile represents the survival measured in 2 mm slices taken from a gel tube which received the indicated *average* peak dose (averaged over 13 to 30 mm). In all, 15 such profiles were measured, 5 of which are shown here. The cell sorter assay was used for these survival measurements. All irradiations were done at ~ 0° C.

A total of 15 gel tubes were exposed to different peak doses of protons from 0.5 to 11.0 Gy, in this experiment. Figure 4 shows 5 of the resulting survival profiles. Cross-plots of those 14 profiles could allow us to plot Survival *vs*. Dose for each slice depth, or data for several slices could be pooled to obtain *average* survival values for a particular

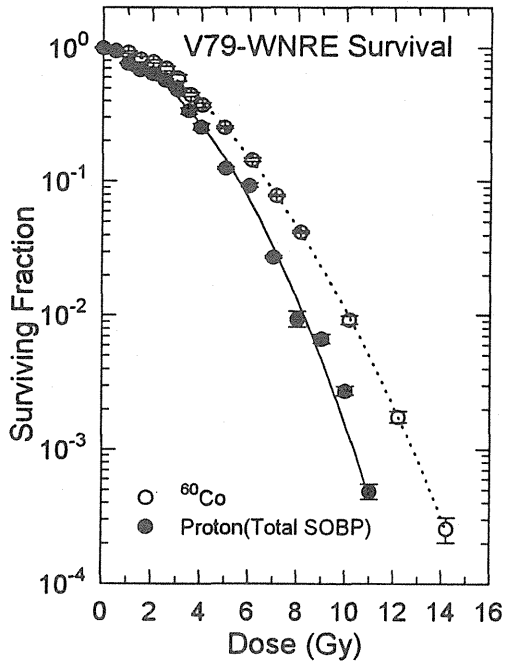

Fig. 5 Survival *vs.* dose for V79 WNRE cells irradiated with single doses of protons or ^{60}Co γ-rays. For protons, data for 8 slices (13.9 to 28.6 mm depth) were averaged together to yield the plotted survival value. All irradiations were done at ~ 0° C. The solid and dotted lines represent fits of equation (1) to the data. Error bars represent standard errors.

range of depths. Figure 5 shows the results of such an averaged response where for each profile, survival values for 8 peak slices at depths 13.9 mm to 28.6 mm have been averaged together. This average excludes the slice at the distal edge of the peak (30.7 mm), which showed the increase in cell kill in figure 4. Also shown in figure 5 is the response of the same cell population to ^{60}Co irradiation, measured at the same time and using the cell-sorting assay. Both data sets have been fitted to a 2-component linear quadratic function of the form

$$s = f\,(e^{-\alpha_1 D - \beta_1 D^2}) + (1-f)\,(e^{-\alpha_2 D - \beta_2 D^2}) \qquad (1)$$

which we have shown is necessary to accurately describe the radiation response of asynchronous cell populations, particularly at low dose from 0.5 to 4.0 Gy (20,26-29). These responses provide the opportunity to determine the RBE of 70 MeV protons relative to ^{60}Co photons, *for the inactivation of Chinese hamster V79-WNRE cells.*

Discussion

The data of figure 4 indicate that the RBE of the 70 MeV proton beam increases somewhat with depth, particularly at the distal edge of the proton stopping distribution, as one would expect from the increased proportion of dose that arises from high LET track-ends, at such depths. This has also been predicted by the model calculations of Scholz and Kraft, reported at this Workshop (17). One can also show from fits of equation (1) to the data in figure 5, that the RBE is dependent on dose and increases at low doses. However, a more detailed analysis of the depth- and dose-dependence of RBE must await the accumulation of more data in our studies, which are continuing. Nevertheless, if the depth-dependence of RBE that is apparent in our present work persists, we expect to shape the proton depth-dose profile at TRIUMF so as to compensate for the changing RBE.

The data of figure 5 allow one to calculate, for inactivation of V79 WNRE cells, a provisional *average* RBE for the 70 MeV proton spread out Bragg peak (SOBP) of 1.22 ± 0.12, valid for doses greater than 3 Gy, approximately.

Conclusions

It is important to remember that laboratory measurements of the RBE of heavy charged particle beams yield numbers that are specific to the cell line, normal tissue or tumour, etc., used in the experiment, as well as on the end-point being measured. One should thus expect clinical RBE values to also be specific to the tumour and normal tissue being irradiated. This complicates the clinical evaluation of the efficacy of any new radiation modality since the therapeutic gain, which is a function of both the normal tissue and tumour response, can clearly be expected to be different for different tumour sites. The challenge will always be to find those sites, if any, which have a significant therapeutic gain.

As well, RBE is dose-dependent and it can also change with depth in a particle stopping distribution. Despite these caveats, radiobiological measurements have become an essential precursor to the clinical use of any new radiation modality. A number of *in vivo* normal tissue systems including skin, lung, kidney,

intestine, spinal cord, etc., as well as experimental tumour systems, have been developed and have been shown to be of value in certain situations. Skin (rodent, pig, human), in particular, has proven to be a practical and useful *in vivo* biological dosimeter for RBE determinations and has provided valuable guidance for the initiation of new clinical protocols.

In vitro biological dosimeters measuring cell survival, offer the most practical method for the development of isoeffective dose distributions, where the dose profile must be shaped to compensate for a depth-dependent RBE. The choice of cell line for this purpose is important: one should avoid cell lines that could lead to over- or under-compensation in shaping the dose profile, as could occur, for example, with some of the human tumour cell lines which have anomalously high or low RBE values.

Our preliminary measurements on the 70 MeV proton beam at TRIUMF suggest that the combination of the gel technique and the cell sorting assay for survival may be uniquely valuable for such measurements.

REFERENCES

1. Battermann, J.J.; Breur, K.; Hart, G.A.M.; van Peperzeel, H.A. Observations on pulmonary metastases in patients after single doses and multiple fractions of fast neutrons and cobalt-60 gamma rays. Europ. J. Cancer 17:539-548; 1981.
2. Britten, R.A.; Warenius, H.M.; Parkins, C.; Peacock, J.H. The inherent cellular sensitivity to 62.5 MeV ($p \rightarrow Be^{+}$) neutrons of human cells differing in photon sensitivity. Int. J. Radiat. Biol. 61:805-812; 1992.
3. Chaplin, D.J.; Douglas, B.G.; Grulkey, W.; Skarsgard, L.D.; Lam, G., Denekamp, J. The response of mouse epidermis to fractionated doses of π mesons. Int. J. Radiat. Oncol. Biol. Phys. 13:1199-1208; 1987.
4. Douglas, B.G. Pion beam studies in mice and in pigs. In: Skarsgard, L.D., ed. Pion and heavy ion radiotherapy: pre-clinical and clinical studies. New York, Elselvier; 1983:299-314.
5. Douglas, B.G.; Grulkey, W.R.; Chaplin, D.J.; Lam, G.; Skarsgard, L.D.; Denekamp, J. Pions and pig skin: preclinical evaluation of RBE for early and late damage. Int. J. Radiat. Oncol. Biol. Phys. 12:221-229; 1986.
6. Durand, R.E. Use of a cell sorter for assays of cell clonogenicity. Cancer Res. 46: 2775-2778; 1986.
7. Field, S.B. An historical survey of radiobiology and radiotherapy with fast neutrons. In: Ebert, M., Howard, A., eds. Current topics in radiation research. Amsterdam, North-Holland; 1976:1-86.
8. Field, S.B. and Hornsey, S. The RBE for fast neutrons: the link between animal experiments and clinical practice. In: Nygaard, O.F., Adler, H.I., Sinclair, W.K., eds. Proceedings of the Fifth International Congress of Radiation Research, Seattle, Washington, July 14-20, 1974, New York, Academic Press, 1975: 1125-1135.
9. Goodman, G.B.; Bowen, J.L.; Dixon, P.; Gaffney, C.; Ogawa, Y.; Pomeroy, M.; Rheaume, D.; Saito, T.; Shirato, H.; Vernimmen, F. Pimeson radiotherapy at TRIUMF. J. Jpn. Soc. Ther. Radiol. Oncol. 2:85-99; 1990.
10. Goodman, G.B.; Douglas, B.G.; Jackson, S.M.; Kornelsen, R.O.; Lam, G.K.Y.; Ludgate, C.M.; Skarsgard, L.D. Pions, Vancouver. Int. J. Radiat. Oncol. Biol. Phys. 8:2187-2190; 1982.
11. Pickles, T.; Bowen, J.; Dixon, P.; Gaffney, C.; Pomeroy, M.; Rheaume, D.; Vernimmen, F.; Goodman, G.B. Pions - the potential for therapeutic gain in locally advanced prostate cancer: dose escalation and toxicity studies. Int. J. Radiat. Oncol. Biol. Phys. 21:1005-1011; 1991.
12. Ito, H., Yamashita, S., Nishiguchi, I., Shigematsu, N., Ka, W-J., Kubo, A., Yatagai, F., Kanai, T. RBEs of various human monolayer cells irradiated with carbon beams. In: proceedings of the third workshop on physical and biological research with heavy ions, September 2-3, 1993. HIMAC report, NIRS-M-99 (HIMAC-006), 1993: 41-43.
13. Ogawa, Y.; Goodman, G.B.; Chaplin, D.J.; Grulkey, W.; Lam, G.K.Y. The response of mouse tumours to fractionated doses of pions: determination of therapeutic gain factor. Oncology 48:81-87; 1991.
14. Sakamoto, K.; Okada, S.; Lam, G.K.Y.; Henkelman, R.M.; Skarsgard, L.D. The comparative survival of clonogenic cells of a murine epithelioma irradiated *in vivo* with 250 kVp x rays, ^{60}Co gamma rays, or negative pions produced by the cyclotron at TRIUMF. Radiology 133:501-505; 1979.
15. Sakamoto, K.; Takai, Y.; Lam, G.K.Y. Survival of murine epithelioma cells exposed at various

positions to pions produced by the cyclotron at TRIUMF. Radiat. Res. 87:159-165; 1981.
16. Sakamoto, K.; Okada, S., Lam, G.K.Y.; Howard, J. Comparison of the effects of pion and heavy ion beams in a mouse tumor system. In: Skarsgard, L.D., ed. Pion and heavy ion radiotherapy: pre-clinical and clinical studies. New York, Elselvier; 1983:325-333.
17. Scholz, M.; Kraft, G. Calculation of RBE for charged particle and neutron beams based on track structure. In: Proceedings of the NIRS International Seminar on the Application of Heavy Ion Accelerators to Radiation Therapy of Cancer - PTCOG XXI, Chiba, Japan, Nov. 14-16, 1994. (These proceedings).
18. Skarsgard, L.D. The biological properties of pions. In: Okada, S. *et al.*, eds. Proceedings of the Sixth International Congress of Radiation Research, Tokyo, Japan, May 13-19, 1979, Tokyo, Japanese Association for Radiation Research; 1979: 788-801.
19. Skarsgard, L.D.; Douglas, B.G.; Denekamp, J.; Chaplin, D.J.; Lam, G.K.Y.; Harrison, R.W.; Kornelson, R.O.; Palcic, B. *In vitro* and *in vivo* studies of the TRIUMF pion therapy beam. Radiat. Res. 104:S135-S144; 1985.
20. Skarsgard, L.D.; Harrison, I.; Durand, R.E. The radiation response of asynchronous cells at low dose: evidence of substructure. Radiat. Res. 127:248-256;1991.
21. Skarsgard, L.D.; Henkelman, R.M.; Eaves, C.J. Pions for radiotherapy at TRIUMF. J. Can. Assoc. Radiol. 31:3-12; 1980.
22. Skarsgard, L.D.; Henkelman, R.M.; Lam, G.K.Y.; Palcic, B.; Eaves, C.J.; Ito, A. Pre-clinical studies of negative pi-mesons at TRIUMF. In: Abe, M., Sakamoto, K., Phillips, T.L., eds. Treatment of Radioresistant Cancers. New York, Elsevier/North-Holland; 1979: 127-144.
23. Skarsgard, L.D.; Henkelman, R.M.; Lam, G.K.Y.; Palcic, B.; Poon, M.N. Pre-clinical studies of the negative pi-meson beam at TRIUMF. Radiat. Environ. Biophys. 16:193-204; 1979.
24. Skarsgard, L.D.; Palcic, B.; Douglas, B.G.; Lam, G.K.Y. Radiobiology of pions at TRIUMF. Int. J. Radiat. Oncol. Biol. Phys. 8:2127-2132; 1982.
25. Skarsgard, L.D.; Palcic, B.; Lam, G.K.Y. RBE mapping in pion beams using the gel technique. In: Skarsgard, L.D., ed. Pion and heavy ion radiotherapy: Pre-clinical and clinical studies. New York, Elsevier, 1983:197-210.
26. Skarsgard, L.D.; Skwarchuk, M.W., Wilson, D.J. Substructure in the cell survival response at low dose: Effect on the fitted parameters α and β . In: Chadwick, K., Moschini, G., Varma, M., eds. Biophysical modelling of radiation effects. Bristol, Institute of Physics Publishing, 1992;277-284.
27. Skarsgard, L.D.; Skwarchuk, M.W.; Wouters, B.G. The survival of asynchronous V79 cells at low radiation doses: modeling the response of mixed cell populations. Radiat. Res. 138:S72-S75; 1994.
28. Skarsgard, L.D.; Wilson, D.J.; Durand, R.E. Survival at low dose in asynchronous and partially synchronized Chinese hamster V79-171 cells. Radiat. Res. 133:102-107; 1993.
29. Skwarchuk, M.W.; Wouters, B.G.; Skarsgard, L.D. Substructure in the radiation survival response at low dose: asynchronous and partially synchronized V79-WNRE cells. Int. J. Radiat. Biol. 64:601-612; 1993.
30. Takai, Y.; Goodman, G.B.; Chaplin, D.J.; Grulkey, W.; Lam, G.K.Y. The response of murine B-16 melanoma to fractionated doses of pions. Int. J. Radiat. Oncol. Biol. Phys. 23:573-578; 1992.
31. Van Peperzeel, H.A.; Breur, K.; Broerse, J.J.; Barendsen, G.W. RBE values of 15 MeV neutrons for responses of pulmonary metastases in patients. Europ. J. Cancer 10:349-355; 1974.
32. Warenius, H.M.; Britten, R.A.; Peacock, J.H. The relative cellular radiosensitivity of 30 human *in vitro* cell lines of different histological type to high LET 62.5 MeV ($p \rightarrow Be^{+}$) fast neutrons and 4 MeV photons. Radiother. and Oncol. 30:83-89; 1994.

INTERPLAY OF DAMAGE COMPLEXITY AND DAMAGE REPAIR DETERMINE RBE.

JOHN F. WARD, PH.D.
Department of Radiology 0610, University of California at San Diego, La Jolla, CA 92093, USA.

ABSTRACT

The lethal potentially lethal model of Curtis (1) for cell survival is considered in terms of the complexity of DNA damage types produced by ionizing radiation. The spectrum of the damage moves to greater complexity as the LET of the radiation increases. Damage of greater complexity has a greater probability of being irretrievably lethal and will be longer lived - and more likely to be fixed as lethal because of the problems it presents to the cellular repair mechanisms.

INTRODUCTION

Curtis (2) and Braby (3) have recently published excellent summaries of the various biophysical models for radiation effects on cellular systems. Some of these models are based on descriptions of energy deposition patterns in low volumes (e.g. 4,5). Others, with the realization that energy deposition *per se* can not account for the post-treatment biochemical response of the cells exposed to the radiation, introduced considerations of repair (1,6). Curtis in his lethal-potentially-lethal (LPL) model invokes the radiation induction of lethal lesions and repairable lesions (both formed linearly with dose). There are two categories of the latter lesion which are distinguished by repair rates, the slow repairing class of which is also subject to fixation or binary misrepair. Curtis (1) shows how this model well fits a broad field of experimental data wherein the radiation response is modified by different protocols. Curtis tentatively identifies the two types of repairable lesions as DNA double strand breaks (DSB) of different severity. However, in this model only three classes of lesion and three rates of lesion progression are permitted. What all of these models omit is a consideration of the biochemical nature of the damage, the spectra of such structures and the different challenges which the different damage complexities present to cell's repair systems. I discuss here the complexities of radiation damage to the genetic material and the probable complexities and the interaction of these lesions with repair phenomena. A consideration of the LMDS idea of radiation damage to cellular DNA (7) indicates a more complex situation, with the damage requiring repair increasing in complexity with the "LET" of the radiation (8). Braby (2) has stated: "a detailed model of mammalian cell survival involving coefficients for the production of half a dozen different forms of DNA damage and the repair kinetics for all known DNA repair systems would probably not be useful because there are no experiments which can be used to test so many variables simultaneously". While this may be true, the alteration in the spectrum of lesions facing the cell as the "LET" varies ought to be taken into account in setting up biophysical models for cell survival.

IONIZING RADIATION DAMAGE

In earlier papers (7,8,9) I have pointed out the parameters of the molecular radiation damage which will vary with the amount of energy deposited in the local volume. With "low LET" radiation the energy deposition events cause low number of ionizations (10) with ~60% causing single damaging reactive species, and 30% two damaging reactive species. Consequently few of the molecular lesions produced involve more than two damages: the majority of the biologically significant damage produced by low

LET radiation consists of DNA doubly damaged sites, having various mixtures of base damages and strand breaks (e.g. a double strand breaks caused by two damaging species reacting on opposite strands. The fact that the majority of significant low LET radiation damage consists of only double lesions may explain why Curtis was able to use his model to satisfactorily fit low LET survival curves. However as the "LET" of the radiation increases, the spectrum of energy deposition events changes, the lesions become more complex and other repair and fixation mechanisms take part.

There is little information about these energy deposition spectra for condensed matter, but, spectra extrapolated from the gaseous state (11) are indicative of the marked increases in higher energy deposition events with increasing LET. From this increasing amount of energy the multiplicity of damaging species per event will increase and hence the with it the potential for greater multiplicity of DNA lesions.

As the LET of the radiation increases, the spectrum of lesion complexity will shift. Differences in damage parameters will occur:

a. The average number of base damages per site will increase.
b. The average number of strand breaks per site will increase.
c.. Spatial separation of the damages in the site will change.

REPAIR OF DNA DAMAGE

The repair of singly damaged sites is readily accomplished by mammalian cells. However, the removal of each lesion requires the concerted action of several enzymes (12): a damaged base is removed by the action of first an endonuclease, then an exonuclease then the correct base is introduced by a polymerase and finally the strand is resealed by a ligase. Strand breaks (which occur with loss of an intact base) require a similar series of enzymes for their repair. The initial enzymatic reaction depends on the structure of the lesion - several base damage specific enzymes have been identified (13), but the steps after removal of the damaged base will be the same for all lesions. It should be pointed out that repair of a base damaged site requires cleavage of the DNA backbone, i.e. a base damaged site is a potential strand break. The mechanisms by which double lesions are repaired are not known, at each single strand break a base moiety is deleted - thus correct repair must include the reintroduction of these bases and then resealing of the strand break ends. However, it is clear that a doubly damaged site of necessity requires the removal of two lesions, each requiring a series of enzyme actions, with the initial enzymatic activity being specific for the individual lesion involved. The sequencing of the multiple enzymatic activities is crucial to the fidelity of the repair process (9). For instance in a site which contains a base damaged site on one strand and a base damage on the other, strand cleavage of the base damaged site prior to strand break rejoining would give rise to a DSB.

As the number of damages per site increase, the requirements of coordination of repair activities increases, the repair enzyme requirements increase - and it is expected that the time taken for the repair will increase. Of course as the complexity of the lesion increases, the possibility that accurate repair is possible decreases. Thus with increased complexity repair is slower, and more prone to am errored result. As the multiplicity of the damages increases, with the probable consequences being increased time required for repair and decreased probability of correct repair.

FIXATION OF DAMAGE

In repair models, accurate repair of DNA lesions are considered to be in competition with lesion fixation, i.e. the progression of a lesion from being repairable to unrepairable or in other parlance from being potentially lethal to being lethal. We have previously shown that singly damaged sites in DNA are inconsequential to cell survival (14). Thus we concentrate here on LMDS.

There are two fundamental mechanisms by which LMDS lesions can become lethal which we have described previously (15,16). An error in base sequence can be introduced during the attempted

repair of a lesion but resealing with the correct end is accomplished. If this error occurs in a crucial part of the genome for instance within an exon of a gene then the error becomes biologically significant. If the error occurs in the intron region of a gene, then it is probably inconsequential. The probability that attempted repair of a lesion leads to an error in base sequence in the DNA will increase with the complexity of a lesion.

The second mechanism which leads to deleterious consequences in attempted repair is that the LMDS (DSB formed directly or by enzyme nicking at base damaged sites) rejoins with an end of another DSB. Such an occurrence would be deleterious whether the lesion rejoining had been produced within an important part of the genome or not. The probability of such a rejoining would increase with the life time of the damaged site, i.e. as the complexity of the damage increases.

From these considerations a modification of the LPL model is necessary particularly for high LET radiation. The modifications of the model (as presented by Weber (17) are shown in Figure 1.

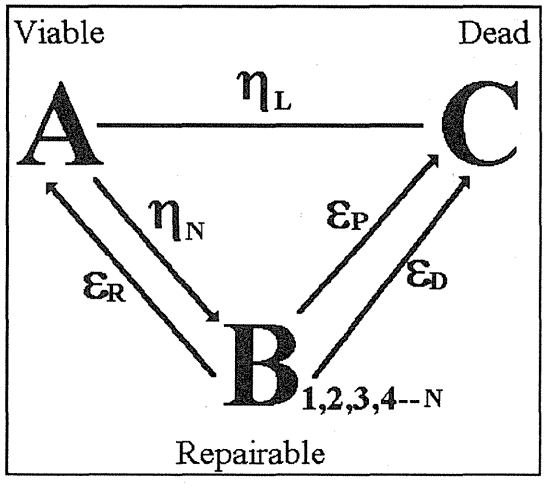

Figure 1. Schematic representation of the competition between repair and fixation of damage.

η_L represents the relative proportion of the damage which is irretrievably lethal. $B_{1,2,3,4\text{-}n}$ indicates the spectrum of repairable lesions produced by the radiation (the range of which depends on the radiation being used). η_N is the relative proportion of the damage of type B_n of which the spectrum depends on the radiation being used. ε_R is the rate of repair of repairable damage, ε_P is the rate of fixation of damage to cause a local error in the DNA sequence, ε_D is the rate of fixation of damage by misrejoining with the wrong DNA end. ε_R, ε_P, and ε_D are all dependent on the form of the damage B_n.

Thus as the spectrum of the damage changes, because of the competition between repair and fixation for each type of lesion (B_n) the fraction of the repairable damage which becomes fixed changes. In addition as the LET increases, the fraction of the initial damage which is irretrievably lethal increases.

CONCLUSIONS

1. As the amount of energy per deposition event increases the complexity of the DNA damage increases.
2. As the complexity of the damage increases:
   a. The difficulties of repairing the damage increase.
   b. The time to repair the damage increases
   c. The probability that the damage is misrepaired increases.
   d. The probability that the damage is not repaired increases.
3. The LET of the radiation is not the important factor, it is the spectrum of the energy deposition events which is prime.
4. The "repairability" of the damage is not a linear function of the amount of energy taken to create it.

ACKNOWLEDGMENTS

Work in the author's laboratory is supported by grant CA46295 from the National Cancer Institute, NIH, and grant DEFG03-93ER61952 from the Department of Energy.

REFERENCES

1. Curtis, S.B. Lethal potentially lethal lesions induced by radiation - A unified repair model. Radiat. Res. 106: 252-270 (1986).
2. Curtis, S.B. Mechanistic models. In "Physical and Chemical Mechanisms on Molecular Radiation Biology (W.A. Glass and M.N. Varma eds.) Plenum Press, New York. pp.367-386 (1990).
3. Braby, L.A. Phenomenological models. In "Physical and Chemical Mechanisms on Molecular Radiation Biology" (W.A. Glass and M.N. Varma eds.) Plenum Press, New York. pp.367-386 (1990).
4. Butts, J.J. and Katz R. Theory of RBE for heavy ion bombardment of dry enzymes and viruses. Radiat. Res. 30: 855-871 (1967).
5. Rossi, H.H., The radiobiological significance of spatial and temporal distribution of energy absorbed from ionizing radiations. In "Physical and Chemical Mechanisms on Molecular Radiation Biology (W.A. Glass and M.N. Varma eds.) Plenum Press, New York. pp.325-337 (1990).
6. Tobias, C.A. Blakely, E.A, Ngo, F.Q.H. and Yang, T.C.H. The repair-misrepair model of cell survival. In "Radiation Biology and Cancer Research. (R.E. Meyn and H.R. Withers eds.) Raven Press, New York, pp. 195-230 (1980).
7. Ward, J.F. Some biochemical consequences of the spatial distribution of ionizing radiation produced free radicals. Radiat. Res. 86, 185-195 (1981).
8. Ward, J.F. DNA damage produced by ionizing radiation in mammalian cells: Identities, mechanisms of formation and repairability. Progress in Nucleic Acids and Molecular Biology, 35, 95-125, (1988).
9. Ward, J.F. The intracellular molecular damage which is dependent on radiation energy deposition patterns at the nanometer level. In "Genes, Cancer and Radiation Protection". N.C.R.P. Proceedings No. 13, pp. 38-48 (1992).
10. Pimblott, S. and Mozumder, A., Structure of electron tracks in water. 2. Distribution of primary ionizations and excitations in water radiolysis. J. Chem. Phys. 95: 7291-7300 (1991).
11. Charlton, D. E., Nikjoo, H. and Goodhead, D.T. Energy deposition in sub-microscopic volumes. In "Radiation Research - a twentieth century perspective." (W.C. Dewey, M. Edington, R.J.M. Fry, E.J. Hall and G.F. Whitmore eds.) Academic Press, San Diego. pp. 421-426 (1992)
12. Friedberg, E.C. DNA Repair. W.H. Freeman and Co. New York (1984).
13. Wallace, S.S. Biological consequences of oxidized DNA bases. Brit J. Cancer 55 Suppl. VIII pp 118-128 (1987).
14. Ward, J.F., Blakely, W.F., and Joner, E.I. Mammalian cells are not killed by DNA single strand breaks caused by hydroxyl radicals from hydrogen peroxide. Radiat. Res. 104, 383-393, (1985).
15. Ward, J.F., Milligan, J.R. and Jones, G.D.D. Biological consequences of non-homogeneous energy depositions by ionizing radiation. Radiation Protection Dosimetry 52, 271-276, (1994).
16. Ward, J.F. The complexity of DNA damage - relevance to biological consequences. Int. J. Radiat. Biol. (In Press, June 1994).
17. Weber, K.J. Models of cellular radiation action - an overview. In "Quantitative Mathematical Models in Radiation Biology" (J.Kiefer ed.) Springer-Verlag, Berlin 1988, pp. 3-26.

A GENERAL APPROACH TO THE RBE EVALUATION IN A THERAPEUTICAL PROTON BEAM: PRELIMINARY RESULTS

MAURO BELLI[1,2], ALESSANDRO CAMPA[1,2], ILARIA ERMOLLI[1]

[1]Physics Laboratory, Istituto Superiore di Sanità
Viale Regina Elena, 299 - 00161 Roma, Italy

[2]INFN, Sezione Sanità, Roma, Italy

We address the problem of the relative biological effectiveness (RBE) evaluation of therapeutical proton beams for cell inactivation. While it is commonly accepted that high energy protons (with energies greater than 10 MeV) have radiobiological properties analogous to those of X- or γ–rays normally used in radiotherapy, there is now experimental evidence that for lower energies the RBE depends on proton energy. We consider a general approach to the evaluation of the lethal effect of protons, which is applicable in different situations, included those in which an extended Bragg peak is obtained via a modulated beam. The results that we present have been obtained combining two kinds of information: a) the experimental results available in the literature for V79 cell response to monoenergetic beams; b) the energy spectrum of the beam in the target volume, computed through the Monte Carlo algorithm implemented by the GEANT simulation code, which was used to describe the dose and energy distribution of the protons inside the target. In this preliminary work we applied this method to a simple Bragg peak produced by a proton beam of about 60 MeV initial energy, such as that typically used for treatment of ocular tumours. We found that the RBE increases with depth, even beyond the Bragg peak, up to a value higher than 2, when evaluated at the same surviving fraction as that given by 2 Gy of X-rays.

INTRODUCTION

The increasing interest for therapeutical applications of hadron beams calls for a better knowledge of their biophysical and biological features.

Most of the advantages associated with proton beams are ascribed to the possibility of delivering the dose in a physically selective way, i.e. in the target tissue while sparing the surrounding tissues. This possibility mainly relies upon the exploitation of the Bragg peak and is related to energy deposition at the macroscopic scale. By contrast, in the field of hadron therapy little attention has been paid so far to the biophysical and biological properties of protons that are related to energy deposition at the microscopic scale and that determine their biological effectiveness. In effect, it is currently accepted the idea that high energy protons are as lethal as (or perhaps less effective than) X- or γ-rays used in radiotherapy (13) and that only at an extended Bragg peak cell lethality is increased by only 10% (4,13). It appears that this increase is related to the presence of low energy particles, as pointed out by Robertson et al. (14), who found an RBE increase in the descending part of the Bragg peak. On the other hand, data on the RBE for cell inactivation as a function of proton energy have been obtained in recent years by extensive experimental studies carried out on cultured V79 cells irradiated with monoenergetic, low energy proton beams (1,2,6,9,12). They have shown that proton RBE may reach values significantly higher than unity at sufficient low energy. Since an important fraction of the dose delivered to cells by a therapeutical proton beam is deposited by low energy particles belonging to the Bragg peak, these results put in evidence the relevance of the low energy, densely ionizing proton components of the beam.

The need for understanding the possible implications for proton therapy of the radiobiological results obtained with low energy protons prompted us to clarify the relationship between these results and those obtained on cultured cells irradiated with pure or spread-out Bragg peaks, that imply a quite large energy spread at the cell position.

As an attempt to reach such an objective, we developed an approach aimed at evaluating the proton RBE at a given depth from the contribution of the different energy components to cell inactivation. It is based on the integration of two types of information:

1) the experimental knowledge of the dependence of cell inactivation on proton energy;

2) the calculation of the energy distribution of the particles at a given depth.

The energy distribution at a given position depends on

several factors that determine the "history" of the particles, such as the initial mean value and distribution of the beam energy, the material traversed by the beam, and the diffusion on collimators. Therefore, the energy distribution, and consequently the RBE, depends on the beam configuration. The relevant beam characteristics can be included in the calculation so as to obtain the particle energy distribution at any position in the volume traversed by the beam. This allows the possibility of calculating the inactivation level inside the target and in the surrounding tissues, provided that suitable radiobiological information is available.

The approach we devised, therefore, could give a general method that can be applied to any configuration and operating conditions, including those where a beam modulation is used (and more generally when the proton beam in the target volume has an arbitrary energy spectrum), for evaluating the RBE and the so-called "biological dose" and their mapping inside the target and in the surrounding tissues.

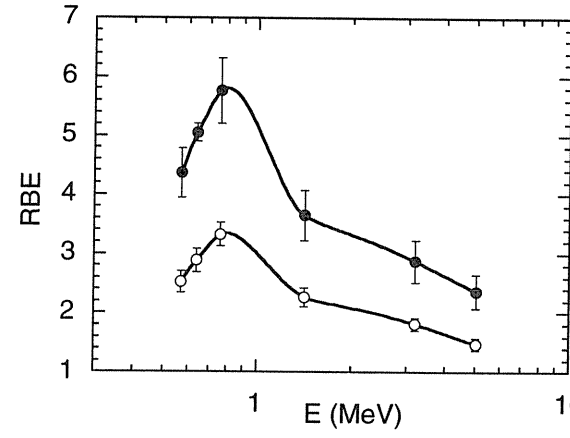

Figure 1. Experimental values of the RBE for monoenergetic protons; open points: surviving fraction given by 2 Gy of X-rays; full points: very low doses.

EXPERIMENTAL RBE-ENERGY RELATIONSHIP

In the approach here described we used the extensive data set on radiobiological effects induced by monoenergetic protons in cultured mammalian cells that has been obtained at Laboratori Nazionali di Legnaro (LNL) of the National Institute for Nuclear Physics (INFN) in the framework of a large co-operation between the National Health Institute (ISS), the INFN and the National Research Council (CNR). Data on cell inactivation, mutation, and DNA damage (double strand breaks), have been collected over several years on V79 cells using a radiobiological facility based on the 7 MeV Van de Graaff accelerator. Here we only consider the inactivation data (1,2), obtained by means of the usual clonogenic assay. They are summarized in the following, while details of the work can be found in the original publications.

The survival curves were obtained at 6 different energies in the range 0.5-5 MeV, and the response with X-rays was used as a reference. The dose-response curves were found to be linear for energies less than about 1 MeV. At higher energy a shoulder appeared, similarly to the dose-response observed for sparsely ionizing radiation.

The experimental points were fitted to a linear, or linear-quadratic, equation in order to obtain the linear (α) and quadratic (β) coefficients. They have been used to evaluate the RBE both at low doses (in terms of the linear coefficient ratios) and at the surviving fraction given by 2 Gy of X-rays. The maximum in the RBE has been found at about 31 keV/μm or 0.76 MeV (figure 1). This maximum RBE depends on the level of inactivation: it is about 6 at low doses and about 3 at the same inactivation level as that given by 2 Gy of X-rays (i.e. at 64% survival).

THE ENERGY DISTRIBUTION OF THE PROTON BEAM

A powerful and suitable tool for attacking the problem of the transport of a proton beam in biological matter is offered by simulation with Monte Carlo procedures, that have extensive application to radiation transport and shielding computations.

There exist several well known Monte Carlo codes that have been developed for use in particle physics experiments. We used one of these, the GEANT code (7), that has become a "*de facto*" standard in recent years. The GEANT code simulates the passage of elementary particles through the matter. The first version of the code has been written in 1974 at CERN, the European Centre for Nuclear Research in Geneva (Switzerland), but it has been developed and constantly updated over the years. Originally the code was developed for high energy physics experiments, but after some improvements it has found applications also outside this domain, in areas such as medical and biological sciences and radiation protection. This constant evolution is one of the reasons for the success of the GEANT code. In fact, although several "home-made" codes exist which allow description of proton transport, they often use drastic approximations for the physical processes described. The GEANT code is able to simulate the physical processes dominant in the range energy from 10 keV up to 10 TeV; in particular, we appreciate that this code takes care of the transport of secondary particles through the matter, allowing very accurate descriptions on the propagation of particle beam through targets.

The design of the code is modular: a main programme has to be provided by the user to allow the insertion of data for the various possible situations as desired. The

target volume where the particles are transported is user-defined through a composition of elementary volumes and traversed material (elements or compounds). The user can easily describe target with any complex geometrical form and composition. Various parameters can also be selected by the user to determine the degree of accuracy used to describe the physical processes and to follow individual secondaries produced into the simulation.

Our present user-code is designed to simulate the track of a pencil beam of protons incident on the central region of a target. This is described as a homogeneous tissue equivalent cube (4x4x4 cm^3) containing small cylindrical volumes ($r \approx 2$ mm, h = 1 mm) aligned with the beam axis, in which we register the energy deposition and other physical particle properties of interest. For any given plane perpendicular to the beam axis, we compute the number and the energy spectrum of the protons crossing the surface defined by the intersection of the target volume with the plane. The absorbed dose is evaluated as the energy released in the small volume encompassed by two consecutive surfaces.

We applied this method to simulate proton beams of relatively low energy ($\approx$ 60 MeV), typically used for treatment of ocular tumours. Figure 2 shows the results obtained with a pencil beam of protons, assuming that their initial energy has a 1 MeV (FWHM) Gaussian distribution around 57.7 MeV, similar to the therapeutical proton beams used at the PSI facility (Paul Scherrer Institute) in Villigen (Switzerland). The simulation has been performed with 10,000 protons, which gives a sufficient statistics for the loss of energy and for the proton energy distribution along the track of the beam. When the depth-dose curves so obtained have been compared with experimental data obtained at the PSI facility (5), a very good agreement was found.

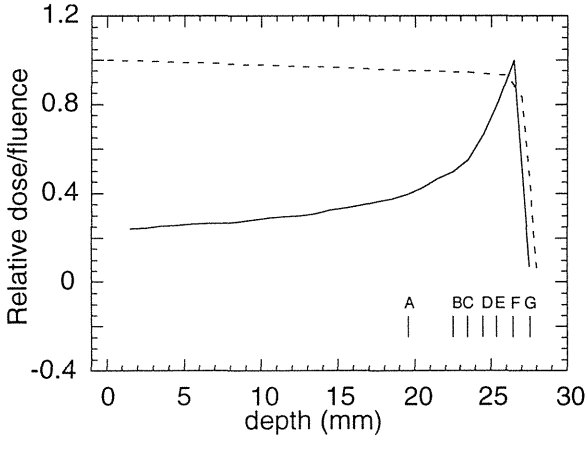

Figure 2. Relative dose (solid curve) and relative fluence (dashed curve) as a function of the depth in the simulation of a proton beam with an average initial energy=57.7 MeV and an initial spread=1 MeV; bars and corresponding letters indicate the plane positions where we have computed the energy distributions shown in figure 3.

The physical processes implemented into the simulation are: excitation, ionisation, multiple scattering, decay in flight, nuclear fission and other hadronic interactions for the hadron transport; photoelectric, Compton and Rayleigh effects, pair production for the photon transport; excitation and ionisation, multiple scattering, bremsstrahlung and annihilation for electron and positron transport.

In figure 3 we show some energy distributions of the particles at several depths along the track. These are described in terms of the Landau theory for the energy lost by the particles.

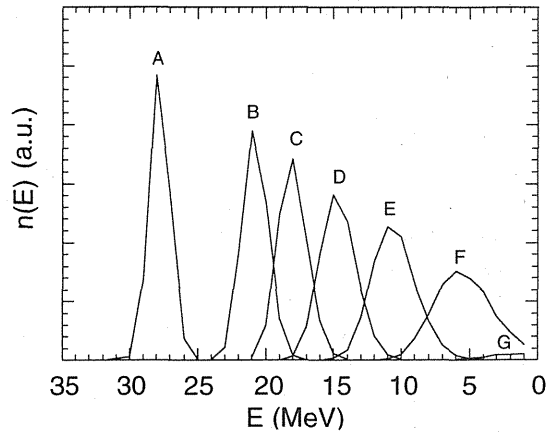

Figure 3. Energy spectra of the simulated proton beam at different positions along the track. The depths where we have computed these spectra are indicated by the corresponding letter in figure 2. The curve with the peak at about 5 MeV refers to the depth at the Bragg peak. The rightmost very low curve (G) refers to the distal part of the Bragg peak, where most of the protons have already been absorbed.

The information obtained with the Monte Carlo simulation (in particular about the energy deposition and the energy distributions along the track) has been used as a basis for calculating the relevant biological effects caused by protons in cells, as described in the following.

INTEGRATION OF THE PHYSICAL AND RADIOBIOLOGICAL DATA

We have devised a method to define the RBE of a given proton energy distribution, such as those obtained by the simulation described above, and shown in figure 3. The method can be summarized as follows. We have used the experimental data which have determined, at various energies of the incident protons in the range from about 0.5 MeV to about 5 MeV, the parameters of the survival curves. From these data we have fitted two functions of the energy, one for the parameter α and one for the parameter β, in order to have these parameters for all the energies involved in the energy spectra of the protons of the simulated beam. Then we have generalized the usual relationship between the surviving fraction and the dose

from monoenergetic protons (with given α and β) in order to handle the effect due to protons of different energies. In this way we can compute the absorbed dose needed to produce a given surviving fraction in the case of protons with the energy distribution given, at any depth along the track, by the simulation. Therefore we can calculate the RBE of the simulated beam at a given depth as the ratio of the dose of X-rays needed to give the same effect with respect to the proton dose calculated as above. In the following we give some details of the procedure.

We have defined the two functions of the energy, α(E) and β(E), starting from the values determined experimentally at 6 different energies in the range 0.5-5 MeV; more precisely, the energies are 0.57, 0.64, 0.76, 1.41, 3.20 and 5.01 MeV. We had also the values of the same two parameters for the dose-response curve for X-rays. For the five energy ranges between each pair of consecutive experimental energies we have defined α and β with a linear fit between the experimental values. We note at this point that for the three lowest energies β was determined to be 0 (linear dose-response curve), and therefore the fit for β was taken as identically 0 for all the energies between 0 and 0.76 MeV. In the case of α, for energy values between 0 and 0.57 MeV we have made a linear fit between the value 0 at 0 MeV and the experimental value at 0.57 MeV; the reason was the experimental indication that the peak of α is at energy values larger than 0.57 MeV. For energy values larger than 5.01 MeV we have adopted the strategy to make α and β tend asymptotically to the X-rays values. We have then chosen to have curves that from the values at 5.01 MeV tend to the asymptotic values with the inverse square of the energy.

The dose absorbed from protons distributed according to an energy distribution function n(E), which is different from zero between E_1 and E_2, is given by:

$$D = K\int_{E_1}^{E_2} n(E)L(E)dE \qquad (1)$$

where L(E) is the LET as a function of the energy, n(E) dE is the number of protons with energies between E and E + dE, and K is the factor of proportionality. In this calculation we used the Tables of the ICRU Report 49 (10) for the LET of protons in tissue equivalent material. The Tables give the LET for a very fine grid of energy values, and for values between the points of this grid we have used a linear fit. The energy integral of n(E) gives the total number of protons N_p. For later convenience it is useful to define the normalized distribution function n'(E) = $(1/N_p)$ n(E) such that the energy integral of n'(E) is equal to 1.

In the linear-quadratic survival curve, the surviving fraction S after the absorption of a dose D from protons of energy E_0 is given by:

$$S = \exp\{-\alpha(E_0)D - \beta(E_0)D^2\} \qquad (2)$$

Now suppose to have an absorption of a dose D_a at energy E_a and of a dose D_b at energy E_b; if β for these two energies were 0 the extension of (2) to this case would give a surviving fraction:

$$S = \exp\{-\alpha(E_a)D_a - \alpha(E_b)D_b\} \qquad (3)$$

The extension is not straightforward when β is different from 0. We have chosen to make the following hypothesis, which has to reduce to (2) when E_a is equal to E_b:

$$S = \exp\{-\alpha(E_a)D_a - \alpha(E_b)D_b - \beta(E_a)D_a^2 - 2\beta(E_a,E_b)D_aD_b - \beta(E_b)D_b^2\} \qquad (4)$$

where the function of two variables β (E_a, E_b) is such that β (E, E) = β(E) for each E . In this way when $E_a = E_b$ eq. (4) reduces to the usual expression (2). The extension of eq. (4) to the case in which there is an energy distribution n(E) between the energies E_1 and E_2 is straightforward: the surviving fraction S is given by:

$$\ln S = -K\int_{E_1}^{E_2} \alpha(E)n(E)L(E)dE - K^2\int_{E_1}^{E_2}\int_{E_1}^{E_2} \beta(E_a,E_b)n(E_a)L(E_a)n(E_b)L(E_b)dE_adE_b \qquad (5)$$

Apart from the condition above mentioned, the function β(E_a, E_b) could be arbitrary. We have chosen the definition $\beta(E_a,E_b) = \sqrt{\beta(E_a)\beta(E_b)}$, which seems quite natural. We will come back to this point in the discussion. With this definition eq. (5) becomes:

$$\ln S = -K\int_{E_1}^{E_2} \alpha(E)n(E)L(E)dE - K^2\left(\int_{E_1}^{E_2} \sqrt{\beta(E)}n(E)L(E)dE\right)^2 \qquad (6)$$

After these definitions it is also possible to compute the RBE of a beam of protons with energies distributed according to a given normalized energy distribution n'(E). In fact one can proceed as follows. Taking, as it is often used, the dose of 2 Gy of X-rays as the dose of reference, one computes the surviving fraction S_X for this dose. Then one substitutes in eq. (6) n(E) = N_p n'(E) , with N_p unknown, and S = S_X to obtain:

$$\ln S_x = -KN_p\int_{E_1}^{E_2} \alpha(E)n'(E)L(E)dE - K^2N_p^2\left(\int_{E_1}^{E_2} \sqrt{\beta(E)}n'(E)L(E)dE\right)^2 \qquad (7)$$

and solves this quadratic equation in KN_p. The value computed is substituted in eq. (1) (after having made the substitution $n(E) = N_p\, n'(E)$), and the dose D is therefore obtained; the ratio D_X/D with, in this case, $D_X = 2$, gives the desired RBE. In the same way it is possible to compute the RBE at a given surviving fraction S_0 : now one has S_0 instead of S_X in (7), while the reference dose D_X to compute the RBE is obtained from eq. (3), with α and β assuming the values for X-rays.

We now consider the problem of assigning an error to the value of the RBE computed for a given normalized energy distribution n'(E). By far the main source of uncertainty is the experimental error in the values of the parameters α and β, which have been determined for protons at the experimental energies given above; also the parameters for X-rays are affected by an error. These uncertainties propagate through the determination of the RBE for a distribution n'(E) in the following way. A different set of values for α and β for protons at the experimental energies gives a different fitting curve for α and β of protons as a function of energy; besides, if one chooses for a given value D_X as the reference dose of X-rays (in our case D_X =2), different values for α and β for X-rays give a different reference surviving fraction S_X. Therefore for a given n'(E) one has different coefficients for the quadratic equation (7); this will give a different dose D and so a different RBE. Analogous is the case where one chooses a given reference surviving fraction S_0: different $\alpha(E)$ and $\beta(E)$ for protons give different coefficients in the right hand side of eq. (7), and different α and β for X-rays give a different reference dose D_X (given S_0).

The experimental errors in α and β are given in the form of standard deviation. We have thus performed a Monte Carlo algorithm, in which we have assumed that each one of the experimental α and β is distributed according to a Gaussian distribution with average value and standard deviation given by the experimental values. We have also assumed, for simplicity, that the distribution of the whole set of parameters is the product of the single Gaussian distributions, implying that the determination of one parameter is independent of that of any other parameter. Although this is not true in general (α and β for a given proton energy should be correlated) it is expected that this simplification would give a conservative evaluation of the error in the RBE. In each step of the Monte Carlo algorithm the functions $\alpha(E)$ and $\beta(E)$ have been determined through the fitting procedure described above, and the RBE at a given X-ray dose D_X or at a given surviving fraction S_0 have been computed via the steps explained in the text after eq. (7). At the end of the Monte Carlo, one can then obtain the average value of the standard deviation of the RBE for a given distribution n'(E).

Figure 4 shows the RBE value as a function of the depth obtained with the procedure described, in the case where the reference dose is 2 Gy of X-rays. It can be seen that the RBE increases with depth even beyond the maximum of the Bragg peak. Also shown in the same figure are the RBE values derived on the basis of the mean energy of the protons at the various depth, i.e. without taking into account their energy distribution. These values are practically the same at the plateau and in the ascending part of the Bragg peak, but, at greater depths, they are systematically lower than those obtained with the complete calculation. This is related to an asymmetry of the response, mainly due to the higher dose delivered by the protons with lower energy. In figure 5 we show the surviving fraction as a function of the depth, in the case where the survival at the Bragg peak is the same as for the reference radiation.

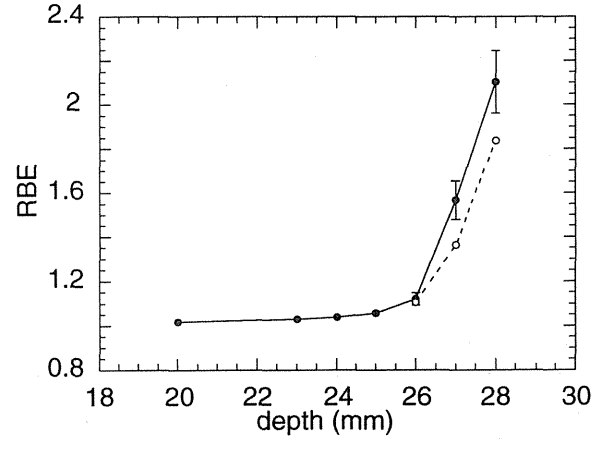

Figure 4. Solid circles : RBE of the distribution functions shown in figure 3, with the abscissa of the points giving the depth of the corresponding distribution. Where the error is not shown it is smaller than the symbol. Also shown, with open circles and without errors, is the RBE for monoenergetic protons having an energy equal to the average energy of the corresponding distributions. The solid and the dashed lines are guides for the eye.

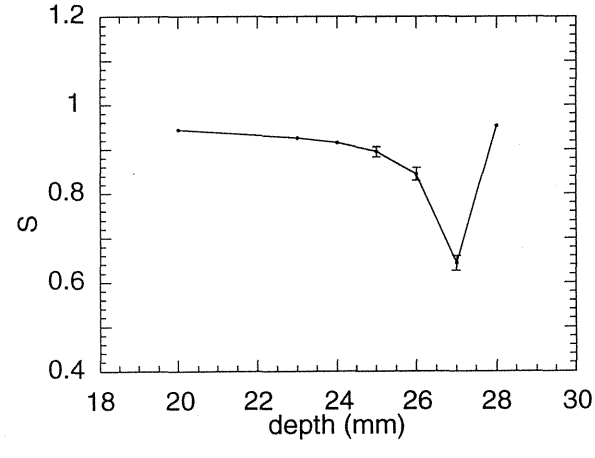

Figure 5. The surviving fraction corresponding to the positions shown in figure 4. It has been computed assuming a beam intensity such that at the Bragg peak the surviving fraction is that given by 2 Gy of X-rays (0.64).

DISCUSSION AND CONCLUSIONS

The code that we have used for simulating proton interaction has proven to be applicable for describing some important features of the transport of therapeutical proton beams through the matter, at least for certain purposes and under certain conditions. In fact, we were able to reproduce in a satisfactory way the experimental Bragg curve of a beam of about 60 MeV initial energy. However, the applicability of the code, that has been developed for high energy physics, must be carefully checked in order to ascertain if different codes are more appropriate for describing beam degradation, particularly for accurate description of the energy distribution of the primary protons and of the secondary particles at very low energy.

With relatively high energy protons, such as those used for treatment of deep-seated tumours, production of other charged particles and neutrons may be significant, and their contribution to the dose and to the biological effect needs to be evaluated, particularly for the low energy, densely ionizing particles. On the other hand, in the present work we simulate proton beams of relatively low initial energy, such as those used for ocular treatments, for which the contribution of nuclear interactions is quite small, so that the energy is mainly deposited by the primary protons. Under these conditions, the possible inaccuracy of the code for low energy secondary particles is not important. In addition, the simulation work helped to highlight how the distribution of energy and atomic number of particles in a therapeutical proton beam depends on several factors, such as the initial mean energy and energy spread of the beam.

A crucial point encountered in putting together the calculation of the energy spectrum of protons with the experimental radiobiological data is the model to use for taking into account the combined effect of doses deposited by protons of different energies. This is not a new point, since it belongs to the general problem of describing or predicting the interaction of mixed radiations as far as biological effects are concerned. Although it can be approached by general methods such as those based on track structure calculations (8,15), these are not yet available in a form suitable to answer this question. We therefore preferred to use a semi-empirical approach based on a reasonable generalization of the usual linear-quadratic expression, eq. (2), to take into account the presence of different energy components in the proton beam. Our assumption about the interaction term, $\beta(E_a,E_b)=\sqrt{\beta(E_a)\beta(E_b)}$, implies that, in the particular case where only two energies are present, eq. (4) becomes:

$$-\ln S = \alpha(E_a)D_a + \alpha(E_b)D_b + \left(\sqrt{\beta(E_a)}D_a + \sqrt{\beta(E_b)}D_b\right)^2 \qquad (8)$$

which is same expression as that used by Leenhouts and Chadwick on the basis of DNA damage (11). Even if it is possible to give a biophysical meaning to this expression (in fact, the quadratic term, which is responsible for deviation from linearity, can be formally regarded as arising from the interaction of two "sublesions", each one with probability given by $\sqrt{\beta(E)D}$), we think that the assumption of eqs. (4) or (8) (and of their generalizations represented by eqs. (5) and (6)), does not necessarily imply that a specified biophysical model of radiation action is assumed.

Some tests that we have performed using other assumptions, indicate that the results, in terms of RBE or surviving fraction, are scarcely dependent on the model used for describing the interaction. This poor sensitivity can be ascribed to the fact that the β term is important only at positions where protons with relatively high energies are present, but at these positions the energy spread is small, so that the results are well described in terms of average energy. On the other hand, near the Bragg peak or in the descending portion of the curve, the α term is predominant, so that the interaction term has no or little effect.

The most important feature derived from this study is the RBE increase with depth, even beyond the maximum of the Bragg peak, up to a value higher than 2, when evaluated at the same survival level (64%) as that given by 2 Gy of X-rays. This is qualitatively consistent with the scarce experimental data so far obtained on V79 and other cells. Robertson et al. (14), irradiating rat hepatoma cells with a spread-out Bragg peak at the Harvard cyclotron, found that the "biological" Bragg peak extended beyond the physical one. The results obtained by Blomquist et al. (3) at the Uppsala facility with V79 cells showed a little increase of cell inactivation with depth in a modulated Bragg peak. They found an RBE at 2 Gy of about 1.3 in the central part of this extended peak, that suggests an important role of the low energy components. Unfortunately, this authors do not give any information for the distal region, that is expected to be the richest one in these components. However, a very recent indication that the RBE sharply rises in the distal part of a modulated Bragg peak was obtained by Skarsgard et al. (16) at TRIUMF using V79 cells .

A detailed knowledge of the RBE for inactivation in the irradiated tissue is fundamental for prevention of late radiation effects in the normal tissue and in general for optimizing the treatment. Information on the RBE distribution in the distal part of the Bragg peak is especially important when critical structures are likely to be involved.

This preliminary study shows the feasibility of a general approach to this problem, based on simulations of the beams and on experimental data with monoenergetic protons. However, some improvements are required, in order to consider more realistic beam geometries, and radiobiological data obtained with human cell lines. For this purpose, we are developing simulations of modulated Bragg peaks with a broad field, that can be used for more

detailed tests of the method with the experimental results obtained in such conditions.

In conclusion, the approach that we have devised, in spite of its present limitations, can be of fundamental and practical value in:

i) establishing the logical relationship between the biological effects of a therapeutical proton beam and those of monoenergetic beams;

ii) developing a methodological tool for obtaining a 3-dimensional mapping of the biological effects in tissues, therefore improving the treatment planning in proton therapy.

REFERENCES

1. Belli, M.; Cera, F.; Cherubini, R.; Haque, A.M.I.; Ianzini, F.; Moschini, G.; Sapora, O.; Simone, G.; Tabocchini, M.A.; Tiveron, P. The RBE of protons for cell inactivation: the experience with V79 cells. In: Proceedings of the International symposium on hadron therapy (Como, Italy, October 18-20, 1993); U. Amaldi and B. Larsson eds.; Excerpta Medica, Elsevier (in press).
2. Belli, M.; Cherubini, R.; Finotto, S.; Moschini, G.; Sapora, O.; Simone, G.; Tabocchini, M.A. RBE-LET relationship for the survival of V79 cells irradiated with low energy protons. Int. J. Radiat. Biol. 55: 93-104; 1989. - Belli, M.; Cera, F.; Cherubini, R.; Haque, A.M.I.; Ianzini, F.; Moschini, G.; Sapora, O.; Simone, G.; Tabocchini, M.A.; Tiveron, P. Inactivation and mutation induction in V79 cells by low energy protons: re-evaluation of the results at the LNL facility. Int. J. Radiat. Biol. 63: 331-337; 1993.
3. Blomquist, E.; Russell, K.R.; Stenerlöw, B.; Montelius, A.; Grusell, E.; Carlsson, J. Relative biological effectiveness of intermediate energy protons. Comparisons with ^{60}Co gamma-radiation using two cell lines. Radiotherapy and Oncology 28: 44-51; 1993.
4. Bonnet, D.E. Current developments in proton therapy: a review. Phys. Med. Biol. 38: 1371-1392; 1993.
5. Egger, E. Private communication; 1994.
6. Folkard, M.; Prise, K.M.; Vojnovic, D.S.; Roper, M.J.; Michael, B.D. The irradiation of V79 cells by protons with energy below 2 MeV. Part I. Experimental arrangement and measurement of cell survival. Int. J. Radiat. Biol. 56: 221-237; 1989.
7. GEANT User's Guide. CERN DD/93/2.
8. Goodhead, D.T; Leenhouts H.P.; Paretzke, H.G.; Terrissol, M.; Nikjoo, H.; Blaauboer, R. Track structure approaches to the interpretation of radiation effects on DNA. Radiat. Prot. Dos. 52 (1-4): 217-223; 1994.
9. Goodhead, D.T.; Belli, M.; Mill, A.J.; Bance, D.A.; Allen, L.A.; Hall, S.C.; Ianzini, F.; Simone, G.; Stevens, D.L.; Stretch, A.; Tabocchini, M.A.; Wilkinson, R.E. Direct comparison between protons and alpha particles of the same LET: I. Irradiation methods and inactivation of asynchronous V79, HeLa and C3H 1OT1/2 cells. Int. J. Radiat.Biol. 61 (5): 611-624; 1992.
10. ICRU Report 49, Stopping powers and ranges for protons and alpha particles. International Commission of Radiation Units and Measurements; Washington D. C.; 1993.
11. Leenhouts, H.P.; Chadwick, K.H. Analysis of the interaction of different radiations on the basis of DNA damage. Paper presented at the workshop on Biophysical Modelling of Radiation Effects, Padua, Italy, 1991; K.H.Chadwick, G. Moschini and M.N. Varma eds., Adam Hilger, Bristol, Philadelphia and New York; 1992.
12. Perris, A.; Pialoglou, P.; Katsanos, A.A.; Sideris, E.G. Biological effectiveness of low energy protons. I. Survival of Chinese hamster cells. Int. J. Radiat. Biol. 50: 1093-1101; 1986.
13. Raju, M.R. Protons. In: Heavy particle radiotherapy. Academic Press, New York, 1980; 188-251.
14. Robertson, J.B.; Williams, J.R.; Schmidt, R.A.; Little, J.B.; Flynn, D.F.; Suit, H.D. Radiobiological studies of a high energy modulated proton beam utilizing cultured mammalian cells. Cancer 35: 1664-1677; 1975.
15. Scholz, M.; Kraft, G. Calculation of heavy ion inactivation probabilities based on track structure, X-ray sensitivity and target size. Radiat.Prot.Dosim. 52 (1-4): 29-33; 1994.
16. Skarsgard, L.D.; Wouters, B.G.; Lam, G.K.Y.; Durand, R.E.; Sy, A. RBE determination for the 70 MeV proton beam at TRIUMF using cultured V79-WNRE cells. Abstracts of the XX PTCOG meeting, held in Chester, England, May 16-18 1994.

CALCULATION OF RBE FOR PROTON BEAMS WITH ENERGIES BETWEEN 70 AND 250 MEV BY USING THE RESPONSE FUNCTION MODEL

H. PAGANETTI[1], P. OLKO[2], H. KOBUS[3], M.P.R. WALIGORSKI[2,4], TH. SCHMITZ[1], D. FILGES[3], AND H.W. MÜLLER-GÄRTNER[1]

1 Institute of Medicine IME, Forschungszentrum Jülich GmbH, Jülich, Germany
2 Institute of Nuclear Physics IFJ, Krakow, Poland
3 Institute of Nuclear Physics IKP, Forschungszentrum Jülich GmbH, Jülich, Germany
4 Center of Oncology, Krakow, Poland

The biological effectiveness of therapeutic pencil proton beams was studied with regard to the initial energy distribution of an extracted beam and to the depth of the beam penetration in water. Such data will be useful to assess the biological effectiveness of protons in future therapy installations with electronically modulated scanned beams, which are planned to be applied on some modern accelerators, e.g. COoler SYnchrotron COSY at Juelich, Germany. Proton transport calculations in water for a proton energy range from 70 to 250 MeV were performed with the Monte Carlo codes PTRAN and MC4 in order to obtain proton energy spectra at a given depth in water. The momentum spread of an input semi-monoenergetic proton beam, Δp/p, was varying from 0 to 0.003. Next, the microdosimetric response function approach was applied to calculate the biological effectiveness of a proton beam at a depth of interest. The biological response function describes the probability of a biological effect after an event of energy deposition with a given lineal energy, y, which is a parameter characterizing ionization density. In the calculation of the relative biological effectiveness for protons, RBE_0, the whole distribution of possible energy deposition events (i.e. so-called yd(y) microdosimetric distribution) was taken into account and normalized to an effect for Co-60 gamma-rays. The biological end-point of the early intestinal tolerance assessed by crypt regeneration in mice was considered. The results show that RBE values depend on the initial energy spread of the input proton beam and on the depth of beam penetration. RBE for intestinal tolerance in mice approaches 1 in the plateau region and gradually increases with the proton penetration depth. In the center of the Bragg peak, at maximum dose delivery, RBE values range from about 1.1 (250 MeV beam) up to 1.9 (70 MeV beam). At the end of the Bragg peak the RBE was found even higher (1.3 for 250 MeV beam to about 2.3 for 70 MeV beam) but only about 1% of dose is delivered with such a high RBE values. In addition an radial increase of the RBE has been found. The above results indicate that for therapy planning with electronically modulated pencil proton beams it would be necessary to account for a depth and radial dependence of proton RBE, especially for low penetrating beams.

Introduction

Medical applications of charged particle beams have significantly increased worldwide during the last twenty years (see e.g. [Sui88]). The use of protons with energies between 70 and 250 MeV in cancer radiotherapy offers significant advantages over radiations conventionally employed. Tumor volumes in the body can be irradiated more precisely than it is possible with photon, electron, pion or neutron beams. Due to the finite range and the sharpness of the dose gradients, the dose to well defined target volumes can be delivered without excessive irradiation of non-target tissue. Range modulated proton beams are used for radiotherapy at several accelerator laboratories to introduce proton therapy as a clinical hospital-based therapy modality.

In proton therapy planning it is necessary to take into account an increased biological effectiveness of slow protons, which transfer their energy to tissue with higher ionization density than conventional therapy modalities as fast electrons or gamma-rays. High-energy protons are considered as low-LET particles because 200 MeV protons stopped in water transfer only about 2% of the dose to the medium with LET higher than 10 keV/μm. In the present proton therapy installations beams are shaped with range modulators (absorbers) in order to produce a uniform dose distribution within the tumor volume. In that case, high-LET ends of proton tracks are uniformly spread over an extended Bragg peak and, while the total high-LET contribution to dose is small, the biological effectiveness increases only slightly. At present, the value of therapeutic RBE applied for proton therapy planning is in the range of 1-1.2 [Raj80]. For therapy planning, the variation of a

biological dose in tissue should be known within an uncertainty not exceeding 5 %.

However, the present methods of beam shaping using absorbers have some disadvantages. Scattering and energy loss straggling in the absorber reduce the sharpness of lateral and distal dose falloffs. An alternative method is offered by a dynamic range modulation system which are able to extract monoenergetic particle beams at different energies. Such an electronic range modulation system of a proton pencil beam is considered to be constructed at the COoler SYchrotron COSY, at Jülich, Germany. This machine should produce highly monoenergetic protons with momentum spread only about $\Delta p/p=10^{-3}$. In that case, when dynamic modulation is applied, a tumor volume will be irradiated with overlapping narrow pencil beams.

In this work the biological effectiveness of semi monoenergetic proton beams, penetrating a water phantom, was studied as a function of an incident proton energy spectrum, depth of penetration and radial distance to the beam axis. Proton energy spectra at different depths were calculated and applied, using a biological weighting function approach, to evaluate the Relative Biological Effectiveness.

Methods of RBE Calculations

It is possible to characterize the biological effectiveness of a given radiation by a determination of its microdosimetric parameters. A main parameter used in experimental microdosimetry, lineal energy, y, describes an actual energy deposition to the target normalized to its mean chord length (for the definition of the basic microdosimetric parameters see [ICRU80]). y can be denoted as the microdosimetric analogon to LET. In contrast to LET, y is a stochastic quantity. Even if the whole system is irradiated with just a single radiation modality the target can experience a whole spectrum of energy deposition events. These spectra of energy deposition events (microdosimetric distributions), denoted e.g. d(y), and their moments are used to describe the ionization density of the radiation in the target. Microdosimetric procedures were succesfully applied to compare the biological effectiveness of fast neutron and proton therapy beams [Men90, Men94, Lon94]. This assessment of RBE is based on an assumption that there exists a biological weighting function, r(y), which relates a given, observed biological effect, R, to measured d(y) distributions. This approach only assumes a correlation between the RBE of a given proton beam and the shape of its microdosimetric distribution. This distribution can be obtained, when the proton energy spectrum at the point of interest is known.
In this paper such a procedure was adopted to investigate the biological effectiveness of proton beams penetrating in a water phantom. Monte Carlo proton transport calculations in water were performed in order to obtain physical information at the depth of interest, particularly dose, fluence and proton energy spectrum. Using these data microdosimetric distributions d(y) were calculated and applied to evaluate the RBE at different depth in water with the use of a biological weighting function for early intestinal tolerance in mice published by Loncol et al. [Lon94].

A. Monte Carlo Calculations

Monte Carlo techniques have proven efficient to study dose deposition in heterogeneous media where exact analytic calculations are impossible or extremly difficult. Statistical fluctuations in energy loss are responsible for the phenomenon of energy straggling. If one replaces tissue by water and neglects differences in the electron collision cross sections, the interaction of protons can be simulated by using cross sections for water vapor. Proton transport calculations with the Monte Carlo programs PTRAN [Ber93b] and MC4 [Clo93] have been performed for water and for a set of energies between 70 and 250 MeV with small energy spreads (up to $\Delta p/p=3x10^{-3}$, see e.g. figure 1 for a 150 MeV beam) as available at COSY (COoler SYnchrotron in Jülich, Germany). PTRAN was used to calculate the depth dependence and MC4 to calculate the radial dependence of the beam characteristics.

The information obtained by PTRAN and MC4 includes energy loss curves as well as energy spectra of protons at various depths.

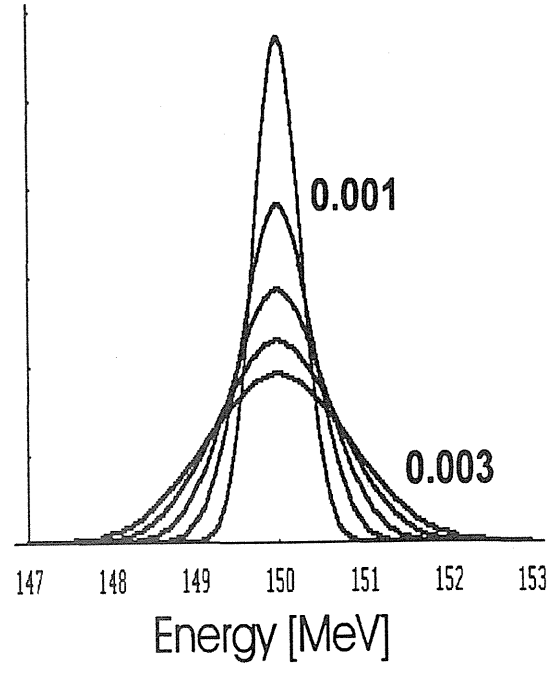

Figure 1: Momentum spread ranging from $1x10^{-3}$ up to $3x10^{-3}$ of a 150 MeV proton beam (in arbitrary units).

The program PTRAN accounts for energy loss, multpile scattering and energy loss straggling, whereas the inelastic nuclear interactions are treated as entirely absorptive effects. The energy lost by primary protons in Coulomb collisions is mostly transferred to secondary electrons and to a lesser extend it is used for molecular excitation and dissociation. Due to the maximum reachable energy in those collisions depending on the proton energy the energy transport by secondary electrons has a significant effect on the depth-dose curve only near the entrance face of the phantom. PTRAN disregards the energy transport by secondary electrons.

Most of the energy lost by primary protons in nuclear reactions is transferred to secondary charged particles (protons, deuterons, alpha particles, heavy recoil nuclei), neutrons and gamma rays. Seltzer [Sel93] recently estimated the number and energy spectra of secondary charged particles and neutrons from nonelastic reactions of protons with ^{16}O for some proton energies (The fraction of gamma-rays was found to be unimportant).

We used Seltzer's results to determine from the calculated spectra of energy loss due to Coulomb and nuclear interactions a depth-dose curve. The method is described in [Ber93c]. The influence of nuclear interactions is nearly vanishing at large depths, especially around the Bragg peak. On average 90% of the energy is lost in Coulomb interactions.

The program MC4 in addition to the PTRAN code is able to calculate not only the proton energy spectra as a function of depth but also as a function of the radial distance to the beam axis. MC4 [Clo93] is based on the Monte Carlo system HERMES [Clo88] which is used in medium and high energy physics detector and beam material interaction studies. Another important feature of the HERMES system is its detailed treatment of nuclear interactions. This is accomplished by using Monte Carlo methods in conjunction with theoretical nuclear interaction models to determine the energy, angle and multiplicity of the particles produced in nucleon-nucleus interactions. The system takes into account charged particle energy loss due to atomic ionization and excitation, multiple Coulomb scattering by the primary and secondary protons, range straggling of the primary protons and the secondary produced protons, elastic and nonelastic nucleon collisions with hydrogen nuclei. The application and performance of the needed particle transport simulations is described in detail elsewhere [Fil92].

We consider a narrow pencil beam incident along the z axis onto a water medium that occupies the region z>0. For each energy a set of 100.000 Monte Carlo histories of primary protons was sampled and analyzed. As the PTRAN code is only able to account for monoenergetic beams we calculated monoenergetic beams in steps of 0.25 MeV. To obtain the Gaussian shape of the incident proton energy distribution one has to add a couple of beams (we used 30) weighted due to an integration of the Gaussian curve.

The required stopping powers are those reported in the ICRU report 49 [ICRU93] basing on the computer program PSTAR [Ber93a] in PTRAN and on the computer program SPAR [Arm73], which is commonly used in nuclear and particle physics, in MC4. This has to be stated because the stopping powers are slightly different from each other. A comparison of the results of the two used Monte Carlo programs and thus the influence of the considered effects and used range tables will be published separately.

B. Calculation of microdosimetric distributions

The calculation of radiation action at a given depth in a water phantom with a biological weighting function approach requires the knowledge of the distribution of lineal energy, d(y). A computer code PMIC has been prepared to analyze the results of the PTRAN calculations in order to obtain microdosimetric characteristics of the proton beam such as e.g. the yd(y) distributions and their moments. PMIC reads an actual proton spectrum at a given depth in a water phantom as obtained by PTRAN or MC4, and calculates microdosimetric distributions of lineal energy for particles entering a sensitive site (crossers and stoppers, see [ICRU83]). The number of stoppers and crossers traversing the site is determined by the spectrum of protons at the surface of the cavity and the chord length distribution of the target. The lineal energy deposited in the target was calculated with the Continues Slowing Down Approximation (CSDA) and does not account for delta-ray effects and straggling of energy loss. For CSDA calculations identical stopping power and range tables were applied as available for PTRAN. Homogeneous spherical targets of a uniform sensitivity, 1μm in diameter, where considered in our calculations. Microdosimetric parameters are related to the defined site and they are quantified in terms of probability distributions that determine the relative frequencies of different lineal energy values in a series of repeated exposures or in a succession of energy deposition events. The method of the PMIC calculations is described in details in Appendix E of the ICRU-Report Nr. 36 [ICRU83].

C. Biological Weighting Function Approach

This concept relates microdosimetry, biological effect and radiation quality by using a response function, r(y) for a biological endpoint which describes the cummulative probability that a subcellular target will respond to a specific target-averaged ionization density. No general assumptions about the mechanisms of radiation action are made. It is assumed that there exists a function r(y), which

correlates the microdosimetric distribution d(y) in the target with a biological effect, R (see e.g. [Mor89]).

$$R = \alpha_i / \alpha_{X-ray} = \int r(y) \cdot d(y) \cdot dy \qquad (1)$$

where R is the maximum RBE for a given radiation modality, calculated as a ratio of initial slope coefficients of dose-response curves of an investigated, i, and standard, X-ray, radiation. In this formula an implicit assumption is made that there exists an initial slope of the dose-response curve.

The approch can be used in the following way. First, results of radiobiological experiments available in the form of dose-response curves (e.g. survival curves) and obtained for N radiation modalities are fitted with linear-quadratic equations in order to obtain initial slopes, α_i, of those curves and the corresponding RBE_{0i}:

$$RBE_{0i} = \alpha_i / \alpha_{X-ray} \qquad (2)$$

For all radiation modalities used, the d(y) distributions have to be measured or calculated. Then, the follwing set of equations, which is usually underdeterminated, is solved by unfolding in the least-square sense to obtain r(y) (see e.g. [Zai85]).

$$RBE_{0i} = \int r(y) \cdot d_i(y) \cdot dy \; ; \; i = 1, N \qquad (3)$$

When r(y) is available for a given biological end-point then RBE_0 for a new type of radiation can be obtained via Eq.1, assuming that the d(y) is available. The determination of the weighting function rests on the assumption that the information of the single event spectra d(y) is sufficient to assess the contribution of the different radiation components to the overall biological effectiveness. A statistical analysis (see [Lon94, Men90, Men94]) indicates the accuracy achievable in estimating the RBE_0. For R values above 2 the RBE_0 could be underestimated up to 10% for the response function given by Loncol et al. We denote in the following text RBE_0 as RBE.

The described method is well known in radiation protection, where the initial slopes are the major point of interest for determining the mean quality factor of a given radiation field at low dose situations. The approach was also already proved satisfactory for fast neutron therapy beams of different energy using a biological weighting function numerically determined using the results of a RBE-microdosimetry intercomparison study [Men90, Men94]. Loncol et al. [Lon94] determined several weighting functions by applying unfolding calculations to different sets of RBE-d(y) data pairs combining high energy gamma rays, protons and neutrons. As a biological end-point the early intestinal tolerance assessed by crypt regeneration in mice was used. Figure 2 shows the weighting function derived by Loncol et al. [Lon94]. The curve was calculated by using separately proton data from Orsay and Louvain-la-Neuve.

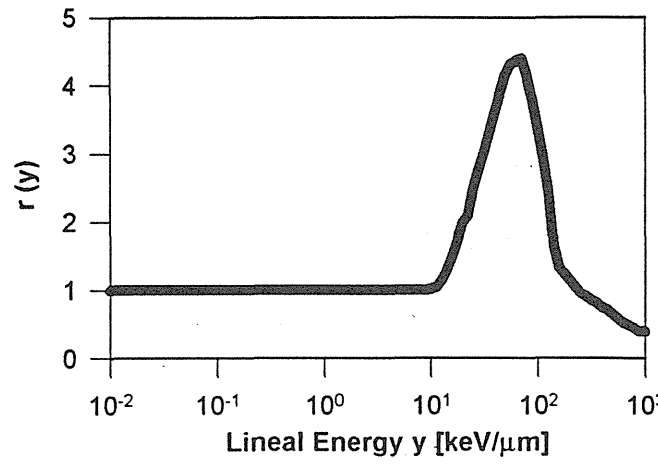

Figure 2: Biological weighting function r(y) for the biological end-point early intestinal tolerance assessed by crypt regeneration in mice for the reference radiation ^{60}Co [Lon94].

We used the biological weighting function r(y) to estimate the radiobiological effectiveness of proton beams. Within this model, the effectiveness of a defined proton beam has been calculated for different positions in the Bragg curve and we studied the influence of the beam energy and energy spread on the biological effectiveness as a function of depth in a water phantom.

Results

A. Monte Carlo Calculations

Figure 3 shows proton energy spectra for some depths and for an incident beam energy of 150 MeV. The results from PTRAN are normalized to one incident proton. Except at large depths the primary proton spectra are almost symmetric and have a shape close to a Gaussian distribution. As the output from PTRAN provides proton energy spectra only for energies down to a cut-off energy of 142 keV, the spectra have to be extrapolated to lower energies.

In figure 4 the radial dependence of the proton energy distribution calculated with MC4 is shown. We defined three rings around the z-axis increasing the radius by 0.5 cm. The first ring, a zylinder with the center on the beam axis has a radius of 0.5 cm, the second starts at 0.5 cm, the third at 1cm. The figure shows the shift to lower proton energies increasing the distance to the beam axis.

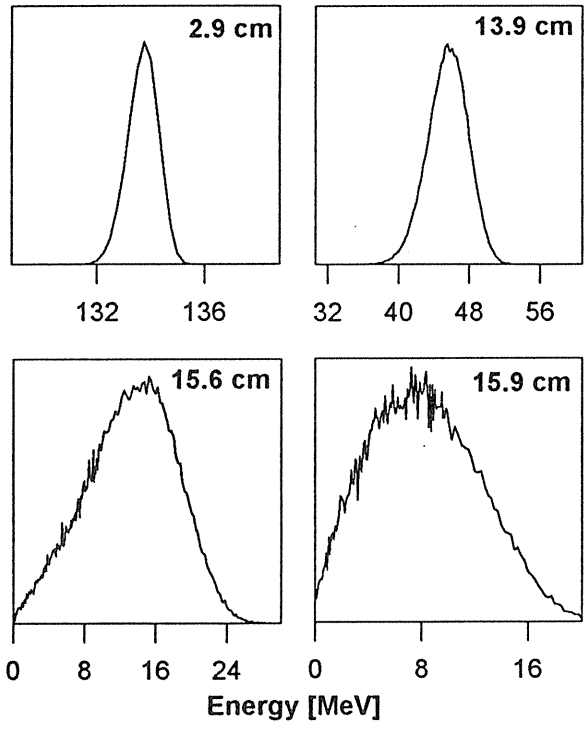

Figure 3: Proton energy spectra as calculated with PTRAN for the depths 2.9 cm (Entrance region), 13.9 cm (plateau region), 15.6 cm (maximum dose, Bragg peak), and 15.9 cm (behind the Bragg peak) for an incident monoenergetic beam with an energy of 150 MeV. The results are given in arbitrary units. Except at large depths the primary proton spectra are almost symmetric and have a shape close to a Gaussian distribution.

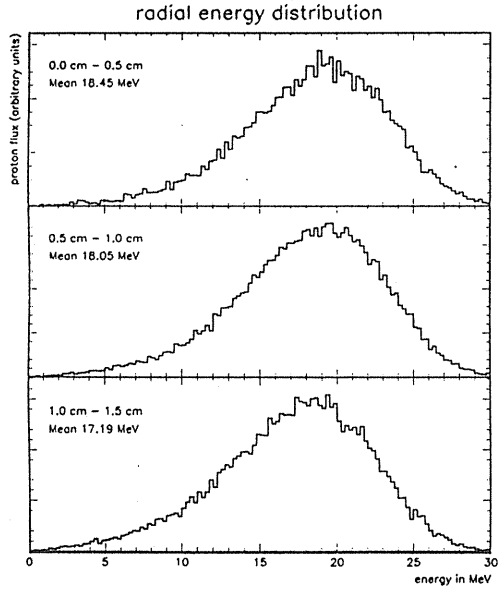

Figure 4: Proton energy spectra in the Bragg peak region for an incident monoenergetic beam with an energy of 150 MeV. The three spectra show the proton energy distribution in three different rings on the beam axis as calculated with MC4. The given mean values illustrate the decreasing proton energy with increasing radial distance.

The chemical and biological effects of radiation are frequently interpreted in terms of average track segment quantities, such as LET pertaining to heavy charged particles. These quantities reflect only indirectly the statistical fluctuations in particle transport that are the subject of microdosimetry. Only for a rapid survey of radiation quality it is of interest to consider average LET values as a function of depth. The contribution to the dose averaged LET from primary protons can be calculated directly from PTRAN output as described in reference [Ber93c]. We found that the lower the beam energy, the greater are the values of $\langle LET \rangle_D$ at depths near and beyond the Bragg peak. The rise of the $\langle LET \rangle_D$ depth dependence decrease with increasing initial proton energy. As shown by Berger [Ber93c] the contributions from secondary charged particles other than protons increases the $\langle LET \rangle_D$ significantly only at depths smaller than 0.95 times the CSDA (Continuous Slowing Down Approximation) range of the proton, that means at depths slightly smaller than the maximum of the Bragg peak. The influence of the secondary charged particles from nuclear reactions is therefore very small in the region where the $\langle LET \rangle_D$ increases rapidly. So it can be expected to lead to only a small enhancement of biological effectiveness.

B. Microdosimetric Distributions

From the proton energy distributions the microdosimetric yd(y)-distributions for different energy spreads of a pencil beam as a function of the depth in a water phantom have been obtained. The lineal energy is the ratio of the energy loss of a charged particle in the sensitive volume and the mean chord length of this volume. In this representation of the spectra, equal areas under the distributions correspond to equal contributions to absorbed dose. The results, given in figure 5 for different positions in the Bragg peak and for a 150 MeV beam, illustrate that in the area of the Bragg peak, the dose, on average, is delivered at higher lineal energies, i.e. at higher radiation quality. The increase of the beam energy spread results in a broadening of the yd(y)-distribution. For successively lower proton energies, the average energy loss increases, and by this yd(y), in a 1 μm segment is shifted to higher lineal energies (see figure 3 to compare the proton energy and yd(y) distribution). The curves become progressively more Gaussian in shape, and the most probable energy loss gets closer to that predicted from the stopping power.

The dose-mean lineal energy $\bar{y}_D$ behaves nearly as their non-stochastic analogon $\langle LET \rangle_D$. As mentioned above the microdosinmetric spectra themselves are complex and do not offer an obvious way to specify radiation quality. The biological effectiveness is not simply linearly or quadratically related to y in a wide range. In fact, the lineal energy spectra show large overlapping components. Due to

the RBE versus LET dependence the contribution of each lineal energy component to the average radiation quality for a given defined beam critically depends on both their contribution to the total absorbed dose and on their relative biological weight. Small differences between two lineal energy spectra can affect a lineal energy interval where the biological weight of the events is most important.

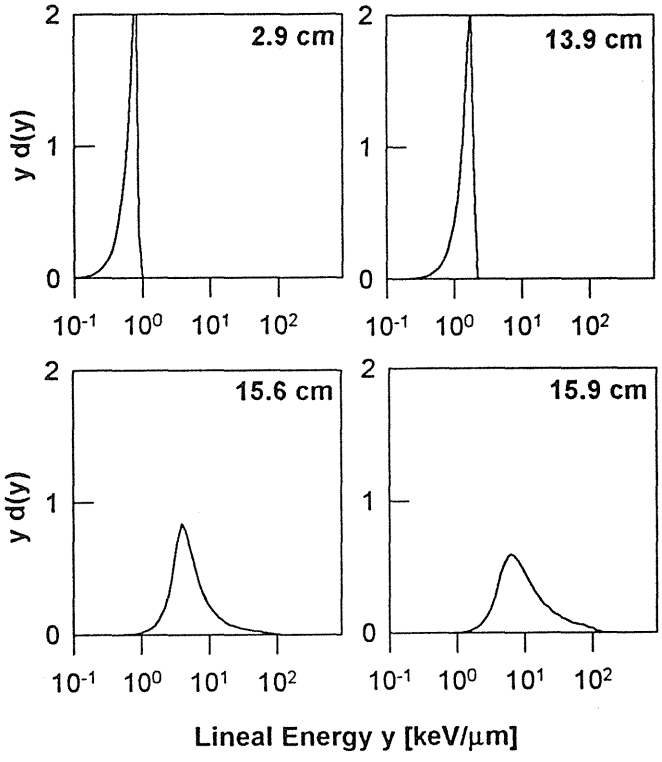

Figure 5: Lineal energy spectra for the depths 2.9 cm (Entrance region), 13.9 cm (plateau region), 15.6 cm (maximum dose, Bragg peak), and 15.9 cm (behind the Bragg peak) for an incident monoenergetic beam with an energy of 150 MeV. The results are normalized to one incident proton.

C. Biophysical Modelling

In figure 6 the RBE depth dependence is shown for the set of energies we used in our calculations. The highest reached RBE value decreases with initial proton energy. The sharp rise of the RBE values at and beyond the Bragg peak is due to the presence of primary protons of very low energy. This sharpeness decreases with initial proton energy.

The increase of the RBE with depth results in a shift of the biological dose distribution to larger depths in comparison to the physical dose distribution, e.g. about 1mm for the 150 MeV beam (see figure 7). The biological dose is given as

$$BIOLOGICAL\ DOSE = RBE \times DOSE \qquad (4)$$

By this, using an average RBE results in an underestimation of the effectiveness of the beam at the end of its range.

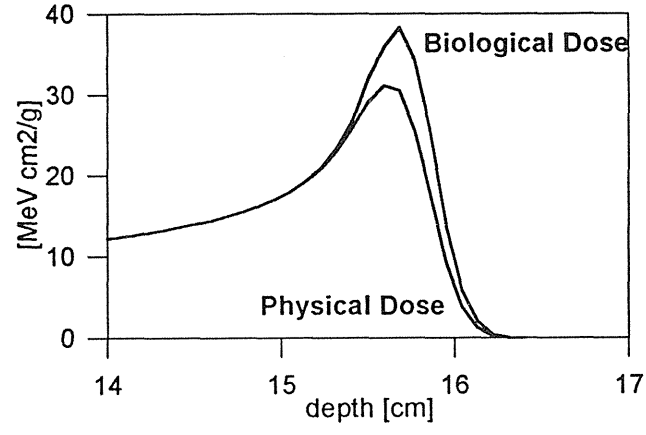

Figure 7: Comparison of the Biological dose (see equation 4) and physical dose for a monoenergetic 150 MeV proton pencil beam.

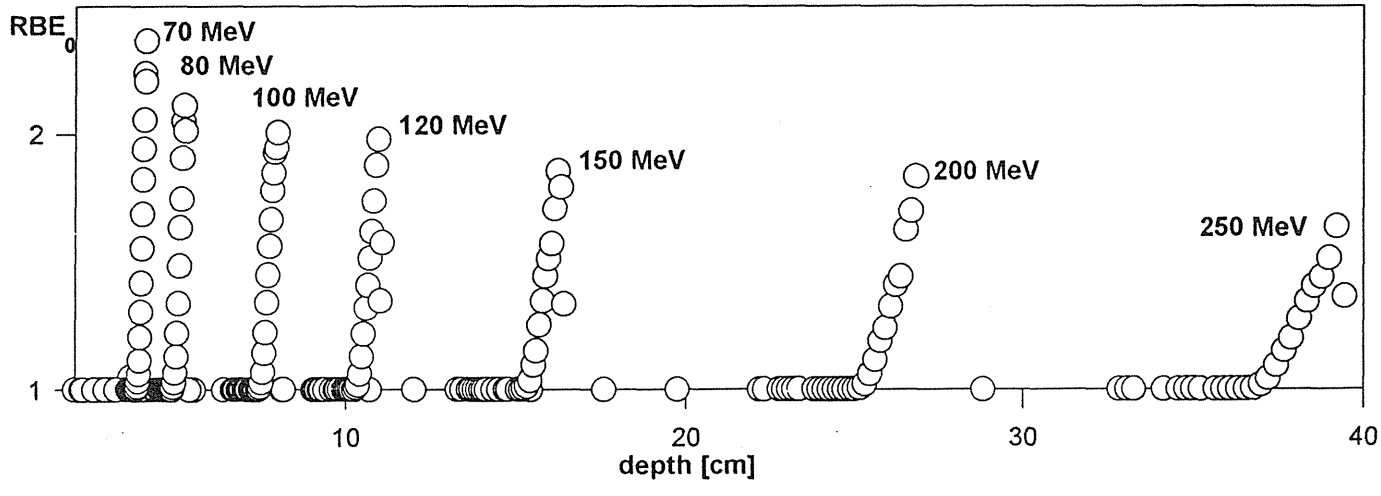

Figure 6: Dependence of the RBE on the depth in a water phantom for monoenergetic proton beams of 70, 80, 100, 120, 150, 200, and 250 MeV. Not only the decrease of the highest RBE value but also a decrease of the rise of the RBE is obvious.

Figure 8 illustrates the depth dependence of the RBE in the region of the Bragg peak for a 150 MeV beam variing the energy spread. The influence of the energy spread on the depth-dose distribution is also shown. It can be seen that the ratio of the Bragg maximum to the entrance dose and the rise of the RBE with depth depends sensitively on the standard deviation of the Gaussian beam spectrum. When increasing the energy spread, we obtained a decrease of the RBE behind the Bragg peak and a slightly RBE increase in the Bragg peak. The broadening of the depth-dose distribution as a function of energy spread will be slightly compensated by the decreasing RBE distal to the Bragg peak in relation to the biological dose distribution.

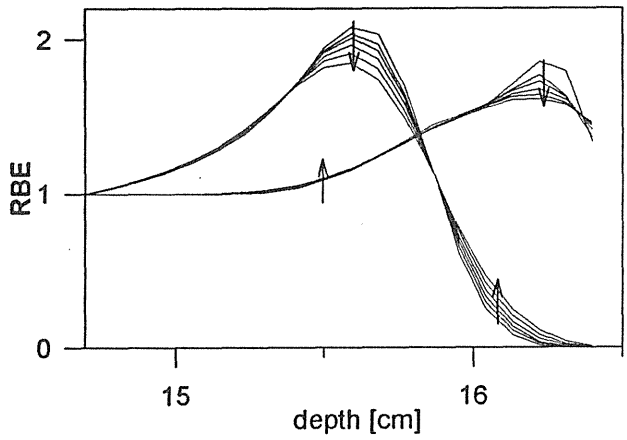

Figure 8: RBE and dose as a function of depth and energy spread. The dose is given in arbitrary units. The energy spread has been varied up to a momentum spread of $\Delta p/p=3x10^{-3}$ in steps of $0.5x10^{-3}$. The arrows indicate the behaviour of the curves increasing the momentum spread.

The tables 1-3 lists our RBE results as a function of beam energy and depth in water. The statistical errors of our RBE values do not exceed 5%. The calculated RBE values are only slightly depending on the energy spread of the proton beam for the small spreads used.

Table 1: Calculated RBE values for the Bragg peak maximum (point of maximum dose delivery) and their dependence on the initial proton energy. The results for two momentum spreads are given.

Beam energy	RBE $\Delta p/p=0$	RBE $\Delta p/p=0.003$
70 MeV	1.94	1.77
80 Mev	1.64	1.63
100 MeV	1.34	1.27
120 MeV	1.22	1.22
150 MeV	1.15	1.17
200 MeV	1.12	1.13
250 MeV	1.09	1.10

Table 2: Calculated RBE values for the Bragg peak (averaged over FWHM (Full Width Half Maximum)) and their dependence on the initial proton energy. The results for two momentum spreads are given.

Beam energy	RBE $\Delta p/p=0$	RBE $\Delta p/p=0.003$
70 MeV	1.56	1.45
80 Mev	1.38	1.34
100 MeV	1.16	1.16
120 MeV	1.14	1.13
150 MeV	1.11	1.10
200 MeV	1.08	1.08
250 MeV	1.07	1.06

Table 3: Calculated RBE values behind the Bragg peak (point of dose delivery equals 1% of the total dose delivery) and their dependence on the initial proton energy. The results for two momentum spreads are given.

Beam energy	RBE $\Delta p/p=0$	RBE $\Delta p/p=0.003$
70 MeV	2.25	2.24
80 Mev	2.08	2.05
100 MeV	1.63	1.64
120 MeV	1.55	1.56
150 MeV	1.47	1.44
200 MeV	1.35	1.35
250 MeV	1.29	1.28

In the center of the Bragg peak we found RBE values of about 1.1 (250 MeV beam) up to 1.9 (70 MeV beam) (see table 1). When averaging the RBE values over the Bragg peak (FWHM) we obtained the results listed in table 2. If this averaging is done dose weighted, the RBE will increase by about 4% compared to the results in table 2. In addition we found values of about 1.3 (250 MeV beam) to about 2.3 (70 MeV beam) a few mm distal to the Bragg peak where the dose is about 1% of the maximum dose. The maximum RBE values (see figure 8) are reached at even greater depths.

The RBE in the center of the Bragg peak and peak averaged is illustrated in figure 9 as a function of incident proton energy.

The evaluation of the radial dependence of RBE based on the proton energy spectra from the Monte Carlo code MC4 (see figure 4) is in progress. However, from the proton energy distributions it can be seen that due to the decrease of the average proton energy there will be an increase of the RBE as a function of the radial distance to the beam axis. This has to be weighted with the decreasing dose. So, the

effect will be comparable to the effect of increasing RBE with depth (see figure 8). Due to the increase of RBE increasing the radial distance to the beam axis, the biological dose will be shifted to higher distances.

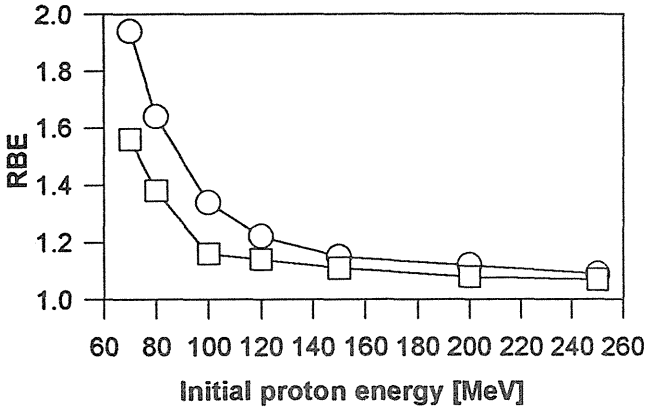

Figure 9: RBE in the center of the Bragg peak (maximum dose) (O) and averaged over FWHM (□) as a function of initial proton energy for a monoenergetic proton beam.

Discussion

Raju [Raj80] summarized most of the available RBE data and demonstrated that, depending on the proton energy, position in the Bragg ionization curve, reference radiation and biological endpoint, the RBE values reported ranged from 0.6 to 1.84. Most of the RBE values reported however are about 1.1. This value has been used for clinical proton radiotherapy worlwide primarily based on the results of several assays on murine tumors in vivo [Tep77, Ura80, Sui82, Ura84]. Studies of the proton RBE of several human tumor cell lines reveal values in excess of 1.1 [Blo91, Blo93]. Recently the mean RBE value for a proton beam with a maximal range of 33 mm, which corresponds to an initial energy of about 67 MeV, was found by Blomquist et al. [Blo93] to be 1.22 with a standard deviation of 0.08. In their experiments the clonogenic cell survival showed only a very small decrease with depth when cells were placed in different positions, along the central axis of the range modulated depth-dose distribution, indicating only a small increase in RBE with depth. An RBE increase in the descending part of the Bragg peak was found by Robertson et al. [Rob75] for a cell killing in cultured mammalien cells. In addition the RBE variates depending on the proton energy, biological endpoint and type of reference radiation [Blo93 and references therein].

A proper comparison of these data with our calculations will be possible if similar calculations will have been done for realistic, i.e. modulated Bragg peaks.

The weakness in our calculations is of course the application of the response function model in radiation therapy. Conventionally it has been established for radiation protection studies. As we used only one parameter to parametrize the RBE, the model is strictly only valid in the low dose region of a survival curve where only linear terms contribute and where the microdosimetric single event spectra can be used. The fact, that the biological weighting function used here has been obtained at the LD_{50} survival level does not overcome these difficulties. However, this should only influence our absolute RBE values but not the RBE behaviour we found as a function of various beam parameters and our qualitative statements.

The accuracy of our calculated data is highly dependent on the accuracy of the used biological weighting function. As already remarked by Loncol et al. [Lon94], more accurate RBE values are required to make the unfolding calculations more accurate and to determine exactly the peak region of the weighting function. The calculated RBE is very sensitive to that region because of its overlap with the yd(y) spectra in the region of the Bragg peak. Therefore the presented results are heavily based on the biological data obtained from a given sets of experiments. This data have to be checked, especially with regard to their relevance for tumor therapy.

It is of interest to unfold biological weighting functions for other endpoints, especially for those which can be verified in radiobiological experiments. When the response function is properly determined the RBE for any new proton beam could be derived for the considered biological systems, provided the microdosimetric spectra had been measured. Up to now there is a lack of sufficient and adequate radiobiological data suited for the analysis to obatin a weighting function by unfolding procedures. This is mainly due to the fact that there is no adequate characterization of the radiation field available for most of the radiobiological results. Biological and dosimetric experiments at COSY are planned to contribute to the solution of this problem. In addition, it has to be proven that a single response function is applicable for the whole range of initial proton energies presented here [Lon94].

Summary

We conclude from this data that the RBE depends strongly on beam characteristics such as the proton energy and the energy spread of the beam. The value of the maximum RBE depends on the initial beam energy and the energy spread. The RBE increases with depth in the phantom with a rise decreasing with beam energy.

Furthermore the depth dependence of the RBE results in a shift of the biological dose distribution (Biological dose = RBE x Dose) to higher depths in comparison to the

physical dose distribution, e.g. about 1mm for the 150 MeV beam. Using an average RBE results therefore in an underestimation of the effectiveness of the beam at the end of his range. The slope of the RBE depth dependence will decrease with increasing energy spread so that for energetically broad beams the described effect will become smaller.

Outlook

Calculations of the RBE dependencies not only for pure beams but also for modulated proton beams to simulate directly the dependence of the RBE on the method of modulation are in progress. With the computer code MC4 range filters of different materials can be defined.

Calculations with the code MC4 with a detailed treatment of nuclear interactions are planned to look for the influence of secondary particles on the RBE. Although the ratio of energy loss due to nuclear interactions is small, this interactions may cause heavy charged particles with a high RBE, especially when high initial proton energies were used.

Furtheron an evaluation of the data in using the `Katz model` [Kat73, Kat74] is also in progress. This model starts from completely different assumptions, e.g. from a vanishing initial slope of the survival curves. With these calculations not only the RBE but also the OER depth dependence can be obtained.

Finally, our planned biological and dosimetric experiments at COSY will give us the possibility of comparing our results with measurements and to look for other biological endpoints relevant for proton therapy.

References

[Arm73] Armstrong, T.W.; Chandler, K.C., Stopping Powers and Ranges for Muons, Charged Pions, Protons and Heavy Ions. Nucl. Inst. Methds. 113: 313-314; 1973

[Ber93a] Berger, M.J., ESTAR, PSTAR and ASTAR: Computer programs for caclculating stopping-power and range tables for electrons, protons and helium ions. National Institute of Standards and Technology Publication NISTIR 4999; 1993

[Ber93b] Berger, M.J., Proton Monte Carlo Transport Program PTRAN. National Institute of Standards and Technology Publication NISTIR 5113; 1993

[Ber93c] Berger, M.J., Penetration of Proton Beams Through Water I. Depth-dose Distribution, Spectra and LET Distribution. National Institute of Standards and Technology Publication NISTIR 5226; 1993

[Blo91] Blomquist, E.; Carlsson, J., Strategy for planned radiotherapy of malignant gliomas: Postoperative treatment with combinations of high dose proton irradiation and tumor seeking radionuclides. Int. J. Radiat. Oncol. Biol. Phys. 22: 259-263; 1991

[Blo93] Blomquist, E.; Russell, K.R.; Stenerlöw, Bo; Montelius, A.; Grusell, E.; Carlsson, J., Relative biological effectiveness of intermediate energy protons. Comparisons with ^{60}Co gamma-radiation using two cell lines. Radiother. and Oncol. 28: 44-51; 1993

[Clo88] Cloth, P.; Filges, D.; Neef, R.D.; Sterzenbach, G.; Reul, Ch.; Armstrong, T.W.; Colborn, B.L.; Anders, B.; Brückmann, H., HERMES A Monte Carlo Program System for Beam Materials Interaction Studies. Report Jülich-2203; 1988

[Clo93] Cloth, P.; Drüke, V.; Filges, D.; Kilian, K.; Röser, A.; Sterzenbach, G., Monte Carlo Simulation of Medium Energy Detectors at COSY Jülich. MC93, Int. Conf. on Monte Carlo Simulation in High Energy and Nuclear Physics, Tallahassee, 129-136; 1993

[Fil92] Filges, D., Modern Monte Carlo Transport Simulation for Safety and Radiation Protection Applications in Accelerator Technology and in Space Science. Report Jül-2609; 1992

[ICRU80] ICRU Report 33, Radiation Quantities and Units. International Commission of Radiation Units and Measurements, Washington D.C. 1980

[ICRU83] ICRU Report 36, Microdosimetry. International Commission of Radiation Units and Measurements, Washington D.C. 1983

[ICRU93] ICRU Report 49, Stopping powers and Ranges for Protons and Alpha Particles. International Commission of Radiation Units and Measurements, Washington D.C. 1993

[Jan82] Janni, J.F., Proton range energy tables, 1 keV - 10 GeV. Atomic Data and Nuclear Data Tables 27: 147; 1982

[Kat73] Katz, R.; Sharma, S.C., Response of cells to fast neutrons, stopped pions, and heavy ion beams. Nucl. Inst. Methds. 111: 93-116; 1973

[Kat74] Katz, R.; Sharma, S.C., Heavy Particles in Therapy: An Application of Track Theory. Phys. Med. Biol. 19: 413-435; 1974

[Lon94] Loncol, T.; Cosgrove, V; Denis, J.M.; Gueulette, J.; Mazal, A.; Menzel, H.G.; Pihet, P.; Sabattier, R., Radiobiological Effectiveness of Radiation Beams with broad LET Spectra: Microdosimetric Analysis using Biological Weighting Functions. Radiat. Prot. Dos. 52: 347-352; 1994

[Men90] Menzel, H.G.; Pihet, P.; Wambersie, A., Microdosimetric specification of radiation quality in neutron radiation therapy. Int. J. Radiat. Biol. 57: 865-883; 1990

[Men94] Menzel, H.G.; Wambersie, A.; Pihet, P., The clinical RBE and microdosimetric characterization of radiation quality in fast neutron therapy. to be published in Acta Oncol. 1994

[Mor89] Morstin, K.; Bond, V.P.; Baum, J.W., Probabilistic approach to obtain hit-size effectiveness functions which relate microdosimetry and radiobiology. Radiat. Res. 120: 383-402; 1989

[Raj80] Raju, M.R., Protons Chapter 4 pp. 188-251 in Heavy Particle Radiotherapy. Academic Press, New York, 1980

[Rob75] Robertson, J.B.; Williams, R.A.; Schmidt, J.B.; Little, J.B.; Flynn, D.F.; Suit, H.D., Radiobiological studies of a high-energy modulated proton beam utilizing cultured mammalian cells. Cancer 35: 1664-1677; 1975

[Sel93] Seltzer, S.M., An assessment of the role of charged secondaries from nonelastic nuclear interactions by therapy proton beams in water. National Institute of Standards and Technology Publication NISTIR 5221; 1993

[Sui82] Suit, H.D.; Goitein, M.; Munzenrider, J.E.; Verhey, L.; Blitzer, P.; Gragoudas, E.; Koehler, A.M.; Urie, M.; Gentry, R.; Shipley, W.; Urano, M.; Duttenhaver, J.; Wagner, M., Evaluation of the clinical applicability of proton beams in definitive fractionated radiation therapy. Int. J. Radiat. Oncol. Biol. Phys. 8: 2199-2205; 1982

[Sui88] Suit, H.D.; Griffin, T.W.; Castro, J.R.; Verhey, L.J., Particle radiation therapy research plan. Am. J. Clin. Oncol. (CCT), 11: 330-341; 1988

[Tep77] Tepper, J.E.; Verhey, L.; Goitein, M.; Suit, H.D.; Koehler, A.M. In vivo determinations of RBE in a higher energy modulated proton beam using normal tissue reactions and fractionated dose schedules. Int. J. Radiat. Oncol. Biol. Phys. 2: 1115-1122; 1977

[Ura80] Urano, M.; Verhey, L.J.; Goitein, M.; Tepper, J.E.; Suit, H.D.; Mendiondo, O.; Gragoudas, E.S.; Koehler, A., Relative biological effectiveness of high energy modulated proton beams using a spontaneous murine tumor in vivo. Int. J. Radiat. Oncol. Biol. Phys. 6: 1187-1193; 1980

[Ura84] Urano, M.; Verhey, L.J.; Goitein, M.; Tepper, J.E.; Suit, H.D.; Mendiondo, O.; Gragoudas, E.S.; Koehler, A., Relative biological effectiveness of modulated proton beams in various murine tissues. Int. J. Radiat. Oncol. Biol. Phys. 10: 509-514; 1984

[Zai85] Zaider, M.; Brenner, D.J., On the microdosimetric definition of quality factors. Radiat. Res. 103: 302-316; 1985

MICRODOSIMETRIC EVALUATION OF HEAVY PARTICLES RBE VERSUS DOSE FRACTIONATION, AND ITS INTERPRETATION IN RADIATION BIOPHYSICS

M. F. Lomanov
The Institute of Theoretical and Experimental Physics, B. Cheremushkinskaya 25, Moscow, 117259, Russia.

SUMMARY

Microdosimetry has too little influence on clinical investigations, in spite of its rich computation potentialities. Actually, the complex spectrum composition of neutral beams (photons, neutrons) is a matter of difficulties even for usual dosimetry. Heavy charged particle beams give a new chance for the development of microdosimetrical concepts. That could give a real opportunity to supplement experimental biological modeling of clinical situation by computer simulation which requires sufficiently smaller time.

In principle, biological effects are more independent of time and space factors of irradiation for beams of heavier ions. Some determinism achieved in this condition is destroyed if conventional radiation is taken as a reference source. This paradoxical use of RBE concept can be overcome if the specific entropy is introduced into consideration. This value is in coincidence with a clinical characteristics used in practice as a time - dose - fractionation (TDF) parameter.

The microdosimetrical approach is applied to initial processes of cell damage. The processes in track core are basically independent of dose fractionation. As for delta electrons, an attractive consideration is proposed on preference of damage events with an additional Auger electron. The dual radiation action theory is used to microdosimetric analyses of all these factors affecting RBE in dose fractionation of different ion beams or mixed (boost) irradiation. As a result of dual radiation action theory, decrease of proton RBE (toward unity) can be significant in single fraction doses above 4 Gy.

Microdosimetry makes also correction for TDF parameter of fractionated irradiation by photons to decrease a difference between Blair Davidson method and experiments with small single fraction doses.

There is a restriction of microdosimetry taking into attention only intracellular radiation processes. Use of thermodynamical functions can advance to overcome this deficiency.

INTRODUCTION

Microdosimetry occupies a comparatively modest place at seminars like this. However it appears that problems of highly effective bombardment of tumour cells give a new chance to show potentialities of microdosimetry. Sometimes it can repeat the result well-known earlier. That would be not only a corroboration at the higher level, but also a very important analysis which confirms the quality assurance in patient treatment.

That could give a real opportunity to supplement experimental biological modeling of clinical situation by computer simulation which requires sufficiently smaller time. In principle, for beams of heavier ions biological effects are more independent of time and space factors of irradiation. If the effect can be considered as a small correction to a primary effect then certain extrapolation seems valuable. The processes in the core of a heavy particle track, are basically independent of dose fractionation. As for delta electrons, an attractive consideration is proposed on preference of damage events with an additional Auger electron. Anyway, the microdosimetric analysis of all these factors affecting RBE confirms contemporary semi-empirical concepts working in terms of TDF parameters.

In this view, the concepts of RBE and TDF will be followed in the sequence as below.

- RBE by a simplest explanation (track model);
- RBE dependent on single fractionation
- Thermodynamical approach: specific entropy and TDF factor as a biological dose;
- Place of microdosimetry in quality assurance (QA);

Another aim is set to find the place of this methodology in general biophysics. The term *radiation biophysics* was used long ago by A.M.Kellerer (1). However no new meaning was added compared to the usual microdosimetry. Even cumulative effects of radiation action were considered at subcellular level only. In the present case such cumulative effects as extracellular interactions affects deeply the irradiated tissue recovery.

METHODS AND MATERIALS

Simplest models of RBE

The microdosimetry is mostly known by measurements with a "Rossi chamber". Harald Rossi designed his spherical proportional counter in 1995 (2). About the same time the bubble chamber was built by Donald Glaser. One of applications of his invention was reported by F.d'Enrico at the XX PTCOG as a superheated drop

(bubble) detector (3). This equipment registers an equivalent dose with an RBE or quality factor.

Two findings anticipated this elaboration. Immediately after Glaser's, a Russian design appeared and its radiation characteristics were calibrated (4). The result was in striking contradiction to the conventional concept. As it is seen in Fig.1, the bubble density rises much stronger with decrease of particle energy than it could be anticipated because of ionization losses. Moreover, its reverse rise in relativistic region seemed absurd, but many experiments confirmed it. The author, being a participant of this work, published later an explanation of this phenomenon (5). If we speak about a metastable stage in liquid, notice that life is a metastable stage as well. It can be suggested that a similar mechanism destroyes it. Frequently, an enormous specific energy (microdosimetric notation is z) is locally absorbed at delta-ray stopping particularly if it is knocked out from the atomic K-shell and is accompanied by an Auger electron. Then the total energy deposition is more than 500 eV in the sensitive volume ("site") of several tens nanometers. The cross-section of the effect differs from the total ionization losses -dE/dx by substitution of reciprocal of the knock-out energy V instead of usual logarithmic term;

$$-dE/dx = \sum_i 2\pi n_i e^4 Z^2 / (mc^2\beta^2) \times [\ln(W/V_i) - \beta^2 - s] \quad \text{(Eq.1)}$$

$$-dN/dx = 15.7/\beta^2 \times \{7.57 + 4.3\times 10^3 \times (1/V - 1/W) + \ln[\beta^2/(1-\beta^2)]\} \quad \text{(Eq.2)}$$

where e, βc and mc^2 are charge, velocity and rest mass of electron, n is the electron number in cm^3, the minimum value of V (or V_i) is the average (or partial) ionization potential of the atom, 125 eV multiplied by nucleus charge Z, the maximum value of V is W, whose values can be up to $2mc^2\beta^2/(1-\beta^2)$. The member s is a small correcture of density effect, non sufficient to heavy particles. Eq.2 is specified for electrons and protons in water only, because heavier ions have additional ionization events in track core.

The efficiency of the bubble track formation along particle tracks can be compared with a typical RBE measured by Barendsen (6) as it is seen in Fig. 2. If V is near the K-shell ionization potential of oxygen atom (500 eV), there is only one parameter V, to come to agreement. The concept (4) also predicts up to 20% enhancement of the RBE for relativistic electron beams (above 2 MeV) which could be disregarded if observed. What was really very often observed and disregarded was strikingly low proton RBE measured in the fifties and sixties whose value was re-evaluated later being at first about a unit, then more. A series of experiments carried out at Harvard proton beam and reported at Moscow Seminar (7) shows the RBE be about 1.10.

Nevertheless there is a reasonable argument to understand the preceding results because conditions were different. Let's return to Eq. 2 where the term 1/V is psesented instead of a logarithmic term in (8). The term 1/W is so small compared to 1/V that the result depends only on particle velocity. Comparing the biological action of electrons equivalent to standard X-rays and protons with the same velocity, the RBE is equal to (9);

$$RBE = dE/dx_{electrons\ 7keV} / (-dE/dx)_{protons\ 13MeV} = 2.9\ (keV/\mu m)/3.6(keV/\mu m) = 0.8 \quad \text{(Eq.3)}$$

As a matter of fact, many results have been around this value while there were two circumstances;

1. 250keV X rays were used as a reference source;
2. A specimen irradiated was thin (cell culture, small animal), and equilibrium state of secondaries was violated.

In the seventies, the cobalt X-rays were usually used as a reference source, and phantom experiments exclude item 2 to have secondary irradiation in equilibrium state, and the result was as above (7).

RBE in fractionation

The above mentioned should be referred to intratrack interactions with matter and it does not depend on neighboring tracks and consequently on dose. The dependence has been formulated by Kellerer and Rossi as a theory of dual radiation action (10). They manifested that combined track effects prevail at clinical dose region for conventional irradiation much more than for neutrons. Hence the neutron RBE depends on dose approximately as the inverse square root. In practice, this dependence is slower and it does not reach unity with high doses. Some discrepancies of this theory can be omitted if the heavy admixture in a proton beam is very small, no more than several percent. There is a better opportunity to evaluate RBE - dose dependence using this theory in its primary formulation. Not going into detail, the result is that in the field of low doses (up to about 1-2 Gy), the proton RBE is constant. However, for higher doses RBE can decrease up to 1.01 or 1.03, what is important for large fractionation which is often used in proton therapy. Single irradiation by protons is often used in radioneurosurgery. Arguments in favour of dose dependence of proton RBE have been reported by the author at the First Seminar on Proton Therapy (8) but sparse experimental data did not confirm it. Some indications are accumulated that this effect really exists (11). Recently the RBE for protons was found to be dose dependent (12, 13).

Is "biological dose" a product of the RBE and absorbed dose?

In principle, we consider the main result of dual radiation action theory as a downfall of the RBE concept

which is a coefficient to calculate dose equivalent, but this coefficient appears to be far from constant (excluding low doses). It is not surprising that radiation therapy has searched for and found other approaches. So, the first problem to solve dose fractionation is a search of additive function of dose which could be summarized in different rhythms for patient irradiation. Next problem is to calculate many components and types of irradiation.

It is desirable that additive value as equivalent to dose could be called a "biological dose". Unlike a standard definition which demands to multiply dose to RBE, there is an old different definition (14). This is a specific entropy as a measure of tissue damage by irradiation which destroys cell division. It is not so difficult to be convinced that this "biological dose" is proportional to a well-known additive value, the TDF parameter. Then a new factor of proportionality between biological dose - TDF and absorbed dose is another value, also well-known, the biologically equivalent factor (BEF). Its thermodynamical analog is the value dS/dE, the derivative of entropy in respect to absorbed energy. It is equivalent to inverse temperature 1/T;

$$dS/dM = dS/dE \times dE/dM = (1/T) \times D \qquad \text{(Eq.4)}$$

where D is the absorbed dose, M the irradiated mass.

There is a principal difference between BEF and RBE. The measurement of heavy particle RBE demands two measured dose - effect curves, one of them is measured at a beam of given radiation, and another with the reference source, repeating all biological conditions at both radiation sources including fractionation. As for BEF, this is defined by survival curve of a given radiation only, while the standard source is used only once, in standard fractionation of 2 Gy per day. The same refers to specific entropy; its definition depends only on the radiation studied at every fractionation operation. In this case some unusual fractionation can not be investigated for photon irradiation if it needs only for the RBE measurement.

Semi-empirical law for heavy charged particles can be the same as it is established for neutrons. For example, L.Cohen (15) gives a split course of photon irradiation followed by neutrons. The nominal single dose (NSD) for treatment with a dose of D cGy delivered in N fraction over T days is given by the conventional Ellis formula. The TDF parameter is calculated by the formula:

$$NSD = D \times N^{-\alpha} \times T^{-\beta}$$
$$TDF = K \times (NSD)^{1/(1-\alpha-\beta)}$$

where K is a normalization constant (0.001 for protons, 0.024 (for neutrons), α=0.24 for protons and 0.04 for neutrons, β = 0.11.

If a course of low LET therapy (marked by index γ) is followed , after a gap of a few days by a neutron boost (index ν):

$$TDF_{SUM} = TDF_{\gamma} \times [T_{\gamma}/(T_{\gamma} + GAP)\}^{0.11} + TDF_{\nu} \qquad \text{(Eq. 7)}$$

Microdosimetry considers heavy ion track as the sum of the track core whose TDF is time independent (the exponent in TDF is equal to unity), and the electronic envelope is described by the same constants as photons. Neutrons could be considered in the same spirit, with weight parameters for spectrum of secondaries. This approach differs from the semi-empirical one which comprises in a choice of constants in expression of the same type as for photons. So at this stage, another expression is found not only for neutrons but for other heavy particles as an approximation of the same data (15) which were used for Eq. 7:

$$TDF_{SUM} = \Sigma(\Sigma a_{ij} \times D_{jCORB} + b_i \times TDF) \quad \text{(Eq.8)}$$

These data are summarized over particle type (index I) and spectrum (index j).

Neutrons generated by 66 MeV protons on a beryllium target are fitted approximately by data of (15) (i=j=1) with coefficients of Eq.8: a= 0.031, b=2.4. Microdosimetric analog of Eq.8 can be constructed for more precise calculation of TDF, as it is discussed in the next section.

Necessity for the application of microdosimetry

Presently, we can only compare two approaches, one usual and another one made through microdosimetric analysis how it has been performed by A.Dolgikh(16) for photon irradiation of skin cancer. The comparison between calculation in terms of Blair - Davidson model (BDM) and two variants of its modification by using microdosimetric distributions is demonstrated in Fig. 3 and 4. The result is different from usual BDM when a factor number is more than 30. The version (variant) 2 is preferable being in better coincidence with experimental data (17). However, an unusual behavior or incorrectness is observed in this version only; when the effective dose can fall with the increase of fraction number. This kind of calculation gives a result for irregular rhythms of irradiation which are out of simple empirical study.

In spite of the achieved agreement, this result suffers from general deficiency of the methodology (see the Introduction). The empirism of the BD method was left as it was but the average dose concept has been substituted with microdistributions. New free parameters appeared, and this provided for a better, but again empirical, choice of an appropriate model. No reasonable argument has been found to explain this choice.

Another appeal to thermodynamics

Having started this issue from bubble experiments, we should return to thermodynamics in its conceptual sense. Our reference to a bubble chamber gives a model of an

incident phase of a radiation process; however it would be unreasonable not to draw a further analogy. First, bubble growth from irradiated bubble embryo diminishes as far as its surface/volume ratio reduces surrounding contacts. Hence the "entropy production" can gradually stop. Second, a leap can come in the process dynamics if the information of the bubble track space distribution is transformed into a stable imprint. The conversion of another kind happens in living media. Irradiation can destroy the reparation mechanism as well as it does with other living functions. On the contrary, reparation capacities switch on and a sound reverse begins to convert the "harm" into the benefit for cancer radiation treatment. This process corresponds to the thermodynamic principle of minimum energy (i.e. reparative flux) dissipation. According to the Prigogine theorem can result in extraordinary rapid tissue recovery. For example, the prolifererative capacity of the epidermis appears so large that the survival of 1 cell per sq.cm allows regeneration of 10^6 cells per sq.cm (19).

The Onsager theorem postulates symmetry, or cross correlation of diffusion forces regulating irreversible processes in nonequilibrium systems. The regenerative processes after irradiation dependent on tissue architecture (20) are under this control. There is a lot of reciprocal effects of tissue degeneration in malignant tumor or its cure. Their analog could be, for example, thermodiffusion (Soret effect) and diffusive heat conductivity (Dufour effect). The first one if a gas mixture is placed in a vessel with temperature gradient, the components separate due to diffusion. The same law results in the directed proliferative cell flux needed to tissue recovery.

The phenomenological equations determine the correlation between causes $X_k \approx 1/T_k$ (here T is the deflection from equilibrium state, analog to changing temperature) and flux J caused by any kind of diffusion exited by them:

$$J_i = \sum_{k=1}^{m} L_{ik} X_k \qquad \text{(Eq.9)}$$

where L_{ik} are kinetic Onsager coefficients (18) which define the contribution of several cell compartment (marked by index I in our case) into the flux.

This approach can be continued to have a quantitative description to connect "microscopic" aspects easy of access to microdosimetry, and "macroscopic" ones of tissue tolerance which begins to be considered in models of tissue architecture.

CONCLUSION

Heavy particle have well-known advantages of high biological efficiency and overcoming the oxygen effect during irradiation of tumor cells. The irradiation response becomes much more predicted due to low sensitivity to a cell cycle. The dose - effect curve is pure exponential. All these peculiarities become the more expressive the heavier ions are. Large fractionation has been well used with protons, and it succeeds still more with heavy ions, much easier than with photons or neutrons.

Use of non-standard irradiation rhythms makes important evaluation of efficiency of various fractionation types and their optimization. The dose dependence of this factor could vanish for heavy ions however they are used in combination with photon irradiation, as a rule.

In this report, we tried to find arguments in favour of using microdosimetry for effective dose calculation. As a result, it is seen that it would favour the successful development of particle therapy. The peculiarities of heavy ions lift ambiguity due to the multitude of parameters characteristic for photons.

In this view, the possibility to develop thermodynamical aspects of radiation action which can connect the microdosimetric modeling with real processes in irradiated media, seems attractive. These approaches exist in biophysics as an application of irreversible processes theory. The NSD - TDF concept used everywhere corresponds completely to this trend; in its turn, this result can bring a new content into systematization of empirical data.

At present, a tissue architecture concept is developed on a large scale, describing tissue organization as an additional reserve for postirradiational recovery.

Microdosimetrical modelling is more developed with mathematical instrument, but it suffers from a shortcoming postirradiated tissue reparation is explained only by processes inside the irradiated cell. There is a real possibility to overcome these deficiencies and to realize potentialities of microdosimetry in direct clinical investigation.

REFERENCES

1.Kellerer,A.M.; A survey of approaches to radiation biophysics. In Proc. of 5th Symp. of Microdosimetry (H.G.Ebert; Ed.) 409-438.

2.Rossi,H.H., Rosenzweig.W. A device for measurement of dose as a function of specific ionization. Radiology. 64: 404-411;1955.

3 d'Errico,F, Egger,E. Superheated drop bubble detector tests with proton therapy beams. Abstracts of the XX PTCOG Meeting. May 16-18, 1994, Chester, England, 12-13.

4. Blinov,G.A.; Krestnikov,Yu.S.; Lomanov,M.F.

Measurement of ionisation capacity of particles in a bubble chamber. Soviet Phys. JETP.31:762-770; 1956. Proc. CERN Symp. on High Energy Accelerators and Pion Physics. Geneva, June 1956, vol.2, 25-27
5. Lomanov,M.F. On a possible relativistic enhancement of biological effectiveness. In Proc. of 1st All-Union Seminar on Microdosimetry Atomizdat, 107-113; 1973 (in Russian)
6. Barendsen,G.W. Relative biological effectiveness as a function of linear energy transfer. In Proc. of the Symp. on Microdosimetry (H.G.Ebert; Ed.) Euratom 3747 d-e-f, Brussels, 249-263; 1968.
7. Suit,H.; Goitein,M.; Tepper,J.; Koehler,A.; Verhey,L.; Friedberg,C.; Schneider,R. Radiobiological evaluation of a modulated energy 160 MeV proton beam. In Proc. 1st Intern. Seminar on the uses of proton beam in radiation therapy. Moscow, Dec. 6-11, 1977. Atomizdat, 2:52-62;1979.
8. Lomanov,M.F. Proton beams dose field formation and measurement. ibid, 1;78-94 (in Russian).
9. Lomanov,M.F. Factors influenced of biological effectiveness of protons. Kosmicheskaja Biologija I Medizina. 3;88-90; 1972 (in Russian).
10. Kellerer,A.M.; Rossi,H.H. The theory of dual radiation action. Current Topics in Rad. Res. Quaterly 8;85-185;1972.
11. Schulte,R.W.M.; The RBE or protons - directions for future clinical trials. In Abstracts of the XVIII PTCOG Meeting. Orsay & Nice, April 16-19, 1993,6.
12. Gueuelette,J.; Gregoire,V.; De Coster,B.M.; Vynckier,E., Wambersie,A. RBE variation as a function of depth in the 85 MeV clinical proton beam produce at Louvain-la-Neuve Comparison with 650 MeV helium ions. Preprint Darmstadt, 1-3; August 14, 1991.
13. Skarsgard,L.D.; Wouters, B.G.; Lam,G.K.Y.; Durand,R.E.; Sy,A. RBE determinations for the 70 MeV proton beam at TRIUMF using cultured V79-WNRE cells. Abstract of the XX PTCOG Meeting, May 16-18, 1994, Chester, England, 30
14. Quastler,H. Information theory in radiation biology Ann Rev. of Nucl. Sci. 8; 387-400; 1958.
15. Cohen,L.; Hendrickson,F.; Mensell,J.; Awschalorn,M.; Hrejsa,A.; Kaul,R.; Rosenberg,L Late reaction and complication in patients treated by with high energy neutrons p (66MeV) Be (49 MeV). Preprint FN 323 1183.000, Fermilab, 1-18; Jan 1981.
16. Dolgikn,A.P. Microdosimetric aspects of irradiation planning in radiation oncology. Doctoral theses. Moscow, 1986. (in Russian).
17. Cohen,L.; Moulder,F.E. Derivation of celluar survival kinetic parameters for experimental fractional irradiations of rat-skin. Rad. Research 76; 250-258; 1978.
18. Davies,R.O. The macroscopic theory of irreversible processes. Reports on progress in physics. 19; 326-367; 1956.
19. Arrchambeau,J.O.; Shymko,R.M. Tissue population configuration as modifier of organ dose response. Intern. J. Rad. Biol. Phys. 15; 727-734; 1988.
20. Jackson,A.; Kutcher,G.J.; Yorke,E.D. Probability of radiation induced complications in normal tissues with parallel architecture under condition of uniform whole or partial irradiation. Radiotherapy and Oncology 26; 226-237; 1993.

FIGURES

1. Dependence of the track density in a bubble chamber g/g_0 on the particle velocity β. ❑- protons, ❑ - deuterons, Δ- pions, + - electrons (upper curve). The ratio of track density to LET (curve 2) simulates RBE. Barendsen's data of RBE measured with human cell culture are below at curve 3.

2. The dependence of bubble yield (experiment) and delta ray yield (calculation) on inverse square of particle velocity 1/b2, LET and particle energy (the last for protons). Experimental data are the same as Fig.1. Points B correspond to Barendsen's RBE Big square - the RBE measured at the ITEP proton beam. These data are in qualitative agreement with the increase of RBE with the power law for LET with an exponent. The effect is also proportional to the number of delta rays with the energy above V divided by LET.

3. Isoeffect curve of total dose dependence on fraction number for skin complication. ------- Model of Ellis, ... Blair - Davidson's model, -.-.-.-.-. and _____ two microdosimetric variants of its modification, experiment by (17).

4. Isoeffect curves for complications of epidermoid cancer treatment, calculated by two modified Blair - Davidson models.

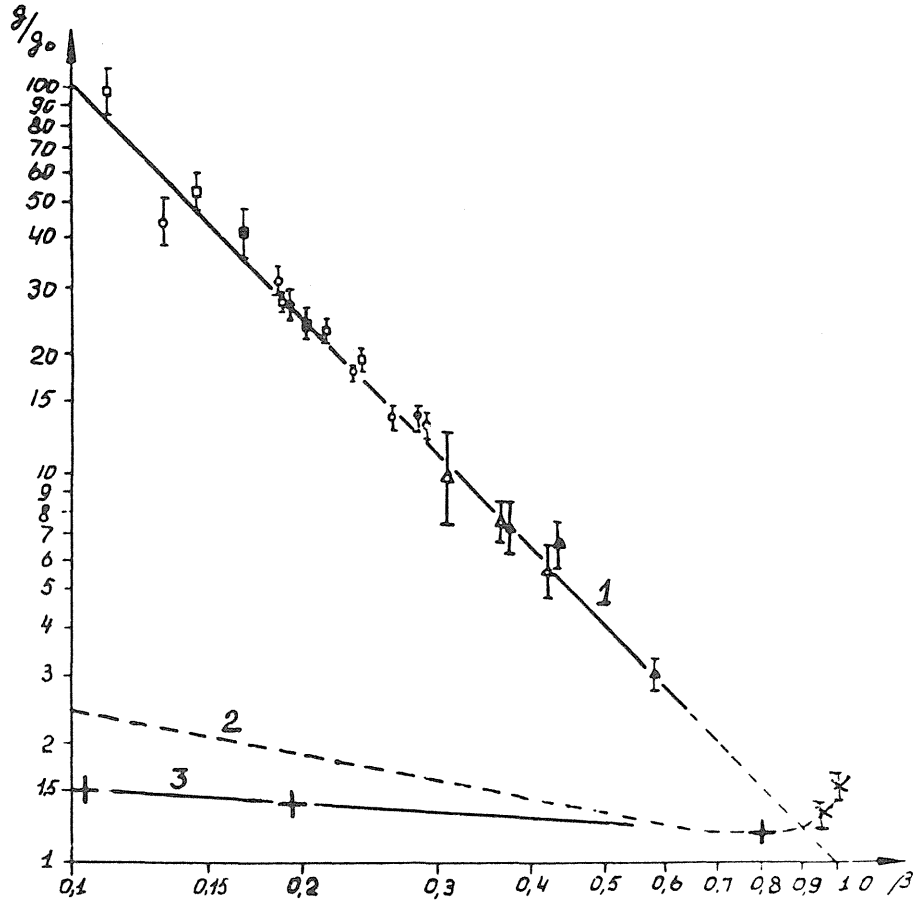
g/g₀
100
90
80
70
60
50
40
30
20
15
10
9
8
7
6
5
4
3
2
1,5
1
0,1
0,15
0,2
0,3
0,4
0,5
0,6
0,7
0,8
0,9
1,0
β
1
2
3

Fig.1

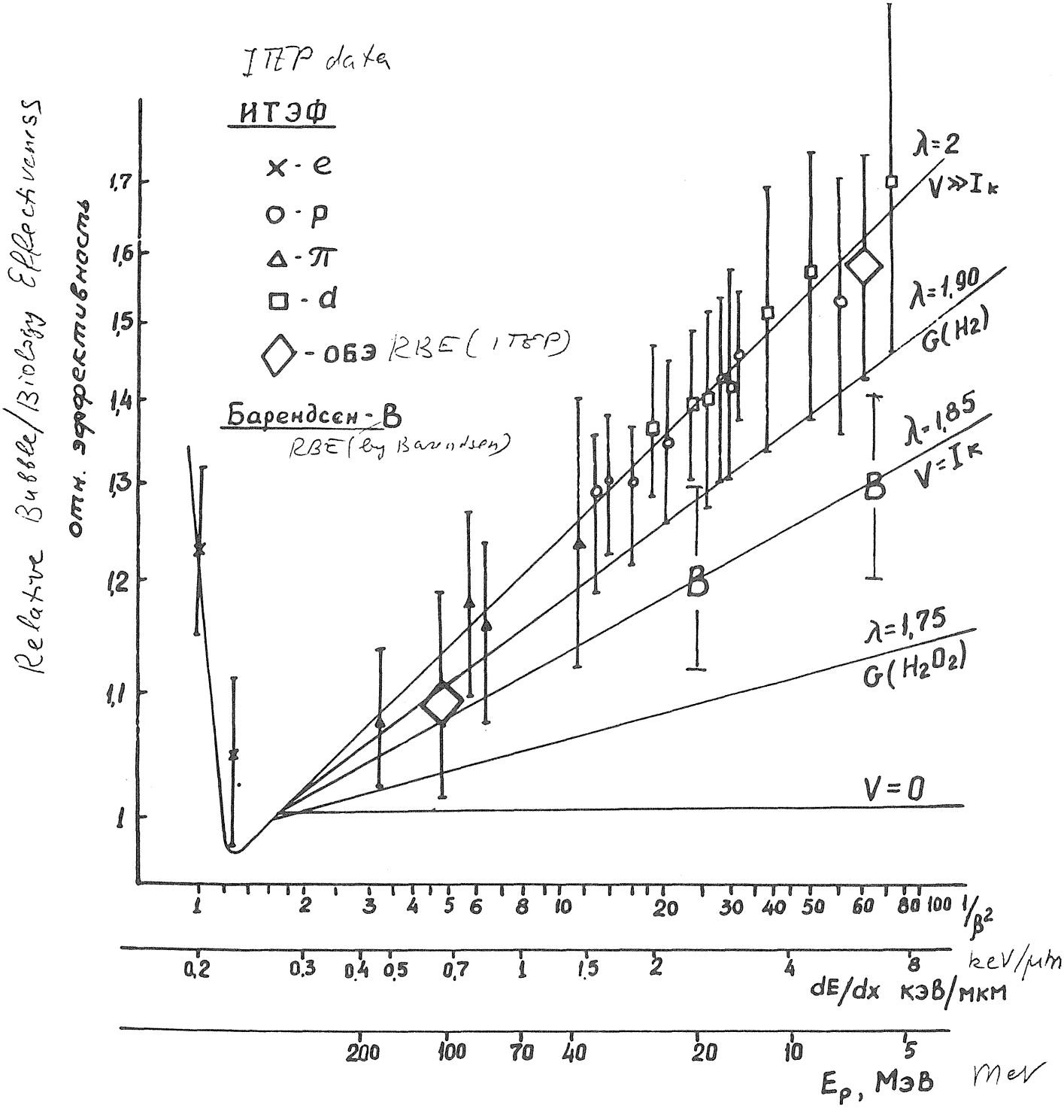
ITEP data
ИТЭФ
x - e
o - p
Δ - π
□ - d
◇ - ОБЭ RBE (ITEP)
Барендсен - B
RBE (by Barendsen)
Relative Bubble/Biology Effectiveness
отн. эффективность
λ=2
V≫Iк
λ=1,90
G(H2)
λ=1,85
V=Iк
λ=1,75
G(H2O2)
V=0
1/β²
keV/μm
dE/dx кэВ/мкм
Ep, МэВ
MeV

Fig.2

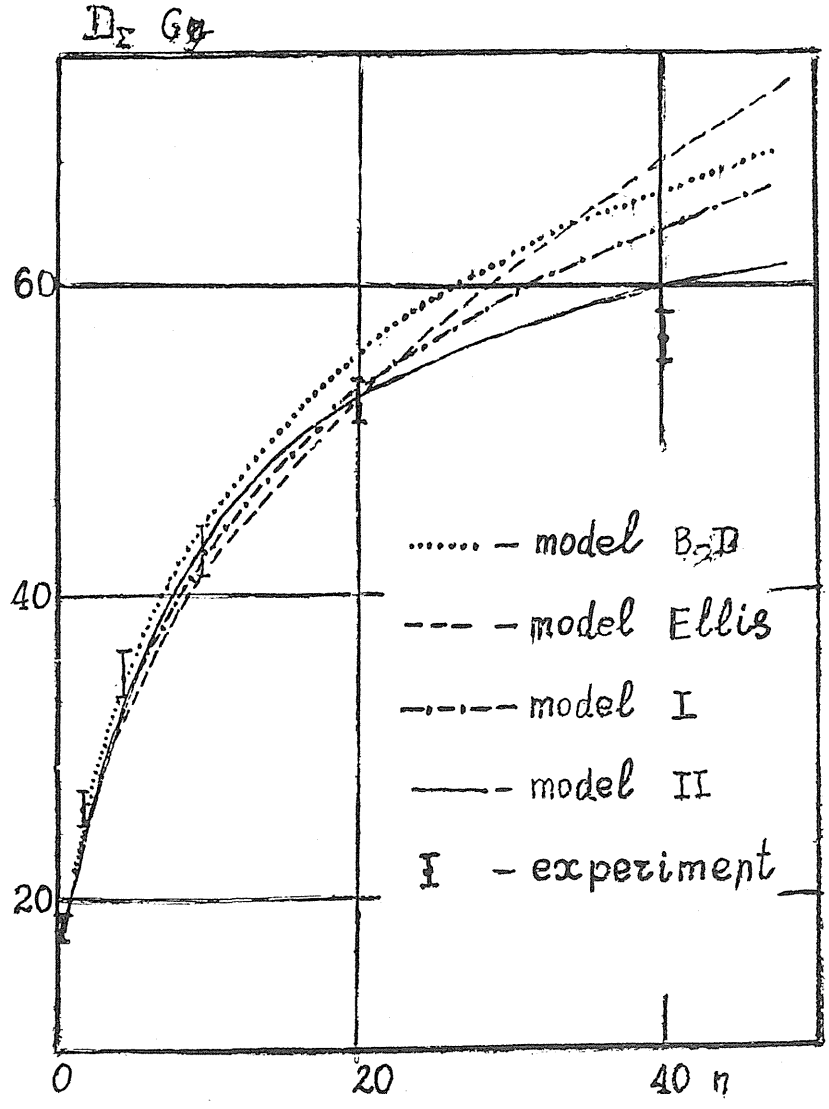
D_Σ Gy
60
40
20
0
20
40 η
..... – model B-D
--- – model Ellis
–·–·– model I
—— – model II
I – experiment

Fig.3

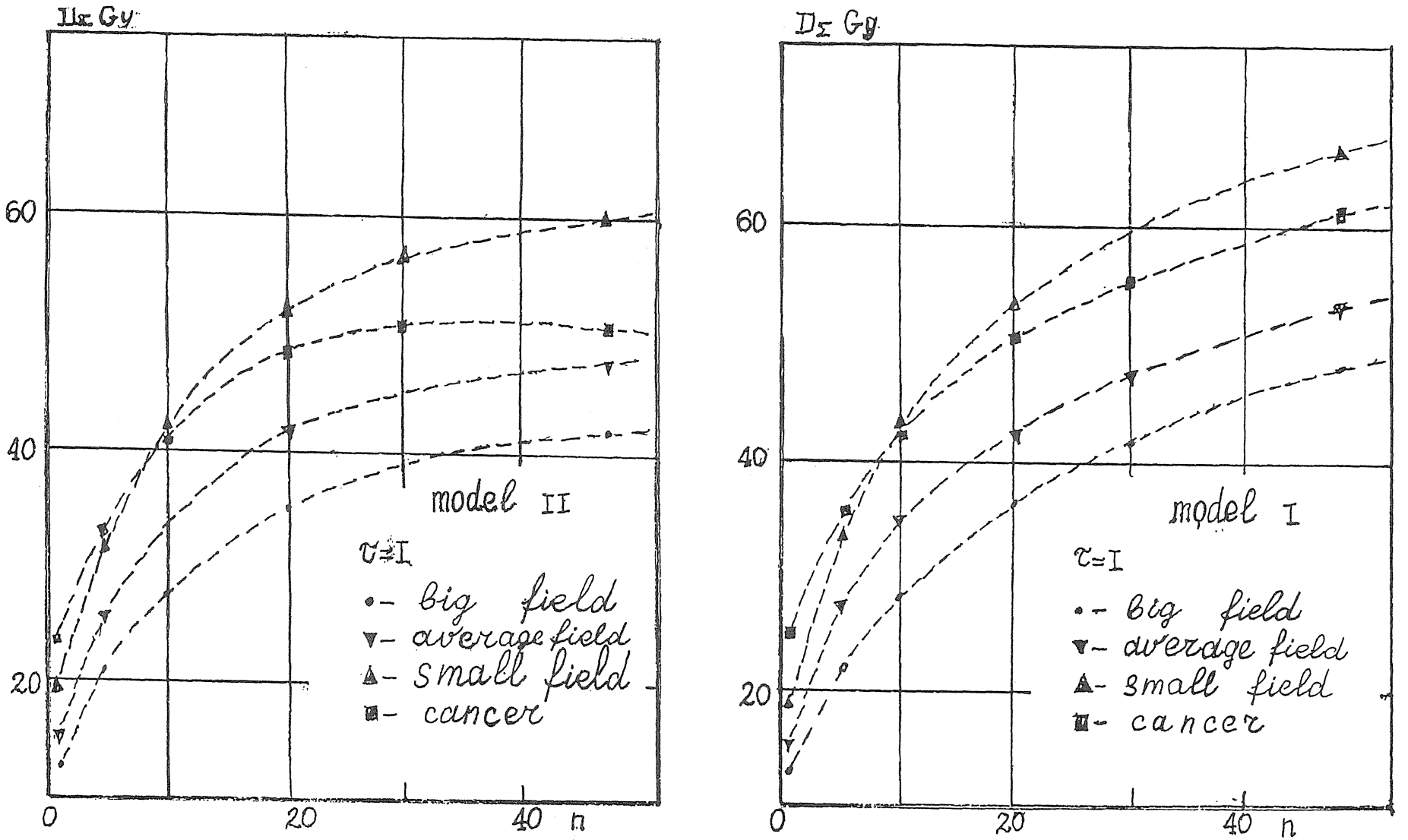
Dx Gy
60
40
20
0
20
40
n
model II
τ=I
• - big field
▼- average field
▲- small field
■- cancer
Dx Gy
60
40
20
0
20
40
n
model I
τ=I
• - big field
▼- average field
▲- small field
■- cancer

Fig.4

Clinical Results and Protocols

Commencing HIMAC Heavy-Ion Clinical Trials at NIRS

H.Tsujii, J.Mizoe, T.Miyamoto, M.Mukai, T.Nakano, S.Morita, K.Morita, K.Kawachi.
National Institute for Radiological Sciences(NIRS), Chiba , Japan

Abstract

Heavy-ion radiotherapy possesses optimal properties for therapy, that is the improved beam localization by the use of the Bragg curve and biological advantages due to an increased density of local high-LET depositions. At National Institute of Radiological Sciences(NIRS), the HIMAC(Heavy-Ion Medical Accelerator in Chiba) project was started in 1984, and construction of the building and installation of all facilities were completed in 1993. This is the first heavy-ion accelerator complex in the world dedicated to medical use in a hospital environment. There are three treatment rooms for vertical, horizontal, and vertical/horizontal beams as well as rooms for physics and radiobiological research studies. The aim of the HIMAC project is to establish clinical advantage of heavy-ion therapy in human cancer treatment. The phase I/II clinical trials was begun on June 21 1994 using carbon-ions to irradiate patients with head and neck tumors. Thereafter, treatment of brain and lung tumors was started, and currently tumors of the liver, uterine cervix, prostate, and other anatomical regions are under consideration. The potential efficacy of heavy-ion therapy is presented.

Heavy-ions, Carbon-ions, Clinical trial, High-LET radiation, Dose distribution, RBE

Introduction

In 1984 the Japanese government put into operation "The Comprehensive 10-year Strategy for Cancer Control". Since then the project for construction of the HIMAC (Heavy Ion Medical Accelerator in Chiba) had been carried out at National Institute of Radiological Sciences(NIRS), Science and Technology Agency(1). At the end of 1993 the construction of the entire facility was completed, and in June 1994 the first patient was treated with 290 MeV/u carbon-ions. The HIMAC facility is the first heavy-ion synchrotron complex dedicated to medical use in a hospital environment. Its aim is to evaluate and establish clinical advantages of heavy-ions in human cancer treatment by carrying out heavy-ion clinical trials on various type of malignancies and by related fundamental research works as well.

In this paper the clinical aspects of HIMAC heavy-ion project are described.

Scientific Background

There has been ample evidence that improvements of cancer cure can be expected from an improvement of local control(2,3). With regard to the efficacy of local treatment, surgery has been considered as the most important modality and recently surgical techniques has become more radical. However, the increase of radical procedures has hardly yielded higher local control and/or cure rates. In contrast, significant progress has been achieved in radiotherapy through technical developments and introduction of a new type of radiation in recent years. Among them, heavy charged particles such as protons and heavy-ions(carbon, neon, silicon ions) have potential advantages in improving local tumor control.

Heavy-ions have a benefit of superior depth-dose localization allowing selective irradiation to the tumor while minimizing irradiation to the surrounding normal tissues. In addition, as heavy-ions are

high-LET radiations, their efficiency will be further augmented by an increased radiobiological effectiveness(RBE) and reduced oxygen enhancement ratio(OER) caused by high-LET components delivered to the tumor. Since normal tissues are considered to be well-oxygenated, differential effects between the tumor and normal tissues are expected that favor the latter. High-LET radiations are also less susceptible to variations in radiosensitivity in the cell cycle, and the sublethal or potentially lethal damage caused by high-LET radiations is less able to be repaired, especially in slow growing tumors. By these properties, heavy-ions are considered to be more effective against hypoxic or anoxic tumor cells which are usually resistant to low-LET radiations(4).

Heavy-ion beam therapy was initiated at the University of California Lawrence Berkeley Laboratory(LBL) using helium-ions. Their clinical effects are similar to protons but they do exhibit somewhat higher RBE values ranging 1.2-1.4 for connective tissues. With helium-ions the improved results observed in specific malignancies include uveal melanoma, skull base tumor, juxtaspinal and sacral tumor, lesions adjacent to or encirculating the brain stem or spinal cord(5). The other effective possibility for helium-ions may be treatment of a bigger target volume including a primary and adjacent lymphatic region, which could be followed by heavier-ion boost irradiation confining to the primary site.

Beginning in 1979, nearly 300 patients were treated with neon-ions at LBL(5,6,7). The patients were selected for treatment when their tumors were not expected to respond favorably to conventional irradiation. Linstadt *et al* (6) reported that, compared with historical data, improved results were observed in selective tumor types including salivary gland tumors, paranasal sinus tumors, advanced bone and soft tissue sarcomas, locally advanced prostate carcinoma and biliary tract carcinoma. However, malignant glioma, pancreatic, gastric, esophageal, lung, and advanced or recurrent head and neck tumors were less successfully treated. It is considered that such unsuccessful results obtained in these tumors are due partly to relatively low dose levels employed and limited capability of the fixed horizontal gantry, possibly prohibiting a precise positioning of internal lesions. Unfortunately, the clinical trials at LBL were discontinued due mostly to financial difficulty in its continuation. Thus, more study is expected in the HIMAC trial, especially for the tumor which exhibited unfavorable results at LBL.

Clinical Trials at NIRS

Selection of Ion beams for clinical applications

Among several ion-beams available at HIMAC facility, we have decided to select carbon-ions in the initial clinical trial because they were considered to have the most optimal characteristics in physical and biological efficiencies, and the RBE value of carbon-ion-peak was similar to the fast neutron therapy which has been also used at NIRS. When critical organs are present in close proximity, it is essential that the multiple scattering be minimized without undue increase in fragmentation exit dose. In this regard, carbon-ion beams may be optimal compared to other particles. In addition, in the course of various studies at LBL, it has become apparent that the ions with atomic number of 6-10 have some advantages when compared to lighter ions(protons or heliums) or heavier ions(Si or Ar)(8), that is their good depth-dose distribution would be augmented by the increase of the RBE with depth(9). This has been demonstrated by survival data that the carbon-ion curves showed the effects of the increasing linear energy transfer(LET) from the plateau to the distal peak, resulting in the increasing RBE with depth in the depth-survival results. This means that for equal biological effect at the plateau region, carbon-ions cause significantly more killing in the extended peak than for other heavy charged particles(8,9,10).

Modulation of Bragg peak

The beam modulation system for shaping the Bragg peak precisely to the tumor contours has been developed(1). This system consists of a pair of beam scanning magnets(wobbler magnets), beam scatterers, range shifter, ridge filters, multileaf collimators and several beam monitoring devices(1). A lateral extension of the beams can be achieved by the wobbler magnets and scatterers, and for depth modulation a range shifter is used. For generating a spread-out Bragg peak(SOBP), various type of ridge filters are used depending on the thickness of tumor. The collimator is a device for shaping the lateral edge of the field. For a small tumor, the collimator is made of brass block for each tumor, but when the irradiation field becomes bigger the multileaf collimator will be used. This is a field-shaping device controlled with a computer according to the perpendicular cross section of the tumor. The compensating bolus that determines the edge of the SOBP corresponding to the distal edge of the tumor is fabricated by a numerically controlled milling machine.

Several ridge filters have been designed to produce the physical dose gradient of the SOBP so that the biological effect along the SOBP becomes uniform. This has been done based on biological response of human salivary gland(HSG) tumor cells at 10% survival level. The biological flatness along the SOBP was checked by measurements of physical dose distributions and dose averaged LET, which were compared with calculated results with satisfactory agreement.

Preclinical studies

Preparatory to starting radiotherapy to human cancers, a variety of preclinical studies have been carried out to confirm the quality of carbon ion-beams for clinical application. This included the evaluation and development of beam-transport system, measurements of the RBE values along the carbon-ion beam path, and evaluation of physical depth-dose distributions using animals and phantom materials.

In order to verify the precision of the treatment planning system for calculation of depth dose distributions, dosimetries were performed in big animals (monkeys) and phantom materials. Firstly, a monkey was irradiated using parameters obtained by CT-planning and an exit dose passing through the animal was checked. Secondly, the dose was measured at several points in the rectum which was outlined as a target volume. The results measured were in satisfactory agreement with those calculated. A phantom was also irradiated based on CT-planning with several semiconductor detectors being placed in it to check dose distributions. Again, the results were satisfactory.

Using 290 MeV/u carbon-ions, we have performed preclinical studies on five human cell lines cultured *in vitro* and mouse skins to estimate RBE values relative to photons and fast neutrons. The skin reactions included acute reactions and late skin contractions. The RBE values relative to ^{60}Co at the 6 cm SOBP have been in the range of 1.5-3.5 depending upon location of the peak, LET, dose fraction size and number of fractions. In single dose irradiation on cultured cells, the RBE values at 10% survival ranged 1.2-2.3 at the proximal(40 KeV/μ) and 2.0-2.7 at the distal part(82 KeV/μ) of the SOBP. In the treatment regimen of 4 fractions in 4 days, the RBE values along the 6 cm SOBP for mouse skin dry desquamation were 2.3 at the proximal and 3.2 at the distal part of the SOBP. The RBE value of 3.2 as determined in a fractionated regimen was almost identical as that of fast neutron. In fact, the carbon-ion SOBP has been basically designed so that it has a similar biological effectiveness as the fast neutron.

Clinical trial organization

The goal of our clinical program is to investigate and demonstrate systematically clinical advantages of HIMAC heavy-ion therapy for various type of human cancers. In order to perform clinical trials most effectively, phase I/II clinical protocols have been designed for each tumor site with assistance by other interested physicians. We have organized an advisory network committee, ethical committee and protocol working groups,

which consists of interdisciplinary group of scientists invited from other institute as well as those of NIRS. We have also an ethical subcommittee consisting of NIRS staff to evaluate the eligibility of each patient referred to us as a possible candidate for heavy-ion treatment.

Design of Clinical trials

In the initial HIMAC clinical trial, we have proposed to investigate the efficacy of carbon-ion beams first on various type of tumors. The phase I/II protocols have been designed by interdisciplinary working groups, and clinical trials were started on tumors of the brain, head and neck, and lung, and the treatment of tumors of the liver, prostate, and uterine cervix is under consideration. The criteria of patient selection and dose fractionations for these tumor sites is shown in Table 1. The general rule for patient selection is to seek patients with locally advanced tumors unlikely to be cured by other modalities. In selected tumor sites, the patients who refuse other treatment will be also included in the study. It is required that the patient would have reasonable length of life so that appropriate follow-up could be obtained. Since our initial trials is directed to the toxicity of heavy-ions on normal tissues together with initial estimate of tumor response, locally advanced and/or recurrent tumors at various sites, localized metastatic tumors, or localized unresectable carcinoma because of medical and/or personal reasons have been considered as the logical tumors in this study.

The treatment protocols designed to date for carbon-ion therapy in several tumor sites are as follows.

1) Head and neck tumors were chosen for the initial pilot study, which included locally advanced and/or recurrent tumors being treated unsuccessfully with other modalities. Since the purpose of this study is to evaluate toxicity and estimate clinical RBE values of carbon-ions, a patient who merely refuses other modality would not be justified to be included in this study.

2) For brain tumors, malignant glioma including glioblastoma multiforme, anaplastic astrocytoma, and lesser grade astrocytoma(G-3) will be treated. In the current protocol, malignant glioma will be initially irradiated by X-rays(50Gy/5wks) with concomitant use of chemotherapy(ACNU), which will be followed by carbon-ion irradiation. The target volume for X-ray irradiation will have generous margins around high signal area on T2 enhanced MRI, and carbon-ion irradiation will be confined to the gross tumor volume. Lesser grade astrocytoma will be irradiated with carbon-ions alone to a T2 high signal area. The patients with metastatic brain tumors will be selected if there is no evidence of active tumors in remote area and the primary site as well.

3) For lung tumors, carbon-ion therapy will be applied to stage I tumor(T1-2,N0,M0) which is inoperable due to medical reasons, and locally advanced tumor with invasion to the adjacent thoracic wall(Stage IIIA or T3N0M0). As such the majority of these tumors would locate in the peripheral lung field, even a new type of radiotherapy could be given without undue morbidity.

4) Primary hepatocellular cancer(HCC) will be selected for T2-4N0M0 tumors. If the major branch of the portal vein is involved with tumor invasion, it will be excluded from the study. The criteria of patient selection is similar to that for head and neck tumors, in that the patient selected for carbon-ion therapy would be hardly treated successfully with other available modalities.

5) Compared with other tumor sites, protocols for carbon-ion therapy of uterine cervix cancer would be more difficult to design because there exists an effective combination of treatment with intracavitary brachytherapy, external whole pelvic irradiation, and external irradiation confined to the primary tumor site. In treatment of stage III tumor, it would be ethically too early to replace brachytherapy by a new treatment modality. Therefore, only a big tumor(>4 cm) will be treated with a whole pelvis carbon-ion irradiation for 4 weeks followed by brachytherapy. But for a patient with stage IVA tumor it would be justified to treat with carbon-ions alone because the most of them are

usually hard to cure with conventional modalities.

6) Prostate cancer has been chosen as one of the most suitable subject for carbon-ion trial, and the patients with Stage B2 or C and pN0-N2 will be selected. The existence of pelvic lymph nodes will be surgically confirmed, then hormone therapy will be given for 2-3 weeks. Thereafter, carbon-ion irradiation will be given only to the primary prostate site and seminal vesicles but not to the pelvic lymph node area.

The initial radiation doses have been determined based upon preclinical studies and the clinical experiences on fast neutron therapy(Table 1) They are considered to be 10-20% lower than the dose level that is possibly tolerable in musculo-connective tissues. In the current trials, the radiation dose will be escalated by 10% interval for every 3-5 patients. On June 21, 1994, the initial phase I/II trials were started on 3 patients with head and neck tumors using 290 MeV/u carbon-ions. Head and neck tumors have been selected because it is easier to perform the initial RBE studies, *i.e.* observation of radiation response of normal tissues . The first patient had adenocarcinoma of the cheek mucosa(T3N0M0), the second had squamous cell carcinoma of the ethmoid sinus with invasion to the skull base(T4N0M0), and the third had post-operative recurrent tumor(adenoid cystic carcinoma) in the oral floor with lung metastasis. They were all treated solely with carbon-ion irradiation with 16.2 physical Gy in 18 fractions over 6 weeks. At about 6 months following the treatment, radiation effects of the skin and mucosal reactions were acceptable with satisfactory tumor response. As of February 1995, 13 patients finished treatment and 8 patients are under treatment.

Summary

As such heavy charged particle therapy possesses a combination of radiobiological and dose localization advantages, it potentially offer increased cure rates in cancer therapy. It has been well known that one of the key factors in radiotherapy for achieving cancer cure is a dose localization property, which has been proven with improved local control obtained by such modalities as brachytherapy, intraoperative radiotherapy, stereotactic radiosurgery, 3D-conformal irradiation technique, etc. Obviously, they were developed to improve dose-localization in the tumor with minimizing irradiation to the surrounding healthy tissues. In this regard, heavy-ions could deliver biologically more effective dose to the tumor. However, it still remains to be demonstrated that in what type of tumors biologically differential effects could be observed between the tumor and normal tissues.

The HIMAC heavy-ion clinical trial has only begun to be studied. Since this is a facility dedicated to radiotherapy in a hospital environment, various type of tumors could be studied for possible candidate for this modality. We decided to use carbon-ions first, but in the next stage helium-ions will be used for eye melanoma and skull base sarcomas, thereafter heavier ions such as silicon or neon ions will be used for relatively superficially located tumors. There are numerous developments that should be done for successful performance of heavy-ion therapy. In addition, organization of the effective networks with the major institutions is also an urgent requirement in carrying out clinical trials successfully. It is without saying that for conducting a definitive dose escalation study, further studies are needed for investigation of tumor response and normal tissue late reactions as well, and worldwide collaborations should be more extensively performed.

Acknowledgments

This work was supported in part by the Grant-in-Aid(Kitagawa-han) for Scientific Research from the Ministry of Education, Science and Culture.

Table 1. Criteria of patient selection and radiation dose in HIMAC carbon-ion radiotherapy at NIRS

Tumor sites	Eligibility	Treatments per week	Carbon-ion dose(Gy) to start with[a] Daily dose	Total Dose/Fx/Wks
Head & neck (9301)	Locally advanced and/or recurrent tumors unlikely to be cured by other modalities	3	0.9	16.2 / 18 / 6 (Pilot study)
Brain (9302)	Malignant glioma (Grade 3-4)	4	0.7	5.6 / 8 / 2 [b] (boost irradiation)
	Low grade astrocytoma(G2)	4	0.7	16.8 / 24 / 6
	Metastatic tumor	4	1.0	16.0 / 16 / 4
Lung(NSCLC) (9303)	Medically inoperable or surgery refused(T1-2N0M0 or Stage I)	3	1.1	19.8 / 18 / 6
	Locally advanced tumor with chest wall invasion (T3N0M0 or Stage IIIA)	3	1.1	19.8 / 18 / 6 (preoperative irrad)
Liver (9501)	T2-4N0M0 tumor unlikely to be cured by other modalities and without involvement of a major branch of the portal vein	3	1.1	16.5 / 15 / 5
Uterine cervix (9502)	Stage III large tumor(≥4cm)	4	0.7	11.2 / 16 / 4 [c] (followed by brachy)
	Stage IVA	4	0.7	16.8 / 24 / 6 [d]
Prostate (9503)	Stage B2-C and pN0-N2	4	0.9	18.0 / 20 / 5 [e]

a) : Described in physical dose(Gy) at the distal part of the SOBP where the RBE value is 3.0 for skin reactions.
Prescribed dose will be escalated by 10% interval.

b) : Carbon-ion irradiation will be preceded by X-ray irradiation(50Gy/25Fx/5wks) with ACNU(100mg/m^2) concomitantly given twice at the 1st and 5h week.

c) : Whole pelvis irradiation with carbon-ions will be followed by remotely afterloading brachytherap

d) : With carbon-ions, whole pelvis irradiation will be given for 16 fractions followed by irradiation with a cone-down field to a total of 24 fractions.

e) : Prior to carbon-ion irradiation, hormone therapy will be given for 2-3 weeks.

References

1. Kawachi,K.; Kanai,T.; Endo,M.; Hirao,Y.; Tsunemoto,H. Radiation oncological facilities of the HIMAC. J.Jpn.Soc.Ther.Radiol.Oncol. 1:19-29; 1989.
2. Suit, H.D.; Miralbell, R. Potential impact of improvements in radiation therapy on quality of life and survival. In.J.Radiat.Oncol.Biol.Phys. 16:891-895; 1989.
3. Leibel, S.A.; Clifton Ling, C.; Kutcher, G.J.; *et.al.* The biological basis for conformal three-dimensional radiation therapy. In.J.Radiat.Oncol.Biol.Phys. 21:805-811; 1991.
4. Wambersie, A. Is there any future for high-LET radiation? Strahlenther.Oncol. 165:348-356, 1989.
5. Castro,J.R.; Phillips,T.L.; Petti,P; et.al. Clinical results of charged particle radiotherapy. Radiation Research. eds. by Fielden,E.M. *et.al.* Volume 2 :910-915, 1987.
6. Linstadt, D.E.; Castro, J.R.; Phillips, T.L. Neon ion radiotherapy: Results of the phase I/II clinical trial. In.J.Radiat.Oncol.Biol.Phys. 20:761-769; 1991.
7. Castro, J. Future studies in heavy ion therapy. The 1st International Conference on Life, Science and Biotechnology. Hyogo 1994.
8. Chapman, J.D.; Blakely, E.A.; Smith, K.C.; Urtasun, R.C. Radiobiological characterization of the inactivating events produced in mammalian cells by helium and heavy ions. I n.J.Radiat.Oncol.Biol.Phys. 3:97-102; 1977.
9. Phillips, T.L.; Fu, K.K.; Curtis, S.B. Tumor biology of helium and heavy ions. In.J.Radiat.Oncol.Biol.Phys. 3:109-113; 1977.
10. Blakely, E.A.; Ngo,F.Q.H.; Curtis, S.B.; Tobias, C.A. Heavy-ion radiobiology: Cellular studies. Adv.Radiat.Biol. 11:295-378; 1984.

THE POTENTIAL USE OF PROTON THERAPY IN THE MANAGEMENT OF PINEAL TUMORS

J.-L. HABRAND, M.D., C. HAIE, M.D., S. HELFRE, M.D., C. LENIR, M.D., D. PONTVERT, M.D., L. SCHWARTZ, M.D., H. RANDRIANARIVELLO, M.D., C. PATTE, M.D., J.-M. ZUCKER, M.D. and A. MAZAL, Ph. D.

Centre de Protonthérapie d'Orsay, Campus Universitaire, 115 rue G. Clemenceau - 91406 Orsay - France

Protontherapy (PT) has proven successful in the management of slow growing, ill-resectable, radio resistant tumors such as base of the skull sarcomas. We have adressed the issue of the potential advantage of PT in the management of pineal area tumors (PAT) through a review of literature and personal experience.

PAT are rare entities mostly seen in children and adolescents in which they count for 3 - 11 % of brain tumors. They are made of 3 major histological subtypes that are germ cell (germinoma, secreting non germinoma and teratoma), parenchymal (pineoblastoma and pineocytoma), and glial tumors with a respective frequency of 85 - 10 and 5 %. Some of them have a high propensity for CSF dissemination. Conventional radio therapeutical management include generally a coverage of the entire CNS up to 30 - 35 Gy followed by a booster to the primary of 15 - 20 Gy. This policy has proven successful in germinomas only (90 % 5 Y - survival) whereas it has remained highly disappointing in the other forms.

Modern approaches aim to improve tumor control as well as to reduce long term neuro-endocrinological toxicity which is critical in this young age group. Main ones are represented by the development of micro surgical techniques, and the combination of polychemotherapy (mostly platinum - based) to radiotherapy. Similarly, the potential advantage of PT in PAT would be two-fold :

1) Improving local failures in non germinomas since they have been associated with the majority of failures.

An increased tumor-dose seems to be justified by the dose-effect relationship (in the range of 40 - 60 Gy) that has been shown by some investigators.

2) Improving long term side-effects like brain and optic pathway damages, hypopituitarism, radiation-induced arteritis and second malignancy.

Preliminary proposals on the design of a multi institutional study will be presented.

The Use of the JINR Proton Beam in Dubna for the Uterus Cervix Cancer treatment.

Astrakhan B.V., Kiseleva V.N., Klochkov I.I., Molokanov A.G., Mytsin G.V., Poidenko V.K., Savchenko O.V., Zorin V.P.

I.Introduction

The method of the uterus cervix cancer treatment was for the first time elaborated at ITEP (Moscow), applied to 160 patients from 1970 to 1985 [1–3] and developed at the JINR proton beam in Dubna [4–5].

At the first stage of investigations we reproduced the method of the preoperative combined proton and γ–irradiation of the uterus cervix cancer and after that went on to the radical (without surgery) radiation treatment.

The clinical and hystological variabilities of tumour and normal tissues after treatment were investigated. The direct result and the distal consequence of the treatment were compared with other investigations.

2. The technique of patient treatment at the JINR medical proton beam.

Patients with the uterus cervix cancer were irradiated in procedure room No.2 of the clinical–physical facility with a horizontal 130 - 160 MeV modified proton beam. The beam of this energy is produced after deceleration of the 660 MeV proton beam ejected from the JINR phasotron in a carbon degrader. The depth-dose distribution is formed with the aid of a ridge filter calculated for the nonmonoenergetic beam [6].

For the dose field shaping we use a set of cylindrical collimators with a set of conical and cylindrical plexiglass heads. The ridge filter is a strong scatterer, and we employ collimators to determine the dose field. These collimators and a central probe are also used to fix the target with respect to the beam axis. The cylindrical heads of different thickness are intended for treatment depth regulation. The conical heads make it possible to irradiate both the uterus cervix and the adjacent region. Examples of isodose distributions with cylindrical and conical heads measured with a small silicon detector in a water phantom are presented in Fig.1. Each line indicates the isodose level with an interval of 10% of the maximum dose.

The stand design makes it possible to fix precisely and quickly the patient's body at the beam axis.

For absorbed dose rate measurements we use a clinical dosimeter KD-27012 with thimble ionization chambers VAK-251 and VAK-253. The dosimeter was calibrated with a ^{60}Co source of the therapeutic γ–unit placed in one of the cabins of our clinical–physical facility, and also used for patient treatment. The ^{60}Co source was calibrated against the primary standard of the Czech Republic placed in the Prague Institute of Radiation Dosimetry. The accuracy of the gamma-unit calibration is 1.3% (one standard deviation) [7].

Using the gamma-unit as a calibrated stand for ionization chambers of our clinical dosimeters was described in [8,9] and practically coincided with recommenda-

tions of the "Code of Practice for Clinical Proton Dosimetry" elaborated by the ECHED (**E**uropean **C**linical **He**avy Particles **D**osimetry) working group [10].

The full error of the JINR phasotron proton beam dosimetry is about 5%. This accuracy meets the international requirements for the therapeutic proton beams.

3. The method of pre-operative combined proton and γ–treatment of the uterus cervix cancer.

3.1 Methods and materials.

At first we reproduced the method of the pre-operative combined proton and γ–treatment of the uterus cervix cancer. This method includes proton irradiation of the uterus and γ–irradiation of the regional lymphatic nodules followed by surgical removal of the uterus. We normally used 3 fractions of proton irradiation. The diameter and depth of the dose field was chosen individually for each patient. The dose in the maximum of the dose distribution was 20 Gy for each irradiation run. The dose rate of the proton beam was about 2 – 5 Gy/min and the proton irradiation procedure was as long as 5 - 10 minutes.

Regional lymphatic nodules were irradiated at the ^{60}Co γ–unit ROCUS–M for 5 weeks with five 2 Gy fractions a week. The method of γ–irradiation is rotation within 4 sectors of 60° each. The full size of the dose field was limited from (4cm*14cm) to (4cm*16cm). The example of the dose distribution is shown in Fig.2a. The full dose of the γ–irradiation at point B was 30 Gy.

2-3 weeks after the end of the radiation therapy an operation was carried out at the Surgery Department of the Cancer Research Center in Moscow.

3.2 Clinical results.

From November 1987 to December 1988 six patients were treated. The age of patients was from 30 to 50 years. All patients had the clinical Stage I uterus cervix cancer.

The full course of the proton treatment was carried out for 3 patients, the other 3 patients had additional γ– irradiation. The postirradiation reactions to critical organs (bladder and intestines) were absent in all patients.

All patients were observed for over 5 years. One patient died of the distant metastasis outside the region of the irradiation, other 5 (83%) are living without recidives, metastases and complications. These results are in good agreement with the analogous results obtained at ITEP [3] and have become the basis for transition to the radical (without surgery) combined proton and γ–treatment.

4. The method of radical combined proton and γ–treatment of the uterus cervix cancer.

4.1. Methods and materials.

For the radical treatment of the uterus cervix cancer we used the same proton and gamma irradiation as for the pre-operative treatment but the dose was increased against the pre-operative treatment. We used four 20 Gy fractions of proton irradiation. For two of the four fractions we used the collimator with a cylindrical head and for the other two a conical

head was used.

For γ–irradiation we used the same rotation within 4 sectors. Additionally we used γ–irradiation within 2 sectors of 180° each, an example of this summarized dose distribution is shown in Fig. 2b.

The full dose from proton and γ–irradiation was 60 – 70 Gy at point A, 50 – 60 Gy at point B. The dose to critical organs (bladder and intestines) was from 8 to 16 Gy.

4.2. Clinical results.

From 1990 to 1994, 25 patients were treated by the radical method. Three of them got a palliative treatment and were excluded from the later analysis. The age of the patients and tumour characteristics are shown in Table 1.

The direct results of the radical treatment confirmed by cytological analysis show that regression of the tumour was observed in all patients. In all patients the tumour cells were not observed.

12 of 22 patients are followed up for over 3 years (see Table 2), 2 of them died. The death of the first patient, 78 years old with Stage III, at the end of the second year after treatment was caused by cerebral thrombosis. The death of the second patient, 58 years old with Stage II, was caused by the recidive of the tumour. The others are living without postradiation complications to the critical organs and without recidives and metastases.

Analysis of the results of the uterus cervix cancer treatment shows that the method of the combined proton and γ–treatment of the uterus cervix cancer has a great advantage over conventional therapy.

5. Conclusions.

1. The clinical probation of the setup for treatment of gynaecological tumours with the JINR proton beam has been done.

2. The results of the clinical probation of the method for the uterus cervix cancer treatment have confirmed the advantage of the proton irradiations over the conventional afterloading method.

3. The most impotent advantage of the proton beam treatment is absence of postradiation reactions to the critical organs (bladder and intestines).

4. Up to now 31 patients with the uterus cervix cancer have been treated at the JINR phasotron. 6 of them had proton and γ–treatment combined with surgery operation and 25 patients had radical treatment (without surgery). The clinical results are in good agreement with the preceding results of the ITEP group.

References

1. Ruderman A.I. et al. Use of High Energy Protons in Complex Treatment of Cervix Utery Cancer. Med. Radiology (Russian), **1**, 1971, p.5.

2. Kiseleva V.N. et al.The Results of the Combined Gamma-Proton Irradiations of Patients with the of Cervix Utery Cancer. Obstertrics and Gynaecology (Russian), 2, 1986, p.37.

3. Kiseleva V.N. et al. Long-Term Results of Cervical Cancer Therapy Using Proton Beam Irradiation. Med. Radiology (Russian). **6**, 1988, p.49.

4. Abazov V.M. et al. Radiation Therapy with JINR Phasotron Beams, JINR, Dubna, 1992.

5. Abazov V.M. et al. Medical Facility for Radiation Therapy with JINR Proton Phasotron Beams. JINR E–18–94–112, Dubna, 1994.

6. Molokanov A.G. Using of Ridge Filters for Nonmonoenergetic Proton Beams. JINR, 9–89–391, Dubna, 1988 (in Russian).

7. Wagner R. et al. Physico–Dosimetric Measurements on the ROCUS–M Gamma–Unit. JINR, 16–87–935, Dubna, 1987 (In Russian).

8. Votochkova I. et al. Measurement of Dosimetric Parameters of Therapeutic Proton Beams. JINR, 16–89–353, Dubna, 1989 (In Russian).

9. Kovar I. et al. Dosimetry of Medical Proton Beams at the JINR Phasotron in Dubna. JINR E–16–93–310. Dubna, 1993.

10. Vynckier S., Bonnett D.E. and Jones D.T.. Code of Practice for Clinical Proton Dosimetry. Radiotherapy and Oncology, 20, 1991, p.53.

11. Pavlov A.C., Kostromina K.N. The Uterus Cervix Cancer. M., 1983. (In Russian).

12. Vishnevskaya V.V. The Combined Treatment of the Uterus Cerviv Cancer. Minsk, 1987 (In Russian).

Table 1. The age of the patients treated with a radical method and tumour characteristics.

Age of patients	Number of patients	Stage I	Stage II	Stage III
50-59 years	6	-	5	1
60-69 years	12	4	7	1
70-79 years	4	2	1	1
Total	22	6	13	3

Table 2. The results of radical proton and γ–treatment of the uterus cervix cancer for patients followed up over 3 years.

Stage	Number of patients	Are living over 3 year	Death from tumour	Death from other reasons
I	5	5	-	-
II	4	3	1	-
III	3	2	-	1
Total	12	10	1	1

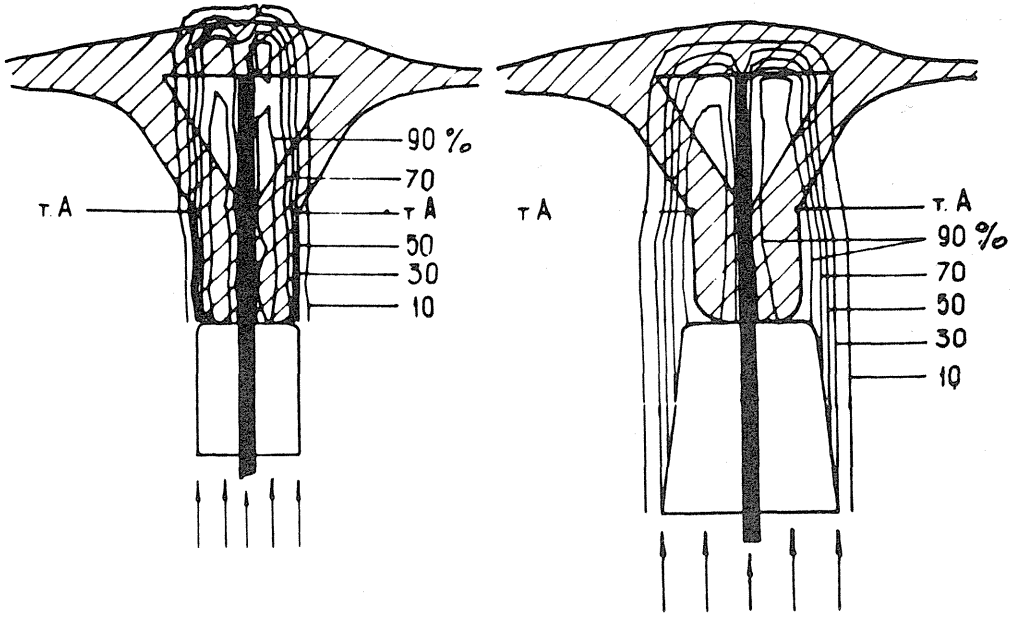

Fig 1. Dose fields for modulated proton beam for conical and cylindrical head with a central probe

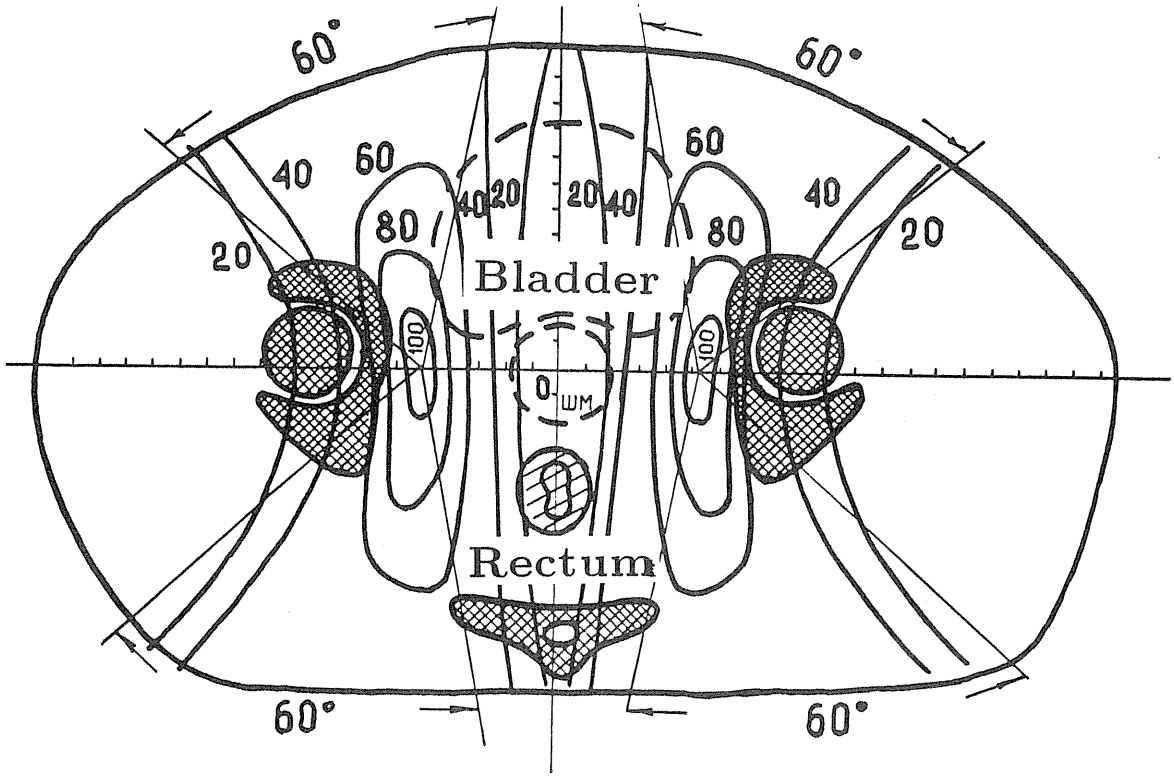

rotation within 4 sectors of 60°.

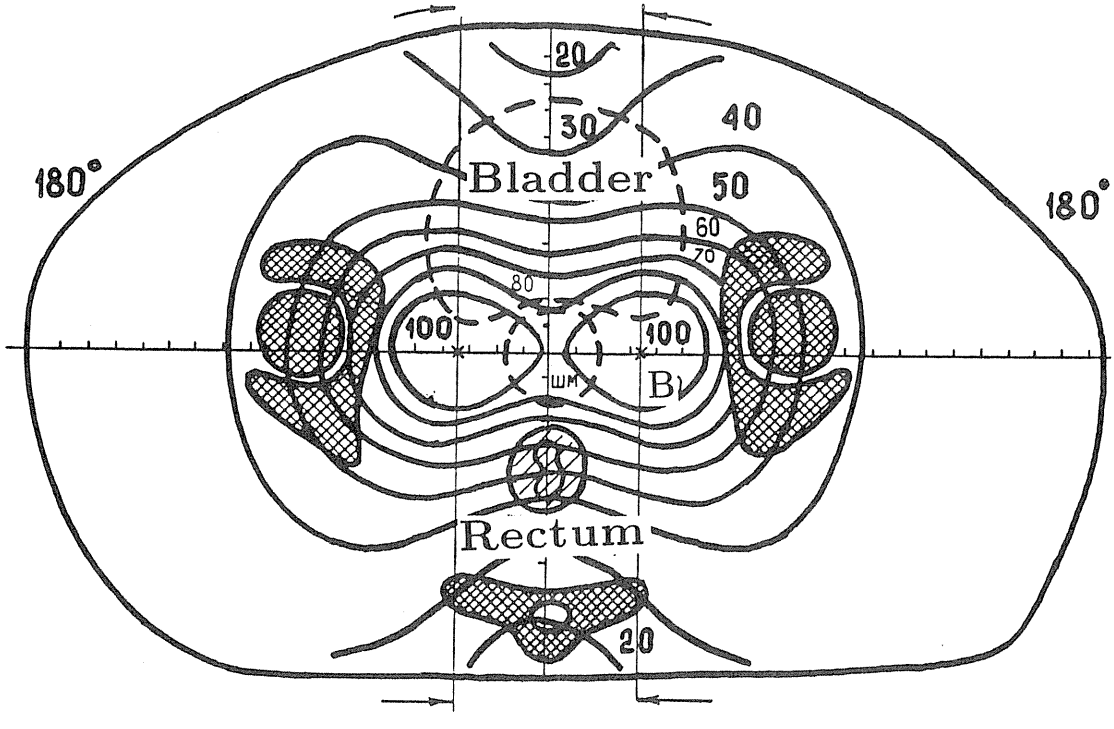

rotation within 2 sectors of 180°.

Fig.2. Dose fields for distant γ–irradiation of regional lymphatic nodules.

Proton Radiation Therapy of Low-grade Chondrosarcomas involving the Cranial Base

NJ Liebsch, LG Renard, JE Munzenrider, EB Hug, HD Suit

Department of Radiation Oncology, Massachusetts General Hospital, Harvard Medical School, Boston, Harvard Cyclotron Laboratory, Cambridge, USA

From 1974 to 1994, 130 adult patients (64 females, 66 males ages 18-70 years, median age = 33 years 9 months) with primary, non-metastatic low-grade chondrosarcomas of the cranial base received high-dose fractionated postoperative proton radiation therapy at the Massachusetts General Hospital and Harvard Cyclotron Laboratory. These tumors are rare neoplasms that originate from cartilaginous remnants in the chondrocranium, i.e. the part of the skull that undergoes endochondrol ossification during fetal life. Among the 130 patients, the tumor originated from the petro-clival junction (64%), the clivus (31%) and the anterior cranial base (5%). The patients presented with a variety of signs and symptoms and clinical findings whose onset preceded the detection of the tumor by 0-14 years (median = 15 months). Most common were a combination of headaches (22%), abducent palsy (50%) and lower cranial nerve deficits (19%).

The 130 patients underwent 182 surgical procedures with gross residual tumor prior to their referral for definitive radiation therapy. Upon histologic review at the MGH, including H & E stains and immunohistochemical staining profile, the tumors were classified as hyaline (8%), myxoid (37%), mixed hyaline-myxoid (47%), not otherwise specified (8%) chondrosarcomas of low grade (grade 1/3, 2/3). Of note, in 53/130 patients = 41% of the referrals, the review resulted in a change of the diagnosis from chordoma to low-grade chondrosarcoma. After detailed clinical evaluation, the patients underwent oncologic imaging to define the residual tumor and delineate neighboring critical, dose-limiting structures. Utilizing 3D CT-based treatment planning, they received fractionated precision radiation therapy with curative intent, employing a combination of photon and proton beam irradiation. The median prescribed total dose was 68.4 Cobalt-Gy-equivalent (CGE) in 38 fractions of 1.8 CGE each with a range of 66.6 to 72.0 CGE. (1 CGE = RBE x 1 pGy, RBE = 1.1 for the 160 MeV proton beam at the Harvard Cyclotron Laboratory). The dose to non-target structures was limited by 60.0 CGE for the optic pathway, 53.0 CGE for the center, and 64.0 CGE for the surface of the brainstem. All patients have been followed. The median follow-up is 30 months (range 0-18 years 5 months) since completion of radiation therapy. Local tumor control (LC) = freedom from tumor progression as judged by clinical and radiographic criteria is 98% at 5 years. In contrast, LC in 125 adult patients with chordomas of the central cranial base who received definitive proton radiation therapy with similar techniques

during the same time period is 54% at 5 years (Figure). None of the patients with low-grade chondrosarcomas of the cranial base has developed metastasis. 8% of the 130 patients had one or more of the following radiation-related complications: blindness, brainstem injury, brain injury with 2 deaths due to brain necrosis.

In summary, primary low-grade chondrosarcomas of the cranial base are uncommon, slowly growing, locally invasive neoplasms with low metastatic potential. They can be distinguished with confidence from chordomas of the central cranial base by virtue of their immunohistochemical staining pattern. They can be successfully controlled with acceptable treatment-related morbidity by a carefully planned combined modality approach. This consists of modern skull base surgery with the aim of establishing the tissue diagnosis and decompressing any neighboring critical anatomic structures that are significantly compromised by the mass effect of the tumor, thereby improving the geometry of the residual tumor for the purpose of postoperative fractionated, high-dose proton radiation therapy.

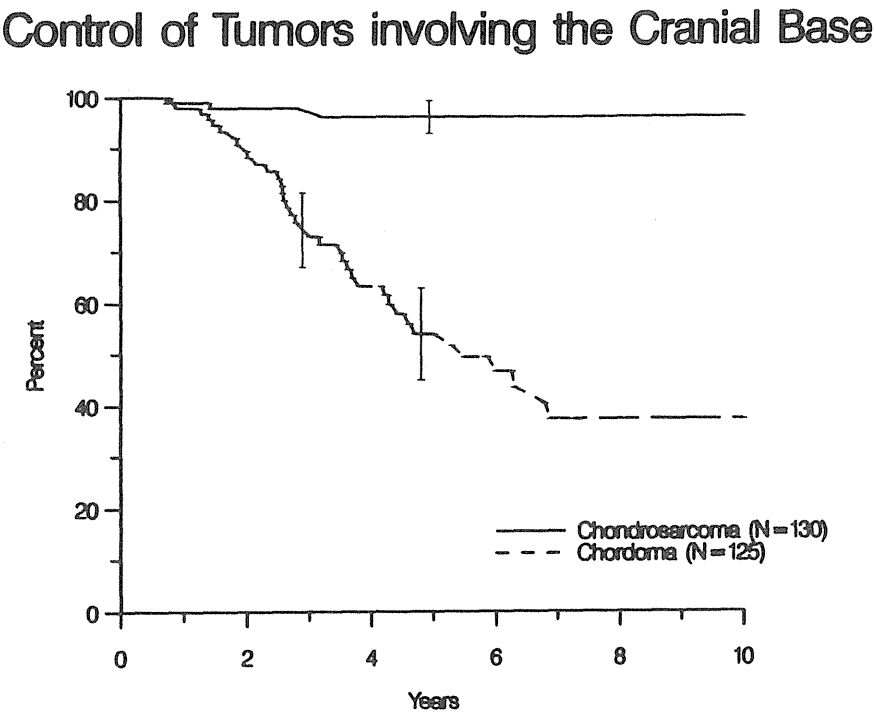

Figure: Local control of low-grade chondrosarcomas (n = 130) and chordomas (n = 125) of the cranial base following proton radiation therapy.

Beam Delivery and Dosimetry

NATIONAL ACCELERATOR CENTRE: PROTON DOSIMETRY INTERCOMPARISONS

D T L Jones, A N Schreuder, J E Symons (NAC); S Vynckier (UCL); A Kacperek (DCC); A Mazal, S Delacroix, C Nauraye (CPO); A Bridier (IGR); M Wagner (HCL); J Beatty, K Gall (MGH); Y Hayakawa (PMRC)

The National Accelerator Centre (NAC) has recently been involved in several proton dosimetry intercomparisons. Measurements were made in the proton therapy beam at the Douglas Cyclotron Centre, UK (DCC), the Université Catholique de Louvain, Belgium (UCL), the Centre de Protonthérapie d'Orsay, France (CPO) [73 and 200 MeV beams] and the Harvard Cyclotron Laboratory, USA (HCL). In addition, measurements involving UCL and the Proton Medical Research Center, Japan (PMRC) were made at NAC. The proton doses were determined according to the Code of Practice for Clinical Proton Dosimetry *[S Vynckier, D E Bonnet and D T L Jones, Radioth. Oncol.* ***20*** *(1991) 53]* using air-filled ionization chambers. In all cases the same procedures were followed, viz. the ionization chambers (IC) were calibrated in ^{60}Co and then irradiated in air and/or in phantom in the respective proton beams. In some cases doses were also determined using a Faraday cup (FC). The results obtained are summarised in the table below. The IC data are in excellent agreement, except for the measurements at DCC where very unstable beam conditions prevailed. Doses determined at HCL according to the AAPM protocol *[AAPM Report 16, 1986]* were 2.2% lower. This can largely be accounted for by the different proton W-values used in the two protocols. The FC measurements are problematic and this can be ascribed to low-energy proton contamination and errors in determining the effective beam area. In the absence of a calorimeter it is clear that ICs calibrated in ^{60}Co are reliable proton dosimeters provided the same protocol is followed.

VENUE	STANDARD DEVIATION OF MEAN DOSE (IC)	DOSE (IC) / DOSE (FC)
NAC at DCC	1.73%	1.056
NAC at UCL	0.35%	1.054
NAC at CPO (73 MeV)	0.55%	0.992
NAC at CPO (200 MeV)	0.33%	-
NAC at HCL	0.54%	1.092
UCL/PMRC at NAC	0.71%	-
Average	0.70%	1.053

PTCOG XXXI, Chiba, Japan, 14 -16 November 1994

PROTON DOSIMETRY PROTOCOL COMPARISONS

Kenneth P. Gall, Ph.D., Stanley J. Rosenthal, Ph.D.,
Alfred R. Smith, Ph.D.

Department of Radiation Oncology, Massachusetts General Hospital, Boston, Massachusetts, 02114, USA.

Purpose: This paper presents the analysis of the variation in the proton beam calibration factor for the Exradin T1 (0.05 cc) ionization chamber SN 194, when each of three protocols are followed. The first two protocols begin with a cavity gas calibration factor for the ionization chamber derived following the protocol popularly known as TG21, and then applying factors for proton beams to arrive at a proton calibration factor for the chamber. The third derives a proton calibration for a chamber using a fluence measurement technique based on a Faraday cup. The measurements were carried out at the Massachusetts General Hospital and the Harvard Cyclotron Laboratory. The measurements are presented in order to demonstrate the change in prescribed dose that would result following any change in protocol undertaken at this institution.

AAPM EXPOSURE BASED PROTOCOL

According to the AAPM protocol known as TG21 (1) the cavity gas calibration factor is defined as

$$N_{gas} = \frac{N_x A_{ion} k\, W_e (A_{wall}\beta_{wall})}{\left(\bar{L}/\rho\right)_{gas}^{wall}\left(\mu_{en}/\rho\right)_{wall}^{gas}}$$

Where,

$$A_{ion} = 1.0$$
$$k = 2.58\times10^{-4}\left(C/R\cdot kg\right)$$
$$W_e = 33.77\left(J/C\right)$$
$$(A_{wall}\beta_{wall}) = 0.983$$
$$\left(\bar{L}/\rho\right)_{gas}^{wall}\left(\mu_{en}/\rho\right)_{wall}^{gas} = 1.037$$

The value of $(A_{wall}\beta_{wall})$ is given in ref. (2) and of $\left(\bar{L}/\rho\right)_{gas}^{wall}\left(\mu_{en}/\rho\right)_{wall}^{gas}$ is given in ref (1). The value of

$$N_{x\,Exradin194} = 5.713\times10^{10}\left(R/C\right)$$

was measured on Aug 30, 1994 by comparing to the MGH standard Farmer chamber with a NIST traceable calibration constant.

The AAPM protocol of TG20 (3) defines the proton calibration factor for an ionization chamber with an exposure calibration as

$$PCF = N_{gas}\frac{W_p}{W_e}\left(\frac{1}{\rho}\frac{dE}{dx}\right)_{air}^{tissue}$$

in which we use

$$W_p = 34.3\left(J/C\right)$$
$$\left(\frac{1}{\rho}\frac{dE}{dx}\right)_{air}^{tissue} = 1.141$$

The value of W_p is taken from ref (3) and the value of $\left(\frac{1}{\rho}\frac{dE}{dx}\right)_{air}^{tissue}$ is derived from the stopping powers in ref (4) evaluated at an energy of

100 MeV. Using these values we obtain

$$PCF_{\text{Exradin194}} = 5.468 \times 10^8 \left({}^{\text{Gy}}/_{\text{C}} \right)$$

which is the proton calibration factor for the ionization chamber following the AAPM protocol.

ICRU Exposure based protocol

The forthcoming ICRU protocol calls for new values of W_p and $\left(\frac{1}{\rho} \frac{dE}{dx} \right)_{\text{air}}^{\text{tissue}}$ as well as stipulating that dose to water be specified rather than dose to tissue. An early draft of the report suggested values of (7)

$$W_p = 35.2 \left({}^{\text{J}}/_{\text{C}} \right)$$

$$\left(\frac{1}{\rho} \frac{dE}{dx} \right)_{\text{air}}^{\text{water}} = 1.131$$

Once again the stopping power ratio is evaluated at 100 MeV, however here using the ICRU stopping power tables (5). Using these values we obtain

$$PCF_{\text{Exradin194}} = 5.562 \times 10^8 \left({}^{\text{Gy}}/_{\text{C}} \right)$$

which is the proton calibration factor for the ionization chamber following the ICRU protocol.

Faraday Cup based protocol

The ionization chamber was calibrated in the HCL Room 2 calibration beam using the protocol also described in the TG20 report (3). We use the stopping powers of ref (6) in evaluating the proton dose. The average calibration constant obtained for three runs (8/30/94, 9/27/94, 10/18/94) is

$$PCF_{\text{Exradin194}} = 5.162 \times 10^8 \left({}^{\text{Gy}}/_{\text{C}} \right)$$

Conclusions

To compare each of these calibration constants to the others we present the comparison matrix at the bottom of the page.

We currently follow the Faraday cup based protocol to derive dose for treatments given to MGH patients. If we were to adopt either the AAPM protocol which is currently followed by the Loma Linda University Medical Center group, or the ICRU protocol which will be issued in the near future, physical dose prescribed for patients would be modified in accordance with the ratios presented in the table. Implications for the RBE of proton beams are such that the value of 1.1 currently stated for delivered proton dose following the Faraday cup protocol would be reduced to a value closer to 1.0 .

Ratio Matrix		AAPM	ICRU	Faraday Cup
		5.468E+08	5.562E+08	5.162E+08
AAPM	5.468E+08	1.0000	1.0172	0.9440
ICRU	5.562E+08	0.9831	1.0000	0.9281
Faraday Cup	5.162E+08	1.0593	1.0775	1.0000

References

1. A protocol for the determination of absorbed dose from high-energy photon and electron beams, Medical Physics, 10(6), 741, 1983.

2. Calculated response and wall correction factors for ionization chambers exposed to ^{60}Co gamma-rays, Nath R. and Schulz R.J., Medical Physics 8(1), 85, 1981.

3. Protocol for Heavy Charged-Particle Therapy Beam Dosimetry, AAPM Report 16, 1986.

4. Atomic Data and Nuclear Data Tables, J. Janni , 27(4,5), 1982.

5. Stopping Powers and Ranges for Protons and Alpha Particles, ICRU Report 49, 1993.

6. Calculations of Energy Loss, Range, Pathlength, Straggling, Multiple Scattering, and the Probability of Inelastic Nuclear Collisions for 0.1-1000 MeV Protons, J. Janni ,Technical Report AFWL-TR-65-150, September 1966.

7. Lynn Verhey, Chairman ICRU Proton Beam Dosimetry Committee, private communication. The value of W is currently under review..

UNEVEN RIDGE FILTER FOR CONFORMAL THERAPY AND VARIABLE BOLUS USING FILTERED BACK PROJECTION TECHNIQUE

Yoshinori Hayakawa, Ph.D.

Inst.Bas. Med. Sci., University of Tsukuba, Tsukuba 305 JAPAN

Purpose: Novel method of beam delivery are proposed for therapy by proton beam and/or heavy ion beam. Proposed are an Uneven Ridge Filter for conformal therapy and a Variable Bolus constructed at the site of irradiation.
A Variable Bolus is proposed to reduce the tedious process of manufacturing bolus for each port of a patient, and in the future, to change the dose distribution inside the patient during irradiation, when the dose distribution monitoring become available.
Methods and Materials: Traditional ridge filter is of uniform width of Spread Out Bragg Peak(SOBP). This however irradiate normal tissue above tumor with the same dose with tumor, when the thickness of the tumor depends on the location. Uneven Ridge Filter has uneven SOBP depending on the thickness of the tumor at the location. The ridge filter should be placed a little upstream of the patient with upstream scatterer to smear out the structure of the ridge filter. A Variable Bolus is to be created with many pairs of wedge shaped strips whose overlapping thickness is adjusted by moving the wedge shaped strips. These pairs of wedge shaped strips are to be used to back project thickness of filtered projection of designed bolus. As the negative thickness dose not exist, filtered projection should be increased by a constant that makes the reconstructed bolus uniformly thicker than the designed one. The increased thickness, however, can be compensated by increasing the energy of incident protons or heavy ions.
Results: Exactly speaking, the resultant dose using Uneven Ridge Filter is not conformal with the tumor but will reduce the unnecessary dose to normal tissue. Variable Bolus is uniformly thicker compared to the bolus designed, which can be compensated easily by increasing incident proton energy.
Conclusion: Concerning about Uneven Ridge Filter a quantitative analysis should be achieved from the point of view of Dose Volume Histogram in the actual treatment, together with more realistic computer simulation before application. Also about Variable Bolus, although the principle is valid, detailed design should be made. These are under development in the laboratory.

Proton beam, Ridge Filter, Bolus, Conformal Therapy.

INTRODUCTION

In the conventional treatment by proton beam, conformal therapy can be achieved by 3D voxel scanning or by changing incident proton energy during irradiation(1). These method have problems of creating inhomogeneity of tumor dose due to the movement of target during irradiation. A novel method of creating approximately conformal dose distribution to target volume is proposed. A Variable Bolus is also proposed, which is to be fitted to the tumor to be irradiated at the site of irradiation, while,traditional, fixed bolus manufactured for each irradiation port for each

patient has been used. As the number of irradiation increases, manufacturing boluses become time consuming and will be eliminated if possible. also, the Variable Bolus will enables to change dose distribution during irradiation, when dose distribution monitoring in the patient body will be available in future(2-5).

METHODS AND MATERIALS

Principle of traditional even ridge filter is shown in Fig.1 with the isodose curves. As can be seen from the figure, normal tissue above the tumor is irradiated by the same dose with the tumor. More desirable conformal therapy can be achieved by 3D voxel scanning or by changing incident proton energy during irradiation(1). These methods have problems of creating inhomogeneity of tumor dose due to the movement of target during irradiation. Proposed Uneven Ridge Filter is to create nearly conformal dose distribution compared to the traditional treatment. The principle of Uneven Ridge Filter is shown in Figs. 2 to 4. The width of Spread Out Bragg Peak(SOBP) is dependent on the location due to the difference of tumor thickness. The ridge filter should be placed a little upstream of the patient. Multi-leaf collimator should be moved during irradiation to make the dose distribution in the tumor uniform. This is due to the fact that necessitated

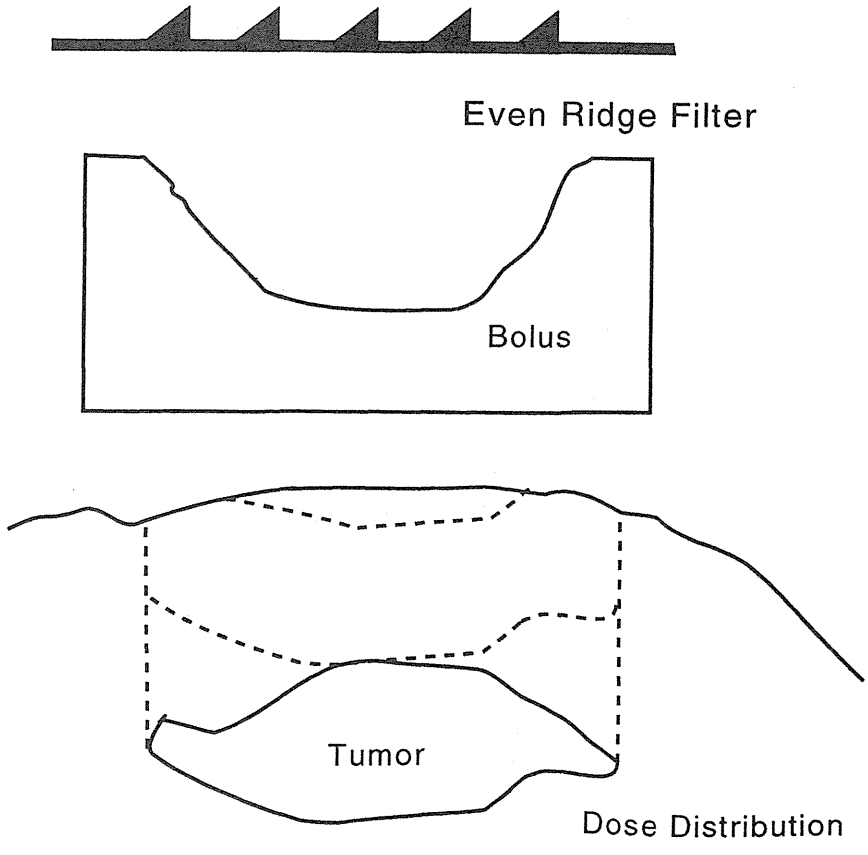

Fig. 1. Traditional even ridge filter and resultant proton dose distribution. Normal tissue near the tumor is irradiated by the same dose with that of the tumor.

proton fluence is less for thinner SOBP compared to thicker SOBP. A scatterer should be placed upstream of the ridge filter to smear out the structure of the ridge filter. The scatterer widens the angular distribution of the beam and increase the penumbra as shown in Fig. 4. Exactly speaking, the resultant isodose distribution is not conformal with the tumor contour.

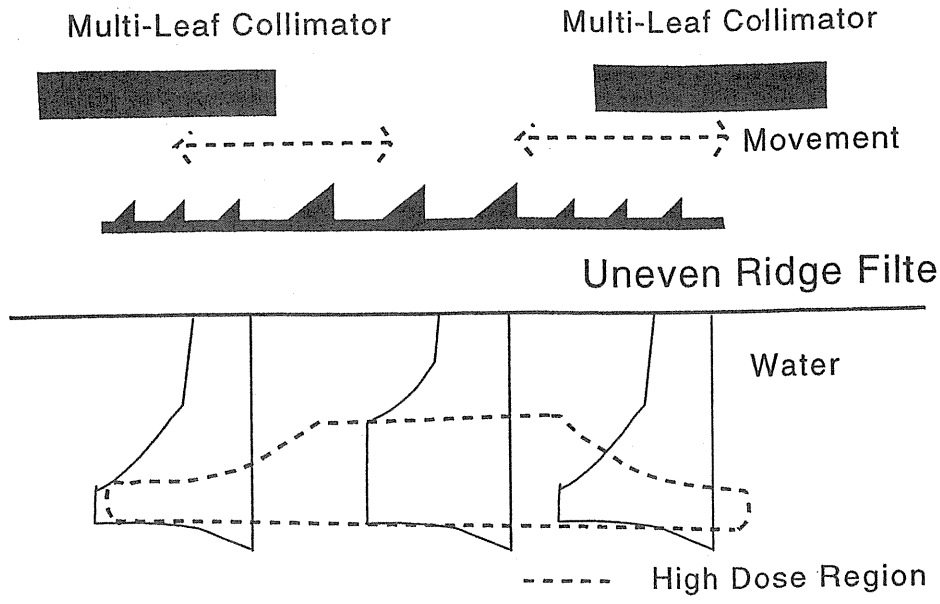

Fig. 2. Principle of the Uneven Ridge Filter(a view perpendicular to the beam).

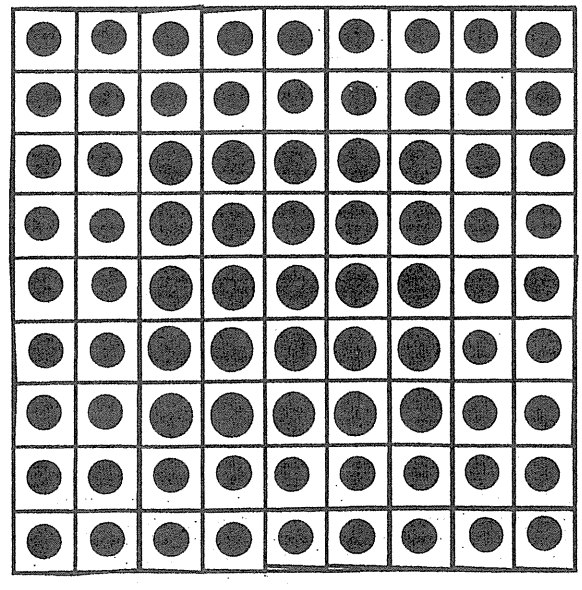

Fig. 3. Principle of the Uneven Ridge Filter(a view parallel to the beam). Each element of the Ridge Filter is square shaped on which cone shaped metal is placed to create energy distribution of proton after passing the filter. Elements is to be connected together to form desired SOBP distribution as types used for the press.

The change of SOBP should be be moderate not to make the dose distribution inhomogeneous due to blurring effect by the scatter. The material of the ridge filter should be of medium Z number such as brass, as high Z material increase the scattering in the ridge filter, while employment of low Z number material increase sharpness of the ridge(cone) and is not suitable for beams with considerable angular distribution to blur the structure of the ridge(cone).
The principle of manufacturing the Variable Bolus is shown in Figs. 5 to 6. First, the thickness distribution of designed bolus due to treatment planing should be lineally integrated to obtain projection data. This process is to be repeated for plural directions. The projections are filtered by suitable mathematical filter, e.g., filter of Shepp and Logan(6). As the filtering process has high frequency enhancing effect, it creates negative value to be back projected. By adding constant value to all the filtered projection, the negative value to be back-projected can be eliminated. The resultant thickness value is then back-projected to create thickness distribution of the Variable Bolus, which is uniformly thicker compared to the original design of the bolus. The

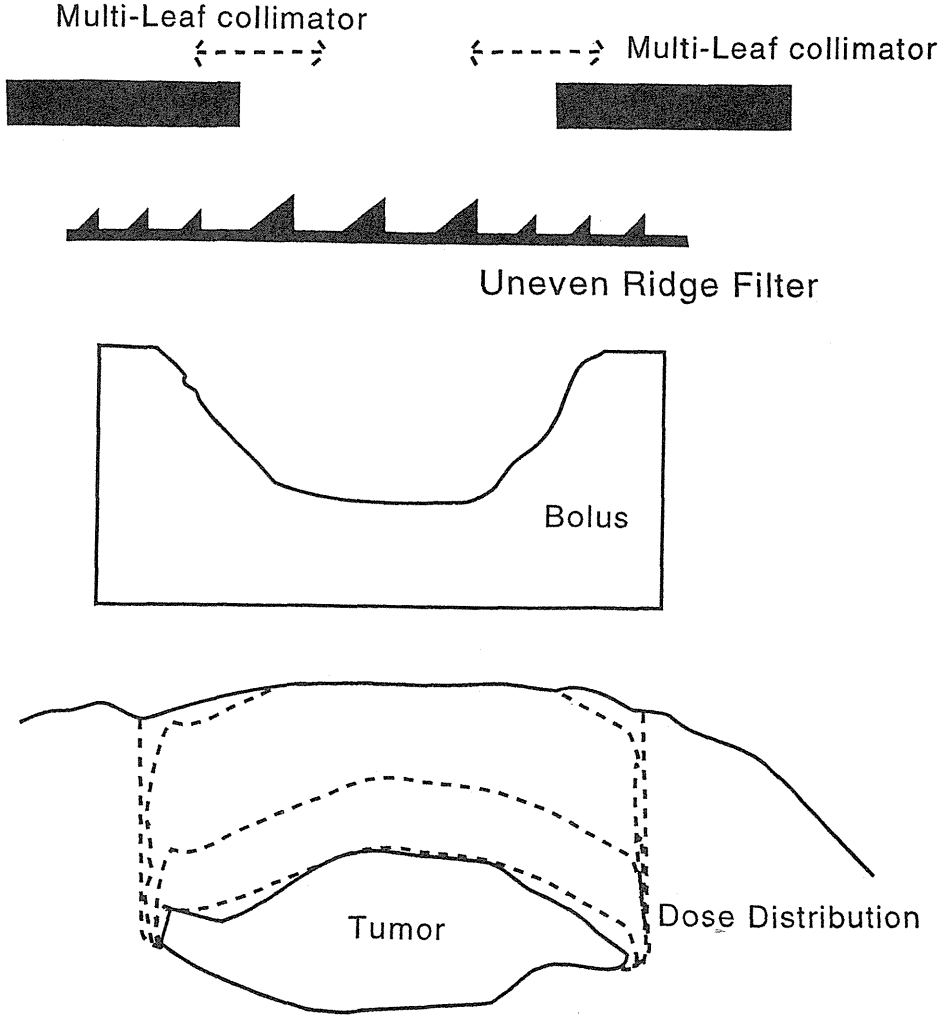

Fig. 4. Uneven Ridge Filter and resultant proton dose distribution.

increased thickens, however, can be compensated simply by increasing the incident proton energy. The back-projection of the thickness is done by strips of wedge pairs, by changing overlapping thickness of them by the movement of ridge pairs(Fig. 7). The materials for wedge pairs should be of low Z number not to increase additional scattering.

RESULTS

Novel methods of beam delivery (ridge filter and bolus) are proposed. The Uneven Ridge Filter seems to be useful for nearly conformal therapy by proton and/or heavy ion irradiation, and the Variable Bolus seems to be useful for efficacy of treatment . The latter seems to cope with the modulation of dose distribution by future dose distribution monitoring inside the patient's body.

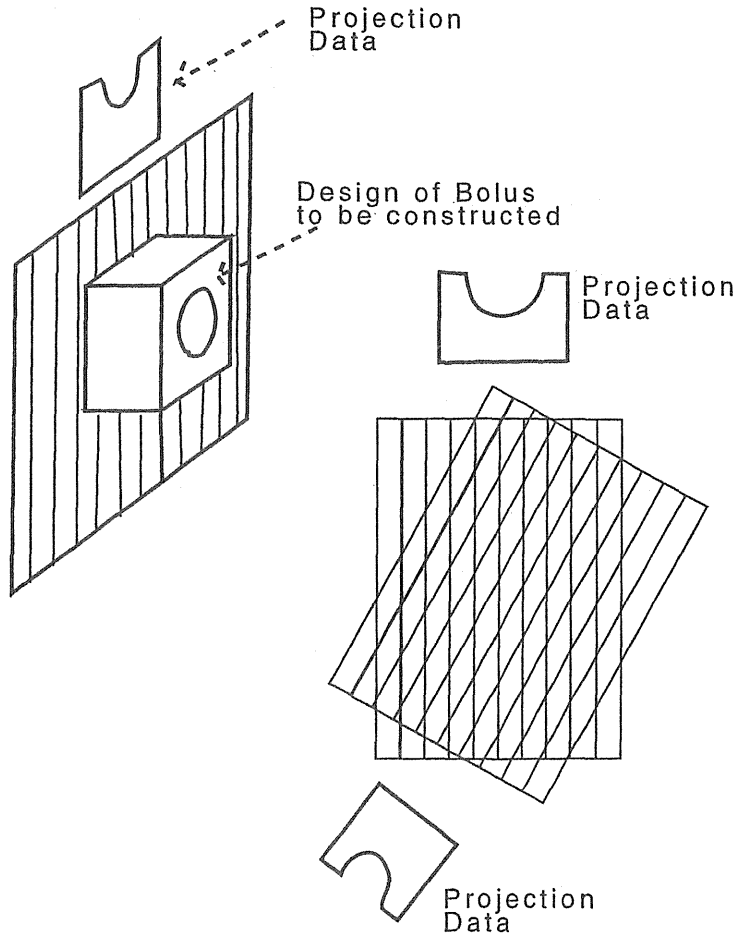

Fig. 5. Data acquisition of Variable Bolus from a designed bolus by treatment planing.

DISCUSSION

In the above, novel methods of creating SOBP and bolus is proposed qualitatively. The problem, however, should be investigated quantitatively. Computer simulation is under development in my laboratory. Especially the effectiveness of Uneven Ridge Filter should be checked from the point of view of Dose Volume Histogram.

REFERENCES

1. Castro, J.R.; Petti, P.L.; Daftsri, I.K.; Collier, J.M.; Renner, T.; Ludwigt, B.; Chu, W.; Pitluck,S.; Glening,T.; Alonso,J.; Blakey, F.; Clinical gain from improved beam delivery system.
   Radiat. Envirom. Biophys. 31 233-240; 1992.

2. Hayakawa, Y.; Tada,J.; Inada, T.; Kitagawa, T.; Wagai, T.; Yosioka, K.; Acoustic pulse generated in excised muscle by pulsed proton beam irradiation and the possibility of clinical application to radiation therapy. J.Acoust. Soc. Jpn.(E) 9 255-257;1988.
3. Hayakawa, Y.; Tada,J.; Inada, T.; Wagai, T.; Yosioka, K.; Acoustic pulse generation in water by pulsed proton beam irradiation and its possible application to radiation therapy. Jpn. J. Appl. Phys. 28(Supple. 28-1) 217-219; 1989.

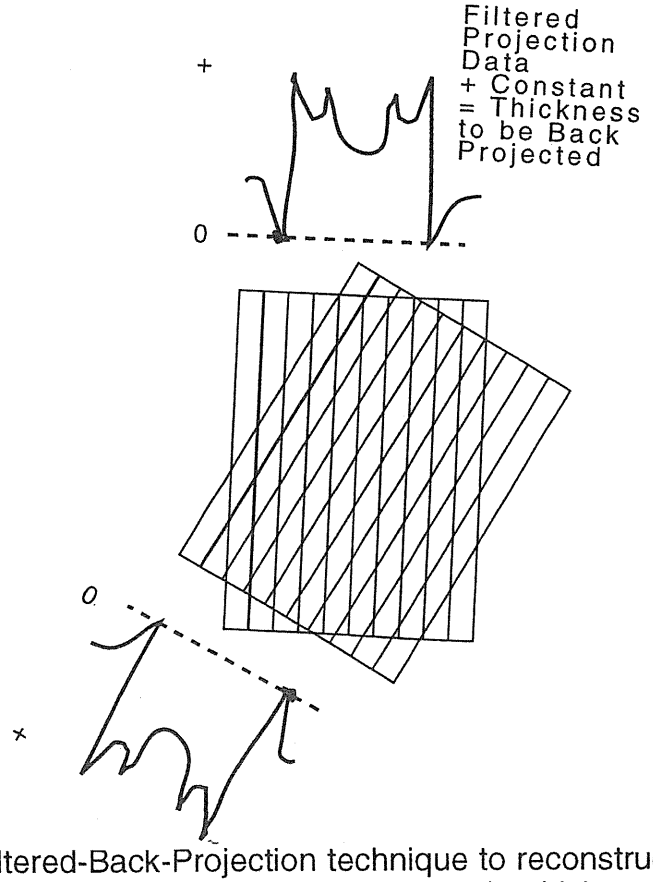

Fig. 6. Filtered-Back-Projection technique to reconstruct designed bolus thickness distribution, where the thickness of the bolus is increased uniformly compared to the designed one. The increased thickness can be compensate by increasing the energy of incident proton energy.

4. Tada, J.; Hayakawa, Y.; Hosono, K.; Inada, T.; Time resolved properties of acoustic pulses generated in water and in soft tissue by pulsed proton beam irradiation-- A possibility of doses distribution monitoring in proton radiation therapy. Medical Physics 18(6) 1100-1104;1991.
5. Hayakawa, Y.; Tada, J.; Inada, T.; Hatanaka, H.; Possibility of application of acoustic pulse generation to dose distribution monitoring during neutron capture therapy. In Advances in Neutron Capture Therapy, edited by Soloway et al., Plenum Press, New York, 1993 pp.181-183.
6. Shepp, L.A.; Logan, B .L.; Proc. IEEE Nucl. Sci. NS-21 21, 1974.

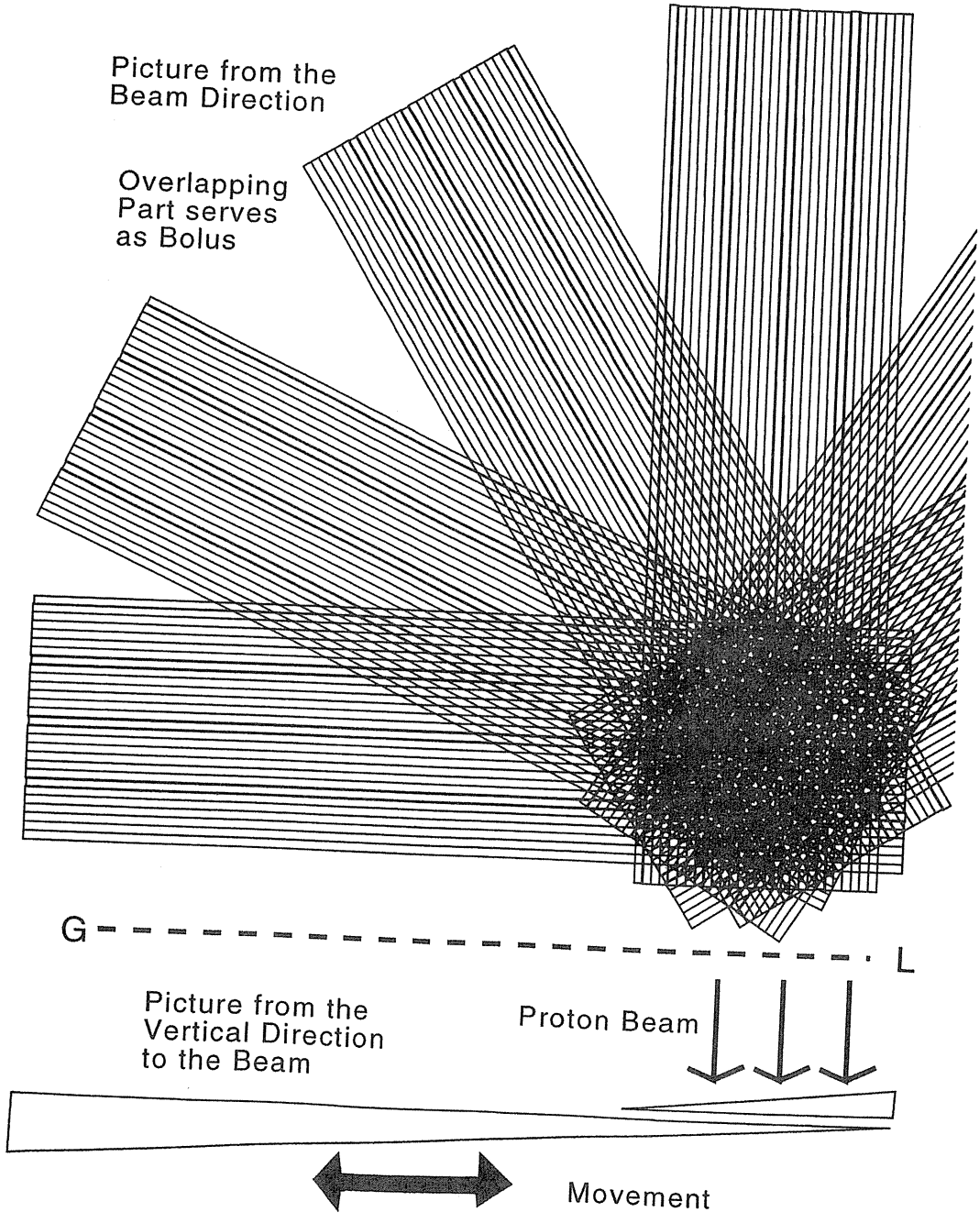

Fig. 7. Structure of a Variable Bolus. Upper part: view from the direction of the beam. Overlapping part serves as bolus.
Lower part: view from the direction perpendicular to the beam.
Pair of wedge strips is moved in a remote manner to adjust the thickness to be back-projected.

Depth-Dose and Fluence Distributions when using Heavy Ion Beams

L. Sihver[1], D. Schardt[1], and T. Kanai[2]

[1]GSI Biophysik, Planckstr. 1, D-64291 Darmstadt, Germany
[2]Division of Accelerator Physics and Engineering, National Institute of Radiological Sciences, 263 Chiba, Japan

ABSTRACT

We have measured the depth-dose distributions for beams of ^{12}C (270 and 330MeV/u), ^{18}O (200, 300 and 400 MeV/u) and ^{20}Ne (670 MeV/u) delivered by the heavy-ion synchrotron SIS using water as a tissue-equivalent absorber. Measurements of depth-dose and LET distributions for ^{12}C at 135 MeV/u were performed at the RIKEN ring cyclotron. We have also developed a one-dimensional model and a computer code for calculating depth-dose, fluence, energy and dose average LET distributions when using either protons or light ions any medium. The calculated depth-dose distributions have been compared to the measured ones and good agreement was obtained for all systems studied.

INTRODUCTION

Energetic heavy ions generally travel in near straight-line trajectories in an absorbing medium and are slowed down by losing their kinetic energy mainly through their multitude of collisions with orbital electrons in the medium. The energy loss per unit path of the absorber traversed by these particles increases with decreasing particle speed, giving rise to a maximum in ionization near the end of their range. Therefore, when a beam of monoenergetic heavy ions slows down, the ionization density rises from a low dose plateau in the entrance region to the Bragg peak near the end of their range, where the ionic charge is reduced by electron pick-up and the ionization falls rapidly to zero when the primary beam stops. For application in radiotherapy, this gives an excellent physical dose distribution. The biological effectiveness (RBE) is also very high in the Bragg peak region, where the ionization density is high and the oxygen effect is reduced or vanished. This gives big advantages when treating deep-seated radio-resistant tumours. For treatment planning, a good knowledge of depth-dose, dose average LET, fluence and energy distributions is very important. We have therefore both developed a one-dimensional model for calculating these distributions when using high-energy protons or heavy ion beams and measured the depth-dose distributions of C to Ne beams at different high energies using water as a tissue-equivalent absorber. These calculations and measurements are also of importance for space missions outside the shielding effect of the Earth's magnetic field where the two main health risks are the highly charged, energetic nuclei in the galactic cosmic rays (GCR) and the sporadic and unpredictable large solar flares. Astronauts exposed to this ionizing radiation will be vulnerable to an increased risk of contracting cancer later in life. To determine this risk of deleterious effects of the GCR to astronauts and the spacecrafts on long missions, one therefore needs a good knowledge of both the radiation environment (particle species, fluence, LET and depth-dose distributions etc.) and the effects of shielding provided by the spacecraft and the bodies of the astronauts.

MEASUREMENTS AND CALCULATIONS

We performed measurements of depth-dose distributions for beams of 270 and 330 MeV/N ^{12}C, 200, 300 and 400 MeV/N ^{18}O and 670 MeV/N ^{20}Ne in water at GSI's heavy-ion synchrotron SIS [1,2] and 135 MeV/N ^{12}C in water at RIKEN ring cyclotron [3]. At GSI, we used two large parallel plate ionization chambers and a narrow circular beam of 5-10 mm width, but at RIKEN, two small ionization chambers and a large uniform irradiation field of around 10 cm in diameter was used. At both

places a computer controlled water target of variable length was placed in between the two ionization chambers.

In our computer code (which will be described in detail elsewhere [4]), the depth-dose, dose-average LET, fluence and energy distributions are calculated simultaneously when using either proton or heavy ion beam in any medium. The user chooses the projectile, beam energy, target, detector material and thickness. The program then reads the atomic weights and the atomic numbers for all fragment isotopes, starting from protons up to Z_{beam}, A_{beam-1}, from an input file. From the same file the program reads the necessary properties of the target and detector material. During the calculation, the target material is first divided into many thin slabs. The thicknesses of these slabs are also set interactively by the user at the beginning of the calculation. The stopping power [5], path-length straggling and the attenuation of the primary beam are calculated in each slab for its whole range. The path-length straggling for the primary particles is calculated by transforming the dE/dx straggling, which is calculated according to a formalism for thick targets developed by Payne [6]. In every slab, i, the dose contribution from the primary beam is calculated according to

$$DOSE(i) = \frac{dE(i)}{dx}\,\phi(i), \qquad (1)$$

where dE(i)/dx is the stopping power of the primary particles in slab i and $\phi(i)$ is the average fluence of these particles in this slab. The program also calculates the energy loss in the detector gas for the primary particles. The production of each possible projectile fragment, the momentum loss and spread due to the fragmentation process and its stopping power (dE/dx) is also calculated in somewhat thicker steps along the beam path. Both the beam attenuation and the production of the secondary and the tertiary fragments are calculated with semiempirical formulas, which will be described in detail elsewhere [7]. The momentum loss and spread are calculated using a model based on the participant-spectator picture of high-energy nuclear collisions [8]. This model uses three empirically-fitted microscopic non-adjustable nuclear-transport parameters. During their path through the target, the secondary fragments are attenuated and tertiary fragments are produced. The production of these tertiary fragments is also calculated in the same way as for the secondary fragments, but these fragments are not attenuated and no particles of higher order are assumed to be created. The path-length straggling for the secondary and the tertiary particles are considered negligible and are not calculated.

When calculating the dose contribution from the secondary and the tertiary fragments, the range, r', for a given energy E'(k,i) is first calculated from the stopping power-range relations for each fragment k. After that, the energy E''(k,i) corresponding to a new range, r''=r'-Δx, is calculated. In each slab, i, the dose contribution from each secondary or tertiary particle k is then calculated according to

$$DOSE(k,i) = \frac{E''(k,i) - E'(k,i)}{\Delta x(i)}\,\phi(k,i), \qquad (2)$$

where E''(k,i) and E'(k,i) are the energies of the particle k at the exit and the entrance of slab i, respectively. Δx(i) is the thickness of slab i and $\phi(k,i)$ is the average fluence of particle k in this slab. The total dose average LET in each slab i is then calculated according to

$$\frac{\sum_k \left[\frac{dE''(k,i)}{dx} + \frac{dE'(k,i)}{dx}\right] DOSE(k,i)}{2\sum_k DOSE(k,i)}, \qquad (3)$$

where dE''(k,i)/dx and dE'(k,i)/dx are the stopping powers of particle k (which both can be a primary particle, a secondary or a tertiary fragment) at the exit and the entrance of slab i, respectively.

In Fig. 1, we show our calculated fluence distributions in comparison with the experimental data from ref. [9]. For the measured depth-dose distributions, the material in the beam line prior to the water target was approximated by a "water equivalent" thickness. Both the total fluence and the total depth-dose distributions are first normalized to 1.0 at zero target depth in our calculations and then the calculated distributions are normalized to the measured ones in the first data point.

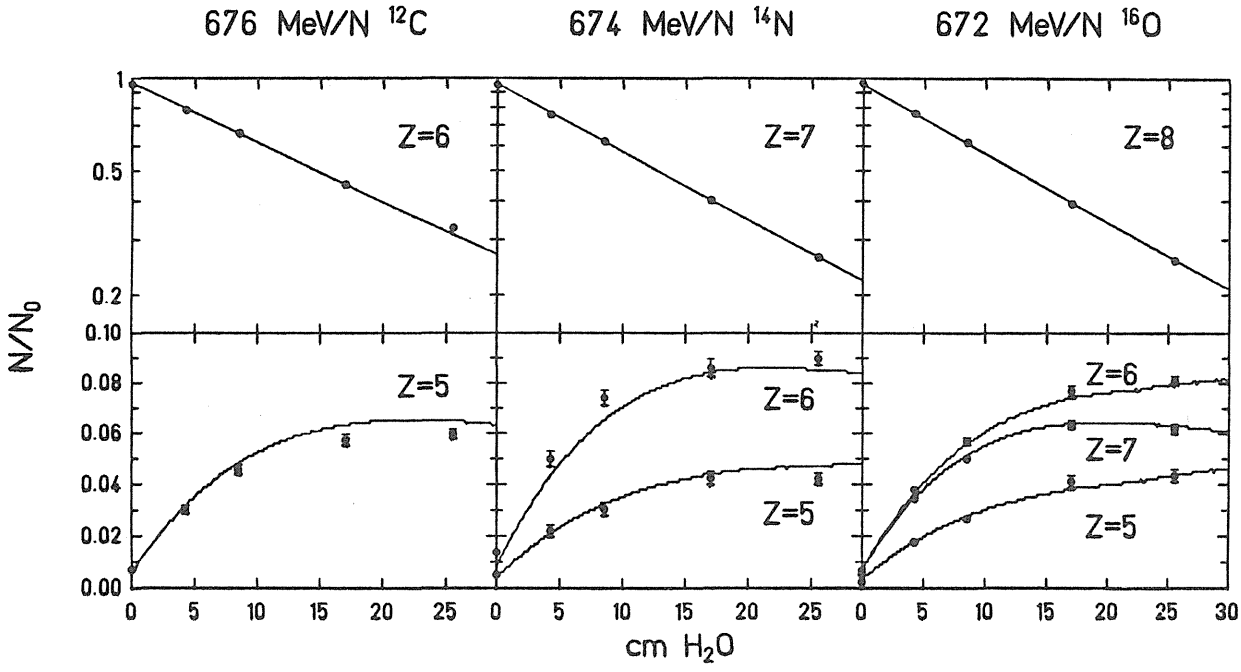

Fig. 1. Measured (solid points) [8] and calculated (solid lines) [2] fluence distributions for 676 V/N ^{12}C, 674 MeV/N ^{14}N and 672 MeV/N ^{16}O in water.

In Fig. 2, we show our calculated depth-dose distributions for 135, 270 and 330 MeV/N ^{12}C in water, together with our measured Bragg curves.

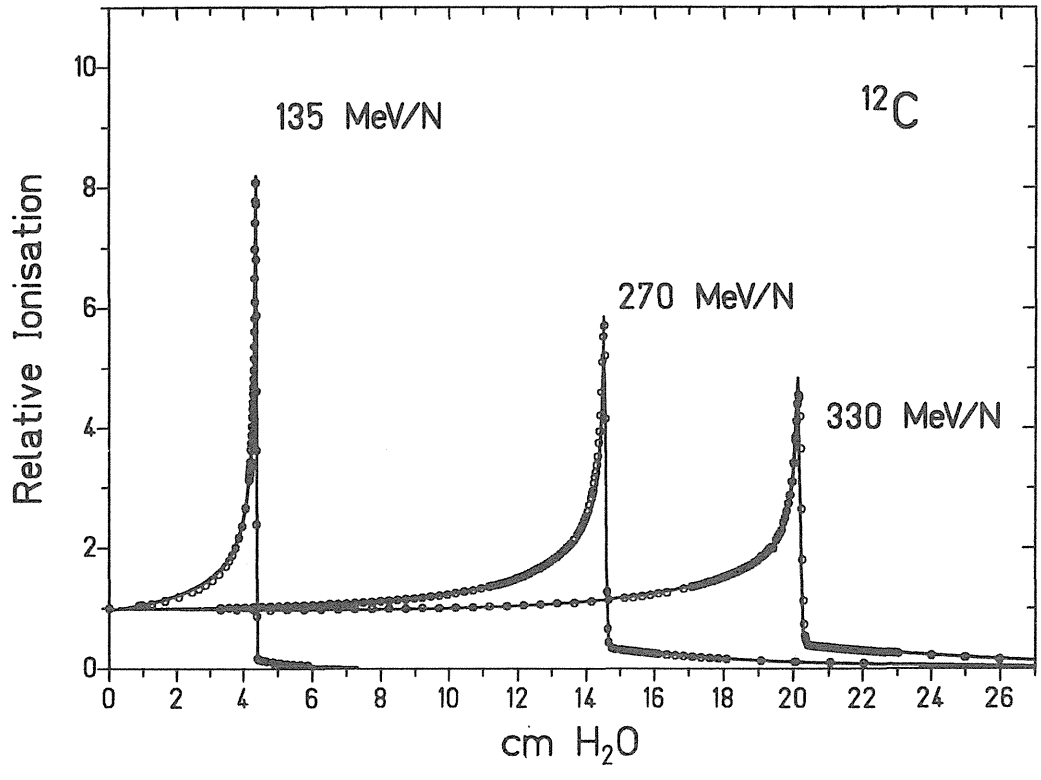

Fig. 2. Calculated depth-dose distributions for 135, 270 and 330 MeV/N ^{12}C in water [1,2] (open circles), together with our measured total Bragg curves (solid lines).

SUMMARY

A one-dimensional physical beam model when using protons or heavy ions in any medium has been developed. This model calculates simultaneously depth-dose, dose-average LET, energy and fluence distributions. We have also measured the depth-dose distributions of ^{12}C, ^{18}O and ^{20}Ne beams in water at different high energies. The measured distributions were compared to the calculated ones and good agreement was obtained for all system studied

REFERENCES

[1] L. Sihver, D. Schardt and T. Kanai, GSI Scientific Report 1993, 233 (1994).

[2] L. Sihver, D. Schardt and T. Kanai (to be published).

[3] T. Kanai, S. Minohara, T. Kohno, M. Sudou, E. Takada, F. Soga, K. Kawachi, A. Fukumura and F. Yatagai, NIRS-M-92, HIMAC-004, NIRS, Japan (1993).

[4] L. Sihver (to be published).

[5] W. Heinrich, B. Wiegel, and G. Kraft GSI Report 91-30 (1991).

[6] M.G. Payne, Phys. Rev. 185 (1969) 611.

[7] L. Sihver (to be published).

[8] C.H. Tsao, R. Silberberg, A.F. Barghouty, and L. Sihver ApJ (submitted).

[9] I. Schall, Ph.D. Thesis, Technische Hochschule Darmstadt, 1994.

PATIENT POSITIONING SYSTEM IN HIMAC

S.Minohara, M.Endo, T.Kanai, H. Koyama-Itoh, N.Miyahara, F.Soga and K.Kawachi
Division Accelerator Physics and Engineering, National Institute of Radiological Sciences,
4-9-1 Anagawa, Inage-ku, Chiba-shi 263 Japan

We developed the computer aided patient positioning system in HIMAC treatment room. In our system, Two each orthgonal X-ray televisions are used to verify the patient position. X-ray images of patient on the treatment couch are immediately displayed on the positioning computer screen, and the difference from the planning position is calculated in the computer. Positioning computer is linked with the control console of treatment couch, and we are able to set the couch semi-automatically. In addition, image data of positioning are digitally stored.

Introduction

In particle radiation therapy, patient positioning means that the target of patient is exactly set along the treatment room coordinate system. It is very important that the patient target figured at treatment planning is always positioned accurately, quickly and easily to the beam iso-center. Various parameters of shaping devices of irradiating field are determined according to the location and shape of target. These parameters follow the coordinate system of beam line in the treatment room. For example, the contour of target from beam's eye view must be fitted accurately to the shape of the beam defined by patient collimator.

Conventionally X-ray films are used to verify the patient position. But daily setup verification of film method is time-consuming because of development of film and calculation of difference from planning position. We developed the computer aided patient positioning system using digital X-ray television. In this system, X-ray TV images are used to verify the patient position. X-ray images of patient are immediately displayed on the computer screen, and the difference from the planning position is calculated in the computer. Furthermore, image data of positioning are digitally stored.

Data flow of positioning

For treatment planning, X-ray CT images of the patient are taken after the patient is immobilized by fixation device. Then three dimensional treatment planning is performed. The program of treatment planning produces the summary data file for irradiation. The summary file includes parameters of port devices and treatment aids of beam's eye view alignment. The aids include digitally-reconstructed radiographs (DRRs), the coordinates of landmarks and contours of target and collimator. The summary file for each patient is transferred to treatment control computer following treatment schedule.

The computer network of positioning system in HIMAC is shown in figure 1. The summary file of each patient is stored in the treatment control computer and the data are referred at each time of treatment. For examples, treatment control computer controls beam port devices and positioning computer mainly handles image data for patient alignment. Most of the operations are performed with touch panel screen switch except for ON-OFF of beam and X-ray. Each image data of positioning is stored digitally in the computer, and will be sent to HIMAC treatment database that we are developing now.

The couch can be operated in six different movements; three translations and three rotations. The couch motion is controlled manually and semi-automatically to preset position. The range, maximum and minimum speed and accuracy of treatment couch is shown in table 1. The mechanical accuracy of couch position is within $\pm$ 0.5 mm.

Before the first irradiation of each patient, we simulate the treatment in the irradiation room to check the patient position and port parameters. If necessary, re-planning is performed and parameters are corrected.

All positions and movements are stated in terms of treatment room coordinate system with its origin at an isocenter.

Process of aligning the patient position

Figure 2 shows the flow chart of the patient positioning in HIMAC treatment room. At first, the patient is immobilized on the treatment couch by using fixation device such as a plastic mask. Then, the couch is moved to align the marks on the fixation device with laser lines indicating the three axes of the coordinate system. At the same time, laser light localizer which spread out the laser light by using the lens system simulates the broad beam , and is used to project the shape of the irradiating field formed by the collimator on the surface of patient.

Final alignment is performed with internal anatomy on the X-ray images. Two each orthogonal X-ray images are taken into positioning computer. Projected X-ray images are compared with DRRs referring landmarks and other anatomical features. After that, radio-technologist move the patient to the correct position. Then, X-ray images are taken repeatedly to check the patient position.

X-ray TV system

Two each orthogonal X-ray TV systems are provided. One is incorporated in the beam port. Distance from the X-ray focus point to the isocenter is 200 cm and distance from the isocenter to the image intensifier (II) is 50 cm. During the patient positioning, X-ray sources and IIs are set on the coordinate axis. X-ray source in the port is inserted into the beam line. Horizontal X-ray TV comes down from the ceiling and vertical X-ray TV is carried under the couch, and set on the center of axis. Two orthogonal X-ray TV images are taken into the positioning computer. X-ray TV image is corrected through the digital image filter in the computer because X-ray TV image is distorted by the characteristic of II. Filter function of each X-ray TV is defined experimentally.

Landmark method

To compare the target position with planning one, our positioning system has three methods. One is a three-dimensional landmark method. Another method are two-dimensional landmark method and two-dimensional manual method. Anatomical features such an edge of bone, or implanted markers are useful as landmarks. DRRs and X-ray TV images are shown on the image screen of positioning console. Referring landmarks on DRRs, radio-technologist sets points of landmarks on X-TV images by digitizer coupled to image screen.

In the three-dimensional landmark method, three-dimensional coordinates of landmarks are reconstructed by two projected images. Figure 3 illustrates the projection geometry. Landmark **R**(x,y,z) is projected on $\mathbf{T_1}(x_1, y_1)$ and $\mathbf{T_2}(y_2, z_2)$. **R**(x,y,z) can be calculated as

$$x = \frac{L_1(L - z_2)}{L^2 - z_2 x_1} x_1 \quad (1), \quad z = \frac{L_1(L - x_1)}{L^2 - z_2 x_1} z_2 \quad (2)$$

$$y = \frac{L_1(L - z_2)}{L^2 - z_2 x_1} y_1 \quad (3), \quad y = \frac{L_1(L - x_1)}{L^2 - z_2 x_1} y_2 \quad (4)$$

$$L = L_1 + L_2 \quad (5)$$

where L_1 is the distance from the X-ray focus spot to the isocenter and L_2 is the distance from the isocenter to X-TV. The three unknowns x, y, z are determined from equations (1)-(4) by using the least-squares method. Because setting points have digitizing errors. The coordinates of landmarks are compared to those of treatment plan, and the displacement length of treatment couch is calculated.

The relation of setting point and planning point are shown as

$$\mathbf{Pi} = \mathbf{M}\ \mathbf{Ri} \quad (6),$$

where **Pi** is the coordinates of planning landmark of i-th and **Ri** is the coordinates of setting one, and **M** is a three dimensional translation matrix as illustrated in figure 4, where

$$Pi = \begin{pmatrix} Xpi \\ Ypi \\ Zpi \\ 1 \end{pmatrix}, \quad Ri = \begin{pmatrix} Xri \\ Yri \\ Xri \\ 1 \end{pmatrix}$$

$$M=\begin{pmatrix} A & B & C & -X0 \\ D & E & F & -Y0 \\ G & H & I & -Z0 \\ 0 & 0 & 0 & 1 \end{pmatrix}$$

$A = \cos\alpha \cos\beta$
$B = \cos\alpha \sin\beta \sin\gamma + \sin\alpha \cos\gamma$
$C = -\cos\alpha \sin\beta \cos\gamma + \sin\alpha \sin\gamma$
$D = -\sin\alpha \cos\beta$
$E = -\sin\alpha \sin\beta \sin\gamma + \cos\alpha \cos\gamma$
$F = \sin\alpha \sin\beta \sin\gamma + \cos\alpha \sin\gamma$
$G = \sin\beta$
$H = -\cos\beta \sin\gamma$
$I = \cos\beta \cos\gamma$

$X0$; move along to X-axis
$Y0$; move along to Y-axis
$Z0$; move along to Z-axis
α ; rotate around the Z-axis (rotation)
β ; rotate around the Y-axis (rolling)
γ ; rotate around the X-axis (pitching).

The best matching between planning landmark and setting landmark is obtained by minimizing S as

$$S=\sum_i (M\,Ri - Pi)^2 \quad (7)$$

The least-squares method calculates **M**. To solve this equation, we need more than three landmarks.

Another method are two-dimensional landmark method and two-dimensional manual method. Two projected X-ray images are used independently. In the two dimensional method, the coordinates of landmarks are calculated on each image, and are compared to corresponding plan in two dimension. However two dimensional method isn't sensitive the rolling error of position.

In the manual method, shift length on each image is set manually by radio-therapist. Following tools to manipulate the image are useful.

(1)Measure of the distance between two points on the each image.
(2)Measure of the distance from the point on the DRR to the corresponding point on the X-ray image in the same coordinate system.
(3)Transfer and rotation of projected image. These simulate the movement of treatment couch.
(4)Overlay of the target and collimator contours.
(5)Magnification of each image.
(6)Adjustment of window and leveling.

Clinical trial and Present study

In this June, we started clinical trial in HIMAC. Treatments of three patients were finished. Each patient was fixed by plastic mask, and we took the X-ray film images at every fraction to record and analyze the positioning in addition to X-ray TV images. In these cases, we used two dimensional manual method for the patient positioning. Because it was difficult to point out the anatomical landmark on two orthogonal images. Point of landmark is clear on one image, but not always clear on the other image. In such a case, we think two dimensional landmark method is useful. However the present console for image isn't comfortable to daily operation, so we are improving now. To use three dimensional landmark method clinically, we think we need more empirical knowledge of a kind of landmark in each irradiating part.

It took about ten to twenty minutes to set the patient and a few minutes to irradiate, and then total treatment time of each patient was about thirty minutes in first clinical trial. But now, it takes about twenty minutes for the treatment of each patient because radio-technologists have been accustomed to operate the consoles and devices. Currently, we are able to treat three patients within one hour in each treatment room.

In addition to X-TV system, we have CT scanner in the treatment room. But we haven't used it yet clinically. It is possible to scan the patient with the treatment condition. The couch on the irradiating position can be displaced to scanning position. Since the coordinate system of each position is defined geometrically, the coordinates of points on CT images can be stated by treatment coordinate system. Now we are investigating the positioning method based on CT image in the treatment room. We think CT image is very important to verify the position of target and critical organ around abdomen.

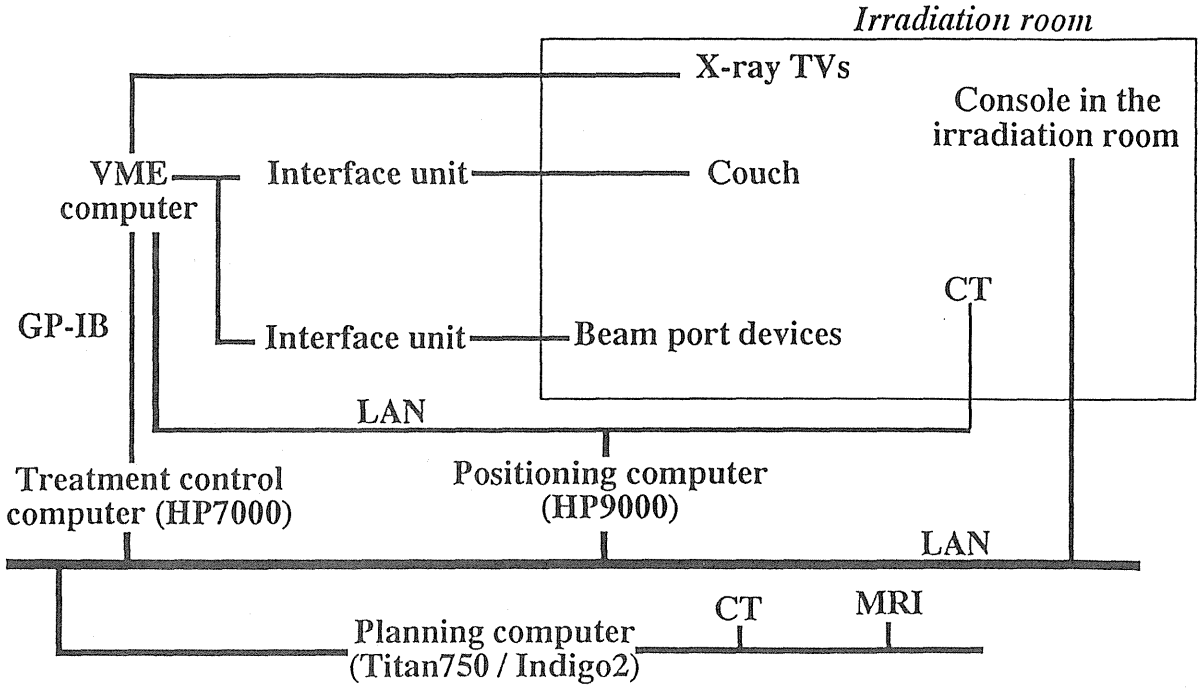

Fig. 1 Network of patient positioning system

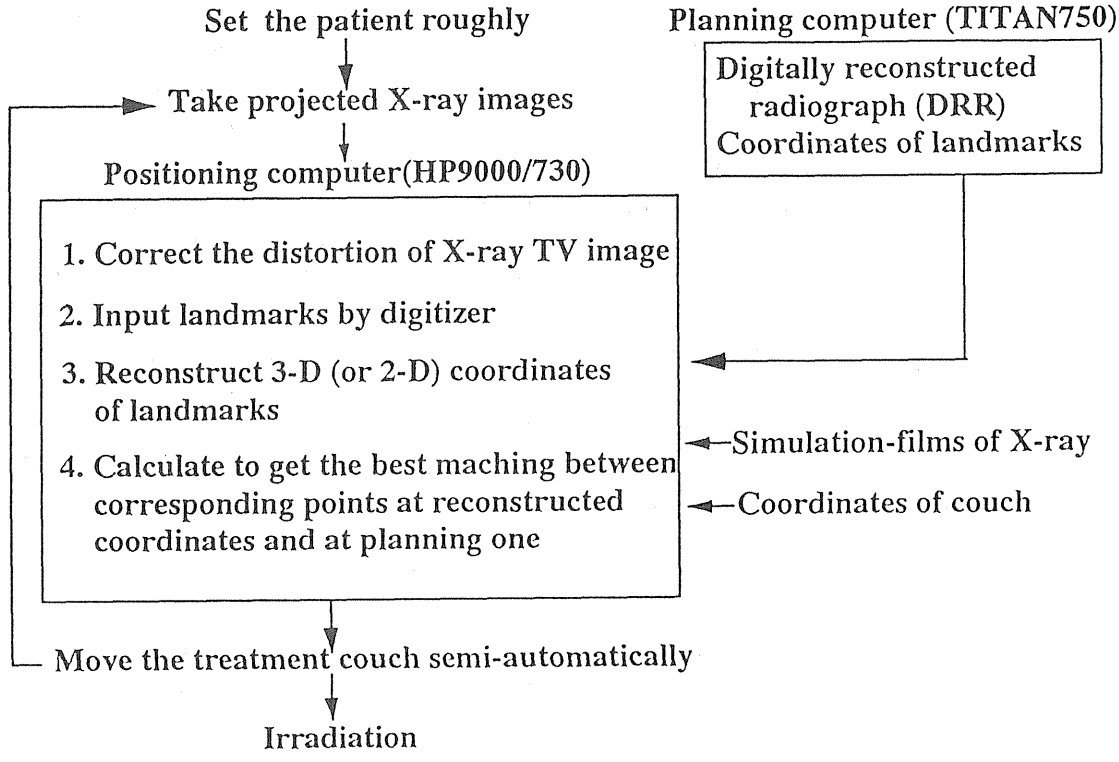

Fig. 2 Flow chart of patient aligning in HIMAC

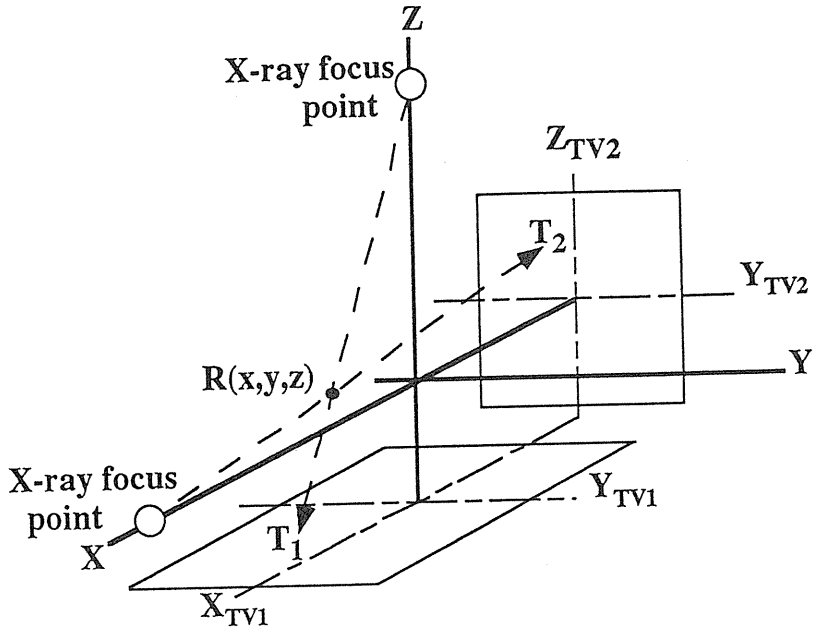

Fig. 3 Projection geometory of landmark

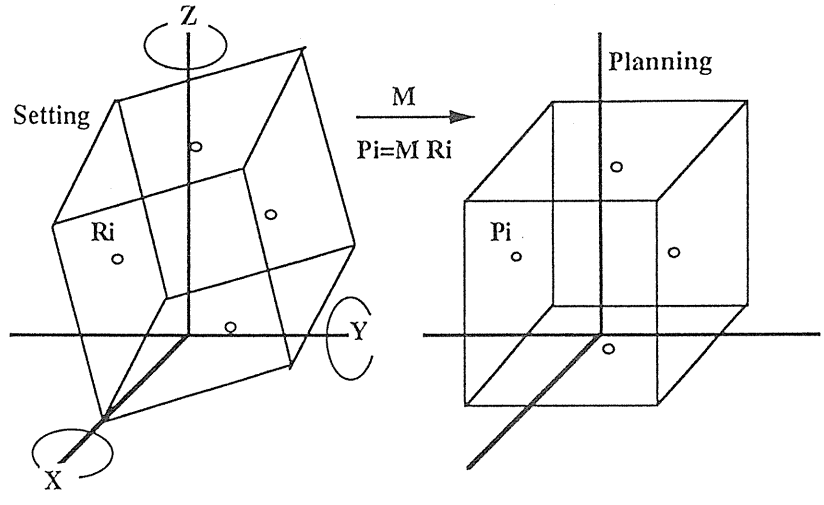

Fig. 4 Relation of setting points and planning points

Table 1 Motion of the treatment couch

	Range	Max.speed	Min. speed	Accuracy
Up and Down	500mm	30mm/s	1mm/s	±0.5mm
Fore and Back	750mm	50mm/s	1mm/s	±0.5mm
Lateral shift	±150mm	20mm/s	1mm/s	±0.5mm
Rotation	260°	12° /s	2° /s	±0.5°
Pitching	±10°	1° /s	1° /s	±0.1°
Rolling	±10°	1° /s	1° /s	±0.1°

Treatment Planning

A convolution model for proton beam treatment planning dosimetry

D. Miller, S. Vatnitsky, J. Siebers, M. Moyers

Loma Linda University Medical Center

A. Model Description

A general convolution equation for synthesizing dose distributions for radiation therapy photon and charged particle treatment beams may be expressed as follows:

$$D = [\,(1 - \beta)\, P \times vs + \beta\, (P \times vs) \times cs] \times mc \qquad (1)$$

where D represents the distribution of radiation dose
- P represents the "primary" dose distribution (defined below)
- β = Compton scatter fraction in photon beams
- vs is a virtual source spread function
- cs is the Compton scatter spread function
- mc is the multiple Coulomb scatter spread function
- x signifies convolution

Primary dose at a point the treatment field is:

$$P(d, x, y) = DD(d)\ OCR(d, r)\ ISL\ I(x, y) \qquad (2)$$

where d = depth in the medium
- r = distance from the beam central axis
- DD = measured, large-field (full scatter) central axis depth dose
- OCR = large field (full-scatter) beam profiles at multiple depths
- ISL = inverse square law correction
- I(x, y) = distribution of intensity modification factors

The convolution approach mathematically scatters dose away from a full-scatter, sharp-edge primary dose distribution in contrast to a pencil beam approach that builds up dose and scatter by superposition of small beams. The primary dose distribution in the convolution model is a shaped portion of radiation field cut from an infinite size (full scatter) dose distribution. Convolution kernels *vs*, *cs* and *mc* from equation (1) are normalized to unity. Therefore, convolutions with these kernels have no effect on integral dose but smear and spread the primary distribution according to the effects of finite source size, Compton scatter and multiple Coulomb scatter. An advantage of this method is its reliance on measured large-field dose distributions for primary characterization of treatment fields. For example, off-axis beam penetrability variation, common in photon beams, is handled by means of the measured OCR table rather than by varying pencil beam characteristics as a function of location in the field.

The model approximates the effects of finite source size and beam scatter by depth-dependent lateral spread convolutions. This is accomplished by application of variable, two-dimensional convolution kernels over the three-dimensional distribution.

For charged particle beams the convolution equation reduces to the following expression:

$$D = [P \times vs] \times mc \qquad (3)$$

For a charged particle beam with no intensity modification other than field shaping, the primary dose intensity modification factor distribution I(x, y) may be replaced by $\delta_{Ap} = 1$ within the projection of the aperture opening and zero elsewhere.

The effects of finite source size are approximated by assuming the existence of a radial distribution of source intensity within a plane passing through an effective source location. The source intensity distribution is projected to a point at the field edge defining device and expands geometrically from that point to form a virtual source convolution kernel that varies with distance from the collimating device. A Gaussian virtual source intensity distribution is assumed. $P \times vs$ is the three-dimensional source-smeared primary dose distribution.

The effect of multiple Coulomb scattering is approximated by convolution of the source-smeared primary distribution with a depth dependent Gaussian spread function. In the current implementation of the model, the multiple scatter spread function for a given incident proton beam energy is precomputed as a function of depth in water and applied according to the water-equivalent depth at the point of scatter within a heterogeneous medium.

B. Results

In clinical practice the distribution of dose within patient treatment fields must be predicted to facilitate treatment planning, and the calibration of treatment portals must be determined for delivery of the prescribed dose. Treatment planning dosimetry models should be capable of predicting both quantities. The convolution model described above was tested by comparing computed treatment field calibration ratios and dose profile shapes with physical measurements for small proton treatment fields produced at the Loma Linda proton therapy facility. Calibration ratio in this study is defined as dose at a reference point in the treatment field relative to dose at a point within a standard calibration field. Small proton treatment fields were selected as a first test of the model because of the growing demand for their use in the clinic and because of the difficulty in modeling their dosimetry characteristics.

Measurements and model computations were compared for a 1 x 1 cm, 155 MeV field with 2 cm range modulation and a 2 x 2 cm, 250 MeV field with 3 cm range modulation. The measurements were performed in water with a diamond detector and Wellhofer field scanner. The results of this comparison are presented below in the form of lateral dose profiles for depths in the entrance region and near the center of modulation. Relative dose in these figures are dose within the test fields normalized to dose on the central axis at the depth of the center of modulation of 14 x 14 cm calibration fields. Note that beam profiles were not corrected for centering in the water phantom. The results indicate prediction of dose on the central axis relative to the large fields to within approximately 2.0 percent and good agreement between measured and computed dose profile shapes.

155 MeV protons, field 1 x 1cm

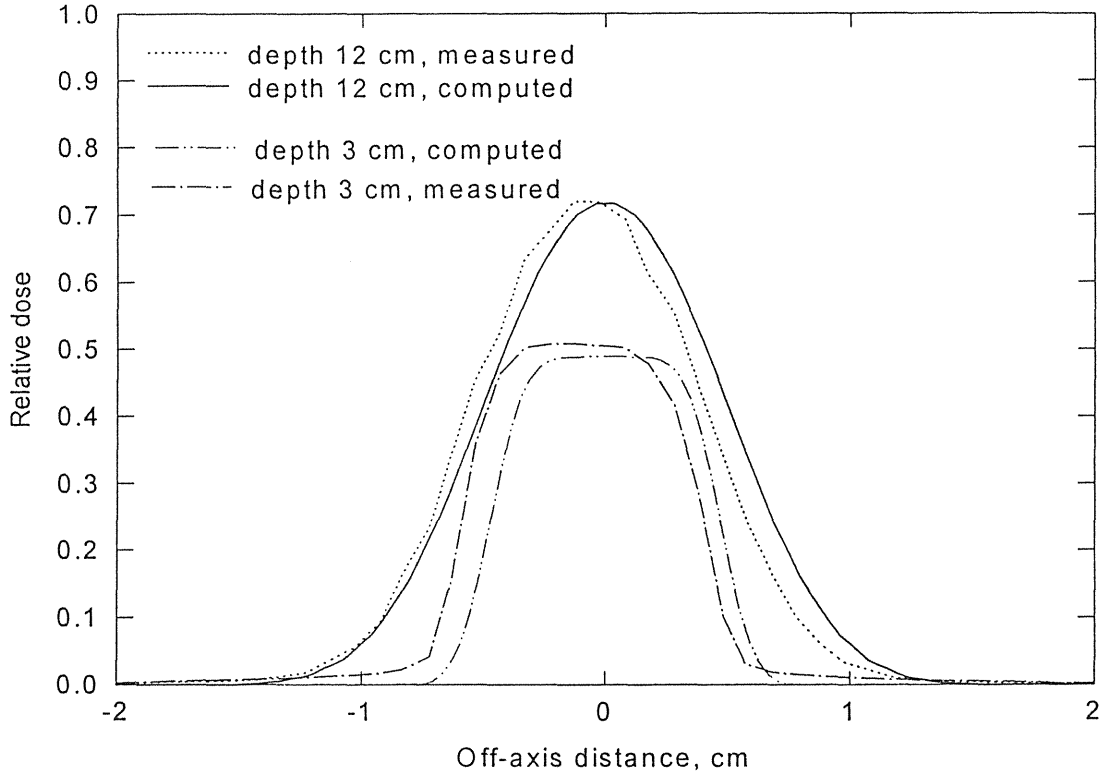

250 MeV protons, field 2 x 2 cm

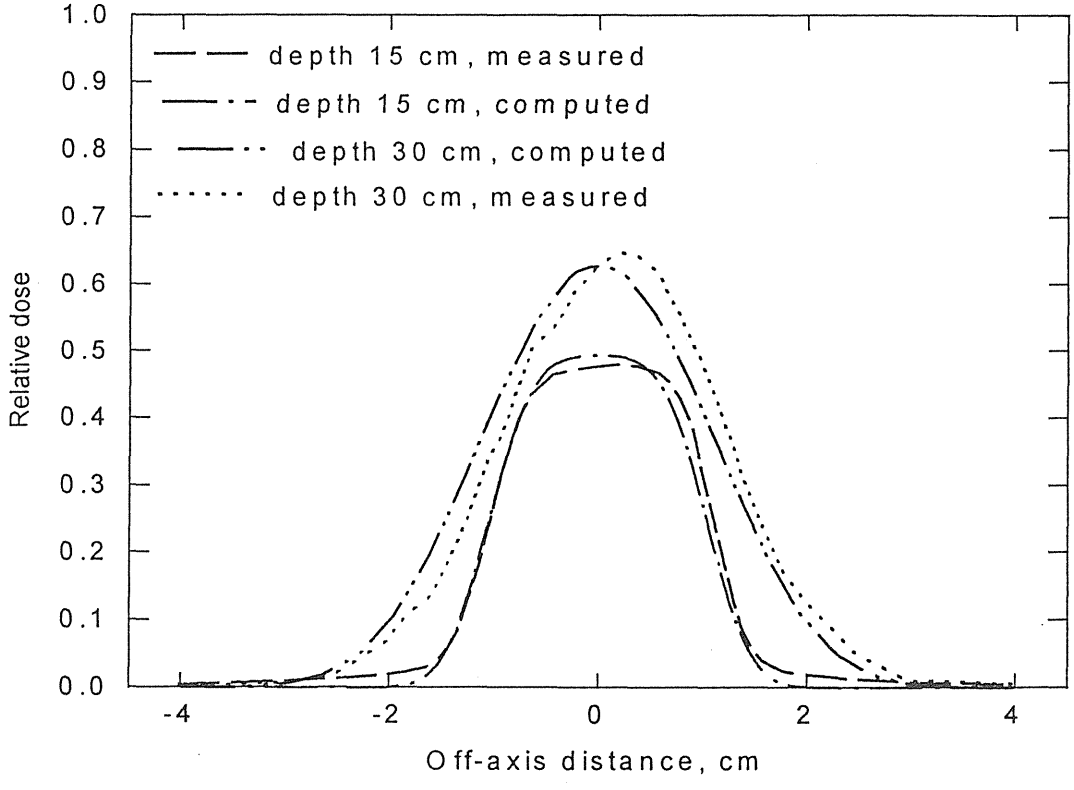

Eye Treatment Planning at Clatterbridge

M. Sheen and A. Kaçperek

Douglas Cyclotron Unit, Clatterbridge Centre for Oncology, UK

Statistics

Some 570 patients have now been treated for uveal melanoma or haemangioma at the Douglas Cyclotron Unit; we give here a description of the normal planning routine.

We plan and treat approximately 120 patients per year, with a staff of 2 or 3 physicists and two radiographers. There are approximately 16 treatment weeks per year, when 1 physicist and 2 radiographers carry out the actual treatment. Simulations are performed by two staff members, normally during the one or two weeks before treatment. We normally perform up to 4 simulations per day. Planning is performed by one of the physicists or radiographers.

Simulations

We usually take simulation radiographs with the fixation light in around 5 different positions.

The rationale for the simulations is:

1) To provide a basis for the computer model

2) To establish the range of fixation angles comfortably achievable by the patient

3) To test the patient's consistency of fixation

4) To measure the eye's degree of twist (torsion) for the final plan

In view of the above, we generally:

1) make a best guess at the final fixation azimuthal angle, and explore the practical limit of polar angle. The azimuthal angle used would normally be opposite the tumour location, so as to present the tumour to the beam

2) use azimuthal angles of 30° either side of 1), and with similar polar angles

3) use a more moderate polar angle if in doubt that the patient is actually reaching the extreme

4) use an opposing azimuthal angle, if there is the possibility of treating <u>through</u> the eye ie. for a small posterior tumour

5) get the patient to look straight ahead, to provide a reference position of nominally zero twist.

Finally we draw the eyelids, with the patient fixating in our best-guess treatment position(s). We use a field-area light with a 20mm diameter collimator to provide a position reference, and draw the lids in lateral, superior and frontal aspects. We may well draw the lids both retracted and unretracted, to be able to choose the most appropriate arrangement for the plan; retraction is performed informally with a finger.

Planning: Equipment

We currently use a Digital MicroVAX II computer, with three graphics terminals, two digitisers and a laser printer. This computer was chosen as it had to be a VAX for compatibility with PSI and this machine was available. Its performance satisfactory if slow, but it is expensive to maintain as it is obsolete. It is used as a stand-alone system.

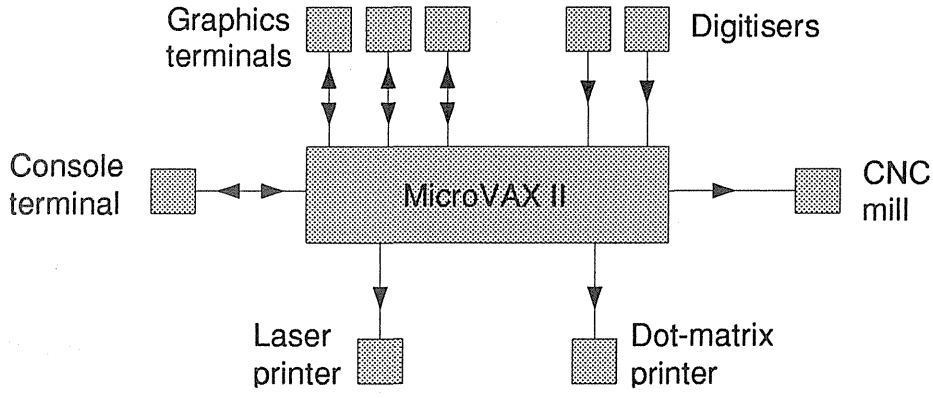

The terminals are Tektronix 4105 emulators, which combine graphics and text on the same screen.

The digitisers are GTCO Digi-pads, with a resolution and accuracy of 0.08mm. We estimate the reproducibility of clip digitisation as around 0.2mm, so the result is not limited by the digitiser.

We are now in process of replacing the MicroVAX with a Digital Alpha AXP 2000/300, which is both faster and cheaper to run; the saving on maintenance costs will pay for it in four years. The MicroVAX will be retained as a back-up, linked with the MicroVAX to port program and data files.

The planning program used is EYEPLAN, as written originally at MGH Boston and developed at PSI and Clatterbridge. It uses the GRAPHX graphics interface from PSI.

Planning: Simulations

Measuring the clip positions by digitiser takes approximately one minute per pair of radiographs. Apart from speed, using the digitiser has the added advantage of providing a cross-check. The clips' vertical positions are measured on both the axial and lateral views, hence if these are not equal within error limits then the clips have probably been mis-identified.

For each simulation we print out a wide-angle fundus view of the resultant eye model. Comparison of these views gives us a measure of the consistency of the patient's fixation. At present this comparison is performed by hand; a future version of the program under development will perform the task automatically.

Comparison between the ophthalmologist's data and each simulation is simplified by tabulating the chi-squared values and the clip-to-limbus and clip-to-clip distances.

One simulation must be selected as a basis for the plan. The following criteria apply:

1) the straight-ahead view is preferred, but subject to ...

2) a reasonably low chi-squared value

3) reasonable correspondance of clip-to-limbus distances

4) reasonable agreement with the majority of other simulations

5) if using healthy-eye fixation, a better fit to the parallel-eye-axes model

6) if in doubt, err on the safe side ie. the model which will give the largest tumour base.

Occasional problems have been encountered with clips that are near to a great circle, as the program is unable to locate the eye's centre along the axis perpendicular to the plane of that circle with any accuracy. We have then to determine the eye centre's position along that axis "by hand" eg. by examination of the apparent orientation of the clips themselves.

Planning: Tumour

The tumour is modelled next; first the base then the apex, as we find it easier to place the apex after the base is delineated. Finally we model the tumour's cross-section profile. We have no firm statistics on which profile-model options have been used, but we estimate:

~50% of tumours have parabolic profiles,

~40% have rotational symmetry but with a hand-drawn profile, and

~10% have individually-drawn profiles, with the remainder being linearly interpolated by program.

Planning: Eyelids

The eyelids are normally modelled while the eye model is still in its original position, so as to be able to use the drawing's measurements directly. Since the facility became available, we have modelled:

21% patients with no eyelid,

34% with an upper lid only,

27% with a lower lid only, and

18% with both.

We have no statistics on which lid model is used, but *very* approximately we use:

10-20% parabolic eyelid rims

10-20% constant-thickness lids; like "orange-peel"

remainder with a constant-thickness rim and straight cross-section

Very occasionally we use a "pseudo-wedge" to model a low brow.

Planning: Fixation

We now decide on a fixation angle. We use the program to calculate the degree of twist in the nearest simulation.

We may change the lid model at this point; for example if retracting the lower lid would put more of its rim into the field, we may leave the lid un-retracted and deliberately treat through it. We may in fact tape the lid UP, to reduce the dose to the rim and shield the optic nerve.

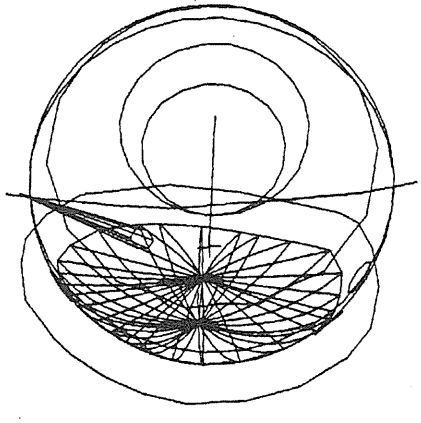

Lower lid unretracted / taped UP

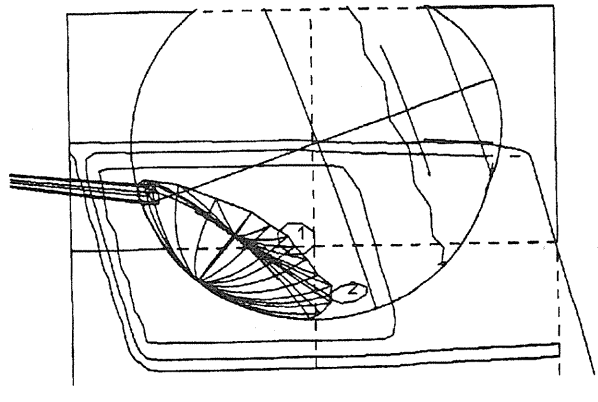

Optic nerve shielded by the lid

Planning: Margins

We rarely use other than 2.5mm round the aperture. If the patient is clearly having difficulty remaining still, we may use 3mm. For a haemangioma we have used 1.5mm.

Our standard margin on the range is 2mm for a bare eye, which we increase to 2.5mm if the eyelids are significantly involved to allow for increased uncertainty. In practice it is usually 2.5mm.

Planning: Isodoses

We first look at isodoses on a plane aligned with the beam, to see if a wedge would be of benefit. In practice we use wedges for two reasons:

1) to reduce the dose to the optic nerve and

2) to reduce the dose to anterior structures, if the combination of a wedge and reduced beam modulation depth can make the isodoses conform better to the tumour volume.

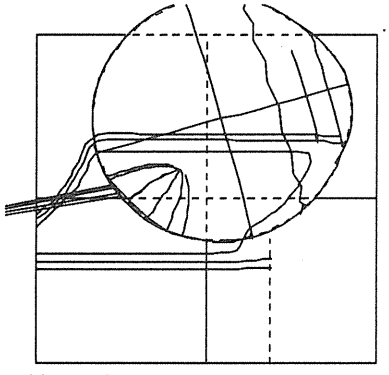

No wedge.
Optic nerve receives large dose.

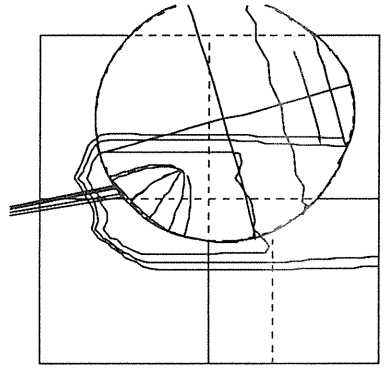

Modulation recalculated after introduction of wedge
Dose to nerve and anterior structures now much reduced.

Our use of wedges over the last five years is:

65% no wedge used

35% one wedge used

1% two wedges.

Planning: Documentation

We normally generate:

The plan protocol

A beam's-eye view

Isodoses on a wide-angle fundus view

Isodoses on a vertical plane in line with the beam

Isodoses on a horizontal plane in line with the beam

A life-size collimator view

A view showing the position of the wedge on the collimator, if relevant

The simulation of the position-verification radiographs (overlay)

Other views as required eg. an eye-axial view for comparison with a photograph of a large anterior tumour.

IMPLEMENTING TREATMENT PLANNING FOR SCANNED PROTON BEAMS ON THE PSI COMPACT GANTRY

E. PEDRONI, H.BLATTMANN, T.BÖHRINGER, A. CORAY, A. LOMAX, S. LIN, G. MUNKEL, S. SCHEIB, U.SCHNEIDER, A. TOUROVSKY
Paul Scherrer Institute
Division of Radiation Medicine
CH-5232 Villigen PSI

In this report we describe the features of the treatment planning system developed at PSI for the spot scanning technique. Special emphasis is given to the practical implementation of treatment planning on the PSI gantry during the last beam period of summer 1994.

1. INTRODUCTION

At PSI we are developing a new application technique, the so-called spot scanning technique. The focused proton pencil beam is applied directly on the patient and is scanned under computer control in all three dimensions in the patient's body. The PSI spot scan method relies on the sequential deposition of a large number of pencil beams (dose spots), with typically 10000 static spot depositions being applied in a few minutes for a reference target volume of 1 liter. By choosing individually the position and dosage of each spot, complex dose distributions with exact conformation of the dose to the target volume can be deposited in the patient, without using patient individual hardware and completely under computer control. The method is designed specifically for the PSI compact gantry, which will be soon the second and the smallest functioning proton gantry in the world. The new proton facility at PSI is presently under commissioning. In April 1994 the first beam was successfully transported through the gantry. During summer 1994 the spot scanning technique was implemented on the gantry and in September 1994 the first veterinary patient (a dog with a lypoma in a leg) was treated. For further details on the general features of the proton therapy project of PSI we refer to the literature [1].

Fig.1 shows a photograph of the PSI compact gantry during the final steps of its installation in October 1994.

2. INPUT FOR TREATMENT PLANNING

2.1 Properties of the Beam on the Gantry

During summer 1994 we limited ourselves to work at only one beam energy, which was chosen to be 177 MeV. The size of the beam was measured at this energy, in air and in the isocenter region to be 1 cm FWHM in both transverse directions. The shape of the beam did not change when changing the setting of the momentum slits in the beam line ahead of the gantry, which demonstrated the achromaticity of the beam transport system of both the NA3 beam line and of the gantry. The momentum band was chosen to be ±0.6%.

By changing the current in the sweeper magnet the beam could be displaced parallel to itself over a range ±9.5cm. It takes about 40 ms to perform a complete sweep of the beam over this range. The parallelism of the swept beam is wrong by about 2 mrad convergence over a 10 cm displacement. We plan to correct this error by shifting the position of the sweeper magnet by a small amount along the beam axis .

The nozzle on the gantry has been designed with a minmal amount of material in the beam. This consists of the exit window of the vacuum beam pipe, about 60 cm of drift space in air and the material for the monitoring of the beam (a dozen of 20-30 μm thin mylar and aluminum foils). The total amount of material in the beam corresponds to only 0.005 radiation lengths and the enlargment of the beam size at the isocenter of the gantry due to multiple Coulomb scattering (MCS) in the material ahead of the patient is calculated to be 4 mm FWHM.

2.2 Pencil Beam Dose Calculation Model

After having found the beam and optimized the beam optics of the gantry, we performed the basic measurements needed for the calculation of the dose distribution of the individual pencil beams deposited by scanning the beam in the patient.

The dose of the proton pencil beam is calculated using two distinct contributions:

[1] The integral depth dose T(w)

This quantity determines essentially the dose in the homogeneous region of a dose field when the beam is scanned regularly in all three dimensions over dimensions larger than the beam size.

This dose was measured very precisely with a plane parallel ionization chamber, which covered completely the transverse extent of the pencil beam and which was scanned in depth in a water phantom.

The integral dose T(w) has been parametrized using a semiempirical physical model, which takes into account following physical effects:

a. dE/dx (slow down approximation),
b. convolution of momentum band and range straggling,
c. beam flux attenuation (using nuclear interaction

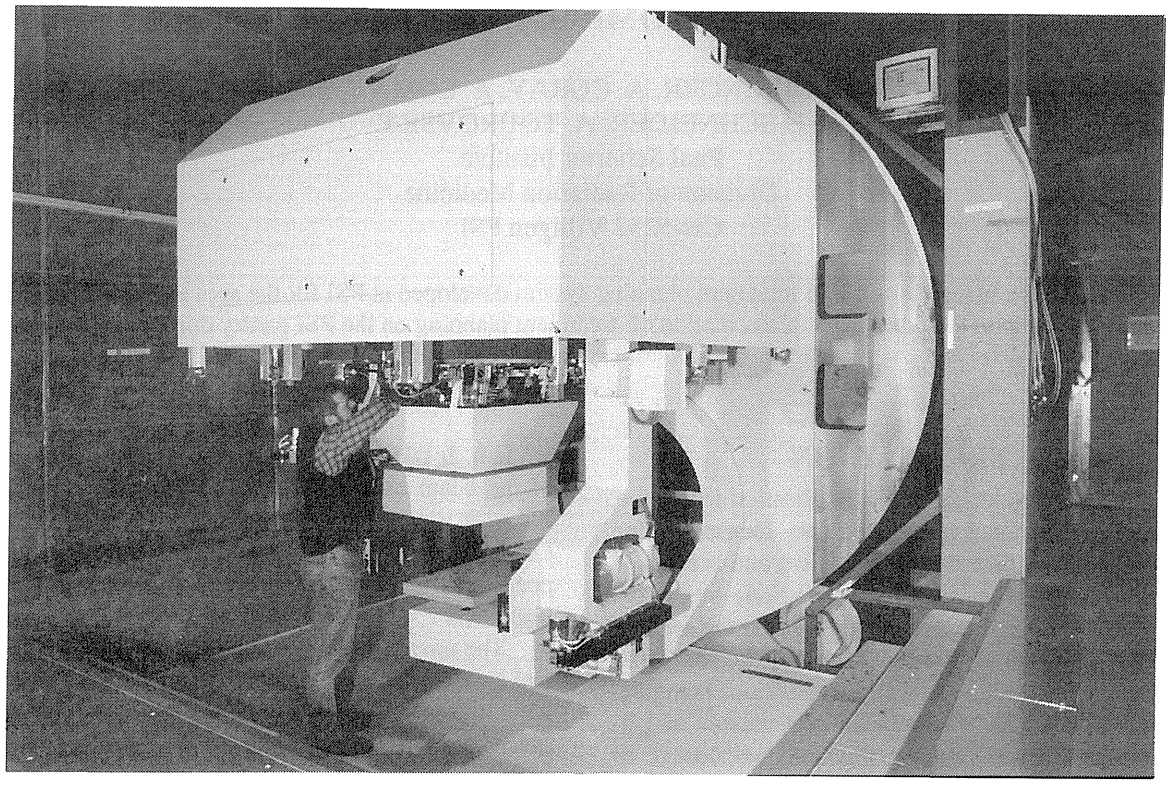

Fig. 1 Photograph of the PSI gantry during final installation in October 1994.

cross sections found in the literature),

d. and an empirical model for the dose deposition of charged secondaries from nuclear interactions.

In fig. 2 we show the comparison between measured (on the gantry) and calculated (using the physical model) dose depth curves T(W).

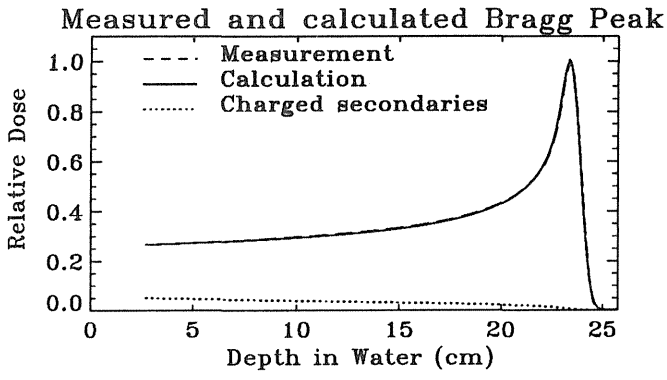

Fig. 2 Integral depth dose T(w) as a function of depth in water. Comparison of the physical dose model with the data measured in summer 1994 on the gantry. The fitted contributions to the dose from nuclear interactions are depicted on the lower part of the figure.

It is interesting to note, that in order to provide a good fit to the data, our model interprets about 19% of the dose in the entrance dose (plateau) region as a direct contribution to the dose from nuclear interactions (the dotted curve in Fig. 2). This value agrees well with the predictions of the PTRAN Monte Carlo code of Berger and Selzer [2]. This is probably a warning not to neglect nuclear interactions when we discuss the problems of changing RBE with depth and the absolute dosimetry of proton beams.

[2] Beam width $\sigma_x(w)$ and $\sigma_y(w)$

The quantity $\sigma(w)$ describes the dose falloff of the dose distribution at the edge of the dose field (resulting from the superposition of the scanned beams).

The spatial dose distribution of the pencil beam has been measured as 2-dimensional xz- and yz- dose maps across the beam axis using a diamond detector. The measured x and y beam profiles were fitted by Gaussians and the resulting beam widths $\sigma_x(w)$ and $\sigma_y(w)$ are plotted as a function of depth in Fig.3. The data has been measured both in air (beam phase space) and in water (propagation of multiple Coulomb scattering in water) and are compared with the predictions of the physical model used for treatment planning in Fig.3.

With the help of the physical model it is possible to calculate the dose of the pencil beam absolutely in Gy /

proton. Using Faraday Cup measurements we will normalize our monitor system in monitor units/ proton. In this way the dose will be normalized in our treatment planning system from the very beginning already for the pencil beam data. The final dose normalization will be however performed using thimble ionization chambers calibrated in a normalized Cobalt source, following the international recommendations.

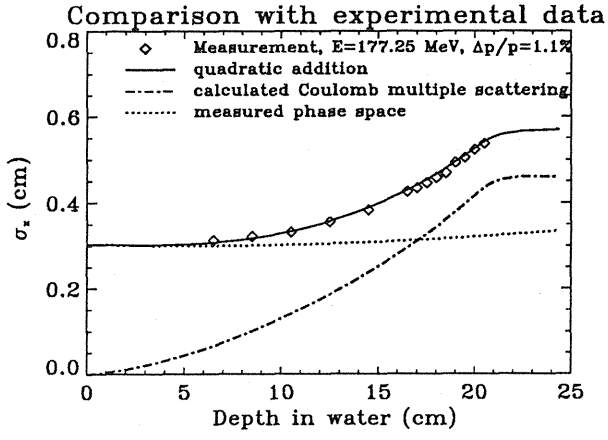

Fig 3. Beam width σ(w) as a function of depth and comparison of the data measured on the PSI gantry with the predictions of the physical model.

3. CT-DATA

3.1 CT Adaptation

The 3D-density information obtained by taking a regular sequence of CT slices will be used in the computer as a volumetric information. The data will be used for diagnostics, for target volume definition, for the dose calculation in the patient including density heterogeneities effects and for the transfer of coordinates between treatment planning and actual dose delivery on the gantry.

In order to fullfill optimally these criteria we have decided to install in our facility a dedicated CT-unit with a modified CT table, which has been designed to allow a reproducible mechanical coupling of the patient couch to a patient transporter system on the CT and to the gantry. In this way the patient will be moved lying in his couch from one room to the other without leaving the mould.

3.2 Calibration of the CT-data.

Before starting the calculation of the dose the CT data must be converted from Hounsfield numbers into proton stopping power.

Here we have some news to report.

The thesis work of U.Schneider "Proton Radiography as a tool for quality control in proton therapy" has been completed [3] and two papers were submitted to Medical Physics for publication [4,5].

We have learned from this work, using a range-calibrated proton radiography of a sheep head, that proton radiographies can be used to check the position of the patient in the beam and to quantify proton range uncertainties (range errors due to the combined effect of density heterogeneities and multiple Coulomb scattering in the patient). In addition, the measured proton ranges can be compared directly with corresponding calculations of treatment planning using calibrated CT data. In this way we can check directly the validity of such calibrations.

Although very preliminary, the results of this work show that the usual calibration of the CT-data based on tissue substitutes measurements is not free of errors and that the situation can be improved by a more refined analysis of the data. By fitting the response of the CT as a function of the chemical composition (the Z-dependence) of the CT-probes used for the calibration, new calibration data points for "real" biological tissues can be calculated and more refined calibration curves can be obtained. Fig. 4 shows as an example the usual calibration curve, which connects the tissue substitute data points, together with an alternative "biological" calibration curve, which takes into account additional calculated "real tissue" data points. In figure 5 we see the range error improvement which can be obtained by using a different calibration curve.

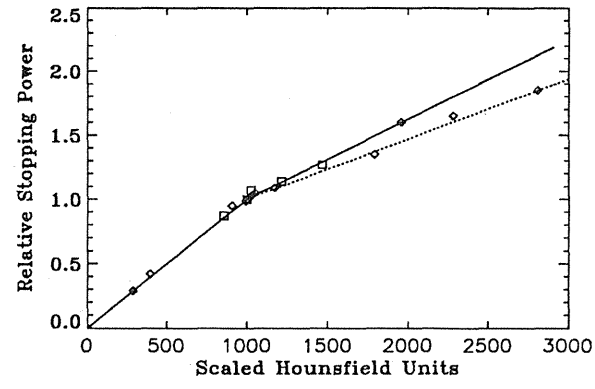

Fig. 4 Calibration curves for the transformation of Hounsfield values into relative stopping power. The solid line shows the tissue-substitute -calibration and the dotted line the "real-tissue" calibration. The squares represent tissue substitute data and the diamonds represent calculated values for biological tissues.

In Fig.5 we plot the histogram (pixel by pixel) of the range differences between measured and calculated proton radiographies of the sheep head (one histogram for either of the calibration curve used). The best agreement between measured and simulated proton ranges in proton radiographies is however obtained by using individual calibration curves for different organs, identified by segmentation on the CT images. For more details we refer here to the original thesis work of U.Schneider.

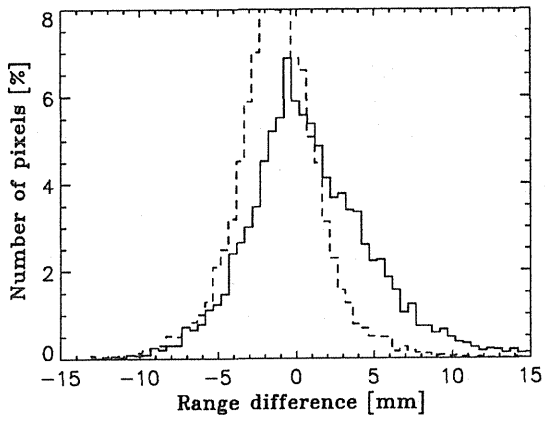

Fig.5 Histogram of (pixel by pixel) range differences between measured and calculated proton radiographies . The solid line and the dashed line are respectively the results obtained using the tissue-substitute and the "real tissues" calibrations of Fig. 4.

4. DENSITY EFFECTS AND DOSE CALCULATION

In the present version of treatment planning the density effects on the dose distribution are calculated only along the beam axis of each pencil beam. To calculate the dose for a given pencil beam at a given point in the patient we calculate first the corresponding integral density $w = \int \rho(z)dz$ along the pencil beam axis. The values T(w) and $\sigma(w)$ are fetched from water look-up tables and the dose is then deposited as a Gaussian with corresponding σ_x and σ_y widths and with T(w) as its content.

The effects of density heterogeneities are therefore treated in first approximation as a simple dilution or compression in depth of the dose of the pencil beam distribution measured in water.

In this model the propagation of MCS of density inhomogeneities in the patient's body is not treated correctly but the analytical implementation of this effect is in principle possible and is planned for a later release. The effect of the beam phase space in air is however treated correctly and added separately in quadrature to the beam width already now and the propagation of MCS due to the range shifter including the air gap between patient and nozzle is also treated correctly.

The approach to treat density effects only on the pencil beam axis relies on the assumption that the phase space of the pencil beam in air is similar or smaller in size than the degree of "confusion" created by the MCS in the patient's body. If MCS is the dominating effect, this approach represents more or less the best which one can do with an analytical calculation. If the scanning is performed with larger beams, the "scan-beam" used for scanning will be calculated as the superposition of many representative "calculational beams" describing the phase space in air. Since there is a practical limit for the precision of such analytical calculations, we have decided at PSI to go directly to the next step and to calculate the dose by tracing individual protons using a dedicated Monte Carlo (see Sec. 8).

5. DOSE OPTIMIZATION

The physician defines a three-dimensionally shaped target volume by entering individual contours on each CT slice displayed on a workstation. After having chosen the energy and angles of incidence (on the gantry) of the beam on the patient, the computer then chooses automatically from the list of all possible dose "spot" positions those which are within some safety margin inside the target volume and defines the dose intensity of each spot according to a predefined Spread-Out-Bragg-Peak scan law. This preliminary list of spots, each defined by its sweeper position t_i, range shifter plates setting s_i, patient table u_i and individual exposure D_i, is used to calculate the total dose resulting from the superposition of the individual pencil beams calculated each in three dimensions using the model described in the previous sections. At the same time a dose distribution "template" is generated on the base of the target contour information using only geometrical criteria. This fictitious dose distribution is chosen to be the goal function for an optimization procedure, in which the dosage D_i of each spot is allowed to vary individually (without becoming negative). The dose distribution is improved in an iterative optimization procedure by minimizing a χ^2-function, defined to be the sum of the squares of the differences between template and calculated 3-D dose distributions.

After the iterative optimization process is concluded, the dose is recalculated using the final optimized exposures D_i. In the present version of the treatment planning we optimize the dose with a fixed beam angle, i.e. the dose is optimized individually for a given single "dose field". At the end the different dose fields are added together, with the option to choose individual weights for each field, the final dose is displayed and the steering file(s) with the commands for the steering system are created.

The simultaneous optimization of spot intensities with different beam angles (simultaneous dose fields optimization) is expected to provide superior dose distributions, especially for concave targets. Work along this direction is under development at PSI.

The basic tools for the PSI treatment planning system were developed by S.Scheib, who has now concluded his thesis work on this subject at the ETH-Zürich. Dr. A. Lomax is now developing the system further. Fig. 6 shows, as an example of treatment planning, the comparison of a proton dose distribution calculated using the PSI proton therapy planning system with the corresponding photon plan calculated using the Voxel-plan of the German Cancer Research Center in Heidelberg. This study is just one of the examples in our treatment planning intercomparison program, which is being performed with the goal to identify new optimal indications for proton therapy.

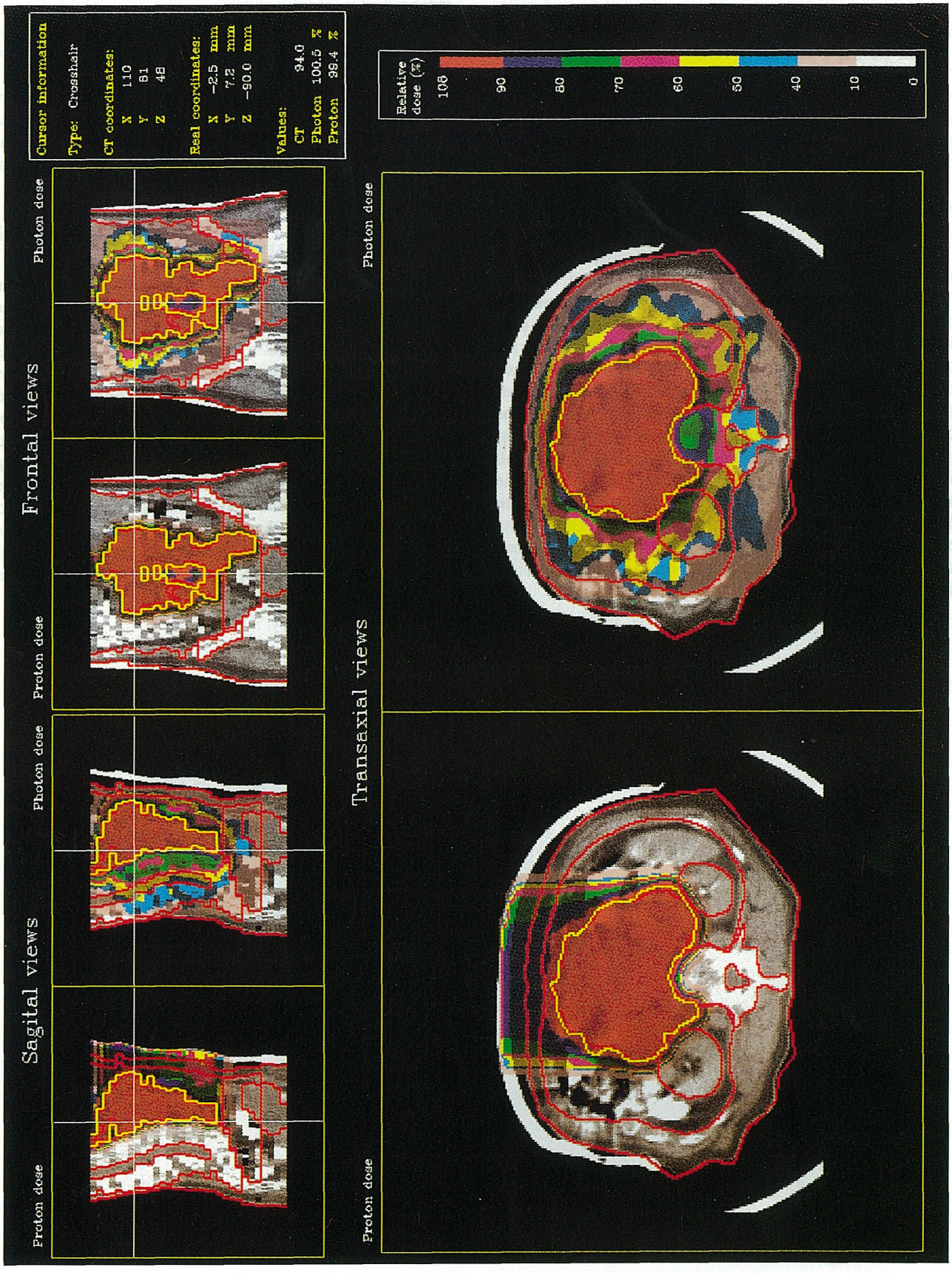

Fig. 6 Example of comparative treatment planning

6. STEERING SYSTEM

The actual treatment will be performed using single static dose spot irradiations. For the fastest varying spot motion we use a deflecting magnet (the sweeper magnet). The motion along the second axis of scanning is realized with a range shifter system, which scans the dose spot in depth. The third direction is covered by the motion of the patient table itself, which is the slowest and the least frequently used motion.

The devices used for scanning were designed for a typical application rate of about 10'000 spots in 2 minutes in a 1 liter volume. An extensive safety system, which is currently under development, should eliminate completely the risk of uncontrolled dose delivery to the patient.

The safety system being realized is based on redundancy and diversity. Two separate computer systems are used independently of each other, to apply, and to check, the deposition of the dose of each spot. This is done on the basis of two different lists of parameters, which are preloaded into the two computer memories before starting the treatment. The first computer (the "active steering" system) performs actively the scanning by controlling directly all scanning devices, including a fast kicker magnet. The time sequence is executed on the basis of the dose information delivered by one of the monitor systems . The second computer (the "dose controller") checks the status of each scanning device using a different set of measured parameters and beam monitors.

Each scanning device is checked at least twice by independent measuring systems.

It is the task of treatment planning to provide all the necessary data of the steering files for each of the two computers.

Each individual treatment plan will be checked before being used for therapy, in one or more test runs with the patient replaced by a dosimetric phantom, following the same strategy used successfully in the last 10 years of dynamic therapy with pions.

7. THE FIRST DYNAMIC TREATMENT ON THE GANTRY

In summer 1994 we put the PSI spot scanning system into operation on the gantry. The practical feasibility of the spot scanning technique was demonstrated by the completed 10 fractions treatment of a lypoma in the leg of a dog. This dog is the first (veterinary) patient treated on the PSI gantry. Although very preliminary, the dose distributions measured with ionization chambers and using densitometric data of films irradiated in a stack of plexiglass plates compared quite well with the data predicted by our treatment planning system. This is shown as an example in Fig. 7 where we compare a measured film (isodose lines) with a calculated dose distribution (gray shades). Since this was the very first attempt to scan the beam in order to produce a useful irregular shape of the dose, this result is considered to be very encouraging.

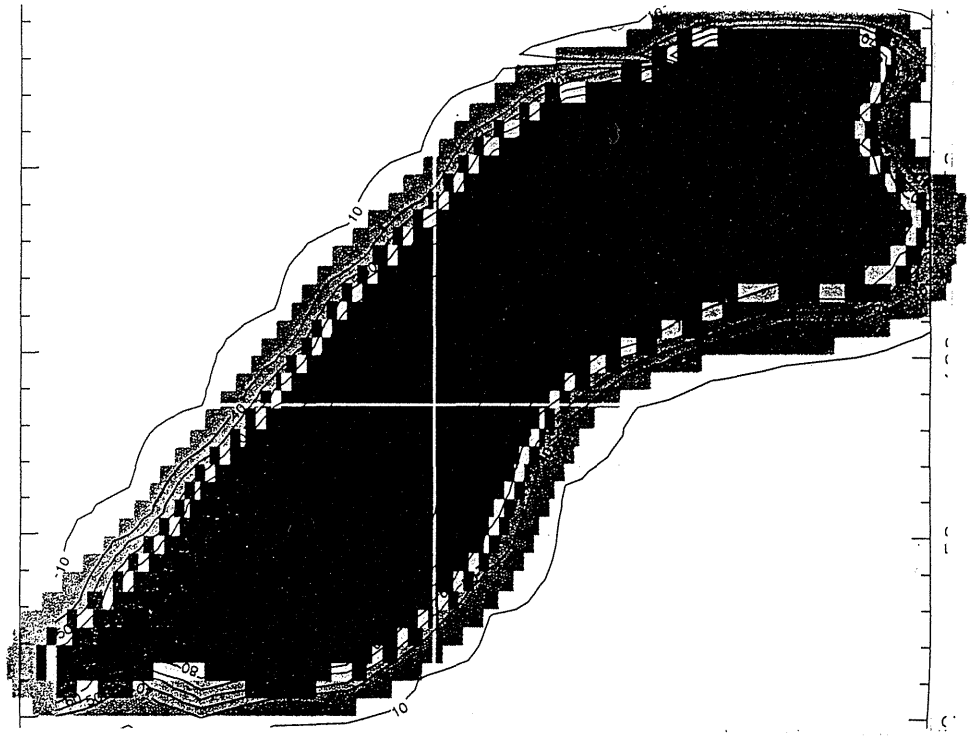

Fig. 7 Comparison of the isodensity lines (solid lines) of a film irradiated by dynamical spot scanning using the steering file for the treatment of the first veterinary patient at PSI with the corresponding dose calculation of treatment planning (gray shades). The picture is reduced in size by about a factor of two.

8. QUALITY ASSURANCE

At PSI we have just started to use the spot scanning on a compact gantry. Both subjects are new challenging technological developments. A lot of work has to be done in order to acquire a complete detailed knowledge of the whole system and in order to achieve the aimed precision of the treatment.

Extensive dosimetry experiments are planned for spring of 1995, when the beam of the PSI accelerator will be available again after a long shut-down (necessary for the installation of new cavities in order to increase the beam current for the new neutron spallation source od PSI). These dosimetry experiments should provide enough confidence to be able to start treatments on human patients before the end of 1995.

The following items are being developed now at PSI in the context of treatment planning and quality assurance :

a) Proton radiography.

This work will be continued in collaboration with the University of Munich (Prof. De Boer and Dr. U. Schneider). The goal is to built a system with scintillators and fibers capable of providing fast radiography images of the patients on the gantry and to use this information especially for "in vivo" range tests before stopping the beam in front of critical structures in the patient.

b) Monte Carlo simulation

A Monte Carlo code, which simulates a full spot scanning treatment by tracing individual protons in the CT volumetric data, has been developed by A. Tourosvky (ITEP Moscow) during his sabbatical year at PSI. The goal here is to specialize the code for speed so as to be able to provide dose distributions in very complex anatomical situations with sufficient proton statistics (at the size of the pixels of the CT data).

c) Error analysis

A new PhD student will study the precision of the PSI treatment planning system, including dose errors arising from density heterogeneities and from motion artifacts. The goal here is to find practical recipes which can be implemented quickly in the treatment planning system in order to provide safety margins and upper limits for error estimates.

This is how we plan to improve our precision and to gain control on all possible errors before applying difficult or critical proton dose plans to the patients.

REFERENCES

[1] Pedroni, E.; Bacher, R.; Blattmann, H.; Böhringer, T.; Coray, A.; Lomax, A.; Munkel, G.; Lin, S.; Scheib, S.; Schneider, U.; Tourovsky, A. The 200 MeV proton therapy project at PSI: conceptual design and practical realization, Medical Physics, January 1995.

[2] Berger, J. M. Penetration of proton beams through water. I. Depth dose distributions, spectra and LET distributions, NISTIR 5226 (1993), National Institute of Standards and Technology, Gaithersburg, MD 20899, USA.

[3] Schneider, U. Thesis Nr. 10780, Proton Radiography: a tool for quality control in proton therapy, ETH-Zürich, 1994.

[4] Schneider, U; Pedroni, E. Multiple Coulomb scattering and spatial resolution in proton radiography, Med. Phys. 21 (11), November 1994.

[5] Schneider, U. ; Pedroni, E. Proton radiography as a tool for quality control in proton therapy, submitted to Med. Phys. in May 1994.

[6] Scheib, S. Thesis Nr. 10451, Spot-Scanning mit Protonen: Experimentelle Resultate und Therapieplanung, ETH-Zürich, 1994.

DOSE OPTIMIZATION OF HEAVY CHARGED PARTICLE THERAPY BY DVHs

J. MIZOE, M.D., M. ENDO, PH.D., H. ITO-KOYAMA, PH.D., Y. MATSUOKA, M.D.
H. TSUJII, M.D. AND K. MORITA, M.D.

Division of Radiation Medicine, Research Center of Charged Particle Therapy, National Institute of Radiological Sciences, Anagawa, Chiba, Japan

Purpose: To simulate the optimal treatment dose of carbon ions using the dose volume histograms(DVHs) of the patients who were treated by Heavy Ion Medical Accelerator in Chiba of National Institute of Radiological Sciences.
Methods and Materials: Materials were 7 patients who consisted of 3 cases of the H&N cancer, 3 cases of the brain and one case of the lung. Dose volume histograms of the target volume and irradiated normal tissues were converted to the complication probability of the patients. The dose which showed most lower value of complication probability was considered as optimal dose. In 3 cases of H&N patients, complication probabilities between carbon ions and fast neutrons were compared at the same time.
Results: Simulated optimal doses of 7 patients was ranged from 77 GyE(Equivalent to the photon dose) to 99 GyE. In 3 cases of H&N cases, complication probabilities of carbon ions showed smaller value than fast neutrons. At optimal dose level of carbon ions, tumor control probability was higher than 0.84 in all 7 cases, but the normal tissue complication probability was also higher than 0.10 in 4 cases.
Conclusion: When the normal tissue complication probability become more improved value which will be acceptable clinically, the tumor control probability will become more low. To improve tumor control probability keeping low probability of normal tissue complication, multi portal irradiation will be need.

Heavy charged particle therapy, DVHs; Dose optimization.

INTRODUCTION

Heavy charged particles have characteristics of having Bragg peak and showing high relative biological effectiveness(RBE). These characteristics produce different effects from conventional irradiation by photon and/or fast neutrons in patients' reaction. Physically, localized dose distribution to the target volume will deliver the treatment results of high tumor control and low incidence of radiation complication. Biologically, high RBE will have possibility to give more effective radiation dose to the tumor and to the normal organs also. Clinical pilot study of National Institute of Radiological sciences(NIRS) using carbon ions of Heavy Ion Medical Accelerator in Chiba(HIMAC) have started on June 1994 with initial treatment dose of 60 GyE(Equivalent to photon dose) for advanced H&N cancer. It will be useful for future clinical study of HIMAC to simulate optimal dose of carbon ions treatment, determined by tumor control and normal organ complication.

METHODS AND MATERIALS

Materials were 7 patients who were treated by carbon ion of HIMAC from June 1994. Patients included 3 cases of the H & N(adenocarcinoma of the minor salivary gland, adenoid cystic carcinoma of the sublingual gland and squamous cell carcinoma of the ethmoid sinus), 3 cases of the brain(astrocytoma grade II) and one case of the lung(squamous cell carcinoma).

After the 3 dimensional(3D) treatment planning, dose volume histograms(DVHs) of the target volume and irradiated organs were calculated. In this study, the brain, the spinal cord, the eyes, the lungs and the skin were listed as surrounding normal organs.

To calculated the complication probability of the organ voxels, following relationship between dose(D: GyE) and complication probability of the voxels(Pv) was used(2).

$$Pv = 1-1/(1+EXP(a+b*D))$$

Coefficients(a and b) of normal organs in the equation were calculated from TD5/5 and TD50/5(Tolerance dose

Table 1. TD5/5 and TD50/5 of normal organs and tumors. RBE was assumed from clinical results of fast neutrons.

Organ	RBE	TD5(GyE)	TD50(GyE)	Comments
Brain	4.5	30	40	Whole volume
Cord	5.0	30	42	10 cm
Eye	4.5	30	43	Whole volume
Lung	3.0	45	65	1/3 volume
Skin	3.0	50	65	100 cm2
ADC	8.0	43	53	Adenoid cystic carcinoma
ADE	4.5	40	50	Adenocarcinoma
SCC	3.0	60	75	Squamous cell carcinoma
AS2	3.0	50	65	Astrocytoma grade II

with 5% and 50% probability at 5 years) from literature(1). Because the average Linear Energy Transfer(LET) of carbon ions was made to be same with fast neutrons, coefficients for the tumors were assumed from out clinical experiences of fast neutrons(Table 1). DVHs were divided to 10 partial volumes and calculated normal tissue complication probability(NTCP) of normal organs using following integral model(3);

$$NTCP = 1-\Pi\{(1-Pv)\}^{1/n}$$

where n is a number of partial volume and 10 was applied in this study.

The complication probability of patient(CP) was calculated from NTCPs of normal organs and tumor control probability(TCP).

$$Pp = 1-\{\Pi(1-Po)\}*TCP$$

To compare the other type of radiation beam, complication probability of the patients simulated by fast neutrons therapy for 3 patients of H & N were calculated at the same time. In this comparative study, port number and directions of fast neutrons beam were same with those of carbon ions..

RESULTS

The DVHs of the ethmoid sinus carcinoma are shown in figure 1 as example. High dose to the left eye(LEY) was delivered because of tumor invasion to the left orbita. Treatment dose(DOSE)-NTCP(and TCP) curves are shown in figure 2 and DOSE-CP curves are shown in

Fig. 1. DVHs of the ethmoid sinus carcinoma treated by carbon ions(a) and simulated fast neutrons(b) .

a.

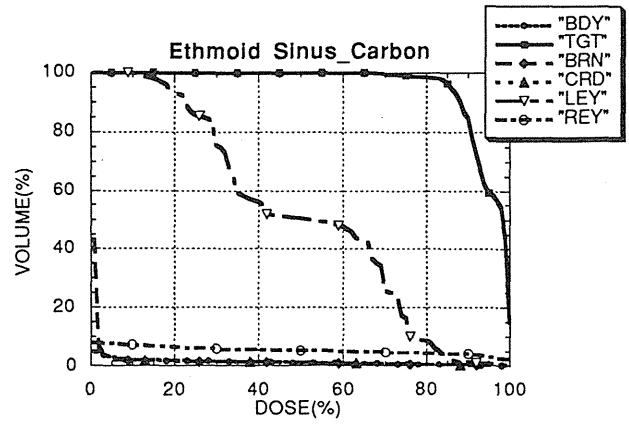

BDY: Body
TGT:Target
BRN:Brain
CRD:Spinal cord
LEY:Left eye
REY:Right eye

b

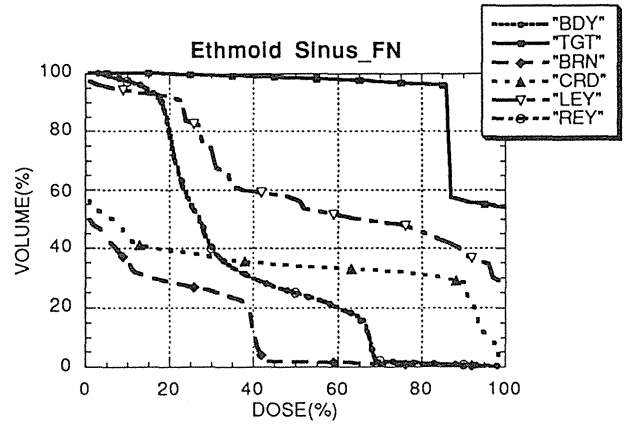

figure 3. Results of comparison between carbon ion and fast neutrons for 3 H&N cancer cases are listed in table 2. CPs of all 3 cases were improved in carbon ions treatment compared to fast neutron therapy with improvement of TCPs and NTCPs simultaneously. Ratios of CP between carbon ions and fast neutrons were 1.36, 1.43 and 15.63 individually.

In 3 cases of the brain, optimal dose were 86, 80 and 99 GyE individually. TCP of 3 cases were 0.97, 0.93 and 0.99, and NTCP were 0.04, 0.15 and 0.00 individually(Table 3). In lung cancer patient, optimal dose was 86 GyE with TCP of 0.92 and NTCP of 0.21(Table 3).

DISCUSSION

Optimal dose of carbon ions therapy, calculated in this study, was ranged from 80 GyE to 99 GyE. Because the

Fig. 2. DOSE-NTCP(and TCP) curves of carbon ions(a) and simulated fast neutrons(b)

a

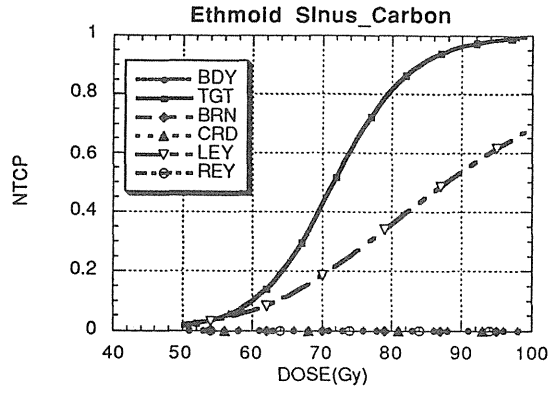

DOSE: Treatment dose
NTCP: Normal tissue complication probability
TCP: Tumor control probability(=NTCP of TGT)

b

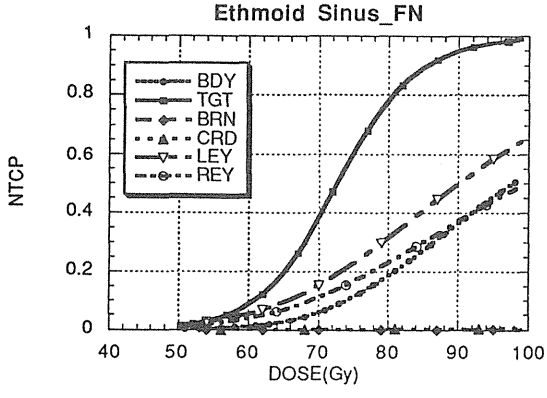

Fig.3. DOSE-CP curves of carbon ions(a) and simulated fast neutrons(b)

a

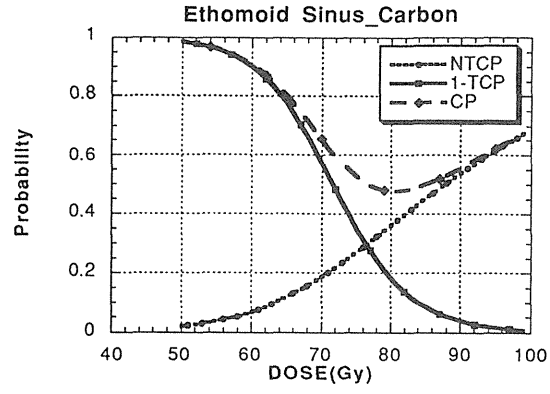

CP: Complication probability

b

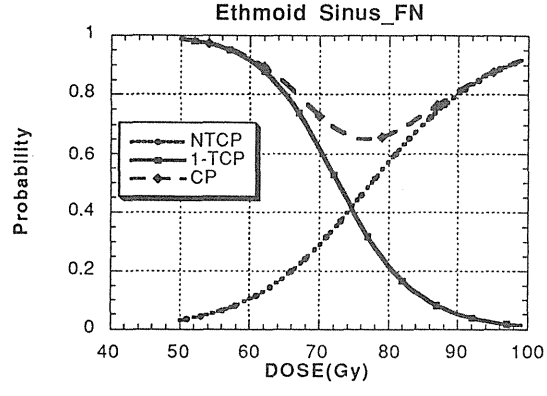

Table 2. Optimal dose, CP, TCP and NTCP of 3 H&N cancer treated by carbon ions and simulated fast neutrons

Case	CP		CP ratio (F/C)	Dose(GyE)		TCP		NTCP	
	C	F		C	F	C	F	C	F
Cheek Mucosa	.007631	.119283	15.63	99	86	.994011	.957192	.001652	.079895
Ethmoid Sinus	.476926	.650578	1.36	81	77	.841362	.681911	.378301	.487584
Subling. Gland	.293221	.418387	1.43	83	80	.899257	.817240	.214041	.288321

CP : Complication Probability
TCP : Tumor Control Probability
NTCP: Normal Tissue Complication Probability
C : 290MeV/u Carbon Ions
N : 30MeV D->Be Fast Neutrons

Table 3. Optimal dose, CP, TCP and NTCP of 3 brain tumors treated by carbon ions

Case	Volume(cm3)			Optimal Dose(GyE)	TCP	NTCP	CPF
	TGT	BRN	BDY				
1	12.8	337.3	712.9	86	0.973378	0.040716	0.0662546
2	15.9	349.2	731.8	80	0.928329	0.149507	0.2104630
3	6.2	373.9	747.4	99	0.996498	0.000631	0.0041311

Table 4. Optimal dose, CP, TCP and NTCP of lung cancer treated by carbon ions

Case	Volume(cm3)				Optimal Dose(GyE)	TCP	NTCP	CPF
	TGT	RLU	LLU	BDY				
1	27.1	607.3	584.1	3932.8	86	0.92380	0.21104	0.27115

dose of initial clinical study of HIMAC was set around 60 GyE, there will be little complication probability of normal tissues. But the optimal doses of this study include somewhat high NTCP value like 0.38 of the ethmoid sinus cancer shown in figures. There will be need of clinical agreement about the probability of normal tissue complication, which will be around 0.03 or 0.05. To avoid such high dose irradiation to the normal organs, more multi portal or conformal therapy will be need in future. The number of ports and the direction of ports will be determined by same methods with this study.

REFERENCES

1) Emami, B.; Lyman, J.; Brown, A,; Coia, L.; Goiten, M.; Munzenrider, J. E.; Shank, B.; Solin, L. J.; Wesson, M. Tolerance of normal tissue to therapeutic radiation. Int. J. Radiat. Oncol. Biol. Phys. 21:109-122;1991.
2) Potish, R.A.; Boen, J.; Jones, T.K.; Levitt, S.H.. Probability models in the analysis of radiation-related complications: Utility and limitations. Therapeutic Radiology 140:203-207; 1981.
3) Schultheiss, T.E.; Orton, C.G.; Peck, R.A. Models in radiotherapy: Volume effects. Med. Phys. 10: 410-415; 1983.

Projects and Status II

ITEP PROTON THERAPY FACILITY
Status Report and Plans for the Future

V.S.Khoroshkov and K.K.Onosovsky
Institute of Theoretical and Experimental Physics
Moscow, Russia

Abstract

The results are summarised for the 25-year functioning of ITEP proton therapy facility based on the 10-GeV proton synchrotron. Status report is presented on the project of a dedicated medical and biological facility based on an H^- synchrotron. The program of work on testing of the proton ejection system by recharge of H^- particles accelerated in the 10-GeV ITEP accelerator is discussed. Plans are reported for the use of the ejected beam for testing the 3D scanning system and the design of the gantry that will be installed in the fourth treatment room of ITEP proton treatment facility.

This year, we have celebrated the 25-th anniversary of irradiating the first patient at ITEP Proton Therapy Facility.

The history of the proton therapy facility is illustrated by Table 1. At present, the facility consists of 3 treatment rooms where 4 treatment units are housed: for neurosurgery, urology & gynaecology, eye treatment, and general oncology [1]. During the 25 years, the treatment units have been upgraded and presently, the second generation units are already in use. Despite certain hardships in our Institute and in the country as a whole, the Proton Therapy Facility continues functioning, and it is handling up to 250 patients per year. Table 2 demonstrates the results of work for 25 years.

Despite the fact that the proton beam of up to 200 MeV is provided independently and simultaneously with running the physical experiments at the accelerator, a number of reasons holds back increasing the number of patients requiring treatment:

1. Only horizontal beams are available - this does not let us provide convergent irradiation which is usually done when other sources of irradiation are used.

2. It is impossible to use a 3D scanning system (ejected beam duration is 100 nsec, with 0.25 Hz repetition rate).

3. The hospitals co-operating with us are far away, and there are complicated problems connected with treatment organisation and patient transportation.

4. High cost of the proton beam resulted from high operating cost of such a big machine.

Therefore, alongside with patient treatment, improvement of methods and equipment, the work is being done on design and construction of a dedicated proton therapy facility based on an H^- synchrotron [2].

We have chosen the H^- synchrotron as the dedicated accelerator for a medical therapeutic facility, for three basic reasons:

First - the possibility to provide the treatment rooms with a "pencil" beam with a very small phase volume that can be used in 3D scanning systems without additional collimation and therefore, without additional activation. We are absolutely convinced that the 3D scanning system is the only way making it possible to use all the advantages of a proton beam. We use the opportunity to note that Japanese scientists made considerable contribution to the development of a 3D scanning technique [3, 4].

Second - the possibility to use small apertures in magnetic channels and in a gantry system which provides for the reduction of both the initial expenses and the running expenses.

Third - the possibility to have several independent ejection points which, generally speaking, may work simultaneously during one accelerator cycle. This provides for the advance in reliability of the facility, and for saving its construction area by means of placing the treatment rooms around the accelerator ring.

Unfortunately, due to the financial hardships, the work on building the facility in Russia is done extremely slowly, and up to this

day, only part of the accelerator systems or their prototypes have been manufactured. The work has advanced further on manufacture of the gantry, 3D scanning systems and on the planning of irradiation with the use of the 3D scanning.

For a 3D scanning system, stability of the external beam parameters, intensity, position, phase volume, are of importance.

Intensity stability of the proton beam ejected from an H^- synchrotron, is provided by the possibility to use the signal from the recharge target where two extra electrons are produced as the result of H^- recharge into H^+. The current of these collected electrons corresponds to the intensity of the ejected protons, and it may be used immediately in the feedback circuit when the H^- beam is aimed at the target for recharge (Fig. 1).

It should be noted however, that the recharge process depends not only on the parameters of the accelerated beam and those of the accelerator; it depends quite substantially on the target design, its material, and on the quality of its mechanical processing and the possibility to measure the current of extra electrons - on the design of the collector device and the amplifying equipment.

Certain experts doubt the possibility of ejecting protons with fair stability of intensity. Therefore we have developed the program for testing the system of ejection of protons after the recharge of the H^-, using the 10 GeV ITEP synchrotron. The program is being performed in close cooperation with TERA group from Italy.

There is a number of stages in the program.

At the first stage, we suggest to accelerate the H^- ions up to 200 MeV energy, eject the proton beam by a recharge target, and test the stability of the ejected proton beam intensity. For this purpose, an H^- source has been designed capable of operating in modes with caesium and without it, magnetic bump systems and a special vacuum chamber for the target have been built, etc.

At the second stage, we are intended to measure the phase volume of the ejected beam and study the phase volume dependence on internal beam parameters and on the target design.

And finally at the third stage, we are planning to eject the beam into a new treatment room of ITEP Proton Therapy Facility where a gantry with 3D scanning systems will be installed (Fig. 2).

The choice of the scanning system depends on the results of the experiment on the ejected beam stability study. For the raster scanning system, a very high stability is required. However the recharge method of beam ejection may also be used with a spot scanning system. In this case, after dose delivery in a spot, the beam can be rapidly deflected from the recharge target and then aimed at it when the delivery system is ready to direct the beam at the next spot. The number of particles per spot may be controlled by an ionisation chamber in addition to intensity measurements by extra electrons, and the beam, besides deflection of the H^- from the target, may be cut off by a chopper in the beam transport channel. Thus the unproductive particle loss will be at minimum. It may be noted here that the particles remaining in the accelerator chamber and not used for the ejection of protons, can be decelerated. Our calculations show that this gives the possibility to reduce a great deal the radiation background and residual activity of the chamber.

Presently, we have completed the work on manufacturing the chopper and its power supply system, and the whole system will be tested in assembly in the nearest future. Also, the power supply system of the sweep magnet has been tested, which is providing a ± 12cm beam scan to the target behind the gantry at 1 kHz seesaw voltage frequency. The work is nearing its completion on manufacture and assembly of the mechanical part of the gantry, and on the design of the fourth treatment room for ITEP Proton Therapy Facility.

We believe that financial support from the INTAS Foundation will be available owing to the activities of our Italian and German colleagues. In this case the first stage of the program is to be completed in 1995 [5]. The second and third stages will be completed in 1996 - 1997 since the construction of the gantry has got the financial support from another source. We also hope that within the nearest years we shall find the money for the construction of the dedicated facility while the work at our grounds with the beam ejected by recharge with the use of the scanning system and the gantry, will save us time during the start-up of the facility.

In conclusion, I would like to make certain points with regard to the importance of the 3D scanning system use.

The problem of choosing either a 3D scanning or a passive method with individual collimators, boluses, and filters, etc. for irradiation, lies in the fact that with the passive method, not only the dose field and the economic indices get worse, but also the psychological danger of artificial reduction of the number of ports used for irradiation occurs for the reasons of saving money and time or manufacturing simplicity. In this case, the clinical results will inevitably get worse. In the end, the advantages of protons compared to other sources of irradiation, will be wasted.

REFERENCES

1. I.V.Chuvilo, L.L.Goldin, V.S.Khoroshkov et al. ITEP Synchrotron Proton Beam in Radiotherapy. Int. J. Rad. Oncol. Biol. Phys., vol. 10, 1984, pp. 185-195.
2. V.S.Khoroshkov, K.K.Onosovsky. H^- Synchrotron for Proton Therapy Facility. Proc. of the NIRS Int. Workshop on Heavy Charged Particle Therapy and Related Subjects, 1991, pp. 204-213.
3. T.Kanai, K.Kawachi, Y.Kumamoto, H.Ogawa, T.Yamada, H.Matsuzawa and Radiotherapy. Med. Phys., vol. 7, pp. 365-369 (1980).
4. K.Kawachi, T.Kanai, H.Matsuzawa, Y.Kutsutani-Nakamura and T.Inada. Proton Radiotherapy Facility Using Spot Scanning method. Jpn Acta Radiol., vol. 42, pp. 467-475 (1982).
5. N.N.Alexeev et al. H^- Acceleration and Proton Beam Recharge Extraction at 10 Gev Proton Synchrotron (Proposed Program). TERA 93/7 ACC 4, June 1993.

Table 1

ITEP Proton Therapy

Beginning of the work	1966
Extraction of proton beam up to 200 Mev	1968
First special treatment room	1969
2 treatment units	1969
First patient treatment	1969
Use of independent magnetic cycle for 200 Mev beam acceleration	1970
Building the two additional treatment rooms	1974

Table 2

Disorders Treated by Proton Beams at ITEP

Pituitary hormone suppression 800

- advanced breast carcinoma
- advanced prostatic carcinoma
- diabetic retinopathy
- adreno-genital syndrome

Pituitary tumors 660

- acromegaly
- Cushing's derease
- Nelson's syndrome
- prolactinoma
- TSH-secreting adenoma
- non-functional adenoma

Vascular disorders of brain 180

- arteriovenous malformation (angiographically demonstr.)
- arteriosinusal fistula (spontaneus)

Intracranial tumors 101

- meningioma of the cavernous sinus
- craniopharyngiomas
- low-grade gliomas
- germinomas
- hamartomas
- pineocytoma
- anaplastic astrocytoma
- solitary metastases in brain

Malignant eye tumors 570

- uveal melanoma
- epibalbar cancer or melanoma
- secondary orbital melanoma (after enucleation)

Oncogynecology 200

- cervix uteri cancer
- vulva tumors (cancer and melanoma)

Oncourology 100

- prostate cancer

General oncology 169

- skin melanoma and cancer
- osteogenic sarcoma
- primary nodal breast cancer
- sceleton and soft tissues metastases
- metastases in salivary gland
- metastases in liver

total ~2800

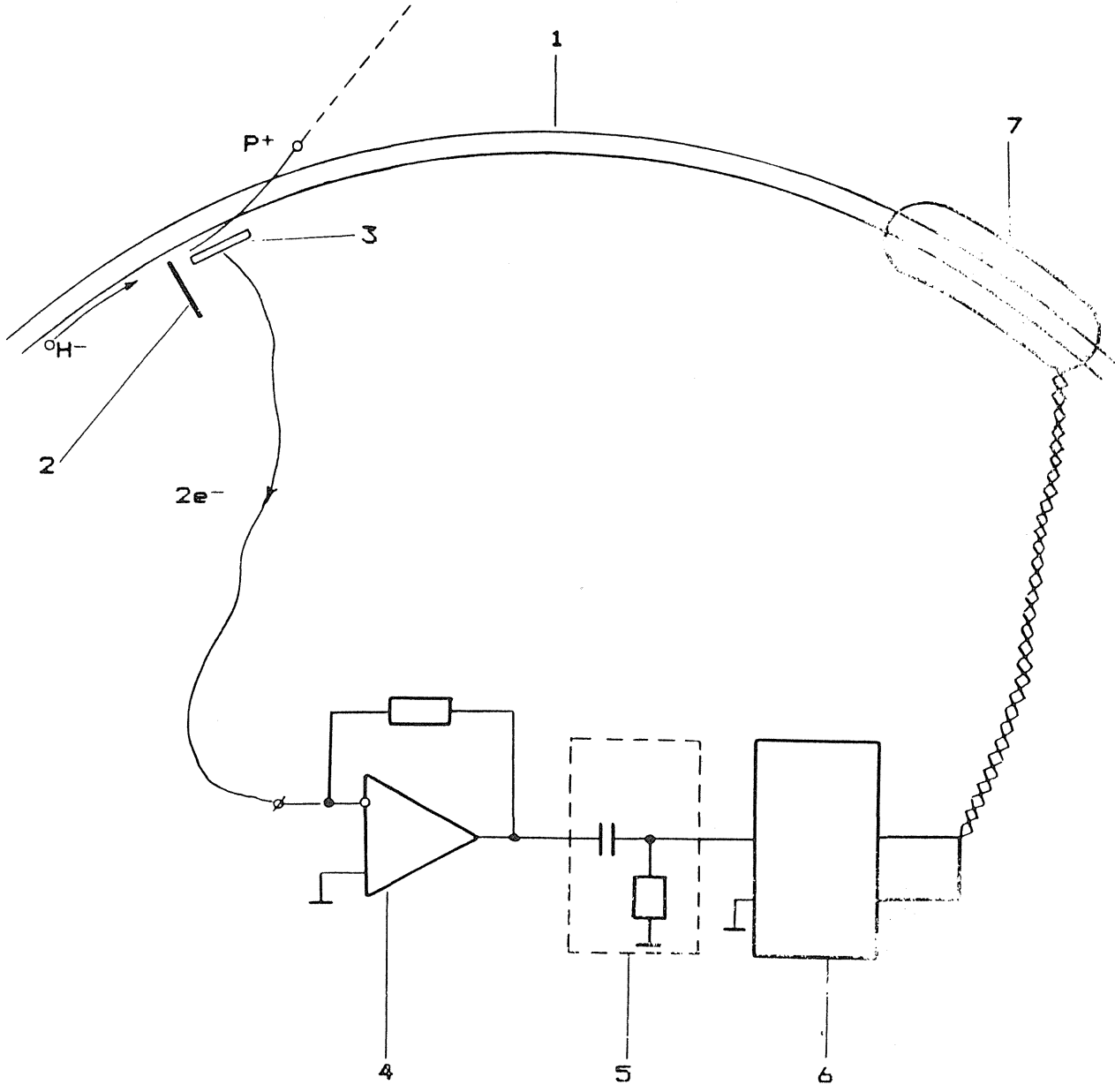

Fig. 1

Block diagram of the system for suppression of intensity pulsations of the external proton beam

1 – H^- ion beam in the accelerator chamber
2 – recharge target
3 – collector of extra electrons
4 – input current amplifier
5 – upper frequency filter
6 – power amplifier
7 – ironless dipole

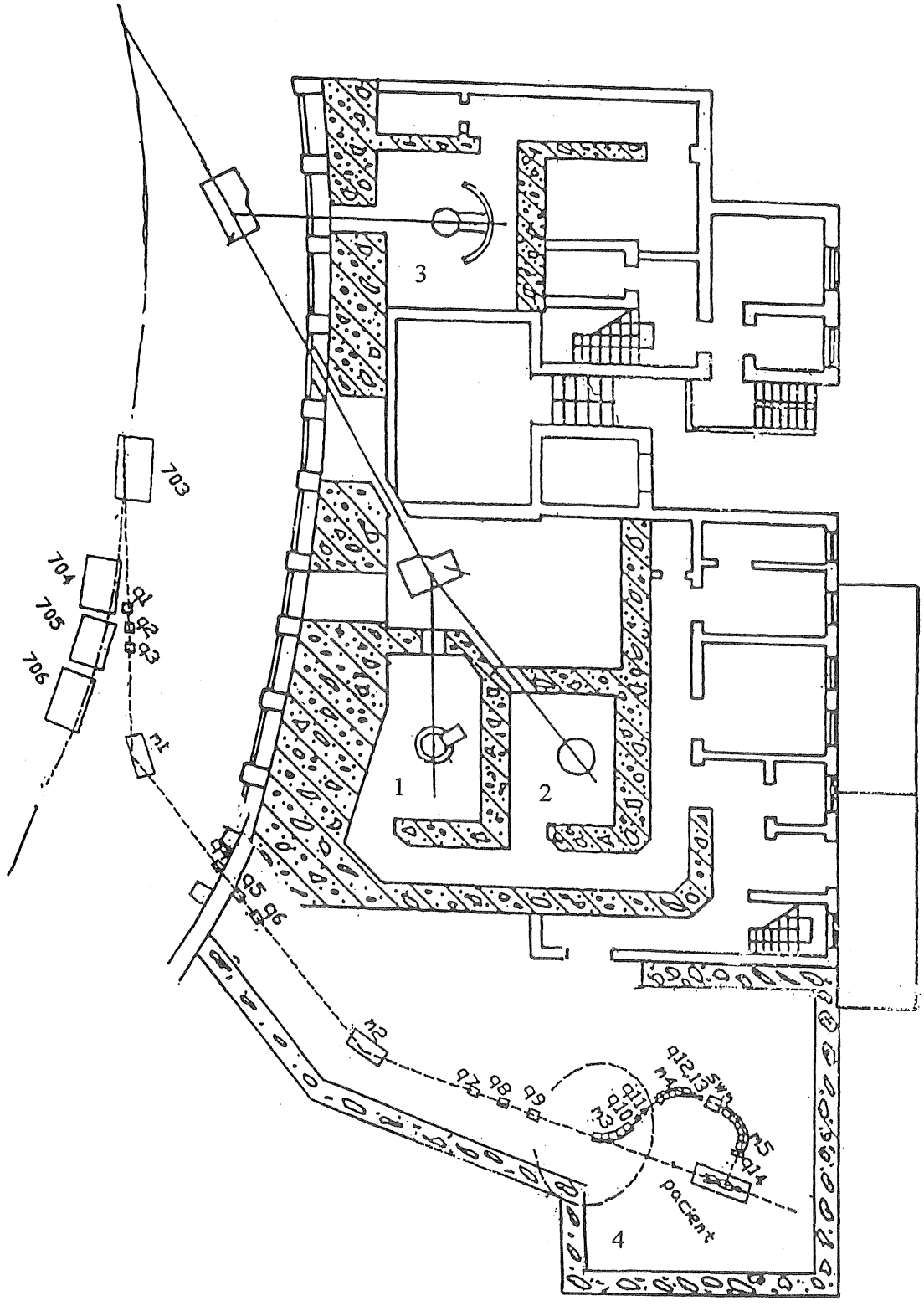

Fig. 2. ITEP Proton therapy Facility: 1-intracranial irradiation unit, 2-eye irradiation unit, 3-uro-gynaecological irradiation unit, 4-planned treatment room for gantry irradiation

PRESENT STATUS OF THE PROGETTO ADROTERAPIA

MARCO SILARI, PH.D.

Consiglio Nazionale delle Ricerche, Istituto Tecnologie Biomediche Avanzate,
Via Ampère 56, 20131 Milano, Italy

The present status of the Progetto Adroterapia is reviewed. The central purpose of the project is to set up a nationwide network of protontherapy centres which has been named RITA (Rete Italiana Trattamenti Adroterapici, Italian Network for Hadrontherapeutical Treatments). This network is made up of a large Hadrontherapy Centre, provided with 5 treatment rooms served by a H^-/light ion synchrotron, and a number of smaller Protontherapy Centres based on compact proton accelerators. The feasibility study for the Hadrontherapy Centre has just been completed and the book describing it has just been published, whilst four different designs which are possible candidates for the "compact accelerator" are presently being evaluated and are the subject of a forthcoming volume. This paper reviews the status of the two studies, starting from the clinical indications and the socio-economical evaluations which form the bases of the overall project.

Hadrontherapy, protons, light ions, synchrotron, compact proton accelerator

INTRODUCTION

The use of hadron beams (protons, neutrons and light ions such as carbon, oxygen and neon) in cancer radiation therapy has grown considerably since the first trials in the mid-fifties and now a few hospital-based facilites are in operation, with a few others being built or designed. A very comprehensive and up-to-date review of the field can be found in the Proceedings of the First International Symposium on Hadrontherapy [1]. The rationale for the use of protons in radiation therapy relies on the better dose distribution which can be achieved with respect to photons and electrons: this is due to the low lateral scattering undergone by protons, their well-defined range and the increasing ionization (i.e., dose deposition) with increasing penetration in tissue, which produces the well known Bragg peak. Ions heavier than protons show an even improved dose distribution and the additional advantage of an increasing biological effect (RBE) at the end of range [2].

The aim of the Progetto Adroterapia (Hadrontherapy Project) is to set up a nationwide network of protontherapy centres which has been named RITA (Rete Italiana Trattamenti Adroterapici, Italian Network for Hadrontherapeutical Treatments) (Fig. 1). The centre of the network is occupied by the Centre for Oncological Hadrontherapy which will have four rooms for proton treatments. This hospital-based *Hadrontherapy Centre* should be a "centre of excellence" and it is conceived to provide, within a hospital which has already available all other facilities, the techniques and the tools that are related to state-of-the-art radiation therapy. The facility will aim at the treatment of 1000 patients/year and is designed with a relatively easy upgrading path to ion treatments. A room for the production and use of thermal and epithermal neutrons for Boron Neutron Capture Therapy is also foreseen. The other nodes of the RITA network are various *Protontherapy Centres*, which should make use of relatively "cheap" and "compact" proton accelerators to be installed, due to their reduced space requirement, in a number of hospitals distributed over the entire nation. The double arrows in Fig. 1 indicate modern multimedia connections which will allow physicians and medical physicists to discuss the cases by exchanging CT, MRI and other diagnostic images and possibly plan the best treatment at a distance. Following such preparatory work, the patients will be referred to the closest or more convenient centre for hadron treatment. Some patients may be treated locally with conventional radiation and receive elsewhere only a proton (or ion) boost.

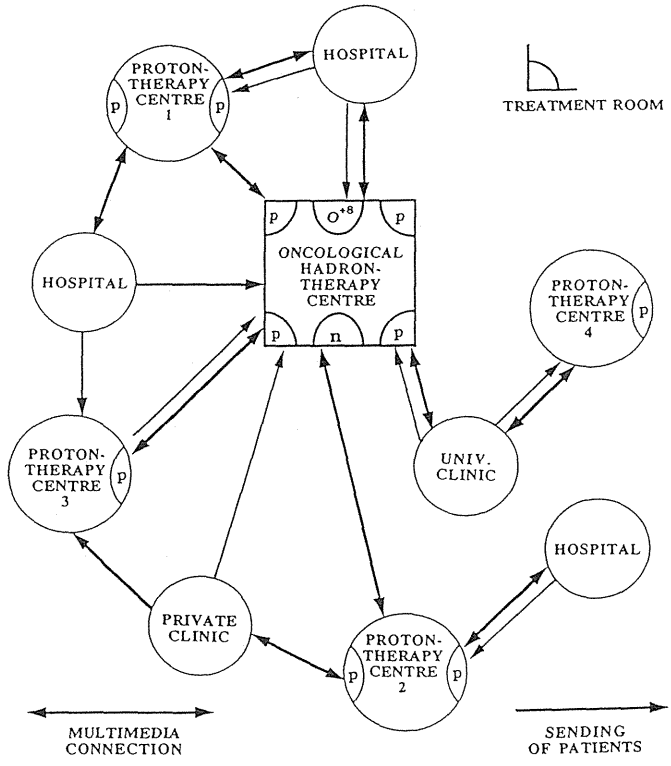

Fig. 1. The Italian network for hadrontherapy treatment RITA

Such a network will maximize the fall-out of the overall investment on public health giving to a large fraction of the patient population the possibility of being treated with hadron beams, for the pathologies for which this modality will be considered to be really advantageous with respect to conventional treatments. The network will also allow a continuous exchange of information among members of a nationwide community of physicians and medical physicists, thus contributing to the development of the needed clinical research and to the estalishment of common agreed protocols. Such a scheme can eventually be extended to the european level.

The RITA project started in October 1993 and is still in a development phase. The feasibility study for the Hadrontherapy Centre [3] has just been completed and has been officially presented to the public and to the press on October 7, 1994, at the presence of the Minister of Health. Four different designs which are possible candidates for the "compact accelerator" are presently being evaluated and are the subject of a forthcoming volume (which will be distributed in spring 1995) which will compare the various solutions. This paper reviews the status of the two studies, starting from the clinical indications and the socio-economical evaluations which form the bases of the overall project.

CLINICAL INDICATIONS AND SOCIO-ECONOMICAL EVALUATIONS

To define a priority scale of clinical indications for proton therapy, four categories of pathologies have been identified [4], named A to D in order of decreasing priority: A) pathologies characterized by their proximity to highly critical structures and for which the use of protons is the only way to administer a radical dose without producing serious side effects; B) pathologies characterized by a prevalently local evolution (for which local control is important) and by low radiosensitivity; C) pathologies for which the main indication in the use of protons is a boost on a restricted volume; D) pathologies with locally advanced conditions and unfavourably prognosis, but which can allow long survival with heavy symptoms and where protons can provide a better palliation than conventional radiotherapy with fewer side effects. Clinical indications have shown that about half of the yearly treatments will be given with curative intents (i.e., to treat patients for whom no other therapy has a reasonable chance of success) and half will be clinical research. An estimate of the patient afflux to the Hadrontherapy Centre, based on the epidemiological data reported in the Tumour Registries of several italian provinces has yielded an overall figure of about 2500 - 3000 patients expected from the North of Italy.

A justification of this advanced treatment modality requires a cost comparison with conventional therapies. The average cost per treatment can be estimated only after having answered the question: should the Centre guarantee the upkeep and/or the remuneration of the value of the financial resources utilized? The answer depends on the origin and the nature of the funds received to build the facility. Four different scenarios have been studied by computer simulations [5]: I) fees charged to the patients are used to cover only the running costs (including the personnel); II) fees are used to cover the running costs and to maintain the real value of the invested capital; III) fees are used to cover the running costs, maintain the real value of the invested capital and give a fair remuneration to half of the invested capital; IV) fees are used to cover the running costs, maintain the real value of the invested capital and give a fair remuneration to the totality of the invested capital. The average patient fee for the four scenarios turned out to be 10400 k$, 12400 k$, 14300 k$ and 15600 k$, respectively, in the assumption of treating 1000 patients per year. These figures should be compared with the cost of the best conventional radiation therapy, i.e. conformal therapy. The results show that the cost of protontherapy is about twice that of conventional conformal therapy. A factor even smaller than 2 applies to scenario II, which is consistent with the present funding system of the Italian National Health Service. This analysis is incomplete because it does not quantify the benefits to the patient, to his family and to society expected from proton therapy. A recent review by Gademann [6] yielded results which are in agreement with the present analysis. It can therefore be concluded that protontherapy is not an abnormally expensive treatment.

THE HADRONTHERAPY CENTRE

To fully exploit the higher ballistic selectivity of protons as compared to photons and electrons, stringent specifications on the dose delivery has to be satisfied. The design of the facility is based on clinical performance specifications which are given in terms of beam range, Bragg peak modulation, range adjustment, dose rate, field size, field homogeneity and symmetry, lateral penumbra, distal dose fall-off, source-to-surface distance, displacement of the beam axis from the isocentre and gantry rotation. These specifications have been translated into physical specifications which have to be met by the accelerator and beam delivery system [7-9].

The Centre for Oncological Hadrontherapy will be provided with:

1) two treatment rooms equipped with an isocentric gantry (see below) capable of transporting protons up to 250 MeV;
2) one treatment room equipped with one horizontal beam and one vertical (downward) beam, also for 250 MeV proton beams;
3) one room equipped with two horizontal beam lines, one for irradiations of eye tumours and one mainly devoted to head and neck treatments;
4) one room with one horizontal beam for experimental activities with both protons and light ions (dosimetry, radiobiology, calibrations, etc.);
5) one room devoted to future light ion treatments;
6) two smaller rooms served by the 11 MeV proton beam from the injector, one for the production of positron emitting radionuclides for PET diagnostics (^{11}C, ^{13}N, ^{15}O and ^{18}F), the other for thermal neutron production for boron neutron capture therapy (BNCT).

The complex will consist of two buildings: an underground, heavily shielded area (the "bunker") housing the accelerators and the treatment rooms, and a surface building above ground with conventional facilities and office space. The bunker has a surface area of about 3500 m^2. Two versions of the facility have been studied. In the first one (version A) the accelerator, the high energy beam transport and the treatment rooms are located at the same level; the maximum height is about 15 m to accommodate the gantry rooms. Besides the basement of the gantry rooms, the lowest floor houses the rooms for BNCT and for radionuclide production.

In the second version (version B) the clinical area is located at a different level than the accelerator and services. The advantages of this solution in terms of optimized patient flow and decoupled clinical and research/service activities have to be balanced against the possible additional complexity of the building, the shielding requirements, a more complex beam transport and the overall cost. Such a solution has been mentioned by Rabin et al [10] and is now being better evaluated. The two layouts are shown in Figs. 2 and 3.

After a sufficient clinical experience has been gained with proton treatments, the accelerator can be upgraded to start treatments with light ions. After initial operation with one horizontal beam line, the building can be expanded with the addition of one or two additional treatment rooms for ions.

ACCELERATOR DESIGN

A 3-D prospect of the accelerators and the complex of beam lines for version A is shown in Fig. 4. The main accelerator is a H^- synchrotron (which will also accelerate protons) capable of providing 60-250 MeV proton beams with an average intensity of about 10 nA [11,12]. The injection energy in the synchrotron is 11 MeV. The injector is an RFQ + DTL structure, delivering average currents of 50-100 μA, sufficient for producing positron emitting radionuclides for PET diagnostics [13] and thermal and epithermal neutrons for BNCT [14].

The design includes the possibility of upgrading the complex to accelerate fully stripped light ions up to ^{16}O to a final energy in the range 120-400 MeV/u with minor interventions on the ring and the addition of a second ion source and injector. A synchrotron has been preferred as it easily provides pulse-to-pulse energy variability over fine steps, as required by the clinicians. In addition, the cyclotron

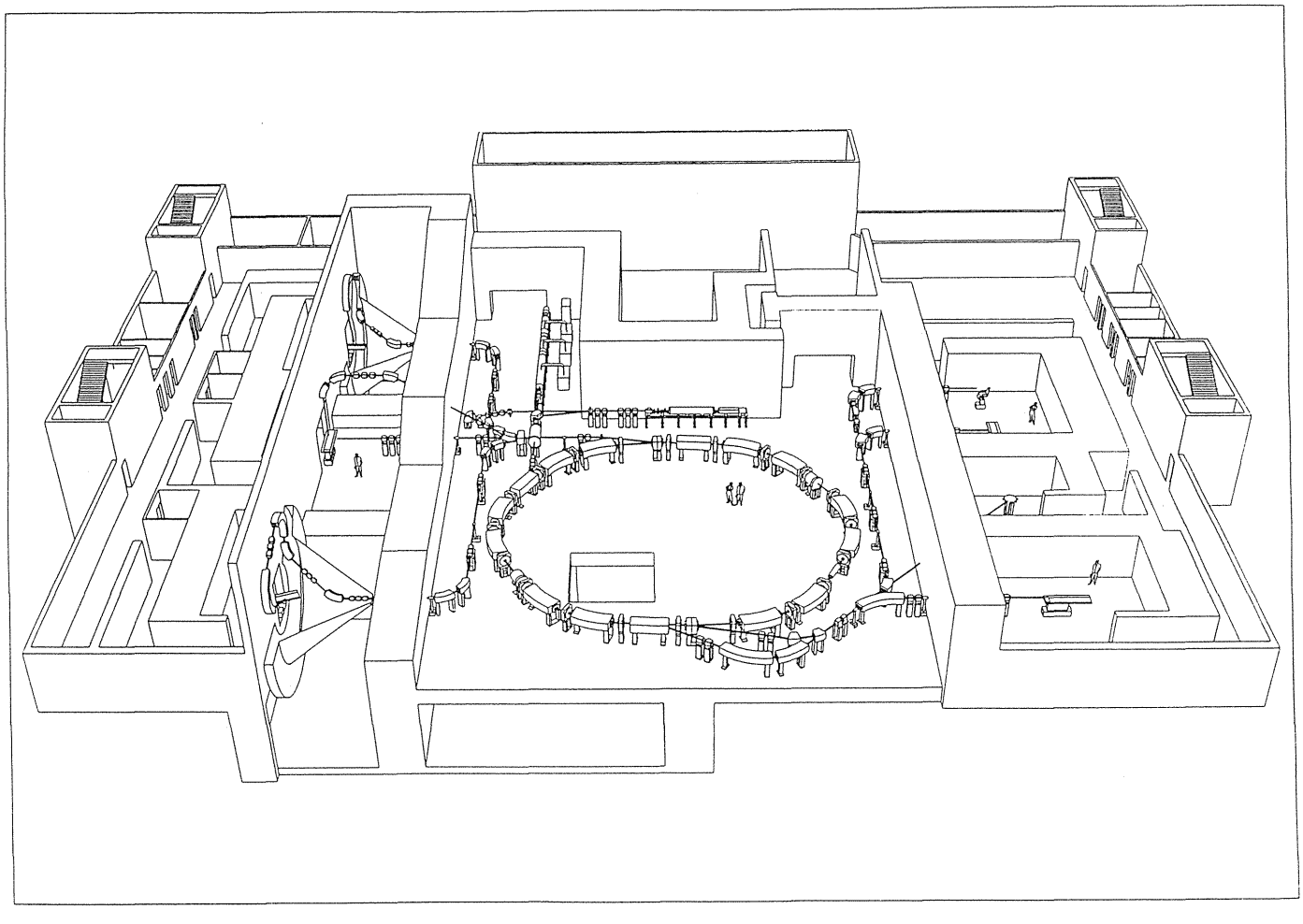

Fig. 2. Version A of the Hadrontherapy Centre

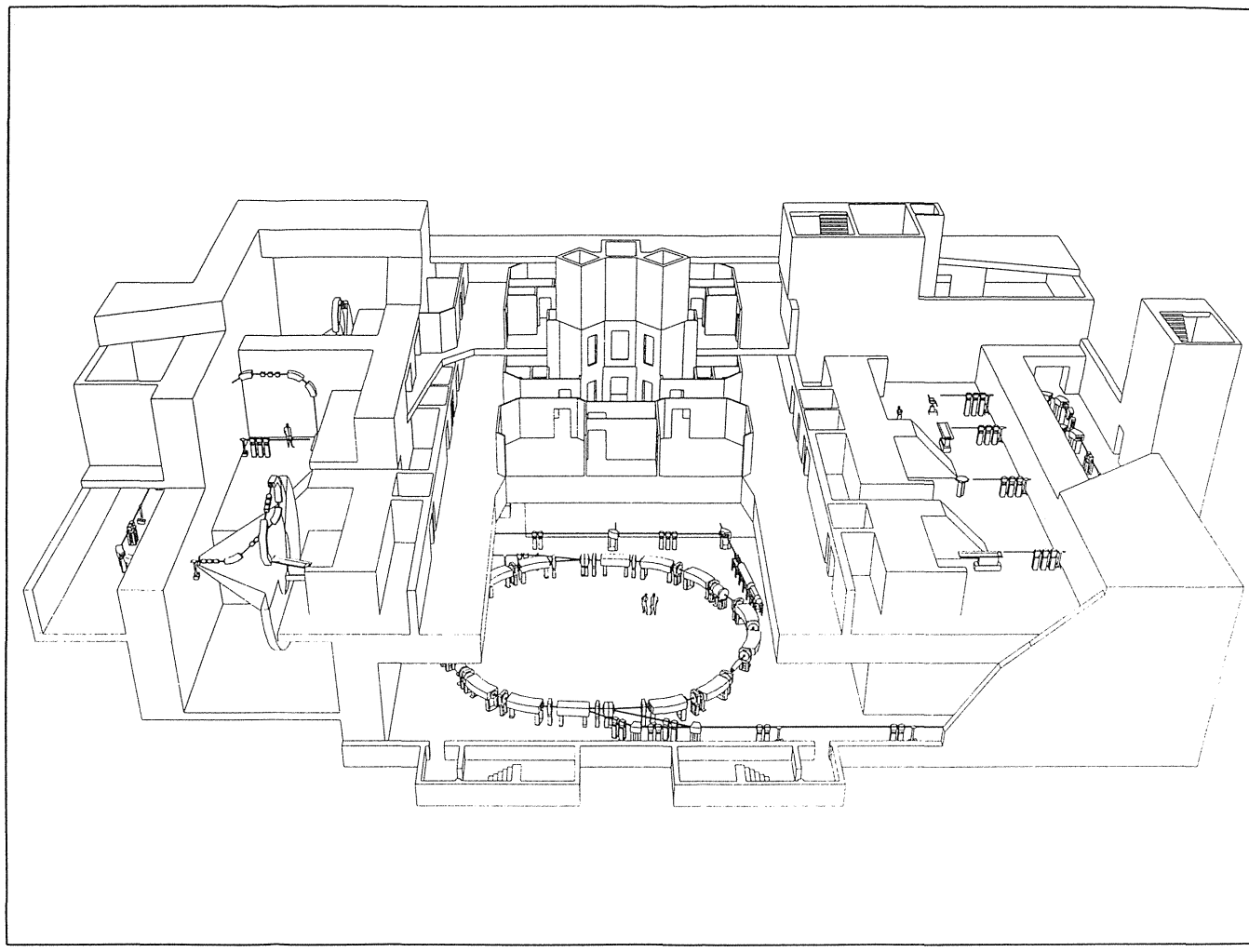

Fig. 3. Version B of the Hadrontherapy Centre

and linac options are ruled out by the request of future upgrade to light ion acceleration.

The advantages of accelerating H^- ions essentially are: 1) the very simple extraction scheme, in which a slow orbit bump drives the beam against a thin stripping foil; the H^- ions undergo charge exchange in the foil, are turned into protons, separated from the circulating beam by a short dipole placed downstream the foil and extracted; 2) the fact that this extraction mechanism is simpler that resonant extraction and should allow a better control of the therapeutic beam, which is particularly important when a scanning technique is adopted; the beam intensity can be controlled by feedback from a monitor in the beam line to the dipoles producing the bump; 3) the very small transverse emittances (of the order of 0.1 π mm·mrad) [15] of the extracted beam which can be obtained if the stripping foil is made very small; a small beam can be better transported and this can be particularly advantageous in a gantry, where a reduction of the magnet gap may translate into substantial weigth and cost savings.

Acceleration of H^- ions instead of protons requires an ultra-high vacuum (of the order of 10^{-10} torr) and a low magnetic field (which translates into a ring of relatively large radius) to prevent beam losses caused by collisional electron detachment and magnetic stripping [16]. These two requirements do not constitute major constraints in the present design, as acceleration of ions needs a residual pressure as low as 10^{-9} torr and a ring of comparable size. Protons can also be accelerated as a back-up capability in case of vacuum deterioration or when energies above 250 MeV are required (e.g., for proton radiography or computed tomography).

The main parameters of the synchrotron are listed in Table 1. Only single-turn injection over half circumference has presently been studied for both H^- and light ions, because it is simpler than multi-turn injection and likely requires a smaller magnet aperture. The same injection elements designed for H^- (septum and fast kicker magnet) will also be adequate for light ions. The space-charge limit, for a Laslett incoherent tune shift ΔQ = -0.25 and an emittance of 20 π mm·mrad at injection, is 4.9×10^{11} particles for 11 MeV H^- and 3.3×10^{10} particles for 3 MeV/u $^{16}O^{+8}$ ions, higher than the design intensity values required for radiotherapeutical applications.

The synchrotron is provided with multiple extraction: two charge exchange extraction systems for H^-, one resonant extraction for protons and one fast extraction port to be used

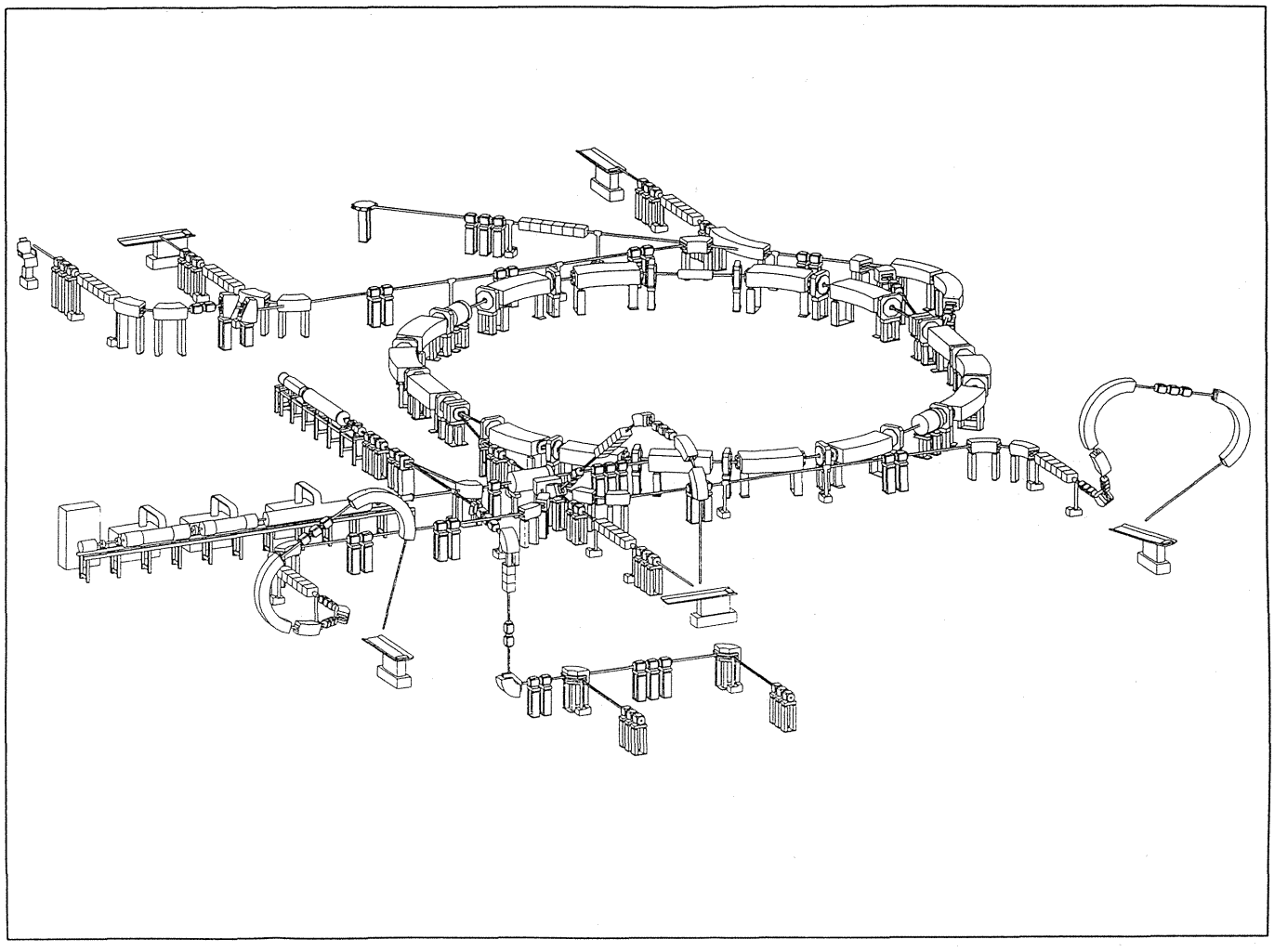

Fig. 4. 3-D view of the accelerators and beam transport (including gantries) for version A of the Hadrontherapy Centre

as beam abort. The extraction of H^- ions is achieved by smoothly driving the circulating beam against a small beryllium or carbon foil, by generating a local orbit bump by means of two small dipoles. An equivalent pair of vertical steerers is used to control the vertical position of the beam. The ions traversing the foil loose their two electrons and are converted to protons. A short bending magnet placed just after the stripping foil separates the protons from the circulating H^- ions. The two extraction channels can be operated on a pulse-to-pulse basis and independently at different energies.

Each of the two stripping foils is located in correspondence of a vertical focussing quadrupole in a straight section of the synchrotron, where the dispersion and the angular dispersion vanish. It has been calculated that small horizontal and vertical emittances (of the order of 0.1 π mm·mrad) can be obtained with this scheme, by using a target a few μm thick and a few tens of μm wide in the vertical direction [15]. The absence of dispersion and angular dispersion at the target position eliminates any correlation between the momentum of a beam particle and its probability of being extracted. Effects such as slewing of the average momentum of the extracted beam during the spill and modulation of the extracted beam current at the frequency of the ripple of the magnetic field in the dipoles are therefore strongly suppressed. Control of the extracted beam intensity is provided by two fast horizontal steering magnets.

The extraction of protons and light ions is achieved by exploiting the third integer resonance line $3Q_x = 7$. The working point is moved to this line by a fast air-core quadrupole and the resonance is excited by means of an adequate set of sextupoles. The resonant extraction system for protons will include an electrostatic septum and a magnetic septum placed about 120° downstream in betatron phase. The upgrading to light ions will likely require the addition of a second septum.

A fast beam abort system can also be implemented by means of a fast extraction system consisting of a fast kicker and a septum magnet located about 120° downstream in betatron phase.

Table 1. Synchrotron parameters.

	H^- / protons / $^{16}O^{+8}$
Injection energy [MeV/u]	11 / 11 / 3
Minimum extraction energy [MeV/u]	60 / 60 / 120
Maximum extraction energy [MeV/u]	250 / 300 / 400
Required average current [pnA]	10 / 10 / 0.21
Circumference [m]	60.677
Focussing scheme	FODO
Maximum magnetic field at extraction [T]	0.537 /0.595 /1.4
Number of FODO cells	10
Number of superperiods	2
Residual pressure [torr]	10^{-10}
Repetition rate [Hz]	2 / 2 / 1
Typical cycle (for maximum energy)	
Acceleration [s]	0.15 / 0.2 / 0.4
Flat-top [s]	0.25 / 0.2 / 0.3
Fall [s]	0.1 / 0.1 / 0.3
Emittance at injection [π mm·mrad]	20
Normalized emittance [π mm·mrad]	3.07 / 3.07 / 1.61
$\Delta p/p$ at injection [%]	± 0.35
Maximum $\Delta p/p$ during acceleration [%]	± 0.6
Frequency at injection [MHz]	0.75 / 0.75 / 0.40
Frequency at extraction [MHz][(a)]	3.03 / 3.22 / 3.53
	horizontal/vertical
Betatron frequency	2.29 / 2.40
γ at the transition energy	2.085
Maximum values of the β functions [m]	10.05 / 9.50
Maximum value of the dispersion [m]	5.30 / 0
Acceptance with dispersion [π mm·mrad]	79 / 56

[(a)] At the maximum energy.

GANTRY DESIGN

As stated above, two treatment rooms will be equipped with an isocentric gantry. This unit allows to rotate the terminal tract of the beam line 360° around the patient in order to vary the direction of irradiation as is done in conventional radiotherapy. It has been decided that the gantry should be isocentric rather than eccentric (such as the unit designed at the Paul Scherrer Institut (PSI), Villigen, Switzerland [17]). This decision is mainly dictated by the choice of avoiding a translation of the patient couch which, while permitting a reduction of the gantry radius, has obvious shortcomings from a clinical point of view. An isocentric gantry of the "corkscrew" type, similar to that installed at the Loma Linda University Medical Center (LLUMC) in California [18], has been chosen (Fig. 5). With this geometry the longitudinal dimension is considerably reduced as compared to a gantry of conventional design and is only fixed by the space needed by the movements of the patient couch. The radial dimension is determined by the minimum source to isocentre distance, which should be at least 2 m as imposed by the necessity of minimizing the skin dose. This geometry achieves a minimization of the overall swept volume.

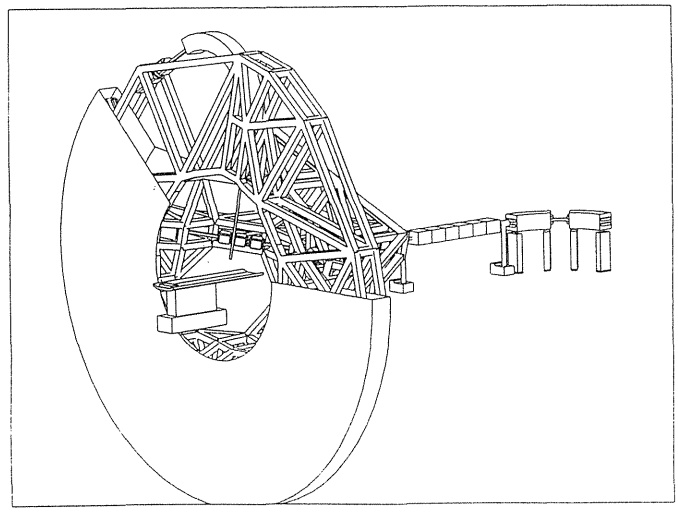

Fig. 5. Isocentric gantry adopted for the Hadrontherapy Centre

The outer diameter of the proposed gantry is about 11 m with a distance between the exit of the last dipole and the isocentre of 3.4 m. The gantry optics is achromatic and designed to fully exploit the small beam size. The estimated vertical aperture of the dipole magnets is 2 cm. The weight of the magnets is estimated to be about 6 t and the overall weight of the gantry is expected not to exceed 25 t, versus a value of 95 t for the LLUMC design and 120 t for the PSI design. Some steering magnets will be needed for final adjustement of the beam position.

THE COMPACT ACCELERATOR PROJECT

A real innovation would be represented by the development of a "compact" accelerator. Such an accelerator should satisfy the following requirements (or at least most of them): 1) it should accelerate a minimum of $2x10^{10}$ protons/s to at least 190 MeV; 2) it should be built (including ancillary systems) in less than 300 m^2 (shielded area and service space); 3) it should consume less than 250 kW and 4) it should cost, with one external beam (but without civil engineering) less than 10 M$; this figure should include the cost of controls and beam delivery, but the cost of the injector can be excluded if it is also used to produce PET radionuclides for the same hospital. An effort has been undertaken within the Progetto Adroterapia in this direction. Four options are presently being considered: 1) a synchrotron using pulsed magnets with a peak field of 4 T; 2) a linear accelerator; 3) a superconducting cyclotron and 4) a weak focussing synchrotron of the LLUMC type but of reduced circumference. These designs are briefly review below. The demonstration of the feasibility of one (or more) of these designs would represent a significant technology transfer from a research organization to industry and the medical field.

Pulsed high field synchrotron. This accelerator (Fig. 6) is based on a design originally developed at the Budker Institute

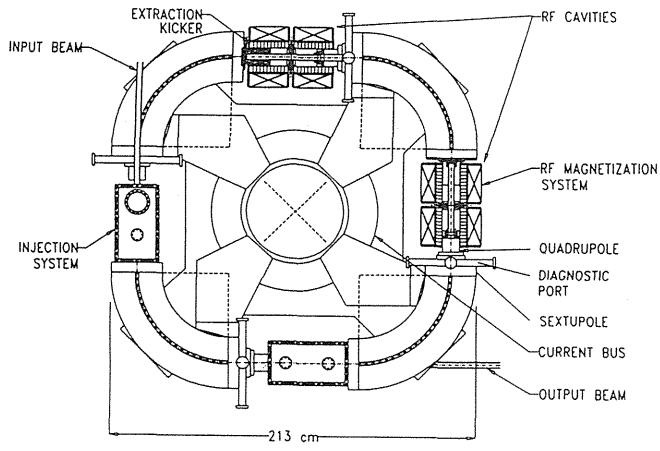

Fig. 6. STAC

of Nuclear Physics in Novosibirsk [19], but recently revised in a more conservative way [20]. The synchrotron uses four room temperature 3.5 ms pulsed dipole magnets providing a maximum field of 4 T. The addition of four short straight sections (to house injection and extraction elements and the RF system) yields a circumference of only 6.4 m. For this reason this accelerator has been called STAC (Synchrotron Technologically Advanced and Compact). The lattice is BODO, in which the horizontal focussing is provided by the dipole bending and the vertical focussing by four quadrupoles. The accelerator cycles at 1 Hz and is designed for a maximum energy of 200 MeV and 10^{10} protons/s. The beam is fast extracted by a shift of the equilibrium orbit towards a septum. The pulse length is very short, only 300 ns, and this may prevent the use of a magnetic scanning system and pose specific requirements on dosimetry. Injection is at 12 MeV from a H^- cyclotron (to be used for PET radionuclide production) using charge exchange. A possible layout for this facility is shown in Fig. 7.

Linear accelerator [21]. This accelerator is also designed for a maximum energy of 200 MeV; the beam intensity is 10-20 nA, which is very low for a linac, so that the accelerator is operated well below its limit. The accelerator structure is made of: 1) an RFQ operating at 750 MHz, accelerating protons to 5 MeV; 2) a 3 GHz Side-Coupled-Drift-Tube-Linac (being patented) divided in 6 sections, to accelerate protons to 70 MeV; each section, less than 2 m long, consists of a number of tanks and requires less than 1.5 MW peak power. Focussing is achieved by permanent magnet quadrupoles; 3) an achromatic magnetic system to bend the beam 180 degrees (either in the horizontal or in the vertical plane - the latter solution is preferred to minimize the surface area required), followed by a re-bunching cavity; 4) a Side-Coupled-Linac accelerating protons from 70 to 200 MeV, with a peak power requirement of 30 MW. The frequency of 30 GHz is considered advantageous because the low beam current should

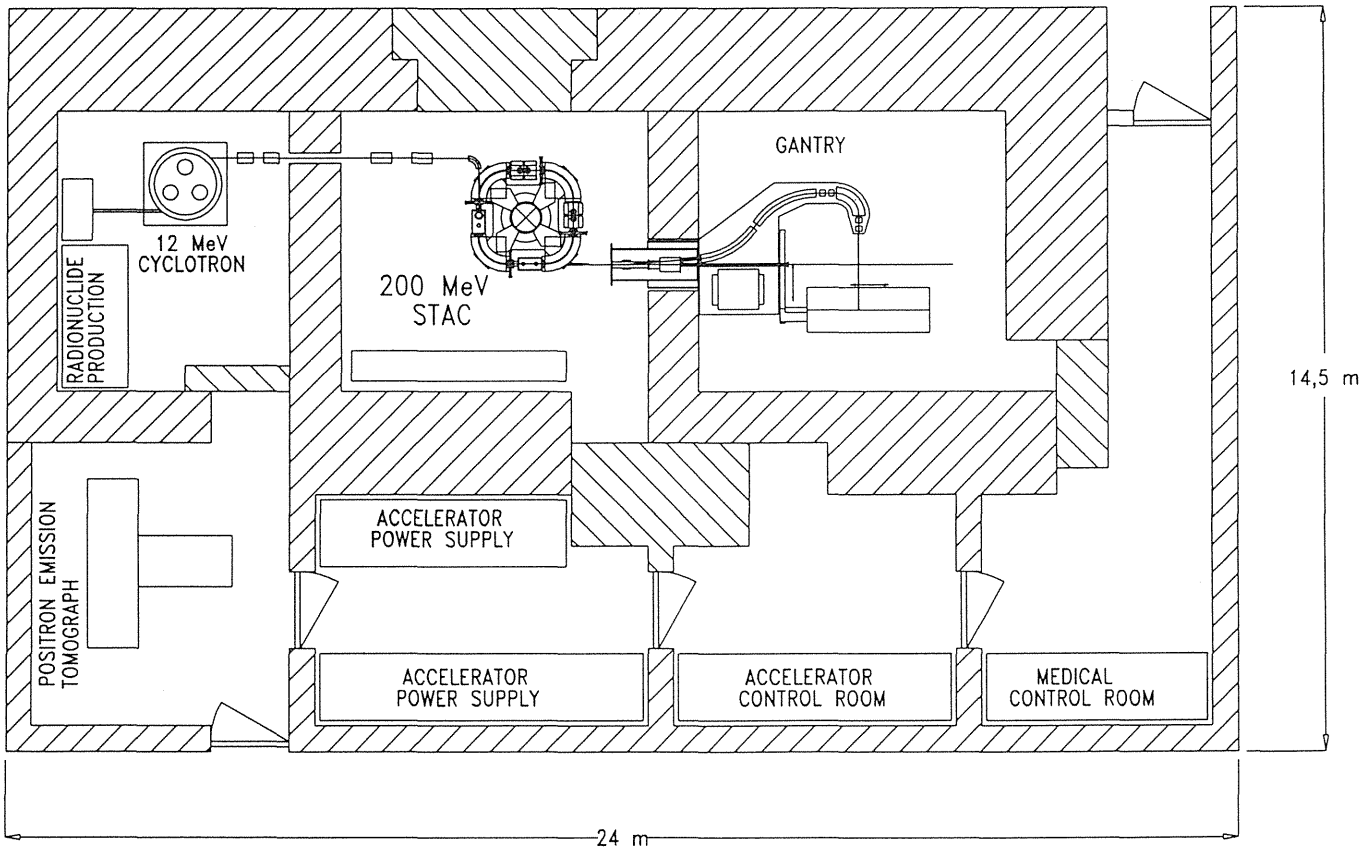

Fig. 7. A possible installation of the STAC inside a conventional radiation therapy department

allow to transport the beam along the small aperture of the linac and make use of low cost RF systems used in electron linacs. The facility should be equipped with one beam at a fixed energy of 70 MeV (from the exit of the SCDTL) for eye treatments and one (two) fixed vertical (horizontal/vertical) beam(s) at 200 MeV from the exit of the SCL (Fig. 8). The energy should be variable in steps by switching off some of the tanks of the SCL structure.

(a joint project between the University of Milan and the Centre Antoine Lacassagne in Nice) R_e has conservatively been chosen to be 0.7 m. The cyclotron (Fig. 9), designed for a fixed energy of 200 MeV, has a three sector configuration and uses three RF cavities located in the valleys and operating in the third harmonic. To simplify operation, two solutions are adopted: 1) the isochronous field is obtained by shimming the poles, thus avoiding the necessity of trim coils; 2) the

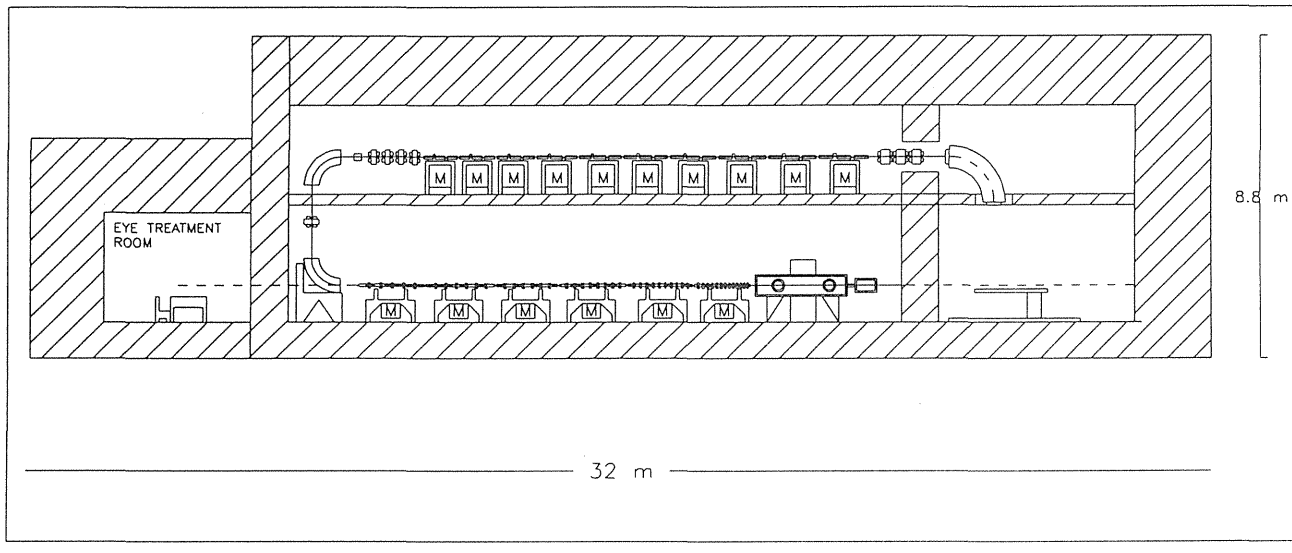

Fig. 8. The 200 MeV linac, folded vertically, supplying two treatment rooms

Superconducting cyclotron. The factors affecting the lower limit in the size of a superconducting cyclotron are related to extraction, injection, current density in the superconducting coils, problems in the magnetic field shaping, etc. Extraction must occur in less than one turn; since the beam displacement is proportional to ER_e^2 (E being the electrostatic field and R_e the extraction radius), and because of the practical upper limit on E (about 140 kV/cm), a reduction of the cyclotron size produces a drastic reduction of the orbit separation at the extraction radius. The lower limit on R_e has been shown to be around 0.6 m [22]. For the cyclotron presently under study

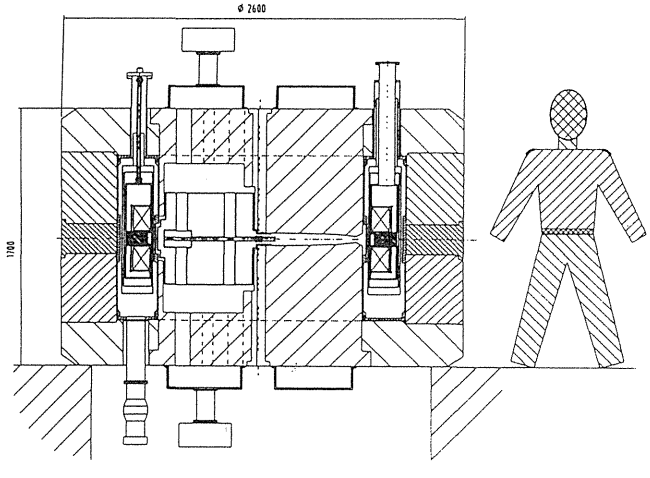

Fig. 9. Superconducting cyclotron

superconducting coils are operated in the persistent mode by shortening them with a superconducting cable. The LHe consumption is thus minimized. The magnet dimensions are 1.7 m (height) x 2.6 m (width), the magnet weight is 65 t and its power consumption is 25 kW.

Weak focussing synchrotron. The accelerator under study at the University of Genova [23] is a weak focussing synchrotron (Q_H=0.692, Q_V=0.866) cycling at 10 Hz, designed for a maximum energy of 200 MeV and a beam intensity of 10^{11} protons/s. The acceleration cycle is 30 ms for acceleration, 40 ms flat-top and 30 ms for field resetting. Four dipoles of 1.43 m bending radius and total weigth of about 12 t provide a maximum magnetic field of 1.5 T. Four straight sections 0.5 m long are foreseen, one for the RF cavity, one for injection, one for installation of a quadrupole which is used to drive the resonance for extraction, and one spare. The machine circumference is 11 m. Injection is at 18 MeV from a H^- cyclotron, using the charge exchange technique over about 100 foil crossings.

CONCLUSIONS

The design of the Hadrontherapy Centre as described in ref. [3] is now being carefully reassessed, with regard to both the building and the accelerator, while waiting for a reply to the request for funding submitted to the authorities. Advantages and costs of version A ad version B are under evaluation, also in consideration of the assigned site (the feasibility study was carried out on a green field basis). The accelerator design is being reviewed, with particular reference to H^- or H^+

acceleration, the lattice (FODO vs doublet scheme) and injection (single turn vs multiturn). The beam diagnostics requirements in the beam transfer lines and the effects of magnetic errors, misalignments and momentum dispersion on the transport of the beam in the gantry are now being studied in more detail.

The four designs which are candidates for the compact accelerator are under study. The volume comparing these four solutions will be issued in spring 1995. If it will not be possible to make a final choice by that date, it is expected that an indication on the two more probable candidates will nevertheless be given; the final choice will have to be made by the end of next year. Funds from the Istituto Superiore di Sanità (ISS) are already available for the construction of a prototype.

ACKNOWLEDGEMENTS

The work reported here is the result of the effort of several people. First, let me mention my group working on the design of the Hadrontherapy Centre: G. Arduini, L. Badano, R. Cambria, F. Gerardi, F. Gramatica, P. Knaus, R. Leone, M. Pullia, S. Rossi, L. Sangaletti and E. Zanolli. The design of the building and plants are under the responsibility of D. Campi (CERN) and M. Nonis, with the support of the CERN ST division, for which I wish to thank F. Ferger and A. Scaramelli. Part of the design of the H^- synchrotron was carried out by AccTek Associates (La Grange, Illinois) on a consultancy basis. The shielding design was performed by S. Agosteo and G. Bodei (Polytechnic of Milano), S. Monti, F. Padoani and R. Tinti (ENEA, Bologna) and A. Rindi and G. Tromba (Sincrotrone Trieste). I am also indebted to E. Acerbi (University of Milano), M. Conte (University of Genova), K. Crandall and M. Weiss (TERA Foundation, Novara) and L. Picardi (ENEA, Frascati) for supplying me with information (mostly still unpublished) on the design of the compact accelerators. I also wish to thank P. Lefèvre, G. Petrucci and A. Susini (CERN) for many useful discussions and advices. Last but not least, I wish to express my gratitude to U. Amaldi (CERN and University of Milano) and G.P. Tosi (Istituto Europeo di Oncologia, Milano) for their continuous encouragement and support.

REFERENCES

[1] Proceedings of the First International Symposium on Hadrontherapy, Como (Italy), October 18-21, 1993, U. Amaldi and B. Larsson (editors), Excerpta Medica, Elsevier (1994).

[2] M.R. Raju, Heavy particle radiotherapy, New York, Academic Press (1980).

[3] U. Amaldi and M. Silari (editors), The TERA Project and the Centre for Oncological Hadrontherapy, INFN Frascati (1994), ISBN 88–86409–01–X.

[4] Ibid. ref. 3, Chapter 4.

[5] Ibid. ref. 3, Chapter 22.

[6] G. Gademann, Socio-economic aspects, ibid. ref. 1, p. 63-71.

[7] W.T. Chu et al., Performance specifications for proton medical facility, LBL-33749 (1993).

[8] Ibid. ref. 3, Chapter 5.

[9] G. Arduini , R. Cambria, C. Canzi, F. Gerardi, B. Gottschalk, R. Leone, L. Sangaletti and M. Silari, Physical specifications of therapeutical proton beams from a synchrotron, to be published.

[10] M.S.Z. Rabin, B. Gottschalk, A. Koehler, J.M. Sisterson and L.J. Verhey, Compact designs for comprehensive proton beam clinical facilities, Nucl. Instr. and Meth. B40/41 (1989) 1335-1339.

[11] U. Amaldi et al., A hospital-based hadrontherapy complex, in: Proceedings of the Fourth European Particle Accelerator Conference, London, June 27-July 1, 1994, in press.

[12] G. Arduini, R. Leone, R.L. Martin, S. Rossi and M. Silari, A H^-/light ion synchrotron for radiation therapy, submitted to Nucl. Instr. and Meth. A.

[13] S. Agosteo, M. Bonardi, A. Foglio Para, M. Lattuada and M. Silari, Radionuclide production by protons, deuterons, and α-particles in the energy range 6 - 70 MeV, INFN/TC- 93/13, July 1993.

[14] S. Agosteo, G. Bodei, R. Leone and M. Silari, Monte Carlo study of neutron production for BNCT, ibid. ref. 1, p. 565-573.

[15] G. Arduini, A.E. Bolshakov, R.L. Martin, K.K. Onosovsky and M. Silari, Emittance and time structure of the proton beam extracted from a H^- synchrotron by the charge exchange technique, to be published.

[16] G. Arduini, R.L. Martin, S. Rossi and M. Silari, Vacuum and magnetic field constraints in a H^-/light ion synchrotron, Nucl. Instr. and Meth. A346 (1994) 557-564.

[17] E. Pedroni et al., Proton Therapy Project, in PSI Life Sciences Newsletter 1992, Villigen: PSI, 1992, p. 11.

[18] R. Little, Initial operation of the LLUMC accelerator and beam transport, Nucl. Instr. and Meth. B56/57 (1991) 1192-1196.

[19] I.I. Averbukh et al., Project of small-dimensional 200 MeV proton synchrotron, in: Proceedings of the First European Particle Accelerator Conference, Rome, June 7-11, 1988, S. Tazzari (editor), World Scientific (1989), p. 413-415.

[20] L. Picardi et al., Preliminary design of a very compact protonsynchrotron for proton therapy, ibid. ref. 11, in press.

[21] K. Crandall, L. Picardi and M. Weiss, private communication.

[22] E. Acerbi, private communication.

[23] M. Conte, private communication.

POSSIBLE USE OF THE AGS LINAC FOR PROTON THERAPY*

J.G. Alessi, A. Chanana, F.A. Dilmanian,
Y.Y. Lee, D. Raparia, J. Tuozzolo, L. Wielopolski

Brookhaven National Laboratory
Upton, NY 11973-5000 USA

Abstract

The BNL 200 MeV linac presently provides beam for the AGS high energy physics program and for isotope production at the Brookhaven Linac Isotope Producer (BLIP)[1] facility. There is now a proposal to develop a proton therapy facility which would also use the linac beam. Approximately 1% of the current in each linac beam pulse would be diverted from BLIP, down an existing transport line, to the proposed new facility. This paper focuses on the basic design of the facility, particularly the accelerator issues. The planned transport line layout is presented, along with a description of the energy and intensity control, and beam delivery systems. In the initial phase, we are planning one 360° vertical gantry and one horizontal treatment room.

Introduction

Following completion of the upgrade of the AGS linac in 1996, 30 mA, 650 μs pulses will be accelerated at a 7.5 Hz rep rate, giving an average linac current of 146 μA (9 x 10^{14} H^-/second). In this paper we present a possibility of using the linac for proton therapy, in a way which would essentially be transparent to the BLIP and AGS operations. We propose to use the already existing 200 MeV transport line as a spur from the BLIP line, which takes the beam to what had been the Radiation Effects Facility (REF), and the Neutral Beam Test Facility (NBTF), both no longer in operation and potentially available for this application.

Figure 1 shows the layout of the existing and proposed facilities. A pulsed dipole magnet switches beam pulses between the AGS Booster injection line and BLIP. The REF/NBTF line branches off the BLIP line, and there is a 116 m transport line, including three 30 degree dipoles, before the beam enters the NBTF experimental hall. The dipoles, quadrupoles, power supplies, and vacuum system are already in place for much of this transport line, but some additional elements will be added to better meet the needs of the therapy facility. The NBTF experimental hall, with a floor space of 9.1 m x 24.4 m, will be converted into a horizontal beam patient treatment room. A new beamline will be added off of the NBTF transport line to deliver beam to a 360° gantry, in a new room. The remainder of the NBTF facility will be converted to offices, patient examination rooms, reception and waiting areas, etc. There is sufficient space to expand the facility for additional horizontal and gantry rooms in the future. The REF experimental hall, also shown in Fig. 1, could be used for beam characterization, detector development, and development of scanning system.

*Work performed under the auspices of the U.S. Dept. of Energy.

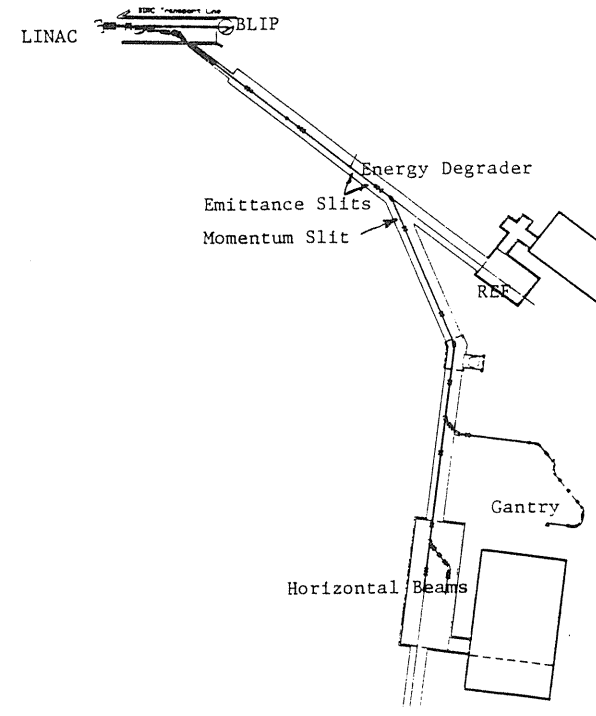

Fig. 1. Schematic of transport lines to therapy facility.

General Design Features

We will utilize a small fraction (1%) of beam from every pulse delivered to BLIP for this purpose. The BLIP beamline will require minor modifications to allow 1% of the beam in every BLIP pulse to be directed to the proton therapy facility. A thin carbon button, suspended in the beam using 5 micron graphite fibers, will be placed just upstream of an already existing dipole magnet. The 1% of the BLIP beam which passes through this stripper is converted to H^+, and in the dipole following this stripper it is deflected 3.75° to the REF/NBTF beamline, while the remaining 99% H^- beam is deflected 3.75° to BLIP. This config-

uration is failsafe in that the stripper breaking/falling would result in no beam to PTF.

Almost the full linac energy of 200 MeV would be required to treat deep tumors in larger patients. Therefore, our design minimizes the loss of beam energy in the beam-spreading and beam-flattening process. "Voxel-by voxel" treatment, while preserving the full beam energy, would lead to treatment times which are too long for medium and large tumors at the 7.5 Hz repetition rate of our linac. Therefore, in order to lose less energy than a conventional double scattering beam-spreading system, we have chosen to replace the first scatterer with spreading via quadrupole magnets. This would be followed by either an occluding ring [2] or contoured scatterer [3] for flattening of the distribution. (A scanning system with a ribbon beam could be implemented at a later time).

Figure 2 shows the relation of the proton range and energy as a function of width of the treatment area from Ref. 4 with possible point from the proposed scheme.

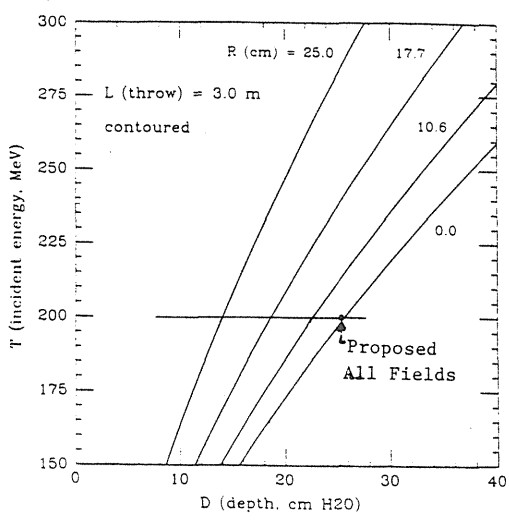

Fig. 2.

Bragg peak spreading can not be done easily during a 650 μs beam pulse, so we will treat the full field first at one depth, and then change the beam energy. Energy modulation will be carried out in two steps - a coarse energy degrader, shown in Fig. 1, located approximately 84 m upstream of the treatment room, and a fine energy degrader, for Bragg peak spreading, located in the nozzle away from the patient.

Collimators downstream of the coarse degrader will be used to produce a beam of small emittance and small energy spread before reaching the beam delivery sections. The beam intensity will be adjusted so that at least 100 pulses are required to treat the distal edge of the tumor. The intensity could then remain the same throughout the treatment, and the number of beam pulses would be controlled to give the desired dose at each range. The fine energy degrader would then be changed for the next energy step. With this scheme, each beam pulse contains no more than 1% of the dose required at a given depth. Total treatment times should be approximately 60 seconds, assuming it takes 1 s to make an energy change with the fine degrader.

Coarse Energy Degrader

We have chosen to do the coarse energy degradation far upstream of the patient, since the intensity is sufficient to allow the use of collimators downstream of the degrader to produce a beam of small emittance and energy spread before reaching the beam delivery sections. This has the advantage of reducing the energy degradation required near the patient, where transverse momentum spread, fast neutrons, and gammas can be a problem. Initially, for simplicity we plan to have the coarse energy degrader give one of four energies, 200, 160, 120, or 80 MeV. (It will be a simple matter to expand the choice of energies in the future, and ultimately one can degrade the energy at this upstream location to match the distal edge of a tumor.)

Emittance and Momentum Slits

An aperture at the degrader exit, and a second aperture 2 m downstream, will define the exit beam position, size, and angular spread, (i.e., emittance). These will be set to provide a beam with a transverse emittance of 20 π mm mrad (unnormalized). A 0.6 mm thick lead foil located in the energy degrader will be used with the 200 MeV beam, so that full-energy beam will also pick up some extra divergence, while losing only 0.2 MeV in energy. (That is, the emittance of the 200 MeV beam is first increased, and then recollimated to 20 π mm mrad).

After a 30° bend, a horizontal collimator at the image point of the exit aperture of the degrader (and the maximum dispersion point) will serve as a spectrometer to produce a well defined beam energy, as well as to limit the momentum spread of the beam to that required to contribute < 2 mm range error (or alternatively 1% maximum dp/p). The beam energy will be independently verified as part of the safety systems, using downstream magnets.

Intensity Control

In the above sections, we have chosen to take 1% of the current in each BLIP pulse for PTF, have limited the emittance entering the beam delivery section to 20 π mm mrad, and have limited the momentum spread to give < 2 mm range error (or 1% dp/p maximum). Table I shows the maximum number of protons that can be delivered to the facility versus energy. The lower intensity at lower energy is generally acceptable, since the beam range is smaller. More pulses can thus be used at a given range since fewer energy steps would

be required, and treatment times remain reasonable. The intensity can be reduced below these maximum values without changing the other beam characteristics by using a set of collimating slits located before the coarse energy degrader. Alternatively, one could reduce the intensity using the momentum slits described in the previous section.

Table I

Beam Energy (MeV)	Max I Delivered to Nozzle (protons/sec)	Max I at Patient (protons/sec)
200	6.6×10^{12}	1.7×10^{12}
160	7.5×10^{11}	3.8×10^{11}
120	2.1×10^{11}	1.1×10^{11}
80	9.1×10^{9}	4.6×10^{9}

Field Size Control

Both the gantry and horizontal beam delivery systems, described below, are designed to transport the beam of 20 π mm mrad into a field of up to 30 cm diameter at the patient, using quadrupole magnets to spread, and an occluding ring or contoured scatterer to flatten the beam profile. A set of horizontal and vertical collimators in the transport line, downstream of the momentum slit, can be used to reduce the transverse emittance of the beam (unnormalized), to below 20 π mm mrad in each plane. The location of these slits has been chosen such that the reduction in emittance results in a reduction in the field size at the patient, with all elements in the beam delivery system remaining the same. These slits can thus be used to reduce the field size to match the desired treatment. The field size could also be adjusted using the spreading magnets. A patient collimator will always be used in addition, for shaping the radiation field proximal to the tumor.

Beam Delivery

Initially, there will be two horizontal and a 360° gantry beam. A similar scheme is used for spreading the beam for the large field horizontal beam and the gantry beam. The maximum size of the field chosen is 30 cm diameter and the beam divergence is magnified by a set of quadrupole triplets. We decided to use a set of occluding rings to flatten the distribution in order to keep maximum depth of penetration. However, for less than 20 cm depth of penetration where one needs more intensity, a contoured scatter can be used to flatten the distribution. For the small field horizontal beam, there is no beam distribution flattening device used; only the flat portion of the beam spread is used.

In selecting the best gantry design, there are trade-offs to consider in room size, gantry weight, power requirements, simplicity of beam optics, etc. After looking at many possible gantry designs, we have selected at this stage, a system that has a very simple beam optics design, with small magnet apertures leading to a low gantry weight. The gantry size is larger than some other designs, but this is not too critical in our case, since there is ample space for the gantry rooms next to the existing NBTF building. The gantry, and its support structure, is shown schematically in Figure 3.

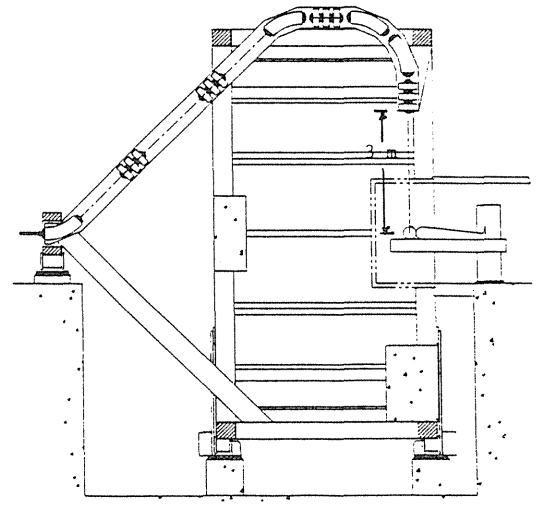

Fig. 3. 360° Gantry.

The incoming beam is deflected by 45°, transported 7.2 m, and then deflected 135° to the isocenter with three more 45° dipoles. The beam is bent by a total of only 180°, which reduces power requirements over other more complicated geometries. The gantry is dispersion free. All four dipoles can be powered in series. A quadrupole triplet after the last dipole spreads the beam in such a way that it diverges to a 30 cm diameter field size 3 m away.

The beam optics through the gantry are shown in Figure 4. We have chosen to use identical 45° dipoles in all four locations. The mechanical parameters of the gantry system are shown in Table II.

Table II

Dipoles	4 @ 45°, 4 cm gap
Quadrupoles	12 @ 4 cm dia. aperture
Total magnet power	92 kW
Total magnet weight	3000 kg

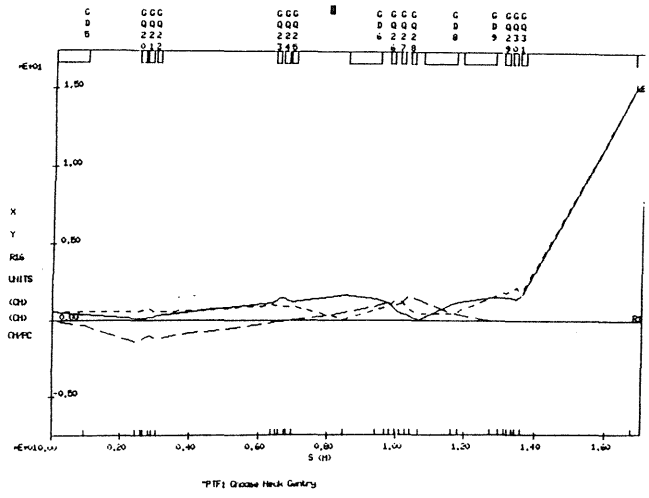

Fig. 4. Optics through gantry.

Acknowledgements

We acknowledge invaluable discussions we have had, during the course of the design of the facility, with our colleagues at the following institutions: Centre Antoine LaCassagne, Nice, France; Harvard Cyclotron Laboratory and Massachusetts General Hospital, Cambridge, MA; Lawrence Berkeley Laboratory, Berkeley, CA; Loma Linda University Medical Center, Loma Linda, CA; Paul Scherrer Institute, Villigen, Switzerland; and Institute of Medicine, Jülich Research Center - KFA, Jülich, Germany. We also thank colleagues at BNL for their contribution at different stages of this design, particularly W.W. MacKay, S.G. Peggs, L.C. Snead, and N. Tsoupas. This research has been supported by the U.S. Department of Energy under the contract DE-AC02-76CH00016.

References

[1] L.F. Mausner, S. Mirzadeh, H. Schnakenberg, and S.C. Srivastava, Appl. Radiat. Isot. 41 (1990) 367.

[2] A.M. Koehler, R.J. Schneider, and J.M. Sisterson, Med. Phys. 4 (1977) 297.

[3] B. Gottschalk, A.M. Koehler, J.M. Sisterson, and M.S. Wagner, Proc. of the Proton Radiotherapy Workshop, PSI, H. Blattmann, Ed. (1991) 50.

[4] B. Gottschalk, private communication.

DEDICATED ACCELERATOR PROJECT FOR PROTON THERAPY AT KYOTO UNIVERSITY

Akira Noda, Ph.D., Yoshihisa Iwashita, Ph.D., Makoto Inoue, Ph.D.,
Institute for Chemical Research, Kyoto University

Mitsuyuki Abe*, M.D., Junji Konishi, M.D.,
Faculty of Medicine, Kyoto University

and

Koji Ono, M.D.
Research Reactor Institute, Kyoto University

Abstract

A proton accelerator dedicated for cancer therapy is designed at Kyoto University as one of major facilities of the proposed Particle-Radiation Tumor-Research Center, Kyoto University. Its output energy can be changed from 70 MeV to 250 MeV, which correspond to the range in muscle from 4 cm to 38 cm. The dose rate up to 5 Gray per min is to be delivered with a combined function type synchrotron utilizing a linear accelerator as an injector. Single treatment room which is facilitated with a horizontal beam line together with a gantry will be provided. An experimental irradiation room for physical and biological basic research is also made in addition. The design of the gantry is based on the principle to use as less scatterer as possible in order to reduce the beam loss. The facility is oriented for clinical use at Kyoto University and open use among universities in whole country. Further the construction itself is expected to give a typical example of a compact proton facility to be widely used at general hospitals.

Proton Therapy, Bragg Peak, Combined Function Synchrotron, Untuned RF Cavity, Single Treatment Room, Gantry

Introduction

The malignant tumor makes largest number of the cause of death in Japan and it amounts to more than one fourth and it is anticipated to increase rapidly from now. So it is required to establish in an early stage an effective and high quality cure and diagnosis preserving the shape and function of the organ. The radiation therapy has such a merit as keeps the shape and function of the human body and is preferable from the point of view of quality of life. However, in the cases of tumor with little sensitivity to radiation and locally developing tumor, it has not been possible to safely irradiate necessary amount of dose into only limited area around the tumor due to the limitation of dose distribution of the X-ray. In order to break though this limit, it is inevitable to utilize the radiation with better physical properties.

In Japan, an excellent facility for heavy ion therapy has been completed this year in National Institute of Radiological Sciences and first clinical treatment has been already started. Considering the urgent needs for such radiation therapy, the needs for such a facility is expected to increase rapidly and in fact, Hyogo Prefecture is now planning to construct similar hadron therapy facility following the success at HIMAC.

At Kyoto University, succeeding the will of late Prof. emeritus H. Yukawa to utilize π-meson for cancer therapy, medical facility of pion therapy had been studied as one of the main items in π-meson Research Facility. However in recent years, stimulated by the success at Loma Linda University and University of Tsukuba, it has become to be known that proton therapy is also very powerful tool to cure the cancer[1,2]. As the Radio-biological Effectiveness (RBE) of proton is similar to that of X-rays (RBE~1.1), the huge amount of experience for clinical treatments with use of X-rays is considered to be applicable to proton therapy[3] in addition to the fact that the proton beam has such a merit as has Bragg peak and dose localization is better than X-ray. Further the cost needed for proton therapy is expected to be within reasonable size, which is large merit for dedicated machine for medical use.

From these reasons, Proton Therapy facility has been proposed at Kyoto University as the *dedicated machine for hadron therapy inherent in the university*, which is named *KUMPF* abbreviating Kyoto University Medical Proton Facility. With proton therapy, it is possible to make such a dose distribution localized to the tumor and dose irradiated into the tumor can be largely raised without increasing the dose in the normal cells. So it is expected to enable the cure of such a tumor as had been uncontrollable up to now. At Kyoto University, fundamental research and clinical application of the thermal neutron capture by ^{10}B has been performed at Fundamental Research Laboratory for Reactor Therapy in Research Reactor Institute. Particle produced by the neutron capture of ^{10}B has a very large RBE and is considered to be effective on the cure of the tumor with little sensitivity to radiation. However short range of thermal neutron gives a severe limit on applicable disease and its stage. Thus the proton therapy with better dose distribution and neutron capture therapy of ^{10}B with large RBE have complementary roles. Combined use of these therapy is considered to provide unique facility for cancer therapy. Thus a new Particle-Radiation Tumor-Research Center has been proposed from Kyoto University as a research center for open use among universities. Here the particle means both proton accelerated by a synchrotron and neutron produced by a research reactor.

* Present address, Kyoto National Hospital

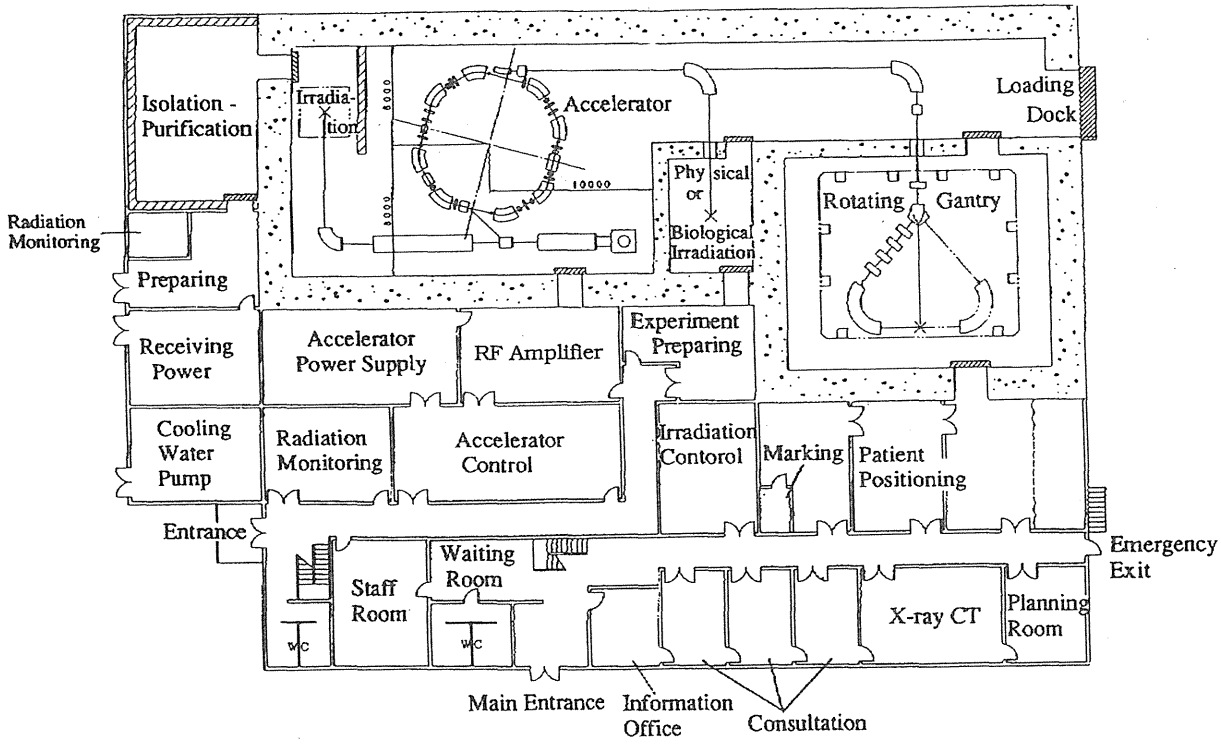

Fig. 1 Layout of the proposed proton therapy facility at Kyoto University (KUMPF)

The roles of the proton accelerator proposed for the center can be divided into the followings; one is to educate a certain amounts of medical students who are well familiar with the hadron therapy with the home machine. This needs is considered to increase much more after full operation of the facilities at NIRS and Hyogo Prefecture. The other is to show a typical example for a compact proton accelerator facility for widespread use in general hospitals. For medical machine, it is highly desirable that the freedom of the machine adjustment is as small as possible in order to make the operation much easier and necessary information to fix the machine parameters should be obtained during construction and running in of this machine. In the present paper, the brief outline of KUMPF is described.

Design Concept

As the main accelerator, a synchrotron is adopted for the merit of energy variability. In order to attain easy control of the magnet system, a combined function type is to be used. By combined function lattice, the tracking problem between dipole and quadrupole magnets can be avoided, which is considered to largely contribute the easy operation. As the combined function type has little flexibility, it is important the machine design is verified to be complete beforehand and to give such an example is one of the present project as already mentioned.

The control of RF acceleration system is the another important item to attain easy operation of the synchrotron. As the needed voltage is rather low as 600V, we are designing the untuned ferrite loaded cavity with wide frequency range, which can be excited with solid state amplifier. The real power system is under construction by the collaboration with Hitachi Energy Research Laboratory, by Grant-in-Aid for Scientific Research from Ministry of Education, Science and Culture.

For the medical machine, the extraction scheme of the beam is also one of the main important item and we are proposing the method which utilize the transverse RF field together with resonant extraction.(4). The method was tested with TARN II at Institute for Nuclear study, University of Tokyo and is more thoroughly investigated this year at HIMAC(5). This method extracts the beam from the ring enlarging the betatron oscillation amplitude by forced oscillation caused by the transverse RF field keeping the separatrix size to be constant. The merit of this method is the fact that the time structure of the extracted beam is rather insensitive to the current ripple of the magnet in the lattice, because the operation tune does not cross the resonance. Further this method can provide an extracted beam with smaller emittance, which will be suited for scanning. Another merit of this extraction is easy control of beam on off by switching the transverse RF field, which is considered to be utilized for synchronization with breathing.

As the injector, a combination of a Radiofrequency Quadrupole (RFQ) and Drift Tube Linac (DTL) with Alvarez type operated with high frequency of 430 MHz is to be utilized.. This type of linac is developed at Institute for Chemical Research and other institutions in these several years(6, 7, 8) and is well considered to have a good reliability. As the power source for the cavity, amplifiers utilizing a lot of vacuum tubes in parallel might be suitable in order to keep the down time to be short. The injection energy should be as low as possible with the condition of the required dose rate of 5 Gy min^{-1}. is attained and considering the space charge limit at injection, the injection energy of 7 MeV is adopted, which should be studied with use of fast tune compensation as HIMAC.(9) In order to facilitate the possibility of radioisotope production, the linac is to be extended to provide 30 MeV beam in the second step, which will enable the analysis of the disease and judge of the therapy effect with use of positron CT.

Irradiation Facility

At the facility of medical treatment in university, the manpower for operation is rather limited and it is not easy to maintain many irradiation rooms. So in the present plan, only one treatment room is to be provided together with an experimental room for physical and biological researches. In order to enable two port irradiation, a horizontal beam course and a rotating gantry are to be facilitated in this treatment room. So as to reduce the beam loss, the gantry is designed to include as small amounts of scatterer as possible.(10).

In order to increase the efficiency of the proton accelerator for radiation therapy with a single treatment room, it is proposed to make precise positioning system at the next rooms outside from the radiation controlled area with use of knock-pins. The next patient to be treated is precisely positioned beforehand on the movable couch which can be fixed exactly at the certain position in the room with knock-pins. After finishing the irradiation of the former patient, he/she is moved on the couch by a stretch to the irradiation room, where the couch is fixed to treatment stage with use of knock-pins. If enough precision of knock-pins is realized between the treatment stage and the next room, where marking with X-ray is applied, well precise positioning of the patient can be attained. With above mentioned methods, idling time of the proton beam during the positioning is considered to be largely reduced even with a single treatment room. Another feature of the present facility is possibility of two ports irradiation, which will reduce the damage of the normal cells. In Table 1, main parameters of KUMPF is listed up.

Conclusion

The Particle-Radiation Tunor-Research Center, Kyoto University will give a unique facility which enables both radiations as proton with good dose distribution and neutron capture with ^{10}B with high RBE. If these methods are selected adequately, such a tumor to be considered unable to be cured today is expected to be conquered. Another goal of the present project is to provide a prototype of compact proton facility to be installed in general hospitals. Without such wide spread use of the facilities, it will be difficult to respond to the desires of so many patients to be cured from the cancer.

Table 1 Main Parameters of KUMPF

Particle	Proton
Beam Energy	70 - 250 MeV
Repetition Rate	0.5 Hz
Dose Rate (Maximum)	5 Gy per Min
Number of Treatment Room	1
Beam Ports	Horizontal and Rotatable
Method of Beam Spreading	Scanning

Acknowledgements

The authors would like to present their sincere thanks to Director General Prof. Y. Hirao and Dr. K. Kawachi at NIRS and Prof. S. Fukumoto at University of Tsukuba for their useful suggestions and discussion. They are also grateful to Drs. M. Nishi, K. Hiramoto and J. Hirota at Hitachi Energy Research Laboratory for their collaboration on accelerator design. This work is partially supported by Grant-in Aid for Scientific Research from the Ministry of Education, Science and Culture of Japan.

References

1. Slater, J M.; Archambeau, J. O.; Miller, D. W.; Notarus, M. I.; Preston, W. and Slater, J. D. The proton treatment center at Loma Linda university medical center: rationale for and description of its development Int. J. Rad. Oncol. Biol. Phys. 22 383-389;1992.
2. Tsujii, H.; Tsuji, H.; Inada, T.; Maruhashi, A.; Hayakawa, Y.;Tada, J. and Fukumoto, S. Clinical results of proton therapy at Tsukuba Proc. of the NIRS Int. Workshop on Heavy Charged Particle Therapy and Related Subjects 73-81 1991.
3. Webb, S. The physics of three dimensional radiation therapy 174 1993.
4. Tomizawa, M.; Yoshizawa, M.; Chida, K.; Yoshizawa, J.; Arakaki, Y.; Nagai, R.; Mizobuchi, A.; Noda, A.; Noda, K.; Kanazawa, M.; Ando, A.; Muto, H.; Hattori, T. Slow beam extraction at TARN II Nucl. Instr. Meth. in Phys. Res. A326 399-406 1993.
5. Noda, K.; Itano, A.; Ogawa, H.; Kanazawa, M.; Kitagawa, A.; Kohno, T.; Kumada, M.; Sato, K.; Sato, Y.; Sudou,, M.; Takada, E.; Yamada, S.; Yoshizawa, J. and Murakami, T. Beam test on ring property in HIMAC synchrotron Proc. of the fourth European Particle Accelerator Conf. in press.
6. Inoue, M.; Dewa, H.; Fujita, H.; Iwashita, Y.; Kakigi, S.; Noda, A.; Okamoto, H. and Shirai, T. Commissioning of the 7 MeV proton linac at ICR Kyoto University Bull. Inst. Chem. Res. Kyoto Univ. , 71, No.1 57-61 1993.
7. Ueno, A.; Yamazaki, Y.; Kubota, C.; Yoshino, K.; Morozumi, Y.; Kawamura, M.; Ono, M.;Anami, S.; Igarashi, Z.; Takagi, A.; Mori, Y. and Kihara, M. The first operation of a 432-MHz, 3-MeV RFQ stabilized with PISLs Proc. of the 17th Int. Linac Conf. 1994 in press.
8. Hasegawa, K.; Ito, N.; Kusano, J.; Mizumoto, M.; Murata, H. and Tatsumi, S. First beam test of the JAERI 2 MeV RFQ for the BTA Proc. of the17th Int. linac conf. 1994 in press.
9. Noda, K. private communication.
10. Hiramoto, K. et al., contribution to this conf.

Perspectives

PTCOG XXI Meeting, and NIRS International Seminar on the Application of Heavy Ion Accelerator to Radiation Therapy of Cancer, Chiba, Japan, Nov. 1994

RBE AND SPECIFICATION OF RADIATION QUALITY IN HEAVY PARTICLE THERAPY

André Wambersie, M.D., Ph.D.[1], Hans G. Menzel, Ph.D.[2] and Reinhard A. Gahbauer, M.D., Ph.D.[3]

[1] *Université Catholique de Louvain (UCL), Cliniques Universitaires St-Luc, 1200 Brussels, Belgium,* [2] *Commission of the European Communities (CEC), Radiation Protection Programme, 1049 Brussels, Belgium,* [3] *Ohio State University Hospitals (OSUH), Division of Radiation Oncology, 43210-1228 Columbus, OH, USA*

The RBE concept is widely used in radiation therapy when non-conventional radiations are used. The definition of RBE, and its application in radiation biology, is clear and unambiguous provided the biological system, type and magnitude of effect, the dose and experimental conditions are specified. Due to the wide variation of RBE with dose and biological system, it is useful when exchanging information or prescribing a treatment, to select reference conditions for RBE specification in radiation therapy. The following conditions are clinically relevant: a dose level of 2 Gy (photon equivalent) per fraction and the "average" or "overall" late tolerance of normal tissues. The RBE for these reference conditions is the reference RBE. The clinical RBE is the ratio of the photon absorbed dose and of the dose of a non-conventional radiation which is actually prescribed at a given facility for a given tumour localisation. Selection of the clinical RBE includes a judgement of the radiation oncologist and his responsability. The RBE problem is important in neutron therapy since high RBE values (up to 5 and even more) are observed. In heavy ion beam therapy an additional difficulty is encountered because the radiation quality (and thus the RBE) varies with depth. For proton beams, although lower RBE values are observed (between 1.0 and 1.2), the selected clinical RBE has to be clearly stated. In BNCT, the highly inhomogeneous spatial distribution of the α-particle tracks and the variation of the radiation quality of the primary beam, with depth, give rise to complex problems in dosimetry and radiobiology. The concept of absorbed dose has necessarily shortcomings in BNCT, as well as the concept of RBE as it is the ratio of two absorbed doses.

INTRODUCTION: Short history

In radiation therapy with low-LET radiations, the biological effects can be predicted from the absorbed dose and the spatial dose distribution (and of course the fractionation scheme). The specification of the type of radiation (gamma-rays, X-rays or electrons) and of the energy is of little importance, since there is almost negligible RBE variation between gamma-ray, X-ray and electron beams from about one MeV to a few tens of MeV, at least for the effects relevant in radiation therapy.

However, in the 1950s-1960s, when 200 kV X-rays (orthovoltage) were progressively replaced by ^{60}Co γ-rays and high-energy X rays (and electrons), a dose weighting factor of 0.85 was introduced to take into account the fact that, at equal absorbed doses, the 200 kV X-rays are more effective than high-energy radiations.

The concept of relative biological effectiveness (RBE) was recommended by the ICRP and the ICRU in 1963 **[22]**, then defined and discussed again in ICRU Report 30 **[17]**. The above conversion factor of 0.85 was considered to be representative of the RBE of 200 kV X-rays relative to ^{60}Co γ-rays.

Radiobiological results documented more and more that the RBE values could vary for different systems, and it has been shown that the RBEs of 200 kV X-rays, relative to ^{60}Co γ-rays, could reach values in excess of 2 for some biological criteria and at low-doses, i.e. in the dose range which is more relevant for radiation protection **[20]**. However, the conversion factor of 0.85 was adequate to take into account the radiation quality differences between 200 kV X-rays and high-energy X-rays or electrons for the dose ranges and the effects relevant in radiation therapy **[16]**. These historical facts must be remembered because of the quite similar problem today with the RBE of proton beams.

The need to take account of RBE differences became much more obvious in fast neutron therapy. As a matter of fact, RBE values of neutrons, relative to γ-rays, ranging from about 1.5 to 5 or more were observed, depending on neutron energy, dose and biological effect. A single conversion factor could not longer be used (a single "RBE value" could not be assumed) to take into account these large RBE differences. <u>In fact, any therapeutic benefit for neutrons can only result from a RBE being larger for the effects on the tumour than for the effects on the normal tissues</u>.

The RBE concept continues to be important in radiation protection where radiation quality has to be taken account of for different types of exposures such as γ-rays and fission neutrons. Indeed, the concepts of equivalent dose and effective dose **[23]** and dose equivalent and effective dose equivalent **[18,19]** take into account the experimentally observed RBE values through the radiation weighting factors W_R or the radiation quality factors respectively.

The relative biological effectiveness (RBE)

When comparing two radiation qualities, one identifies the test radiation and the reference radiation. If D_{test} and D_{ref} are the absorbed doses necessary to reach a given biological effect for the test radiation and the reference radiation respectively, the Relative Biological Effectiveness (RBE) of the test

radiation relative to the reference radiation is given by:

$$RBE_{test/ref} = \frac{D_{ref}}{D_{test}}$$

A RBE value is the result of an experiment and is thus associated with an experimental uncertainty. The definition of RBE and its application in radiation biology is clear and unambiguous provided the biological system, type and magnitude of effect, the dose and the experimental conditions are specified.

When comparing two radiation qualities, there is no single but a large number of RBE values, i.e. one RBE value for every set of system, effect, and experimental conditions (with the corresponding confidence intervals). Therefore, if two experiments with a given set of two radiations result in different RBE values, of course one has to check the dosimetry and the experimental conditions, but the difference between the observed RBE values does not imply that there is a disagreement (or that one of the results is wrong): it could simply reflect the variation of RBE with dose, biological system and effect, and experimental conditions.

Strictly speaking, the commonly used jargon that a certain radiation (e.g. fast neutrons from a given nuclear reaction) have a certain RBE is fundamentally incorrect and misleading. RBE values cited in this way are usually not the result of a given experiment but are judgments based on experimental RBE's and sometimes clinical experience (see below). Although this practice is widely spread and reflects some convenience of procedure for a complex issue, it has to be stressed very clearly that the use of such comparative values for different types of radiations should not be confused with RBE values.

In the present discussion, and except when specifically mentioned, RBE values are always expressed relative to ^{60}Co γ-rays.

The RBE in fast neutron therapy will be discussed in detail in the next section. The specific problems of RBE in clinical heavy-ion beams, proton beams and in BNCT will be discussed in the following sections.

THE RBE IN FAST NEUTRON THERAPY

In the 1960s, in preparation of the clinical neutron therapy programs and in order to start this new therapy modality in safe and optimal conditions, a large number of RBE determinations were performed for fast neutrons. In some centres, comprehensive sets of RBE measurements were made, e.g. the complete RBE/dose relationships for different normal tissues and different types of tumours. In other centres, a more limited number of RBE determinations were performed which were however considered to be sufficient for starting neutron therapy in safe conditions. Experimental RBE determinations, for conditions as close as possible to the clinical conditions, are of particular relevance and are therefore especially needed **[6,7,13,33]**.

1. RBE data

Large differences in RBE values for fast neutrons, compared to γ-rays, were reported with a range between about 1.5 and 5. As examples, the Hammersmith data for different normal tissues irradiated with d(16)+Be neutrons **[6]** and some of the TNO data obtained
with a (d+T) generator **[33]** are presented in **figures 1 and 2**, respectively.

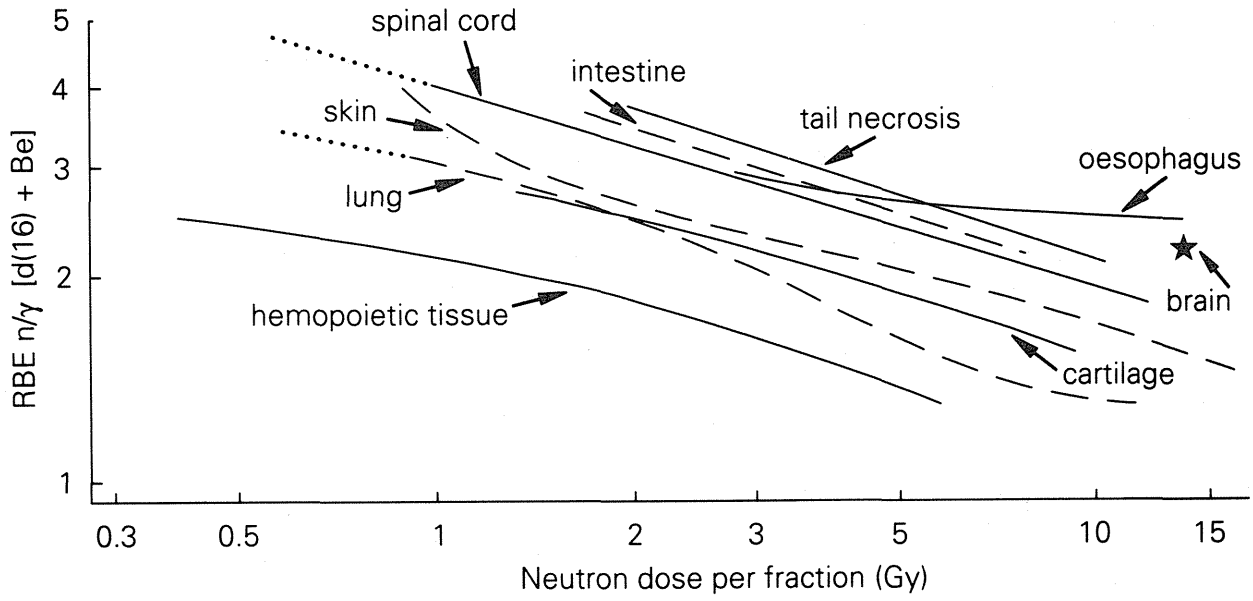

Figure 1
RBE of d(16)+Be neutrons relative to ^{60}Co γ rays plotted as a function of neutron dose per fraction. The RBE/dose relationships obtained for different normal tissues are compared. Data obtained at the Hammersmith cyclotron.
Redrawn from Field and Hornsey **[6]**.

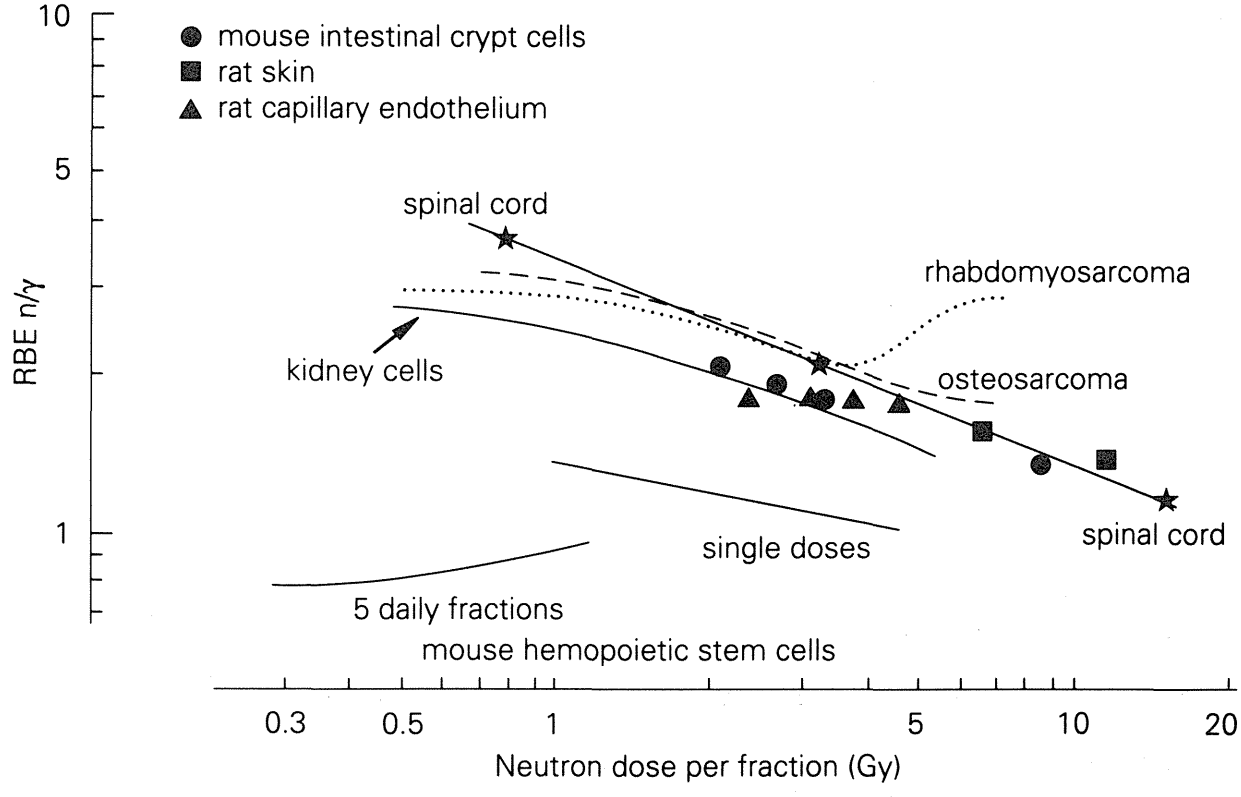

Figure 2
RBE of 15 MeV neutron [(d,T) generator] relative to γ rays, plotted as a function of neutron dose per fraction for different biological endpoints in normal tissues and tumours. For late tolerance on spinal cord, RBE increases for 1.2 to 3.7 when neutron dose per fraction decreases from 16 to 0.8 Gy
Redrawn from van der Kogel [**33**].

Some general conclusions can be derived from the available experimental data:

a) The neutron RBE increases with decreasing dose, tends to level off and reaches a plateau value for (photon) doses per fraction of about 2 Gy **[8,32]**.

b) The RBE varies to a large extent with the biological system and criterion, even for a given tissue. For example, for late effects on the spinal cord, Van der Kogel **[33,34]** has reported different RBE values for damage on white matter, blood vessels or for functional effects. In general, the neutron RBE values are larger for late responding tissues than for early responding tissues. As far as the clinical consequences are concerned, this implies that the neutron RBE's are larger for late complications than for early tolerance.

c) The RBE also varies to a large extent with neutron energy, in the energy range used in therapy : for some systems, RBE variations as large as 40% have been observed **(Figure 3) [1,2,7]**.

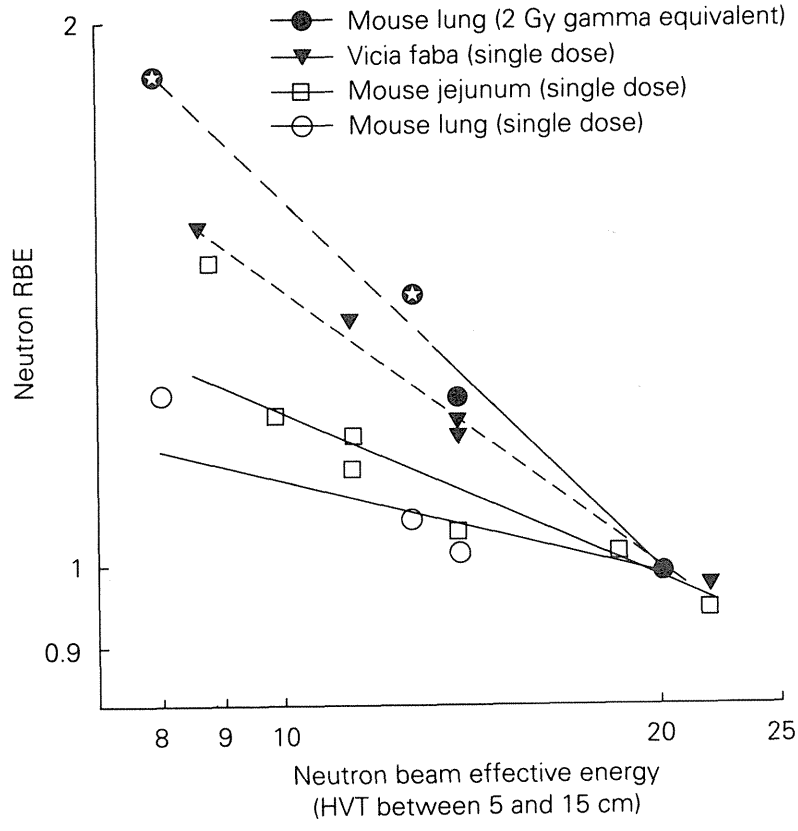

Figure 3
Variation of neutron RBE as a function of neutron beam effective energies expressed by their Half Value Thickness (HVT 5/15) for different biological systems and irradiation conditions. The reference is the p(65)+Be neutron beam produced at the variable-energy cyclotron of Louvain-la-Neuve (LLN). For the different biological systems, the neutron beams are (from left to right):

- mouse lung : d(16)+Be (Hammersmith data), d(42)+Be (Harwell data), p(45) +Be (LLN) and p(65)+Be (LLN);
- Vicia faba : d(20)+Be, p(34)+Be, p(45)+Be, d(50)+Be, p(65)+Be and p(75)+Be (all LLN data);
- mouse jejunum : d(14,5)+Be (Gent, Belgium), p(26)+Be (Riyadh, Saudi Arabia), p(34)+ Be (Orléans, France), p(34)+Be (LLN), p(45)+Be (LLN), d(50)+Be (LLN), p(65)+Be (LLN), p(66)+Be (Capetown, South Africa) and p(75)+Be (LLN).

Redrawn from Grégoire et al. **[7]**.

Therefore, the neutron energy has to be specified. This can be done by indicating the energy of the incident particles and the nuclear reaction, but also more usefully by the Half Value Thickness (HVT) of the neutron beam measured in reference conditions **[21]** and the full microdosimetric spectra **(Fig 4) [30,37]**.

The RBE variation with neutron energy raises difficulties when exchanging information between different neutron therapy facilities.

d) On the other hand, for a given energy and at a given facility, the neutron RBE does not vary significantly with depth, field size and distance to the beam axis (except in the penumbra region). However, some RBE increase has been reported in the first centimetres of the irradiated medium for neutrons produced by protons on beryllium when no polyethylene filter was inserted **[14]**.

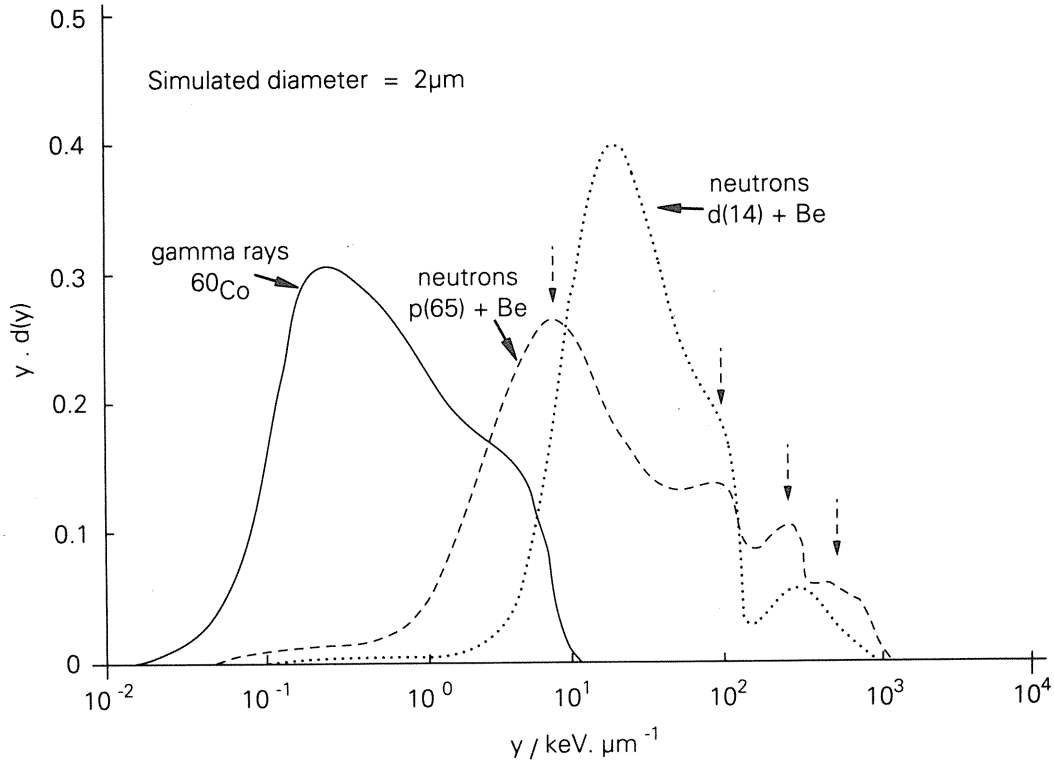

Figure 4
Microdosimetric spectra of p(65)+Be and d(14)+Be neutron beams (the highest and the lowest energies used in neutron therapy respectively). The corresponding spectrum for ^{60}Co γ rays is shown for comparison. The curves indicate distributions of individual energy-deposition events in a simulated volume of tissue 2 µm in diameter; the parameter *y* (lineal energy) represents the energy deposited by a single charged particle traversing the sphere, divided by the mean cord length. The maximum with γ rays is at 0.3 keV μm^{-1} and with d(14)+Be neutrons at 20keV μm^{-1}. The spectrum for p(65)+Be neutrons shows 4 peaks: the first is at 8 keV μm^{-1} and corresponds to high energy protons, the second at 100 keV μm^{-1} corresponds to low energy protons, the third at 300 keV μm^{-1} is due to α-particles and the last is due to recoil nuclei at 700 keV μm^{-1}.
After Pihet et al. [**30**].

Most of the RBE determinations performed in the frame of the radiobiological pretherapeutic programs were using biological systems chosen because they were suitable for this type of experiment: well codified, reliable, easy to transport, providing reproducible and quick results (e.g. mammalian cells in vitro, Vicia faba, intestinal crypt regeneration, etc) **[10,11]**.

Of course, these RBE values cannot be used directly by the radiation oncologist when prescribing the neutron dose to the patient. Data obtained for late tolerance of normal tissues and for fractionations close to the current fractionation schemes are obviously more relevant. This leads to the concept of the "reference RBE" which will be discussed in the next section.

Although these large variations between experimental RBE values raise considerable practical problems in neutron therapy, one has to stress again that any therapeutic benefic resulting from the replacement of photons by neutrons can only exist if the neutron RBE for the effects on the tumour is higher than the neutron RBE for the effects on normal tissues.

2. The reference conditions for specifying RBE

Due to the wide variation of RBE with the biological system and criterion, dose and experimental conditions, it is useful when exchanging information or prescribing the neutron dose, to select reference conditions for RBE specification. These reference conditions should be as relevant as possible to the clinical situations and in that respect the following conditions appear to be the most suitable:

- dose level : 2 Gy (photon equivalent) per fraction;
- biological system : a system and endpoint which can be considered to be relevant to represent the "average" or "overall" late tolerance of normal tissues.

The RBE for these reference conditions is the **reference RBE.**

The reference RBE values are derived from experiments performed e.g. for late CNS (brain and spinal cord) tolerance **[33,34]**, late lung tolerance **[7]** or late skin tolerance [e.g. the system presented by ANDO at the PTCOG XXI meeting in Chiba, 1994].

The definition of reference RBE implies that a single RBE value can represent the "overall" or "average" late tolerance for the normal tissues in patients. However, the fact that the alpha/beta ratios for late tolerance of different normal tissues are similar supports this approach. The reference RBE is still a radiobiological concept, although it implies some judgement on how to weight the different experimental RBE values. It also implies assumptions on the radiobiological mechanisms which could influence the observed RBE values.

3. The Clinical RBE

In contrast to the reference RBE which is a radiobiological concept, the clinical RBE is a clinical and operational concept.

The term "clinical RBE" has been used, especially in the US, and is understood as a ratio of the absorbed dose which would be prescribed in a photon treatment and of the neutron dose which is actually prescribed, at a given neutron therapy facility, and for a given tumour localisation [**36**].

It is a value that the radiation oncologist has to select when prescribing the irradiation in order to take into account the RBE differences between neutrons and photons. The selection of a clinical RBE will directly influence the number of monitor units, i.e. the dose actually prescribed to the patient. As a matter of fact, if the clinical RBE is increased by 10%, the dose to the patient will be decreased by 10%.

Although the clinical RBE is a dose ratio for two radiation qualities, it is not in a strict sense a RBE. It is chosen on the basis of the reference RBE but several additional weighting factors may have to be applied by the radiation oncologist (see below). Selection of the clinical RBE is part of the treatment prescription in the same way as a selection of the target volume and dose and the fractionation. It implies a judgement of the radiation oncologist and thus his responsibility.

Since the RBE values observed for fast neutrons are significantly higher than unity, the prescribed neutron doses will obviously be lower than the currently prescribed photon doses. A first indication about the neutron dose to be prescribed will be obtained by dividing the photon dose by the reference RBE. This implies that the doses are adjusted to give the same late tolerance (or late complication rate).

However, other factors may need to be taken into account and require much care before transferring the animal data into the clinical situation: i.e. the volume effect (mouse data vs partial organ irradiation in humans), dose homogeneity, "time factor" (difference between animals and humans), etc.

For the interpretation of the outcome of a treatment, it is important to know if the neutron dose has been selected on the basis of the reference RBE only, or if, in addition, other factors were taken into account.

Of course, when non-conventional fractionations are used, the appropriate corrections must be applied to the prescribed neutron and photon doses to comply with the definition of the reference RBE.

Finally, as more and more clinical experience becomes available, this should be used when selecting the neutron dose to be delivered to the patient (and thus selecting the clinical RBE) **[35]**. Relevant information can be obtained from dose-escalation studies or from transferring information from one centre to another one. However, in the latter case, a conversion factor taking into account radiation quality differences between the two neutron beams involved may have to be applied.

RBE IN HEAVY ION BEAM THERAPY

The problem of RBE is more complex with heavy ions than with neutrons.

First of all, the observed RBE values are high, sometimes higher than for neutrons, and they vary significantly with dose and biological system and effect. Heavy ions and neutrons are very similar concerning the evaluation of the reference RBE and the selection of the clinical RBE <u>at a given point in the beam, i.e. for the radiation quality at that point</u>.

However, there is a specific problem with heavy ions, due to the fact that the radiation quality (and thus the RBE) dramatically varies within the irradiated volume, especially as a function of penetration depth.

With heavy ions, it is no longer possible to speak about the radiation quality (or the clinical RBE) of the beam as such: one has to add at what point within the irradiated medium, the radiation quality or the RBE is specified.

In contrast, for neutrons the radiation quality (and the RBE) can be assumed to remain constant as a function of depth (except in some situations close to the surface, as mentioned above [14]) (Figure 5).

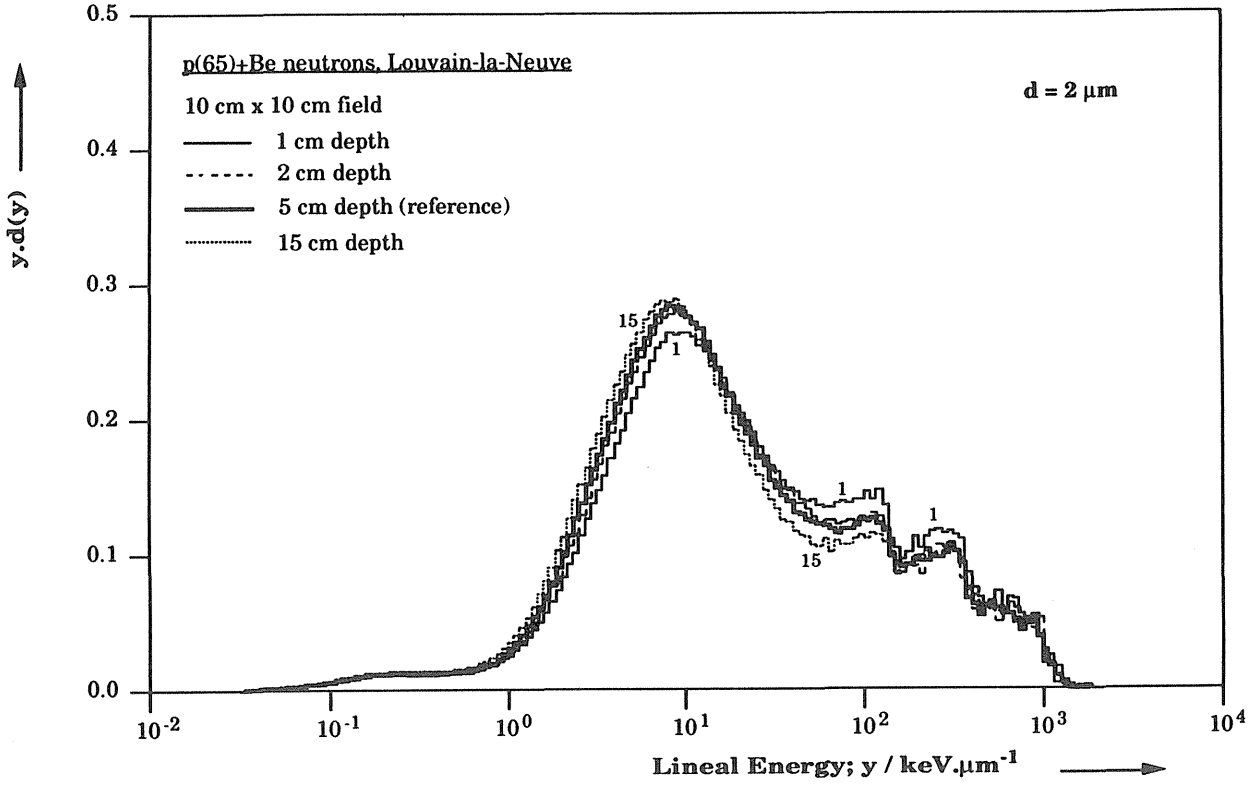

Figure 5
Microdosimetric spectra (*y* spectra) measured as a function of depth in the p(65)+Be neutron beam at Louvain-la-Neuve. A 2 cm polyethylene filter was added in order to eliminate the low-energy component of the incident neutron spectrum.
Comparison of the microdosimetric spectra measured at 1, 2, 5 and 15 cm in depth indicates only a small hardening of the beam. However, no significant RBE variation in depth was observed so far [29].

For heavy ions, it is thus necessary to define a clinically relevant "reference point", where the dose, the radiation quality and the RBE could be specified. This reference point should be selected in such a way that the dose as well as the RBE, at that point, could be considered as representative of the dose and RBE distributions in the target volume. It should be defined in a clear and unambiguous way in relation to the target volume and the beam, i.e. in the centre (or in the central part) of the target volume and, when possible, on the beam axis in the middle of the spread out Bragg peak (SOBP). The treatment prescription comprises the (physical) dose at the reference point (which is related to the number of monitoring units) and the clinical RBE at that point (and of course the fractionation scheme).

In normal conditions, the type of particles, their energy and the width of the SOBP are selected in such a way that SOBP fully covers the target volume. The point located at the centre of the SOBP on the beam axis is thus at (or close to) the centre of the target volume: it is thus the obvious choice for the reference point.

In addition, before prescribing a heavy ion treatment, it is necessary to evaluate the physical dose but also the best estimate of the reference RBE at different clinically relevant points in the target volume.

The treatment should ideally be planned in such a way that the product (physical dose x reference RBE) should be rather uniform within the target volume.

As a minimum, the dose on the beam axis at the beginning and at the end of the SOBP, and the corresponding RBE, should be determined before treatment prescription is decided.

It should be stressed again that RBE values obtained using current radiobiological systems (such as mammalian cells in vitro irradiated at high dose levels, intestinal crypt regeneration after single fraction irradiation, etc.) may significantly differ from the clinically relevant RBE, i.e. the reference RBE.

RBE IN PROTON BEAM THERAPY

The problem of RBE is qualitatively similar for protons as for heavy ions to the extent that the particle energy decreases with depth, that the beam quality changes with depth and then also the RBE.

However, quantitatively, the situation is different because the magnitude of the RBE variation is much smaller with protons than with heavy ions. Most of the experimental RBE values for proton beams, relative to gamma rays, are between 1.0 and 1.2 **[9,31]**. As examples, some experimental data obtained with the 85 MeV proton beam of Louvain-la-Neuve are presented on Figure 6.

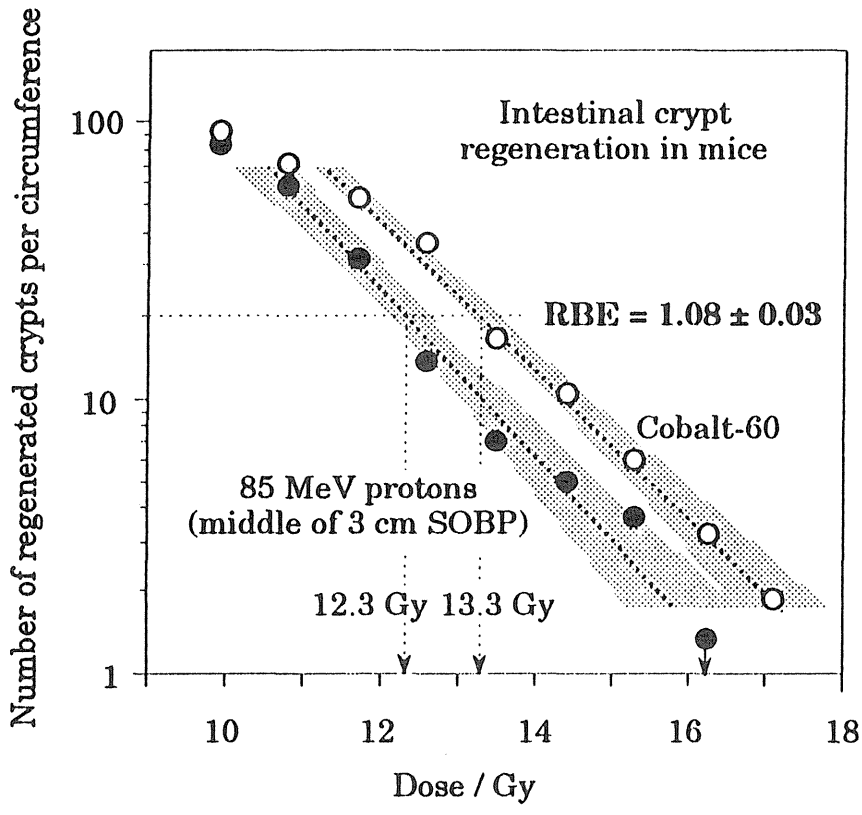

Figure 6
RBE of the 85 MeV proton beam of Louvain-la-Neuve compared to cobalt-60 γ rays. RBE is determined at the middle of a 3 cm width spread-out Bragg peak (SOBP), using as biological system the intestinal crypt regeneration in mice. Twenty regenerated crypts per circumferance are counted after 12.3 Gy and 13.3 Gy for protons and γ rays respectively, which gives a RBE value of 1.08 ± 0.03. The grey areas correspond to the confidence intervals of the exponential curves **[9]**.

Higher RBE values were reported at depths near the end of the spread out Bragg peak (SOBP) or close to the surface, but this is of little clinical significance **[3]**. Low-energy (< 1 MeV protons) have a higher RBE: indeed, the high RBE of fast neutrons (3 to 5) is mainly due to low-energy recoil protons **[28]**.

The small RBE of clinical proton beams within the volume covered by the spread out Bragg peak, in spite of maximum LET values of around 100 keV μm^{-1}, is explained by the fact that the protons have a high LET (> 10 keV μm^{-1}) for only a small fraction of their total range (some ten μm residual range). In other words, at any given point of a volume irradiated by a spread out proton beam, the spectral distribution of protons contains only a small fraction with protons below 1 MeV and thus high LET (Figure 7) **[26]**.

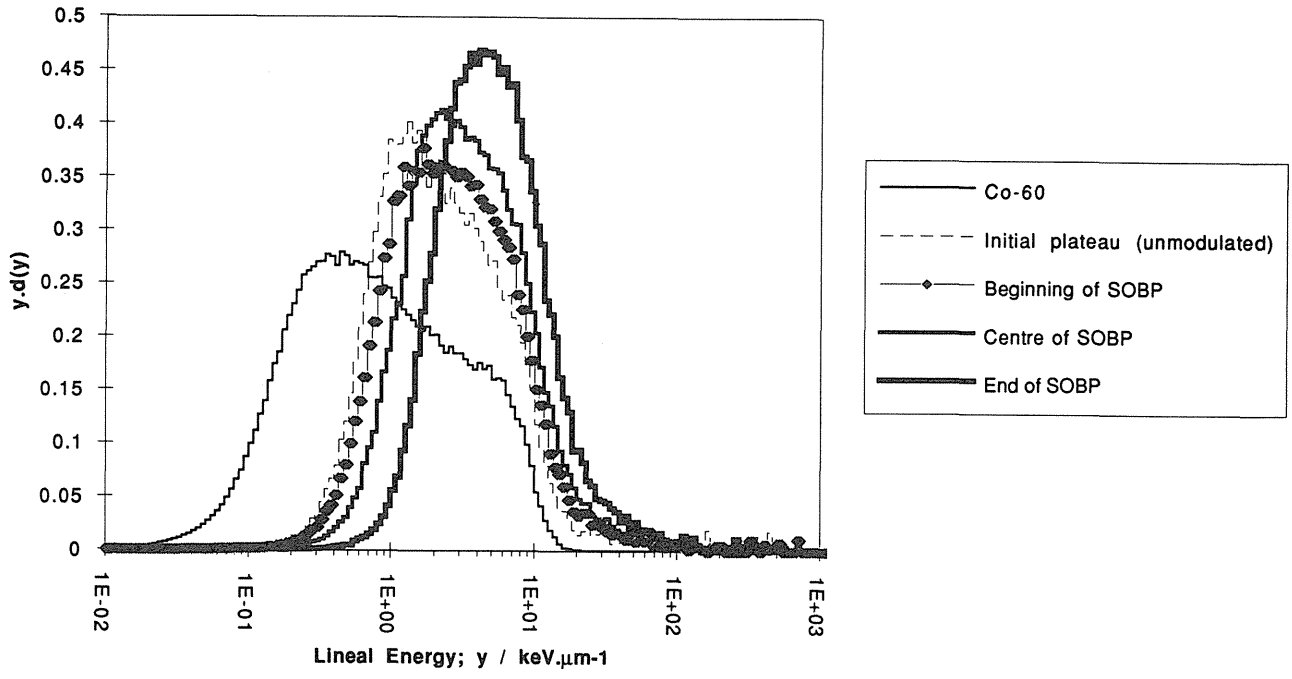

Figure 7
Microdosimetric spectra (*y* spectra) measured at different depths in the 85 MeV proton beam at Louvain-la-Neuve. The Bragg peak is spread-out over a width of 3 cm. The spectra are slightly shifted towards the high *y* values, but most of the variation occurs in a *y* region where the RBE/*y* relationship does not vary significantly.

The curves correspond to the initial plateau, the beginning, middle and end of the spread-out Bragg peak. The *y* spectrum for cobalt-60 γ rays is given for comparison **[26]**.

It is, however, this fraction which gives rise to the observed RBE values between 1.0 and 1.2.

High RBE values (> 2) have also been reported for very high energy (> 1 GeV) protons for several biological endpoints **[24,25]**. These observations are presumably related to nuclear reactions of very high-energy protons.

From a clinical point of view and for the energies commonly used in proton beam therapy, the fact that RBE of protons is only 1.0-1.2 makes the problem in principle much less critical than for heavy ions. However, it can not be ignored because the accuracy requirement in dose delivery is at least 5% **[15,22]**. A high accuracy in dose is required especially with protons since high doses are prescribed to target volumes close to radiosensitive organs. At least the same accuracy is needed for the RBE than for the dose, because a 5% change on the selected clinical RBE will bring a 5% change in the dose received by the patient.

It is reasonable to assume that the conclusions derived from neutrons can be extended to protons, i.e. that the RBE increases with decreasing dose, and that the RBE for late effects is higher than the RBE for early effects. However it is difficult to obtain clear evidence for this assumption because the RBE variations are small for protons and difficult to quantify: they are nearly of the same order of magnitude as the experimental uncertainties.

For therapy applications, selection of a clinical RBE of 1.1, as proposed by the MGH in Boston seems quantitatively reasonable **[4]**, but it has to be clearly indicated when reporting the treatment. The selection of the clinical RBE of 1.1 is a medical decision based on experimental data (and available clinical data) but is not the direct result of a radiobiological experiment. The factor of 1.1 is a weighting factor used to take into account the fact that the RBE values are in general somewhat higher for protons than for photons. Other values have been selected for the clinical RBE in some centres (e.g. 1.0 in Japan). The appropriate correction can easily be made when comparing the clinical results provided that the selected clinical RBE's are clearly stated.

The product of the absorbed dose and of the clinical RBE (sometimes expressed as cobalt-gray-equivalent, CGE) is intended to facilitate comparison with cobalt or X-ray data. However, in a strict sense, the true radiobiological "equivalence" exists, only for a given dose level and biological effect, and probably not for other dose levels and biological effects.

RBE IN BORON NEUTRON CAPTURE THERAPY (BNCT)

The BNCT beam is complex and consists of different components: epithermal and thermal neutrons and gamma rays **[5,12]**. Thermal neutrons produce protons through the ^{14}N (n, p)^{14}C reaction and gamma rays through the ^{1}H (n, γ) ^{2}H reaction, but mainly they induce an irradiation by α-particles selectively in those cells who have incorporated the boron compounds.

Part of the discussion about RBE presented above for fast neutron therapy could be repeated for BNCT applications. However, there are two additional problems which are specific to BNCT : the first one is related to the poor penetration of the thermal and epithermal neutrons, the second one is related to the heterogeneous distribution of the alpha-particles.

We will restrict the discussion to the applications of BNCT in the treatment of brain gliomas.

1. Absorbed dose and RBE variations in depth

The dose distribution resulting from the irradiation by the BNCT beam decreases rapidly with depth, mainly due to the poor penetration of the epithermal and thermal neutrons (let us exclude for the moment the α particles from boron disintegration). As a consequence in a human brain, the dose distribution but also the radiation quality will significantly change in depth, even if several irradiation fields are applied.

Therefore, when a RBE determination is performed at a given point in depth in the brain (or brain phantom), the RBE value is true only for the radiation quality at that point. The radiation quality could be characterized e.g. by its microdosimetric spectra in the same way as in fast neutron therapy.

RBE values for late tolerance of brain in different species of mammals are of course most relevant for BNCT of gliomas, especially when they are obtained in conditions similar to that planned in the clinical applications (e.g. number of fractions). However, there may be

serious limitations to the extrapolation to the clinical situation. Spatial variations of absorbed dose and radiation quality (and thus RBE) depend critically on geometry and composition of the irradiated volumes and
thus on brain sizes, location of nuclei and irradiation geometries.

On the other hand, the brain tolerance to radiation varies from one brain region to another one and it is specially low for the grey central nuclei (poorer vascularisation). The depth of these critical regions are of course different for different brain sizes and animal species.

2. *The alpha-particles*

The radiation quality problem of the disintegration products from the neutron capture in boron has two aspects :

a) the range of the alpha particles is 9 μm (and the range of the ^{7}Li particles is only 6 μm), so that each particle traverses only a few cells (diameter about 10 μm). These cells have a very high energy deposition whereas neighbouring cells will have no energy deposition at all. The dose distribution, on a cellular and subcellular level, is therefore highly inhomogeneous and any macroscopic dose quantity or concept must necessarily have shortcomings. In addition, the LET of the particles varies along the particle tracks and therefore corresponding variations of radiation quality have to be expected.

b) the spatial origin of the disintegration products is also highly inhomogeneous and depends on the concentration and distribution of ^{10}B nuclides and on the spatial fluence distribution of thermal and epithermal neutrons. This inhomogeneity, paired with the short range of the released charged particles, must put any dose concept based on macroscopically defined quantities into serious question.

It should be noted that as RBE is the ratio of two absorbed doses, i.e. macroscopically defined quantities, the existence of an appropriate averaging procedure is implied **[18,19]**. The large local inhomogeneities of absorbed dose in BNCT pose big problems if the conventional quantities and concepts are to be used.

Systematic radiobiological investigations are now being performed in different centres preparing BNCT applications, in order to assess the brain tolerance first to the BNCT beam (without boron), then after administration of different concentrations of different boronated compounds.

At a certain point in the programme, a decision will have to be made on the prescribed irradiation, which could be expressed e.g. in terms of "monitor units" or exposure time to the neutron flux and amount of administered boron compound. To take that decision in optimal conditions, all available data will have to be taken into account, including RBE data which are however only part of the information needed. The final decision will remain a medical decision depending on the clinical judgment of the radiation oncologist.

CONCLUSION

Before introducing non-conventional radiations in therapy, "pretherapeutic" radiobiological programs are usually carried out (RBE determinations) in order to start

the clinical applications in safe and optimal conditions.

In radiation therapy, the RBE concept is important and widely used if different radiation qualities are compared or combined. At equal doses, different radiation qualities (e.g. fast neutrons, heavy ions, to a lesser extent protons, BNCT beams) produce different effects or alternatively different dose levels have to be delivered to produce the same effects. The situation is complicated by the fact that the RBE of a given beam relative to ^{60}Co γ-rays is not constant but varies with dose and biological effect. Any potential therapeutic benefit of a non-conventional radiation quality (except protons) rests on RBE differences for local tumour control and for normal tissue complications respectively.

Some of the RBE determinations are carried out with rather simple, well codified radiobiological systems such as mammalian cells in vitro, Vicia faba, intestinal crypt regeneration, etc.. These systems are suitable for RBE determinations, easy to handle and provide quick and reproducible results. They are recommended for obvious safety reasons, they provide an overall check of dosimetry and irradiation procedures, and they allow for intercomparisons between therapy centres. In addition, correlations with microdosimetric data provide further confidence in both sets of data and contribute to a better specification of radiation quality.

Unfortunately, these systems are of limited help for the radiation oncologist to select the clinical RBE. For that aim, other systems should be used which provide an evaluation of RBE for an "average" or "overall" late tolerance of normal tissues. Among these, late CNS tolerance, lung and skin late tolerance have been used. The RBE for these systems obtained under reference conditions (for the current 2 photon Gy per session fractionation scheme) is the reference RBE.

In neutron therapy, introduction of the concept of reference RBE has shown to be useful because it facilitates a clearer exchange of information between centres.

However, the reference RBE provides only a first step and a quantitative basis for chosing the neutron dose to be prescribed to the patient. The prescribed dose should in general not be simply the ratio of the currently applied photon dose by the reference RBE. It is rather the result of a clinical judgement (and experience) of the radiotherapist, and takes into account not only the reference RBE but also other factors (which can not be assessed from animal experiments) as well as the clinical experience when available (especially late sequellae).

The main difference between the reference RBE and the clinical RBE is that the first one is a radiobiological concept, implying a judgement value on how to weight experimental data, the second one expresses a medical decision of the radiation oncologist and implies his responsibility.

Of course, the clinical RBE must rest on sound and accurate radiobiological data. Therefore, one can say that today it is impossible to run a therapy program with non-conventional radiations in safe conditions without the collaboration of a competent radiobiological team, in the same way as it is impossible to apply any radiation therapy without a competent physics team.

The RBE problem in heavy ion beam therapy is more complex than in neutron therapy since the

radiation quality, and thus also the RBE, changes with depth. A reference point has to be selected for prescribing and reporting the dose and also for prescribing and reporting the clinical RBE.

In proton beams, the radiation quality changes with depth as in heavy ion beams, but to a much lesser extent. A single RBE value (e.g. 1.1 or 1.0) can then be used to take into account the RBE difference between protons and photons. This clinical RBE should be clearly stated, but it should be kept in mind that it is not a RBE in a strict sence, but a weighting factor on which one has agree.

In BNCT, the highly inhomogeneous spatial distribution of the alpha-particle tracks and the substantial variation of radiation quality of the primary beam with depth, raise difficult problems in dosimetry and radiobiology. In particular, the concept of absorbed dose which is a macroscopically defined quantity has then necessarily shortcomings. The same is true for the RBE which is defined as a ratio of two absorbed doses.

However, the available radiobiological data on alpha particles (RBE, OER, repair capacity, etc.) are definitely useful to help to select the optimum conditions of application of BNCT. In addition, the RBE of the BNCT beam (without boron) for late tolerance of the brain is another useful information, although it may change with depth in terms of the radiation quality due to the poor penetration of the epithermal and thermal neutron beams.

A final decision on the prescribed irradiation will have to be taken at a certain point of the BNCT programme. From a very practical point of view, the prescribed irradiation could be expressed e.g. in terms of "monitor units" or exposure time of the neutron flux and amount of administered boron (as well as fraction number and eventually dose rate). This approach, however, must necessarily have limitations as far as transfer of clinical experience between different centres is concerned. As in fast neutron therapy, the final decision will always imply a clinical judgement. However, all the available information (physical, pharmacological, radiobiological, etc.) will help to select the irradiation conditions in an optimal way. The RBE data are needed, but could play as such only a limited role in the final decision.

REFERENCES

1. Beauduin M., Gueulette J., De Coster B.M., Grégoire V., Octave-Prignot M., Vynckier S. and Wambersie A. Radiobiological intercomparisons of fast neutron beams used in therapy, *Strahlentherapie Onkologie*, 165, 263-267, 1989.
2. Beauduin M., Laublin G., Octave M., Gueulette J. and Wambersie A. Variation of RBE between p(75)+Be and d(50)+Be neutrons determined for chromosome aberrations in Allium cepa. *Radiat. Res.*, 130, 275-280, 1992.
3. Belli M., Cherubini R., Finotto S., Moschini G., Sapora O., Simone G. and Tabocchini M.A. RBE-LET relationship for the survival of V79 cells irradiated with low energy protons, *Int.J.Radiat.Biol.*, **55**, 93-104, 1989.

4. Benk V.A., Adams J.A., Shipley W.U., Urie M.M., McManus P.L., Efird J.T., Willett C.G. and Goitein M. Late rectal bleeding following combined X-ray and proton high dose irradiation for patients with stages T3-T4 prostate carcinoma, *Int.J.Radiation Oncology Biol.Phys.*, **26**, 551-557, 1993.

5. Fairchild R.G., Bond V.P., Woodhead A.D. (Eds). Clinical Aspects of Neutron Capture Therapy. Plenum Press, New York, 1989.

6. Field S. B., Hornsey S. Neutron RBE for normal tissues. In: G.W. Barendsen, J.J. Broerse, K. Breur (Eds), High-LET Radiations in Clinical Radiotherapy, Pergamon Press, Oxford, 1979, pp. 181-186.

7. Grégoire V., Beauduin M., Gueulette J., De Coster B.M., Octave-Prignot M., Vynckier S., Wambersie A. Radiobiological intercomparison of p(45)+Be and p(65)+Be neutron beams for lung tolerance in mice after single and fractionated irradiation, *Radiation Research*, 1993, **133**, 27-32.

8. Gueulette J. Efficacité Biologique Relative (EBR) des neutrons rapides pour la tolérance de la muqueuse intestinale chez la souris. Thèse de Doctorat de l'Université Paul Sabatier, Ordre des Sciences, Spécialité Physique Radiologique, Toulouse, 1982.

9. Gueulette J., Grégoire V., Octave-Prignot M. and Wambersie A. RBE measurements in the 85 MeV proton beam produced at the cyclotron CYCLONE of Louvain-la-Neuve (Belgium), *Radiation Research* (in press).

10. Hall E.J., Kellerer A. Review of RBE data for cells in culture. In : G.W. Barendsen, J.J. Broerse, K. Breur (Eds), High-LET Radiations in Clinical Radiotherapy, Pergamon Press, Oxford, 1979, pp. 171-174.

11. Hall E.J., Astor M., Brenner D.J. Biological intercomparisons of neutron beams used for radiotherapy generated by p→Be in hospital-based cyclotrons. *The British Journal of Radiology*, **65**, 1992, 66-71.

12. Harling O.K., Zamenhof R.G., Solares G.R., Yanch J.C., Wazer D.E., Rogus R.D., Chabeuf J-M., Yam S.C., Bernard J.A., Cano G., DiPetrillo T. and Madoc-Jones H. Preparations for Phase I clinical trials of boron neutron capture therapy at the MIT reactor and the New England Medical Centre, Radiation Oncology Investigations, 2, 109-118, 1994.

13. Hornsey S. Experimental central nervous system injury from fast neutrons. In: P.H. Gutin, SA.A. Leibel and G.E. Sheline (Eds), Radiation Injury to the Nervous System, Raven Press, Ltd., New York, 1991, pp; 137-148.

14. Hornsey S., Myers R., Parnell C.J., Bonnett D.E., Blake S.W., Bewley D.K.. Changes in relative biological effectiveness with depth of the Clatterbridge neutron therapy beam. *The British Journal of Radiology*, **61**, 1058-1062, 1988.

15. International Commission on Radiation Units and Measurements (ICRU). Determination of absorbed dose in a patient irradiated by beams of X or gamma rays in radiotherapy procedures, ICRU Report 24, 1976. ICRU Publications 7910 Woodmont avenue, Suite 800, Bethesda, Maryland 20814-3095,USA.

16. International Commission on Radiation Units and Measurements (ICRU). Dose specification for reporting external beam therapy with photons and electrons. ICRU Report 29, 1978. ICRU Publications 7910 Woodmont avenue, Suite 800, Bethesda, Maryland 20814-3095, USA.

17. International Commission on Radiation Units and Measurements (ICRU). Quantitative concepts and dosimetry in radiobiology. ICRU Report 30, 1979. ICRU Publications 7910 Woodmont avenue, Suite 800, Bethesda, Maryland 20814-3095, USA.

18. International Commission on Radiation Units and Measurements (ICRU). Radiation quantities and units. ICRU Report 33, 1980. ICRU Publications 7910 Woodmont avenue, Suite 800, Bethesda, Maryland 20814-3095, USA.

19. International Commission on Radiation Units and Measurements (ICRU). Determination of dose equivalents resulting from external radiation sources. ICRU Report 39, 1985. ICRU Publications 7910 Woodmont avenue, Suite 800, Bethesda, Maryland 20814-3095, USA.

20. International Commission on Radiation Units and Measurements (ICRU). The quality factor in radiation protection. ICRU Report 40, 1986. ICRU Publications 7910 Woodmont avenue, Suite 800, Bethesda, Maryland 20814-3095, USA.

21. International Commission on Radiation Units and Measurements (ICRU). Clinical Neutron Dosimetry. Part I: Determination of Absorbed Dose in a Patient Treated by External Beams of Fast Neutrons. ICRU Report 45, 1989. ICRU Publications 7910 Woodmont avenue, Suite 800, Bethesda, Maryland 20814-3095, USA.

22. International Commission on Radiation Protection (ICRP). Report of the RBE Subcommittee to the International Commission on Radiation Protection and the International Commission on Radiation Units and Measurements. *Health Physics*, **9**, 357-386, 1963.

23. International Commission on Radiological Protection (ICRP), *1990* Recommendations of the International Commission on Radiation Protection, ICRP Publication 60, Annals of the ICRP **21**, no 1-3, Pergamon Press, 1991.

24. Kabachenko A.N., Fedorenko B.S. and Smirnova O.A. Evaluation of the cataractogenic effect of 9 GeV protons (Russ.), *Radiobiologiia*, **26**, 318-322, 1986.

25. Leont'eva G.A., Fomenko B.S., Antipov A.V. and Mantsygin I.A. Action of secondary radiation from 70 GeV protons on the cellular DNA of mammals (Russ.), *Radiobiologiia*, **24**, 9-12, 1984.

26. Loncol T., Cosgrove V., Denis J.M., Gueulette J., Mazal A., Menzel H.G., Pihet P. and Sabattier R. Radiobiological effectiveness of radiation beams with broad LET spectra: microdosimetric analysis using biological weighting functions, *Radiation Protection Dosimetry*, **52**, 347-352, 1994.

27. Mijnheer B.J., Battermann J.J., Wambersie A. What degreee of accuracy is required and can be achieved in photon and neutron therapy? *Radiother.Oncol.*, **8**, 237-252, 1987.

28. Perris A., Pialoglou P., Katsanos A.A. and Sideris E.G. Biological effectiveness of low-energy protons. I. Survival of Chinese hamster cells, *Int.J.Radiat.Biol.*, **50**, 1093-1101, 1986.

29. Pihet P. Etude microdosimétrique de faisceaux de neutrons de haute énergie. Applications dosimétriques et radiobiologiques. Thèse de Doctorat en Sciences, Université Catholique de Louvain, 1989.

30. Pihet P., Norman C., Gueulette J., Menzel H.G., Wambersie A. Microdosimétrie des faisceaux de neutronthérapie d(50)+Be et p(65)+Be à Cyclone, Louvain-la-Neuve. In Radiophysique, XXIV Congrès de la Société Française des Physiciens d'Hôpital, Tours, 1985, 269-277.

31. Robertson, J.B., Williams J.R., Schmidt R.A., Little J.B., Flynn D.F. and Suit H.D. Radiobiological studies of a high-energy modulated proton beam utilizing cultured mammalian cells, *Cancer*, **35**, 1664-1677, 1975.

32. Tubiana M., Dutreix J., Wambersie A. Introduction to radiobiology. London: Taylor and Francis, 1990.

33. Van der Kogel, A.J. Late effects of radiation on the spinal cord: dose-effect relationships and pathogenesis. Thesis. University of Amsterdam. Publication of the Radiobiological Institute TNO, Rijswijk, The Netherlands, 1979.

34. Van der Kogel A.J., Sissingh H.A. and Zoetelief J. Effect of X-rays and neutrons on repair and regeneration in the rat spinal cord, *Int.J.Rad.Oncol.Biol.Phys.*, **8**, 2095-2097, 1982.

35. Wambersie A. Neutron therapy from radiobiological expectation to clinical reality. *Radiation Protection Dosimetry*, **44**, 379-395, 1992.

36. Wambersie A., Battermann J.J. Practical problems related to RBE in neutrontherapy. In: K.H. Kärcher, H.D. Kogelnik and T. Szepesi (Eds), Progress in Radio-Oncology III, ICRO (International Club for Radio-Oncology), Vienna, Austria, 1987, pp. 155-162.

37. Wambersie A. Contribution of microdosimetry to the specification of neutron beam quality for the choice of the 'clinical RBE' in fast neutron therapy, *Radiation Protection Dosimetry*, **52**, 453-460, 1994.

38. Wambersie A. and Menzel H.G. RBE in fast neutron therapy and in boron neutron capture therapy. A useful concept or a misuse? *Strahlentherapie Onkologie*, **169**, 57-64, 1993.

PRESENT AND FUTURE OF HIGH-LET RADIATIONS IN CANCER TREATMENT

Pierre CHAUVEL, MD

Head Radiotherapy Department and Biomedical Cyclotron
Centre Antoine-Lacassagne, 227 avenue de la Lanterne 06200 Nice - France

Summary: High-LET (Linear Energy Transfer) particles are mainly represented by neutrons and light ions (as carbon, oxygen, neon or heavier particles). Compared to those two groups, π mesons and particles issued from boron neutron capture are presently more exotic but are also adressed.
The potential advantages of all these high-LET particles are different. The advantage of neutrons comes from biological considerations as they present a depth dose distribution comparable to photons. The use of heavy charged particles in radiotherapy is mainly linked to their finite range at a depth which is function of their energy. It represents a potential progress towards a better local tumor control and a decrease in morbidity related to radiation injury of healthy tissues surrounding the target volume. Light ions join the two types of advantage: biology and physical selectivity. But this assertion is only true if treatment planning systems can provide an accurate 3-D dose distribution taking into account both physical and biological aspects especially for heavier ions. The influence of LET on the biological effects, its variations related to the depth, particle, target tissue, position in the Bragg peak, inhomogeneities and other factors make the possible models for treatment planning extremely complex. The use of π mesons was based on the same rationale as light ions, but the results were disappointing, confirming in facts that their physical selectivity and LET were not sufficient.
Boron neutron capture therapy (BNCT) is based on the high cross section of the stable boron-10 nuclide for thermal neutrons. At the time of capture, the boron nucleus desintegrates into highly energetic alpha (^{4}He) and lithium-7 (^{7}Li) particles which range is in the order of a cell diameter. Assuming a preferential uptake of the boronated compound in the tumor cells, these cells will be killed by intracellular irradiation.
Since the fourties high-LET particles are more or less used in cancer treatment and a lot of questions related to their usefulness remain unsolved after fifty years. Presently high-LET particles areused in less than twenty neutron facilities around the world, three BNCT installations, one π mesons facility, and one light ions facility recently opened. The immediate future of neutrons is uncertain. The π mesons facility is closing. Some BNCT facilities are on the verge of opening and one charged particles installation will start treatments in a few months. New projectsand developments exist for high-LET particles and classical radiotherapy: relevant applied research and clinical trialshave to be organized to assess the place of each technique.

INTRODUCTION

«Advance in radiotherapy can be achieved by obtaining a greater tumor control and by reducing the morbidity of treatment, both early and late» (S.Dische).
Use of charged particles in radiotherapy represents indisputable progress in localization of the dose delivered to tumour masses and reduction of the dose received by adjacent healthy tissues. For example, protons improve the physical selectivity of the irradiation, i.e. the dose distribution, while high LET (Linear Energy Transfer) radiation produce different biologic effects, decreasing the differences in radiosensitivity, and allowing radiation therapy to control radioresistant tumours.
Fast neutrons represent the most known of these high LET particles, but they suffer of a relatively poor physical selectivity. The two approaches (physical selectivity and biological advantages) are met when using light ions as Carbon, Oxygen, Neon. For the purpose of this paper we call "heavy charged particles" protons and heavier ions and "light ions" the charged particles from nitrogen to argon, in order to agree with physicist language. Using these particles a highly selective high-LET radiation therapy can be performed for radioresistant tumours without damaging healthy tissues. This enhances the therapeutic ratio for tumour lying in or close to critical structures such as the brain and the spinal cord. Preliminary results obtained at the Lawrence Berkeley Laboratory (LBL) Berkeley (USA) demonstrate an improved local control of unresectable, slowly growing tumours, confirming what could be extrapolated from proton and neutrontherapy. Furthermore, radioactive light ion beams or spontaneous positron emission in a particle beam can be used to verify the accuracy of treatment planning by checking the range of the particle with a PET camera: this allows a feedback control of the depth dose deposition (13). One of the main problems in using these ions remains the ability to take into account all their characteristics and their variations in a reliable treatment planning system. Thissystem would have to depict not only the physical dose distribution but also the dose corrected for the biological effects of these particles. For conformal radiotherapy techniques using charged particles or not, patients cure passes through an accurate delivery of the treatment, which implies the possibility of performing an accurate treatment planning (50, 38).
Los Alamos (USA), Vancouver (Canada) and

Villigen(Switzerland) were involved in π mesons therapy and have treated some hundreds of patients. At present time, only Vancouver is still treating and it seems that protons will be the future option of the facility. In facts π mesons did not give the expected results: their physical selectivity is not as satifying as the one of proton beams and the real LET in the tumor volume is closer to protons than to clinical neutron beams. They will not be considered in this review.
BNCT has experienced a lot of trouble initially and suffered from a very bad fame: a very high complication rate was observed. This was due to the properties of boronated compounds used which concentrated more in the vessels than in the tumor cells. Secondary to tumor neovascularization and lack of measurements of intratumoral uptake, it was thought that the tumoral concentration was excellent. This led to a poor dose distribution with overdosage of vascular healthy tissues and underdosage of the tumor. The works of the japanese teams allowed a "second début" of this sophisticated irradiation technique and the future of BNCT seems more favourable than twenty years ago.
All these techniques are not accessible to a large number of radiation oncologists and patients, which leads to a subcritical mass of informations compared to main stream radiotherapy. Furthermore this situation results in a lack of interest from physicians, patients, politicians, and industry. Furthermore, the present developments in conformal therapy and alternative fractionation raise a major interest in the radiation oncology community, which could jeopardize the future of more exotic particles unless their present applications are better defined and are also improved through more sophisticated techniques.

PRESENT STATUS OF HIGH-LET PARTICLES

Neutrons

Neutrons have been and are mainly used to treat radioresistant tumors, radioresistance being initially attributed to poor oxygenation (52) and later to more complicated cellular phenomena related to intrinsic sensitivity (4) and/or to cell kinetics and sensitivity. Neutrons and more generally high-LET particles tend to reduce the individual differences in radiosensitivity (10). Neutrons are more efficient against cells in S or G_0 phase of the cell cycle. Moreover sublethal damage repair after neutron irradiation is less important than after X ray (19), due to the high frequency of lethal lesions occuring after neutron irradiation.
From the clinical experience accumulated during the last 20 years neutrons may be used as a standard treatment in some clinical situations. They generally concern inoperable or unresectable tumors, slowly growing, well differentiated. This was established from randomized clinical trials for locally advanced inoperable and/or relapsing salivary gland tumors (34), locally advanced prostate carcinomas (35, 45), inoperable squamous cell carcinomas of the lung (32), unresectable head and neck squamous cell carcinomas with fixed nodes (26, 28, 18). For some other tumors the indications rely only on clinical experience and are not supported by randomized studies: inoperable tumors of paranasal sinuses (14), soft tissue, osteo and chondrosarcomas (36, 14), melanomas (55) are in this situation. Presently inoperable salivary gland tumors are the only one for which the NCI strongly recommends the use of neutrons (39).
Disappointing results were obtained for brain tumors (48). This is in agreement with the radiobiological data and especially the high RBE value observed for central nervous system.The possibility for these tumors to benefit from a small neutron boost has been suggested and is under investigation (7).
For some other tumor types highly radiosensitive to low-LET radiations as seminomas, lymphomas and more generally rapidly growing, poorly differentiated tumors, neutrons are contraindicated. Their use in these cases would reduce the favourable differential effect between tumor and normal tissue radiosensitivities.
A last group of tumors includes those types for which further studies are necessary (55, 48, 17, 37). This group mainly includes bladder, rectum, cervix, stomach and biliary duct tumors.
Two factors need to be considered when evaluating the results: - the lack of individual predictive tests, which make impossible the identification of «subgroups» or individuals for which neutrons could bring a benefit or on the other hand give adverse effects - the «poor technical conditions» of the treatments applied in many centres for which the neutron beam was closer to a 200kV than to a modern photon Linac. A large number of complications related to the use of neutron beams are due to a poor depth dose distribution (27). We know from the results of the RTOG trial on prostate cancer that the treatment technique plays a major role in the complications and sequellae (45) and the improvement of neutrontherapy technique must be one of our goals for the future.
Consequently, an accurate picture of the merit of neutrons irradiation will require many clinical trials.

Neutron Capture Therapy

The first clinical experiments to use a bimodal treatment modality combining a thermal neutron beam and a boron compound to selectively destroy cancer cells by the alpha radiation induced by the neutron capture in the boron-10, were set-up by neurosurgeons in the 1950s (51). As for fast neutrons the first results are controversial but new developments are sufficiently encouraging to justify a European Concerted Action for the treatment of glioblastomas using the european nuclear reactor located in Petten (Netherlands) and to

allow United States to start again with medical programs at Brookhaven and MGH/MIT/Harvard. There is a large interest throughout the world for this type of targeted radiation treatment as summarized in a recent special issue of the International Journal of Radiation Oncology, Biology and Physics (40). This new interest is mainly due to a better understanding of the past experience, to the elaboration of better boron compounds demonstrating an intracellular uptake as sodium borocaptate (BSH) and boronophenylalanine (BPA), to the successes of the japanese teams of Hatanaka for brain tumors and Mishima for skin melanomas, and to the construction of new thermal and epithermal beams.

The bad results obtained at the very beginning of BNCT (all patients died) are explained by: 1-the poor penetration of the thermal neutron beam through the scalp giving skin and bone complications, 2-the radiation damage in the blood vessels of the brain where the boron compound was circulating at a high concentration while almost no cellular uptake was possible, leading to almost exclusive intra-vascular interactions and irradiation, 3-underdosage of the tumor bed leading to a lack of local control, 4-poor understanding of the biology, pharmacology and pharmacokinetics of boron compounds. Hopefully, while treatments were stopped in the United States, they continued in Japan and fundamental research also continued in the North America.

Even if the interpretation of recent results is sometimes difficult or controversial, the 20% survival at 5 years obtained by Hatanaka from a series of 120 patients treated for glioblastomas cannot be ignored.

New methods of investigations led to acquire the certitude that the BPA intracellular uptake is sufficient to ensure a favorable tumor to normal tissue ratio while giving a sufficient dose in the tumor cells (43). These experiments confirm the possibility to achieve an interesting differential effect.

In the same way, it should be interesting to use boron compounds in the fast neutron beams in order to create a concomitant tumor boost (46). This combination of fast and thermal and epithermal neutrons seems to encounter an increasing interest in the teams involved in neutron therapy.

Charged particles

The last seventy years in radiation oncology have shown that each amelioration in the radiation depth dose distribution is correlated with an improvement in therapeutic results, both in term of increasing tumor control and decreasing side effects of treatments. This was established by the works of Bush and Allt for cancer of the cervix: going from 200kV to Cobalt 60 and further from Cobalt 60 to 22MV photons increase the survival of patients by a factor of two for each step. This was also the case for Hodgkin's disease, as shown by Kaplan, for oropharynx, as shown by Fletcher, and for prostate carcinomas, as shown by Bagshaw. All these results were summarized and presented during the «NCI Proton Workshop» in April 1989 (54) in Bethesda.

In parallel to the progressive enhancement of radiotherapy accuracy, a new kind of possibilities appeared in the 50"s, with the therapeutic use of the first charged particle beams. Due to their charge and heavy mass, protons present favorable absorption characteristics known as the Bragg curve. The protons energy at the entrance and the tissue density along their track, determine the depth of penetration of the beam and the position of the Bragg peak. Spreading out the Bragg peak, using modulating devices, permits to obtain a plateau which correspond to the thickness of the treatment volume. The heavy mass of the particle results in minimal deviation and therefore minimal side scattering. This results in sharp fall-off and penumbra. These main characteristics permit the radiation oncologist to give a dose in depth superior or at less equal to the entrance dose in case of a Bragg peak spread-out on the total range.

The first proton beams were used in Berkeley (University of California San Francisco, Lawrence Berkeley Laboratory)(UCSF/LBL) in 1954, followed in 1957 by Uppsala (Uppsala University, the Svedberg Laboratory)(UU/SL) and in 1959 by Boston (Massachussets General Hospital, Harvard Cyclotron Laboratory)(MGH/HCL). These pioneers paved the way of charged particle therapy and demonstrated their superiority for some tumor sites untreatable by standard radiation techniques. Following these pioneers, some more facilities were opened for partial medical use, in previous USSR (Dubna 1967, Moscow 1969, Gatchina 1973), in Japan (Chiba 1979, Tsukuba 1983) and in Switzerland (Paul-Scherrer Institute, Villigen 1985)(PSI). Despite the fact that these accelerators were not installed in a medical environment but in Universities or Nuclear Physics Research Laboratories, several thousands patients were treated. The usefulness of proton beams was established and thanks to this experience and hospital-based machines now begin to be available for clinical purposes. But even considering the LET increase at the end of the range in a proton beam, protons cannot be considered as high-LET particles and the RBE currently used for clinical applications is close to 1.1. Nevertheless they are the most widely used heavy charged particle demonstrating the interest of an accurate depth dose distribution allowing to increase the total dose in the tumor volume while sparing healthy tissues. The clinical results obtained confirm the relevance of this assertion (3).

Light ions, from nitrogen to neon, join in the same particle the physical advantages of protons and the biological advantages of neutrons. Their use is

presently limited by the very small number of facilities available. In the recent past Berkeley made the pioneer work, establishing the rules for using these particles in medicine. A lot of fundamental and clinical research was performed and applied to the treatment of around 1500 patients before the facility was closed for budgetary reasons. The results obtained confirmed the interest to use these particles in treating radioresistant tumors close to critical normal tissues (9). The weaknesses of this program were mainly due to the relatively small numbers of patients included for each pathology but particularly to the low proportion of cases fully treated with neon. This demonstrates the importance of the reliability of the accelerator for medical applications and the need for a large number of patients treated homogeneously over a relatively short period.

But these particles were considered by the large majority of radiation oncologists as a "dream car" and they prefered to investigate more cost effective alternatives. For this reason the EULIMA (EUropean Light Ion Medical Accelerator) project (12) was not really supported by the radiotherapy community nor by politicians and failed by the end of the feasibility study on the grounds that the project was too expensive and complex. The 400MeV/nucleon accelerator recommended was a synchrotron with a circumference of 50 to 60 m, the other solution studied being a supraconductive cyclotron less than 5m diameter and 4m height (16).

Hopefully the situation in Japan allowed to design and build the HIMAC (Heavy Ion Medical Accelerator in Chiba) facility in Chiba, despite the major costs.

Some few teams keep interest in light ions and are presently involved in fundamental and radiobiological research and/or development of a medical beamline. In Germany a close collaboration between the Heidelberg Cancer Center and the GSI in Darmstadt is on the verge of opening a treatment facility able to treat a hundred patients/year. Some of the solutions elaborated for beam delivery systems were studied in the framework of the EULIMA project. As in Darmstadt with whom there is a close collaboration, a radiobiological program is running at the GANIL (Grand Accélérateur National d'Ions Lourds) in Caen, France and should perhaps lead to the use of the Saturne synchrotron (Saclay - France) for some experimental treatments, but no formal decision has yet been taken by french authorities.

In Italy the feasibility study of the TERA project (TERapia con Adroni) has been completed (2) and the group hopes to find funds soon. The project differs from the EULIMA by incorporating beside light ions treatments, protons and BNCT. As the EULIMA project the facility is designed to treat 1000 patients/year. The estimated cost per patient varies from 10,400 to 15,600 US$ to be compared to the estimate of 9,000US$ for the EULIMA project three years ago! These provisional costs do not exceed the mean cost of present cancer treatments as estimated during the feasibility study of the EULIMA project (16).

WHAT FUTURE FOR THESE PARTICLES ?

After this review of the present situation of high-LET particles, we have to briefly introduce the situation of low-LET particles in order to better understand in what context the future of high-LET has to be investigated.

New developments not only occured in the field of charged particles and high-LET but also in standard radiotherapy. Stereotaxy, conformation, biology, alternative fractionation should compete with high-LET conformation. This tendancy was reflected by the program of the last ESTRO meeting in september 94: from 80 sessions, 1 was partly devoted to heavy particles, 4 to fractionation problems, 7 to conformal therapy and 13 to cell kinetics and biological approaches in radiation oncology (1). The same problem has to be underlined during the training of radiation oncologists: very few of them have any exposure to heavy particles. The future of high-LET particles has to deal with this apparent lack of interest from the profession at large and in this context a major effort is indicated.

But these problems are not the only one affecting the potential future of high-LET particle. Mostly the techniques of treatments and the treatment planning have to be improved to be competitive with new developments occuring in photon beam radiotherapy.

Neutrons

We saw that neutrontherapy suffers from a lack of accurate criteria for the selection of patients who could benefit. Many hopes were based on predictive assays but it is clear now that we need more than one test to evaluate the radiosensitivity of a tumor. But important developments are in progress in this field and in a near future it should be possible to discriminate between tumors of the same type those which could benefit from one or another type of radiation and/or fractionation.

The second problem concerns the dose distribution of neutrons and healthy tissues protection. This means that tumor volume and treated volume have to be very carefully assessed using all imaging procedures available in order to increase the accuracy of dose distribution and sparing of normal tissues. We know that a large part of neutron complications resulted from poor techniques and that not only there are great differences in the complication rates between low and high energy machines, but also between the different beam delivery systems. Neutrons will be safe and credible if the trend towards a general use of isocentric gantries and multileaves collimators continues.

In that way it should be relevant to consider the possibilities to realize conformal neutrontherapy using gantries and multileaves in non coplanar multiple fields arrangements. 3-D treatment planning sytems used for photons should be slightly modified for neutron beams by introducing the proper physical data. Considering the improvements achieved in photon dose delivery, it is quite clear that we should obtain from neutron beams something close to light ions dose distribution with less variation of LET than in the spread-out Bragg peak of ions. Neutrons could therefore better compete with photons for their own indications.

Another promising avenue is the possibility of creating through the use of neutron capture in boron-10 a concomitant boost in the tumor volume.

Neutron Capture Therapy

After a long latency this technique is reintroduced in clinical oncology in the USA and shortly in Europe. Two approaches have to be considered: 1) pure neutron capture therapy (NCT) in thermal and/or epithermal neutron beams, 2) neutron capture potentialization (NCP) (i.e. concomitant boost) of a fast neutron beam treatment by giving boronated compounds all along the neutron sessions.

Pure NCT suffers from the same potential troubles as other high-LET treatment modalities: very few facilities available for patients, time sharing with nuclear industry or research, almost no hospital-based project, high cost for new installations. Added to these problems are specific ones: importance of pharmacokinetics and measurement of intracellular uptake of the drug, high cost and low availability of some compounds as BPA, necessity to improve tumor selectivity of the drugs by refining the conception of boron carriers in close collaboration with biology and chemistry, possible interest in alternative compounds. Some teams presently involved in high-LET and/or charged particles therapy are also interested in NCT and are studying the possibility to adapt their beams for the production of epithermal neutron beams as Uppsala, Villigen and Nice. If these projects succeed at an acceptable cost, the future of NCT should be better and a more general interest could rise-up in teams performing neutrontherapy and presently interested (or not) in NCP.

This NCP modality seems to stimulate a lot of reflexions in the small world of neutrontherapy. These reflexions certainly pave the way for NCT developments if the NCP experiments demonstrate their feasibility and a clinical advantage.

Charged particles

Despite the new project AUSTRON (44) under development in Austria, the future of light ions in radiation oncology is not very clear, due to the economic problems encountered in all developped countries. In addition, if light ions share some problems with protons, they also have their specific troubles mainly in the field of treatment planning.

A perfect definition of the different structures related to tumor, normal or critical tissues has to be elaborated from multimodality imaging documents (CT scan, magnetic resonance imaging, positron emission tomography), including corrections for geometric discrepancies between the sets of images (30, 23, 22). The calculation of tissues densities along the particles path, their influence on the dose distribution are much more critical than for neutrons and photons. While a 3 cm thick bone reduces the intensity of a Cobalt 60 beam by some 11% at all depth beyond the bone, the effect on a charged particle beam is to reduce the range by around 2 cm (25). In the latter situation the inadequate correction of tissue inhomogeneities can easily cause a geographic miss. Also if aeric cavity is included in the beam, its contour has to be taken into account accurately. If it is underestimated, the range will be longer than calculated and if a critical structure lies at the end of the range, it will partly receive full dose. On the other hand if this cavity is partially filled by an exsudate (as a maxillary antrum during radiotherapy or an influenza) the range will be diminished. The status of these cavities has to be often verified along the radiation course in order to avoid over or underdosage, a simple sinusitis being able to destroy a sophisticated treatment plan! This example demonstrates the interest of beam-monitoring systems based on PET. The first measurements made in the LBL underlined the relevance of the method (11). All inhomogeneities have not only to be known but to be compensated to shape the target volume (53).

Up to now heavy charged particle beams are spread-out using ridge filters or modulating wheels in order to conveniently cover the whole length of the target volume in the beam direction (31). These devices achieve a fixed passive modulation of the beam. They produce extra-irradiation of healthy tissues located upstream of the target volume. Moreover, the introduction of these elements in the beam increases the scattering and the lateral penumbra. Several methods have been proposed to reduce these effects. The treatment volume may be divided in many layers and the size of each layer adapted to the target volume using a variable collimator avoiding unecessary irradiation of normal tissues by reducing the surface exposed to the beam to the necessity of each layer. The beam is modulated to cover the thickness of the layer and the distal surface is shaped by a compensator to conform with the shape of the distal surface of the volume. In a near future this technique will likely be supplanted by beam scanning (24, 42, 47) or pixel

scanning (6). In beam scanning the contour of each layer is given either using a variable collimator limiting the surface exposed to the beam or a variable speed raster scanner conforming the scanning to this surface. The energy variation allowing to pass from layer to layer may be given actively by the accelerator or passively by a range stacking system. The pixel scanning or pencil beam technique is close to the raster scanner system. The elementary pencil beam varies in energy and position from a pixel to another in the volume to be treated. As for the raster scanner, the speed of the scanning can be adjusted in order to compensate for the doses previously given in a part of a layer by the entrance plateau of the deeper layers. The physical homogeneity of the dose distribution achieved is almost perfect and gives the maximal protection of normal tissues in depth and laterally.

Future treatment planning systems will have to demonstrate their capability and reliability in this 3-D conformal charged-particle therapy. But the problem is more simple for protons than for heavier ions. We know that the LET increases at the end of the Bragg peak of a proton beam enhancing the biological efficiency of the dose delivered in the last few millimeters of the target volume. It is necessary to spread-out the peak in order to cover the length of the tumor with an homogeneous dose. This is obtained through modulation which consists in superimposing Bragg peaks at different energies. This leads to irradiate the proximal part of the tumor by the summation of the entrance plateau of these Bragg peaks more than by the peak itself. This could be relatively easy to correct by diminishing the physical dose deposited in these pixels because the RBE gradient along the spread-out Bragg peak is smaller and less complex for protons than for light ions. The correction for different RBE becomes quite complex for light ions.

Problems adressed by light ions :

From a physical point of view light ions are less affected by multiple scattering and the lateral penumbra of these beams is less than for proton beams. Due to this particularity the profiles in depth are better for heavier ions and the lateral penumbra is less affected. On the other hand, due to fragmentation, light ions present a "tail of dose" increasing with the Z of the particle. Along the path ions break up due to nuclear interactions as they pass through tissue. Lighter fragments such as protons and helium ions have larger ranges than the parent ion and so deposit energy beyond the theoretical range. The fragmentation depends upon the tissue composition and it is of real interest to be able to know precisely the proportion of the different elements and their energy in the "tail of dose" in order to estimate their biological effect in normal tissues hit by these components.

The biological effect is in facts the main difference between protons or helium and heavier particles for which the biological efficiency is in close relationship with the LET, the particle, the energy of the particle, the position in the entrance plateau or in the peak, the position in the spread-out Bragg peak, the dose/fraction, the type of tissue, the size of cell nucleus, and the same parameters for each fragment of the secondary beam. This complexity explains why the existing treatment planning systems calculate the physical dose distribution and not a "biological" dose (15, 8, 5, 41, 21) which is extrapolated in a point to point calculation from clinical experience and some biological models. The LBL made an attempt to incorporate RBE (Relative Biological Efficiency) in the calculations of dose distribution but this was abandonned. It has to be noted that RBE is a controversial concept, inadequate for a dose equivalence calculation.

Another problem has to be underlined regarding treatment planning with heavy ions: the beam delivery system used. As it was previously described, the different devices influence the dose distribution and the composition of the beam with more or less fragmentation depending on the use or not of compensators, bolus, and fixed modulation. All these factors influence the biological effect of heavy ion beams and must be entered in a reliable model if one wants to calculate a biological equivalent dose. The works in progress in GSI, Darmstadt (20, 29, 33, 49) are of great importance both for dose distribution monitoring and biological equivalence calculations. The energy of the GSI synchrotron may be varied from pulse to pulse as well as the speed of the beam scanning. This allows to compensate the physical dose distribution in each layer of the target volume to take into account for example the dose given in a part of slice B by the irradiation of slice A. The LET in the portion of slice B irradiated by the beam of slice A is less important than in the peak located in slice A. The dose has to be corrected not only for the physical dose but also for biological equivalence. This effect expands along the track of the particles. A substantial part of the irradiation is given by low-LET in the entrance-plateau. This phenomenon increases with the thickness of the target volume resulting in a uniform physical dose given by a mosaic of different LET. The complexity of the problem increases when the irradiation is given through multiple ports. The external part of the target volume may then receive a higher mean LET than the central part. Considering that the external part of the volume is mainly constituted of healthy tissues, this could result in a normal tissue complication probability enhancement and a diminished tumor control probability.

Sparing normal and critical tissues from the high-LET components of the beam is the main objective, but it is

also relevant to put the high-LET part of the beam in the tumor: this is only partly solved by the geometry of irradiation, the problem being complicated by the existence of the "tail of dose" which does not exists for protons or helium. This means that the most critical organs have often to be located on the lateral part of heavy ions beams which is less affected by scattering and fragmentation.

We could say that if for proton beam therapy the problems of treatment planning are almost solved, for heavier ions a lot of uncertainties remain presently unsolved. Therefore, many experiments are required to have a better understanding of the biological effects and dose equivalence in humans. A comprehensive and cautious biological and clinical research program are mandatory before treating a large number of patients.

Logistics

To facilitate further analyses, it could be relevant to be extremely selective in the number of tumor sites and histology referred for light ion treatment instead of accepting to treat a relatively large number of heterogeneous tumors. This policy could allow a faster and better understanding of the treatment results. It necessitates to set-up an international network for patients referral.

The research effort to answer the many questions on the utility of high-LET particles in cancer care will require 1) an international cooperation 2) a simplification of the referral process and its administrative hurdles 3) a priorization of research efforts defining the patient population 4) appropriate long term funding effort.

We have to keep in mind that in some clinical situations an alternative to high-LET exists, for example stereotaxic radiotherapy for base of skull tumors, and we must organize comparative studies. When there is no alternative, we have to prove it and let it know to the clinical oncology community or in other words refine the unique indications for high-LET particle beam therapy.

In order to be helpful for public health authorities, clinical trials will have to encompass both clinical and economic endpoints. It is important to have a clear understanding of the efficacy and costs of different treatments in order toadvise health decision makers of a country. The example of the use ofchemotherapy versus palliative care in non-small cell lung cancer illustrates the risk of ill advised bias. Costs analysis demonstrated that it is more cheaper to treat advanced patients with chemotherapy than with strict palliative care (56). We have to assess the real cost of high-LET particle treatments and to establish genuine comparisons with other cancer treatments, considering all factors from running costs to patient hosting and transportation. The comparison must include as endpoints quality of life, overall treatment time, acute and long term morbidity including socio-economic disruption from the patients point of view. On the other hand it should be relevant to compare different radiotherapy modalities able to answer the question: does a higher low-LET tumor dose delivered by protons or photons conformal therapy achieve the same tumor cure as the use of a high-LET beam? This question certainly complicates the set-up of clinical trials but the answer is so important that it would be a pity not to encourage the realization of such multicentric studies.

An essential point would be toinitiate cooperative radiotherapy groups to evaluate a fair comparison between the different radiotherapy modalities. These groups would have to elaborate together, as a matter of consensus, the techniques of irradiation to be used with the different particles and to install multidisciplinary international pannels in charge of establishing and controlling the tumor volumes, safety margins and quality control procedures.

This kind of international organization mixing-up low and high-LET users should facilitate the mutual comprehension, education and knowledge in order to give to future patients the best chances for cure at the best cost for society.

CONCLUSIONS

To draw an evident conclusion about the future of high-LET particles throughout the world is rather uneasy, but it is obvious that the existing facilities still have to carry on a lot of fundamental and clinical research. The light ion beam installations will have to demonstrate that the advantages related to their use in terms of local control, survival, quality of life, and reinsertion of patients are optimal for the costs involved. The existing neutron facilities should be upgraded to provide isocentric gantries and multileaf collimators. The final goal should be to develop neutron conformal therapy (with or without NCP) and organize a multicentric comparison between this technique and light ions. This comparison would include clinical and economic endpoints in order to establish the more appropriate treatment for some unfrequent but radioresistant tumors. Those trials would also have to include in the comparison photon conformal therapy and protontherapy, both with a dose escalation with regard to normal photon treatments, in order to appreciate the value of higher tumor dose delivered with low-LET radiations compared to standard tumor dose delivered with high-LET particles. Such international studies involving both low and high-LET should raise interest of the radiation oncology community for particles considered as "exotic" and expensive .

REFERENCES

1. Abstract book of the 13th Annual ESTRO Meeting, Granada, Spain, sept. 26-29, 1994. Radiother Oncol 32(suppl 1): 1-106; S1-S196, 1994
2. Amaldi U, Silari M (editors). The TERA project and Centre for Oncological Radiotherapy. INFN-LNF, SIS Eds, Frascati (Roma) Italy, 1994
3. Austin-Seymour M, Urie M, Munzenrider J et al. Considerations in fractionated proton radiation therapy: clinical potential and results. Radiother. Oncol. 17: 29-35, 1990
4. Barendsen GW, Broersen JJ. Differences in radiosensitivity of cells from various types of experimental tumors in relation to the RBE of 15 MeV neutrons. Int J Radiat Oncol Biol Phys 3: 211-14, 1977
5. Berson AM, Castro JR, Petti P et al. Charged particle irradiation of chordoma and chondrosarcoma of the base of skull and cervical spine: the Lawrence Berkeley Laboratory experience. Int J Oncol Biol Phys 15: 559-565, 1988
6. Brahme A, Källman P, Lind BK. Optimization of proton beam and heavy ion therapy using an adaptive inversion algorithm. Radiother Oncol 15, 189-197, 1989
7. Breteau N, Destembert B, Favre A et al. Fast neutron boost for the treatment of grade IV astrocytomas. Strahlenther Onkol 165: 320-323, 1989
8. Castro JR, Saunders WM, Woodruff et al. Clinical radiotherapy with heavy charged particles at the Lawrence Berkeley Laboratory. In Karcher KH, Kogelnick HD, Reinartz G eds. Progress in radio-oncology II. NY: Raven Press; 1982
9. Castro JR. Review of medical treatment with heavy charged particle beams. In Proceedings of the 2nd European Particle Accelerator Conference EPAC 90, P.Marin, P.Mandrillon Eds, pp 369-373, Ed. Frontières, Gif/Yvette, France, 1990
10. Chapman JD. Biophysical Models of Mammalian Cell Inactivation by Radiation. In Meyn RE & Withers HR (Eds). Radiation Biology in Cancer Research, Raven Press, New York, 21-32, 1988
11. Chatterjee A., Llacer J., Collier M. et al. in «Proceedings of the Vth PTCOG Meeting and International Workshop on Biomedical Accelerators», Berkeley, California, December 1-2, 1986. LBL 22962, April 1987, 213
12. Chauvel P, Wambersie A (editors). EULIMA workshop on the Potential Value of Light ion Beam Therapy. Publication EUR 12165 EN of the Commission of the European Communities, cECS-EEC-EAEC, Brussels-Luxembourg and CAL Edition, 1989
13. Chauvel P. in «Proceedings of the EULIMA workshop on the Potential Value of Light Ion Beam Therapy» (P.Chauvel & A.Wambersie, Eds), Centre Antoine-Lacassagne, Nice-France, Nov 3-5, 1988. Publication n° EUR 12165EN of the Commission of the European Communities, cECSC-EEC-EAEC, Brussels-Luxembourg, 1989 and CAL Edition (526 p), LXIII
14. Chauvel P. Osteosarcomas and soft tissue sarcomas: is there a place for high-LET radiation therapy ? Ann Oncol 3(suppl 2): S107-S110, 1992
15. Chen GT, Singh RP, Castro JR et al. Treatment planning for heavy ion radiotherapy. Int J Oncol Biol Phys 5: 1809-1812, 1979
16. Concerted Action: Cancer Treatment with Light Ionsin Europe - EULIMA. Final report. 1992
17. Duncan W, Arnott SJ, Jack WJL et al. A report of a randomized trial of d(15)+Be neutrons compared with megavoltage X-ray therapy of bladder cancer. Int J Radiat Oncol Biol Phys 11: 2043-9, 1985
18. Errington RD, Snee MP Locally advanced malignant tumors of the paranasal sinuses treated with high energy fast neutrons. In Johnson JT & Didolkar MS Eds, Head and Neck Cancer, vol. III, Excerpta Medica, Amsterdam, 939-944, 1993
19. Fertil B, Deschavanne PJ, Gueulette J et al. In vitro radiosensitivity of six human cell lines. II. Relation to the RBE of 50 MeV neutrons. Radiat Res 90: 526-37,1982
20. Gademann G, Hartmann G, Kraft G et al. The medical heavy ion therapy project at the Gesellschaft für Schwerionenforschung facility in Darmstadt. Strahlenther. 166: 34-39, 1990
21. Gademann G, Wannenmacher M. Charged particle therapy to pediatric tumors of the retroperitoneal region: a possible indication. Int J Oncol Biol Phys 22: 375-381, 1992
22. Goitein M, Abrams M, Rowell D. et al. Multi-dimensional treatment planning: II. Beam's eye view, back projection and projections through CT sections. Int J Oncol Biol Phys 9: 789-797, 1983
23. Goitein M, Abrams M. Multi-dimensional treatment planning: I Delineation of anatomy. Int J Oncol Biol Phys 9: 777-787, 1983
24. Goitein M, Chen GTY. Beam scanning for heavy charged particle radiotherapy. Med Phys 10: 831-840, 1983
25. Goitein M, Suit H. The influence of tissue inhomogeneities on the dose distribution of charged particle beams. In «Particle Radiation Therapy» Proceedings of an International Workshop, oct 1-3, 1975, Key Biscayne, Florida, American College of Radiology Ed.
26. Griffin TW, Davis R, HendricksonFR et al. Fast neutron radiation therapy for unresectable squamous cell carcinomas of the head and neck: the results for a randomized RTOG study. Int J Radiat Oncol Biol Phys 10: 2217-2223, 1984
27. Griffin TW, Pajak TF, Laramore GE et al. Analysis of neutron radiotherapy treatment complications. Bull

Cancer (Paris) 73: 582-586, 1986.
28. Griffin TW, Pajak TF, Maor GE et al. Mixed neutron/photon irradiation of unresectable squamous cell carcinomas of the head and neck: the final report of a randomized cooperative trial. Int J Radiat Oncol Biol Phys 17: 959-965, 1989
29. Haberer T, Becher W, Schardt D, Kraft G. Magnetic scanning system for heavy ion therapy. Nucl Instrum Meth Phys Res A330: 296-305, 1993
30. Kessler ML, Pitluck S, Petti P, Castro JR. Integration of multimodality imaging data for radiotherapy treatment planning. Int J Oncol Biol Phys 21: 1653-1667, 1991
31. Koehler AM, Schneider RJ, Sisterson JM. Range modulators for protons and heavy ions. Nucl Instr Meth 131: 437-440, 1975
32. Koh WJ, Krall LJ, Peters LJ et al. Neutron vs. photon radiation therapy for inoperable non-small cell lung cancer: results of a multicenter randomized trial. Int J Radiat Oncol Biol Phys 27: 499-505, 1993
33. Kraft G, Haberer T, Schardt D, Scholz M. Physics and radiobiology of heavy charged particles in relation to the use of ion beams for therapy. GSI, Report 93-50, Gesellschaft für Schwerionenforschung, 1993
34. Laramore GE, Krall JM, Griffin TW et al. Neutron versus photon irradiation for unresectable salivary gland tumors; final report of an RTOG-MRC randomized clinical trial. Int J Radiat Oncol Biol Phys 27: 235-240, 1993
35. Laramore GE, Krall JM, Thomas KJ et al. Fast neutron radiotherapy for locally advanced prostate cancer: final report of a Radiation Therapy Oncology Group randomized clinical trial. Am J Clin Oncol (CCT) 16: 164-167, 1993
36. Laramore Ge, Griffith JT, Boespflug M et al. Fast neutron raditherapyfor sarcomas of soft tissue, bone and cartilage. Am J Clin Oncol(CCT) 12: 320-326, 1989
37. Maor MH, Gillespie BW, Peters LJ et al. Neutron therapy in cervical cancer: results of a phase III RTOG study. Int J Radiat Oncol Biol Phys 14: 885-891,1988
38. Miralbell R, Urie M. Potential improvement of three dimension treatment planning and proton beams in fractionated radiotherapy of large cerebral arteriovenous malformations. Int J Oncol Biol Phys 25: 353-358, 1993
39. National Cancer Institute (NCI). Fast neutron radiation therapy in the United States: a twenty-year NCI sponsored research program (NCTWG Annual Report, 1991), National Cancer Institute, Bethesda, MD 20892, USA, 1991
40. New developments in Neutron Capture Therapy. Int J Radiat Oncol Biol Phys 28: 1055-1218, 1994 24.
41. Nowakowski, VA, Castro JR, Petti PL et al. Charged particle radiotherapy of paraspinal tumors. Int J Oncol Biol Phys 22: 295-303, 1992
42. Pedroni E, Blattmann H, Börhinger T et al. Dynamic scanning for proton therapy. In Proceedings of the Proton Radiotherapy Workshop at PSI Feb 28th-March 1st, 1991, ed H Blattmann. PSI - Bericht Nr 111: 29-33, dec 1991
43. Pignol JP, Abbe JC, Thellier M et al. Neutron Capture Radiography applied to the investigations of boron-10 biodistribution in animals: improvement in techniques of imaging and quantitative analysis. Nucl Instr Meth (accepted, in press)
44. Preliminary AUSTRON Feasibility Study, AUSTRON Planning Office, Vienna, August 1994
45. Russell KJ, Caplan RJ, Laramore GE et al. Photon versus neutron external beam radiotherapy in the treatment of locally advanced prostate cancer: results of a randomized prospective trial. Int J Radiat Oncol Biol Phys 28: 47-54, 1993
46. Sauerwein W, Ziegler W, Olthoff K et al. Neutron capture therapy using a fast neutron beam: clinical considerations and physical aspects. Strahlenther Onkol 165: 208-210, 1989
47. Scheib S, Pedroni E. Treatment planning for dynamic proton therapy. In Proceedings of the Proton Radiotherapy Workshop at PSI Feb 28th-March 1st, 1991, ed H Blattmann. PSI - Bericht Nr 111: 67-70, dec 1991
48. Schmitt G, Wambersie. A Review of the clinical results of fast neutron therapy. Radiother Oncol 17: 47-56, 1990
49. Scholz M, Kraft G. Radiobiological aspects of therapy planning for heavy charged particles beams. GSI, Report 93-51, Gesellschaft für Schwerionenforschung, 1993
50. Suit H, Du Bois W. The importance of optimal treatment planning in radiation therapy. Int J Oncol Biol Phys 21: 1471-1478, 1991
51. Sweet WH. The uses of nuclear disintegrationin the diagnosis and treatment of brain tumor. N Engl J Med 245: 875-878, 1951
52. Tubiana M, Dutreix J, Wambersie A. Introduction to Radiobiology. Taylor & Francis, London, 1990
53. Urie M, Goitein M, Wagner M. Compensating for heterogeneities in proton radiation therapy. Phys Med Biol 29: 553-566, 1983
54. Urtasun RC. Does improved dose characteristics and treatment planning correlate with a gain in therapeutic results? Evidence from past clinical experience using conventional radiation sources. Int J Radiat Oncol Biol Phys 22: 235-239, 1991
55. Wambersie A, Bewley D, Lalanne CM Prospects for the application of fast neutrons in cancer therapy. Radiobiological bases and survey of the clinical data Bull Cancer (Paris) 73: 546-61, 1986
56. Evans WK Management of metastatic NSCLC and consideration of cost. Chest 103:68-71S, 1993

Closing

Closing Address

Director of Research Center of Charged Particle Therapy
Kouzou Morita, MD

Mr. Chairman, dear colleagues and ladies and gentlemen, it is my great honor and pleasure to be able to invite a many famous quests to this international seminar, and to discuss earnestly in these three days about the charged particle therapy. I deeply appreciate for your wonderful cooperation in carrying out this seminar, and I would like to encourage your further interest in and attention to this problem. Also, I am most grateful for the hearty cooperation with IAEA and PTCOG.

It is our great pleasure to present you the integral activity of HIMAC-project including some clinical experiences, and at the same time to be able to show you the facility of HIMAC. In near future, we can show you the clinical results in detail.

During this seminar, I was able to deepen my knowledge about the charged particle therapy. In these more than 20 years, my main clinical research field was conformal radiotherapy technique using photon beam. At present, I am sure that the ideal conformal radiotherapy can be obtained by proton and heavy-ion therapy.

In conclusion, I would point out that, although we have made gratifying process during this seminar, much still remains to be done. I sincerely hope that the PTCOG meeting will get more fruitful results in near future. We would like to meet together in April next year in San Francisco.

Thank you for your kind cooperation.

Appendix

NIRS International Seminar on the Application of Heavy Ion Accelerator to Radiation Therapy of Cancer

organized by the National Institute of Radiological Sciences
in cooperation with International Atomic Energy Agency

(The meeting is in conjunction with the PTCOG XXI.)

November 14 -16, 1994, the Auditorium, NIRS, Chiba, Japan

Program

11/14(Mon.)

9:20 Opening [K. Sato, DDG (NIRS)]
Address — Y. Hirao, DG (NIRS)
Address — J. Mircheva (IAEA)
Address — M. Goitein (PTCOG)
Address — Y. Tabata, Commissioner (Atom.Ene.Com.)
9:40 Lecture (30+10) — M. R. Raju (Los Alamos)
"Some historical aspects of heavy ion radiotherapy with reference to other particles"
10:20 *Break*

10:40 Special Session on HIMAC [J. Alonso (LBL)]
10 Overview of HIMAC construction --a decade history — K. Kawachi (NIRS)
20 HIMAC accelerator --performance and feature — S. Yamada (NIRS)
10 Accelerator/facility operations — K. Ueda (Acc.Eng.Co.)
10 Q&A, Discussion on accelerator aspects of HIMAC
15 HIMAC beam delivery system --physical characteristics — T. Kanai (NIRS)
15 Pre-clinical biology at HIMAC — K. Ando (NIRS)
15 Treatment planning system at HIMAC
--present facility and future prospective — M. Endo (NIRS)
15 Q&A, Discussion on clinical irradiation facility aspects of HIMAC
12:30 **Lunch** *(IAEA Consultants' Meeting)*

14:00 Projects & Status I [E. Blakely (LBL)]
- Update on the Northeast Proton Therapy Center at MGH — A. Smith (MGH)
- Progress report on the construction of the MGH NPTC equipment — Y. Jongen (IBA)
- Heavy ion therapy at GSI — G. Kraft (GSI)
- LIGHT-ION THERAPY WITHIN THE AUSTRON PROJECT — R. Pötter (Vienna)
- Eye treatment facility at the Crocker Nuclear Facility — T. Renner (LBL)
- World experience in proton/ion therapy '94 — J. Sisterson (HCL)

15:30 One-minute-each oral presentation of Posters (see next page for poster titles.)
15:45 *Break*

16:00 Guided Tour to HIMAC facility
or Video movie of HIMAC construction and NIRS introduction (in Japanese)
17:30 *(Buffet) Reception at HIMAC building patio*

Oral presentation: **10 minutes** + 5 min.-discussion, default. **Posters** at Auditorium **Lobby.**

[Posters] (*: unable to attend)

-Heavy Ion Medical Accelerator Project by Hyogo Prefectural Government — A. Itano (HPG)
-Measurements of heavy ion beam qualities — N. Matsufuji (NIRS)
-Result of penumbra measurement in HIMAC — H. Tomura (NIRS)
-A compact proton synchrotron of combined function lattice for medical use — K. Hiramoto (Hitachi)
-Application of the dual-ring double scattering method for proton field enlargement to beam with finite emittance — Y. Takada (Tsukuba)
-Proton beam therapy at NIRS — T. Nakano (NIRS)
-Inverse problem in light ion therapy — M. Lomanov (ITEP)
-The leakage of protons between plane collimator leaves in a multileaf collimator — *E. Grusell (Uppsala)
-Preliminary measurements of auto activation of ^{12}C beams with a commercially available PET — T. Tomitani (NIRS)
-Current Status of Clinical Trial at PMRC, Tsukuba — T. Okumura (Tsukuba)

11/15 (Tue.)

9:00 Proton therapy and facility [W. Chu (LBL)]
- Emerging international consensus on clinical proton dosimetry — L. Verhey (UCSF)
- The basic principle and the interpretation of protontherapy with physics — K.E. Chiang (CUHK)
- Commissioning the TRIUMF eye facility — E. Blackmore (TRIUMF)
- Developments at the Clatterbridge Cyclotron Unit — A. Kacperek (CCO)
- Recent developments at COSY - Jülich — U. Linz (KFA Jülich)

10:30 *Break*

10:50 Biology I [van der Kogel (Nijmegen)]
- Volume effects in the rat spinal cord: assessment in vivo & in vitro — A. van der Kogel (Nijmegen)
- An RBE study of a proton beam at University of Tsukuba (vs. Co-60) — H. Tatsuzaki (Tsukuba)
- Tumor microcirculation function by proton activation positron emission — F. Ngo (Taipei)
- Assessment of late effects to high-LET radiation — E. Blakely (LBL)
- Calculation of RBE for charged particle and neutron beams based on track structure — M.Scholz/G.Kraft (GSI)
- RBE vs LET of cultured mammalian cells for heavy ion beams — Y. Furusawa (NIRS)
- LET dependence of cell death, mutation induction & chromatin breaks by accelerated C ion beams — M.Suzuki (NIRS)

12:35 **Lunch** *(PTCOG Steering Committee Meeting)*

14:05 Biology II [Skarsgard (Vancouver)]
- Biological dosimetry for heavy charged particle beams using an in vitro system — L. Skarsgard (BCCRC)
- Interplay of damage complexity and damage repair determine RBE. — J. Ward (UCSD-LaJolla)
- A general approach to the RBE evaluation in a therapeutical proton beam — M. Belli (Rome, ISS)

- Estimation of radiobiological effectiveness: proton beam 70-250 MeV
H. Paganetti (Jülich)
- Microdosimetric evaluation of heavy particle RBE vs. dose fractionation
M. Lomanov (ITEP)
- Radiobiological activities with the charged particles at Legnaro Nat'l Lab.
R. Cherubini (LNL)

15:35 *Break*

16:00 Clinical Results & Protocols [P. Chauvel (Nice)]
- COMMENCING HEAVY-ION CLINICAL TRIAL AT HIMAC
H. Tsujii (NIRS)
- The potential use of protontherapy in pineal tumors J. Habrand (Orsay)
- The use of the JINR proton beam for the uterus cervix cancer treatment
A. Molokanov (Dubna)
- Proton therapy of low-grade chondrosarcomas involving the cranial base
N. Liebsch (MGH)
- A Medical network for a non-hospital based proton facility G. Munkel (PSI)

17:30 Transport to Banquet Site
18:30 *Conference Banquet* (Buffet style) at Chiba-Kyosai-Kaikan

11/16 (Wed.)

9:00 Beam Delivery and Dosimetry [Renner (LBL)]
- NAC: Progress & dosimetry intercomparisons D. Jones (NAC)
- Absorbed dose calibrations for the MGH-HCL proton therapy program
A.Smith/M.Goitein (MGH)
- Upstream absorber and modulator M. Wagner (HCL)
- Progress report on the Berlin eye therapy project (Beam Delivery)
H. Homeyer (HMI)
- Uneven ridge filter for conformal therapy and variable bolus
using filtered back projection technique Y. Hayakawa (Tsukuba)
- Depth-dose and fluence distributions when using heavy ion beams
L. Sihver (GSI)
- Patient positioning system in HIMAC S. Minohara (NIRS)

10:45 *Break*

11:05 Treatment Planning [Verhey (UCSF)]
- A convolution algorithm for proton beam treatment planning dosimetry
D. Miller (LLUMC)
- Review of eye treatment planning at Clatterbridge M.Sheen/A.Kacperek (CCO)
- Present status of MGH/HCL proton treatment planning system M. Goitein (MGH)
- Implementing treatment planning for scanned proton beams
on the PSI compact gantry E. Pedroni (PSI)
- Present status of treatment planning and operation of the PSI
proton therapy device G. Munkel (PSI)
- Dose optimization of heavy charged particle therapy by DVHs
J.-E. Mizoe (NIRS)

12:35 **Lunch**

14:05 Projects & Status II [V. Khoroshkov (ITEP)]

- APPLICATIONS OF PROTONS IN CANCER TREATMENT
  J.M. Slater (LLUMC)
- The Bavarian hospital based proton therapy at Regensburg
  M. Herbst (Regensburg)
- Proton therapy in Moscow K.Onosovsky/V.Khoroshkov (ITEP)
- Compact 200 MeV proton synchrotron based on 5T magnets
  G. Silvestrov (Novosibirsk)
- Present status of the Progetto Adroterapia M. Silari (CNR, Milan)
- Brookhaven linear accelerator proton therapy facility plan Y.Y. Lee (BNL)
- Dedicated accelerator project for proton therapy at Kyoto University
  A. Noda (Kyoto)

15:35 *Break*

16:10 *PTCOG Business Meeting [PTCOG Steering Com.]*

16:30 Perspectives [Tsujii (NIRS)]

- Specification of RADIATION QUALITY AND RBE PROBLEM IN HIGH-LET RADIOTHERAPY A. Wambersie (UCL)
- ROLE OF HIGH-LET ION THERAPY IN CANCER J. Castro (UC/LBL)
- Prospect of charged particle therapy K. Kawachi (NIRS)

17:15 Closing
Address K. Morita, D-RCCPT (NIRS)
Address M. Goitein (MGH)

17:25 Adjourn

Post-conference activity
11/17 (Thu.)

8:30 Bus Departure to Tsukuba from NIRS
11:00 Visit Proton Therapy Center of Tsukuba University located in KEK
S. Fukumoto (Tsukuba)
12:30 ***Lunch***
13:30 Bus *tour to Mt. Tsukuba* (-15:30 / Leaving Tsukuba for return)
18:00 Bus Arrival to Hotel

List of Participants

Name	E-mail address Affiliation, Dept. Mailing address	phone number Mail Stop	Fax number Country

Note: Participants from NIRS are listed without Mailing address. See the end of the list for detail.

Abe, Y		+81-22-273-9505	Fax:+22-275-7324
	Tohoku Univ., Inst. Devel. Aging & Cancer, Dept. Radiol. & Nucl. Med. 2-1 Seiryo-cho, Sendai-shi 980		Japan
Akine, Y.		+81-3-3542-2511	Fax:3-3542-3815
	NCC Hospital, Rad. Therapy 5-1-1 Tsukiji, Chuo-ku, Tokyo		Japan
Alonso, J.R.	JRAlonso@lbl.gov	+1-510-486-4206	Fax:510-486-5788
	LBL, Acc. & Fusion Res. Div. 1 Cyclotron Rd, Berkeley, CA 94720	MS 71-259	USA
Ando, K.	C	+81-43-251-2111	Fax:43-256-9616
Arai, Y.	yarai@dokkyomed.ac.jp	+81-282-87-2171	Fax:282-86-4940
	Dokkyo U. Med. School, Radiology 880 Kitakobayashi, Mibumachi, Shimotsuga-gun, Tochigi		Japan
Araki N.	A araki@nirs.go.jp		
Asai, O.		+81-78-682-6126	Fax:78-682-6209
	MELCO, Kobe Works 1-1-2 Wadazaki, Hyogo-ku, Kobe-shi		Japan
Beeckman, W.		+32-10-47-5890	Fax:10-47-5810
	IBA 6 Rue Jean Lenoir, Louvain-La-Neuve, B-1348		Belgium
Belli, M.	BELLI@sanita.infn.it	+39-6-4990-2916	Fax:6-4462872
	ISS, Lab. di Fisica Viale Regina Elena 299, Roma, I-00161		Italy
Blackmore, E.W.	EWB@triumf.ca	+1-604-222-1047	Fax:604-222-1074
	TRIUMF 4004 Wesbrook Mall, Vancouver, B.C., V6T 2A3		Canada
Blakely, E.A.	EABlakely@lbl.gov	+1-510-486-6595	Fax:510-486-4475
	LBL, Life Science Div. 1 Cyclotron Rd, Berkeley, CA 94720	MS 70A-1118	USA
Castro, J.R.	JRCastro@Biovax.lbl.gov	+1-510-486-6325	Fax:510-486-4170
	UC-LBL, Radiation Oncology 1 Cyclotron Rd, Berkeley, CA 94720	MS 55-121	USA
Chauvel, P.		+33-93-18-8022	Fax:93-71-0479
	CAL, Biomedical Cyclotron, Dept. Med. Appl. 227 Avenue de la Lanterne, Nice, F-06200		France
Chen, K.Y.		+886-2-875-7015	Fax:2-873-2815
	Veterans General Hospital - Taipei, Cancer Center		

	201 Shihpai Road, Section II, Taipei		Taiwan
Chen, Y.	C		
Cherubini, R.	Cherubini@legnaro.infn.it INFN, LNL Via Romea n.4, Legnaro(Padova), I-35020	+39-49-8292393	Fax:49-641925 Italy
Chiang, K.E.	CUHK, Physics Dept. 50 Grove Street, Wellesley, MA 02181	+1-617-237-2299	USA
Chu, W.T.	WTChu@lbl.gov LBL 1 Cyclotron Rd, Berkeley, CA 94720	+1-510-486-7735 MS 64-227	Fax:510-486-5788 USA
Endo, M.	A endo@nirs.go.jp		
Fukumoto, S.	fukumoto@medvax.kek.jp NLHEP 1-1 Oho, Tsukuba-shi, Ibaraki-ken 305	+81-298-64-1171x3759	F:298-64-2575 Japan
Fukumura, A	P fukumura@nirs.go.jp		
Furusawa, Y.	A		
Goitein, M.	MGH, Radiation Oncology 75 Blossom Court NPTC, Boston, MA 02114	+1-617-724-9529	Fax:617-724-9532 USA
Gueulette, J.R.	UCL, Radiobiology & Radioprotection 54 Ave. Hippocrate, Brussels, B-1200	+32-2-764-5480	Fax:2-764-9425 Belgium
Gunel, N.	Gazi Univ. Ankara, Oncology Dept. Sehit Danis Tunaligil Sok. 10/14, Maltepe Ankara	+90-312-229-1711	Fax:312-212-4647 Turkey
Habrand, J.-L.	CPO 15 Rue Georges Clemenceau, Orsay Cedex, F-91406	+33-1-6941-7165 BT-101	Fax:1-6941-6470 France
Hayakawa, Y.	U. Tsukuba, Inst. Basic Med. Sci. Tennoudai, Tsukuba-shi, Ibaraki-ken 305	+81-298-64-2571	Fax:298-64-2575 Japan
Herbst, M.	Med. Univ. Regensburg, Rad.Onc. Dept. Franz-Josef-Strauss-Allee 11, Regensburg, D-93042	+49-941-944-7601	Fax:941-944-7602 Germany
Hiramoto, K.	hiramoto@hrl.hitachi.co.jp Hitachi Ltd., Energy Research Lab., Second Div. 7-2-1 Oomika-cho, Hitachi-shi, Ibaraki-ken 319-12	+81-294-53-3111	Fax:294-53-2830 Japan
Hiraoka, T.	P		
Hirota, J.-I.	Hitachi Ltd., Energy Research Lab., Second Div. 7-2-1 Oomika-cho, Hitachi-shi, Ibaraki-ken 319-12	+81-294-53-3111	Fax:294-53-2830 Japan

Hishikawa, Y. +81-78-362-3265 Fax:78-362-3913
Hyogo Pref. Gov., Regional Hygiene Div., Charged Particle Treatment
5-10-1 Shimoyamate-Dori, Chuo-ku, Kobe-shi, Hyogo 650 Japan

Homeyer, H. Homeyer@vax.hmi.d400.de +49-30-8062-2414 Fax:30-8062-2097
HMI-Berlin, Festkorperphysik
Glienlicker-Str. 100, Berlin Germany

Ichitani, T. +81-3-5488-8319 Fax:3-5488-8321
SHI, Quantum Equipment
5-9-11 Kitashinagawa, Shinagawa-ku, Tokyo 141 Japan

Inoue, M. +81-774-32-5806 Fax:774-33-5509
Kyoto U., Inst. Chem. Res., Nucl. ci. Res. Fac.
Gokanosho, Uji-city, Kyoto 611 Japan

Inoue, T. +81-479-86-4721 Fax:479-86-5412
Daiichi Radioisotope Lab., Ltd.
453-1 Shimoohkara, Matuo-machi, Sanbu-gun, Chiba 289-15 Japan

Irie, Y. iriey@kekvax.kek.jp +81-298-64-5607 Fax:298-64-3202
NLHEP, Booster Synchrotron Utilization Facility
1-1 Oho, Tsukuba-city, Ibaraki 305 Japan

Ishikawa, A. M

Ishikawa, T. +81-3-5269-5328 Fax:3-5269-5329
Fujita Corp., SR project
5-23-15 Sendagaya, Shibuya-ku, Tokyo 151 Japan

Itano, A. itano_a@nirs.go.jp +81-78-341-7711x3302 F:78-362-3913
Hyogo Pref. Gov., Regional Hygiene Div., Charged Particle Treatment
5-10-1 Shimoyamate-Dori, Chuo-ku, Kobe-shi, Hyogo 650 Japan

Jones, D.T. Jones@nac.ac.za +27-24-843-3820 Fax:24-843-3525
NAC, Med. Rad. Div.
POBox 72, Faure 7131 South Africa

Jongen, Y. +32-10-47-5890 Fax:10-47-5810
IBA
Rue Jean Lenoir 6, Louvain-la-Neuve, B-1348 Belgium

Kacperek, A. Andrzejk@smtpgate.ccotrust.co.uk +41-51-334-6366 Fax:51-334-2845
CCO, Douglas Cyclotron Unit
Bebington, Wirral L63 4JY UK

Kamada, T. M

Kanai. T. A kanai@nirs.go.jp

Kanazawa, M. A

Karashima, H. +81-78-341-7711x3301 F:78-362-3913
Hyogo Pref. Gov., Regional Hygiene Div., Charged Particle Treatment
5-10-1 Shimoyamate-Dori, Chuo-ku, Kobe-shi, Hyogo 650 Japan

Kato, H. M

Kawachi, K. A

Khoroshkov, V.S. Bolshakov@vitep2.itep.msk.su +7-095-123-8092 Fax:095-123-6584
ITEP, Medical Physics
Bolshaya Cheremushkinskaya 25, Moscow 117259 Russia

Khorprasert, C.
Chulaalongkom Hospital, Div. Radiotherapy
Thailand

Kitagawa, A. A kitagawa@nirs.go.jp

Kobayashi, S. Safety Anal. Unit

Koike, S. C

Kojima, E. H

Kostova, P.G. +359-2-7123-320 Fax:2-720-651
National Oncology Center, Gynecology Clinic
6 Plovdivsko pole str., Sofia 1756 Bulgaria

Koyama-Ito, H. A. koyama@nirs.go.jp

Kraft, G. G.Kraft@GSI.DE +49-6159-71-2607 Fax:6159-71-2106
GSI, Biophysik
Planckstr. 1, Darmstadt D-64291 Germany

Kutsutani-Nakamura, Y. M Fax:43-256-8301

Lee, Y.Y. yylee@bnl.gov +1-516-282-4663 Fax:516-282-5954
BNL, AGS Dept. Bldg. 911B
Upton, NY 11973 USA

Li, J.
ShanXi Province Tumour Hospital, Radiotherapy
China

Liebsch, N.J. +1-617-726-8153 Fax:617-726-3603
MGH, Dept. Rad. Onc.
Boston, MA 02114 USA

Lin, F.-J. +886-2-834-5429 Fax:2-834-5428
ShinKong Memorial Hospital, Dept. Rad. Therapy & Oncol.
95 Wen Chang Road, Shih Lin, Taipei 111 Taiwan

Linz, U. +49-2461-61-2651 Fax:2461-61-3930
KFA-Juelich, IKP
Postfach 1913, Juelich D-52425 Germany

Liu, Y.-C. +886-35-783822 Fax:35-783892
SRRC
No.1, R&D Road VI, Hsinchu Science-Based Industrial Park Taiwan

Lomanov, M. lomanov@vxitep.itep.ru +7-095-125-9045 Fax:095-123-6584
ITEP, Dept. Medical Physics
B. Cheremushkinskaya 25, Moscow 117259 Russia

Ludewigt, B. BALudewigt@lbl.gov +1-510-486-7733 Fax:510-486-5788
LBL, Life Science Div.
1 Cyclotron Rd, Berkeley, CA 94720 USA

Manatrakul, N.	National Cancer Institute, Div. Rad. Onc. Rama VI Rd., Bangkok 10400	+66-2-246-1297	Thailand
Martin, R.	Acctek Associates 901 S. Kensington, LaGrange, IL 60525	+1-708-252-6786	Fax:708-252-4007 USA
Matsubara, H.	Chiba U., Dept. Surgery II 1-8-1 Inohana, Chuo-ku, Chiba 260	+81-43-226-2110	Fax:43-226-2113 Japan
Matsufuji, N.	A matufuji@nirs.go.jp		
Matsuoka, Y	M		
Matsushita, S.	Lab. Animals Sec.		Fax:43-251-6404
Miller, D.W.	dmiller@prolit.llu.edu LLUMC, Dept. Rad. Med. 11234 Anderson St., Loma Linda, CA 92354	+1-909-824-4257	Fax:909-824-4083 USA
Minohara, S.	A		
Mircheva, J.	rlm@iaea1.iaea.or.at IAEA, Human Health Div. POBox 100, Vienna, A-1400	+43-1-2360-1667	Fax:1-234564 Austria
Miyahara, N.	A		
Miyamoto, T.	M		
Mizoe, J.-E.	M j_mizoe@nirs.go.jp		
Molokanov, A.G.	molok@lnpvx2.jinr.dubna.su JINR, Lab. Nuclear Problems 141980 Dubna, Moscow Region	+7-09621-65563	Fax:09621-66666 Russia
Morita, K.	Director, Res. Center Charged Particle Therapy		
Mowat, R.	mowat@pyvax.physics.ncsu.edu NCSU, Physics Dept. Box 8202, Raleigh, NC 27695-8202	+1-919-515-4492	Fax:919-515-4496 USA
Mukai, M.	M		
Munkel, G.	munkel@vax.psi.ch PSI, Dept. Rad. Med. Villigen-PSI, CH-5232	+41-56-99-3512	Fax:56-99-3515 Switzerland
Myomin	U. Tsukuba, Proton Med. Res. Center 1-1-1 Tennoudai, Tsukuba-shi, Ibaraki-ken 305	+81-298-53-3210	Fax:298-64-2575 Japan
Nakabushi, H.	SHI, Quantum Equipment 5-9-11 Kitashinagawa, Shinagawa-ku, Tokyo 141	+81-3-5488-8319	Fax:3-5488-8321 Japan
Nakajima, H.	Aloka Co. Ltd., Osaka branch	+81-6-344-5391	Fax:6-344-5396

	1-4-28 Doujimahama, Kita-ku, Osaka-shi 530		Japan
Nakano, T.	M		
Nemoto, K.	Physiol. & Pathol. Div.		
Ngo, F. Q.H.		+886-2-826-7198	Fax:2-821-7446
	National Yang Ming Univ., Med. Tech., Div. Radiol. Sci. 155 Li Nung St., Shih-Pai, Taipei		Taiwan
Noda, A.	noda@jpnkekvx.bitnet	+81-774-32-5806	Fax:774-33-5509
	Kyoto U., Inst. Chem. Res., Nucl. ci. Res. Fac. Gokanosho, Uji-city, Kyoto 611		Japan
Noda, K.	A		
Nohara, N.	P		
Ogawa, H.	A		
Ogino, T.		+81-471-33-1111	Fax:471-31-4724
	NCC Hosp. East, Dept. Radiology 6-5-1 Kashiwa-no-ha, Kashiwa-shi, Chiba 277		Japan
Okada, O.		+81-3-3258-1111	Fax:3-3258-2348
	Hitachi Ltd., Fusion & Accel. Div. 4-6 Kanda Surugadai, Chiyoda-ku, Tokyo 101		Japan
Okada, S.		+81-3-3506-9071	Fax:3-3506-9075
	Nucl. Systems Assoc.	4F Nakai Bldg.	
	2-13-6 Shimbashi, Minato-ku, Tokyo 105		Japan
Okumura, T.		+81-298-53-3210	Fax:298-64-2575
	U. Tsukuba, Proton Med. Res. Center 1-1-1 Tennoudai, Tsukuba-shi, Ibaraki-ken 305		Japan
Omata, K.	P		
Ono, K.		+81-724-52-0901x2317	F:724-52-8194
	Kyoto U., RRI, Rad. Onc. Res. Lab. Kumatori-cho, Sennan-gun, Osaka 590-04		Japan
Onosovsky, K.K.	bolshakov@vitep2.itep.msk.su	+7-095-123-8092	Fax:095-125-5806
	ITEP, Ring Accelerators Bolshaya Cheremushkinskaya 25, Moscow 117259		Russia
Otsu, H	Physiol. & Pathol. Div.		
Paganetti, H.	h.paganetti@kfa-juelich.de	+49-2461-61-4643	Fax:2461-61-2820
	Forschungszentrum-Juelich, IME Juelich D-52425		Germany
Pedroni, E.S.	pedroni@cageir5a.bitnet	+41-56-99-3518	Fax:56-99-3515
	PSI, Dept. Rad. Med. Villigen-PSI, CH-5232		Switzerland
Pötter, R.		+43-1-40400x2692	Fax:1-40400x2693
	GH Vienna, Div. Radiotherapy & Radiobiol. Waehringer Guertel 18-20, Vienna A-1090		Austria

Raju, M.R.		+1-505-667-2750	Fax:505-665-3024
	LANL, Life Science Div., Cell Growth, Damage & Repair		
	MS M888, Los Alamos, NM 87545		USA
Renner, T.R.	TRRenner@lbl.gov	+1-510-486-7730	Fax:510-486-7696
	LBL, Acc. & Fusion Res. Div.	MS 2-400	
	1 Cyclotron Rd, Berkeley, CA 94720		USA
Sakamoto H.		+81-6-497-5471	Fax:6-497-5613
	MELCO, Mechatronics Eng. Sec. D, Comm. Equip. Works		
	8-1-1 Tsukaguchi-honmachi, Amagasaki-city, Hyogo 661		Japan
Sangaletti, L.	Sangaletti@mi.infn.it	+39-2-7064-3356	Fax:2-266-3030
	ITBA		
	Via Ampere 56, Milano, I-20131		Italy
Sato, T.		+81-3-5488-8319	Fax:3-5488-8321
	SHI, Quantum Equipment		
	5-9-11 Kitashinagawa, Shinagawa-ku, Tokyo 141		Japan
Sato, Y.	A		
Scholz, M.	as09@ddagsi3.gsi.de	+49-6151-359-2627	Fax:6151-359-2106
	GSI, Biophysik		
	Planckstr. 1, Darmstadt D-64291		Germany
Shamim, A.		+80-02-50-7278	
	Dhaka Medical College Hospital, Radiotherapy Dept.		
	Dhaka		Bangladesh
Shimizu, W.	wshimizu@ncc.go.jp	+81-471-33-1111	Fax:471-31-4724
	NCC Hosp. East, Dept. Radiology		
	6-5-1 Kashiwa-no-ha, Kashiwa-shi, Chiba 277		Japan
Shino, M.		+81-422-45-5129	Fax:422-45-2214
	Aloka Ltd.		
	6-22-1 Mure, Mitaka-shi, Tokyo 181		Japan
Shiono, S.	shiono@bio.crl.melco.co.jp	+81-6-497-7066	Fax:6-497-7294
	MELCO, Central Res. Lab.		
	Amagasaki-shi, Hyogo 661		Japan
Shiragai, A.	P		
Sihver, L.	bio@vscn.gsi.de	+49-6151-359-2432	Fax:6151-359-2785
	GSI, Biophysik		
	Planckstr. 1, Darmstadt D-64291		Germany
Silari, M.	silari@cernvm.cern.ch	+39-2-7064-3356	Fax:2-266-3030
	CNR-ITBA		
	Via Ampere 56, Milano, I-20131		Italy
Silvestrov, G.	silvestrov@inp.nsk.su	+7-3832-35-6031	Fax:3832-35-2163
	Budker Inst. Nucl. Phys.		
	Novosibirsk 630090		Russia
Sisterson, J.M.	sisterson@huhepl.harvard.edu	+1-617-495-2885	Fax:617-495-8054
	HCL		
	44 Oxford St., Cambridge, MA 02138		USA

Skarsgard, L.D.		+1-604-877-6010x3010	F:604-877-0743
	BCCRC, Medical Biophys. 601 West 10th Avenue, Vancouver, B.C. V5Z 1L3		Canada
Slater, J.M.	74053,21	+1-909-824-4644	Fax:909-824-4824
	LLUMC, Dept. Rad. Med. 11234 Anderson St., Loma Linda, CA 92354		USA
Smith, A.R.		+1-617-724-1197	Fax:617-724-1095
	MGH, Rad. Onc. Fruit Street, Boston, MA 02114		USA
Soga, F.	A		
Suzuki, M.	A		
Tagami, J.S.		+1-909-599-7769	Fax:909-599-1399
	Tagami & Assoc. 316 San Simeon Road, San Dimas, CA		USA
Takada, E.	A takada@nirs.go.jp		
Takada, Y.	takada@kekvax.kek.jp	+81-298-64-2571	Fax:298-64-2575
	U. Tsukuba, Inst. Appl. Phys. 1-1-1 Tennoudai, Tsukuba-shi, Ibaraki-ken 305		Japan
Takeda, A.		+81-75-702-1141	Fax:75-702-2141
	Health Research Foundation	5F Pasteur Bldg.	
	103-5 Tanakamonzen-cho, Sakyo-Ku, Kyoto-shi 606		Japan
Taniguchi, M.		+81-3-5381-5191	Fax:3-3345-8330
	Taisei Corp., Nucl. Facility 1-25-1 Nishi-Shinjuku, Shinjuku-ku, Tokyo 163-05		Japan
Tatsumi, K.	Biology		
Tatsuzaki, H.	tatsu@sakura.cc.tsukuba.ac.jp	+81-298-53-3210	Fax:298-53-3039
	U. Tsukuba, Inst. Clinic. Med., Dept. Rad. Onc. Tennoudai, Tsukuba-shi, Ibaraki-ken 305		Japan
Terahara, A.	M GED00620@niftyserve.or.jp		
Tomitani, T.	P tom@nirs.go.jp		
Tomura, H.	A tomura@nirs.go.jp		
Torikoshi, M.	A		
Tsuboi, A.	H		
Tsuji, H.		+81-298-53-3210	Fax:298-64-2575
	U. Tsukuba, Proton Med. Res. Center 1-1-1 Tennoudai, Tsukuba-shi, Ibaraki-ken 305		Japan
Tsujii, H.	M		
Ueda, K		+81-43-251-6440	Fax:43-251-6623
	Accelerator Engineering Corp. 2-10-14-302 Konakadai, Inage-ku, Chiba-shi 263		Japan

van der Kogel, A.J. RADPIE_AK@aznvx1.azn.nl +31-80-615354 Fax:80-568350
UH Nijmegen St Radboud, Inst.Radiotherapy
POBox9101, Geert Grooteplein 32, Nijmegen, 6500HB The Netherlands

Verhey, L.J. verhey@radonc4.ucsf.edu +1-415-476-1208 Fax:415-476-8734
UCSF, Rad. Onc. Dept. Long Hospital
L-08 Box 0226, San Francisco, CA 94143-0226 USA

Wagner, M.S. wagner@huhepl.harvard.edu +1-617-495-2885 Fax:617-495-8054
HCL
44 Oxford St., Cambridge, MA 02138 USA

Wambersie, A.C.M. +32-2-764-4726 Fax:2-764-3703
UCL- Cliniques St. Luc, Unit Radiother. Neutron & Curiether.
Av. Hippocrate 54 69, Brussels, B-1200 Belgium

Ward, J.F. +1-619-534-4918 Fax:619-534-0265
UCSD, Radiology Dept. 0610
UCSD, La Jolla, CA 92093 USA

Yamada, S. A

Yamada, T. +81-292-82-5644
JAERI-Tokai, JRR4 Operation
Tokai-mura, Naka-gun, Ibaraki 319-11 Japan

Yamashita, S. +81-48-462-1101 Fax:48-464-1138
National Saitama Hospital, Dept. Radiology
2-1 Suwa, Wako-shi, Saitama 351-01

Guest participants include:

Tabata, Y	Terashima, T.	Matsudaira, H.	Umegaki, Y.
Inada, T.	Ito, A.	Suzuki, N.	Hashimoto, N.
Maezawa, H.	Kawashima, K.	Tateno, Y.	Tsunemoto, H.

NIRS address and abbreviated symbols for division in the above list are:

+81-43-251-2111 Fax:43-256-9616
4-9-1 Anagawa, Inage-ku, Chiba-shi 263 Japan

Division symbols:

A=Accel. Phys. & Eng. Div. +81-43-256-0122 Fax:43-251-1840 or 287-0417
M=Rad. Med. Div. Fax:43-256-6506 or 256-6507
P=Physics Div. Fax:43-284-0918
C=Clinic. Res & Rad. Health Div.
H=Rad. Hazards Div.